Hashemite Kingdom of Jordan

Jordan Journal of Biological Sciences

An International Peer-Reviewed Scientific Journal

Financed by the Scientific Research and Innovation Support Fund

This title is indexed in Scopus

http://jjbs.hu.edu.jo/

المجلة الأردنية للعلوم الحياتية
Jordan Journal of Biological Sciences (JJBS)
http://jjbs.hu.edu.jo

Jordan Journal of Biological Sciences (JJBS) (ISSN: 1995–6673 (Print); 2307-7166 (Online)): An International Peer- Reviewed Open Access Research Journal financed by the Scientific Research and Innovation Support Fund, Ministry of Higher Education and Scientific Research, Jordan and published quarterly by the Deanship of Scientific Research , The Hashemite University, Jordan.

Editor-in-Chief

Professor Wedyan, Mohammed A.
Environmental Biochemistry,
The Hashemite University

Assistant Editor

Professor Muhannad, Massadeh I.
Microbial Biotechnology,
The Hashemite University

Editorial Board (Arranged alphabetically)

Professor Al-Eitan, Laith
Biotechnology and Genetic Engineering
Jordan University of Science and Technology

Professor Al-Khateeb , Wesam M.
Plant Genetics and Biotechnology
Yarmouk University

Professor Al-Ghzawi , Abdul Latief A.
Plant biotechnology
The Hashemite University

Professor Al-Najjar , Tariq Hasan Ahmad.
Marine Biology
The University of Jordan/ Aqaba

Professor Khleifat, Khaled M.
Microbiology and Biotechnology
Mutah University

Professor Odat , Nidal
Plant biodiversity
Al Balqa Applied University

Associate Editorial Board

Professor Al-Farawati, Radwan K.
Oceanography Laboratories ,King Abdulaziz University,Saudi Arabia

Professor Dheeb, Batol I.
Medical Mycology, University of Samarra, Iraq

Professor El-Tarabily, Khaled A.
Microbiology, United Arab Emirates University, United Arab Emirates

Professor Radu, Marius-Daniel
Biochemistry and physiology, Ovidius University of Constanta, Romania

Dr Ahmadi, Rahim
Avicenna International College, Hungary

Dr BĂNĂDUC, Doru S.
Ecology and environment protection and biology, University of Sibiu, Romania

Editorial Board Support Team

Language Editor
Professor Shadi Neimneh

Publishing Layout
Eng.Mohannad Oqdeh

Submission Address

Professor Wedyan, Mohammed A.
The Hashemite Universit y
P.O. Box 330127, Zarqa, 13115, Jordan
Phone: +962-5-3903333 ext.4147
E-Mail: jjbs@hu.edu.jo

المجلة الاردنية للعلوم الحياتية
Jordan Journal of Biological Sciences (JJBS)
http://jjbs.hu.edu.jo

International Advisory Board (Arranged alphabetically)

Professor Abdelaziz M. Hussein
Mansoura University, Egypt

Professor Abhik Gupta
School of Environmental Sciences, Assam University, India

Professor Adnan Bashir Al- lahham
German Jordanian University, Jordan

Professor Ahmed Deaf Allah Telfah
Leibniz-Institut für Analytische Wissenschaften- ,Germany

Professor Ahmed Amri
genetic resources ICARDA in Morocco, Morocco

Dr. Amalia A Tsiami
University of West London, London

Professor Amir Menwer Al-Hroob
Al-Hussein Bin Talal University, Jordan

Professor David Modry
Masaryk University, Science Department, Czech

Professor Elif Demirkan
Bursa Uludag University Turkey, Turkey

Professor Emad Hussein Malkawi
Yarmouk University, Jordan

Professor Erhan Nurettin ÜNLÜ
Turkey Dicle University,Turkey

Professor Gottfried Hartmut Richard Jetschke
Friedrich-Schiller-University of Jena, Germany

Professor Hassan Mohammed M. Abd El-Rahman Awad
National Research Centre, Egypt

Professor Ihsan Ali Mahasneh
Al al-Bayt University, Jordan

Professor Khalid M. Al-Batayneh
Yarmouk University, Jordan

Professor Khalid Majid Hameed
Dept. of Biological Sciences, Duke University, USA

Professor Laith Abd Jalil Jawad
School of Environmental and Animal Sciences, Unitec Institute of Technology Auckland ,New Zealand

Professor Maizirwan Bin Muhammad Mel
International Islamic University Malaysia, Malaysia

Professor Maroof A. Khalaf
Jordan University/ Aqaba , Jordan

Professor Mohamed Emara
Chartered Management Institute, UK

Professor Mohammed H. Abu-Dieyeh
Biological and Environmental Sciences, Qatar University, Qatar

Professor Nabil Joseph Awadalla Girgis
King Khalid University, Saudi Arabia

Professor Nour Shafik Emam El-Gendy
Egyptian Petroleum Research Institute, Egypt

Professor Olga Anne
Marine Technology and Natural Sciences of Klaipėda University, Lithuania

Professor Omar F. Khabour
Jordan University of Science and Technology, Jordan

Professor Roy Hendroko Setyobudi
University of Muhammadiyah, Indonesia

Professor Saleem Hmood Aladaileh
Al-Hussein Bin Talal University, Jordan

Dr. Salem M Akel
St, Jude's Children's Research Hospital, USA

Professor Walid Al Zyoud
German Jordanian University, Jordan

Professor Yacob Hassan Yacob
Al al-Bayt University, Jordan

Instructions to Authors

Scopes

Study areas include cell biology, genomics, microbiology, immunology, molecular biology, biochemistry, embryology, immunogenetics, cell and tissue culture, molecular ecology, genetic engineering and biological engineering, bioremediation and biodegradation, bioinformatics, biotechnology regulations, gene therapy, organismal biology, microbial and environmental biotechnology, marine sciences. The JJBS welcomes the submission of manuscript that meets the general criteria of significance and academic excellence. All articles published in JJBS are peer-reviewed. Papers will be published approximately one to two months after acceptance.

Type of Papers

The journal publishes high-quality original scientific papers, short communications, correspondence and case studies. Review articles are usually by invitation only. However, Review articles of current interest and high standard will be considered.

Submission of Manuscript

Manuscript, or the essence of their content, must be previously unpublished and should not be under simultaneous consideration by another journal. The authors should also declare if any similar work has been submitted to or published by another journal. They should also declare that it has not been submitted/ published elsewhere in the same form, in English or in any other language, without the written consent of the Publisher. The authors should also declare that the paper is the original work of the author(s) and not copied (in whole or in part) from any other work. All papers will be automatically checked for duplicate publication and plagiarism. If detected, appropriate action will be taken in accordance with International Ethical Guideline. By virtue of the submitted manuscript, the corresponding author acknowledges that all the co-authors have seen and approved the final version of the manuscript. The corresponding author should provide all co-authors with information regarding the manuscript, and obtain their approval before submitting any revisions. Electronic submission of manuscripts is strongly recommended, provided that the text, tables and figures are included in a single Microsoft Word file. Submit manuscript as e-mail attachment to the Editorial Office at: JJBS@hu.edu.jo. After submission, a manuscript number will be communicated to the corresponding author within 48 hours.

Peer-review Process

It is requested to submit, with the manuscript, the names, addresses and e-mail addresses of at least 4 potential reviewers. It is the sole right of the editor to decide whether or not the suggested reviewers to be used. The reviewers' comments will be sent to authors within 6-8 weeks after submission.
Manuscripts and figures for review will not be returned to authors whether the editorial decision is to accept, revise, or reject. All Case Reports and Short Communication must include at least one table and/ or one figure.

Preparation of Manuscript

The manuscript should be written in English with simple lay out. The text should be prepared in single column format. Bold face, italics, subscripts, superscripts etc. can be used. Pages should be numbered consecutively, beginning with the title page and continuing through the last page of typewritten material.

The text can be divided into numbered sections with brief headings. Starting from introduction with section 1. Subsections should be numbered (for example 2.1 (then 2.1.1, 2.1.2, 2.2, etc.), up to three levels. Manuscripts in general should be organized in the following manner:

Title Page

The title page should contain a brief title, correct first name, middle initial and family name of each author and name and address of the department(s) and institution(s) from where the research was carried out for each author. The title should be without any abbreviations and it should enlighten the contents of the paper. All affiliations should be provided with a lower-case superscript number just after the author's name and in front of the appropriate address.
The name of the corresponding author should be indicated along with telephone and fax numbers (with country and area code) along with full postal address and e-mail address.

Abstract

The abstract should be concise and informative. It should not exceed **350 words** in length for full manuscript and Review article and **150 words** in case of Case Report and/ or Short Communication. It should briefly describe the purpose of the work, techniques and methods used, major findings with important data and conclusions. No references should be cited in this part. Generally non-standard abbreviations should not be used, if necessary they should be clearly defined in the abstract, at first use.

Keywords

Immediately after the abstract, **about 4-8 keywords** should be given. Use of abbreviations should be avoided, only standard abbreviations, well known in the established area may be used, if appropriate. These keywords will be used for indexing.

Abbreviations

Non-standard abbreviations should be listed and full form of each abbreviation should be given in parentheses at first use in the text.

Introduction

Provide a factual background, clearly defined problem, proposed solution, a brief literature survey and the scope and justification of the work done.

Materials and Methods

Give adequate information to allow the experiment to be reproduced. Already published methods should be mentioned with references. Significant modifications of published methods and new methods should be described in detail. Capitalize trade names and include the manufacturer's name and address. Subheading should be used.

Results

Results should be clearly described in a concise manner. Results for different parameters should be described under subheadings or in separate paragraph. Results should be explained, but largely without referring to the literature. Table or figure numbers should be mentioned in parentheses for better understanding.

Discussion

The discussion should not repeat the results, but provide detailed interpretation of data. This should interpret the significance of the findings of the work. Citations should be given in support of the findings. The results and discussion part can also be described as separate, if appropriate. The Results and Discussion sections can include subheadings, and when appropriate, both sections can be combined

Conclusions

This should briefly state the major findings of the study.

Acknowledgment

A brief acknowledgment section may be given after the conclusion section just before the references. The acknowledgment of people who provided assistance in manuscript preparation, funding for research, etc. should be listed in this section.

Tables and Figures

Tables and figures should be presented as per their appearance in the text. It is suggested that the discussion about the tables and figures should appear in the text before the appearance of the respective tables and figures. No tables or figures should be given without discussion or reference inside the text.

Tables should be explanatory enough to be understandable without any text reference. Double spacing should be maintained throughout the table, including table headings and footnotes. Table headings should be placed above the table. Footnotes should be placed below the table with superscript lowercase letters. Each table should be on a separate page, numbered consecutively in Arabic numerals.

Each figure should have a caption. The caption should be concise and typed separately, not on the figure area. Figures should be self-explanatory. Information presented in the figure should not be repeated in the table. All symbols and abbreviations used in the illustrations should be defined clearly. Figure legends should be given below the figures.

References

References should be listed alphabetically at the end of the manuscript. Every reference referred in the text must be also present in the reference list and vice versa. In the text, a reference identified by means of an author's name should be followed by the year of publication in parentheses (e.g.(Brown,2009)). For two authors, both authors' names followed by the year of publication (e.g.(Nelson and Brown, 2007)). When there are more than two authors, only the first author's name followed by "*et al*." and the year of publication (e.g. (Abu-Elteen *et al*., 2010)). When two or more works of an author has been published during the same year, the reference should be identified by the letters "a", "b", "c", etc., placed after the year of publication. This should be followed both in the text and reference list. e.g., Hilly, (2002a, 2002b); Hilly, and Nelson, (2004). Articles in preparation or submitted for publication, unpublished observations, personal communications, etc. should not be included in the reference list but should only be mentioned in the article text (e.g., Shtyawy,A., University of Jordan, personal communication). Journal titles should be abbreviated according to the system adopted in Biological Abstract and Index Medicus, if not included in Biological Abstract or Index Medicus journal title should be given in full. The author is responsible for the sccuracy and completeness of the references and for their correct textual citation. Failure to do so may result in the paper being withdraw from the evaluation process. Example of correct reference form is given as follows:-

Reference to a journal publication:

Bloch BK. 2002. Econazole nitrate in the treatment of *Candida vaginitis*. *S Afr Med J.* , **58**:314-323.

Ogunseitan OA and Ndoye IL. 2006. Protein method for investigating mercuric reductase gene expression in aquatic environments. *Appl Environ Microbiol.*, **64**: 695-702.

Hilly MO, Adams MN and Nelson SC. 2009. Potential fly-ash utilization in agriculture. *Progress in Natural Sci.*, **19**: 1173-1186.

Reference to a book:

Brown WY and White SR.1985. **The Elements of Style**, third ed. MacMillan, New York.

Reference to a chapter in an edited book:

Mettam GR and Adams LB. 2010. How to prepare an electronic version of your article. In: Jones BS and Smith RZ (Eds.), **Introduction to the Electronic Age**. Kluwer Academic Publishers, Netherlands, pp. 281–304.

Conferences and Meetings:

Embabi NS. 1990. Environmental aspects of distribution of mangrove in the United Arab Emirates. Proceedings of the First ASWAS Conference. University of the United Arab Emirates. Al-Ain, United Arab Emirates.

Theses and Dissertations:

El-Labadi SN. 2002. Intestinal digenetic trematodes of some marine fishes from the Gulf of Aqaba. MSc dissertation, The Hashemite University, Zarqa, Jordan.

Nomenclature and Units

Internationally accepted rules and the international system of units (SI) should be used. If other units are mentioned, please give their equivalent in SI.

For biological nomenclature, the conventions of the *International Code of Botanical Nomenclature, the International Code of Nomenclature of Bacteria,* and the *International Code of Zoological Nomenclature* should be followed.

Scientific names of all biological creatures (crops, plants, insects, birds, mammals, etc.) should be mentioned in parentheses at first use of their English term.

Chemical nomenclature, as laid down in the *International Union of Pure and Applied Chemistry* and the official recommendations of the *IUPAC-IUB Combined Commission on Biochemical Nomenclature* should be followed. All biocides and other organic compounds must be identified by their Geneva names when first used in the text. Active ingredients of all formulations should be likewise identified.

Math formulae

All equations referred to in the text should be numbered serially at the right-hand side in parentheses. Meaning of all symbols should be given immediately after the equation at first use. Instead of root signs fractional powers should be used. Subscripts and superscripts should be presented clearly. Variables should be presented in italics. Greek letters and non-Roman symbols should be described in the margin at their first use.

To avoid any misunderstanding zero (0) and the letter O, and one (1) and the letter l should be clearly differentiated. For simple fractions use of the solidus (/) instead of a horizontal line is recommended. Levels of statistical significance such as: $^{*}P < 0.05$, $^{**}P < 0.01$ and $^{***}P < 0.001$ do not require any further explanation.

Copyright

Submission of a manuscript clearly indicates that: the study has not been published before or is not under consideration for publication elsewhere (except as an abstract or as part of a published lecture or academic thesis); its publication is permitted by all authors and after accepted for publication it will not be submitted for publication anywhere else, in English or in any other language, without the written approval of the copyright-holder. The journal may consider manuscripts that are translations of articles originally published in another language. In this case, the consent of the journal in which the article was originally published must be obtained and the fact that the article has already been published must be made clear on submission and stated in the abstract. It is compulsory for the authors to ensure that no material submitted as part of a manuscript infringes existing copyrights, or the rights of a third party.

Ethical Consent

All manuscripts reporting the results of experimental investigation involving human subjects should include a statement confirming that each subject or subject's guardian obtains an informed consent, after the approval of the experimental protocol by a local human ethics committee or IRB. When reporting experiments on animals, authors should indicate whether the institutional and national guide for the care and use of laboratory animals was followed.

Plagiarism

The JJBS hold no responsibility for plagiarism. If a published paper is found later to be extensively plagiarized and is found to be a duplicate or redundant publication, a note of retraction will be published, and copies of the correspondence will be sent to the authors' head of institute.

Galley Proofs

The Editorial Office will send proofs of the manuscript to the corresponding author as an e-mail attachment for final proof reading and it will be the responsibility of the corresponding author to return the galley proof materials appropriately corrected within the stipulated time. Authors will be asked to check any typographical or minor clerical errors in the manuscript at this stage. No other major alteration in the manuscript is allowed. After publication authors can freely access the full text of the article as well as can download and print the PDF file.

Publication Charges

There are no page charges for publication in Jordan Journal of Biological Sciences, except for color illustrations,

Reprints

Ten (10) reprints are provided to corresponding author free of charge within two weeks after the printed journal date. For orders of more reprints, a reprint order form and prices will be sent with article proofs, which should be returned directly to the Editor for processing.

Disclaimer

Articles, communication, or editorials published by JJBS represent the sole opinions of the authors. The publisher shoulders no responsibility or liability what so ever for the use or misuse of the information published by JJBS.

Indexing

JJBS is indexed and abstracted by:

DOAJ (Directory of Open Access Journals)	CABI
Google Scholar	EBSCO
Journal Seek	CAS (Chemical Abstract Service)
HINARI	ETH- Citations
Index Copernicus	Open J-Gat
NDL Japanese Periodicals Index	SCImago
SCIRUS	Clarivate Analytics (Zoological Abstract)
OAJSE	Scopus
ISC (Islamic World Science Citation Center)	AGORA (United Nation's FAO database)
Directory of Research Journal Indexing (DRJI)	SHERPA/RoMEO (UK)
Ulrich's	

المجلة الأردنية للعلوم الحياتية
Jordan Journal of Biological Sciences (JJBS)
ISSN 1995- 6673 (Print), 2307- 7166 (Online)
http://jjbs.hu.edu.jo

The Hashemite University

Deanship of Scientific Research

TRANSFER OF COPYRIGHT AGREEMENT

Journal publishers and authors share a common interest in the protection of copyright: authors principally because they want their creative works to be protected from plagiarism and other unlawful uses, publishers because they need to protect their work and investment in the production, marketing and distribution of the published version of the article. In order to do so effectively, publishers request a formal written transfer of copyright from the author(s) for each article published. Publishers and authors are also concerned that the integrity of the official record of publication of an article (once refereed and published) be maintained, and in order to protect that reference value and validation process, we ask that authors recognize that distribution (including through the Internet/WWW or other on-line means) of the authoritative version of the article as published is best administered by the Publisher.

To avoid any delay in the publication of your article, please read the terms of this agreement, sign in the space provided and return the complete form to us at the address below as quickly as possible.

Article entitled:----------

Corresponding author: ----------

To be published in the journal: Jordan Journal of Biological Sciences (JJBS)

I hereby assign to the Hashemite University the copyright in the manuscript identified above and any supplemental tables, illustrations or other information submitted therewith (the "article") in all forms and media (whether now known or hereafter developed), throughout the world, in all languages, for the full term of copyright and all extensions and renewals thereof, effective when and if the article is accepted for publication. This transfer includes the right to adapt the presentation of the article for use in conjunction with computer systems and programs, including reproduction or publication in machine-readable form and incorporation in electronic retrieval systems.
Authors retain or are hereby granted (without the need to obtain further permission) rights to use the article for traditional scholarship communications, for teaching, and for distribution within their institution.

☐ **I am the sole author of the manuscript**

☐ **I am signing on behalf of all co-authors of the manuscript**

☐ **The article is a 'work made for hire' and I am signing as an authorized representative of the employing company/institution**

Please mark one or more of the above boxes (as appropriate) and then sign and date the document in black ink.

Signed:_____ **Name printed:** _____
Title and Company (if employer representative) : _____
Date: _____

Data Protection: By submitting this form you are consenting that the personal information provided herein may be used by the Hashemite University and its affiliated institutions worldwide to contact you concerning the publishing of your article.

Please return the completed and signed original of this form by mail or fax, or a scanned copy of the signed original by e-mail, retaining a copy for your files, to:

Hashemite University
Jordan Journal of Biological Sciences
Zarqa 13115 Jordan
Fax: +962 5 3903338
Email: jjbs@hu.edu.jo

Editorial Preface

Jordan Journal of Biological Sciences (JJBS) is a refereed, quarterly international journal financed by the Scientific Research and Innovation Support Fund, Ministry of Higher Education and Scientific Research in cooperation with the Hashemite University, Jordan. JJBS celebrated its 12th commencement this past January, 2020. JJBS was founded in 2008 to create a peer-reviewed journal that publishes high-quality research articles, reviews and short communications on novel and innovative aspects of a wide variety of biological sciences such as cell biology, developmental biology, structural biology, microbiology, entomology, molecular biology, biochemistry, medical biotechnology, biodiversity, ecology, marine biology, plant and animal biology, plant and animal physiology, genomics and bioinformatics.

We have watched the growth and success of JJBS over the years. JJBS has published 14 volumes, 60 issues and 800 articles. JJBS has been indexed by SCOPUS, CABI's Full-Text Repository, EBSCO, Clarivate Analytics- Zoological Record and recently has been included in the UGC India approved journals. JJBS Cite Score has improved from 0.7 in 2019 to 1.4 in 2021 (Last updated on 6 March, 2022) and with Scimago Institution Ranking (SJR) 0.22 (Q3) in 2021.

A group of highly valuable scholars have agreed to serve on the editorial board and this places JJBS in a position of most authoritative on biological sciences. I am honored to have six eminent associate editors from various countries. I am also delighted with our group of international advisory board members coming from 15 countries worldwide for their continuous support of JJBS. With our editorial board's cumulative experience in various fields of biological sciences, this journal brings a substantial representation of biological sciences in different disciplines. Without the service and dedication of our editorial; associate editorial and international advisory board members, JJBS would have never existed.

In the coming year, we hope that JJBS will be indexed in Clarivate Analytics and MEDLINE (the U.S. National Library of Medicine database) and others. As you read throughout this volume of JJBS, I would like to remind you that the success of our journal depends on the number of quality articles submitted for review. Accordingly, I would like to request your participation and colleagues by submitting quality manuscripts for review. One of the great benefits we can provide to our prospective authors, regardless of acceptance of their manuscripts or not, is the feedback of our review process. JJBS provides authors with high quality, helpful reviews to improve their manuscripts.

Finally, JJBS would not have succeeded without the collaboration of authors and referees. Their work is greatly appreciated. Furthermore, my thanks are also extended to The Hashemite University and the Scientific Research and Innovation Support Fund, Ministry of Higher Education and Scientific Research for their continuous financial and administrative support to JJBS.

Professor Wedyan ,Mohammed A.
March, 2024

JJBS

Volume 17, Number 3, September 2024
ISSN 1995-6673

Jordan Journal of Biological Sciences

CONTENTS

Original Articles

© 2024 Jordan Journal of Biological Sciences. All rights reserved - Volume 17, Number 3

JJBS

Volume 17, Number 3,September 2024
ISSN 1995-6673
Pages 389 – 396
https://doi.org/10.54319/jjbs/170301

Jordan Journal of Biological Sciences

Metabolism and Antifungal Activity of Coumarin and its Derivatives

Luisa M. Castaño[1], José E. Cuellar[1], Jesús H. Gil[2,*] , Diego L. Durango[1]

[1]*Universidad Nacional de Colombia-Sede Medellín, Facultad de Ciencias, Escuela de Química, Carrera 65, 59ª-110, Medellín, Colombia;*
[2]*Universidad Nacional de Colombia-Sede Medellín, Facultad de Ciencias Agrarias, Departamento de Ingeniería Agrícola y Alimentos, Carrera 65, 59ª-110, Medellín, Colombia.*

Received: April 24, 2023; Revised: September 28, 2023; Accepted: October 20, 2023

Abstract

In the present article, the inhibitory activity against the postharvest fungi *Lasiodiplodia* spp., *Botrytis* spp., and *Fusarium* spp. of coumarin was evaluated. Coumarin exhibited a significant antifungal effect (at concentrations of 1.5 mM and above), with inhibition percentages ranging from 24.8% to 66.4% for *Lasiodiplodia* spp., 55.5% to 78.8% for *Fusarium* spp., and 75.6% to 88.9% for *Botrytis* spp. Additionally, the metabolism of coumarin by phytopathogenic fungi was studied. Coumarin was found to be transformed into two main metabolic products, which were purified by chromatographic techniques and identified by spectroscopic methods (^{1}H and ^{13}C NMR), corresponding to dihydrocoumarin and 3-(2-hydroxyphenyl) propanoic acid. According to the structure of metabolic products, coumarin was hydrogenated at the carbon-carbon double bond and the lactone system was opened, which affects the α,β-unsaturated carbonyl system. Additionally, the effect of different substituents on both the aromatic ring and the α, β-unsaturated carbonyl system in the antifungal activity was evaluated. The results indicate that the presence of substituents such as 3-acetyl and 3-ethyl carboxylate on the double bond moiety significantly enhances the inhibitory effect on the radial growth of postharvest pathogen *Lasiodiplodia* spp.

Keywords: fungitoxicity, metabolic products, *Botrytis* spp., bioreduction, dihydrocoumarin.

1. Introduction

Coumarins constitute a broad group of natural products present in a wide variety of plants. These substances are heterocyclic molecules of the 1,2-benzopyrone type, also known as 2H-chromen-2-ones, and exhibit different biological and pharmacological properties. In particular, various natural coumarins and their derivatives have been found to be active molecules (Mustafa, 2023), especially against fungi and bacteria (Patil *et al*., 2023; Brooker *et al*., 2008; Franco *et al*., 2021; Prusty and Kumar, 2000). Some coumarins have been considered as phytoalexins: low-molecular weight compounds that are biosynthesized *de novo* by plants after exposure to biotic (infection by fungi and bacteria) or abiotic stress (wounds, radiation, freezing) (Stringlis *et al*., 2019; Mansfield, 2000). In the Apiaceae (Umbelliferae) family, coumarin-type phytoalexins such as coumarin, xanthotoxin, isoscopoletin, umbelliferone, isopimpinellin, and bergaptene have been identified (Yang et al., 2022). In the Rutaceae family, particularly Citrus spp., coumarin-type phytoalexins such as scoparone, scopoletin, and xanthyletin, among others, have been reported (Ramírez-Pelayo et al., 2019). The chemical structures of these phytoalexins are shown in Figure 1. For example, accumulation of scopoletin has been directly related to increased resistance against different pathogens (Stassen *et al*., 2021). Otherwise, coumarins can also be constitutive antimicrobial compounds (called phytoanticipins) and act as a first defensive chemical barrier of the plant (Fernandes *et al*., 2022; Stringlis *et al*., 2019). Thus, coumarins with a hydroxyl group in C-7 may present a defensive role against the *Orobanche cernua* parasite, preventing germination, penetration, and connection with the vascular system of the host (Serghini *et al*., 2001).

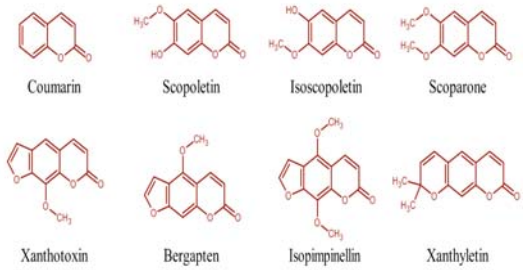

Figure 1. Coumarin-like phytoalexins from Apiaceae and Rutaceae (Yang *et al*., 2022; Ramírez-Pelayo *et al*., 2019)

Due to the antimicrobial activity of defensive compounds found in plants, such as coumarins, expectations have been raised about their potential use. This includes: *i.*) the direct application of phytoalexins or phytoanticipins as antifungal agents in crops, taking advantage of their antibiotic potential; and *ii.*) the design of new antibiotics for plants based on their structural core, which differs from that currently used in fungicides (Song *et al*., 2021; Oros and Kállai, 2019). Unfortunately, in many cases, fungi have adapted through the evolution of

* Corresponding author. e-mail: jhgilg@unal.edu.co.

tissues to tolerate and metabolize the defensive compounds of their hosts using a variety of enzymatic reactions that lead to products innocuous against the fungus (Westrick *et al*., 2021). The elucidation of microbial metabolism and detoxification of plant defensive compounds could provide insight into structural modifications that may be necessary if certain compounds are to be further developed as selective fungal control agents (Pedras and Thapa, 2020; Pedras and Ahiahonu, 2005). Therefore, an environmentally attractive strategy for controlling plant pathogens could be using inhibitors of these fungal detoxifying enzymes or blocking certain functional groups modified by the microorganism to protect the plant against pathogens. In the present study, the antifungal activity of coumarin, as well as its microbial metabolism in three fungi isolated from Tahiti lime (*Citrus latifolia* T.), was evaluated. Additionally, the effect of different substituents on the coumarin nucleus on antifungal efficacy was examined.

2. Materials and Methods

2.1. Chemical and biological materials

Phytopathogenic fungi were isolated from Tahiti lime fruits (*Citrus latifolia* T.) infected and with evident symptoms of the stem-end rot, grey mold, and root rot diseases, and kept on deposit at the National University of Colombia Medellín (Laboratory of Phytopathology vouchers number: L. Castaño-CL01 (*Lasiodiplodia* spp.), L. Castaño-CL12 (*Botrytis* spp). and L. Castaño-CL14 (*Fusarium* spp). Fungi were maintained at 24±2°C and subcultured monthly in Petri dishes containing Potato Dextrose Agar media (PDA, Merck-KGaA, Darmstadt, Germany). A mycelial dispersion (1 mL) of each fungus was used to inoculate sterile Petri plates (15 cm in diameter) and tests the antifungal activity. The suspension was uniformly spread over the medium using a bent glass rod. Then, the inoculated medium was incubated at 25°C for 48 hours and mycelial disc (6 mm diameter) was used for the fungitoxicity assay. Coumarin (1,2-benzopyrone), umbelliferone, coumarin-3-carboxylic acid, salicylaldehyde, ethyl acetoacetate, malonic ester, and piperidine were purchased from Sigma-Aldrich (St. Louis, MO, USA). Carbendazim (methyl benzimidazol-2-yl carbamate, Colizym®) was from Colinagro S.A. (Bogotá, Colombia). Thymol (2-isopropyl-5-methylphenol) was acquired from Abaquim Ltda. (Medellín, Colombia). Acetic anhydride was from Merck (Darmstadt, Germany). Organic solvents *n*-hexane, CH_2Cl_2, ethyl acetate, and methanol were purchased from Protokimica S.A.S. (Medellín, Colombia). The ingredients of the culture medium for metabolic study were purchased from Oxoid Ltd. (Hampshire, England).

2.2. Equipment and analytical methods

The microbial metabolism of coumarin was monitored using Thin Layer Chromatography (TLC) on Merck Kiesegel 60 F_{254} (0.25 mm thick) plates, with mixtures of *n*-hexane-ethyl acetate as the mobile phases, and High Performance Liquid Chromatography (HPLC system Shimadzu, Kyoto, Japan) equipped with: Prominence Auto Sampler (SIL-20A), reciprocating pumps (LC-20AT), degasser (DGU 20A5), integrator (CBM 20A), diode array detector (SPD-M20A) and LC solution software (1.22 SP1). Reverse phase chromatographic analyses were performed under acetonitrile-water gradient conditions using a C18 guard cartridge (Phenomenex, 4.0 x 3.0 mm) followed by a C18 column (Zorbax Eclipse Plus, 4.6 x 150 mm, 5 µm, Agilent, USA). The gradient program was: 0-5 min, 80% A; 5-10 min, 80-60% A; 10-15 min, 60-40% A; 15-20 min, 40-20% A; and finally, reconditioning the column with 80% A isocratic for 5 min. The flow-rate was 1.0 mL/min. For the purification of the metabolic and synthetic products, different chromatographic techniques were used (column chromatography, CC, and preparative thin layer chromatography). For the CC, silica gel 60 (0.040-0.063 mm, Merck) and Sephadex® LH-20 were used as stationary phases. The compounds were detected in TLC by fluorescence under the UV lamp (254 and 366 nm) or by spraying with oleum reagent followed by heating. For the identification of the metabolic and synthetic products, ^1H (300 MHz) and ^{13}C (75 MHz) Nuclear Magnetic Resonance (NMR) spectroscopy were used in a Bruker AMX 300 spectrometer with deuterochloroform ($CDCl_3$) as solvent. The chemical shifts (δ) were expressed in ppm and the coupling constants (*J*) in Hertz. The attribution of the multiplicities for the carbons was carried out using the DEPT experiments. Notations: s = singlet, d = doublet, t = triplet, m = multiplet, dd = double of doublet, q = quintet.

2.3. Antifungal activity of coumarin and derivatives

The toxicity of coumarin 1 against *Lasiodiplodia* spp., *Botrytis* spp., and *Fusarium* spp. was determined using the Poisoned Food Technique (Velasco *et al*., 2010; Al-Rawashdeh *et al*., 2022). Different concentrations of coumarin (0.5, 1.0, 1.5 and 3.0 mM) dissolved in ethanol (less than 0.2%, v/v) were diluted in Petri dishes with PDA medium. All concentrations were evaluated in triplicate, and the results are shown as mean values of the colony diameters (± standard deviation, SD). Petri dishes without compound were used as a negative control, which contained only ethanol (0.2%, v/v) in the PDA medium. The common fungicide carbendazim (methyl benzimidazol-2-yl carbamate), at a concentration of 0.250 mM, was used as a positive control. The Petri dishes were maintained at room temperature under diffuse light, and the mycelial diameter was measured every 24 h. When the mycelial mass of the control was almost fully grown (*Lasiodiplodia* spp (3.5 days), *Botrytis* spp. (10 days) and *Fusarium* spp (11 days)), the incubation was stopped. The fungitoxicity of 1, in terms of the percentage of inhibition of radial growth, was calculated as (%) = [1- (T / C)] x 100; where, C = diameter of the colony (mm) of the control and T = diameter of the colony (mm) of the treatments (coumarin and derivatives). Additionally, compound 1 was used to determine the IC_{50} according to the methodology of Rivillas-Acevedo and Soriano-Garcia (2007). The antifungal activity evaluation of coumarin derivatives 4-9 was determined at 1 mM, using the fungus *Lasiodiplodia* spp.

2.4. Metabolism of coumarin

2.4.1. Preculture:

The methodology described by Castaño *et al*. (2021) was employed with slight modifications. Briefly, the fungi were inoculated in Erlenmeyer flasks containing Czapek-Dox and incubated at room temperature for 72 hours. The

resulting mycelium was filtered, washed with water, and used in the preparative-scale biotransformation and time-course experiments.

2.4.2. Time-course experiments:

The methodology described by Castaño *et al*. (2021) was used with slight modifications. Briefly, the precultured of each fungus was transplanted into Erlenmeyer flasks containing Czapeck-Dox medium (125 mL) and compound 1 at a final concentration of 1.5 mM. The ratios between compound 1 and metabolic products were preliminarily determined based on HPLC peak areas (wavelength: 254nm), and the results were expressed as relative abundances. Controls (without substrate) were carried out to verify the presence of similar compounds in the fungi culture.

2.4.3. Preparative scale metabolism:

The methodology described by Castaño *et al*. (2021) was followed with some modifications. Briefly, mycelia of *Lasiodiplodia* spp. from a 3-day old culture was used, and the final concentration of the compounds 1 in the culture medium was 1.5 mM. A control was performed to verify the presence of similar compounds in fungal cultures without the substrate.

2.5. Isolation and identification of metabolic products

The culture medium was saturated with NaCl and extracted with CH_2Cl_2 (3 x 2.0 L). The organic extracts were combined, dried over anhydrous Na_2SO_4, and concentrated in vacuo. The extract was chromatographed on a column using silica gel as the stationary phase. The elution was performed using a gradient system of *n*-hexane-CH_2Cl_2. The resulting extracts were fractionated to yield six fractions, which were grouped according to their TLC profile. The second fraction (eluted with *n*-hexane-CH_2Cl_2, 10:1) was chromatographed by column on SiO_2 using as eluent *n*-hexane-CH_2Cl_2, 10:1 to give the metabolic product 2. The fourth fraction (eluted with *n*-hexane-CH_2Cl_2, 7:3) was chromatographed by column on SiO_2 using as eluent *n*-hexane-CH_2Cl_2, 8:2 to yield the metabolic product 3. The identification of these metabolites was based on the interpretation of their NMR spectra. Metabolic product 2: it was isolated as an oily liquid. UV (MeOH-H_2O, 1:1) λ_{max} (nm): 273 nm. ^{1}H NMR: δ 7.32-7.22 (m, 2H, H-5, H-7), 7.19-7.10 (m, 2H, H-6, H-8), 3.05-2.90 (t, *J* = 7.2, 2H, H-4), 2.86-2.81 (t, *J* = 7.2, 2H, H-3). ^{13}C NMR: δ 168.9 (C-2), 152.0 (C-8a), 128.3 (C-7), 128.1 (C-5), 127.0 (C-6), 124.5 (C-4a), 117.0 (C-8), 29.3 (C-3), 23.7 (C-4). Metabolic product 3: it was isolated as a crystalline solid. UV (MeOH-H_2O, 1:1) λ_{max} (nm): 269 nm. ^{1}H NMR: δ 7.31-7.11 (m, 2H, H-6', H-4'), 6.94-6.87 (m, 2H, H-5', H-3'), 5.80 (s, 1H, -OH), 2.96 (t, 2H, *J* = 6.9, H-3), 2.81 (t, 2H, *J* = 6.9, H-2). ^{13}C NMR: δ 179.6 (C-1), 154.0 (C-2'), 130.5 (C-6'), 128.0 (C-4'), 126.9 (C-1'), 121.0 (C-5'), 116.6 (C-3'), 34.5 (C-2), 24.7 (C-3).

2.6. Preparation of derivatives

3-acetylcoumarin (4): Salicylaldehyde (2-hydroxybenzaldehyde, 2 mmol), ethyl acetoacetate (2 mmol) and a few drops of piperidine were mixed for 5 min at room temperature and without solvent. The reaction was neutralized with HCl (0.1 M) and finally the product was isolated by filtration. Subsequently, the final compound was recrystallized from ethanol. Yield: 95%. Pale yellow solid. ^{1}H NMR: δ 8.55 (s, 1H, H-4), 7.73-7.67 (m, 2H, H-5, H-7), 7.43-7.36 (m, 2H, H-6, H-8), 2.77 (s, 3H, CH_3). ^{13}C NMR: δ 195.6 (-C=O), 160.3 (C-2), 155.4 (C-8a), 147.6 (C-4), 134.5 (C-7), 130.3 (C-5), 125.0 (C-6), 124.5 (C-3), 118.3 (C-4a), 116.7 (C-8), 30.6 (-CH_3). Ethyl coumarin-3-carboxilate (5): Salicylaldehyde (2 mmol), malonic ester (2 mmol) and a few drops of piperidine were mixed for 5 min at room temperature and without solvent. The reaction was neutralized with HCl (0.1 M) and finally the product was isolated by filtration. Subsequently, the final compound was recrystallized from ethanol. Yield: 90%. Pale yellow solid.^{1}H NMR: δ 8.57 (s, 1H, H-4), 7.72-7.64 (m, 2H, H-5, H-7), 7.41-7.31 (m, 2H, H-6, H-8), 4.45 (q, 2H, -CH_2-), 1.45 (t, 3H, -CH_3). ^{13}C NMR: δ 163.1 (-C=O), 156.8 (C-2), 155.2 (C-8a), 148.7 (C-4), 134.4 (C-7), 129.5 (C-5), 124.9 (C-6), 118.3 (C-3), 117.9 (C-4a), 116.8 (C-8), 62.0 (-CH_2-), 14.27 (-CH_3). 7-acetyloxy coumarin (6): A mixture of umbelliferone (1 mmol), acetic anhydride (2 mmol) and a few drops of pyridine were refluxed for 30 min. The reaction was neutralized with NaOH solution (0.1 M) and extracted with CH_2Cl_2. The organic phase was dried with anhydrous Na_2SO_4 and distilled under reduced pressure in a rotoevaporator. Yield: 88%. White crystalline solid. ^{1}H NMR: δ 7.74 (d, *J* = 9.6, 1H, H-4), 7.54 (d, *J* = 8.4, 1H, H-5), 7.16 (d, *J* = 2.3, 1H, H-8), 7.10 (dd, *J* = 8.4, 1H, H-6), 6.45 (d, *J* = 9.6, 1H, H-3), 2.39 (s, 3H). ^{13}C NMR: δ 168.8 (-C=O), 160.4 (C-2), 154.2 (C-8a), 153.2 (C-7), 142.9 (C-4), 128.6 (C-5), 118.5 (C-6), 116.7 (C-4a), 116.1 (C-3), 110.5 (C-8), 21.2 (CH_3). 7-hydroxy-4-methyl coumarin (7): A mixture of resorcinol (1 mmol), ethyl acetoacetate (1 mmol) and a few drops of piperidine was mixed for 5 min at room temperature and without solvent. The reaction was neutralized with HCl solution (0.1 M), and finally the product was isolated by filtration. ^{1}H NMR: δ 7.55 (d, *J* = 8.4, 1H, H-5), 6.99 (d, *J* = 2.1, 1H, H-8), 6.90 (dd, *J* = 8.4, 2.1, 1H, H-6), 6.21 (s, 1H, H-3), 2.47 (s, -CH_3). ^{13}C NMR: δ 162.1 (C-2), 159.5 (C-7), 154.9 (C-8a), 153.1 (C-4), 126.0 (C-5), 114.2 (C-4a), 113.0 (C-3), 111.8 (C-6), 103.4 (C-8), 18.8 (-CH_3). 6-Nitrocoumarin (8): Coumarin (1.1 mmol) was nitrated using a mixture of concentrated sulfuric acid (96%) and nitric acid (65%) and stirring for 1 hour at 25°C. After neutralization with NaOH solution (0.1 M), an extraction with CH_2Cl_2 was carried out. The organic phase was dried with anhydrous Na_2SO_4, filtered, and evaporated to dryness (Yield: 75%). ^{1}H NMR: δ 8.48 (dd, *J* = 2.4, 9.0, 1H, H-7), 8.43 (d, *J* = 2.4, 1H, H-5), 7.85 (d, *J* = 9.6, 1H, H-4), 7.52 (d, *J* = 9.0, 1H, H-8), 6.64 (d, *J* = 9.6, 1H, H-3). ^{13}C NMR: δ 158.9 (C-2), 157.6 (C-8a), 144.1 (C-6), 142.3 (C-4), 126.7 (C-7), 123.8 (C-5), 118.9 (C-4a), 118.8 (C-8), 118.2 (C-3).

2.7. Statistical analysis

The data underwent analysis of variance (ANOVA), and the means were contrasted using the Least Significant Difference test (LSD) with a significance level of $p < 0.05$.

3. Results and Discussion

3.1. Antifungal activity

The fungistatic properties of 1 were analyzed using the technique of mycelial growth inhibition. The inhibitory

effects of 1 against *Botrytis* spp., *Lasiodiplodia* spp., and *Fusarium* spp. are shown in Figure 2. In general, compound 1 exhibited significant antifungal activity against all three fungi at concentrations of 1.5 mM and above. The results showed that the mycelial growth of these fungi varied according to the amount of compound 1 in the growth medium. At 3.0 mM, the percentages of inhibition of 1 against *Botrytis* spp., *Lasiodiplodia* spp., and *Fusarium* spp. ranged between 88.9 (day 1) and 75.6 (day 9), 66.4 (day 1) and 24.8 (day 3), and 78.8 (day 1) and 55.5% (day 9), respectively. The inhibitory effect of 1 was lower than that shown by the natural antifungal thymol (98-87% inhibition at 1.0 mM) and the synthetic antifungal Carbendazim (all fungi were inhibited 100% at 0.25 mM). In summary, the findings suggest that compound 1 displayed moderate to low antifungal activity against *Botrytis* spp., *Fusarium* spp., and *Lasiodiplodia* spp., with IC_{50} values of 2.19 (on the fourth day), 1.78 (on the third day), and 2.81 mM (on the second day), respectively. Accordingly, the lowest activity of compound 1 was observed against *Lasiodiplodia* spp. The moderate antifungal activity of 1 against *Candida albicans* (3.42 mM), *Aspergillus fumigatus* (6.84 mM) and *Fusarium solani* (3.42 mM) was also reported by Montagner *et al*. (2008). According to Qin *et al*. (2020), the 1,2 benzopyrone skeleton is essential for the antimicrobial activity of 1 and its derivatives. Studies of structure-activity relationship have suggested that the α, β-unsaturated carbonyl system, which is present in the coumarin core, is an important structural feature for exhibiting antifungal activity (El Ouadi *et al*., 2017; Meepagala *et al*., 2003). Compounds having the α, β-unsaturated carbonyl motif can act as Michael acceptors for biological nucleophiles (for example, a cysteine residue) and react irreversibly with biomolecules (for example, proteins) that are relevant to microorganisms, exhibiting the antimicrobial activity attributed to coumarins.

In general, for all fungi, the inhibitory effect of 1 decreased over time, a fact suggesting that the fungus has a detoxification route. To study this metabolic route, the microorganism was incubated with 1 at a concentration of 1.5 mM for 9 days.

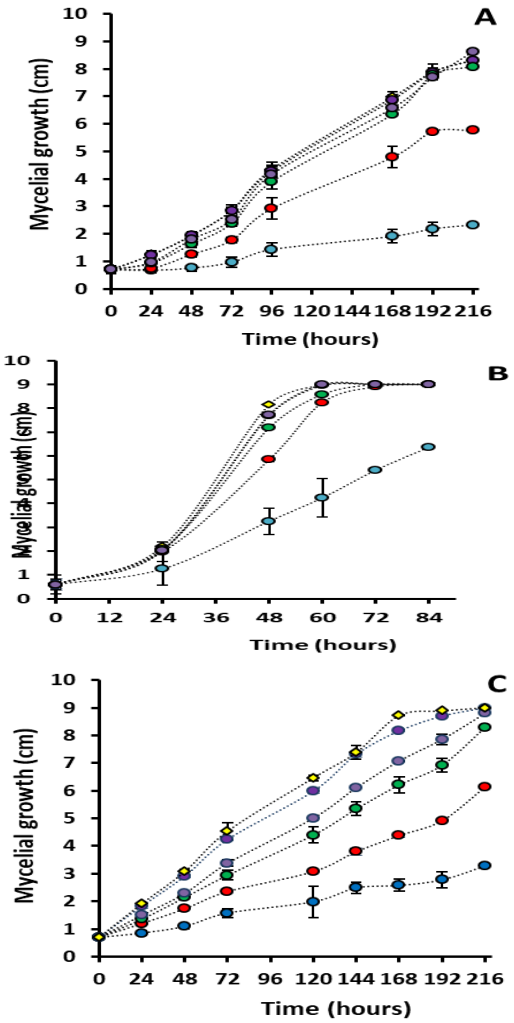

Figure 2. Radial growth of *Botrytis* spp. (**A**), *Lasiodiplodia* spp. (**B**), and *Fusarium* spp. (**C**) without (·····◇·····, Absolute control; ·····●·····, Solvent control) and with coumarin **1** at 0.5 (·····●·····), 1 (·····●·····), 1.5 (·····●·····), and 3 mM (·····●·····).

3.2. Metabolism of compound 1

A comparison of the HPLC-DAD chromatographic profiles obtained from biotransformation is presented in Figure 3. As shown, all fungi metabolized 1 into several metabolic products. *Lasiodiplodia* spp. transformed 1 into approximately 8 metabolic products. The products that are present in greater abundance correspond to the peaks with retention times (RT) of 6.6, 11.5, and 16.6 min. The peak with a retention time of 6.8 min was detected in the controls (data not shown), indicating that it corresponds to a metabolite from the fungus.

The HPLC-DAD chromatograms, obtained of the biotransformation of 1 by *Botrytis* spp. and *Fusarium* spp., exhibited minor similarities showing a single major compound at 9.0 and 19.8 min, respectively. In order to isolate the main metabolic products, a preparative-scale biotransformation of 1 in Czapeck-Dox liquid medium using the fungus *Lasiodiplodia* spp. was performed. Two metabolic products (2 and 3) were isolated and purified by means of column and preparative TLC.

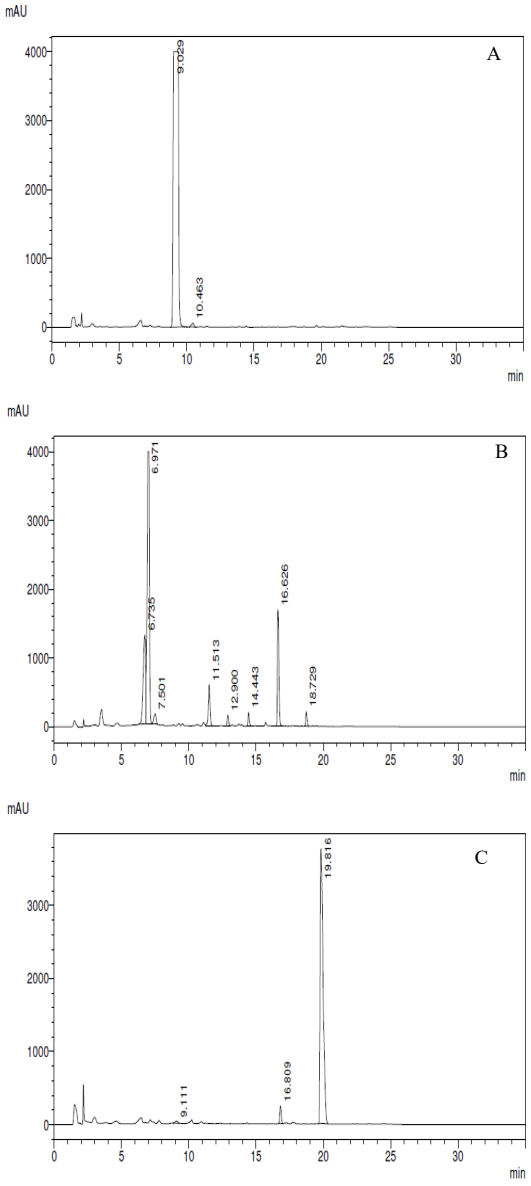

Figure 3. HPLC-DAD profile of the metabolism of **1**, after 6 days of fermentation, by *Fusarium* spp (A), *Lasiodiplodia* spp (B), and *Botrytis* spp (C). Wavelength: 254nm.

The structure of the isolated compounds was elucidated through interpretation of the spectroscopic data. Compound 2: The ^{1}H NMR spectrum showed signals for eight protons. Two upfield signals (at δ 2.86-2.81 and 3.05-2.90 ppm) that integrate each one for two protons. This indicates a reduction in the double bond of coumarin. At downfield, two multiple signals were observed (δ 7.32-7.22 and 7.19-7.10 ppm), corresponding to the four aromatic protons. In the ^{13}C NMR spectrum, nine signals corresponding to nine carbons were found. According to the DEPT-135 spectrum, the upfield signals, δ 29.3 and 23.7 ppm, correspond to two methylenic carbons. Additionally, it is observed that there are six carbon signals at downfield, consisting of four CH carbons at δ 117.0, 124.5, 128.1 and 128.3 ppm, and two quaternary carbons at δ 152.0, 124.5 ppm, belonging of the aromatic ring. There is also one quaternary carbon signal of the ester group at δ 168.9 ppm. From the spectroscopic data, the metabolic product 2 was identified as dihydrocoumarin (RT = 11.5 minutes).

Compound 3: Signals for nine protons were observed in the ^{1}H NMR spectrum. Two upfield signals were observed at δ 2.81 and 2.96 ppm, each integrating for two protons. A broad singlet signal was observed near 5.8 ppm, which corresponds to the hydroxyl group. At the downfield, two multiple signals were observed (δ 7.31-7.11 and 6.94-6.87 ppm), corresponding to the four aromatic protons. The two upfield signals allow us to infer that there was a reduction in the double bond of coumarin, while the presence of the broad singlet suggests that the lactone system was opened. In the ^{13}C NMR spectrum, nine signals corresponding to nine carbons are observed. According to the DEPT-135 spectrum, the low field signals, δ 24.7 and 34.5 ppm, correspond to two methylenic carbons. At lower fields, four CH carbons (δ 116.6, 121.0, 128.0, 130.5 ppm) of the aromatic ring are observed. In addition, 3 signals are observed at δ 179.6, 154.0 and 126.9 ppm, corresponding to the quaternary carbons C-1 (carbonyl group of carboxylic acid), C-2', C-1', respectively. From the spectroscopic data, the metabolic product (3) was identified as 3-(2-hydroxyphenyl) propanoic acid (RT = 6.6 minutes).

The metabolism of compound 1 with *Lasiodiplodia* spp., was monitored for 12 days by taking samples every 1, 3, 6, 9 and 12 days (Figure 4). The relationship between substrate 1 and the metabolic products 2 and 3 in the course of time was determined based on the area of the HPLC peaks.

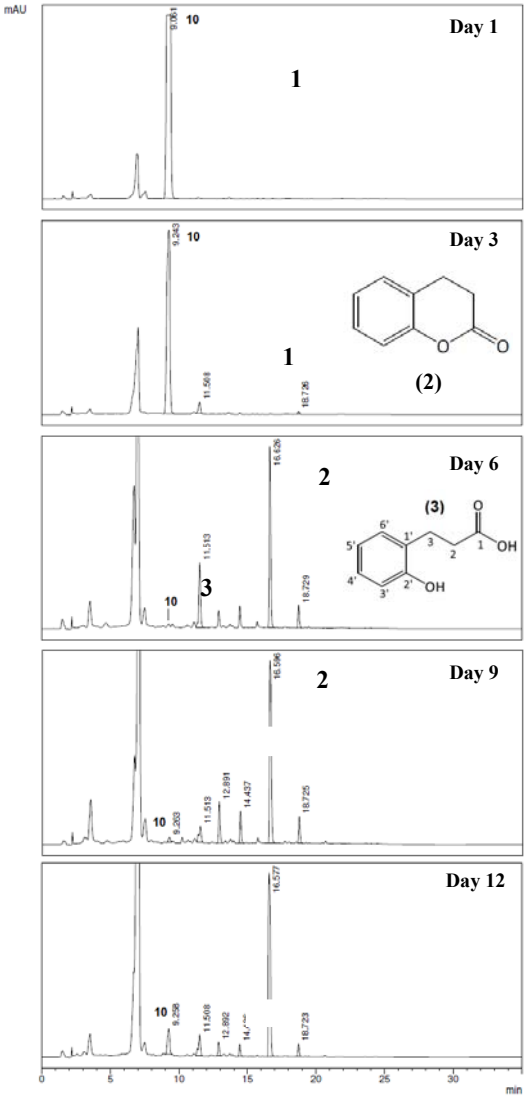

Figure 4. Time-course study for the metabolism of **1** by *Lasiodiplodia* spp. Wavelength: 254 nm.

The results, expressed as relative abundances, are shown in Figure 5. The fungus *Lasiodiplodia* spp. rapidly consumed the compound 1. After 6 days, about 94% of 1 was modified by *Lasiodiplodia* spp., being converted mainly to compound 3. The relative abundance of 2 and 3 was always less than 42%; possibly, these products are further transformed during metabolic biotransformation to generate other compounds.

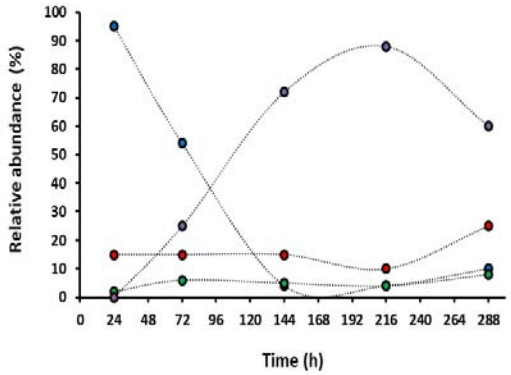

Figure 5. Relative abundance over time for microbial transformation of coumarin (**1**, ·····●·····) by *Lasiodiplodia* spp. Microbial products: compound (**2**, ·····●·····), dihydrocoumarin; compound (**3**, ·····●·····), 3-(2-hydroxyphenyl)propanoic acid; and others (·····●·····). Analysis wavelength: 254 nm.

The conversion of 1 is probably carried out by the action of ene-reductases, which are enzymes capable of reducing the activated C-C double bond to obtain 2. Subsequently, lipase-type hydrolases could act to open the lactone ring and produce 3 (Serra *et al*., 2019). The production of 2 from 1 was also reported by different yeasts and filamentous fungi; the authors found that all the tested strains were able to selectively reduce the compound 1, but with different conversion rates and sensitivity to substrate concentration (Serra *et al*., 2019). According to the structures of metabolic products 2 and 3, it is possible to affirm that the conversion of 1 initially affected the α, β-unsaturated carbonyl system, which is related to its antimicrobial activity. This would suggest a detoxification mechanism of 1 by *Lasiodiplodia* spp. through the action of ene-reductase enzymes. In fact, compound 1 is considered a toxic compound, while compound 2 is classified as a substance safe or GRAS, indicating lower toxicity to living organisms (Serra *et al*., 2019). It seems that the lower antifungal activity of 1 against *Lasiodiplodia* spp., compared to the other two microorganisms, may be a result of its greater ability to convert 1 to other metabolic products. *Lasiodiplodia* spp. modified almost all of 1 in only 6 days (Figure 4 and 5). Therefore, the ene-reductase enzymes could be important metabolic targets for developing new antifungal agents.

Unfortunately, it was not possible to purify and identify other metabolic products, which reached a maximum abundance around 90% for day 9 under the given conditions. According to Aguirre-Pranzoni *et al*. (2011), the biotransformation of 1 by *A. ochraceus* and *A. flavus*, afforded the compound 2 and 5-hydroxycoumarin, respectively. Furthermore, when *A. niger* was used, a mixture of compounds including 2, 3, 6-hydroxy-3,4-dihydrochromen-2-one, 3-(2-hydroxyphenyl) propanal, and 2-(3-hydroxypropyl)phenol was obtained.

3.3. Antifungal activity of coumarin derivatives

The microbial transformation of 1 showed significant structural changes produced by *Lasiodiplodia* spp.; consequently, the antifungal activity of synthetic coumarin derivatives was evaluated to obtain information about the relationship between structure and activity (Figure 6 and 7).

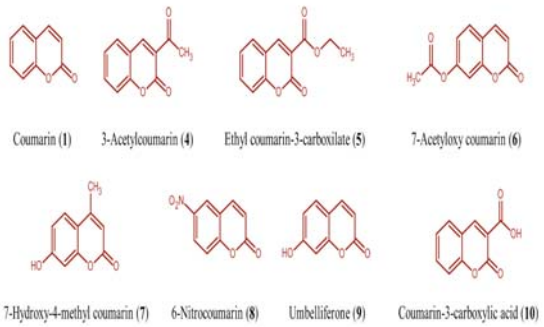

Figure 6. Coumarin derivatives employed to determine the antifungal activity against *Lasiodiplodia* spp.

A series of coumarin derivatives was prepared by standard chemical methods and tested against the fungus *Lasiodiplodia* spp. at a concentration of 1 mM. The percentages of inhibition of radial growth are shown in Figure. 7.

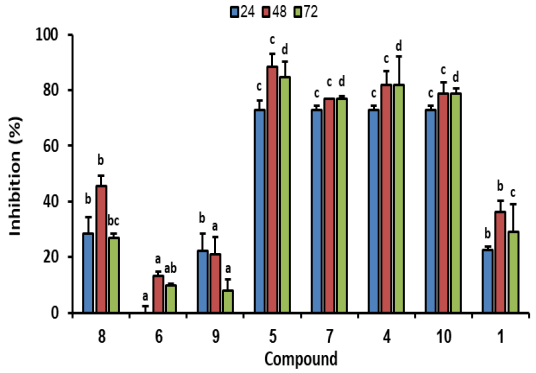

Figure 7. Inhibition (%) of radial growth of *Lasiodiplodia* spp. with **1** and derivatives. Different letters for the same time correspond to significant differences at a confidence level of 95%.

Results showed that substitution in the aromatic ring to afford 8 (with an electron-withdrawing group, -NO_2 in C6), 6 (with a *O*-acetyl group in C7) and 9 (with a hydroxyl group in C7) only slightly affected the antifungal activity with respect to 1. Compound 8 exhibited growth inhibition values for *Lasiodiplodia* spp similar to 1, while compounds 6 and 9 displayed a decrease in antifungal activity.

Remarkably, compounds 4, 5 and 10, which are substituted at C3 of the coumarin, showed a significant increase in fungal inhibition at 48 (~1.8-fold) and 72 h (~2.5-fold). Since the C-C double bond of 4, 5 and 10 is affected by two carbonyl systems (two electron-withdrawing groups), these compounds are better Michael acceptors than 1, and the β carbon (C4) is more electron deficient and therefore more electrophilic. The presence of these structural features would increase the reactivity of compounds 4, 5 and 10 towards biological nucleophiles, making them more active against the fungus. In addition, the presence of substituents on the α,β-unsaturated carbonyl system can change the selectivity or kinetics of the ene-reductase enzymes and, consequently, the ability of the microorganism to detoxify the compounds. Substituents can prevent the reduction of the C-C double bond by ene-reductase enzymes, enhancing the biological activity of compounds 4, 5 and 10 because the pathogenic fungus does not easily detoxify them. The ene-reductase enzymes are flavin-dependent, and the mechanism involves hydride transfer from flavin (cofactor) to the β-carbon of the C-C double bond; then, a tyrosine residue donates a proton on the opposite side of the α carbon, producing an anti-addition. Therefore, steric factors could affect the reduction of the C-C double bond (Vaz *et al*., 1995; Hult and Berglund, 2007).

Similarly, derivative 7, which is substituted at C4 and C7 with a methyl and a hydroxyl group, respectively, exhibited greater antifungal activity than 6 and 9 (substituted only in C7) and comparable fungistatic properties than 4, 5, and 10. The presence of a methyl substituent at the β carbon (C4) of the α,β-unsaturated carbonyl system significantly increased the inhibition of the fungus, as demonstrated by the comparison between compounds 7 and 9. The substituent at C3 or C4 of the coumarin core could contribute to the antifungal activity by decreasing the detoxification by the microorganism. This is possibly due to it steric hindrance, which hinders the transfer of hydride from flavin. Guerra *et al*. (2018) found that by introducing the acetate group in C4 of the coumarin, a derivative with promising antifungal activity was obtained; specifically, the derivative inhibited the mycelial growth and spore germination of *A. fumigatus* and *A. flavus*, affecting the cell structure and virulence of the fungus. According to Sahoo *et al*. (2021), substituents at C3 and C4 of coumarins are appreciated for the development of new antimicrobial agents. It is suggested that modifications at the C3 and C4 positions of coumarin could restrict or block metabolic conversions, thus improving antifungal activity.

The fact that compounds 4, 5 ,7, and 10 maintained high levels of inhibition with slight variations suggests that the toxic effects of these compounds were not immediately mitigated or reduced over time (24 to 72 h). The slow metabolism may be due to the of the fungus´s inability to reduce substituted coumarins at the α o β positions of the activated double bond.

4. Conclusions

Coumarin exhibited moderate antifungal activity against *Botrytis* spp., *Lasiodiplodia* spp., and *Fusarium* spp., which decreased over time. The evaluation of coumarin metabolism shows that fungi rapidly transform the compound into a species- and time-dependent form. In particular, *Lasiodiplodia* spp. affects the α,β-unsaturated carbonyl system, producing dihydrocoumarin and 3-(2-hydroxyphenyl)propanoic acid through reduction and hydrolysis reactions. Structural modification of coumarin at C3 and C4 increases antifungal activity against *Lasiodiplodia* spp. It is suggested that some electronic (improving character as acceptors Michael) and steric characteristics (blocking the double bond) can increase antifungal activity and reduce detoxification of coumarin derivatives by the microorganism.

Acknowledgment

This work was supported by Universidad Nacional de Colombia–Sede Medellin (project 201010027028; Hermes 50200).

References

Aguirre-Pranzoni C, Orden AA, Bisogno FR, Ardanaz CE, Tonn CE and Kurina-Sanz M. 2011. Coumarin metabolic routes in *Aspergillus* spp. *Fungal Biol*., **115(3)**: 245-252. https://doi.org/101016/jfunbio201012009

Al-Rawashdeh ZB, Karajeh MR, Al-Ramamneh EADM and Al-Rawashdeh MS. 2022. A comparative study of onion purple blotch (caused by *Alternaria porri*) and tomato early blight (caused by *A. solani*) diseases in southern ghors of Jordan. *Jordan J Biol Sci*., **15(1)**: 37-43.

Brooker N, Windorski J and Bluml E. 2008. Halogenated coumarin derivatives as novel seed protectants. *Commun Agric Appl Biol Sci.,* **73(2)**: 87-89.

Castaño L.M, Gómez AF, Gil J and Durango D. 2021. Perinaphthenone and derivatives as control agents of phytopathogenic fungi: fungitoxicity and metabolism. *Heliyon,* **7(3)**: e06354. https://doi.org/10.1016/j.heliyon.2021.e06354

El Ouadi Y, Manssouri M, Bouyanzer A, Majidi L, Bendaif H, Elmsellem H and Hammouti B. 2017. Essential oil composition and antifungal activity of *Melissa officinalis* originating from north-Est Morocco against postharvest phytopathogenic fungi in apples. *Microb pathog*., **107(1)**: 321-326. https://doi.org/10.1016/j.micpath.2017.04.004

Fernandes HP, Salomé-Abarca LF, Gonçalves R, Brandão Seibert J, Silva-Junior GJ, Das Graças Fernandes da Silva MF and Choi YH. 2022. Metabolomic investigation of *Citrus latifolia* and the putative role of coumarins in resistance to Black Spot Disease. *Front Mol Biosci*., **9(1)**: 1-13. https://doi.org/10.3389/fmolb.2022.934401

Franco DP, Pereira TM, Vitorio F, Nadur NF, Lacerda RB and Kümmerle AE. 2021. A importância das cumarinas para a química medicinal e o desenvolvimento de compostos bioativos nos últimos anos. *Quím Nova*, **44(1)**: 180-197. https://doi.org/10.21577/0100-4042.20170654

Guerra FQ, Araújo RS, Sousa JP, Silva VA, Pereira O, Mendonça-Junior FJ and Lima EO. 2018. A new coumarin derivative 4-acetatecoumarin with antifungal activity and association study against *Aspergillus* spp. *Braz J Microbiol.,* **49(1)**: 407-413. https://doi.org/10.1016/j.bjm.2017.06.009

Hult K and Berglund P. 2007. Enzyme promiscuity: mechanism and applications. *Trends Biotechnol*., **25(5)**: 231-238. https://doi.org/10.1016/j.tibtech.2007.03.002

Mansfield JW. 2000. Antimicrobial compounds and resistance. In: Slusarenko Aj, Fraser RSS and van Loon LC (Eds.), **Mechanisms of resistance to plant diseases.** Springer, Dordrecht, pp. 325-370.

Meepagala KM, Kuhajek JM, Sturtz GD and Wedge DE. 2003. Vulgarone B the antifungal constituent in the steam-distilled fraction of *Artemisia douglasiana*. *J Chem Ecol*., **29(1)**: 1771-1780. https://doi.org/10.1023/a:1024842009802

Montagner C, de Souza SM, Groposo C, Delle Monache F, Smânia EF and Smânia Jr A. 2008. Antifungal activity of coumarins. *Z Naturforsch C*., **63(1-2)**: 21-28. https://doi.org/10.1515/znc-2008-1-205

Mustafa YF. 2023. Synthesis, characterization, and biomedical assessment of novel bisimidazole–coumarin conjugates. *Appl Nanosci*., **13(3):** 1907-1918. https://doi.org/10.1007/s13204-021-01872-x

Oros G and Kállai Z. 2019. Phytoanticipins: The constitutive defense compounds as potential botanical fungicides. In: Jogaiah S and Abdelrahman M (Eds.), **Bioactive Molecules in Plant Defense: Signaling in Growth and Stress**. Springer, Cham, pp. 179-229. https://doi.org/10.1007/978-3-030-27165-7

Patil SA, Nesaragi AR, Rodríguez-Berrios RR, Hampton SM, Bugarin A and Patil SA. 2023. Coumarin triazoles as potential antimicrobial agents. *Antibiotics* **12(1)**: 160. https://doi.org/10.3390/antibiotics12010160

Pedras MSC and Ahiahonu PW. 2005. Metabolism and detoxification of phytoalexins and analogs by phytopathogenic fungi. *Phytochemistry*, **66(4)**: 391-411. https://doi.org/10.1016/j.phytochem.2004.12.032

Pedras MSC and Thapa C. 2020. Unveiling fungal detoxification pathways of the cruciferous phytoalexin rapalexin A: Sequential L-cysteine conjugation acetylation and oxidative cyclization mediated by *Colletotrichum* spp. *Phytochemistry*, **169(1)**: 1-11. https://doi.org/10.1016/j.phytochem.2019.112188

Prusty JS and Kumar A. 2020. Coumarins: antifungal effectiveness and future therapeutic scope. *Mol Divers*., **24(4)**: 1367-1383. https://doi.org/10.1007/s11030-019-09992-x

Qin HL, Zhang ZW, Ravindar L and Rakesh KP. 2020. Antibacterial activities with the structure-activity relationship of coumarin derivatives. *Eur J Med Chem*., **207(1)**: 1-17. https://doi.org/10.1016/j.ejmech.2020.112832

Ramírez-Pelayo C, Martínez-Quiñones J, Gil J and Durango D. 2019. Coumarins from the peel of citrus grown in Colombia: composition elicitation and antifungal activity. *Heliyon*, **5(6)**: e01937. https://doi.org/10.1016/j.heliyon.2019.e01937

Rivillas-Acevedo LA and Soriano-García M. 2007. Isolation and biochemical characterization of an antifungal peptide from *Amaranthus hypochondriacus* seeds. *J Agri Food Chem*., **55(25)**: 10156–10161. https://doi.org/10.1021/jf072069x

Sahoo CR, Sahoo J, Mahapatra M, Lenka D, Sahu PK, Dehury B and Paidesetty SK. 2021. Coumarin derivatives as promising antibacterial agent(s). *Arab J Chem*., **14(2)**: 2-57. https://doi.org/10.1016/j.arabjc.2020.102922

Serghini K, de Luque AP, Castejón-Muñoz M, García-Torres L and Jorrín JV. 2001. Sunflower (*Helianthus annuus* L) response to broomrape (*Orobanche cernua* Loefl) parasitism: induced synthesis and excretion of 7-hydroxylated simple coumarins. *J Exp Bot*., **52(364)**: 2227-2234. https://doi.org/10.1093/jexbot/52.364.2227

Serra S, Castagna A and Valentino M. 2019. Biocatalytic synthesis of natural dihydrocoumarin by microbial reduction of coumarin. *Catalysts*, **9(8)**: 2-12. https://doi.org/10.3390/catal9080665

Song P, Yu X and Yang W. 2021. Natural phytoalexin stilbene compound resveratrol and its derivatives as anti-tobacco mosaic virus and anti-phytopathogenic fungus agents. *Sci Rep*., **11(1)**: 16509. https://doi.org/10.1038/s41598-021-96069-1

Stassen MJ, Hsu SH, Pieterse CM and Stringlis IA .2021. Coumarin communication along the microbiome–root–shoot axis. *Trends Plant Sci*., **26(2)**: 169-183. https://doi.org/10.1016/j.tplants.2020.09.008

Stringlis IA, De Jonge R and Pieterse CM. 2019. The age of coumarins in plant–microbe interactions. *Plant Cell Physiol*., **60(7)**: 1405-1419. https://doi.org/10.1093/pcp/pcz076

Vaz AD, Chakraborty S and Massey V. 1995. Old yellow enzyme: aromatization of cyclic enones and the mechanism of a novel dismutation reaction. *Biochemistry*, **34(13)**: 4246-4256. https://doi.org/10.1021/bi00013a014

Velasco R, Aristizabal DA, García CM, Gil JH and Durango DL. 2010. Biotransformación de *trans*-cinamaldehído con el hongo filamentoso *Aspergillus* sp. *Vitae*, **17(3)**: 281-290.

Westrick NM, Smith DL and Kabbage M. 2021. Disarming the host: detoxification of plant defense compounds during fungal necrotrophy. *Front Plant Sci*., **12(1)**: 651716. https://doi.org/10.3389/fpls.2021.651716

Yang L, Ni N, Hong Y and Shen L. 2022. A novel sight of the primary active compounds from Umbelliferae: focusing on mitochondria. *Med Chem Res*., **32(1)**: 1-15. https://doi.org/10.1007/s00044-021-02822-6

JJBS

Volume 17, Number 3,September 2024
ISSN 1995-6673
Pages 397 – 412
https://doi.org/10.54319/jjbs/170302

Jordan Journal of Biological Sciences

Inhibition of IgE and IgG1 expression in BALB/c mice and clionasterol potential bioactivity evaluation in *Dioscorea alata* extract, in vivo and in silico studies

Sri Nabawiyati Nurul Makiyah[1,*], Sri Tasminatun[2], Muhammad Sasmito Djati[3], Muhaimin Rifa'i[3], Widodo[3]

[1]*Histology and Molecular Biology Department, School of Medicine, Faculty of Medicine and Health Sciences, Universitas Muhammadiyah Yogyakarta, Indonesia;* [2]*School of Pharmacy, Faculty of Medicine and Health Sciences, Universitas Muhammadiyah Yogyakarta, Jl. Brawijaya, Tamantirto, Kasihan, Bantul, Daerah Istimewa Yogyakarta 55183;* [3]*Biology Department, Faculty of Mathematics and Natural Science, Brawijaya University, Malang, East Java, Indonesia*

Received: May 24, 2023; Revised: October 9, 2023; Accepted: November 8, 2023

Abstract

The prevalence of allergic diseases worldwide is rising dramatically in both developed and developing countries. Dioscorea alata (DA) contains flavonoids and saponin steroid which have potential as anti-allergic agents. This research aims to examine the anti-allergy potential of the ethanol extract of *Dioscorea alata* (EEDA) through IgE and IgG1 levels and to investigate the bioactivity of the phytocompound of hexane extract of *D. alata* (HEDA) in silico. Allergy-induced BALB/c mice used Ovalbumin and were treated with EEDA for 30 days. The levels of B220IgE and B220IgG1 were evaluated. In silico analysis was conducted with HEDA, phytocompound from previous research, 3D structure from PubChem (https://pubchem.ncbi.nlm.nih.gov/), Chemspider (http://www.chemspi-der.com/), Bioactivity analysis on Molinspiration (https://www.molinspiration.com/), PassOnline (http://www. way2drug.com/passonline/predict.php) webservers, target proteins from SwissTarget (http:// www.swisstargetprediction.ch/), STRING (https://string-db.org/), and analyzed with Cytoscape ver 3.9.1. The docking analysis utilizes Vina, a built-in tool in PyRx 0.9, and the results are visualized using Biovia Discovery Studio. B220IgE and B220IgG1 levels decreased in the EEDA treatment significantly ($p<0,05$). The bioactivity predictions showed the activity of enzyme inhibitors, anti-inflammation agents, and cholesterol antagonists. Clionasterol, 9,12-octadecadienoic, and triosanol-1 are the phytocompounds with the highest average bioactivity scores. PSEN1, NR1C1, MAPK14, PTGS2, NR1C2, F2, FABP1, KDR, CNR1, and UGT2B7 are target proteins. Molecular docking results showed that clionasterol had the lowest average binding energy, followed by caryophyllene oxide and 11-pentan-3-ylhenicosane. Clionasterol had a high potential to interact with PPAR-α, PPAR-γ, and MAPK14 as an inhibitor. There was a decrease in B220IgE and B220IgG1 levels in mice given EEDA. Furthermore, Clionasterol could potentially inhibit PPAR and MAPK14, potentially leading to anti-inflammatory activity.

Keywords: *Dioscorea alata*, clionasterol, immunoglobulin E, anti-allergic, in silico

1. Introduction

Dioscorea alata L. (DA) is a plant used to investigate due to its high phytocompound content and potential as a primary food ingredient. Research on the tubers of DA has been conducted to identify the activity of capturing reactive oxygen species, antioxidants, antidiabetic, anticlastogenic, and antiosteoporotic (Amarasekara & Wickramarachchi 2021; Makiyah et al. 2022; Peng et al. 2011; Wang et al. 2011). Meanwhile, early research studying DA as an antiallergic agent has so far been conducted by Makiyah et al. (2014). Therefore, a study related to the expression of immunoglobulin (Ig) E and G1 was carried out to investigate more deeply the potential of the flavonoid and saponin steroid (diosgenin) of DA (Jesus et al. 2016; Wang et al. 2023) on IgE. Flavonoid has potential as an antiallergic agent (Rakha et al. 2022). The antiallergic activity of saponin steroid (diosgenin) in vivo is associated with the suppression of IgE production (Huang et al. 2009). IgE is a crucial molecule as a mediator of allergic responses (asthma, rhinitis, food allergy, atopic dermatitis, etc.) (Gould & Sutton 2008). Moreover, the understanding of the IgE concept is that IgE will act as an initial response to antigen or allergen exposure and will change the immune response to IgG (whose dominant isotypes are IgG1 and IgG4) and IgA after repeated exposure to the same antigen or allergen. (Brazdova et al. 2015). Numerous studies have shown that the majority of food allergies are immunoglobulin E (IgE)-mediated type 1 hypersensitivity reactions, which depend on the antigen-specific differentiation of T helper (Th) 2 cells in the sensitization and degranulation phases and the cytokine production of mast cells and basophil cells in the phase effect (Kumar et al. 2012; Sampson 1999; Yu et al. 2016). However, because the allergy signaling pathway is

* Corresponding author. e-mail: nurul.makiyah@umy.ac.id.

complex, in silico analysis is required to identify target proteins that can be used to decrease allergies.

This research is essential because allergy is one of the diseases with quite a lot of prevalence. Globally, 240 – 550 million people may suffer from food allergy (Pawankar et al. 2013). Research models for inducing allergies in experimental animals have been carried out using Ovalbumin (Barlianto et al. 2013). Ovalbumin sensitization as an allergen in mice can increase IgE and IgG1 levels in blood serum (Saldanha et al. 2004). In this study, DA tuber simplicia was dissolved in 70% ethanol solvent and we also analyzed the data from hexane extraction in previous studies (Makiyah & Djati 2018) to further explore the compound's wider potential in silico. Extraction with a solvent is based on the polarity of the substance in the solvent (Leksono et al. 2018). In this research, ethanol is a polar solvent used to extract flavonoid compounds from *D. alata* tubers. Ethanol is a polar to semi-polar solvent and is universal so it can extract all classes of secondary metabolite compounds; it can also extract many polar, semi-polar compounds and some non-polar compounds (Sasidharan et al. 2011) including flavonoids, which are polar, and diosgenin, which is non-polar. Ethanol can dissolve flavonoid compounds (Hakim & Saputri 2020) in *D. alata* tubers. Diosgenin was obtained from GC-MS analysis of N-hexane extract (Arya et al. 2023). N-hexane is a solvent with a low polarity level, so it is able to extract more non-polar compounds in Dioscorea alata tubers, especially Diosgenin (Hotmian et al. 2021).

The mechanism of action of Dioscorea alata as an antiallergic agent is difficult to understand, because it contains many complex compounds and metabolites. By combining the discovery of potential actionable compound targets and the isolation of active compounds, systems pharmacology approaches together with high-throughput computational analyzes provide a powerful tool to study the underlying mechanisms of DA as an antiallergic agent.

This study aims to examine the effect of the ethanol extract of DA tuber (EEDA) on B220IgE and B220IgG1 levels in the spleen of the mice BALB/c model of gastrointestinal allergy. Also, it further explores the potential of the phytocompound in the hexane extract of DA tuber using in silico to provide a high-throughput computational explanation of phytocompound bioactivity at the molecular level.

2. Materials and Method

2.1. Dioscorea alata L. sample collection.

DA tubers were obtained from the Sumberrahayu area, Moyudan, Sleman, Yogyakarta Special Region. Taxonomic identification of *Dioscorea alata* L. has been carried out in the Plant Taxonomy Laboratory, Faculty of Biology, Gadjah Mada University, with certificate number 0368/S.Tb.

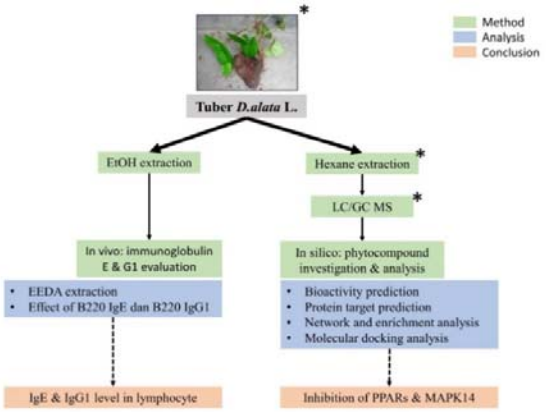

Figure 1. Graphical method for this study. ***** labeled from previous research (Makiyah & Djati 2018)

2.2. Dioscorea alata L. tuber ethanol extraction method

The preparation of ethanol extract of *DA* tubers (EEDA) refers to Badaring et al. (2020). The tubers were sliced and dried under exposure to sunlight covered with black cloth at a temperature of ± 30^0C and then mashed into simplicia. The simplicia was macerated with 70% ethanol with a simplicia: EtOH ratio of 1:70, room temperature, 5 x 24 hours. Remaceration was done using the same steps with a simplicia: EtOH ratio of 1:30 for 2 x 24 hours. Evaporation was carried out at 50ºC in a water bath using a vacuum pump evaporator.

2.3. Dosage formulation and mice model allergy with Ovalbumin

A dose conversion formula based on body weight determined the dose of the EEDA tubers (Ngatidjan 2007). The dose of EEDA was 0.17 g/kg body weight, 2.01 g/kg body weight, and 10.04 g/kg body weight orally in mice with a volume of 0.5 ml. The antihistamine drug used was Fexofenadine (Telfast®) at a dose of 0.4 mg/mice/day (Diding et al. 2008) in 0.5 ml of distilled water = 0.8 mg/ml. The dose of diosgenin is 200 mg/kg of body weight (Huang et al. 2010). Sixty-three male mice (*Mus musculus*) BALB/c strain, body weight ± 20 grams, age ± 6 weeks were divided into 7 groups (control; EEDA 0,00; EEDA 0,17; EEDA 2,01; EEDA 10,04; Drug (OAH), and diosgenin) with 9 mice in each group. Mice were kept in plastic cages measuring 30x40x20 cm. They were acclimated for 10 days in the Animal Physiology cage in the Biomol Building, floor I UB. Furthermore, for 30 consecutive days, groups I – VI were given treatment according to the group. (Table 1).

EEDA, OAH and diosgenin was induced for 30 days on day 1 until day 30. The mouse model of allergy to Ovalbumin, mice were injected intraperitoneally on day 15 with 0.15 cc of Ovalbumin in Al(OH)3/mouse from 2.5 mg of Ovalbumin dissolved in 7.75 ml of aluminum hydroxide and on day 22 with a dose of 0.15 cc of Ovalbumin in distilled water/mice from 2.5 mg of Ovalbumin dissolved in 10 ml of distilled water. On days 23 to 30, mice were exposed orally to 0.15 cc of Ovalbumin in distilled water from 2.5 mg of Ovalbumin in 2.5 ml of distilled water (Fischer et al. 2005). Mice are declared allergic if there is an increase in specific antibody levels, especially those related to Th2 immune responses

such as B220IgE and B220IgG2 after being induced by Ovalbumin. (Abril-Gil et al. 2015; Sun et al. 2013).

Table 1. Mice model and treatment

Group	Ovalbumin induction	EEDA dosage (g/kg bw/day)	Antihistamine drug dosage (mg)	Diosgenin (mg/kg bw/day)
Control	No	-	-	-
I	Yes	0	-	-
II	Yes	0.17	-	-
III	Yes	2.01	-	-
IV	Yes	10.04	-	-
V	Yes	-	0.4	-
VI	Yes	-	-	200

2.4. Flow cytometry analysis

Lymphocyte cells were isolated from the spleen of mice. The spleen was homogenized with PBS and filtered until the lymphocytes were collected in the PBS solution. Lymphocyte cell suspension was centrifuged at 2500 rpm at 4°C for 5 minutes. The supernatant obtained was discarded, and the cell suspension was resuspended with PBS and then homogenized to obtain a homogenate. The homogenate was separated based on the number of groups, and dye antibodies were added according to the protein used and standard procedures in the laboratory. The homogenate and antibody mixtures were incubated in the dark at 4°C for 20 minutes. Next, the mixture was centrifuged at 2500 rpm, temperature 4^0C, for 5 minutes. The resulting lymphocyte pellet was resuspended with 50 µL antibody (1:50) in sterile PBS, then transferred to a cuvette and mounted on a flow cytometry nozzle (BD FACS CaliburTM). The setting was done on the computer with the BD Cell Quest ProTM software and connected to the flow cytometer (acquiring mode). Flow cytometer results stored in the Cell Quest ProTM software were analyzed for the measured cytokine profile in the form of dot plots with percentage figures for the relative number of lymphocytes expressing the estimated cytokine profile and then recapitulated and analyzed (Rifa'i et al. 2023).

2.5. Hexane extract DA sample collection and GCMS method

The HEDA compound was collected based on the results of previous studies (Makiyah & Djati 2018). N-hexane extract of *DA* tuber for GC-MS test was prepared from DAE, which was dissolved in n-hexane (Merck) with the maceration method. GC-MS analysis of bioactive compounds from an n-hexane extract of *DA* L. tuber was carried out using a GC (Shimadzu Europa Gmbh) equipped with Column DB 1 (30 m long x 250µm diameter x 0.25 mm film thickness) and injection temperature 3100C as an injection split method. The mobile phase utilized Helium gas, and the stationary phase was a non-polar Agilent J&W DB-1 column with a flow rate of 39.3 mL/min. The column temperature was programmed with the initial temperature at 800C and held for 5 minutes, then increased to 3000C and held for 15 minutes. The Mass Spectrophotometer (MS) was operated on the electron impact model (EI, 70 Ev). The mass range was from 28-600 Atomic Mass Units (AMU). The results of the spectra of each peak were interpreted by the suitability method of the compound library in the database National Institute of Standards and Technology (NIST) and Wiley (Iheagwam et al. 2019).

2.6. Compound and protein 3D structure mining, bioactivity prediction, and ADME analysis

The 3D structure and canonical SMILES of HEDA were downloaded from the PubChem database (https://pubchem.ncbi.nlm.nih.gov/) and Chemspider (http://www.chemspider.com/). Furthermore, the physicochemical structure of the compound was analyzed through SwissADME (http://www.swissadme.ch/index.php) to determine the ADME score and drug-likeness based on Ro5. Bioactivity prediction of 33 compounds was carried out using the Molinspiration webserver (https://www.molinspiration.com/), and 6 compounds with the highest nuclear receptor ligand and bioactivity prediction scores of enzyme inhibitor were selected for further bioactivity analysis on the PassOnline webserver (http://www.way2drug.com/passonline/predict.php)(Daina et al. 2017; Filimonov et al. 2014).

2.7. Allergic Mice induced by Ovalbumin

The P I - P VI group mice were induced with an allergy model of Ovalbumin. Mice were sensitized and challenged intraperitoneally with Ovalbumin. They were injected intraperitoneally on day 15 with 0.15 cc Ovalbumin in Al(OH)3/mice from 2.5 mg Ovalbumin dissolved in 7.75 ml aluminum hydroxide and on day 22 with a dose of 0.15 cc Ovalbumin in distilled water/mice from 2.5 mg Ovalbumin which was dissolved in 10 ml of distilled water. On the 23rd to the 30th day, the mice were exposed orally to 0.15 cc of Ovalbumin in distilled water from 2.5 mg of Ovalbumin in 2.5 ml of distilled water (Fischer et al. 2005) with modification by Diding et al., 2008. On the 18th day, 25th day, and 31st day, three mice per group were sacrificed by neck dislocation. The mice were dissected, and their spleens were taken to isolate the lymphocytes.

2.8. Protein target prediction and network analysis

Eleven compounds (10-nonadecanone, 9-octadecenamide, caryophyllene oxide, clionasterol, ethyl oleate, 11-pentan-3-ylhenicosane, methyl linolelaidate, methyl octadec-10-enoate, 9,12-octadecadienol, palmitic acid, and tricosanol-1) were subjected to network analysis for further investigation of protein targets through the Swiss Target Prediction webserver (http://www.swisstarget prediction.ch/). The proteins with probability scores > 0 were taken to analyze further interactions, and the network formed through the STRING webserver (https://string-db.org/) (Szklarczyk et al. 2019). A total of 265 proteins were analyzed using STRING, with the parameter used being a high confidence score (0.700) on each edge connecting nodes. Proteins that had no interaction with the main network were selected so that there were 118 proteins for molecular docking analysis. Next, the STRING network data was analyzed in Cytoscape ver. 3.9.1. using the NetworkAnalyzer plugin to determine the score betweenness and closeness centrality and the degree of each node. Ten proteins with the highest betweenness centrality score and two additional proteins were selected for further analysis and became protein candidates for molecular docking analysis targets.

Functional annotation analysis in the form of Gene Ontology (GO) and Pathway (KEGG) was performed on the 118 proteins using the DAVID web server (https://david.ncifcrf.gov/tools.jsp) for their bioactivity in cells. Furthermore, the enrichment related to the bioactivity of 12 proteins was carried out using ClueGO with the following settings: Load marker, Homo sapiens [9606], GOterm and KEGG, Network specificity, medium, pV < 0.05 (Bindea et al. 2009; Shannon et al. 2003; Xia et al. 2014)

2.9. Molecular docking analysis

Six proteins were selected as docking target proteins and downloaded from the RCSB PDB (https://rcsb.org/) with 11 selected compounds, namely PPARA (PDB ID: 6LX4), PPAR-Γ (PDB ID: 4XLD), MAPK14 (PDB ID: 1DI9), PTGS2 (PDB ID: 5IKR), CYP19A1 (PDB ID: 5JKW), and HRH1 (PDB ID: 3RZE). The control compounds were standard drugs registered in the drug bank (https://go.drugbank.com/drugs). Sequentially, the control compounds used were Fenofibric Acid (CID: 64929), Rosiglitazone (CID: 445655), 4-[3-methylsulfanylanilino]-6,7-dimethoxyquinazoline (MSQ) (CID: 1714), Rofecoxib (CID: 5090), testosterone (CID: 6013), and Doxepin (CID: 667477) (Table 2). Protein was prepared using Biovia Discovery Studio ver 19.1.0.18287 to remove ligands, water, and Chimera ver. Alpha to construct the missing residue using a modeler (Webb and Sali, 2016). Molecular docking analysis was triplicated using AutodockVina on PyRx 0.9.7 with standard procedures. The binding site was determined based on the experimental results of interacted residue on PDB as seen through PDBsum (https://www.ebi.ac.uk/). Next, the binding energy score was recorded, and 3D visualization was performed using Biovia Discovery Studio ver 19.1.0.18287.

Table 2. The list of proteins and drugs used as a control group

No	Protein	PDB ID	Drug Name	Drug CID	Drug Pharmacology	Reference
1	PPARA	6LX4	Fenofibric acid	64929	Agonist	(Kamata et al. 2020)
2	PPAR-Γ	4XLD	Rosiglitazone	445655	Agonist	(Mirza et al. 2019) (Gelin et al. 2015)
3	MAPK14	1DI9	4-[3-methylsulfanylanilino]-6,7-dimethoxyquinazoline	1714	Inhibitor	(Shewchuk et al. 2000)
4	PTGS2	5IKR	Rofecoxib	5090	Inhibitor	(Nuvoli et al. 2021)
5	CYP19A1	5JKW	Testosterone	6013	Substrate	(Ghosh et al. 2018)
6	HRH2	3RZE	Doxepin	667477	Antagonist	(Shimamura et al. 2011)

2.10. Statistical analysis

Data in the form of B220IgE and B220IgG1 profiles in B cells were analyzed using the One-Way ANOVA test followed by the Tukey test (Pratiknya 2000). Statistical analysis of One-Way Anova and Two-Way Anova with Dunnett's multiple comparisons were utilized to provide statistical evidence based on the significance of the difference in scores obtained from the docking results.

2.11. Ethical Clearance

This research has received approval for ethical clearance by the Research Ethics Committee of the Universitas Muhammadiyah Yogyakarta with a certificate number 002/EP-FKIK-UMY.

3. Results

3.1. Effect of EEDA on body weight and B220IgE and B220IgG1 cytokine profiles

There was a change in body weight and cytokine profiles of B220IgE and B220IgG1 in the gastrointestinal tract's sensitivity, challenge, and allergic phases after treatment with *D. alata* tuber ethanol extract (EEDA) in Balb/C mice model of digestive tract allergy induced by Ovalbumin (Figure 2 and 3).

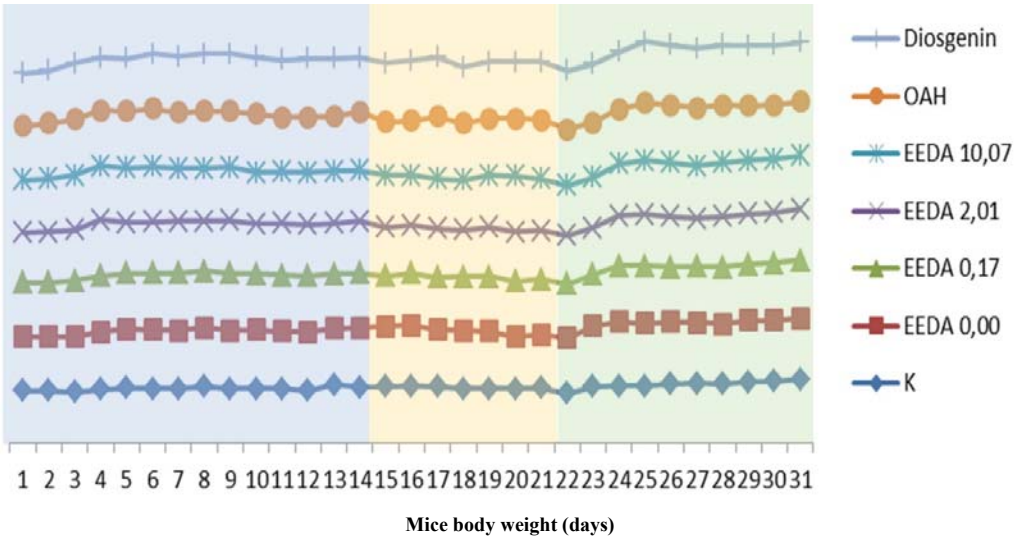

Figure 2. Comparison of representative mice body weight (g) in the sensitivity phase (blue area), challenge phase (yellow area) and digestive tract allergy phase (green area) after administration of *Dioscorea alata* L. tuber ethanol extract (EEDA) in the control group (K), negative control (KN), EEDA 0.17 g/kg; EEDA 2.01 g/kg; EEDA 10.04 g/kg, Antihistamines (OAH) and Diosgenin.

The body weight of the mice in this study increased every day for 30 consecutive days. The body weight of mice can be seen in the sensitivity phase, challenge phase, and allergic phase of the digestive tract after intraperitoneal induced Ovalbumin on day 15 and 22 and Ovalbumin induced orally on day 23 to day 30 (Figure 2). It indicated a slight decrease in body weight from day 16 to day 17, on day 23 to day 24, and on day 24 to day 26.

According to (Dourado et al. 2010), Ovalbumin sensitization in Balb/C mice increased IgE and IgG1 levels. During the sensitization phase, there was an increase in the cytokine profiles B220IgE and B220IgG1 in all groups induced by Ovalbumin. The highest profile of cytokine B220IgE and B220IgG1 was in the EEDA treatment group of 10.04 g/kg. Intraperitoneal injection of low doses of Ovalbumin as an antigen and aluminum hydroxide as an adjuvant resulted in increased formation of high levels of IgE antibodies (Aguilar-Pimentel et al. 2010; Barwig et al. 2010; He et al. 2015; Lee et al. 2013). In the challenge phase, there was an increase in the profile of cytokine B220IgE and IgG1 in all Ovalbumin-induced mice. Controls had the lowest profiles of B220IgE and B220IgG1 cytokines. The highest profile of B220IgE and B220IgG1 cytokines at 0.17 g/kg EEDA was higher than 0.00 g/kg EEDA which was only induced by Ovalbumin. In the allergic phase of the gastrointestinal tract, there was a significant decrease in the profile of cytokines B220IgE and B220IgG1 in EEDA and anti-histamine drugs ($p < 0.05$) (Figure 3). The profile of cytokine B220IgE and B220IgG1 was highest at 0.00 g/kg EEDA and Diosgenin. It showed that Ovalbumin as an allergen had made mice model allergies, proving that administering Ovalbumin can increase IgE and IgG1 levels of Balb/c mice in the sensitivity, challenge, and allergic phases of the digestive tract. One of the clinical symptoms of food allergy is increased levels of IgE and IgG1 (Gocki & Bartuzi 2016).

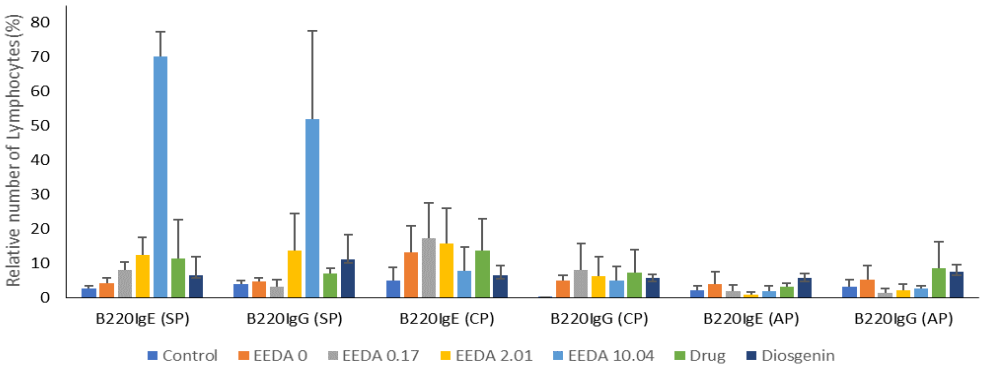

Figure 3. Comparison of the relative number of mice spleen lymphocytes expressing B220IgE and B220IgG1 in the sensitivity phase (A), challenge phase (B) and digestive tract allergic phase (C) after administration of EEDA in the control group, EEDA 0 g/kg as negative control, EEDA 0 .17g/kg; EEDA 2.01 g/kg; EEDA 10.04 g/kg, antihistamines drug and Diosgenin

3.2. Phytocompound based on GCMS and drug-likeness analysis

Research related to the potential of *D.alata* phytocompound is still interesting due to the active compound content and other macromolecules that make it suitable as a staple food. (Makiyah & Djati 2018; Makiyah et al. 2022; Salehi et al. 2019). Based on the GCMS results, 40 peaks were obtained with a total of 33 secondary metabolites from the hexane extract of *DA*

(HEDA) (Table 3). Based on the peaks, the 33 phytocompounds ranged from Tetradecane (13,324) to clionasterol (37,544). Hexadecanoic acid, ethyl ester, and 9-Octadecenamide (Z) were the constituents with the lowest abundances of 0.34% and 0.47%, while methyl palmitate and methyl stearate were the phytocompounds with the highest abundances of 11.59% and 11.75% as revealed from our previous studies (Makiyah & Djati 2018). Phytocompounds with the lowest molecular weight (168 Da) are 1-undecane, 7-methyl- and 1-nonene, 4,6,8-trimethyl. Clionasterol is a phytocompound with a molecular weight of 414 Da. All phytocompounds have a Rule of five (Ro5) violation of less than two, which means they have good drug-likeness. The Ro5 parameter is formulated to assess the absorbance potential of drugs orally based on their physicochemical structure (Leeson et al. 2021). However, it is less relevant to see the potential for drugs that are applied by injection or in other ways other than orally. Still, at least 90% of the compounds from the Available Chemical Directory follow the Ro5 parameter (Benet et al. 2016).

3.3. Bioactivity prediction result

An orally active drug clionasterol, 9,12-octadecadienoic, and tricosanol-1 are the compounds with the highest average probability scores (Tables 4 and 5). Specifically, clionasterol had the highest bioactivity score as a nuclear receptor ligand (0.734), 9,12-octadecadiol as an ion channel modulator (0.152), and tricosanol-1 with scores above the average on several bioactivities. Based on the high bioactivity scores of the nuclear receptor of ligands and enzyme inhibitors compared to other bioactivities, it can be concluded that the compounds contained in HEDA had high potential as nuclear receptor ligands and enzyme inhibitors so that from this bioactivity, six phytocompounds were investigated further in the next analysis.

Furthermore, we also predicted the bioactivity of the six phytocompounds using PassOnline as an anti-inflammatory, non-steroidal inflammatory agent, immunosuppressant, anti-hypercholesterolemic, and cholesterol antagonist. In anti-inflammatory bioactivity, 9,12-octadecadienoic, methyl linolelaidate, and caryophyllene oxide had scores that stood out from the other three phytocompounds. Furthermore, non-steroidal inflammatory agents were the bioactivities with the lowest average predictive scores of the other four bioactivities, followed by anti-hypercholesterolemic and immunosuppressant. Meanwhile, for the two bioactivities related to anti-cholesterol, clionasterol seemed to have the highest score of the other phytocompounds. The predictive score for the bioactivity of clionasterol was increased, indicating that this phytocompound was interesting to identify its anti-cholesterol role in further studies. (Table 4).

Table 3. Prediction of the active compounds of D.alata hexane extract based on GCMS analysis in previous studies (Makiyah & Djati 2018)

Line	Compound	Retention time (min)	Area (%)	MW	Formula	CAS	Lipinski #violations
1	Clionasterol	37.544	6.99	414	C29H50O	83-47-6	1
2	9,12-octadecadienol	23.598	2.67	266	C18H34O	1577-52-2	1
3	Tricosanol-1	24.053	5.4	340	C23H48O	3133-01-5	1
4	Methyl linolelaidate	22.936	4.03	294	C19H34O2	2566-97-4	1
5	Caryophyllene oxide	18.487	1.81	220	C15H24O	1139-30-6	0
6	11-Pentan-3-ylhenicosane	19.617	0.87	366	C26H54	55282-11-6	1

Table 4. Phytocompound bioactivity prediction by MolInspiration

No	Compound Name	GPCR Ligand	Ion Channel Modulator	Kinase Inhibitor	Nuclear receptor ligand	Protease Inhibitor	Enzyme Inhibitor	Mean
1	Clionasterol	0.136	0.045	-0.51	0.734	0.071	0.509	0.164
2	9,12-octadecadienol	0.152	0.152	-0.086	0.142	-0.03	0.306	0.106
3	tricosanol-1	0.08	0.021	0.006	0.126	0.088	0.102	0.071
4	methyl linolelaidate	0.147	0.069	-0.195	0.135	0.027	0.225	0.068
5	caryophyllene oxide	-0.081	0.144	-0.861	0.621	0.003	0.567	0.066
6	11-pentan-3-ylhenicosane	0.089	0.049	-0.107	0.113	0.138	0.061	0.057

Table 5. Phytocompound bioactivity prediction by PassOnline

No	Compound Name	Anti-inflammation	Non-steroidal anti-inflammatory agent	Immunosuppressant	Antihyper-cholesterolemic	Cholesterol antagonist
1	Clionasterol	0.467	0.000	0.762	0.960	0.957
2	9,12-octadecadienol	0.745	0.355	0.484	0.644	0.751
3	tricosanol-1	0.498	0.275	0.430	0.452	0.654
4	methyl linolelaidate	0.728	0.402	0.538	0.691	0.792
5	caryophyllene oxide	0.759	0.414	0.758	0.000	0.281
6	11-pentan-3-ylhenicosane	0.402	0.174	0.336	0.522	0.599
	Mean	0.600	0.270	0.551	0.545	0.672

3.4. Protein-protein network and enrichment analysis

Based on the results of network enrichment of 118 proteins, it is revealed that 10 proteins encoded by the genes Presenilin1 (PSEN1), nuclear receptor subfamily 1, group C, member 1 (NR1C1) or Peroxisome Proliferator Activated Receptor Alpha (PPARA), mitogen-activated protein kinase 14 (MAPK14), prostaglandin-endoperoxide synthase 2 (PTGS2) or Cyclooxygenase 2 (COX-2), nuclear receptor subfamily 1, group C, member 2 (NR1C2) or Peroxisome Proliferator Activated Receptor Gamma (PPAR-Γ), Coagulation Factor II (F2), Fatty Acid-Binding Protein-1 (FABP1), Kinase Insert Domain Receptor (KDR), Cannabinoid Receptor 1 (CNR1), and UDP-Glucuronosyltransferase-2B7 (UGT2B7) had a role as a hub on networks. The majority of proteins in the network were known to have a role in metabolic pathways, various signaling in cells, and several disease pathways, such as cancer and Alzheimers. The results of a functional analysis of the interactions between GOTerm and KEGG on 12 selected proteins (10 hub proteins, H1R (HRH1), and Aromatase (CYP19A1)) showed parental bioactivity related to the production of inflammatory-related molecules, regulation of fatty acid and small molecule metabolism, and oxidation of fatty acids (Figure 4). Six (6) proteins Peroxisome Proliferator Activated Receptor Alpha (PPARA), Peroxisome Proliferator Activated Receptor Alpha (PPAR-Γ), MAPK14, COX2, CYP19A1, H1R) were selected for molecular docking analysis as they had a dominant role in the inflammatory process and were proteins targeted by more than 3 phytocompounds (Nuvoli et al. 2021; Pawlak et al. 2015).

3.5. Molecular docking analysis result and visualization

The molecular docking analysis results demonstrate that the binding energy (kcal/mol) required for interactions between the six compounds and the six protein is higher on average than the binding energy necessary for interactions between the control compounds and the proteins (Table 5). However, clionasterol and caryophyllene oxide were the active compounds with the lowest average binding energy than control. Clionasterol has significantly lower binding energy than MSQ (CID: 1714) (P<.0001) and requires binding energy that is not significantly different from that of fenofibric acid (CID: 64929) and rosiglitazone (CID: 445655) to interact with PPARA and PPAR-Γ. Specifically, clionasterol has a high potential to interact with PPAR, CYP19A1, and MAPK14.

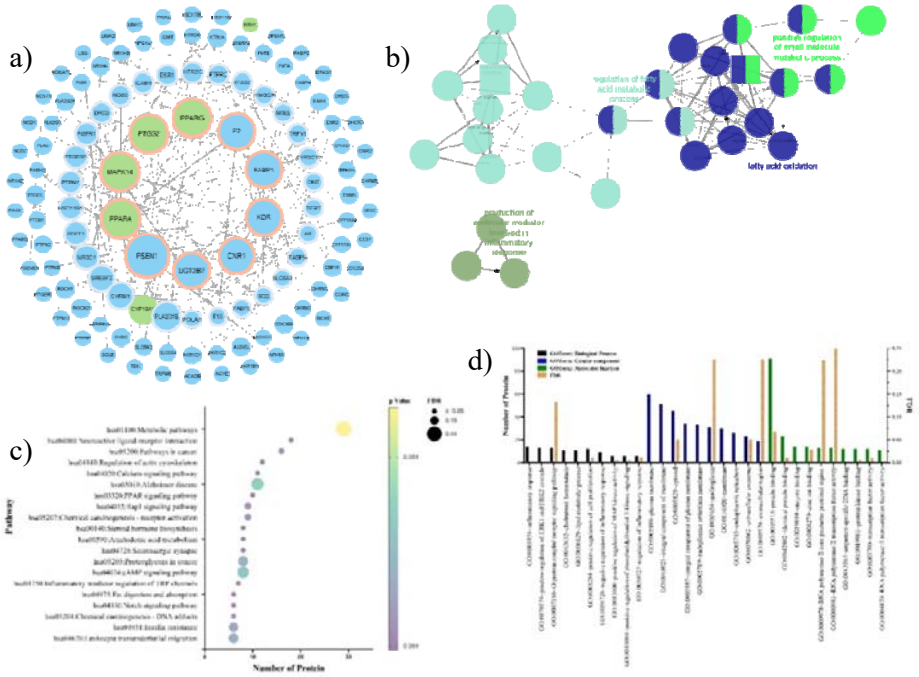

Figure 4. Target protein interaction network of 11 HEDA compounds and their biological activities. a) Network of 118 target proteins. The green proteins were the target proteins in molecular docking analysis. They were selected based on the literature regarding their bioactivity in inflammation and their suitability as proteins for molecular docking analysis. The size of the protein nodes scaled with the betweenness centrality (BC) score. 10 proteins with the highest BC scores had red border nodes. b) Bioactivity of 12 related protein genes (PSEN1, PPARA, MAPK14, PTGS2, PPAR-Γ, F2, FABP1, KDR, CNR1, UGT2B7, HRH1, and CYP19A1) based on GOTerm (round nodes) and KEGG pathway (square nodes). c) GOTerm enrichment analysis of 118 proteins. d) Pathway formed from 118 proteins based on KEGG.

Table 6. Protein and ligand binding energy (kcal/mol)

No	Ligand	PPARA	PPAR-Γ	MAPK14	PTGS2	CYP19A1	HRH1
1	Control	-9.67 ± 0.23	-8.70 ± 0.00	-6.73 ± 0.06	-8.40 ± 0.00	-10.10 ± 0.00	-10.83 ± 1.33
2	Clionasterol	-9.60 ± 0.00	-8.57 ± 0.06	-8.13 ± 0.12	-4.67 ± 0.06	-9.17 ± 0.23	-4.47 ± 0.90
3	Caryophyllene oxide	-7.23 ± 0.40	-6.30 ± 0.00	-6.97 ± 0.06	-6.00 ± 0.00	-7.10 ± 0.00	-7.77 ± 0.32
4	11-Pentan-3-ylhenicosane	-6.70 ± 0.17	-6.37 ± 0.15	-5.40 ± 0.17	-7.27 ± 0.06	-5.90 ± 0.10	-7.40 ± 0.10
5	Methyl linolelaidate	-6.67 ± 0.15	-6.37 ± 0.21	-5.07 ± 0.06	-6.97 ± 0.06	-6.03 ± 0.06	-7.40 ± 0.10
6	9,12-octadecadienol	-6.40 ± 0.10	-6.13 ± 0.31	-5.07 ± 0.12	-6.70 ± 0.10	-6.20 ± 0.17	-7.20 ± 0.00
7	Tricosanol-1	-6.43 ± 0.21	-5.90 ± 0.20	-4.87 ± 0.15	-6.60 ± 0.17	-5.90 ± 0.10	-7.33 ± 0.06

The visualization results on three proteins (PPARA, PPAR-Γ, and MAPK14) with low binding energy when interacting with HEDA compounds showed some interesting data. Clionasterol had a binding energy score that was not significantly different from binding energy control in PPARA and PPAR-Γ. Second, the number of hydrogen bonds formed during interaction did not always contribute to lowering the binding energy. (Figure 5; Supplementary table 1).

A

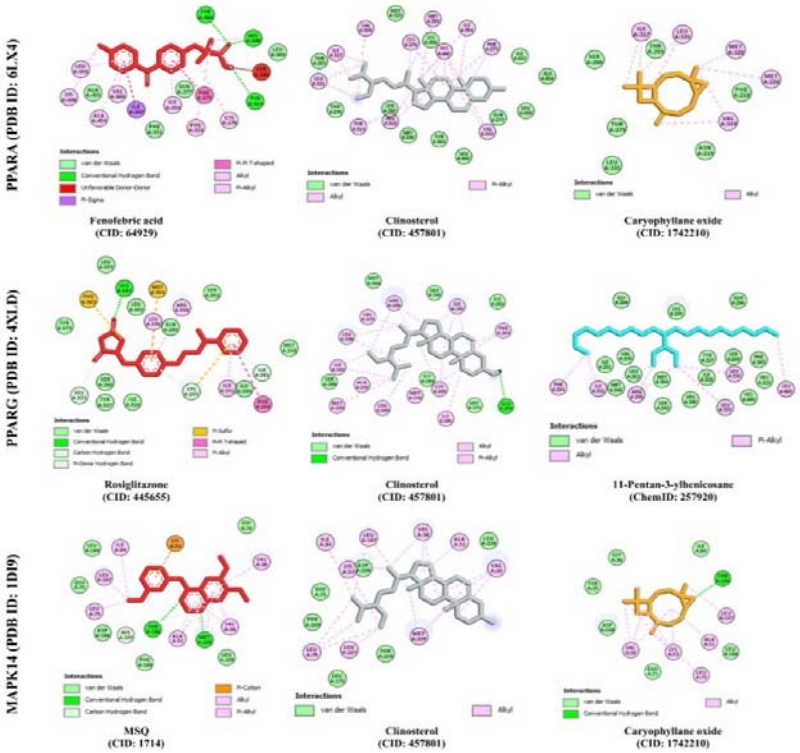

B

Figure 5. Ligand binding position and 2D interaction with the receptor. A) The location of the binding site of each receptor and the comparison of the interaction positions of each compound with the control B) Ligand interaction with receptor amino acid residues in 2D

4. Discussion

The body weight variable is a marker of the success of the gastrointestinal allergy model mice, indicated by diarrhea in mice characterized by watery feces and weight loss. This study successfully made mice models of canal allergy through a slight decrease in body weight after administration of the Ovalbumin allergen. It aligns with the results of research by Mollica et al. (2013). This study showed no difference in feed consumption between groups

of mice, but the mice treated with Ovalbumin lost a little weight due to hypercatabolism caused by the production of inflammatory cytokines (Cara et al. 1997; Dourado et al. 2010). This study did not evaluate whether the weight loss in the Ovalbumin treatment group was due to a decrease in feed consumption or water retention, as found in a (Moreira 2006) study on Ova-sensitized test animals.

The research results of Jan et al. (2007) also showed that the body weight of mice treated with Diosgenin doses of 200 mg/kg and 400 mg/kg did not differ significantly from the body weight of the control group mice. After the sensitization phase with Ovalbumin, re-exposure to the antigen causes local or systemic manifestations of food allergy. Systemic antigen sensitization using intraperitoneal adjuvants is conducted to induce antigen sensitization and food hypersensitivity responses to antigen challenges. This process provides essential insights into the mechanisms of the effector phase of food allergies. (Link et al. 2020; Yoo et al. 2014). Furthermore, the results of this study indicated that EEDA had a variety of active compounds that had the potential as anti-allergenic agents. It is proven that EEDA could reduce IgE and IgG1 levels of Balb/c mice in the allergic phase of the digestive tract. Ovalbumin stimulated an allergic reaction and repeated exposure to Ovalbumin activates CD4+ lymphocytes, stimulating B cells to increase IgE production. IgE is essential in developing allergic reactions (Akdis et al. 2020; Majewska-Szczepanik et al. 2016). Research by Mine et al., (2019) and Wu et al., (2020) showed that giving Ovalbumin orally to mice induced the production of Th2 and IgE cytokines. It will result in an immune response to allergic inflammation. One of the parameters to analyze the development of the allergic process is IgE levels. IgE binds to the FcεRI receptor on the surface of mast cells. In line with allergen exposure, inflammatory mediators are released to trigger allergic symptoms. Administration of EEDA doses of 0.17, 2.01, and 10.04 g/kg in allergic model BALB/c mice in the allergic phase of the gastrointestinal tract in this study reduced the profile of cytokines B220IgE and B220IgG1.

In addition, regarding hub proteins that are not the target of molecular docking analysis, the role of UGT2B7, PSEN1, F2, FABP1, and CNR1 in the inflammatory process is still under further research. UGT2B7 is an enzyme commonly found in the liver that plays an important role in phase II metabolic pathway of chemical compounds, including drugs and endogenous compounds. (Abdullah & Ismail 2018; Yang et al. 2017) Presenilin-1 (PSEN1) is a protein part of the γ-secretase complex which plays a role in the production of amyloid peptide and amyloid precursor protein (APP) which is widely recognized for its effect on Alzheimer's disease (AD) where more than 300 mutations have been known to be involved in the neurodegenerative pathway (Arber et al. 2021; Bagaria et al. 2022; Kelleher & Shen 2017). Besides, prothrombin (F2) is an unstable coagulation protein. It will be cleaved into a small functional protein called thrombin. Thrombin has pro-inflamm atory activity by activating protease-activating receptors on immune cells such as monocytes, dendritic cells, endothelium, and lymphocytes (Palta et al. 2014). Kinase Insert Domain Receptor (KDR), also known as vascular endothelial growth factor receptor-2 (VEGFR-2), is a receptor protein in the endothelium. KDR plays a major role in signaling processes through angiogenesis, cell proliferation, and neovascularization growth factors. (Modi & Kulkarni 2019; Yeo et al. 2019). Next, fatty acid binding protein-1 (FABP1) and Cannabinoid receptor-1 (CNR1) play a role in the endocannabinoid system (ECS). FABP1 plays an important role in lipid metabolism. It is a cytoprotectant and minimizes oxidative damage in hepatocytes (Schroeder et al. 2016; Wang et al. 2015). Meanwhile, CNR1 is abundant in cells in the cerebral cortex, basal ganglia, hippocampus, and cerebellum, which cause the brain to experience psychotropic effects due to the presence of cannabis. (Im 2013; Ye et al. 2019)

COX-2 (*PTGS2*) is an inducible enzyme whose excessive activity will exacerbate inflammation as it is the main source of prostaglandins (PGs) and is also associated with CYP19A1 related to inflammatory processes in malignant pleural mesothelioma (MPM) cells. CYP19A1 (aromatase) is a cytochrome P450 enzyme complex co-translated with COX-2 by expressing PKA-CREB-dependent genes (Ju et al. 2022; Nuvoli et al. 2021). Human histamine receptor H1 (HRH1) plays a role in signaling, resulting in allergies, anaphylaxis, asthma, and autoimmune disease. HRH1 inhibition can inhibit the TH2 response, form IL-4 and IL-13, and prevent airway inflammation and hyperactivity reactions by allergens (Wang et al. 2014). Peroxisome proliferator-activated receptors of alpha and gamma (PPAR-A and PPAR-Γ) are inducible nuclear transcription factors that can induce adipocytokine signaling pathways related to metabolisms, such as keto-lipogenesis, lipid, fatty acid, and cholesterol metabolism, adipocyte differentiation, and cell survival (Michalik & Wahli 2008; Pawlak et al. 2015; Tan et al. 2021). MAPK14 (Mitogen activation protein kinase-14), also known as p38 / p38a, regulates the biosynthesis of inflammatory cytokines such as TNF-a, IL-1, IL-6, and IL-1b. Furthermore, MAPK14 is an important protein in initiating inflammatory disorders, cardiovascular cases, neurodegenerative disease, and cancer, where inhibition of MAPK14 can be an alternative to overcome these disorders (Ali et al. 2021; Ariey-Bonnet et al. 2020; Madkour et al. 2021).

Clionasterol, also known as γ-sitosterol, is a phytosterol compound that is the epimer of β-sitosterol. Clonasterol has high potential as a hypolipidemic agent as it can have low binding energy when interacting with acetoacetyl thiolase, 3-(HMG-CoA) reductase, HMG-CoA synthase, squalene synthase, and oxide-squalene cyclase. In addition, the activity of clionasterol as an anti-hyperlipidemic was also shown by lowering blood cholesterol and triglyceride levels in streptozotocin-induced rats. (Balamurugan et al. 2015). Reducing cholesterol levels in the blood can reduce inflammatory activity, thereby reducing the possibility of diseases such as chronic inflammation, atherosclerosis, and obesity. (Tall & Yvan-Charvet 2015) Elective cytotoxicity activity by clionasterol from *Strobilanthes crispus* on colon cancer cell lines (Caco-2), liver cancer cell lines (HepG2), and hormone-dependent breast cancer cell lines (MCF-7) has low and high IC50 in normal cells (Chang liver cell line). Cytotoxicity occurs since clionasterol can induce apoptosis in Caco-2 and HepG2 and suppress the c-myc gene expression in all cell lines (Endrini et al. 2015). Another study evaluated the clionasterol-rich hexane fraction (CRHF2) of Caulerpa racemosa (CR) against particulate

matter-induced skin damage using a zebrafish model. CRHF2 of CR demonstrated superior protective activity by downregulating ROS and mitochondrial levels, inhibiting oxidative stress, and inhibiting mitochondrial-mediated apoptosis. This result supported the idea that clionasterol has the potential for pharmaceutical development to attenuate inflammation-related diseases. (Liyanage et al. 2022)

MAPK signaling plays an important role in cell differentiation, cell activation, cell proliferation, degranulation and migration of various immune cells (Duan & Wong 2006). MAPK signaling is involved in mast cells that regulate cytokine production in response to specific extracellular stimuli and then initiate biological reactions (Li et al. 2016). Apart from MAPK, Peroxisome proliferator-activated receptor-γ (PPAR-γ) also plays an important role in the response to allergies. PPAR-γ is a nuclear receptor that has emerged as an important regulator of multiple cell types involved in the inflammatory response to allergens; from airway epithelial cells to T Helper (TH) cells. Over the past 10 years, it has become clear that PPAR-γ is a critical component of the type 2 immune response to allergens. In particular, PPAR-γ is important in driving allergic responses in tissue, for instance by promoting IL-33R expression on TH2 cells and ILC2. PPAR-γ may be a critical environmental sensor that modulates allergic immune responses (Stark et al. 2021).

The molecular docking results were interesting as the binding sites were located in different locations even though they were close together. Clionasterol could interact with Phe273 residue as an active site with insignificant differences in binding energy with fenofebric acid, indicating it could interfere with the activation of PPAR-A. (Kamata et al. 2020). Rosiglitazone could form bonds with Cys285 and His323 residues, which were the active sites of PPAR-Γ but not with clionasterol or pentane (Gelin et al. 2015). Based on these results, clionasterol could potentially reduce drug use due to its efficacy as a PPARA and PPAR-Γ agonist. PPAR-γ agonists can mitigate allergic inflammation by suppressing pro-inflammatory gene expression in epithelial cells. PPAR-γ promotes type 2 immune responses by regulating lipid metabolism and inducing effector gene expression. Preclinical models implicate PPAR-γ in driving allergic inflammation (Stark et al. 2021). It was known from the interaction of MSQ with MAPK14, which formed three hydrogen bonds on His107, Thr106, and Met109 residues. They had higher binding energy than clionasterol, which did not form hydrogen bonds in its interactions, but hydrophobic (Met109) and van der Waals bonds (Thr106).

MAPK signaling plays an important role in cell differentiation, cell activation, cell proliferation, degranulation and migration of various immune cells (Duan & Wong 2006). MAPK signaling is involved in mast cells that regulate cytokine production in response to specific extracellular stimuli and then initiate biological reactions (Li et al. 2016). Apart from MAPK, Peroxisome proliferator-activated receptor-γ (PPAR-γ) also plays an important role in the response to allergies. PPAR-γ is a nuclear receptor that has emerged as an important regulator of multiple cell types involved in the inflammatory response to allergens; from airway epithelial cells to T Helper (TH) cells. Over the past 10 years, it has become clear that PPAR-γ is a critical component of the type 2 immune response to allergens. In particular, PPAR-γ is important in driving allergic responses in tissue, for instance by promoting IL-33R expression on TH2 cells. ILC2. PPAR-γ may be a critical environmental sensor that modulates allergic immune responses (Stark et al. 2021).

5. Conclusion

There was a decrease in IgE and IgG1 levels in mice given EEDA. Clionasterol in HEDA had the potential to become PPAR agonist and MAPK14 inhibitors due to its bioactivity as an anti-inflammatory. This research has provided information on the possible potential efficacy of the active and secondary compound content of DA. Further research for its development as a standard herbal medicine or health supplement requires more research and evaluation of the adverse effects that may result from long-term consumption.

Acknowledgment

The authors would like to thank the Directorate of Research and Community Service of the Ministry of Higher Education and Culture through contract number: DIPA-023.04.1.673453 for funding this research (in vivo research). Thanks also go to Yuyun Ika Christina and Ahmad Hafidul Ahkam as laboratory technicians who have helped in compiling and collecting in vivo and in silico data.

References

Abdullah NH, Ismail S. 2018. Inhibition of UGT2B7 Enzyme Activity in Human and Rat Liver Microsomes by Herbal Constituents. *Molecules*. 23(10):2696. DOI: https://doi.org/10.3390/molecules23102696

Abril-Gil M, Garcia-Just A, Pérez-Cano FJ, Franch À, Castell M. 2015. Development and characterization of an effective food allergy model in Brown Norway rats. *PLoS One*. 10(4):e0125314. DOI: https://doi.org/10.1371/journal.pone.0125314

Aguilar-Pimentel JA, Alessandrini F, Huster KM, Jakob T, Schulz H, et al. 2010. Specific CD8 T Cells in IgE-mediated Allergy Correlate with Allergen Dose and Allergic Phenotype. *Am J Respir Crit Care Med*. 181(1):7–16. DOI: https://doi.org/10.1164/rccm.200902-0190OC

Akdis CA, Arkwright PD, Brüggen M-C, Busse W, Gadina M, et al. 2020. Type 2 immunity in the skin and lungs. *Allergy*. 75(7):1582–1605. DOI: https://doi.org/10.1111/all.14318

Ali EMH, Abdel-Maksoud MS, Hassan RM, Mersal KI, Ammar UM, et al. 2021. Design, synthesis and anti-inflammatory activity of imidazol-5-yl pyridine derivatives as p38α/MAPK14 inhibitor. *Bioorganic & Medicinal Chemistry*. 31:115969–115969. DOI: https://doi.org/10.1016/j.bmc.2020.115969

Amarasekara R, Wickramarachchi SR. 2021. Antioxidant Activity of Phenolic Compound in Dioscorea alata L. (Raja Ala) Tuber Cooking Water. Acta Chemica IASI. 29(2):183–200. DOI : DOI: https://doi.org/10.47743/achi-2021-2-0013

Arber C, Lovejoy C, Harris L, Willumsen N, Alatza A, et al. 2021. Familial Alzheimer's Disease Mutations in PSEN1 Lead to Premature Human Stem Cell Neurogenesis. *Cell Reports*. 34(2):108615–108615. DOI: https://doi.org/10.1016/j.celrep.2020.108615

Ariey-Bonnet J, Carrasco K, Le Grand M, Hoffer L, Betzi S, et al. 2020. In silico molecular target prediction unveils mebendazole as a potent MAPK14 inhibitor. *Molecular Oncology*. 14(12):3083–99. DOI: https://doi.org/10.1002/1878-0261.12810

Arya P, Munshi M, Kumar P. 2023. Diosgenin: Chemistry, extraction, quantification and health benefits. *Food Chemistry Advances*. 2:100170. DOI: https://doi.org/10.1016/j.focha.2022.100170

Bagaria J, Bagyinszky E, An SSA. 2022. Genetics, Functions, and Clinical Impact of Presenilin-1 (PSEN1) Gene. *International Journal of Molecular Sciences*. 23(18):10970–10970. DOI: https://doi.org/10.3390/ijms231810970

Balamurugan R, Stalin A, Aravinthan A, Kim J-H. 2015. γ-sitosterol a potent hypolipidemic agent: In silico docking analysis. *Medicinal Chemistry Research*. 24(1):124–30. DOI: https://doi.org/10.1007/s00044-014-1075-0

Barlianto W, Kusuma MSC, Karyono S, Mintaroem K. 2013. Pengembangan Model Mencit Alergi dengan Paparan Kronik Ovalbumin. *Jurnal Kedokteran Brawijaya*. 25(1):1–5.

DOI: https://doi.org/10.21776/ub.jkb.2009.025.01.1

Barwig C, Raker V, Montermann E, Grabbe S, Reske-Kunz AB, Sudowe S. 2010. Antigen dose-dependent suppression of murine IgE responses is mediated by CD4−CD8− double-negative T cells: IgE regulation by CD4−CD8− double-negative T cells. *Clinical & Experimental Allergy*. 40(6):891–901. DOI: https://doi.org/10.1111/j.1365-2222.2010.03476.x

Benet LZ, Hosey CM, Ursu O, Oprea TI. 2016. BDDCS, the Rule of 5 and drugability. *Advanced Drug Delivery Reviews*. 101:89–98. DOI: https://doi.org/10.1016/j.addr.2016.05.007

Bindea G, Mlecnik B, Hackl H, Charoentong P, Tosolini M, et al. 2009. ClueGO: a Cytoscape plug-in to decipher functionally grouped gene ontology and pathway annotation networks. *Bioinformatics*. 25(8):1091–93. DOI: https://doi.org/10.1093/bioinformatics/btp101

Brazdova A, Senechal H, Peltre G. 2015. Immunodominant Semen Proteins III : IgG1 and IgG4 Linkage in Female Immune Infertility. *JJBS*. 8(1):17–21. DOI: https://doi.org/10.12816/0026943

Cara DC, Conde AA, Vaz NM. 1997. Immunological Induction of Flavour Aversion in Mice. II. Passive/Adoptive Transfer and Pharmacological Inhibition. *Scandinavian Journal of Immunology*. 45(1):16–20. DOI: https://doi.org/10.1046/j.1365-3083.1997.d01-363.x

Daina A, Michielin O, Zoete V. 2017. SwissADME: a free web tool to evaluate pharmacokinetics, drug-likeness and medicinal chemistry friendliness of small molecules. *Scientific Reports*. 7(1):42717–42717. DOI: https://doi.org/10.1038/srep42717

Diding, Listyaningsih E, Subijanto A. 2008. Pengaruh Probiotik Terhadap Gambaran Histologis Mukosa Usus Pada Mencit Balb/C Model Alergi. *YARSI medical Journal*. 16(1):6–12. DOI: https://doi.org/10.33476/JKY.V16I1.219

Dourado LPA, Saldanha JC da S, Gargiulo DL, Noviello M de LM, Brant CC, et al. 2010. Role of IL-4 in aversion induced by food allergy in mice. *Cellular Immunology*. 262(1):62–68. DOI: https://doi.org/10.1016/j.cellimm.2009.12.010

Duan W, Wong WSF. 2006. Targeting mitogen-activated protein kinases for asthma. *Curr Drug Targets*. 7(6):691–98. DOI: https://doi.org/10.2174/138945006777435353

Endrini S, Rahmat A, Ismail P, Taufiq-Yap YH. 2015. Cytotoxic effect of γ-sitosterol from Kejibeling (Strobilanthes crispus) and its mechanism of action towards c-myc gene expression and apoptotic pathway. *Medical Journal of Indonesia*. 23(4):203–8. DOI: https://doi.org/10.13181/mji.v23i4.1085

Filimonov DA, Lagunin AA, Gloriozova TA, Rudik AV, Druzhilovskii DS, et al. 2014. Prediction of the Biological Activity Spectra of Organic Compounds Using the Pass Online Web Resource. *Chemistry of Heterocyclic Compounds 2014 50:3*. 50(3):444–57. DOI: https://doi.org/10.1007/S10593-014-1496-1

Fischer R, McGhee JR, Vu HL, Atkinson TP, Jackson RJ, et al. 2005. Oral and nasal sensitization promote distinct immune responses and lung reactivity in a mouse model of peanut allergy. *The American journal of pathology*. 167(6):1621–30. DOI: https://doi.org/10.1016/S0002-9440(10)61246-1

Gelin M, Delfosse V, Allemand F, Hoh F, Sallaz-Damaz Y, et al. 2015. Combining "dry" co-crystallization and in situ diffraction to facilitate ligand screening by X-ray crystallography. *Acta Crystallogr D Biol Crystallogr*. 71(Pt 8):1777–87. DOI: https://doi.org/10.1107/S1399004715010342

Ghosh D, Egbuta C, Lo J. 2018. Testosterone complex and non-steroidal ligands of human aromatase. *J Steroid Biochem Mol Biol*. 181:11–19. DOI: https://doi.org/10.1016/j.jsbmb.2018.02.009

Gocki J, Bartuzi Z. 2016. Role of immunoglobulin G antibodies in diagnosis of food allergy. *pdia*. 4:253–56. DOI: https://doi.org/10.1038/nri2273

Gould HJ, Sutton BJ. 2008. IgE in allergy and asthma today. *Nat Rev Immunol*. 8(3):205–17. DOI: https://doi.org/10.1038/nri2273

Hakim AR, Saputri R. 2020. Narrative Review: Optimasi Etanol sebagai Pelarut Senyawa Flavonoid dan Fenolik. *Jurnal Surya Medika*. 6:177–80. DOI: https://doi.org/10.33084/jsm.v6i1.1641

He P, Zou Y, Hu Z. 2015. Advances in aluminum hydroxide-based adjuvant research and its mechanism. *Human Vaccines & Immunotherapeutics*. 11(2):477–88. DOI: https://doi.org/10.1080/21645515.2014.1004026

Hotmian E, Suoth E, Umar F, Tallei T. 2021. Analisis GC-MS (Gas Chromatography-Mass Spectrometry) Ekstrak Metanol dari Umbi Rumput Teki (Cyperus rotundus L.). *PHARMACON*. 10:849. DOI: https://doi.org/10.35799/pha.10.2021.34034

Huang C-H, Ku C-Y, Jan T-R. 2009. Diosgenin attenuates allergen-induced intestinal inflammation and IgE production in a murine model of food allergy. *Planta Med*. 75(12):1300–1305. DOI: https://doi.org/10.1055/s-0029-1185578

Huang C-H, Liu D-Z, Jan T-R. 2010. Diosgenin, a Plant-Derived Sapogenin, Enhances Regulatory T-Cell Immunity in the Intestine of Mice with Food Allergy. *J. Nat. Prod.* 73(6):1033–37.
DOI: https://doi.org/10.1021/np900690z

Iheagwam FN, Ogunlana OO, Chinedu SN. 2019. Model Optimization and In Silico Analysis of Potential Dipeptidyl Peptidase IV Antagonists from GC-MS Identified Compounds in Nauclea latifolia Leaf Extracts. *International Journal of Molecular Sciences*. 20(23):5913.
DOI: https://doi.org/10.3390/ijms20235913

Im D-S. 2013. Intercellular Lipid Mediators and GPCR Drug Discovery. *Biomolecules and Therapeutics*. 21(6):411–22.
DOI: https://doi.org/10.4062/biomolther.2013.080

Jan T, Wey S, Kuan C, Liao M, Wu H. 2007. Diosgenin, a plant-derived sapogenin, enhances regulatory T-cell immunity in the intestine of mice with food allergy. *Planta Med*. 73:421–26. DOI: 10.1021/np900690z

Jesus M, Martins APJ, Gallardo E, Silvestre S. 2016. Diosgenin: Recent Highlights on Pharmacology and Analytical Methodology. *J Anal Methods Chem*. 2016:4156293.
DOI: https://doi.org/10.1155/2016/4156293

Ju Z, Li M, Xu J, Howell DC, Li Z, Chen F-E. 2022. Recent development on COX-2 inhibitors as promising anti-inflammatory agents: The past 10 years. *Acta Pharmaceutica Sinica B*. 12(6):2790–2807. DOI: https://doi.org/10.1016/j.apsb.2022.01.002

Kamata S, Oyama T, Saito K, Honda A, Yamamoto Y, et al. 2020. PPARα Ligand-Binding Domain Structures with Endogenous Fatty Acids and Fibrates. *iScience*. 23(11):101727–101727.

DOI: https://doi.org/10.1016/j.isci.2020.101727

Kelleher RJ, Shen J. 2017. Presenilin-1 mutations and Alzheimer's disease. *Proceedings of the National Academy of Sciences*. 114(4):629–31.
DOI: https://doi.org/10.1073/pnas.1619574114

Kumar S, Verma AK, Das M, Dwivedi PD. 2012. Molecular mechanisms of IgE mediated food allergy. *Int Immunopharmacol*. 13(4):432–39.
DOI: https://doi.org/10.1016/j.intimp.2012.05.018

Lee HS, Schlereth S, Khandelwal P, Saban DR. 2013. Ocular Allergy Modulation to Hi-Dose Antigen Sensitization Is a Treg-Dependent Process. *PLoS ONE*. 8(9):e75769.
DOI: https://doi.org/10.1371/journal.pone.0075769

Leeson PD, Bento AP, Gaulton A, Hersey A, Manners EJ, et al. 2021. Target-Based Evaluation of "Drug-Like" Properties and Ligand Efficiencies. *J. Med. Chem.* 64(11):7210–30.
DOI: https://doi.org/10.1021/acs.jmedchem.1c00416

Leksono W, Pramesti R, Santosa G, Setyati W. 2018. Jenis Pelarut Metanol Dan N-Heksa... preview & related info | Mendeley. . 21(1):9.

DOI: https://doi.org/10.14710/jkt.v21i1.2236

Li L, Zhang X-H, Liu G-R, Liu C, Dong Y-M. 2016. Isoquercitrin suppresses the expression of histamine and pro-inflammatory cytokines by inhibiting the activation of MAP Kinases and NF-κB in human KU812 cells. *Chin J Nat Med*. 14(6):407–12.
DOI: https://doi.org/10.1016/S1875-5364(16)30036-X

Link CWM, Rau CN, Udoye CC, Ragab M, Korkmaz RÜ, et al. 2020. IL-2-Agonist-Induced IFN-γ Exacerbates Systemic Anaphylaxis in Food Allergen-Sensitized Mice. *Front Immunol*. 11:596772.
DOI: https://doi.org/10.3389/fimmu.2020.596772

Liyanage NM, Nagahawatta DP, Jayawardena TU, Jayawardhana HH a. CK, Lee H-G, et al. 2022. Clionasterol-Rich Fraction of Caulerpa racemosa against Particulate Matter-Induced Skin Damage via Inhibition of Oxidative Stress and Apoptosis-Related Signaling Pathway. *Antioxidants*. 11(10):194.
DOI: https://doi.org/10.3390/antiox11101941

Madkour MM, Anbar HS, El-Gamal MI. 2021. Current status and future prospects of p38α/MAPK14 kinase and its inhibitors. *European Journal of Medicinal Chemistry*. 213:113216–113216.
DOI: https://doi.org/10.1016/j.ejmech.2021.113216

Majewska-Szczepanik M, Askenase PW, Lobo FM, Marcińska K, Wen L, Szczepanik M. 2016. Epicutaneous immunization with ovalbumin and CpG induces TH1/TH17 cytokines, which regulate IgE and IgG2a production. *Journal of Allergy and Clinical Immunology*. 138(1):262-273.e6.
DOI: https://doi.org/10.1016/j.jaci.2015.11.018

Makiyah SNN, Djati M. 2018. Potency of Purple Yam (Dioscorea alata L.) as An Immunomodulatory Agent. *Berkala Kedokteran*. 14(1):89–98.
DOI: http://dx.doi.org/10.20527/jbk.v14i1.4589

Makiyah SNN, Kita M, Setyawati I, Tasminatun S. 2022. Dioscorea alata L. Tubers Improve Diabetes through Anti-hyperglycemia, Anti-inflammation, Ameliorate Insulin Resistance and Mitochondrial Dysfunction. *The Indonesian Biomedical Journal*. 14(4):365–75. DOI: https://doi.org/10.18585/inabj.v14i4.1966

Makiyah SNN, Noor Z, Widodo, Rifa'i M, Djati MochS. 2014. Ethanol Extracts of Tubers Dioscorea Alata L. As Antiallergic Agent on Mice Balb/C Induced with Ovalbumin. *International Journal of Pharma and Bio Sciences*. 5(3):214–20

Michalik L, Wahli W. 2008. PPARs Mediate Lipid Signaling in Inflammation and Cancer. *PPAR Research*. 2008:1–15. DOI: https://doi.org/10.1155/2008/134059

Mine Y, Jin Y, Zhang H, Rupa P, Majumder K, et al. 2019. Prophylactic effects of isomaltodextrin in a Balb/c mouse model of egg allergy. *NPJ Sci Food*. 3:23. DOI: https://doi.org/10.1038/s41538-019-0057-5

Mirza AZ, Althagafi II, Shamshad H. 2019. Role of PPAR receptor in different diseases and their ligands: Physiological importance and clinical implications. *European Journal of Medicinal Chemistry*. 166:502–13. DOI: https://doi.org/10.1016/j.ejmech.2019.01.067

Modi SJ, Kulkarni VM. 2019. Vascular Endothelial Growth Factor Receptor (VEGFR-2)/KDR Inhibitors: Medicinal Chemistry Perspective. *Medicine in Drug Discovery*. 2:100009. DOI: https://doi.org/10.1016/j.medidd.2019.100009

Moreira LF. 2006. *Estudo dos componentes nutricionais e imunolo´gicos na perda de peso em camundongos com alergia alimentar. (Mestrado)*. Thesis thesis. Federal University of Minas Gerais

Ngatidjan. 2007. *Metode Laboratorium Dalam Toksikologi*. GMU Press

Nuvoli B, Antoniani B, Libener R, Maconi A, Sacconi A, et al. 2021. Identification of novel COX-2 / CYP19A1 axis involved in the mesothelioma pathogenesis opens new therapeutic opportunities. *Journal of Experimental & Clinical Cancer Research*. 40(1):257–257. DOI: https://doi.org/10.1186/s13046-021-02050-1

Palta S, Saroa R, Palta A. 2014. Overview of the coagulation system. *Indian Journal of Anaesthesia*. 58(5):515–515. DOI: https://doi.org/10.4103/0019-5049.144643

Pawankar R, Holgate ST, Canonica GW, Lockey RF, Blaiss MS, eds. 2013. *WAO White Book on Allergy | World Allergy Organization. https://www.worldallergy.org/wao-white-book-on-allergy*

Pawlak M, Lefebvre P, Staels B. 2015. Molecular mechanism of PPARα action and its impact on lipid metabolism, inflammation and fibrosis in non-alcoholic fatty liver disease. *Journal of Hepatology*. 62(3):720–33. DOI: https://doi.org/10.1016/j.jhep.2014.10.039

Peng K-Y, Horng L-Y, Sung H-C, Huang H-C, Wu R-T. 2011. Antiosteoporotic Activity of *Dioscorea alata* L. cv. Phyto through Driving Mesenchymal Stem Cells Differentiation for Bone Formation. *Evidence-Based Complementary and Alternative Medicine*. 2011:1–12. DOI: https://doi.org/10.1155/2011/712892

Pratiknya AW. 2000. *Dasar-Dasar Metodologi Penelitian Kedokteran Dan Kesehatan*. Jakarta: Grafindo Persada.

Rakha A, Umar N, Rabail R, Butt MS, Kieliszek M, et al. 2022. Anti-inflammatory and anti-allergic potential of dietary flavonoids: A review. *Biomed Pharmacother*. 156:113945.
DOI: https://doi.org/10.1016/j.biopha.2022.113945

Rifa'i M, Djati MS, Makiyah SNN, Tasminatun S, Widodo W. 2023. Steroidal Saponin Isolated from Dioscorea alata L. Extract Improve Digestive Tract Allergy in Balb/C Mice Induced by Ovalbumin. *Indonesian Journal of Pharmacy. DOI: https://doi.org/10.22146/ijp.4614*

Saldanha JCS, Gargiulo DL, Silva SS, Carmo-Pinto FH, Andrade MC, et al. 2004. A model of chronic IgE-mediated food allergy in ovalbumin-sensitized mice. *Braz J Med Biol Res*. 37(6):809–16. DOI: https://doi.org/10.1590/S0100-879X2004000600005

Salehi B, Sener B, Kilic M, Sharifi-Rad J, Naz R, et al. 2019. Dioscorea Plants: A Genus Rich in Vital Nutra-pharmaceuticals-A Review. *Iranian Journal of Pharmaceutical Research : IJPR*. 18(Suppl1):68–68. DOI: https://doi.org/10.22037/IJPR.2019.112501.13795

Sampson HA. 1999. Food allergy. Part 1: immunopathogenesis and clinical disorders. *J Allergy Clin Immunol*. 103(5 Pt 1):717–28. https://doi.org/10.1016/s0091-6749(99)70411-2

Sasidharan S, Chen Y, Saravanan D, Sundram KM, Yoga Latha L. 2011. Extraction, isolation and characterization of bioactive compounds from plants' extracts. *Afr J Tradit Complement Altern Med*. 8(1):1–10.

Schroeder F, McIntosh AL, Martin GG, Huang H, Landrock D, et al. 2016. Fatty Acid Binding Protein-1 (FABP1) and the Human FABP1 T94A Variant: Roles in the Endocannabinoid System and Dyslipidemias. *Lipids*. 51(6):655–76. DOI: https://doi.org/10.1007/s11745-016-4155-8

Shannon P, Markiel A, Ozier O, Baliga NS, Wang JT, et al. 2003. Cytoscape: A Software Environment for Integrated Models of Biomolecular Interaction Networks. *Genome Research*. 13(11):2498–2504. DOI: https://doi.org/10.1101/gr.1239303

Shewchuk L, Hassell A, Wisely B, Rocque W, Holmes W, et al. 2000. Binding Mode of the 4-Anilinoquinazoline Class of Protein Kinase Inhibitor: X-ray Crystallographic Studies of 4-Anilinoquinazolines Bound to Cyclin-Dependent Kinase 2 and p38 Kinase. *J. Med. Chem.* 43(1):133–38. DOI: https://doi.org/10.1021/jm990401t

Shimamura T, Shiroishi M, Weyand S, Tsujimoto H, Winter G, et al. 2011. Structure of the human histamine H1 receptor complex with doxepin. *Nature*. 475(7354):65–70. DOI: https://doi.org/10.1038/nature10236

Stark JM, Coquet JM, Tibbitt CA. 2021. The Role of PPAR-γ in Allergic Disease. *Curr Allergy Asthma Rep*. 21(11):45. DOI: https://doi.org/10.1007/s11882-021-01022-x

Sun N, Zhou C, Pu Q, Wang J, Huang K, Che H. 2013. Allergic reactions compared between BN and Wistar rats after oral exposure to ovalbumin. *J Immunotoxicol*. 10(1):67–74.
DOI: https://doi.org/10.3109/1547691X.2012.693546

Szklarczyk D, Gable AL, Lyon D, Junge A, Wyder S, et al. 2019. STRING v11: protein–protein association networks with increased coverage, supporting functional discovery in genome-wide experimental datasets. *Nucleic Acids Research*. 47(D1):D607–13.
DOI: https://doi.org/10.1093/nar/gky1131

Tall AR, Yvan-Charvet L. 2015. Cholesterol, inflammation and innate immunity. *Nature reviews. Immunology*. 15(2):104.
DOI: https://doi.org/10.1038/nri3793

Tan Y, Wang M, Yang K, Chi T, Liao Z, Wei P. 2021. PPAR-α Modulators as Current and Potential Cancer Treatments. *Frontiers in Oncology*. 11.

DOI: https://doi.org/10.3389/fonc.2021.599995

Wang G, Bonkovsky HL, de Lemos A, Burczynski FJ. 2015. Recent insights into the biological functions of liver fatty acid binding protein 1. *Journal of Lipid Research*. 56(12):2238–47. DOI: https://doi.org/10.1194/jlr.R056705

Wang M, Wei X, Shi L, Chen B, Zhao G, Yang H. 2014. Integrative genomic analyses of the histamine H1 receptor and its role in cancer prediction. *International Journal of Molecular Medicine*. 33(4):1019–26.
DOI: https://doi.org/10.3892/ijmm.2014.1649

Wang T-S, Lii C-K, Huang Y-C, Chang J-Y, Yang F-Y. 2011. Anticlastogenic effect of aqueous extract from water yam (Dioscorea alata L.). *Journal of Medicinal Plants Research*. 5(26):6192–6202.
DOI: https://doi.org/10.5897/JMPR11.1126

Wang Z, Zhao S, Tao S, Hou G, Zhao F, et al. 2023. Dioscorea spp.: Bioactive Compounds and Potential for the Treatment of Inflammatory and Metabolic Diseases. *Molecules*. 28(6):2878.
DOI: https://doi.org/10.3390/molecules28062878

Wu M, Gao L, He M, Liu H, Jiang H, et al. 2020. Plasmacytoid dendritic cell deficiency in neonates enhances allergic airway inflammation via reduced production of IFN-α. *Cell Mol Immunol*. 17(5):519–32. DOI: https://doi.org/10.1038/s41423-019-0333-y

Xia J, Benner MJ, Hancock REW. 2014. NetworkAnalyst - integrative approaches for protein–protein interaction network analysis and visual exploration. *Nucleic Acids Research*. 42(W1):W167–74.
DOI: https://doi.org/10.1093/nar/gku443

Yang G, Ge S, Singh R, Basu S, Shatzer K, et al. 2017. Glucuronidation: driving factors and their impact on glucuronide disposition. *Drug Metabolism Reviews*. 49(2):105–38.
DOI: https://doi.org/10.1080/03602532.2017.1293682

Ye L, Cao Z, Wang W, Zhou N. 2019. New Insights in Cannabinoid Receptor Structure and Signaling. *Current Molecular Pharmacology*. 12(3):239–48. DOI: https://doi.org/10.2174/1874467212666190215112036

Yeo NJY, Chan EJJ, Cheung C. 2019. Choroidal Neovascularization: Mechanisms of Endothelial Dysfunction. *Front. Pharmacol.* 10:1363.
DOI: https://doi.org/10.3389/fphar.2019.01363

Yoo J, Manicone AM, McGuire JK, Wang Y, Parks WC. 2014. Systemic sensitization with the protein allergen ovalbumin augments local sensitization in atopic dermatitis. *J Inflamm Res*. 7:29–38.
DOI: https://doi.org/10.2147/JIR.S55672

Yu W, Freeland DMH, Nadeau KC. 2016. Food allergy: immune mechanisms, diagnosis and immunotherapy. *Nat Rev Immunol*. 16(12):751–65.
DOI: https://doi.org/10.1038/nri.2016.111

Attachment

Supplementary table 1. Binding energy which needed (kcal/mol)

Protein	Ligand	Binding Energy (kcal/mol)	Interacted residue					
			Hydrogen bond	Hydro-phobic bond	Electro-static bond	van der Waals bond	Unfavor-able bond	Others bond
PPARA	Control (Fenofebric acd)	-9.7 ± 0.23	TYR314 HIS440 TYR464	PHE273 CYC276 PHE318 ILE354 VAL444 ILE447 LYS448 ALA454 LEU456		GLN277 PHE351 ALA455 LEU460	SER280	
	Clionasterol	-9.6 ± 0.00		PHE273 CYS276 TYR314 ILE317 PHE318 LEU321 VAL324 ILE354 MET355 HIS440 VAL444		GLN277 THR279 SER280 THR283 MET320 MET330 LYS358 ILE447 ALA454 LEU456 LEU460 TYR464		
	Caryophyllene oxide	-7.2 ± 0.40		MET220 ILE317 MET320 LEU321 VAL324		PHE218 ASN219 THR273 SER280 THR283 LEU331		
PPARG	Control (Rosiglitazone)	-8.7 ± 0.00	ILE281 CYS285 HIS323 HIS449	PHE264 ARG288 LEU330 ILE341		GLY284 GLN286 SER289 ILE326 TYR327 SER342 MET348 LEU453 LEU469 TYR473		CYS285 (Pi-sulfur) PHE363 (Pi-sulfur) MET364 (Pi-sulfur)
	Clionasterol	-8.6 ± 0.00	GLU259	PHE264 ILE281 CYS285 ARG288 ALA292 ILE326 MET329 LEU330 LEU333 VAL339 ILE341 MET348		LEU255 ILE262 GLY284 SER289 SER342 MET364		

© 2024 Jordan Journal of Biological Sciences. All rights reserved - Volume 17, Number 3

	11-Pentan-3-ylhenicosane	-6.4 ± 0.15		PHE264 ARG288 LEU330 LEU333 ILE341 LEU469		ILE281 GLY284 CYS285 GLN286 SER289 HIS323 ILE326 TYR327 VAL339 LEU340 SER342 MET348 LEU353 PHE363 MET364 HIS449
MAPK14	Control (MSQ)	-6.7 ± 0.06	THR106 HIS107 MET109	VAL30 VAL38 ALA51 LYS53 LEU75 ILE84 MET109	LYS53	GLY31 GLU71 LEU104 LEU108 ASP168 PHE169
	Clionasterol	-8.1 ± 0.12		VAL30 VAL38 ALA51 LYS53 LEU75 ILE84 LEU104 MET109 LEU167		GLU71 THR106 LEU108 ASP168 PHE169 LEU171
	Caryophyllene oxide	-7.0 ± 0.06	THR106	VAL38 ALA51 LYS53 LEU75 LEU167		THR35 GLY36 GLU71 ILE84 LEU104 ASP168

* The bold residue shows the same residue as the control.

JJBS

Volume 17, Number 3,September 2024
ISSN 1995-6673
Pages 413 – 422
https://doi.org/10.54319/jjbs/170303

Jordan Journal of Biological Sciences

Evaluation of the Potential of Immobilized Cyanide-Degrading Bacteria for the Bioremediation of Cassava Mill Effluent

Ajao[1,*], Abdullahi Taiwo, Jimoh-Hamza[2], Oluwabukola Kudirat, Aborisade[1], Wakili Tope and Jimoh[1], Fausat Abimbola

[1]*Department of Microbiology, Faculty of Pure and Applied Sciences, Kwara State University, Malete, Nigeria;*[2]*Department of Biological Sciences,Faculty of Natural and Applied Sciences, Al-Hikmah University, Ilorin, Nigeria.*

Received: May 26, 2023; Revised: September 10, 2023; Accepted: November 8, 2023

Abstract

This study aimed to assess the feasibility of employing indigenous cyanide-degrading bacterial strains for the treatment of cassava mill effluent (CME) in Nigeria, a hazardous waste material posing significant public health risks. The physicochemical properties and heavy metal concentrations in CME were determined through standard methodologies. Cyanide-degrading bacteria were isolated, characterized, and identified using molecular techniques. These strains were immobilized within a porous network of cross-linked biochar, confirmed through SEM imaging, and evaluated alongside free cells for CME bioremediation. Multiple variables were examined to assess the effluent's pollution load, including pH, electrical conductivity (EC), chemical oxygen demand (COD), biochemical oxygen demand (BOD5), total dissolved solids (TDS), nitrate (NO3), phosphate (PO4), and cyanide levels, falling within respective ranges of (4.00–4.02), (2394–2618 S/cm), (985–1219 mg/L), (1556–1667 mg/L), (3459–3705 mg/L), (2709–2812 mg/L), (251-311 mg/L), (87.25–118 mg/L), and (25.00–28 mg/L). Copper was the most prevalent heavy metal in the effluent, while chromium was detected at the lowest levels, with mean values of 10.00-12.39 mg/L and 0.00-0.27 mg/L, respectively. The study revealed severe contamination of the effluent, above the Federal Environmental Protection Agency (FEPA) threshold limit. The 16S rDNA of the cyanide degrading bacteria were deposited at the NCBI database and the following GenBank accession numbers were assigned (MK71248O, MK71281, MK712482, and MK712483) for *Pseudomonas putida*, *Bacillus subtilis*, *Alcaligenes faecalis* and *Leuconostoc mesenteroides* respectively. Results of the bioremediation approach demonstrated a substantial reduction in physicochemical parameters and heavy metal contents, indicating a promising biological treatment strategy to mitigate CME's adverse effects on public health. In conclusion, despite elevated physicochemical parameters and heavy metal concentrations in CME, this study offers a promising avenue for employing biological treatments to mitigate environmental and public health impacts. Further research and application of this technique hold substantial potential for cassava mill effluent management in Nigeria and other regions facing similar challenges.

Keywords: Bioremediation; Cassava; cyanide; immobilization; physicochemical; heavy metals

1. Introduction

According to Afuye and Mogaji (2015), cassava (Manihot esculenta Crantz) is regarded as a crucial food crop, particularly in African nations, with Nigeria serving as a notable example. Cassava production and processing are largely dominated by a number of small-scale farmers as their source of livelihood (Izah *et al*., 2017a-c). Nigeria was ranked as the top cassava producer in the world in 2016 with a production of 5, 7134,478 tonnes (Izah *et al*., 2018). Moreover, Cassava is the next significant contributor to gross domestic product to the Nigeria economy after petroleum (Jickson *et al*., 2013).

One of the procedures in the processing of cassava is cassava milling, which generates a substantial amount of hazardous waste typically disposed of untreated into nearby farmland and water bodies, posing a risk to public health (Obueh and Odesiri-Erunteyan, 2018; Izah *et al*., 2018). Additionally, the cassava processing industries produce a significant volume of toxic wastewater, constituting a serious environmental threat to both soil biota and aquatic life. This wastewater contains cyanogenic glycosides, primarily linamarin and lotaustralin, which constitute the majority of the hazardous and acidic elements in cassava mill effluent (CME) (Okunade and Adekalu, 2014). According to earlier studies (Oluwafemi *et al*., 2011; Ezeigbo *et al*., 2014; Eboibi *et al*., 2018; Izah, 2018), this wastewater has the potential to cause toxicological effects and have an impact on the biodiversity of soil biota and vegetation if it is not properly treated. Cassava processing has always been regarded with a reputation of a major environment pollutant. Expansion of cassava from subsistence to commercial production, and to the second largest crop production in the country, raised many concerns especially in its relation to the waste management.

Indiscriminately releasing waste products from Cassava processing factories into the environment has been a common practice, thereby polluting the agricultural soil,

* Corresponding author. e-mail: abdullahi.ajao@kwasu.edu.ng.

surface and underground waters (Ezeigbo *et al.,* 2014) induces changes in soil health index such as physicochemical properties, microbial community, building up of toxic metals, and numerous factors associated with plant development (Patrick *et al*.,2011: Chinyere *et al*., 2013: Izah *et al*., 2017). As such, these wastes could even be more difficult to handle in future with the scale-up in the cassava production and processing (Izah *et al*., 2017: Eneriviofi *et al*., 2017).

Considering cassava's economic and agricultural importance, along with its contribution to enhancing food security in Nigeria, it is essential to prioritize the management and processing of cassava waste in urban areas of the country (Oluwatosin *et al*., 2017). Most of the available physicochemical methods for the removal of cyanide are not satisfactory in terms of the cost, toxicity and generation of hazardous chemical end products. Given the limitations of physicochemical methods, there is a pressing need for a robust and economically viable strategy for treating cyanide-contaminated natural ecosystems (Kandasawy et al., 2015; Akinpelu et al., 2017). The degradative capacity of microbes to control environmental pollution has been explored (Bioremediation). Apparently, bioremediation strategy has become method of choice due to its inexpensive, environmentally friendly and efficient nature (Ugochukwu *et al*., 2014; Sarkar *et al*., 2016; Oluwatosin *et al*., 2017; Gupta *et al*., 2017). The study introduces novelty through the utilization of immobilized cells, a method not previously applied for the bioremediation of cassava mill effluents due to its unique design and methodology. To the best of our knowledge, this work is pioneering in introducing such an approach for processing cassava mill effluents. These findings represent the first preliminary evidence for this innovative solution, and this would be of great advantage in terms of its simplicity and appropriate choice to explore for the waste treatment and management that can be adopted by small-scale farmers to detoxify contaminated CME before being released into the environment.

2. Materials and Methods

2.1. Study Area

The study areas are the selected Cassava processing Factories located within Ilorin Metropolis, the capital of Kwara State, located between the latitude 8º5′-10º4′N and longitude 4º55′-6º5′E (NPC, 2006) as shown in Fig. 1. The region lies in the rainforest zone in the South and Guinea Savannah in the North Zone. The average temperature and rainfall are within (27 ^{O}C - 35 ^{O}C) and (1,000 – 1500 mm) respectively. The total land surface area is 35,705 square kilometer (Sqm). Kwara State is Cassava, Millet, Yam, Cowpea producing area due to the vegetation cover, climatic condition and soil types that support the cultivation.

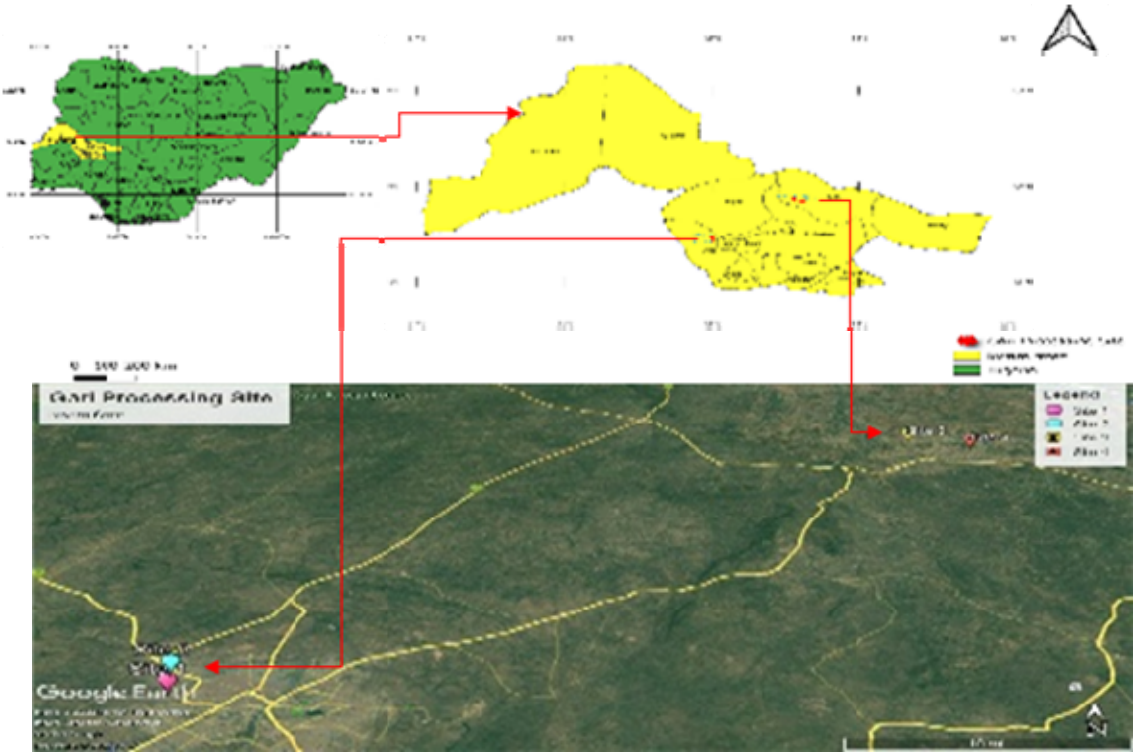

Figure 1.Map of the sampling sites

"Footnote: This map displays four distinct sites representing various Gari Processing Factories from which cassava wastewater samples were collected."

2.2. Sample Collection

This investigation adhered to the methodology outlined by Oljiira *et al*. (2018). Wastewater samples were obtained from the selected cassava processing factories located in the Ilorin metropolis. One-liter samples were aseptically collected from beneath the hydraulic press into clean plastic bottles, which had been cleaned with detergent and rinsed with acid. The samples were then quickly transported to the lab and kept cool at 4 °C in a cooler with ice blocks. To establish a baseline for the assessment in this study, the Agoro *et al*. (2018) method was used to evaluate the physicochemical properties of the wastewater samples.

2.3. Determination of Physicochemical Characteristics of CME

The methodology outlined by Oljiira *et al*. (2018) was employed to examine and measure the physicochemical properties and heavy metal concentrations in CME. TS, TSS, and TDS were determined using the Gravimetric method. The pH was assessed using a pH meter (Model HI9024, HANNA Instrument, UK), and EC was measured with an Oyster conductivity meter during the grab-sampling procedure conducted at the sampling site. Nitrate (ultraviolet spectrophotometric screening methods), Sulfate (Turbidimetric method), Phosphate (Vanadomolybdophosphoric acid) Chloride (argentometric), were determined using standard procedure (APHA, 1998). The determination of COD was performed using a closed reflux method. BOD_5 was measured from the dissolved oxygen content estimated in a BOD5 bottle at 20 °C for 5 days before and after incubation. The CME samples were digested in concentrated nitric acid before being diluted, centrifuged, and filtered using 0.45 m pore size membrane filter. The levels of heavy metals found in wastewater sample were determined using atomic absorption spectroscopy (AAS), including lead, chromium, nickel, copper, manganese, and zinc with a Perkin-Elmer Analyst 300 instrument.

2.4. Determination of the Cyanide Contents in Cassava wastewater

The quantification of cyanide content in cassava wastewater followed the methodology outlined by Eke-Emezia *et al*. (2022) study. In this approach, 2 ml of an alkaline picrate solution was combined with 2 ml of the cassava wastewater sample. The resulting mixture underwent a 10-minute incubation period at 60 °C within a water bath. Following incubation, an absorbance measurement was performed on the resulting deep orange-colored solution using a U-V Spectrophotometer (SHIMADZU UV-1800). The cyanide concentration was determined by extrapolating the values from a previously established potassium cyanide curve, serving as a reference standard.

2.5. Isolation of Cyanide-Degrading Bacteria Using Enrichment Techniques

Cyanide-degrading bacteria were isolated from the soil samples impacted with the cassava mill effluents obtained from the cassava processing factories. These samples were cultivated and enriched in a growth medium that included glucose as the carbon source and KCN as the nitrogen source. The procedure for preparing the medium and isolating bacteria was carried out in accordance with Kandasawy *et al*. (2015) method. The bacterial colonies suspected of degrading cyanide were streaked onto agar slants and then classified based on cultural morphology and biochemical test

2.6. Molecular Identification of Bacterial Isolates.

The genomic DNA was extracted from pure colonies of cyanide-degrading bacteria and suspended in lysis buffer supplemented with Proteinase K to facilitate the extraction process. Subsequently, amplification was performed using universal primers in a thermal cycler, following the conditions specified in Table 1, using established according to the protocol described by Bhutia et al. (2021).

Table 1.16S Primer Sequences

Name of Primers	Target	Sequences (5'-3')
16-518F	Universal primers	5' – CGCTTGTTGATTTGCTGCTGTTCGC – 3'
16S-800R	Universal primers	5-TACCAGGGTATCTAATCC-3
PCR Conditions	Denaturation at 92°C, Annealing at 54°C, and Extension at 72°C,	25 cycles

After purification with the QIA quick PCR purification kit from Qiagen, USA, 1% (w/v) agarose gels were used to evaluate the PCR product. Subsequently, 16S rRNA gene partial sequencing was conducted using Applied Biosystems' BIG-DYE terminator kit for the ABI 310 Genetic Analyzer. Homologous bacteria were identified, and bacterial sequences were aligned using the BLAST Search program from the National Center for Biotechnology Information. To construct the phylogenetic tree, the neighbor-joining technique was employed. The obtained bacterial sequences were deposited into the Genbank of the National Center for Biotechnology Information (NCBI) and assigned accession numbers.

2.7. Preparation of Biochar as a carrier for the cell Immobilization

The preparation of biochar was done according to the method described by Chen and Chen (2009). About 5g of the Activated cow dung was utilized as the biochar material and heated to a temperature of 500 ^{0}C for duration of 4 hours. After cooling for 12 hours, the biochar was then ground and sieved into a fine particle (2mm NO. 60 U.S. Std. mesh). The resultant powder was kept for later use in an airtight container.

2.8. Preparation of Immobilized consortium on carrier

The pre-sterilized biochar, sodium alginate and calcium chloride at 121 °C for 15 mins was used to immobilize the consortium of highest cyanide degrading bacteria as described by (Chen *et al*., 2017). In 100 mL of the mixed culture of the 0.1 at OD_{600} of the cell density of the bacteria, 5 g of the biochar was added and vortexed for 15 minutes. Then, the mixture was added to and mixed for 15 minutes with a 2% (w/v) solution of sodium alginate. The resultant mixture, an adsorption-carrier suspension, was

extruded through a 20 mL syringe and introduced into a sterilized solution of 2% (w/v) calcium chloride to undergo cross-linking for 12 hours, resulting in the formation of spherical beads. The immobilized microsphere was washed with sterile distilled water and subsequently stored in a similar environment.

2.9. Preparation of Microsphere for SEM

The entrapped cells within the porous network of the cross linked biochar characterized using scanning electron microscopy (SEM; KYKY-2800B) as follows: The immobilized cells were fixed for 2 hours with 2.5% glutaraldehyde while the bio-carriers were dried and coated with gold using the method of CO_2-critical point drying. According to protocol, an electron microscope was used to examine the morphology of immobilized bacterial cells.

2.10. SEM Focusing of Microsphere

The samples were mounted onto an aluminum holder stub by utilizing a double sticky carbon tape. Subsequently, gold was applied to the sample, and it was electrically grounded. In order to prevent confusion between samples, the sample stub was marked or inscribed since it can be difficult to distinguish between similar samples in the SEM. Before being loaded into the SEM holder, the sample was completely dried for a minimum of three hours in a drying oven at 60 °C as described by Khashei *et al*. (2018). The sample was focused and magnified as per standard operating procedure with the holder in place on the microscope stage.

2.11. Bioremediation of Cassava Mill Effluent (CME)

Free cells and Immobilized cyanide degrading bacterial Consortium were selected for the bioremediation strategy used for the treatment of CME using modified method of Sonune and Garode's (Sonune and Garode, 2009). The cell density was adjusted to 0.5 at $O.D_{600}$ and inoculum size of 10 % was inoculated into 250 mL Enlenmeyer flask containing 90 mL presterilized cassava wastewater (free cells). Afterwards, 10 ml of the microsphere of immobilized cells was added into 90 ml of presterilized cassava mill effluent in the flasks. Simultaneously, control flasks contained only sterilized Cassava Mill effluent. Each of the flasks was placed on an orbital shaker, where they were maintained at a temperature of 30 °C and rotated at a speed of 120 revolutions per minute for duration of 12 days. All samples were withdrawn at every 72 hrs interval, centrifuged at 4000 rpm for 20 mins and determined the variables in triplicates. The efficiency of the treatment strategy was evaluated by the decrease in the physicochemical parameters and the concentration of heavy metals over the course of treatment.

2.12. Statistical Analysis

One way, variance analysis (ANOVA) has been used to compare the mean of the parameters evaluated. Using the Social Sciences Statistical System (SPSS) Duncan Multiple Range Analysis at $p<0.05$ between the mean values of the calculated parameters.

3. Results

The physicochemical parameters of the sampled Cassava Mill Effluent were determined experimentally, with mean values falling within the ranges of pH (4.00-4.20), EC (2550-2580 µs/cm), BOD5 (980-1215 mg/L), COD (1550-1660 mg/L), Phosphate (87-118 mg/L), and Nitrate (300-310 mg/L). The cyanide content ranged from (28.74-25.00 mg/L), all of which exceeded the permissible limits set by Fedral Environmental Protection Agency (FEPA) (Table 2). The statistical analysis revealed that the mean values obtained from each of the sampling stations were not significantly different, according to the Duncan multiple range tests ($p<0.05$).

Total heterotrophic bacterial counts were (2.7 log CFU/g) and (6.0 log CFU/g) in the Cassava Mill Effluent and the soil impacted by the effluent, respectively, while the heavy metals detected were Lead (0.53-1.15 mgL^{-1}), Chromium (0.16-0.27 mgL^{-1}), Nickel (1.86-2.89 mgL^{-1}), and Copper ions (10.00-12.39 mgL^{-1}) (Table 3).

The four highest cyanide-degrading bacterial strains were tentatively identified as *Pseudomonas* sp, *Lactobacillus* sp, *Bacillus* sp, and a member of *Enterobacteriaceae* for HM1, HM2, HM5, and HM2a, respectively. The 16S rRNA gene sequences of these strains were deposited in the NCBI database under the accession numbers MK712480, MK712481, MK712482, and MK712483, respectively. Strain HM1 showed the highest homology (100%) with *Pseudomonas putida* strain NBRC14164, while strain HM2a was closely related to *Alcaligenes feacalis* strain IAM (100%). Strain HM2 was most closely related (100%) to *Lactobacillus mesenteroides* subsp jonggjibkimchii strain DRC1506, and strain HM5 showed the highest homology with *Bacillus subtilis* strain IAM 12118. These cyanide-degrading bacterial isolates clustered with members of the genera *Pseudomonas, Alcaligenes, Leuconostic*, and *Bacillus* (as shown in Fig. 1).

3.1. SEM of Bio-carriers of calcium Alginate and immobilized Bacterial Consortium

Plate 1 depicts scanning electron microscope (SEM) photomicrographs of calcium alginate that have not been subjected to the attachment of cyanide-degrading bacterial cells. Plate 2 displays a photomicrograph of a consortium of immobilized cells attached to the surface of the biocarrier, which is composed of calcium alginate.

3.2. Physicochemical Parameters of Cassava Wastewater Analysis after 12 Days Treatment

Table 4 presents the physicochemical parameters of the Cassava Mill Effluent (CME) before and after undergoing treatment. Both Free Bacterial Cells (FBC) and Immobilized Cell Consortium (ICC) treatments resulted in a significant reduction in all physicochemical parameters. The analysis of variance revealed that the ICC treatment had the greatest impact on the treatment compared to the control set-up. Conversely, FBC-treated wastewater exhibited minimal removal of heavy metals, whereas immobilized cells demonstrated effective remediation results for heavy metals. Analysis of variance revealed significant differences among the three treatments, with significant differences observed in Pb^{2+} (0.06 ± 0.37 mg/L), Cr^{6+} (00.00 mg/L), and Ni^{2+} (0.02 ± 0.01 mg/L) when compared to the control and FEPA limit. Both treatments were unable to reduce Cu^{2+} to the FEPA limit value specified in Table 5.0.

Table 2. Physicochemical and Bacteriological Characteristics of the Wastewater from Cassava Processing Factories in Ilorin Metropolis

Parameters	A	B	C	D	FEPA (mg/l).	C. S	5.9[a]	5.7[a]	5.8[a]	6.0[a]
						WW	2.4[a]	2.7[a]	2.3[a]	2.3[a]
PH	4.00 ± 0.03 [a]	4.02 ± 0.00 [a]	4.01 ± 0.57 [a]	4.00 ± 0.00 [a]	6-9					
EC(us/cm)	2555 ± 7.07[ab]	2394 ± 5.66[b]	2618 ± 3.54 [a]	2586 ± 1.41 [ab]	1000					
BOD (mg/l)	1107 ± 3.54[b]	1219 ± 1.41 [a]	985 ± 2.12 c	1003 ± 071 c	50					
COD (mg/l)	1556 ± 2.83[b]	1667 ± 2.83 [a]	1577 ± 2.12 [b]	1602 ± 1041 [ab]	160					
TSS (mg/l)	3470 ± 3.54[bc]	3705 ± 2.12 [a]	3556 ± 2.12 [b]	3459 ± 5.66 [bc]	30					
TDS (mg/l)	2751 ± 3.54[b]	2812 ± 4024 [a]	2707 ± 5.66 [b]	2789 ± 1.41 [a]	2000					
PO_4 (mg/l)	106 ± 0.71[a]	97 ± 0.71 [a]	87.25 ± 0.35 [a]	118 ± 0.00 [a]	5.0					
NO_3(mg/l)	302 ± 1.45[a]	251 ± 0.71 [b]	287 ± 2.12 [ab]	311 ± 1.41 [a]	20					
Cyanide (mg/l)	25.00 ± 0.57[a]	28.74 ± 0.45 [a]	28.70 ± 0.00 [a]	27.11 ± 0.14 [a]	0.2					
C.S. (log CFU/g)	5.9 ± 0.00[a]	5.7 ± 0.00 [a]	5.8 ± 0.00[a]	6.0 ± 0.02[a]						
WW (log cfu/ml)	2.4 ± 0.00[a]	2.7 ± 0.05[a]	2.3 ± 0.00[a]	2.3 ± 0.00[a]						

Keys: A-Alagbado; B-Adeta; C- Pakata; D-Okelele.C.S- Contaminated soil; WW- Wastewater; EC-Electrical Conductivity; BOD-Biochemical Oxygen Demand;COD- Chemical Oxygen Demand; TSS-Total Suspended Solid; PO_4-Total Phosphate; NO_3-Total Nitrate; TDS-Total Dissolved Solid, CN^{-}- Cyanide contents.

Turkey's test, columns (with a sample size of n = 3) marked with distinct lowercase letters indicate statistically significant variations ($P < 0.05$) among the different treatments.

Table 3. Heavy Metal Concentrations of the Wastewater from Cassava Processing Factories in Ilorin Metropolis (mg/mL) (Mean ± SEM; n = 3).

Heavy metals	A	B	C	D	FEPA
Cr^{2+}	0.18 ± 0.00[a]	0.27 ± 0.00a	0.00 ± 0.00a	0.16 ± 0.00a	0.5
Pb^{2+}	0.54 ± 0.01b	1.15 ± 0.00a	0.67 ± 0.01b	0.83 ± 0.08b	0.5
Ni^{2+}	2.89 ± 0.03a	2.05 ± 0.07b	1.86 ± 0.01bc	2.10 ± 0.00b	1.0
CU^{2+}	12.39 ± 0.04a	10.48 ± 0.03b	10.00 ± 0.00b	11.89 ± 0.02a	1.5

Keys : Pb^{2+}-Lead ion, Cr^{6+}-Chromium ion, Ni^{2+}- Nickel ion Cu^{2+}- Copper ion

Alagbado; **B-**Adeta; **C**-Pakata; **D**-Okelele.

* Turkey's test, columns (with a sample size of n = 3) marked with distinct lowercase letters indicate statistically significant variations ($P < 0.05$) among the different treatments.

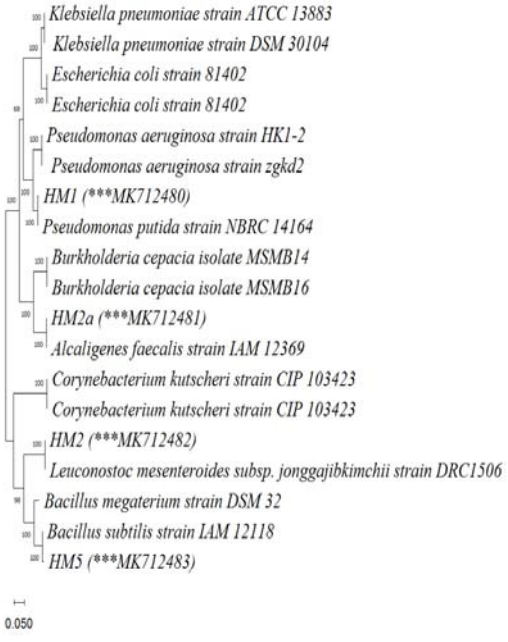

Figure 1. The phylogenetic tree of cyanide-degrading bacterial isolates. The numbers in parenthesis and asterisks indicate the GenBank accession numbers.

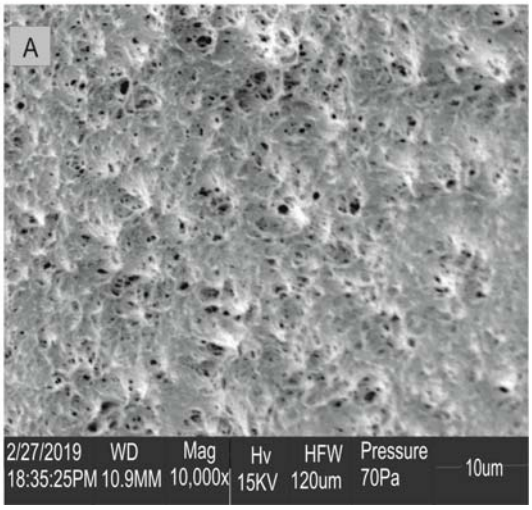

Plate 1. Biocarrier-calcium alginate in SEM photomicrography without the cell consortium

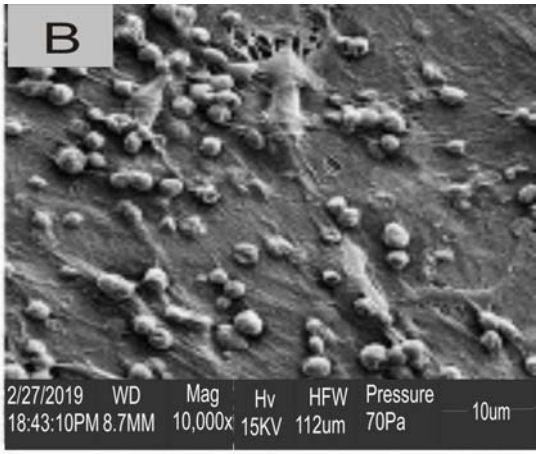

Plate 2. SEM photomicrograph of the immobilized cyanide-degrading bacterial cells consortium on the surface of the biocarrier of calcium alginate.

3.3. Pollution Reduction Efficiency (%) of FBC and ICC

The results depicted in Figure 2 demonstrated the effectiveness of the immobilized consortia (FBC and ICC) in reducing the levels of pollutants (physicochemical parameters) during the treatment process. The immobilized cells exhibited substantial removal efficiencies, as indicated by the high percentage removal values. The removal percentages for various parameters were higher for ICC compared to FBC. Specifically, for BOD5 and COD, ICC achieved removal percentages of 89.01% and 87.10%, while FBC achieved 71.10% and 67.10%, respectively. For NO_3 and TDS, ICC showed removal percentages of 68.00% and 59.60%, whereas FBC achieved 60.00% and 43.20%, respectively. In the case of PO_4 and cyanide concentrations, ICC demonstrated removal percentages of 70.00% and 84.25%, while FBC achieved 47.17% and 60.62%, respectively.

3.4. Heavy Metal Removal Efficiency (%) of Immobilized Cell Consortium and Free Bacteria Consortium

Table 4 summarizes the percentage efficiency of two treatment methods: immobilized cell consortium (ICC) and free bacterial cells (FBC), in addressing heavy metal contamination. Both treatments showed significant reductions in heavy metal concentrations. Specifically, for Pb^{2+} and Cr^{6+}, ICC achieved reductions of 56.60% and 88.68%, while FBC achieved 16.67% and 100%, respectively. For Ni^{2+} and Cu^{2+}, ICC demonstrated reductions of 62.37% and 99.65%, while FBC achieved 30.42% and 73.7%, respectively. These findings highlight the effectiveness of the immobilized cell consortium, particularly in reducing heavy metal concentrations, indicating its efficacy as a treatment process.

Table 4: Physiochemical Characteristics of the Treated Wastewater from Cassava Processing Factory (Means ± SD; n=3)

Treatment	pH	EC (mS/cm)	BOD (mg/l)	COD (mg/l)	TSS (mg/l)	PO_4 (mg/l)	NO_3 (mg/l)	TDS (mg/l)	CYANIDE (mg/l)
FBC	6.20±0.55^{ab}	2770±6.35^{ab}	310±2.9^{b}	510±1.87^{b}	1550±9.4^{b}	56±1.6^{b}	122±20^{b}	990±7.20^{b}	10±1.10^{b}
ICC	7.50±0.00^{a}	2830±12.8^{a}	120±2.1^{c}	200±1.00^{c}	1100±8.0^{c}	32±1.1^{c}	96±2.66^{c}	710±3.50^{c}	4±0.11^{c}
Control	4.40±0.0^{b}	24500±10^{b}	1000±3.4^{a}	1450±5^{ab}	3400±12^{a}	93±3.0^{ab}	290±2.1^{a}	2670±16^{a}	23.90±1.0^{a}
FEPA Limit	6-9	1000	50	160	30	5	20	2000	0.2

Turkey's test, columns (with a sample size of n = 3) marked with distinct lowercase letters indicate statistically significant variations ($P < 0.05$) among the different treatments.

BOD: Biochemical Oxygen Demand; FBC :Free Bacterial Consortium; COD: Chemical Oxygen Demand; TSS: Total Suspended Solid; ICC: Immobilized Cell Consortium; TDS: Total Dissolved Solids; CN^-:Cyanide, PO_4 :Phosphate; NO_3:Nitrate; EC: Electrical Conductivity and TSS:Total suspended solids; FEPA: Federal Environmental Protection Agency.

Table 5. Heavy Metals Concentration of the Treated Wastewater from Cassava Processing Factory (mg/L)

Treatment	Pb^{2+}	Cr^{6+}	N_i^{2+}	Cu^{2+}
FBC	0.22±0.01^{b}	0.15±0.01^{a}	1.40±0.57^{b}	8.58±0.04^{b}
ICC	0.06±0.37^{c}	0.0±0.00^{b}	0.02±0.01^{c}	3.24±0.01^{c}
Control	0.51±0.01^{a}	0.16±0.01^{a}	2.87±0.01^{a}	12.33±0.03^{a}
FEPA	0.5	0.5	1.0	1.5

Key :FBC – Free Bacterial Consortium, ICC – Immobilized Cell Consortium, Pb^{2+} - Lead ion, Zn^{2+} - Zinc ion, Cu^{2+} – Copper ion, Ni^{2+} – Nikel ion, Mn^{2+} – Manganese, Cr^{6+}– Chromium ion .

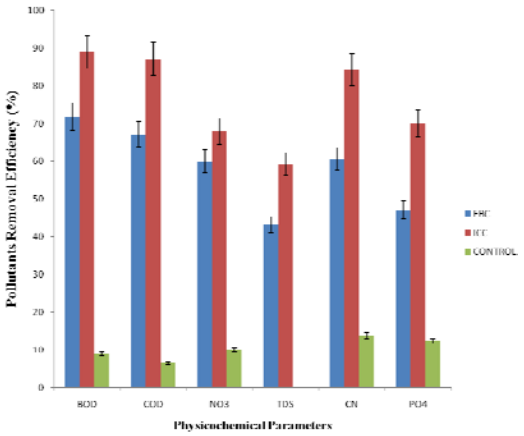

Figure 2. Pollutant Removal Efficiency (%) of FBC and ICC

Keys: FBC –Free Bacteria Consortium, ICC- Immobilized Cell Consortium, BOD-Biochemical Oxygen Demand, COD-Chemical Oxygen Demand, TSS-Total Suspended Solid, PO^{4-}Total Phosphate,NO^{3-}Total Nitrate, TDS-Total Dissolved Solid, CN^--Cyanide

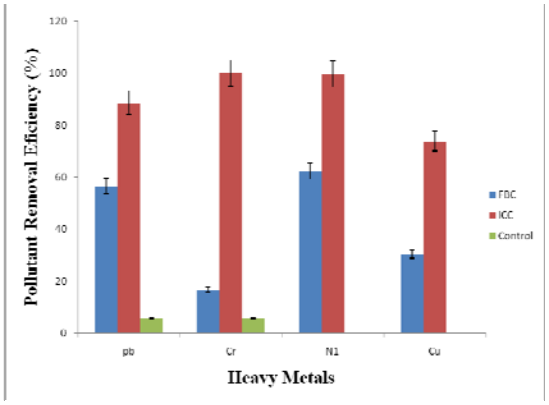

Figure 3.: Heavy Metal Removal Efficiency (%) of Free Bacteria Consortium and Immobilized Cell Consortium
Keys : Pb^{2+} -Lead ion, Cr^{6+} -Chromium ion, Ni^{2+} - Nickel ion Cu^{2+} -Copper ion

4. Discussion

The presence of cyanide, high values of the physicochemical parameters, the effluents' acidic pH, and the presence of heavy metals have earlier all been linked to their toxicity obtained in the current study (Izah, 2018). The pH of the cassava wastewater, which was in the range of 4.00 to 4.20, indicated the acidic nature of the cassava mill effluent (CME). This concurs with the findings of Uzochukwu *et al.* (2001), who noted comparable pH ranges. Nevertheless, aquatic life is reportedly impacted by pH levels between 3.5 and 4.5 (Adarsh and Mchantesh, 2006). Similarly, the mean values of EC, phosphate and TDS recorded in the CME exceeded the established regulatory limit.

The BOD5 and COD values derived from the cassava mill effluent (CME) exceeded the allowable threshold, with readings ranging from 985 to 1219 mg/l and 1556 to 1667 mg/l, respectively (Adewumi *et al*., 2006; Rum-Rukeh, 2016). Moreover, cyanide levels in the CME ranged from 25.00 to 28.74 mg/L, exceeding the allowable limit, as reported by Obueh and Odesiri-Eruteyan (2018). This result was in line with earlier research that showed cassava mill effluent to contain high levels of cyanide. (Okafor and Nwankwegu, 2016; Adewumi *et al*., 2016).

Furthermore, the soil polluted with the CME had high mean values of heavy metals, consistent with previous studies (Aiyegoro *et al*., 2007; Osakwe, 2012; Izah *et al*., 2017). The hazardous waste generated from cassava milling operations poses a significant risk to the environment, particularly soil and surface water, due to the presence of cyanide, high levels of physicochemical parameters, the acidic pH of the effluent, and the presence of heavy metals (Izah, 2018).

The primary sources of heavy metals in cassava mill effluent include agricultural machinery and appliances, soil biosorption, tool wear during harvesting and peeling, metal milling machine parts, and heavy metal contamination from water used in washing or processing. Heavy metal toxicity of this nature could potentially impact soil fertility and the population and diversity of soil biota (Ayansina and Olubukola, 2017). The bacterial strains designated as HM1, HM2a, HM2, and HM5 isolated in this study are closely related to *Pseudomonas putida, Enterococcus faecalis, Leuconostoc mesenteroides jonggajibkimchii,* and *Bacillus subtilis*, respectively, as determined by 16S rDNA sequencing and phylogenetic analysis (as shown in Figure 1). Those taxa showed 100 % similarity in their 16S rRNA-gene sequences to those of GenBank type species. The literature has described the cyanide-degrading ability of *P. putida* (Chatpawala *et al*., 1998; Kandasawy *et al*., 2015).Similarly, several other authors have also reported *Bacillus and Pseudomonas* in their study from cassava mill effluent (Obueh and Odesiri-Erunteyan, 2018: Enerijiofi *et al*., 2017).

The findings of this bioremediation study are consistent with the earlier studies (Ajao *et al*., 2011; Eneriviofi *et al*., 2017; Obueh and Odesiri-Erunteyan, 2018), despite differences in wastewater compositions. This investigation demonstrates the efficacy of both encapsulated and planktonic bacterial species in treating cyanide-laden wastewater, achieving substantial reductions in physicochemical parameters and heavy metal levels below regulatory thresholds. These findings represent an initial step in substantiating the practicality of this innovative approach. Notably, the immobilization of cells is a novel technique, previously unexplored in this context.

In both the free and immobilized treated wastewater, the pH of the cassava mill effluent increased from an initial value of 4.00 to 6.20 and 7.50, respectively; following 12 days of treatment, it fell within the permissible limit of 6-9 in both treatments as recommended for effluent to be discharged (FEPA, 1991). Several authors (Chuvudhary *et al*., 2011; Gaikwad *et al*., 2014; Izah *et al*., 2017) have reported comparable results.

Before treatment, the initial BOD5 and COD values were 985 mg/L and 1556 mg/L, respectively. After treatment with immobilized and free cells, these values decreased to 310 mg/L and 510 mg/L respectively; there was significant variation at $p<0.05$ among the treatments. The better performance recorded in immobilized cells could be attributed to the carriers' ability to impart cell potency, which results in high bioutilization effectiveness. This investigation confirmed the work of Enerjiofi *et al.* (2017) and (Sonune and Garode, 2015) who reported the remarkable decline in COD and BOD_5 in cassava wastewater and industrial wastewater treated with bacterial mixed culture. Several other authors also reported the reduction in BOD_5 and COD during bioremediation of wastewater (Gaikwad *et al*., 2014).

The TSS of the CME was 2751 mg/l before treatment, but subsequently decreased to 990 mg/L and 710 mg/L respectively when treated with planktonic cells and immobilized cells during the 12-day bioremediation process. There is no significant variation in both treatment except in control samples at $p<0.05$. Similarly, the initial value of Total Dissolve Solid was (3470 mg/L) prior to bioremediation, which was remarkably reduced to (1550 mg/L) when treated with free cells, while (1100 mg/L) was recorded when treated with the immobilized cells. This trend vis-à-vis the total dissolve solid corroborated with the report of (Okoduwa *et al*., 2017; Izah *et al*., 2017) who reported reduction in total dissolve solid in Tannery effluent and cassava mill effluent respectively during bioremediation.

The initial value of phosphate recorded was 106 mg/L prior to bioremediation process, which later declined to 56 mg/L and 32 mg/L, when treated with planktonic cells and

immobilized cells respectively. A statistically significant difference was observed in both treatments at a significance level of $p<0.05$. This study agrees the work of Ajao *et al*. (2011) who reported remarkable reduction in phosphate content of textile effluent treated with immobilized *Bacillus* sp and *Pseudomonas* spp. The final phosphate concentration obtained after bioremediation process was within the permissible limit of FEPA.

The initial cyanide concentration in the cassava mill effluent used in this study was 25 mg/l before the bioremediation process. After 12 days of treatment, it decreased to 10 mg/L when free cells were used and to 4 mg/L when immobilized cells were employed. There was a significant difference between the two treatments ($p>0.05$). The initial nitrate concentration was 302 mg/L, and it reduced to 122 mg/L when treated with free cells and 96 mg/L with immobilized cells after the 12-day treatment. Significant variation was observed among the treatments ($p>0.05$).

This reduction in nitrate is consistent with the findings of Sonune and Garode (2015), who demonstrated the ability of *B. licheniformis* to reduce nitrate in municipal wastewater ($p>0.05$).

The cyanide reduction in this study agrees with the work of Nwokoro and Dibua, (2014) who reported remarkable reduction in cyanide in soil contaminated with cassava effluent using *P. stutzeri* and *B. subtilis* (Sankararayana and Gowthami, 2015) reported cyanide degradation up to 98 % using microbial consortia.

Incidentally, Ahmed *et al*. (2005) and Gupta *et al*. (2017) reported that the bacterial cells evolve different mechanisms in the presence of high levels of heavy metals in their environment, which could help to eliminate heavy metals from polluted sites. The heavy metals detected in the cassava mill effluent prior to bioremediation were Pb^{2+}, Ni^{2+}, Cr^{6+}, and Cu^{2+} with the initial mean values of 0.54 mg/l, 2.89 mg/l, 0.18 mg/l and 12.39 mg/l respectively. The concentrations were declined to 0.22 mg/l, 1.40 mg/l, 0.15mg/l and 8.58 mg/l when treated with free cells, while the following results were obtained when treated with the immobilized cells (0.06 mg/l), (0.02mg/l), (0.00mg/l) and (3.24 mg/l) and the values were below the permissible limit (Abo-Amer *et al.*, 2015), In their recent study, it was confirmed that *Alcaligenes faecalis* isolated from wastewater has a co-resistance capability to Cd^{2+}, Pb^{2+}, Ag^{2+} and Al^{3+}.

Mechanisms of metal removal capability of the microbes have been proposed to include the following: Redox transformations, metal-binding peptide and protein production, solubilization through secretion of siderophores and other complexing agents. Cell walls and other structural components have substantial metal-binding capabilities, while precipitation may result from metabolite release such as sulfide, oxalate or reduction (Gadd, 2004).

The remarkable outcomes of this study are in line with most of the published articles regarding the bioremediation of CME by several authors (Enerjiofi *et al.*, 2017; Izah *et al*., 2018) though this is the first report on the bioremediation of CME using immobilized cyanide degrading bacterial cells for the removal of physicochemical parameters and heavy metals with unprecedented findings.

5. Conclusion

Despite the high levels of physicochemical parameters and heavy metal concentrations in the CME, the immobilized and free cells showed a remarkable reduction in physicochemical parameters and heavy metal concentrations, indicating a promising approach for utilizing biological treatments to mitigate the negative consequences of CME on the environment and human health. Further research and application of this technique could lead to significant progress in managing cassava mill effluent in Nigeria and other regions facing similar challenges.

References

Abo-Amer AE, El-Shanshoury AR and Alzahrani OM 2015. Isolation and molecular characterization of heavy metal-resistant *Alcaligenes faecalis* from sewage wastewater and synthesis of silver nanoparticles. *Geomicrobiol J*, **32**:836–845. https://doi.org/10.1080/01490451.2015.1010754

Adarsh S and Mahantesh B 2006. Personal Communication. Resident Doctors of Medicine. Hanagal Shree Kumareshwara Hospital, Bagalkot, Karnataka, India.

Adewumi, JR, Babatola JO and Olayanju OK 2016. The Impact of Cassava Wastewater from Starch Processing Industry on Surrounding Soil: A Case Study of Matna Foods Industry, Ogbese. *Fuoye J Eng Technol,* **1**(1). https://doi.org/10.46792/fuoyejet.v1i1.12

Afuye GG and Mogaji KO 2015. Effect of cassava effluents on domestic consumption of shallow well' water in Owo Local Government Area, Ondo State, Nigeria. *Phys Sci Res Int*, **3**(3): 37-43.

Agoro, M.A., Okoh, O.O., Adefisoye, M.A. and Okoh, A.I. (2018) Physicochemical Properties of Wastewater in Three Typical South African Sewage Works. *Pol. J. Environ. Stud*., 27: 2 491-499.

Ahmed N, Nawaz A and Badar U 2005 Screening of copper tolerant bacterial species and their potential to remove copper from the environment. *Bulletin Environ Contamination Toxicol*, **74**: 219– 226. https://doi.org/10.1007/s00128-004-0573-z

Aiyegoro OA, Akinpelu DA Igbinosa EO and Ogunmwonyi HI 2007 Effect of cassava effluent on the microbial population dynamic and physicochemical characteristic on soil community. *Sci Focus*, **12**: 98-101.

Ajao AT, Adebayo GB and Yakubu SE 2011 Bioremediation of textile industrial effluent using mixed culture of *Pseudomonas aeruginosa* and *Bacillus subtilis* immobilized on agar agar in a bioreactor. *J Microbiol Biotechnol Res.* (3): 50-56.

Akinpelu EA, Amodu OS Mpongwana N Ntwampe SKO and Ojumu TV 2015 Utilization of *Proteus vulgaris* Agrowaste in Biodegradation of Cyanide. Contam. Wastewater. *Biotechnol*., 59-75. https://doi.org/10.5772/59668

APHA 1998 **Standard methods for the examination of water and waste water**, 20th Edition. American Public Health Association.

Ayansina SA.and Olubukola OB 2017 Review A New Strategy for Heavy Metal Polluted Environments: A Review of Microbial Biosorbents. *Int J Environment Res Public Health*, **14**: 94. https://doi.org/10.3390/ijerph14010094

Bhutia MO, Thapa N and Tamang JP 2021 Molecular characterization of bacteria, detection of enterotoxin genes, and screening of antibiotic susceptibility patterns in traditionally processed meat products of Sikkim, India. *Frontiers Microbiol*, **11**: 599606. https://doi.org/10.3389/fmicb.2020.599606

Chatpawala KD, Babu GRV Vijaya OK Kumar KP and Wolfram JH 1998 Biodegradation of cyanides, cyanates and thiocyanates to ammonia and carbon dioxide by immobilized cells of *Pseudomonas putida*. *J Industrial Microbiol Biotechnol*, **20**:28-33. https://doi.org/10.1038/sj.jim.2900469

Chen B and Chen Z 2009 Sorption of naphthalene and 1-naphthol by biochars of orange peels with different pyrolytic temperatures. *Chemosphere,***76**(1):127-133. https://doi.org/10.1016/j.chemosphere.2009.02.004

ChenY, Liu Y Li Y Wu Y Chen Y Zeng G and Li H 2017 Influence of biochar on heavy metals and microbial community during composting of river sediment with agricultural wastes. *Biores Technol*, **243**: 347-355. https://doi.org/10.1016/j.biortech.2017.06.100

Chinyere CG, Iroha AE and Amadike UE 2013 Effect of altering palm oil and cassava mill effluents pH before dumping on dumpsite soils physicochemical parameters and selected enzyme activities. *J Biodivers Env Sci*, **3**(4): 46-58.

Choudhary R, Rawtani P and Vishwakarma M 2011 Comparative study of drinking water quality parameters of three manmade reservoirs i.e. Kolar, Kaliasote and Kerwa Dam. *Current World Env*, **6**(1): 145-149. https://doi.org/10.12944/cwe.6.1.21

Ebbs S 2004 Biological degradation of cyanide compounds. *Current Opinion Biotechnol*, **15**: 231-236. https://doi.org/10.1016/j.copbio.2004.03.006

Eboibi O, Akpokodje OI and Uguru H 2018 Bioremediation of soil contaminated with cassava effluent using organic soap solution. *J Env Sci, Toxicol Food Technol*, **12**(6 Ver. II): 2319-2399.

Eke-emezie N., Etuk, B. R., Akpan, O. P., & Chinweoke, O. C. 2022. Cyanide removal from cassava wastewater onto H_3PO4 activated periwinkle shell carbon. *Applied Water Science*, *12*(7): 157.Enerijiofi KE, Ekhaise FO and Ekomabasi IE 2017 Biodegradation Potentials of Cassava Mill Effluent (CME) by Indigenous Microorganisms. *J. Appl. Sci. Environ. Manage.*,**21**(6): 1029-1034. https://doi.org/10.4314/jasem.v21i6.5

Ezeigbo, O. R., Ike-Amadi, C. A., Okeke, U. P. and Ekaiko, M. U. (2014). The effect of cassava mill effluent on soil microorganisms in Aba, Nigeria. *International Journal of Current Res Biosci Plant Biol,* **1**(4): 21-26.

Fawole MO and Oso BA 2007 **Laboratory manual of Microbiology**, 5th Edition. Spectrum Books Limited.

FEPA (Federal Environmental Protection Agency) 1991 **Guidelines and standards for environmental pollution control in Nigeria**. 238 pp.

Gadd GM 2004 Microbial influence on metal mobility and application for bioremediation. *Geoderma,* **122**:109–119. https://doi.org/10.1016/j.geoderma.2004.01.002

Gaikwad GL, Wate SR Ramteke DS and Roychoudhury K 2014 Development of microbial consortia for the effective treatment of complex wastewater. *J Biorem Biodeg*, **5**(4): 227. https://doi.org/10.4172/2155-6199.1000227

Huertas MJ, Saez LP Roldan MD Luque-Almagro VM Martinez-Luque M Blasco R Moreno-Vivian C Castillo F and Garcia-Garcia I 2010. Alkaline cyanide degradation by *Pseudomonas pseudoalcaligenes* CECT5344 in a batch reactor: Influence of pH. *J Hazard Mat*, **179**: 72-78. https://doi.org/10.1016/j.jhazmat.2010.02.059

Ingvorsen K, Højer-Pedersen B and Godtfredsen SE 1991 Novel cyanide hydrolyzing enzyme from *Alcaligenes xylosoxidanssubsp. denitrificans*. *App Env Microbiol*, **57**:1783-1789. https://doi.org/10.1128/aem.57.6.1783-1789.1991

Izah SC, Bassey SE and Ohimain EI 2017a Changes in the treatment of some physico-chemical properties of cassava mill effluents using *Saccharomyces cerevisiae*. *Toxicol*, **5**(4): 28. https://doi.org/10.3390/toxics5040028

Izah SC, Bassey SE and Ohimain EI 2017b Cyanide and macro-nutrients content of *Saccharomyces cerevisiae* biomass cultured in cassava mill effluents. *Int J Microbiol Biotechnol*, **2**(4): 176-180. https://doi.org/10.5376/mmr.2017.07.0003

Izah SC, Bassey SE and Ohimain EI 2017c Geo-accumulation index, enrichment factor and quantification of contamination of heavy metals in soil receiving cassava mill effluents in a rural community in the Niger Delta region of Nigeria. *Mol Soil Biol*, **8**(2): 7-20. https://doi.org/10.5376/msb.2017.08.0002

Izah SC, Bassey SE and Ohimain EI 2018 Impacts of cassava mill effluents in Nigeria. *J Plant Animal Ecol*, **1**(1):14-42. https://doi.org/10.14302/issn.2637-6075.jpae-17-1890

Izah SC 2018 Estimation of Potential Cassava Mill Effluents Discharged into Nigerian Environment. *Env Anal Ecol Stud*, **2**(5).

JacksonBA, Oladipo NO and Agaja MO 2013 Cassava: A potential crop for industrial raw material in Nigeria. *Int J Life Sci*, **3**(3): 105-112.

Kandasamy S, Dananjeyan B Krishnamurthy K and Benckiser G 2015 Aerobic cyanide degradation by bacterial isolates from cassava factory wastewater. *Brazilian J Microbiol*, **46**(3), 659-666.

https://doi.org/10.1590/s1517-838246320130516

Khashei S, Etemadifar Z and Rahmani HR 2018 Immobilization of *Pseudomonas putida P*T in resistant matrices to environmental stresses: A strategy for continuous removal of heavy metals under extreme conditions. *Ann Microbiol*, **68**(12): 931-942. https://doi.org/10.1007/s13213-018-1402-7

Luque-Almagro VM, Huertas MJ Martinez-Luque M Moreno-Vivia C Roldan MD Garcia-Gil L. J and Blasco R 2005 Bacterial degradation of cyanide and its metal complexes under alkaline conditions. *App Env Microbiol*, **71**: 940-947.

https://doi.org/10.1128/aem.71.2.940-947.2005

Nwokoro O and Uju DibuaME 2014 Degradation of soil cyanide by bacteria. *Arh Hig Rada Toksikol*,**65**: 113-119.

Obueh HO and Odesiri-Eruteyan EA 2016 Study on the effects of cassava processing wastes on the soil environment of a local cassava mill. *J Poll Effects Control*,**4**: 177. https://doi.org/10.4172/2375-4397.1000177

Okafor UC and Nwankwegu AS 2016 Effect of woodchips on bioremediation of crude oil-polluted soil. *Br. Microbiol. Res. J*., **15**(4): 1-7.

https://doi.org/10.9734/bmrj/2016/27027

Okoduwa SIR, Igiri B Udeh CB Edenta C and Gauje B 2017 Tannery effluent treatment by yeast species isolates from watermelon. *Toxics*, **5**:6. https://doi.org/10.3390/toxics5010006

Okunade DA and Adekalu KO 2014 Characterization of cassava-waste effluents contaminated soils in Ile-Ife, Nigeria. *European Int J Sci Technol*, **3**(4): 173-182.

Oljira T, Muleta D and Jida M 2018 Potential applications of some indigenous bacteria isolated from polluted areas in the treatment of brewery effluents. *Biotechnol Res Int*, 2018. https://doi.org/10.1155/2018/9745198

Olorunfemi DI and Lolodi O 2011 Effect of cassava processing effluents on antioxidant enzyme activities in *Allium cepa L. Biokemistri*, **23**(2): 49-61.

Oluwatosin AA, Omolara TA Oluwaseyi AF and Rapheal EO 2017 Bioefficiency of Indigenous Microbial Rhodanese in Clean-up of Cyanide Contaminated Stream in Modakeke, Ile-Ife, Osun State, Nigeria. *J. Bioremediat. Biodegrad.*, **8**: 390. https://doi.org/10.4172/2155-6199.1000390

Osakwe SA 2012 Effect of Cassava Processing Mill Effluent on Physical and Chemical Properties of Soils in Abraka and Environs, Delta State, Nigeria. *Chem Mat Res*, **2**(7): 27-40.

Park D, Lee DS and Kim YM 2008 Bioaugmentation of cyanidedegrading microorganisms in a full-scale cokes wastewater treatment facility. *Biores Technol*, **99**: 2092-2096. https://doi.org/10.1016/j.biortech.2007.03.027

Patrick UA, Egwuonwn N and Augustine OA 2011 Distribution of cyanide in a cassava-mill-effluent polluted eutric tropofluvent soils of Ohaji Area, South-eastern Nigeria. *J Soil Sci Env Manag*, **2**(2): 49-57.
https://doi.org/10.3923/rjes.2011.342.353

Rim-Rukeh J 2016 Biodegradability Assessment of Cassava Processing Mill Wastewater Effluent, Akpofure. *Agr Env Sci*, **16**(5): 946-951.

Sankaranarayanan A. and Gowthami 2015 Cyanide degradation by consortium of bacterial species isolated from sago industry effluent. *J Env Treatment Tech*, 3(1):41-4.

Sarkar J, Kazy SK Gupta A Dutta A Mohapatra B Roy A Bera P Mitra A and Sar P 2016 Biostimulation of indigenous microbial community for bioremediation of petroleum refinery sludge. *Front. Microbiol*., **7**(1407): 1-20.
https://doi.org/10.3389/fmicb.

Seteno KON, Ntwampe SKO and Santos AQB 2013 Potential of Agro-Waste extract as supplements for the continuous Bioremediation of free Cyanide contaminated Wastewater. *Int J Env Ecol Eng*, **7**: 7.

Sonune NA and Garode AM. 2015 Bioremediation potential of bacterial isolates for municipal wastewater treatment. *Curr World Env*, **10**(2):619-625.
https://doi.org/10.12944/cwe.10.2.27

Sonune NA and Garode AM. 2018 Isolation, characterization and identification of extracellular enzyme producer *Bacillus licheniformis* from municipal wastewater and evaluation of their biodegradability. *Biotechnol Res Inn*, **2**: 1-8.
https://doi.org/10.1016/j.biori.2018.03.001

Ugochukwu UC, Manning DA and Fialips CI 2014 Microbial degradation of crude oil hydrocarbons on organoclay minerals. *J. Environ. Manag.*, **144:**197-202.
https://doi.org/10.1016/j.jenvman.2014.06.002

Uzochukwu S, Oyede RA and Ayanda O 2001 Utilization of garri industry effluent. *Nigerian J Microbiol*, **15**:87-92.

JJBS

Volume 17, Number 3,September 2024
ISSN 1995-6673
Pages 423 – 433
https://doi.org/10.54319/jjbs/170304

Jordan Journal of Biological Sciences

The Anti-angiogenic Potential of Thiosemicarbazide Derivative of Captopril (8) in Breast Cancer Cell Lines

Baan. M. AL-Jasani[1,*], Hayder. B. Sahib [2] and Hiba. N. Al-Saad[3]

[1]Department of Pharmacology & Toxicology, College of Pharmacy, University of Basrah, Basrah, Iraq ; [1]College of pharmacy, The university of Mashreq, Baghdad,10021,Iraq, [2]Department of Pharmacology, College of Pharmacy, Al-Nahrain University, Baghdad, Iraq; [3] Department of Pharmaceutical Chemistry, Pharmacy College, University of Basrah, Basrah, Iraq

Received: July 14, 2023; Revised: October 1, 2023; Accepted: November 8, 2023

Abstract

Angiogenesis is essential for many tumours to grow and metastasise, including breast tumours. Captopril, an Angiotensin-Converting Enzyme inhibitor is known to have anti-angiogenic activity. Recently, novel derivatives of captopril that include thiosemicarbazide moiety have shown enhanced ACE inhibition activity compared to captopril. This study aimed to assess the anti-angiogenic activity of one of these derivatives designated as (8) in the Estrogen receptor-positive MCF-7, and the Estrogen-Progesterone receptor-negative AMJ13 breast cancer cells. The study included a microarray screening for 24 angiogenic factors, and genes were confirmed by RT-qPCR. Results demonstrated a stronger anti-angiogenic effect in the MCF-7 cells compared to those on AMJ13. In MCF7, the derivative caused a significant decrease in the pro-angiogenic bFGF mRNA, VEGF-A mRNA expression, thrombopoietin protein level, PECAM -1 (*CD*31) mRNA, G-CSF protein, and a significant increase in the anti-angiogenic factors MIG mRNA level, IL-13 protein level, PF-4 both protein and mRNA level. The derivative also significantly decreased TIMP-1 mRNA and IFN-γ protein levels, whereas in AMJ13, a significant increase in MIG protein expression (but not mRNA), a significant decrease in IL-β protein expression, as well as thrombopoietin and PECAM-1 mRNA were documented. This work has shown the thiosemicarbazide derivative of captopril (8) as a potential anti-angiogenic agent targeting multiple factors in the angiogenesis of breast cancer cells. This study has demonstrated derivative (8) as a very promising molecule to be further investigated in other modes of angiogenesis and types of cancer.

Keywords: Thiosemicarbazide Derivative of Captopril (8), MCF-7, AMJ13 Breast Cancer Cell Line, Angiogenesis, VEGF, bFGF, MIG, PF4.

1. Introduction

In 2020, the prevalence of breast cancer exceeded that of lung cancer among females globally (Sung et al., 2021). Even though there has been a decrease in the mortality rate (DeSantis et al., 2019)along with an increase in the relative five-year survival rates for invasive breast cancer patients(CO, 2015), challenges still exist, particularly cancer metastasis which continues to be at the lead of these challenges (Gupta and Massagué, 2006). Evidence describing the dependency of cancer growth and metastasis on angiogenesis is accumulating (Vinson et al., 2012;Madu et al., 2020).

Angiogenesis supplies oxygen and nutrients to growing cells, facilitating their metastasis (Bouquet et al., 2006; Sahib, 2022). The tumor is believed to launch this process by activating the angiogenic switch by shifting the balance between the pro-angiogenesis and anti-angiogenesis factors to the direction that serves the tumor progression (Hanahan and Folkman, 1996).

In breast cancer, this shift has been documented as overexpression or up-regulation of angiogenic inducers, particularly in vascular endothelial growth factor (VEGF) which correlated with the aggressiveness of the tumor(Relf et al., 1997). Moreover, breast cancer's increased risk of being invasive and more aggressive is associated with the increased expression of pro-angiogenic growth factors, including both the VEGF and bFGF (Hanahan and Folkman, 1996; Linderholm et al., 1999; George et al., 2001). The same is observed with the down-regulation of the angiogenic inhibitors(Volpert et al., 1997).

Hence, targeting the angiogenesis by systemic inhibitors, specifically those that inhibit VEGF in the management of metastatic cancer, is considered one of the standard modalities (Larkins et al., 2015;Tabernero et al., 2015). Few approaches have been extensively investigated, including VEGF, VEGFR monoclonal antibodies, and tyrosine kinase inhibitors; however, several challenges arose with the implication of these, most importantly the side effects and resistance(Madu et al., 2020).

Another approach that awaits to be fully elucidated is targeting factors affecting the up or downstream cellular signalling, such as the Renin-Angiotensin System (RAS)(Herr et al., 2008). RAS components are found to be involved in most carcinogenic processes, including angiogenesis, and metastasis (Ager et al., 2008;George et

* Corresponding author. e-mail: aljasanibaan@yahoo.com.

al., 2010;Pinter and Jain, 2017; Vinson et al., 2012;Wegman-Ostrosky et al., 2015).

Moreover, many studies have explored the anti-angiogenic potentials of angiotensin-converting enzyme inhibitors ACEi and angiotensin II type I receptor blockers ARBS in various types of cancer (Patel and Nakka, 2017; Kosaka et al., 2007).

Captopril, the first member of the ACEis was among those extensively investigated for its antiangiogenic effect. Studies attributed the antiangiogenic effects of captopril mainly to the inhibition of matrix metalloproteinase MMP-2 and MMP-9(Prontera et al., 1999;Williams et al.,2005;Volpert et al., 1996). As well as, to the reduction of VEGF (Napoleone et al., 2012;Cho et al., 2016).

Recently, Al-Saad*et al.* (2019) have synthesized novel derivatives of captopril, which integrate thiosemicarbazide moiety in an attempt to improve the ACE inhibition activity rationalizing their synthesis to the fact that these structures are versatile with a broad spectrum of activity including anti-inflammatory, antioxidants, antifungal and antibacterial (Al-Saad et al., 2019; Al-Saad et al., 2020). Higher anti-platelet (Al-Saad et al., 2019) and ACE inhibition activity (Al-Saad et al., 2020) over captopril were demonstrated by most of the derivatives, and the improvement was accredited to the thiosemicarbazide moiety that replaced the carboxylic acid group of captopril rather than thiol group (Al-Saad et al., 2019).

Recently thiosemicarbazide/ thiosemicarbazone and their derivatives attracted great interest in their biological activity against various types of cancers(Küçükgüzel and CoŦ, 2016;Dincel and Guzeldemirci, 2020). Concerning breast cancer, many derivatives have been synthesized and investigated displaying remarkable antitumor activity both on hormonal receptors positive (Malki et al., 2015) and hormonal receptors negative breast cancer cells(El Majzoub et al., 2019;Siwek et al., 2013;Yee et al., 2017;Sólimo et al., 2020, Afrasiabi et al., 2013;Bai et al., 2021).

Based on these studies and having in mind the implication of RAS in breast cancer and the fact that captopril possesses an antiangiogenic effect, it was postulated that thiosemicarbazide derivatives of captopril(Al-Saad et al., 2019;Al-Saad et al., 2020)might embrace the anti-angiogenesis activity of captopril and the anticancer effect of thiosemicarbazide creating potentially improved anti-proliferative, anti-angiogenic agents than their parent captopril and targeting multiple factors in carcinogenesis. This work sought to investigate one derivative in particular designated as derivative (8)(Al-Saad et al., 2019) (Figure 1.1) in the estrogen receptor-positive MCF-7 and the estrogen/ progesterone receptor negative AMJ13.The selection of this derivative is based on our previous work (unpublished data) that documented the highest anti-proliferative effect on both types of breast cancer cells.

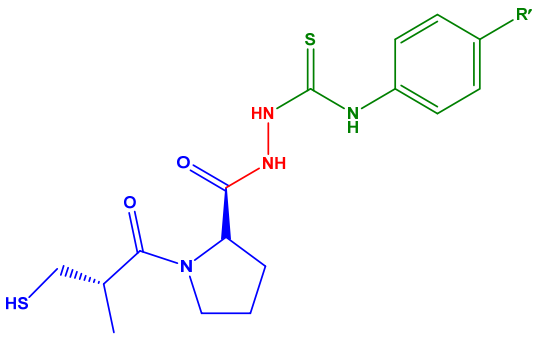

Thiosemicarbazide derivatives (5,7, &8)

Compound	R'
(5)	H
(7)	Cl
(8)	OCH_3

Figure (1.1): Chemical structure of Thiosemicarbazide Derivatives of Captopril (compounds 5, 7 and 8) (Al-Saad et al., 2019).

2. Materials and Methods

2.1. Chemicals and Cell Lines

The derivative was routinely synthesized and supplied by Dr. Hiba. Najeh. AL-Saad,Department of Pharmaceutical Chemistry, College of Pharmacy, Basrah University, Basrah, Iraq. The molecular weight of derivative (8) is 380.46 and is characterized as a highly pure compound with ^{1}HNMR analysis validation(supplementary materials)(Al-Saad et al., 2019). The compound demonstrated promising results concerning the safety profile with *in vivo*histological evidence (unpublished data)

Cell Bank Unit of Experimental Therapy Department, ICCMGR, AL- Mustansiriyah University,Baghdad, Iraq supplied the cells (MCF-7 and AMJ13). AMJ13 cells were grown in RPMI-1640 medium (Gibco/USA), whereas MCF-7 were grown in MEM (U.S Biological, USA). Both were supplied with (10%) fetal bovine serum (Bio West/ USA) and 1% of (Penicillin–Streptomycin) (Capricorn-Scientific, Germany) and Incubated at 37 C^0 and (5%) CO_2.

The concentration chosen for the following experiments is based on the IC50 of derivative (8) (from our unpublished data). MCF-7 cells were treated with (IC_{50}=88.06 µM), whereas AMJ13 was treated with (IC_{50}=66.82µM) of derivative (8) for 36 hours.

2.2. Microarray

A mouse angiogenesis G1 microarray glass chip (Ray Biotech.inc USA) was used for this analysis. All steps were done according to the manufacturer's instructions. In a simple illustration, the plate was incubated with Biotin-conjugated Anti-Cytokines that were preceded and followed by several washing cycles with washing buffers. Then in a dark room, incubation with Streptavidin-Fluor was commenced and was succeeded by another washing cycle until eventually washed with deionized water and left to dry. Data were analyzed by Labworks software (UVP, USA)(Al-Shammari et al., 2015).

2.3. Reverse Transcription – quantitative Polymerase Chain Reaction (RT-qPCR)

The procedures were conducted according to the manufacturer's instructions.GENEzol™ Reagent (Geneaid Biotech Ltd) was used to extract total RNA and was reverse transcribed into cDNA by using AccuPower® RocketScript™ Cycle RT PreMix (Bioneer/USA). The specificprimers (Angiogenic oligo ^{TM} primers / Korea)design was based on a published sequence bythe National Center for Biotechnology Information (NCBI).

Table (2.1): Angiogenicoligo ^{TM} primers / Korea

Primer	Forward	Reverse
VEGF-A	5'-CTTCAAGCCATCCTGTGTGC-3'	5'-TCTCTCCTATGTGCTGGCCT-3'
bFGF	5'-CTTCCCCAAGGATTTCAAGATGA-3'	5'-ATGTCTTCAAACCTATAAAACAGCA-'3
TIMP-1	5'-TTGTGGGACCTGTGGAAGTA-3'	5'-CTGTTGTTGCTGTGGCTGAT-3'
MIG	5'-CTGTTCCTGCATCAGCACCAAC-3'	5'-TGAACTCCATTCTTCAGTGTAGCA-3'
THPO	5'-CCAGAGGTTCACCCTTTGCCTA-3'	5'-CCAGAATGTCCTGTGCCTTGGT-3'
PF4	5'-TCCTGCCACTTGTGGTCGCCT-3'	5'-CCTTGATCACCTCCAGGCTGG-3'
CD31	5'-AAGTGGAGTCCAGCCGCATATC-3'	5'-ATGGAGCAGGACAGGTTCAGTC-3'
Hs-GAPDH	5-'GAGTCAACGGATTTGGTCGT-3'	5'- GACAAGCTTCCCGTTCTCAG-3'

Mx Pro Mx 3500 CYBER Green software/ Agilent/USA was used for qPCR by applying the following reaction: first cycle with 25 - 95° for two minutes, followed by 45 cycles with 95° for 15 seconds, 60° for 30 seconds and 72° for 30 seconds(Ridnour et al., 2012). Data were analyzed by relative quantitation delta delta Ct method ($2^{-\Delta\Delta Cq}$) where they were normalized to GAPDH as the housekeeping gene. The method is calculated based on relative quantitation approach which is the ratio between the RG (reference gene which in this case is GAPDH) and GOI (gene of interest) from the following formulas: ΔCt= average of GOI Ct – Average RG Ct

ΔΔCt= treated ΔCt – average control group ΔCt

2.4. Statistical analysis

GraphPad Prism®, version 9 was used to analyze the data. Unpaired t-test was used to compare between two groups with a significance of < 0.05, One – way ANOVA with Tukey's multiple comparison test was used to compare the means of more than two groups. All results in this work were presented as mean ± SD.

3. Results

3.1. Non-treated cells Microarray analysis

The normal protein signal intensity in each cell line was first established. Results demonstrated different protein expressions in each cell line. In the Estrogen-positive MCF-7 cells, the high signal intensity of bFGF and TIMP2 with low if no signal at all for the other factors was reported (Figure 3.1, A). On the other hand, the highly metastatic ER/PR receptor-negative breast cancer cell line AMJ13 has demonstrated strong expression of many angiogenic factors in particular VEGF and TIMP 1 and 2(Figure 3.1, B).

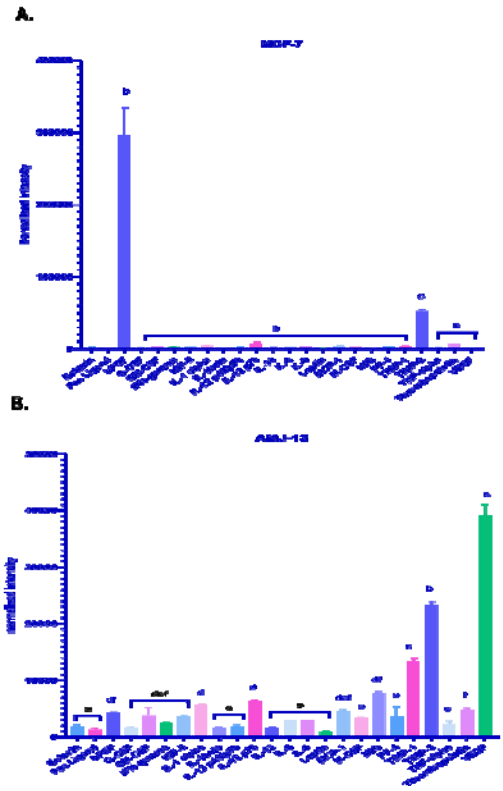

Figure (3.1): Normal signal intensity of 24 angiogenic factors in (A) Control (untreated) MCF-7 cell line. B) Control (untreated) AMJ13 cell line. The experiment was done once in two replicates.

3.2. Effect of Derivative (8) on MCF7 angiogenic factors (Microarray and RT-qPCR analysis)

Derivative (8) has imposed several alterations in the expression of many angiogenic factors. The derivative significantly decreased the protein levels of G-CSF (p-value 0.0472), IFN-gamma (p-value 0.0394), and Thrombopoietin (p-value 0.0213). In addition to that, the derivative significantly increased the protein level of the anti-angiogenic factor PF4 (p-value 0.0236) along with a significant increase in the pro and anti-inflammatory cytokines (IL-1 α and IL-13) (0.0394, 0.036 respectively) (Figure 3.2).

Reverse transcriptase–quantitative polymerase chain reaction (RT-qPCR) results showed a significant increase in PF4 (p-value 0.0169) and MIG mRNA (0.0118) (Figure 3.3 C, D). In addition to that, the derivative significantly and highly significantly decreased the most important contributors in the angiogenic process (VEGF-A, bFGF) mRNA (p-value 0.0119, 0.0008 respectively) (Figure 3.3. A, B) along with a significant decrease in TIMP-1 (p-value = 0.0283) and CD31mRNA level (p-value = 0.0109) (Figure 3.3.E, F). Derivative (8), however, insignificantly decreased Thrombopoietin (Figure 3.3. *G).*

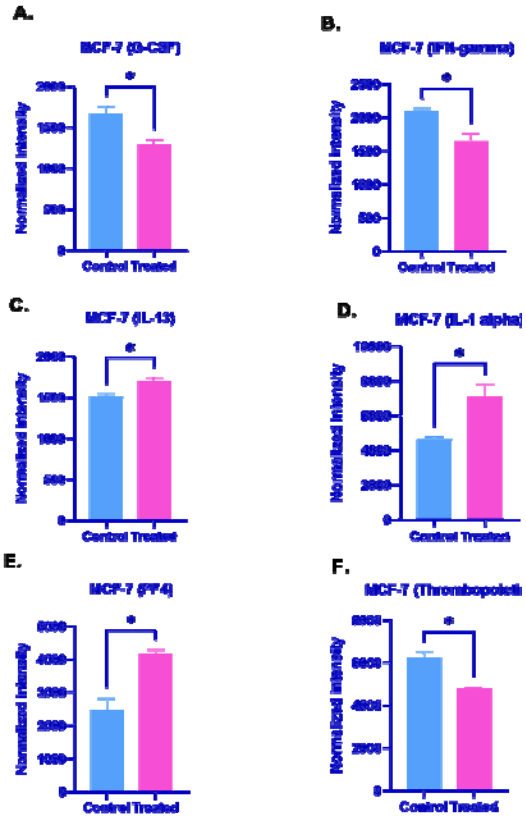

Figure (3.2): Microarray analysis of MCF-7 cell line demonstrating the significant effect of derivative (8) on various angiogenic factors. The cells were treated with (IC_{50}=88.06 µM) of captopril derivative (8) for 36 hours. The experiment was done once with two replicates. An unpaired t – testwas conducted on each angiogenic factor. All results are represented as mean ± SD.

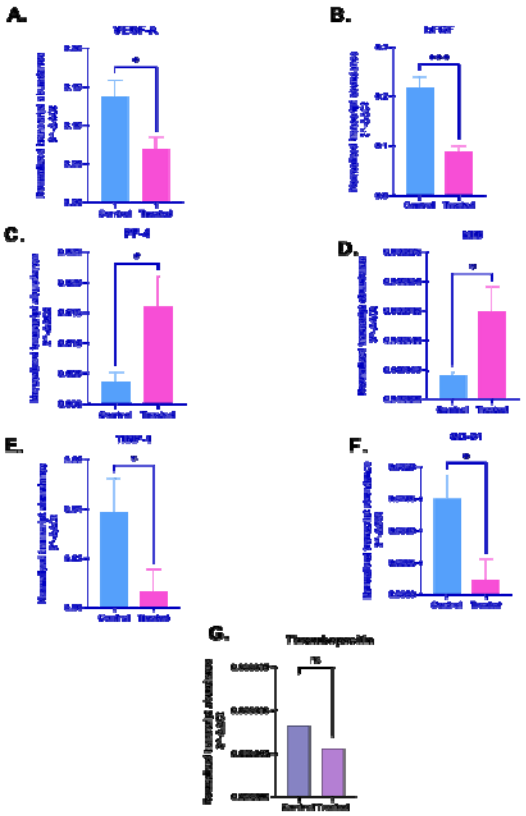

Figure (3.3): RT-qPCR analysis for seven-angiogenic gene expression in MCF-7 cell line after being treated for 36 hours with (IC_{50}= 88.06µM) of derivative (8). The experiment was conducted with three biological replicates for each GOI (control and treated) with duplicate Ct values and was normalized to GAPDH. All results represented here are mean ± SD.

3.3. 3.3 Effect of derivative (8) on AMJ13 angiogenic factors (Microarray and RT-qPCR analysis

The derivative did not cause significant changes in all of the angiogenic factors except a significant increase in MIG (p-value 0.0412), and a significant decrease in IL-1 β (p-value 0.0222) (Figure 3.4 a).

The RT-qPCR analysis for AMJ13 showed that the compound as in the microarray screening insignificantly decreased VEGF-A (Figure 3.4b/A), with an insignificant increase on bFGF, MIG, TIMP-1, (Figure 3.4b/B, D, E) and no significant effect on PF-4 (figure 3.4 b/C). The compound, however, significantly decreased thrombopoietin (p-value 0.0222) and PECAM-1 (p-value 0.0138) (Figure 3.4 b/ G, F)

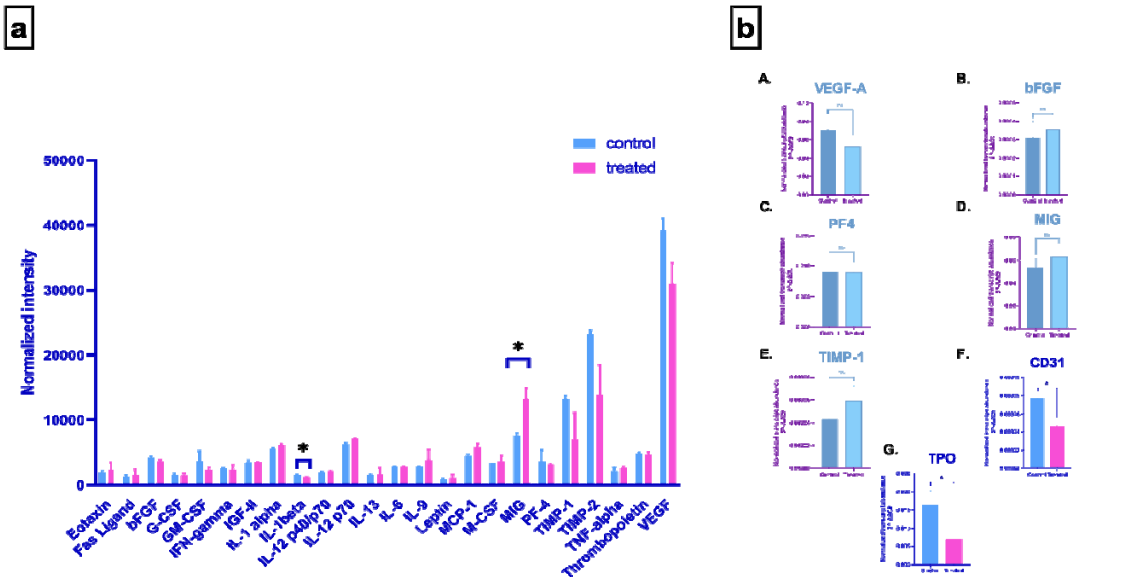

Figure (3.4): Assessment of the anti-angiogenic potential of derivative (8) in AMJ13 breast cancer cells. a) Microarray analysis of AMJ13 demonstrating the effect of compound (8) on various angiogenic factors after being treated with (IC_{50}=66.82µM) of derivative (8) for 36 hours. A significant effect was documented on IL-β and MIG. The experiment was done once with two replicates. An unpairedt–test was conducted on each angiogenic factor. b) RT-qPCR analysis for seven-angiogenic gene expression in AMJ13 cell line after being treated for 36 hours with (IC_{50}=66.82µM) of derivative (8). The experiment was conducted with three biological replicates for each GOI (control and treated) with duplicate Ct values. All results represented here are mean ± SD.

4. Discussion

Studies have proven angiogenesis as a crucial step for breast tumors to metastasize and acquire a more aggressive form (Relf et al., 1997). Thus, several approaches have been developed to target breast cancer angiogenesis. One of these approaches that awaits full elucidation is targeting the Renin-Angiotensin System (RAS) by the use of RAS blockers such as the ACE inhibitor captopril(Napoleone et al., 2012;Cho et al., 2016).

This study investigated the antiangiogenic activity of a thiosemicarbazide derivative of captopril termed derivative (8) in the estrogen receptor-positive MCF-7 and the estrogen/progesterone receptor-negative AMJ13 breast cancer cell lines.

The anti-angiogenesis activity of captopril derivative (8) was investigated based on two main reasons. First, the compound is a derivative of captopril that is known for its anti-angiogenic action in various types of cancer beyond the ACE activity(Hii et al., 1998;Napoleone et al., 2012;Nakagawa et al., 1995;Prontera et al., 1999;Volpert et al., 1996;Williams et al., 2005;Wang et al., 2008;Yoshiji et al., 2001).

Second,Tumour angiogenesis modulation is one of the major mechanisms proposed for RAS to induce the pro-tumour effect and most of its components have been implicated in angiogenesis*(Ager et al., 2008;George et al., 2010;Pinter and Jain, 2017;Vinson et al., 2012;Wegman-Ostrosky et al., 2015)*. Diverse human tumours demonstrated an association between VEGF, VEGFR expression as well as microvessel density with the expression of AT1R (Arrieta et al., 2015;Ino et al., 2006;Shirotake et al., 2011).

4.1 Effect of derivative (8) on angiogenic inducers (VEGF, bFGF, thrombopoietin and, PECAM-1, G-CSF, and IL-β)

Derivative (8) significantly decreased VEGFA mRNA expression in the MCF-7 cell line; if this result would be rationalized based on the fact that the compound is a derivative of captopril and might target RAS components, then it is consistent with many studies that documented the decrease in VEGFA expression in response to captopril. This decrease was observed in many types of cancer, such as triple-negative breast cancer(Napoleone et al., 2012), gastric cancer (Wang et al., 2008), and hepatocellular carcinoma (Yoshiji et al., 2002).

In addition to VEGFA, the compound exerted a stronger effect on the pro-angiogenic factor basic fibroblast growth factor. Various tumors have documented deregulated bFGFsignalling, including breast, lung, prostate, and colon cancer(Lieu et al., 2011).

This growth factor is a very powerful inducer of angiogenesis, where it induces the endothelial cells to invade and form capillary-like tubules with a potency twice that of VEGF(Pepper et al., 1992). Unlike VEGF, the factor was correlated with the angiogenesis maintenance rather than in its initiation (Compagni et al., 2000).

In addition to that, FGF induces angiogenesis synergistically with VEGF, an action that was believed to be achieved by up-regulating VEGF and VEGFR in the endothelial cells. However, each factor imposes a distinct effect on the vessel function and tumor survival(Giavazzi et al., 2003). Furthermore, FGF and FGFR are upregulated in response to anti-VEGF therapies as a resistance mechanism to these therapies(Casanovas et al., 2005); hence, targeting both growth factors and their kinases is a very tempting goal(Lieu et al., 2011).

In this study, Derivative (8) successfully and significantly decreased both growth factors, with a more potent effect on the bFGF, such an effect might decrease the likelihood of resistance rising as a potential future issue.

In addition to that, Captopril derivative (8) also significantly decreased the hematopoietic cytokine thrombopoietin. Hematopoietic cells are known to differentiate and mature to be megakaryocytes by the action of this cytokine, these cells will eventually become platelets(Lin et al., 2014).

It is thought that the platelets potentiate the tumor growth; meanwhile, the tumor hijacks some of the most important activities of the platelet, creating a feedback loop. One of the most important activities is potentiating angiogenesis through the release of their α – granules which are enriched with pro- and anti-angiogenic factors(Battinelli et al., 2014).

Perhaps the greatest proof of this relationship is the correlation between paraneoplastic thrombocytosis and the significant reduction in survival/ and or response that has been recorded in many types of solid tumours(Buergy et al., 2012). Among the many studies that displayed this correlation was that of Stone and colleagues (2012), where not only did they describe this correlation in recently diagnosed ovarian cancer women, but they also demonstrated that both IL-6 and thrombopoietin levels were higher in patients displaying thrombocytosis compared to those without. Moreover, they revealed a reduction in these two factors and restoration of normalized platelet count upon treatment with small interfering RNA(Stone et al., 2012).

In another study, silencing of the hepatic TPO gene in MMTV-PyMT mice significantly reduced TPO, platelet, PF4, and VEGF levels, as well as tumor growth and pulmonary metastasis(Shirai et al., 2019).

Interestingly, in this study, TPO level was decreased in both the estrogen receptor-positive MCF-7 cells, as well as the ER/PR receptor-negative AMJ13 cell lines. In addition to that, a closer look at the microarray results (supplementary materials) would demonstrate a decrease in IL-6 particularly in the MCF-7 cell line even though it is not a significant result; it does warrant further investigation.

Noteworthy, both ACE and RAS components were found to be implicated in the hematopoietic system evolution at the earliest stages, where hematopoietic potential was observed in ACE (+) cells of cultured chicken yolk embryo, while such observation was not detected in ACE(-) cells(Okwan-Duodu *et al.*, 2013).

Another platelet-related factor that has been affected by captopril derivative (8) is the platelet endothelial cell adhesion molecule – 1 (PECAM -1) or (CD31). The compound significantly decreased the mRNA level of this glycoprotein in both cell lines the MCF-7 and the AMJ13. It is worth mentioning that PECAM-1 is considered a reflection of the level of tumor angiogenesis, as well as the presence of tumor endothelial cells since both young and mature endothelial cells tend to express it on their surfaces(Feng et al., 2016).

Several studies have described a reduction in PECAM-1 level upon blocking AT1R, among which one displayed a reduction in tumor growth of the murine melanoma model by losartan. This was justified by the reduction in the mRNA level of both CD31 and VEGFR1 (Flt-1) rather than of VEGF itself(Otake et al., 2010). In another study, angiogenesis and proliferation of nasopharyngeal xenograft tumors were inhibited in response to apoptosis induced by valsartan and losartan; moreover, the AT1R blockers reduced the level of both VEGF and CD31(Lin et al., 2021).

Captopril derivative (8) also significantly reduced the protein level of Granulocyte- Colony Stimulating Factor (G-CSF). Even though this factor is a known mobilizer of hematopoietic progenitor stem cells, yet recently it was found to be implicated in tumour growth, angiogenesis, metastasis and resistance to chemotherapypromotion (Liu et al., 2020). In breast cancer, G-CSF expression was found to be upregulated, specifically in triple-negative breast cancer cells, where higher levels were detected than those in T47D and MCF-7 cells(Lee et al., 2013). It is worth mentioning that AngII has a Stimulatory effect on G-CSF(Jiang et al., 2013).

IL-1β is a pro-angiogenic cytokine that can stimulate angiogenesis(Fahey and Doyle, 2019). The cytokine was also found to be associated with chemoresistance to tamoxifen in TNBC(Jiménez-Garduño et al., 2017). In colorectal cancer, IL-1β release was stimulated by Ang II and its level was successfully decreased by ARBs [reviewed in(Asgharzadeh et al., 2020). Captopril and lisinopril also decreased the expression of IL-β as demonstrated by several studies in several cell types(Nemati et al., 2011;Miguel-Carrasco et al., 2010).

Microarray results displayed a significant increase in IL-1α protein level. Studies have demonstrated a promoted release of this cytokine by AngII(Zaidi and Research, Smith and Missailidis, 2004;George et al., 2010). It is difficult to explain this increment without further investigations, yet two hypotheses can be suggested. First, the derivative did display time-dependent ROS generation (unpublished data). Second, this change might be induced by the derivative independent action from RAS as a system or from the Ang II abrogated effect specifically.

4.2 Effect of captopril derivative (8) on angiogenic inhibitors (PF-4, MIG, TIMP-1, IL-13, and IFN-γ)

Platelet factor 4 is a very potent anti-angiogenic chemokine that was found to bind with VEGF and bFGF in a heparin and heparin – and heparin-independent manner(Teleanu et al., 2019;Belperio et al., 2000). It is suggested that PF4 mainly target microvasculature during angiogenesis owing to its selective binding to the endothelium of the active angiogenesis area only (Hansell et al., 1995). Moreover, high levels of the factor were detected in pre- metastatic stage of lung cancer that later decreased as the tumor progressed to metastasis. In addition to that, the factor inversely correlated with tumour grade and positively with survival(Jian et al., 2017).

In MCF-7 cells, derivative (8) significantly increased both the protein level, as well as the mRNA expression of PF4, with a concurrent decrease in both VEGFA and bFGF.

Another potent anti-angiogenic factor affected by compound (8) is the monokine induced by interferon-gamma (MIG) or (CXCL9). As the term designated, the soluble protein is released from the dendritic cells and macrophage located in the tumour microenvironment in response to interferon–gamma (IFN-γ) (Belperio et al., 2000;Rossi and Zlotnik, 2000).

The anti-angiogenic activity of this protein has been described by several studies; for instance, tumour growth and metastasis inhibition of NSCLC have been correlated with the overexpression of CXCL9 and justified by the decrease of vessel density (Addison et al., 2000). In addition to that, Th1–dependent immunity is promoted by CXCL9 through recruitment of T cells and NK that express CXCL9 receptor (CXCR3) (Groom et al., 2011).

Interestingly, derivative (8) exerted a significant increase in the mRNA level of MIG, but not the protein in MCF-7. This can be correlated with decreased IFN-gamma expression observed in the microarray results (supplementary materials). This might be attributed to the observation that ACE increase the release of the pro-inflammatory mediators independently from Ang II in ACE 10/10 (overexpress ACE) mice compared to ACE KO mice (ACE knock out)(Okwan-Duodu et al., 2013;Bernstein et al., 2018). Whatever the cause might be, it does warrant further investigation.

On the other hand, in AMJ13 cells the derivative increased the MIG protein level, but not the mRNA with no apparent effect on IFN-gamma.

IFN-γ anti- tumour immune response is well documented; however, recent studies have displayed paradoxical effects of this factor promoting tumour genesis. This effect was specifically recognized in the equilibrium and escape phases of the tumor immunoediting paradigm [reviewed in (Zaidi and Research, 2019).The cytokine can be either a pro-apoptotic or proliferative inducer in human lymphocytes depending on the expression of IFN-γR2, where IFN-γ stimulated proliferation and inhibited apoptosis in cells expressing low levels of IFN-γR2. Contrary to that, the pro-apoptotic effect of IFN-γ was seen in cells expressing high levels of IFN-γR2(Bernabei et al., 2001). Studies displayed the involvement of this pro-inflammatory mediator in the suppression of T cells and NK cell activity. This suppression is exerted through the activation and induction of immune checkpoint genes particularly PD-L1 and 2 expressed on the tumour cells as well as due to stimulation of binding to their immune inhibitory receptors PD-1(Abiko et al., 2015;Bellucci et al., 2015;Sharma et al., 2017).

Noteworthy, immune checkpoint inhibitors (ICI) have been investigated by several studies to address this type of immune evasion and were found to act synergistically with anti-VEGF in various types of tumours(Yi et al., 2019).

In this work, it is suggested that compound (8) might exert potent anti-angiogenic action by affecting multiple factors including the most important angiogenesis contributors (VEGF and bFGF). Simultaneously, the derivative might minimize immune evasion by decreasing IFN-γ.

Another factor affected by compound (8) was the Tissue inhibitor of matrix metalloproteinase – 1. TIMP-1 has been known to exert its anti-angiogenic activity by inhibiting MMPs proteolytic activities; however, recent studies have shifted the attention to the complicated roles of TIMP-1 in carcinogenesis that is imposed independently from MMPs inhibition activity. Various types of cancers, including breast have been associated with high levels of TIMP-1; the factor was also correlated with both advanced-stage and fast-relapse tumors(Jackson et al., 2017). Moreover, immunostaining free of TIMP-1 was associated with an improved prognosis of positive node high-grade breast tumours(Kuvaja et al., 2005). Contrary, pre-treatment high serum level of TIMP-1 was associated with endocrine therapy poor response in hormonal-positive breast cancer patients(Lipton et al., 2008). In addition to that, an upregulation in VEGF has been observed in the MCF-7 cell line after being transfected with TIMP-1 cDNA (Yoshiji et al., 1998;Campochiaro et al., 2001). Recently, TIMP-1 has been found to be implicated in tumour cell proliferation through PECAM-1 modulation of the tumour microenvironment, where it is suggested that TIMP-1 might be released from the endothelium in response to PECAM-1 homophilic-dependent binding(Abraham et al., 2018).

In this work, derivative (8) significantly decreased TIMP-1, VEGFA, and PECAM-1 mRNA in the MCF-7 cell line. Noteworthy, AngII has been found to be involved in the regulation of TIMP-1 expression in various cell types (Chen et al., 2003).

Lastly, captopril derivative (8) significantly increased IL-13. It is believed that this anti-inflammatory pro-fibrotic cytokine induces an anti-angiogenic effect similar to those produced by the closely related IL-4, an effect that was attributed to signaling through JAK2/ STAT6(Nishimura et al., 2008).

This study has documented different anti-angiogenic effects of derivative (8) on breast cancer cell lines. As such raised an important question of whether these differences arise because of the distinct characteristics of each cell line, or because the derivative tends to behave differently based on the assumption of its versatility of targets that may or may not involve RAS components.

Without a doubt, the cells are both distinct from each other in their histological characteristics (Al-Shammari et al., 2015;Lee et al., 2015), as well as in RAS involvement. Differences in RAS regulation to angiogenesis have been documented between the two sub-types (hormonal positive and negative receptors)(Herr *et al.*, 2019). Moreover, it was revealed that both cell lines hormonal receptor-positive and receptor-negative express components of RAS(Chen et al., 2003;Herr et al., 2008), yet only in negative cells were the VEGF, HIF-2-α, and TIMP-1 gene expression increased in response to AngII stimulation, which was abolished by candesartan (Herr *et al*., 2008).

Interestingly, in this research derivative (8) exerted an action on the MCF-7 cell line that was likely more dependent on the inhibition of the AngII/ AT1R pathway. At the same time, a different effect was seen on the AMJ13 cell line.

Perhaps, the most essential issue to be mentioned here is the actual expression of RAS components in AMJ13 since, until this date and to our knowledge, no paper has investigated the presence of RAS components in the AMJ13 cell line. This limitation is in fact a very appealing area for future investigation. Examining the expression of RAS components in AMJ13 and exploring the effect of thiosemicarbazide derivatives on these components can provide robust information both on these cells as well as on captopril derivatives' potential mechanism of action.

5. Conclusion

Breast cancer angiogenesis continues to be one of the major challenges in the treatment of this disease as it fuels

the tumor to an invasive and more aggressive form. One of the approaches that recently attracted interest to tackle this challenge is targeting the Renin-Angiotensin System by the use of ACEinhibitors. This study investigated the antiangiogenic activity of a thiosemicarbazide derivative of the ACEi Captorpril. Results of this work have demonstrated the thiosemicarbazide derivative of captopril (8) as a very promising agent with high anti-angiogenic activity, especially in the Estrogen receptor-positive breast cancer cell line (MCF-7). The derivative decreased many vital pro-angiogenic factors specifically VEGF and bFGF, and increased several anti-angiogenic factors such as MIG and PF4.The derivative is a very promising leading molecule for the development of other derivatives. Further investigations will provide robust information on the action of this derivative, revealing potential targets and pathways involved in the regulation of breast cancer angiogenesis.

Funding

The work has been achieved without specific funding**.**

Data Availability Statement

Data is within the article and can be provided by the corresponding author upon reasonable request.

Acknowledgements

The authors acknowledge the support from the Department of Experimental Therapy, Iraqi Center for Cancer and Medical Genetic Research, Mustansiriyah University**.**

Conflict of Interests

The authors declare no conflict of interest**.**

References

ABIKO, K., MATSUMURA, N., HAMANISHI, J., HORIKAWA, N., MURAKAMI, R., YAMAGUCHI, K., YOSHIOKA, Y., BABA, T., KONISHI, I. & MANDAI, M., 2015. IFN-γ from lymphocytes induces PD-L1 expression and promotes progression of ovarian cancer. Br. J. Cancer,**112:** 1501-1509.

ABRAHAM, V., CAO, G., PARAMBATH, A., LAWAL, F., HANDUMRONGKUL, C., DEBS, R. & DELISSER, H. M., 2018. Involvement of TIMP-1 in PECAM-1-mediated tumor dissemination. Int. J. Oncol.,**53:** 488-502.

ADDISON, C. L., ARENBERG, D. A., MORRIS, S. B., XUE, Y.-Y., BURDICK, M. D., MULLIGAN, M. S., IANNETTONI, M. D. & STRIETER, R. M. J., 2000. The CXC chemokine, monokine induced by interferon-gamma, inhibits non-small cell lung carcinoma tumor growth and metastasis. Hum. Gene Ther.,**11:** 247-261.

AFRASIABI, Z., STOVALL, P., FINLEY, K., CHOUDHURY, A., BARNES, C., AHMAD, A., SARKAR, F., VYAS, A., PADHYE, S., 2013. Targeting triple negative breast cancer cells by N3-substituted 9, 10-phenanthrenequinone thiosemicarbazones and their metal complexes. spectro Spectrochim Acta A Mol Biomol Spectrosc SAA, **114:** 114-119.

AGER, E. I., NEO, J. & CHRISTOPHI, C., 2008. The renin–angiotensin system and malignancy. J. Carcinog.**29:** 1675-1684.

AL-SAAD, H. N., KUBBA, A. A., 2020. Evaluation of New Thiosemcarbazides Derived from Captopril as Angiotensin-Converting Enzyme Inhibitors with Docking Study, and Predicted-ADMET Analysis. Res J Pharm Technol.,**13:** 2733-2741.

AL-SAAD, H. N., MAHMOOD, A. A. R. & AL-BAYATI, R. I., 2019. Design, synthesis, docking study and antiplatelet evaluation of new thiosemicarbazide derivatives derived from captopril. Orient. J. Chem.**35:** 829.

AL-SHAMMARI, A. M., ALLAK, W. J. K., UMRAN, M., YASEEN, N. Y. & HUSSIEN, A., 2015. Angiogenesis factors associated with new breast cancer cell line AMJ13 cultured in vitro. *Advances in Breast Cancer Res.,***4:**100.

ARRIETA, O., VILLARREAL-GARZA, C., VIZCAÍNO, G., PINEDA, B., HERNÁNDEZ-PEDRO, N., GUEVARA-SALAZAR, P., WEGMAN-OSTROSKY, T., VILLANUEVA-RODRÍGUEZ, G.& GAMBOA-DOMÍNGUEZ, A., 2015. Association between AT1 and AT2 angiotensin II receptor expression with cell proliferation and angiogenesis in operable breast cancer. Tumour Biol., **36:** 5627-5634.

ASGHARZADEH, F., MOSTAFAPOUR, A., AMERIZADEH, F., AVAN, A., RAHMANI, F., SABBAGHZADEH, R., HASSANIAN, S. M., FAKHRAEI, M., FARSHBAF, A. & FERNS, G. A. 2020. Inhibition of angiotensin II type I pathway reduced tumor growth and ameliorates fibrosis/inflammation associated with colorectal cancer. doi: 10.20944/preprints202007.0508.v1

BAI, C., WU, S., REN, S., ZHU, M., LUO, G., XIANG, H., 2021. Synthesis and evaluation of novel thiosemicarbazone and semicarbazone analogs with both anti-proliferative and anti-metastatic activities against triple negative breast cancer Bioorg. Med. Chem.,**37:** 116107.

BATTINELLI, E. M., MARKENS, B. A., KULENTHIRARAJAN, R. A., MACHLUS, K. R., FLAUMENHAFT, R. & ITALIANO JR, J. E. J. B., 2014. Anticoagulation inhibits tumor cell–mediated release of platelet angiogenic proteins and diminishes platelet angiogenic response. Am. J. Hematol.,**123:** 101-112.

BELLUCCI, R., MARTIN, A., BOMMARITO, D., WANG, K., HANSEN, S. H., FREEMAN, G. J. & RITZ., 2015. Interferon-γ-induced activation of JAK1 and JAK2 suppresses tumor cell susceptibility to NK cells through upregulation of PD-L1 expression. *Oncoimmunology* **4,** e1008824.

BELPERIO, J. A., KEANE, M. P., ARENBERG, D. A., ADDISON, C. L., EHLERT, J. E., BURDICK, M. D.& STRIETER, R. M., 2000. CXC chemokines in angiogenesis. J. Leukoc. Biol,**68:** 1-8.

BERNABEI, P., COCCIA, E. M., RIGAMONTI, L., BOSTICARDO, M., FORNI, G., PESTKA, S., KRAUSE, C. D., BATTISTINI, A. & NOVELLI, F., 2001. Interferon-γ receptor 2 expression as the deciding factor in human T, B, and myeloid cell proliferation or death. J. Leukoc. Biol,**70:** 950-960.

BERNSTEIN, K. E., KHAN, Z., GIANI, J. F., CAO, D.-Y., BERNSTEIN, E. A. & SHEN, X. Z., 2018. Angiotensin-converting enzyme in innate and adaptive immunity. Nat. Rev. Nephrol." **14:** 325-336.

BOUQUET, C., LAMANDÉ, N., BRAND, M., GASC, J.-M., JULLIENNE, B., FAURE, G., GRISCELLI, F., OPOLON, P., CONNAULT, E. & PERRICAUDET, M., 2006. Suppression of angiogenesis, tumor growth, and metastasis by adenovirus-mediated gene transfer of human angiotensinogen. Mol. Ther.,**14:** 175-182.

BUERGY, D., WENZ, F., GRODEN, C. & BROCKMANN, M. A., 2012. Tumor–platelet interaction in solid tumors. Int. J. Cancer Res., **130:** 2747-2760.

CAMPOCHIARO, P. A., YAMADA, E., TOBE, T., YAMADA, H., OKAMOTO, N., ZACK, D., WERB, Z., SOLOWAY, P., 2001. TIMP-1 promotes VEGF-induced neovascularization in the retina. Histol. Histopathol., **16:** 87-97.

CASANOVAS, O., HICKLIN, D. J., BERGERS, G. & HANAHAN, D., 2005. Drug resistance by evasion of antiangiogenic targeting of VEGF signaling in late-stage pancreatic islet tumors. *Cancer cell*,**8:** 299-309.

CHEN, X., WANG, J., ZHOU, F., WANG, X. & FENG, Z., 2003. STAT proteins mediate angiotensin II–induced production of TIMP-1 in human proximal tubular epithelial cells. Kidney Int.,**64:** 459-467.

CHO, W. K., SHIN, S.-W., KIM, S.-Y., HONG, C.-W., CHOI, C., PARK, W. & NOH, J. M., 2016. Immunomodulatory effect of captopril and local irradiation on myeloid-derived suppressor cells. Radiat. Oncol. J.,**34:** 223.

American Cancer Society. Breast Cancer Facts & Figures 2015-2016. Atlanta: American Cancer Society, Inc. 2015.

COMPAGNI, A., WILGENBUS, P., IMPAGNATIELLO, M.-A., COTTEN, M. & CHRISTOFORI, G., 2000. Fibroblast growth factors are required for efficient tumor angiogenesis. Cancer Res.,**60:** 7163-7169.

DESANTIS, C. E., MA, J., GAUDET, M. M., NEWMAN, L. A., MILLER, K. D., GODING SAUER, A., JEMAL, A. & SIEGEL, R. L., 2019. Breast cancer statistics, 2019. CA: Cancer J. Clin.,**69:** 438-451.

DINCEL, E. D. & GUZELDEMIRCI, N. U., 2020. Synthesis and computer-aided drug design studies of novel thiosemicarbazide derivatives as potent and target-oriented anti-cancer agents. *Medicine,***9:** 305-13.

EL MAJZOUB, R., FAYYAD-KAZAN, M., NASR EL DINE, A., MAKKI, R., HAMADE, E., GRÉE, R., HACHEM, A., TALHOUK, R., FAYYAD-KAZAN, H., BADRAN, B., 2019. A thiosemicarbazone derivative induces triple negative breast cancer cell apoptosis: possible role of miRNA-125a-5p and miRNA-181a-5p. *Genes & genomics*, **41:** 1431-1443.

FAHEY, E. & DOYLE, S. L. 2019. IL-1 Family Cytokine Regulation of Vascular Permeability and Angiogenesis. Front. Immunol.,**10**.p.1426.

FENG, Y., CHEN, X. & ZHANG, X., 2016. Roles of PECAM-1 in cell function and disease progression. *Eur Rev Med Pharmacol Sci*, **20:** 4082-4088.

GEORGE, A. J., THOMAS, W. G. & HANNAN, R. D., 2010. The renin–angiotensin system and cancer: old dog, new tricks. Nat. Rev. Cancer",**10:** 745-759.

GEORGE, M. L., TUTTON, M. G., JANSSEN, F., ARNAOUT, A., ABULAFI, A. M., ECCLES, S. A. & SWIFT, R. I., 2001. Vegf-a, vegf-c, and vegf-d in colorectal cancer progression. *Neoplasia,* **3(5)**: pp. 420-427.

GIAVAZZI, R., SENNINO, B., COLTRINI, D., GAROFALO, A., DOSSI, R., RONCA, R., TOSATTI, M. P. M. & PRESTA, M., 2003. Distinct role of fibroblast growth factor-2 and vascular endothelial growth factor on tumor growth and angiogenesis. Am. J. Pathol. **162:** 1913-1926.

GROOM, J. R., LUSTER, A. D., 2011. CXCR3 ligands: redundant, collaborative and antagonistic functions. ICB,**89:** 207-215.

GUPTA, G. P. & MASSAGUÉ, J., 2006. Cancer metastasis: building a framework.*Cell*, **127:** 679-695.

HANAHAN, D. & FOLKMAN, J., 1996. Patterns and emerging mechanisms of the angiogenic switch during tumorigenesis.*Cell*, **86:** 353-364.

HANSELL, P., MAIONE, T. E., BORGSTROM, P., 1995. Selective binding of platelet factor 4 to regions of active angiogenesis in vivo. Am. J. Physiol. Heart Circ. Physiol.,**269:** H829-H836.

HERR, D., RODEWALD, M., FRASER, H., HACK, G., KONRAD, R., KREIENBERG, R. & WULFF, C. J. G. O. 2008. Potential role of renin–angiotensin-system for tumor angiogenesis in receptor negative breast cancer. Gynecol. Oncol., **109:** 418-425.

HERR, D., SAUER, C., HOLZHEU, I., SAUTER, R., JANNI, W., WÖCKEL, A. & WULFF, C. J. G. U. F. 2019. Role of renin-angiotensin-system in human breast cancer cells: is there a difference in regulation of angiogenesis between hormone-receptor positive and negative breast cancer cells? GebFra, **79:** 626-634.

HII, S., NICOL, D., GOTLEY, D., THOMPSON, L., GREEN, M. & JONSSON, J. J. B., 1998. Captopril inhibits tumour growth in a xenograft model of human renal cell carcinoma. Br. J. Cancer, **77:** 880-883.

INO, K., SHIBATA, K., KAJIYAMA, H., YAMAMOTO, E., NAGASAKA, T., NAWA, A., NOMURA, S. & KIKKAWA, F., 2006. Angiotensin II type 1 receptor expression in ovarian cancer and its correlation with tumour angiogenesis and patient survival. Br. J. Cancer,**94:** 552-560.

JACKSON, H. W., DEFAMIE, V., WATERHOUSE, P. & KHOKHA, R., 2017. TIMPs: versatile extracellular regulators in cancer. Nat. Rev. Cancer,**17:** 38-53.

JIAN, J., PANG, Y., YAN, H. H., MIN, Y., ACHYUT, B. R., HOLLANDER, M. C., LIN, P. C., LIANG, X. & YANG, L., 2017. Platelet factor 4 is produced by subsets of myeloid cells in premetastatic lung and inhibits tumor metastasis.*Oncotarget*, **8:** 27725.

JIANG, H.-M., WANG, H.-X., YANG, H., ZENG, X.-J., TANG, C.-S., DU, J. & LI, H.-H., 2013. Role for Granulocyte Colony Stimulating Factor in Angiotensin II–Induced Neutrophil Recruitment and Cardiac Fibrosis in Mice. Am. J. Hypertens. **26** 1224-1233.

JIMÉNEZ-GARDUÑO, A. M., MENDOZA-RODRÍGUEZ, M. G., URRUTIA-CABRERA, D., DOMÍNGUEZ-ROBLES, M. C., PÉREZ-YÉPEZ, E. A., AYALA-SUMUANO, J. T., MEZA, I., 2017. IL-1β induced methylation of the estrogen receptor ERα gene correlates with EMT and chemoresistance in breast cancer cells. Biochem. Biophys. Res. Commun., **490:** 780-785.

KOSAKA, T., MIYAJIMA, A., TAKAYAMA, E., KIKUCHI, E., NAKASHIMA, J., OHIGASHI, T., ASANO, T., SAKAMOTO, M., OKITA, H. & MURAI, M., 2007. Angiotensin II type 1 receptor antagonist as an angiogenic inhibitor in prostate cancer. *The Prostate*,**67:** 41-49.

KÜÇÜKGÜZEL, G. & COŦ, P., 2016. Macromolecular Drug Targets in Cancer Treatment and thiosemicarbazides as anticancer agents. *Anti-Cancer Agents Med. Chem.,***16:** 1288-1300.

KUVAJA, P., TALVENSAARI-MATTILA, A., PÄÄKKÖ, P. & TURPEENNIEMI-HUJANEN, T. 2005. The absence of immunoreactivity for tissue inhibitor of metalloproteinase-1 (TIMP-1), but not for TIMP-2, protein is associated with a favorable prognosis in aggressive breast carcinoma. *Oncology*,**68:** 196-203.

LARKINS, E., SCEPURA, B., BLUMENTHAL, G. M., BLOOMQUIST, E., TANG, S., BIABLE, M., KLUETZ, P., KEEGAN, P. & PAZDUR, R., 2015. US Food and drug administration approval summary: ramucirumab for the treatment of metastatic non-small cell lung cancer following disease progression on or after platinum-based chemotherapy. The Oncologist.**20:** 1320-1325.

LEE, A. V., OESTERREICH, S. & DAVIDSON, N. E., 2015. MCF-7 cells—changing the course of breast cancer research and care for 45 years. J. Natl. Cancer Inst, **107:** p.djv073.

LEE, C.-H., LIN, S.-H., CHANG, S.-F., CHANG, P.-Y., YANG, Z.-P. & LU, S.-C., 2013. Extracellular signal-regulated kinase 2 mediates the expression of granulocyte colony-stimulating factor in invasive cancer cells. Oncol. Rep. **30:** 419-424.

LIEU, C., HEYMACH, J., OVERMAN, M., TRAN, H. & KOPETZ, S., 2011. Beyond VEGF: Inhibition of the Fibroblast Growth Factor Pathway and AntiangiogenesisInhibition of the FGF Pathway and Antiangiogenic Therapy. Clin. Cancer Res.**17:** 6130-6139.

LIN, R. J., AFSHAR-KHARGHAN, V. & SCHAFER, A. I. J. B., 2014. Paraneoplastic thrombocytosis: the secrets of tumor self-promotion. Am. J. Hematol., **124:** 184-187.

LIN, Y. T., WANG, H. C., TSAI, M. H., SU, Y. Y., YANG, M. Y. & CHIEN, C. Y. J. C. 2021. Angiotensin II receptor blockers valsartan and losartan improve survival rate clinically and suppress tumor growth via apoptosis related to PI3K/AKT signaling in nasopharyngeal carcinoma. Cancer, **127:** 1606-1619.

LINDERHOLM, B., TAVELIN, B., GRANKVIST, K. & HENRIKSSON, R., 1999. Does vascular endothelial growth factor (VEGF) predict local relapse and survival in radiotherapy-treated node-negative breast cancer?. Br. J. Cancer", **81(4):** pp. 727-732.

LIPTON, A., LEITZEL, K., CHAUDRI-ROSS, H. A., EVANS, D. B., ALI, S. M., DEMERS, L., HAMER, P., BROWN-SHIMER, S., PIERCE, K. & GAUR, V., 2008. Serum TIMP-1 and response to the aromatase inhibitor letrozole versus tamoxifen in metastatic breast cancer. J. Clin. Oncol.**26:** 2653-2658.

LIU, L., LIU, Y., YAN, X., ZHOU, C. & XIONG, X., 2020. The role of granulocyte colony-stimulating factor in breast cancer development: a review. Mol. Med. Rep. **21:** 2019-2029.

MADU, C. O., WANG, S., MADU, C. O. & LU, Y. J., 2020. Angiogenesis in breast cancer progression, diagnosis, and treatment. J. Cancer, **11:** 4474.

MALKI, A., ELBAYAA, R. Y., ASHOUR, H. M., LOFFREDO, C. A., YOUSSEF, A. M., 2015. Novel thiosemicarbazides induced apoptosis in human MCF-7 breast cancer cells via JNK signaling. J. Enzyme Inhib. Med. Chem.,**30:** 786-795.

MIGUEL-CARRASCO, J. L., ZAMBRANO, S., BLANCA, A. J., MATE, A. & VÁZQUEZ, C. M., 2010. Captopril reduces cardiac inflammatory markers in spontaneously hypertensive rats by inactivation of NF-kB. J. Inflamm., **7:** 1-9.

NAKAGAWA, T., KUBOTA, T., KABUTO, M. & KODERA, T., 1995. Captopril inhibits glioma cell invasion in vitro: involvement of matrix metalloproteinases. Anticancer Res.,**15:** 1985-1989.

NAPOLEONE, E., CUTRONE, A., CUGINO, D., AMORE, C., DI SANTO, A., IACOVIELLO, L., DE GAETANO, G., DONATI, M. B. & LORENZET, R., 2012. Inhibition of the renin-angiotensin system downregulates tissue factor and vascular endothelial growth factor in human breast carcinoma cells. Thromb. Res., **129:** 736-742.

NEMATI, F., RAHBAR-ROSHANDEL, N., HOSSEINI, F., MAHMOUDIAN, M., SHAFIEI, M., 2011. Anti-inflammatory effects of anti-hypertensive agents: influence on interleukin-1β secretion by peripheral blood polymorphonuclear leukocytes from patients with essential hypertension. Clin. Exp. Hypertens.,**33:** 66-76.

NISHIMURA, Y., NITTO, T., INOUE, T. & NODE, K., 2008. IL-13 attenuates vascular tube formation via JAK2-STAT6 pathway. *Circulation J.*, **72:** 469-475.

OKWAN-DUODU, D., LANDRY, J., SHEN, X. Z., DIAZ, R., 2013. Angiotensin-converting enzyme and the tumor microenvironment: mechanisms beyond angiogenesis. Am. J. Physiol. Regul. Integr. Comp. Physiol.,**305:** R205-R215.

OTAKE, A. H., MATTAR, A. L., FREITAS, H. C., MACHADO, C. M. L., NONOGAKI, S., FUJIHARA, C. K., ZATZ, R., CHAMMAS, R., 2010. Inhibition of angiotensin II receptor 1 limits tumor-associated angiogenesis and attenuates growth of murine melanoma. Cancer Chemother. Pharmacol., **66:** 79-87.

PATEL, S. S. & NAKKA, S., 2017. Protective effect of perindopril on tumor progression and angiogenesis in animal model of breast cancer. Anti-Cancer Agents Med. Chem., **17:** 955-960.

PEPPER, M., FERRARA, N., ORCI, L., MONTESANO, R., 1992. Potent synergism between vascular endothelial growth factor and basic fibroblast growth factor in the induction of angiogenesis in vitro. Biochem. Biophys. Res. Commun., **189:** 824-831.

PINTER, M. & JAIN, R. K., 2017. Targeting the renin-angiotensin system to improve cancer treatment: Implications for immunotherapy. Sci. Transl. Med. **9**: eaan5616.

PRONTERA, C., MARIANI, B., ROSSI, C., POGGI, A. & ROTILIO, D., 1999. Inhibition of gelatinase A (MMP-2) by batimastat and captopril reduces tumor growth and lung metastases in mice bearing Lewis lung carcinoma. Int. J. Cancer, **81:** 761-766.

RELF, M., LEJEUNE, S., SCOTT, P. A., FOX, S., SMITH, K., LEEK, R., MOGHADDAM, A., WHITEHOUSE, R., BICKNELL, R. & HARRIS, A. L., 1997. Expression of the angiogenic factors vascular endothelial cell growth factor, acidic and basic fibroblast growth factor, tumor growth factor β-1, platelet-derived endothelial cell growth factor, placenta growth factor, and pleiotrophin in human primary breast cancer and its relation to angiogenesis. Cancer Res.**57:** 963-969.

RIDNOUR, L. A., BARASCH, K. M., WINDHAUSEN, A. N., DORSEY, T. H., LIZARDO, M. M., YFANTIS, H. G., LEE, D. H., SWITZER, C. H., CHENG, R. Y. & HEINECKE, J. L. 2012. Nitric oxide synthase and breast cancer: role of TIMP-1 in NO-mediated Akt activation.plos.org https://doi.org/10.1371/journal.pone.0044081.

ROSSI, D.& ZLOTNIK, A., 2000. The biology of chemokines and their receptors. Annu. Rev. Immunol.**18:** 217-242.

SAHIB, H. B., 2022. The Anti-Angiogenic and Anti-Proliferative Activity of Methyl Hydroxychalcone. Asian Pac J Cancer Prev, **23:** 2071-2077.

SHARMA, P., HU-LIESKOVAN, S., WARGO, J. A. & RIBAS, A. J. C. 2017. Primary, adaptive, and acquired resistance to cancer immunotherapy. *Cell*,**168:** 707-723.

SHIRAI, T., REVENKO, A. S., TIBBITTS, J., NGO, A. T., MITRUGNO, A., HEALY, L. D., JOHNSON, J., TUCKER, E. I., HINDS, M. T. & COUSSENS, L. M., 2019. Hepatic thrombopoietin gene silencing reduces platelet count and breast cancer progression in transgenic MMTV-PyMT mice. Blood Adv.,**3:** 3080-3091.

SHIROTAKE, S., MIYAJIMA, A., KOSAKA, T., TANAKA, N., MAEDA, T., KIKUCHI, E. & OYA, M., 2011. Angiotensin II type 1 receptor expression and microvessel density in human bladder cancer. *Urol*,**77:** 1009. e19-1009. e25.

SIWEK, A., STĄCZEK, P., WUJEC, M., BIELAWSKI, K., BIELAWSKA, A. & PANETH, P., 2013. Cytotoxic effect and molecular docking of 4-ethoxycarbonylmethyl-1-(piperidin-4-ylcarbonyl)-thiosemicarbazide—a novel topoisomerase II inhibitor. J. Mol. Model.**19:** 1319-1324.

SMITH, G. R. & MISSAILIDIS, S., 2004. Cancer, inflammation and the AT1 and AT2 receptors. J. Inflamm.**1:** 1-12.

SÓLIMO, A. M., SANTACRUZ, M. S., VANZULLI, S., COGGIOLA, O., DE KIER JOFFÉ, E. B., FINKIELSZTEIN, L. & CALLERO, M. A., 2020. Anti-metastatic action of an N4-aryl substituted thiosemicarbazone on advanced triple negative breast cancer. *Heliyon*,**6:** e05161.

STONE, R. L., NICK, A. M., MCNEISH, I. A., BALKWILL, F., HAN, H. D., BOTTSFORD-MILLER, J., RUPAIMOOLE, R., ARMAIZ-PENA, G. N., PECOT, C. V. & COWARD, J., 2012. Paraneoplastic thrombocytosis in ovarian cancer. NEJM.**366:** 610-618.

SUNG, H., FERLAY, J., SIEGEL, R. L., LAVERSANNE, M., SOERJOMATARAM, I., JEMAL, A. & BRAY, F., 2021. Global cancer statistics 2020: GLOBOCAN estimates of incidence and mortality worldwide for 36 cancers in 185 countries. CA Cancer J Clin,**71:** 209-249.

TABERNERO, J., YOSHINO, T., COHN, A. L., OBERMANNOVA, R., BODOKY, G., GARCIA-CARBONERO, R., CIULEANU, T.-E., PORTNOY, D. C., VAN CUTSEM, E. & GROTHEY, A., 2015. Ramucirumab versus placebo in combination with second-line FOLFIRI in patients with metastatic colorectal carcinoma that progressed during or after first-line therapy with bevacizumab, oxaliplatin, and a fluoropyrimidine (RAISE): a randomised, double-blind, multicentre, phase 3 study. Lancet Oncol.,**16:** 499-508.

TELEANU, R. I., CHIRCOV, C., GRUMEZESCU, A. M. & TELEANU, D. M., 2019. Tumor angiogenesis and anti-angiogenic strategies for cancer treatment. J. Clin. Med. **9:** 84.

VINSON, G. P., BARKER, S. & PUDDEFOOT, J. R., 2012. The renin–angiotensin system in the breast and breast cancer. Endocr. Relat. Cancer., **19:** R1-R19.

VOLPERT, O. V., DAMERON, K. M. & BOUCK, N., 1997. Sequential development of an angiogenic phenotype by human fibroblasts progressing to tumorigenicity.Oncogene,**14:** 1495-1502.

VOLPERT, O. V., WARD, W. F., LINGEN, M. W., CHESLER, L., SOLT, D. B., JOHNSON, M. D., MOLTENI, A., POLVERINI, P. J. & BOUCK, N. P., 1996. Captopril inhibits angiogenesis and slows the growth of experimental tumors in rats. J. Clin. Investig., **98:** 671-679.

WANG, L., CAI, S.-R., ZHANG, C.-H., HE, Y.-L., ZHAN, W.-H., WU, H. & PENG, J., 2008. Effects of angiotensin-converting enzyme inhibitors and angiotensin II type 1 receptor blockers on lymphangiogenesis of gastric cancer in a nude mouse model. Chin. Med. J.,**121:** 2167-2171.

WEGMAN-OSTROSKY, T., SOTO-REYES, E., VIDAL-MILLÁN, S. & SÁNCHEZ-CORONA, J., 2015. The renin-angiotensin system meets the hallmarks of cancer. J. renin-angiotensin-aldosterone syst.,**16:** 227-233.

WILLIAMS, R., PARSONS, S., MORRIS, T., ROWLANDS, B. & WATSON, S., 2005. Inhibition of matrix metalloproteinase activity and growth of gastric adenocarcinoma cells by an angiotensin converting enzyme inhibitor in in vitro and murine models. Eur J Surg Oncol., **31:** 1042-1050.

YEE, E. M., BRANDL, M. B., BLACK, D. S., VITTORIO, O., KUMAR, N. J. B. & LETTERS, M. C. 2017. Synthesis of isoflavene-thiosemicarbazone hybrids and evaluation of their anti-tumor activity. Bioorg. Med. Chem. Lett.,**27:** 2454-2458.

YI, M., JIAO, D., QIN, S., CHU, Q., WU, K. & LI, A., 2019. Synergistic effect of immune checkpoint blockade and anti-angiogenesis in cancer treatment. Mol. Cancer., **18:** 1-12.

YOSHIJI, H., HARRIS, S. R., RASO, E., GOMEZ, D. E., LINDSAY, C. K., SHIBUYA, M., SINHA, C. C. & THORGEIRSSON, U. P., 1998. Mammary carcinoma cells over-expressing tissue inhibitor of metalloproteinases-1show vascular endothelial growth factor expression. Int. J. Cancer., **75:** 81-87.

YOSHIJI, H., KURIYAMA, S., KAWATA, M., YOSHII, J., IKENAKA, Y., NOGUCHI, R., NAKATANI, T., TSUJINOUE, H. & FUKUI, H., 2001. The angiotensin-I-converting enzyme inhibitor perindopril suppresses tumor growth and angiogenesis: possible role of the vascular endothelial growth factor. Clin. Cancer Res., **7:** 1073-1078.

YOSHIJI, H., YOSHII, J., IKENAKA, Y., NOGUCHI, R., YANASE, K., TSUJINOUE, H., IMAZU, H. & FUKUI, H., 2002. Suppression of the renin-angiotensin system attenuates vascular endothelial growth factor-mediated tumor development and angiogenesis in murine hepatocellular carcinoma cells. Int. J. Oncol.,**20:** 1227-1231.

ZAIDI, M. R., 2019. The interferon-gamma paradox in cancer. J Interferon Cytokine Res., **39:** 30-38.

JJBS

Volume 17, Number 3, September 2024
ISSN 1995-6673
Pages 435 – 442
https://doi.org/10.54319/jjbs/170305

Jordan Journal of Biological Sciences

Grape Seed Extract Enhances Antioxidant Capacity and Attenuates the Ochratoxin A-Induced Genotoxicity and Oxidative Stress in Albino Rats

Shenouda M. Girgis[1, *], Mahrousa M. Hassanane[1], and Somaia A. Nada[2]

[1]Department of Cell Biology, Biotechnology Research Institute, National Research Centre, 33 ElBohouth St. (former El Tahrir St.) Dokki, Giza, P.O. 12622, Affiliation ID: 60014618, Egypt;[2]Department of Pharmacology, Medical Research Institute, National Research Centre, 33 ElBohouth St. (former El Tahrir St.) Dokki, Giza, P.O. 12622, Affiliation ID: 60014618, Egypt.

Received: July 2, 2023; Revised: September 26, 2023; Accepted: November 8, 2023

Abstract

Ochratoxin A (OTA) is highly toxic to animals and humans within mycotoxins. Some studies have reported that Grape Seed Extract (GSE) has a protective role on these toxicities. The aim of the present study is to determine the antioxidant effect of GSE against genotoxicity, and oxidative stress induced by OTA in albino rats. Forty mature Wistar albino male rats with similar body weight were randomly divided into four groups (10 rats each): 1- untreated control group, 2- OTA treated group (1.7 mg/Kg b w, i. p), 3- OTA + 75 mg/Kg b w GSE group, 4- OTA + 150 mg/Kg bw GSE group. Rats were treated for 15 days and at the end of experiments, liver and kidney tissue homogenate, as well bone marrow cells were prepared to determine the antioxidant capacity and ameliorate role of GSE on genotoxicity, DNA damage and oxidative stress was induced by OTA in albino rats. The results show that GSE could significantly improve genotoxicity and DNA damage induced by OTA. SOD and GSH-Px as antioxidant enzymes were increased, as well, MDA and NO as oxidative stress parameters were significantly decreased, and effectively alleviating the oxidative stress caused by OTA and enhance the antioxidant capacity. These results suggest that GSE has a protective effect against OTA induced genotoxicity, DNA damage and oxidative stress in rats through its antioxidant effect. Thus, clinical application of GSE as therapy should be considered to prevent and treat oxidative damage in cases of ochratoxicosis.

Keywords: Ochratoxin A (OTA), genotoxicity, DNA damage, oxidative stress, grape seed extract (GSE), antioxidant, liver; kidney, rats

1. Introduction

Ochratoxin A (OTA) is highly toxic to animals and humans within mycotoxins (Wang et al., 2016), and it is the most potent carcinogenic (Duarte et al., 2011; Malir et al., 2016). The mechanism of toxicity may be attributed to oxidative stress, inhibition of protein synthesis, interference of cell signal transduction and apoptosis (Zhang et al., 2022). Oxidative stress is an increase in oxidation as a result of imbalance between oxidation and antioxidant systems (Yoshikawa and Naito, 2002). Under oxidative stress, overproduction of malondialdehyde (MDA), genotoxicity and DNA damage, and on the other side, antioxidant enzymes activity: superoxide dismutase (SOD), glutathione peroxidase (GPx), reduced glutathione (GSH), and Glutathione reductase (GR)can be estimated (Eken, 2017; Kıran et al., 2023)

OTA exposure increases the production of reactive oxygen species (ROS) and consequently induces genetic damage in rats and mice, indicating that the genotoxic effect may be secondary to oxidative stress due to the formation of DNA-adducts as a result of ROS generation. OTA also induces single and double strand breaks (SSBs and DSBs), gene mutations, chromosomal aberration and DNA damage in mammals (Schrenk et al., 2020). It was found to induce micronucleus (MN) formation and hypodiploid (a measure of aneugenicity) and DNA damage in Chinese hamster. The association between oxidative DNA damage and OTA exposure suggests its involvement in aneugenicity and clastogenicity production (Ali et al., 2011). The methods that measure chromosome aberrations and DNA fragmentation indicate that OTA gives positive results such as single-strand DNA breaks in rat and mice kidney and liver (Mally *et al*., 2005 ; Schrenk *et al.,* 2020) and induces micronuclei in cells of different origins(Degen *et al*., 1997; Ali *et al*., 2014; Campra *et al.,* 2020).

Oxidative stress is one of the main mechanisms of OTA toxicity showing genotoxicity, hepatotoxicity, teratogenicity and carcinogenicity (Heussner and Bingle 2015; Zhang *et al*., 2022). Excessive oxidants accumulation exceeds the scavenging ability of the body, leading to a significant increase of MDA (lipid peroxidation) levels in various tissues, resulting in DNA

* Corresponding author. e-mail: shenoudag2009@hotmail.com.

** **Abbreviations:** OTA: Ochratoxin A; GSE: Grape seed extract; DNA: Deoxyribonucleic acid; SOD: Superoxide dismutase; GPx: glutathione peroxidase; GSH: Reduced glutathione; GR: Glutathione reductase; MDA: Malondialdehyde; NO: Nitric oxide; ROS: Reactive oxygen species; MN: Micronucleus; DTNB: 5, 5′-dithio-bis (2-nitrobenzoic acid); NaCl: Sodium chloride; KCl: Potassium chloride; TCA: Trichloroacetic acid; Mn PCE: Micronucleated polychromatic erythrocytes.

damage (Sharifi-Rad *et al*., 2020). If any amount of OTA enters the body, the antioxidant defense system is destroyed, leading to a significant increase in nitric oxide (NO) and malondialdehyde (MDA) levels (marker of lipid peroxidation) and a significant decrease in antioxidant enzymes: (SOD, GSH and GPx) levels. However, antioxidant supplementation may activate antioxidant enzymes (SOD and GSH-Px) in the liver and kidney, and decrease toxicity-induced oxidative damage in rats (Wang *et al.,* 2019)

Antioxidants are reported to prevent cells from genotoxicity and cytotoxicity induced by OTA (Ramyaa *et al*., 2014; Costa et al., 2016; Damiano *et al.,* 2020). Grape seed extract (GSE), a polyphenolic flavonoid, is an excellent antioxidant, and can protect the activities of various antioxidant enzymes and work as antioxidant enhancement. In the rat, GSE increased antioxidant enzymes (SOD, GSH and GPx) levels, decreased oxidative stress or lipid peroxidation parameters (NO and MDA) expression and enhanced antioxidant capacity (Chis *et al.,* 2009). As well, Taghizadeh et al. (2016) proved that the scavenging properties of GSE were clear in the lipid peroxidation inhibition by reducing the high levels of MDA (oxidative stress indicator) and increasing the antioxidant enzymes activity especially the GPx. Therefore, this study was designed to investigate the antioxidant effect of GSE on genotoxicity, DNA damage and oxidative stress induced by OTA in albino rats.

2. Materials and Methods

2.1. Animals

Adult albino male rats of Wistar strain weighing 180-220 g were obtained from animal house colony of the National Research Centre, Dokki, Giza, Egypt. They were kept for 1 week of adaptation under the hygienic conditions, controlled temperature and humidity and fed with well-balanced diet and water *ad libitum*. The experiments were carried out according to the National regulations on animal welfare and Institutional Animal Ethical Committee guidelines (IAEC) and conform the requirement of the ethics committee of the Institutional Animal Care and Use Committee (IACUC), approval no: 01122022587.

2.2. Experimental groups

Forty mature Wistar albino male rats with similar body weight were randomly divided into four groups (10 rats each): 1- untreated control group; 2- OTA (1.7 mg/Kg, i.p.) treated group; 3- OTA (1.7 mg/Kg bw, i.p.) + GSE (75 mg/kg bw, orally) treated group; and 4- OTA (1.7 mg/Kg bw, i.p.) + GSE (150 mg/kg bw, orally) treated group. Rats were treated for 15 days and at the end of experiments, blood, liver and kidney tissue, as well bone marrow cells were harvested to determine the antioxidant capacity and ameliorative role of GSE on genotoxicity and oxidative stress induced by OTA in the liver and kidney of albino rats.

2.3. Preparation of tissue homogenate

At the end of experiment, a piece of whole liver and kidney was taken freshly from each animal on ice and homogenized by blender in 20% cold saline for determination of oxidative stress parameters: malondialdehyde (MDA) level and nitric oxide (NO) activity, and antioxidant defense system: reduced glutathione (GSH), glutathione peroxidase (GPX), and the activity of superoxide dismutase (SOD) in liver and kidney homogenates.

2.4. Antioxidants and oxidative stress parameters assay

Reduced glutathione (GSH) was determined using the spectrophotometric/microplate reader assay method which involves oxidation of GSH by the sulfhydryl reagent 5, 5′-dithio-bis (2-nitrobenzoic acid) (DTNB) to form the yellow derivative 5′-thio-2-nitrobenzoic acid (TNB), measurable at 412 nm. The activity of GSH was expressed as µg/g tissue (Rahman *et al.,* 2006).

Spectrophotometric assay of superoxide dismutase (SOD) was applied. The assay was based on the SOD-mediated inhibition in the rate of nitroblue tetrazolium reduction to the blue formazan at alkaline pH. The optimized assay of SOD was performed in 50 mM glycine-Na OH buffer, pH 9.5, at 25 degrees C. The SOD concentration was determined from the V/v ratio of rates measured in the absence (V) or the presence (v) of SOD. One unit of SOD has been defined as the concentration that decrease the rate to 50% (V/v = 2) as described by (Nagi *et al.,* 1995). The activity of GPx in the serum and aliquots of the liver and kidney was assayed using the Glutathione Peroxidase Assay Kit by Cayman Chemical Company (Ann Arbor, MI, USA) according to the kit instruction.

MDA levels in the supernatant of the homogenates were determined using a spectrophotometric assay kit according to the manufacturer's instruction. The absorbance of the resultant pink product was measured at 534 nm according to (Ohkawa *et al.,* 1979). Tissue MDA levels were calculated as nmol MDA/g tissue. NO levels were determined using a specialized kit purchased from Assay Designs, Ann Arbor, MI, USA, according to manufacturer's instructions (Jablonska *et al.,* 2007). Results were expressed as µmol/g tissue.

2.5. Cytogenetic and DNA damage analysis

2.5.1. Chromosomal analysis in somatic cells

Rats were subjected to cytogenetic analysis from bone marrow cells (Preston et al., 1983). Briefly, rats were injected with Colchicine (0.05 mg/kg bw) for two and a half hours before sacrifice. Animals were sacrificed and femoral bone marrow cells were flushed with isotonic solution (0.9% NaCl). Hypotonic solution (0.56% KCl) was added to the cell pellet and incubated at 37°C for 30 minutes and the solution was fixed, slides were air dried and stained with 10% Giemsa stain for 20 minutes. 50 metaphases were studied per animal scoring different types of structural and numerical aberrations in bone marrow cells.

2.5.2. Micronucleus assay

Bone marrow slides were prepared according to the method described by Krishna and Hyashi (2000). The bone marrow were washed with 1ml of fetal calf serum and then smeared on clean slides. The slides were left to air dry and then fixed in methanol for 5 minutes, followed by staining in 5% Giemsa stain for 5 minutes then washed in distilled water and mounted. For each animal, 1000 polychromatic

erythrocytes (PCEs) were examined for the presence of micronuclei.

2.5.3. DNA fragmentation

Liver samples were collected immediately after sacrificing the animals. The tissues were lysed in 0.5 ml lysis buffer containing 10mM tris-HCL (PH.8), 1mM EDTA, 0.2 % triton X-100, centrifuged at 10000 rpm (Eppendorf) for 20 minutes at 4°C. The pellets were re-suspended in 0.5 ml of lysis buffer to the pellets (P) and supernatants (S). 1.5 ml of 10% Trichloroacetic acid (TCA) was added and incubated at 4°C for 10 minutes. The samples were centrifuged for 20 minutes at 10000 rpm (Eppendorf) at 4°C and the pellets were suspended in 750µl of 5 % TCA, followed by incubation at 100°C for 20 minutes. Subsequently, to each sample, 2 ml of diphenylamine (DPA) solution [200 mg DPA in 10 ml glacial acetic acid, 150µl of sulfuric acid and 60µlacetaldehyde] were added and incubated at room temperature for 24 hours (Gibb *et al.,* 1997). The proportion of fragmented DNA was calculated from absorbance reading at 600 nm using the formula:

% DNA fragmentation = [OD(S)/ OD(S) + OD (P)] X 100

Where: OD(S) optical density of supernatant; OD (P) optical density of pellet.

2.6. Statistical analysis

Results were represented as mean ± SE, and the data analysis was performed using SPSS 20.0 software. Statistical analysis was carried out using one way analysis of variance (ANOVA) followed by Student-Newman-Keuls multiple comparisons test. Differences between groups were considered significant at $P \leq 0.05$.

3. Results

In this study, the ameliorative effect of GSE on geno-, hepato-, and renal toxicity induced by OTA in albino rats was estimated by measuring oxidative stress parameters (MDA and NO levels) and antioxidant activity (GSH, GPX and SOD activities) as recorded in Materials and methods section and the results are presented in Table (4). In addition, genotoxicity (chromosomal aberration analysis, DNA damage and incidence of micronucleus) in albino Wistar male rats was determined. The results presented in Table (1) and Figure (1), revealed that OTA treatment induced a significant increase in chromosomal aberration especially in gap, fragment, deletions and breaks as well total structural aberration compared to control. In addition, OTA was found to induce aneugenic aberration where it caused numerical variation (5.80±0.37, 7.40±0.60 and 13.2±0.86^{d} vs. 0.40±0.24, 0.00±0.00 and 0.4±0.2^{a}, for hypo polyploidy, hyper polyploidy and total numerical aberration in OTA and control groups, respectively). However, GSE administration in combination with OTA, reduced significantly all types of these aberrations especially with high dose of GSE (150 mg/kg bw).

Table 1. Percentage of chromosomal aberrations in rat bone marrow cells after treatment with OTA and GSE.

	Structural aberrations							Numerical variations		
Treatment	Chromatid gap	Break	Fragments	Deletions	Endomitosis	End to end association	Total structural aberration	Hypo polyploidy	Hyper polyploidy	Total Numerical variations
Control	0.60±0.24	0.00±0.00	0.00±0.00	0.00±0.00	0.40±0.24	0.20±0.20	1.20±0.58^{a}	0.40±0.24	0.00±0.00	0.4±0.2^{a}
OTA	5.40±0.92	3.20 ±0.37	4.80 ±1.06	3.60 ±0.67	3.00 ±0.31	4.60 ±0.50	25.40 ±2.27^{d}	5.80 ±0.37	7.40 ± 0.60	13.2 ±0.86^{d}
GSE1 + OTA	3.40 ±0.50	3.20 ±0.20	3.40 ±0.40	4.80 ±0.20	2.20 ±0.37	2.80 ±0.20	19.80 ±0.48^{c}	2.20 ±0.58	3.20 ± 0.58	9.8 ±0.9^{c}
GSE2 + OTA	1.80 ±0.37	2.20 ±0.20	1.60 ±0.24	1.80 ±0.37	1.00 ±0.00	2.00 ±0.31	10.20 ±0.66^{b}	1.40 ±0.50	2.20 ± 0.66	3.6 ±1.2^{b}

Means with different small letters (a, b, c, d) are differ significantly($P \leq 0.05$).

GSE1 + OTA= 75 mg/kg bw GSE + OTA; GSE2+ OTA = 150 mg/kg bw GSE + OTA.

 © 2024 Jordan Journal of Biological Sciences. All rights reserved - Volume 17, Number 3

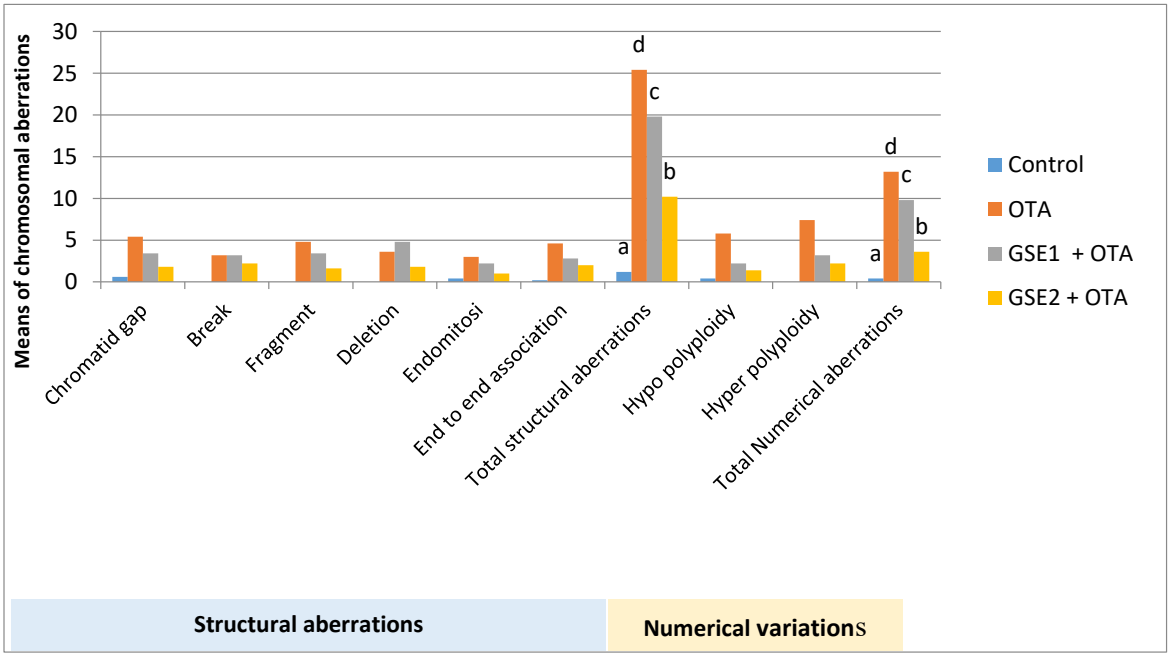

Figure 1. Comparison of chromosomal aberrations in rats after treatment with OTA and GSE.

Micronuclei (MN) frequency results (Table 2 and Figure 2) revealed that MN increased significantly in OTA group compared to control (18.20±2.48^{d} and 4.80±1.78^{a} for OTA and control groups, respectively). However, the treatment with GSE in combination with OTA, lowered significantly Mn frequency, especially in the treated group with high dose of GSE (150 mg/kg bw) compared to control, where it was found to be (12.40±1.51^{c} and 8.0±1.41^{b} and 4.80±1.78^{a} for GSE1+ OTA, GSE2+ OTA and control groups; respectively).

Table 2. Effect of OTA and GSE treatment on the incidence of micronucleated polychromatic erythrocytes (MnPCE) and the relation of PCE to NCE in rats.

Treatment	PCE Screened	Mn PCE / 1000 PCE		NCE scored	PCE / NCE	
		Number	Mean ±SD		Ratio	Mean ±SD
	1000	3		372	2.68	
	1000	5		376	2.65	
Control	1000	7		505	1.98	
	1000	6		543	1.84	
	1000	3	4.80±1.78^{a}	381	2.62	2.35±0.4^{a}
	1000	14		267	3.74	
	1000	19		134	7.46	
OTA	1000	20		149	6.71	
	1000	18		195	5.12	
	1000	20	18.20±2.48^{d}	223	4.48	5.50±1.54^{d}
	1000	13		074	13.51	
	1000	12		263	3.80	
GSE1 + OTA	1000	13		124	8.06	
	1000	14		126	7.93	
	1000	10	12.40±1.51^{c}	222	4.50	7.56±3.85^{c}
	1000	6		747	1.82	
	1000	8		742	1.34	
GSE2 + OTA	1000	10		7.73	1.26	
	1000	8		119	8.40	
	1000	8	8.0±1.41^{b}	651	1.53	2.87±3.09^{b}

Means with different small letters (a, b, c, d) are differ significantly(P≤0.05)

Mn PCE = micronucleated polychromatic erythrocytes; PCE=polychromatic erythrocytes; NCE= normochromatic erythrocytes. GSE1 + OTA= 75 mg/kg bw GSE + OTA; GSE2+ OTA = 150 mg/kg bw GSE + OTA.

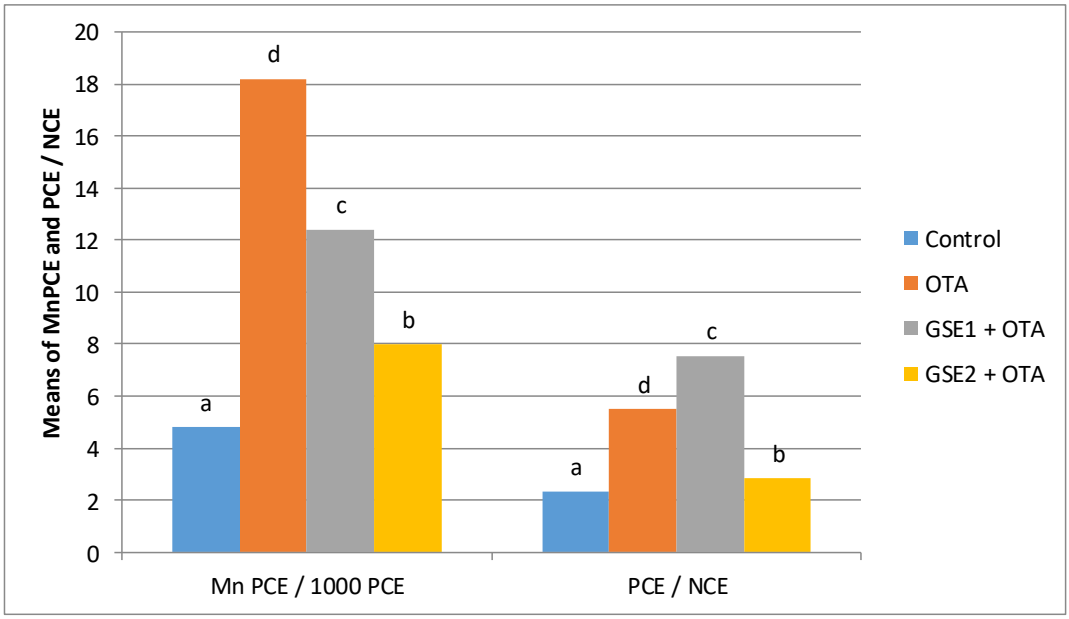

Figure 2. Incidence of micronucleated polychromatic erythrocytes (MnPCE) and the relation of PCE to NCE in rats treated with OTA and GSE.

DNA Fragmentation results (Table 3) revealed that DNA fragmentation frequency was increased significantly in OTA group compared to control (29.69 ± 0.48^{d} and 7.25 ± 0.60^{a} for OTA and control groups, respectively). However, the treatment with GSE in combination with OTA, lowered significantly DNA fragmentation frequency especially in the treated group with high dose of GSE (150 mg/kg bw) compared to OTA treated group (29.69 ± 0.48^{d}, 19.90 ± 0. 68^{c} and 10.86 ± 0.42^{b} for OTA, GSE1 and GSE2, respectively).

Table 3. Effect of OTA and GSE treatment on the incidence of DNA fragmentation in rats.

GSE1 + OTA= 75 mg/kg bw GSE + OTA; GSE2+ OTA = 150 mg/kg bw GSE + OTA

Treatment	% of DNA Fragmentation
	Mean ± SE
Control	7.25 ± 0.60^{a}
OTA	29.69 ± 0.48^{d}
GSE1 + OTA	19.90 ± 0.68^{c}
GSE2 + OTA	10.86 ± 0.42^{b}

Means with different small letters (a, b, c, d) are differ significantly(P≤0.05).

Table (4) and Figure (3), showing that administration of OTA reveals a significant decrease (P ≤ 0.05) in GSH enzyme activity (µg/ g tissue) compared to control group in both liver and kidney tissues (3.24± 0.051, 1.18 ±0.03 vs. 12.78±0.076; 4.85±0.02, for OTA and control group in both liver and kidney, respectively). However, Oral administration of GSE in combination with OTA, increased significantly (P ≤ 0.05) GSH level, especially in the treated group with high dose of GSE (150 mg/kg bw) in both liver and kidney tissue compared to OTA group (8.8±0.077, 2.51±0.02, 10.7±0.09, 4.00±0.02, and 3.24± 0.051, 1.18 ±0.03, for GSE1+OTA, GSE2+OTA and OTA groups in liver and kidney tissues, respectively).

Similarly, GPX concentration (mg/mg tissue) decreased significantly in OTA group compared to control group in both liver and kidney tissues (183.20±2.19, 150.50±0.91, and 269.40± 1.60, 232.12±1.55, for OTA and control groups in liver and kidney, respectively). However, Oral administration of GPX in combination with OTA, increased significantly (P ≤ 0.05) GPX level, especially in the treated group with high dose of GSE (150 mg/kg b w) in both liver and kidney tissues compared to OTA group (183.20±2.19, 150.50±0.91, 275.50±1.92, 221.30±1.52, 289.40±1.67, 249.80±1.17, for OTA, GSE1 and GSE2 groups in liver and kidney tissues, respectively).

There was also a significant inhibition in SOD activity in OTA group in both liver and kidney tissues (24.70± 1.10, 20.62±1.90 and 64.30± 1.94, 61.20± 1.55, respectively) compared to the control group. But, co-treatment with both doses of GSE (75 and 150 mg/kg bw.) leading to a significant increase in SOD level in both kidney and liver tissue compared to OTA group (41.80±1.22, 53.80±1.03, 58.30±1.62, 64.70±1.88, and 24.70±1.10, 20.62±1.90, for GSE1, GSE2 and OTA groups in liver and kidney tissues, respectively).

OTA significantly increased (P ≤ 0.05) MDA in both liver and kidney tissues (809.00±2.18, 973. 20±2.74, vs 250.30±2.13, 250.30±2.75, respectively) compared to control group. On the other oral administration with the 2 doses of GSE (75 and 150 mg/kg bw) groups in combination to OTA, a significant decrease in MDA in both kidney and liver tissues (481.70±1.95, 463.80± 2.42, and 332. 60± 1.78, 302.70±2.71 vs. 809.00±2.18. 973. 20±2.74, respectively) compared to OTA group was accomplished.

The results of NO show that OTA significantly increased (P ≤ 0.05) NO in both liver and kidney tissue (973.20± 2.74 and 114.70±2.15 vs. 250.30± 2.75 and 59.30±1.21, respectively) compared to control group. However, on the other groups treated with the 2 doses of GSE (75 and 150 mg/kg bw) in combination to OTA, a significant decrease in NO in both kidney and liver tissues

(463.80±2.42, 66.40±1.26 and 302.70±2.71, 50.30±1.19 vs. 973.20±2.74 and 114.70±2.15, respectively) compared to OTA group was revealed.

Table 4. Effect of Grape seed extract (75 and 150 mg/Kg bw GSE, POs) in concomitant with Ochratoxin A (OTA) (1.7 mg/Kg, i.p) on oxidative stress and antioxidant parameters in liver and kidney homogenates.

Parameters	GSH –Liver µg/ g tissue	GSH Kidney µg/ g tissue	GPX Liver mg/ mg tissue	GPX Kidney mg/ mg tissue	SOD Liver nmol/g tissue	SOD Kidney nmol/g tissue	MDA Liver nmol/g tissue	MDA Kidney nmol/g tissue	NO Liver µmol/g tissue	NO Kidney µmol/g tissue
Control	12,78±0,076^{a}	4,85±0,02^{a}	269,40±1,60^{a}	232,12±1,55^{a}	64,30±1,94^{a}	61,20±1,55^{a}	250,30±2,13^{a}	250,30±2,75^{a}	250,30±2,75^{a}	59,30±1,21^{a}
OTA	3,24±0,051^{b}	1,18±0,03^{b}	183,20±2,19^{b}	150,50±0,91^{b}	24,70±1,10^{b}	20,62±1,90^{b}	809,00±2,18^{b}	973,20±2,74^{b}	973,20±2,74^{b}	114,70±2,15^{b}
GSE1+OTA	8,8±0,077^{c}	2,51±0,02^{c}	275,50±1,92^{a}	221,30±1,52^{c}	41,80±1,22^{c}	53,80±1,03^{c}	481,70±1,95^{c}	463,80±2,42^{c}	463,80±2,42^{c}	66,40±1,26^{c}
GSE2+OTA	10,7±0,09^{d}	4,00±0,02^{d}	289,40±1,67^{d}	249,80±1,17^{d}	58,30±1,62^{d}	64,70±1,88^{a}	332,60±1,78^{d}	302,70±2,71^{d}	302,70±2,71^{d}	50,30±1,19^{d}

Results are expressed as mean ± SEM (n=8). Different capital letters are differ significantly at $p < 0.05$.GSE1 + OTA= 75 mg/kg bw GSE + OTA; GSE2+ OTA = 150 mg/kg bw GSE + OTA.

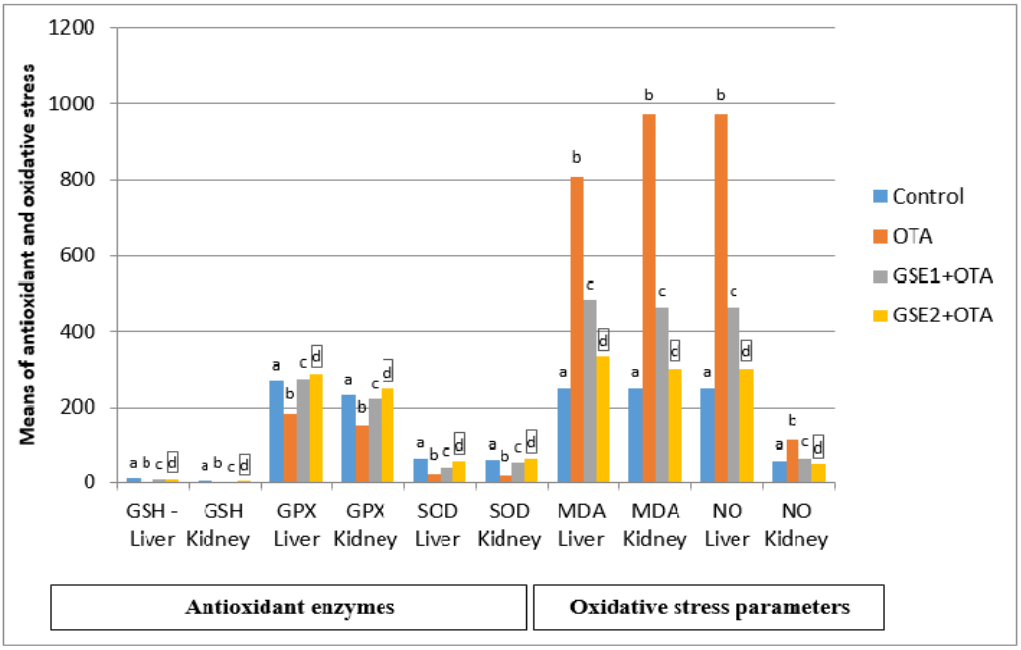

Figure 3. Effect of Grape seed extract (75 and 150 mg/Kg bw GSE) in concomitant with Ochratoxin A (OTA) on oxidative stress and antioxidant parameters in liver and kidney

4. Discussion

Induction of oxidative stress by OTA has a critical role in several kidney and liver toxicity, and many complications of these toxicities such as DNA and genetic damage are mediated by this oxidative stress (Ozbek, 2012; Gong *et al.,* 2019). However, the protective role of GSE on OTA-induced liver and kidney injury has not been reported. Therefore, this study was designed to investigate the antioxidant capacity and ameliorate role of GSE as antioxidant on ochratoxin A-induced genotoxicity and oxidative stress in adult albino male rats.

Oxidative stress and generation of reactive oxygen species (ROS), consequently induce genetic damage in rats, due to the formation of DNA-adducts (damage) as a result of ROS generation (Kamp *et al.,* 2005). OTA was reported to induce MN, hypopolyploidy, single and double strand breaks (SSBs and DSBs), gene mutations, deletions, chromosomal aberration and DNA damage leading to genotoxicity (Mally *et al*., 2005; Ali *et al*., 2011; Hibe *et al*., 2013; Schrenk *et al*., 2020). However, treatment with GSE antioxidant increased cell viability and decreased ROS level after OTA exposure (Schaaf *et al*., 2002), and this coincides with our results as presented in tables (1-3).

Our findings prove that GSE has improved all types of the chromosomal aberrations (structural and numerical) compared to OTA treated group, suggesting its ameliorative the genotoxic effect of OTA. Similar findings were obtained by Ramyaa *et al*. (2014); Costa *et al*. (2016) and Damiano *et al.* (2020), who proved that this extract possessed antimutagenic properties. In agreement with our results, Sorrenti *et al.* (2013) reported that GSE significantly ameliorated the DNA damage induced by OTA, as revealed by lowering of the occurrence of chromosomal aberrations, micronucleus and hepatic DNA fragmentation.

Glutathione in the reduced form (GSH), with GPx, and GR together bring about an important antioxidant defense system (Lu, 2013). In the present study, GSE was found to increase the GSH values significantly in liver and kidney tissues in both GSE+OTA treated groups especially with the high dose of GSE (150 mg/kg bw) compared to OTA treated group ($p<0.05$). In consistent to our results, GSE

supplementation may activate antioxidant enzyme GSH in the liver and kidney, indicating that GSE attenuated toxicity-induced oxidative damage in liver and kidney of the rats (Nagi *et al.,* 1995; Kıran *et al*., 2023).

In the same line as our results, Chis *et al.* (2009) found that GSE as an excellent antioxidant, can enhance the activities of various antioxidant enzymes, play an antioxidant role and increased antioxidant enzymes (GSH, SOD and GPx) levels due to polyphenolic flavonoid content. GPx is an important enzyme in the antioxidant system that works with GSH and SOD to prevent the formation of lipid peroxidation (Meki and Hussein, 2001). In our study, GPx and SOD levels were significantly high in liver and kidney tissues of both GSE+OTA treated groups compared to OTA treated group, and that clearly indicates the enhancement role of antioxidant enzyme activity for GSE in rats, matching those of (Taghizadeh *et al*., 2016; Zhang *et al.,* 2022).

Lipid peroxidation is an oxidative stress indicator resulting from MDA. The MDA level in both kidney and liver of OTA treated group was highly significant compared to control. However, GSE treatment reduced significantly MDA level especially with the 2nd dose of GSE. That is in the same line with Meki and Hussein, (2001), who found that OTA induced oxidative stress in rat liver and kidney by increasing lipid peroxidation (MDA level), and suppressing GPx, GSH and SOD. At the same time, treatment with GSE as antioxidant, can ameliorate the oxidative stress status of OTA toxicity by prevention of free radicals formation or at least by reducing their levels, and that coincides with the findings of Kuyumcu and Aycan, (2018). This indicates that the protective role of GSE on rat kidney injury might be related to prevention of lipid peroxidation.

It is important to say that OTA also increases the reactive nitrogen species (RNS). OTA increases nitric oxide (NO) production, inducible nitric oxide synthase (iNOS) expression, and protein nitration eventually leads to nitrosative stress (overproduction of nitric oxide) in kidney and liver cells (Cavin *et al.,* 2009; Sorrenti *et al*., 2013; Crupi *et al.,* 2020). So, oxidative and nitrosative stress are related to OTA-induced DNA damage and provide additional evidence for their role in this mechanism of toxicity (Tao *et al*., 2018). This is in the same line with our findings. However, GSE supplementation improved the NO levels and restored it nearly to the normal control.

5. Conclusion

In conclusion, we confirm that OTA could increase oxidation products (MDA and NO), genotoxiciy, reduce liver and kidney antioxidant capacity, and induce their injury. GSE displayed an obvious protective effect on OTA induced-genotoxicity, oxidative stress through antioxidant capacity. The beneficial effects of GSE on the toxicity induced by OTA have been proved for the first time in our study. The supposed mechanism of actions includes decrease in genotoxicity, oxidative stress, lipid peroxidation, and enhancement of antioxidant parameters such as GSH, GP-x and SOD. Thus, clinical application of GSE as therapy should be considered to prevent and treat oxidative damage in cases of ochratoxicosis.

References

Ali R, Mittelstaedt RA, Shaddock JG, Ding W, Bhalli JA, Khan QM and Heflich RH. 2011. Comparative analysis of micronuclei and DNA damage induced by Ochratoxin A in two mammalian cell lines. *Mutat Res.,***723 (1):** 58-64.

Ali R, Guo X , Lin H , Khan QM , Ismail M , Waheed U, Ali T and Bhalli JA. 2014. Mutant frequency in comparison to oxidative DNA damage induced by ochratoxin A in L5178Y tk+/ (3.7.2C) mouse lymphoma cells. *Drug Chem Toxicol*., **37(2):** 227–232.

Campra NA, Cariddi LN, Escobar FM, Sabini MC, Freire-deLima CG, Decote-Ricardo D, Roma D, Mañas F and Dalcero AM. 2020. Protective role of chlorogenic acid on DNA damage caused by ochratoxin A exposure. *Analecta Vet.,* **40(2)**, July-December, ISSN: 1514-2590

Cavin C, Delatour T, Marin-Kuan M, Fenaille F, Holzhäuser D, Guignard G, Bezençon C, Piguet D, Parisod V and RichozPayot J et al. 2009. Ochratoxin A-mediated DNA and protein damage: Roles of nitrosative and oxidative stresses. *Toxicol Sci.,***110**: 84–94.

Chis IC, Ungureanu MI, Marton A, Simedrea R, Muresan A, Postescu ID and Decea N .2009. Antioxidant effects of a grape seed extract in a rat model of diabetes mellitus. *DiabVasc Dis Res.,***6(3):** 200–204.

Costa JG, Saraiva N, Guerreiro PS, Louro H, Silva MJ, Miranda JP, Castro M, Batinic-Haberle I, Fernandes AS and Oliveira N. 2016. Ochratoxin A-induced cytotoxicity, genotoxicity andreactive oxygen species in kidney cells: An integrative approach of complementary endpoints. *Food ChemToxicol*., **87**: 65–76.

Crupi R, Palma E, Siracusa R, Fusco R, Gugliandolo E, Cordaro M, Impellizzeri D, De CaroC, Calzetta L and Cuzzocrea S et al. 2020. Protective Effect of Hydroxytyrosol Against Oxidative Stress Induced by the Ochratoxin in Kidney Cells: In vitro and in vivo Study. *Front Vet Sci.,***7**:136 .

Damiano S, Iovane V, Squillacioti C, Mirabella N, Prisco F, Ariano A, Amenta M, Giordano A, Florio S and Ciarcia R. 2020. Red orange and lemon extract prevents the renal toxicity induced by ochratoxin A in rats. *J Cell Physiol*., **235**:5386–5393.

Degen GH, Gerber MM, Obrecht-Pflumio S and Dirheimer G. 1997. Induction of micronuclei with ochratoxin A in ovine seminal vesicle cell cultures. *Arch Toxicol.,***71**: 365–371.

Duarte SC, Lino CM and Pena A. 2011. Ochratoxin A in feed of food-producing animals: An undesirable mycotoxin with health and performance effects. *Vet Microbiol.*, **154**: 1–13.

Eken A. 2017. Rat kan ve Doku Örneklerinde Oksidatif Stres Parametreleri. *J of Clin and Analyt Med Online.* ET: 03/01/2017.

Gibb RK, Taylar DD, Wan T, Oconnar DM, Doering DL and Gercel-Taylor C. 1997. Apoptosisas a measure of chemosensitivity to cisplation and taxol therapy in ovarian cancer cell lines. *Gynecol Oncol J.,***65**: 13-22 .

Gong L, Zhu H, Li T, Ming G, Duan X, Wang J and Jiang Y. 2019. Molecular signatures ofcytotoxic effects in human embryonic kidney 293cells treated with single and mixture of ochratoxin A and citrinin. *Food Chem Toxicol*., **123**: 374–384.

Heussner AH and Bingle LE. 2015. Comparative Ochratoxin Toxicity: A Review of the Available Data. *Toxins,***7**: 4253–4282.

Hibi D, Kijima A, Suzuki Y, Ishii Y, Jin M, Sugita-Konishi Y, Yanai T, Nishikawa A and Umemura T. 2013. Effects of p53 knockout on ochratoxin A-induced genotoxicity in p53-deficient gpt delta mice. *Toxicol.,***304:** 92–99 .

Jablonska E, Kiersnowska-Rogowska B and Ratajczak W. 2007. Reactive oxygen and nitrogen species in the course of BCLL. *Adv Med Sci*., **52**:154–158.

Jeswal P. 1998. Antidotal effect of grape juice (Vitisvinifera) on ochratoxin A caused hepatorenal carcinogenesis in mice (Mus musculus). *Cytobios.,***93:** 123–128.

Kamp HG, Eisenbrand G, Janzowski C, Kiossev J, Latendresse JR, Schlatter J and Turesky RJ. 2005. Ochratoxin A induces oxidative DNA damage in liver and kidney after oral dosing to rats. *Mol Nutr Food Res*., **49:** 1160–1167 .

Kıran TR, Otlu O. and Karabulut AB. 2023. Oxidative stress and antioxidants in health and disease: Review. *J Lab Med.,* **47(1)**: 1–11.

Krishna G and Hyashi M. 2000. In vivo rodent micronucleus assay: protocol, conduct and datainterpretation. *Mutat Res*., **455(1-2)**: 155-166 .

Kuyumcu F and Aycan A. 2018. Evaluation of Oxidative Stress Levels and Antioxidant Enzyme Activities in Burst Fractures. *Med Sci Monit*., **24**: 225-234.

Lu SC. 2013. Glutathione synthesis. *Biochim et Biophys Acta.,***1830**:3143–53.

Malir F, Ostry V, Pfohl-Leszkowicz A, Malir J and Toman J. 2016. Ochratoxin A: 50 Years of Research. *Toxins*, **8(7):** 191.

Mally A, Pepe G, Ravoori S, Fiore M, Gupta RC, Dekant W and Mosesso P. 2005. Ochratoxin A causes DNA damage and cytogenetic effects but no DNA adducts in rats. *Chem Res Toxicol*., **18**: 1253–1261 .

Meki AR and Hussein AA. 2001. Melatonin reduces oxidative stress induced by ochratoxin A in rat liver and kidney. *Comp Biochem Physiol C Toxicol Pharmacol.,***130**: 305–313 .

NagiMN, Al-Bekairi AM and Al-Sawaf HA. 1995. Spectrophotometric assay for superoxidedismutase based on the nitrobluetetrazolium reduction by glucose-glucose oxidase. *Biochem Mol Biol Int.,***36(3):** 633-8.

Ohkawa H, Ohishi N and Yeagi K. 1979. Assay for lipid peroxides in animals' tissues by thiobarbituric acid reaction. *Anal Biochem.,***95(2):** 351-358.

Ozbek E. 2012. Induction of Oxidative Stress in Kidney. Review Article. *Int J of Nephrol.,* Volume **2012,** Article ID 465897, 9 pages.

Polito L, Iriti M, Martins N, Martorell M, Docea AO, Setzer WN, Calina D, Cho WC and Sharifi Rad J. 2020. Lifestyle, Oxidative Stress, and Antioxidants: Back and Forth in the Pathophysiology of Chronic Diseases. *Front Physiol*., **11**:694 .

Preston FJ, Au W, Bender MA, Brewen JC, Carrano AV, Heddle JA, McFee AF, Wolff S andWassom JS. 1983. Mammalian in vivo and in vitro cytogenetics assays: A report of the Gene-Tox Program. *Mutat Res*., **87**: 143-188 .

Rahman I, Kode A and Biswa SK. 2006. Assay for quantitative determination of glutathioneand glutathione disulfide levels using enzymatic recycling method. *Nat Protocols,***1(6):** 3159-3165.

Ramyaa P, Krishnaswamy R and Padma VV. 2014. Quercetin modulates OTA-induced oxidative stress and redox signalling in HepG2 cells—Up regulation of Nrf2 expression and downregulation of NF-kappaB and COX-2. *Biochim Biophys Acta*, **1840:** 681–692 .

Schaaf GJ, Nijmeijer SM, Maas RF, Roestenberg P, de Groene EM and Fink-Gremmels J. 2002. The role of oxidative stress in the ochratoxin A-mediated toxicity in proximal tubular cells . *Biochim Biophys Acta*., **1588**: 149–158 .

Schrenk D, Bodin L, Chipman JK and del Mazo J et al. 2020. Risk assessment of ochratoxin A in food. *EFSA J*., **18(5)**: 6113.

Schrenk D, Bodin L, Chipman JK, del Mazo J, Grasl-Kraupp B, Hogstrand C, Hoogenboom L, Leblanc J-C, NebbiaCS,Nielsen E, Ntzani E, Petersen A, Sand S, Schwerdtle T, Vleminckx C, Wallace H, Alexander J, Dall'Asta C, Mally A, Metzler M, Binaglia M, Horvath Z, Steinkellner H and Bignami M. 2020. Scientific Opinion on the risk assessment of ochratoxinA in food. *EFSA J.,***18(5):** 6113, 150 pp.

Sharifi-Rad M, Anil Kumar NV, Zucca P, Varoni EM, Dini L, Panzarini E, Rajkovic J, Tsouh Fokou PV, et al. 2020. Lifestyle, oxidativestress and Antioxidants: Back and Forth in the Pathophysiology of Chronic Diseases. *Front Physio*l.,**11**: 694.

Sorrenti V, Di Giacomo C, Acquaviva R, Barbagallo I, Bognanno M and Galvano F. 2013. Toxicity of Ochratoxin A and Its Modulation by Antioxidants: A Review. *Toxins*, **5**: 1742-1766.

Taghizadeh M, Malekian E, Memarzadeh MR, Mohammadi AA and Asemi Z. 2016. GrapeSeed Extract Supplementation and the Effects on the Biomarkers of Oxidative Stress and Metabolic Profiles in Female Volleyball Players: A Randomized, Double-Blind, Placebo-Controlled Clinical Trial. *Iran Red Crescent Med J.,***18(9):** e31314.

Tao Y, Xie S, Xu F, Liu A, Wang Y, Chen D, Pan Y, Huang L, Peng D, Wang X and Yuan Z . 2018. Ochratoxin A: Toxicity, oxidative stress and metabolism: Review. *Food and Chem Toxicol.,***112**: 320–331

Wang EH, Yu ZL, Bu YJ, Xu PW, Xia JY and Liang HY. 2019. Grape seed proanthocyanidin extract alleviates high-fat diet induced testicular toxicity in rats. *RSC Adv.,***9**: 11842–11850.

Wang Y, Wang L, Liu F, Wang Q, Selvaraj JN, Xing F, Zhao Y and Liu Y. 2016. Ochratoxin A Producing Fungi, Biosynthetic Pathway and Regulatory Mechanisms. *Toxins*, **8**: 38 .

Yoshikawa T and Naito Y. 2002. What is oxidative stress? *JMAJ*, **45(7):** 271–76 .

Zhang Z, Xu J, Zhang X, Wang J, Xie H, Sun Y, Zhang Q, Chang Z and Liu Y. 2022. Protective Effect of SeMet on Liver Injury Induced by Ochratoxin A in Rabbits. *Toxins*, **14(9):** 628

.

JJBS

Volume 17, Number 3,September 2024
ISSN 1995-6673
Pages 443 – 452
https://doi.org/10.54319/jjbs/170306

Jordan Journal of Biological Sciences

Protective Properties of Milk Thistle in Aquaculture: A Study on its Role in Mitigating Supracide-Induced Stress in Fish

Raid Al-Jawasreh[1,*], Tariq Al-Najjar[2], Giovanni Rizzato[3], Gabriele Capodaglio[3], and Mohammad Wahsha[1]

[1]*Marine Science Station, The University of Jordan, Aqaba branch, Jordan;* [2]*Faculty of Basic and Marine Sciences, The University of Jordan, Aqaba branch, Jordan;*[3]*Department of Environmental Sciences, Informatics, and Statistics, Ca' Foscari University of Venice, Italy.*

Received: September 5, 2023; Revised: November 5, 2023; Accepted: November 16, 2023

Abstract

This investigation sought to comprehensively evaluate the protective properties of Milk Thistle seeds against Supracide-induced oxidative stress in the Marbled Spinefoot fish. Liquid chromatography–mass spectrometry (LC–MS) was employed to identify metabolites present in *Silybum marianum* seeds. The LC_{50} value of organophosphorous insecticide was determined as 7.5 µg L^{-1} through a 24-hour bath exposure. The experimental setup involved a 14-day dietary supplementation of *S. marianum* seeds followed by exposure to the determined Supracide LC_{50}. Various physiological parameters, including lipid degradation, Alanine aminotransferase (ALT), Lactate dehydrogenase (LDH), and Total cholesterol (T.ch) levels, were measured to assess fish health and stress. Additionally, histopathological examinations were conducted on the hepatopancreas tissues of both normal and stressed fish. The obtained results indicated significant increases ($P<0.05$) in serum ALT and LDH activities in the group of fish exposed to the toxin. Moreover, the levels of lipid peroxidation products in hepatopancreas homogenates were significantly higher ($P<0.05$) in the exposed fish group, except for total cholesterol, which exhibited a significant decrease. Histological analysis further revealed notable tissue modifications in the examined organs, while the control group of fish exhibited normal appearance. Taken together, these findings suggest that Milk thistle seeds may possess protective effects against Supracide-induced oxidative stress in challenged *S. rivulatus* fish. As a result, this study provides valuable insights into potential alternative ameliorating agents for addressing aquaculture contamination caused by organophosphate insecticides.

Keywords: Malonaldehyde; Supracide; *Silybum marianum*; Oxidative stress; *Siganus rivulatus.*

1. Introduction

Aquaculture production is a crucial contributor in meeting the global demand for fish food, providing more than 46.8% of the total supply (FAO, 2020). Aquaculture production is susceptible to contamination, resulting in significant losses. However, contaminants originating from industrial chemicals that kill insects, rodents, pests, fungi, and their byproducts raise concerns about the potential health risks for aquatic organisms (Tudi et al., 2021). In particular, insecticides are highly impactful environmental contaminants that have been increasingly released into the environment in recent decades (Rad et al., 2022). Synthetic insecticides, has raised concerns about their impact on non-target organisms, particularly aquatic life. Among the synthetic insecticides, organophosphates (OPs) have gained attention due to their high toxicity and potential threat to the environment (Mali et al., 2023).The inhibition of acetylcholinesterase by OPs is well-established and explains their acute neurotoxic effects. However, recent studies have revealed that OPs can also generate reactive oxygen species (ROS), leading to oxidative stress. This occurs through various mechanisms, including the disruption of cellular redox balance, inhibition of antioxidant enzymes, and induction of lipid peroxidation (Sule et al., 2022).

An important factor influencing the development of pathological conditions in farm animals is oxidative stress, which results from an imbalance between the productions of reactive oxygen species (ROS) and antioxidant defenses. This condition can significantly affect animal production and overall well-being. It is crucial to comprehend the connection between oxidative stress and its consequences for farm animals to implement effective management strategies and enhance animal welfare (Song et al., 2023). Stressors, which can be internal or external in nature, trigger the activation of neurohormonal regulatory mechanisms aimed at maintaining homeostasis. These factors, combined with the body's ability to adapt, determine the alterations in animal maturation, productivity, growth, and all-around healthiness quality (Wahsha et al., 2023). Disruptions in homeostasis result in the overproduction of molecular species known as free radicals, overwhelming the organs' detoxification capacity (Trachootham et al., 2008). Excess free radicals can cause oxidative deterioration to lipid membranes and different organelles within cells (Martemucci et al., 2022). Animals have evolved mechanisms to counteract oxidative stress by enhancing their cellular defenses, primarily through the

* Corresponding author. e-mail: r.jawasreh@ju.edu.jo.

activation of antioxidant enzymes (Halliwell and Gutteridge, 2015). Moreover, certain dietary antioxidants have been shown to help mitigate the damaging consequences of ROS and promote overall health (Sies and Jones, 2020). As a result, medical plants with antioxidant properties have been considered as potential candidates for animal diets, as they may offer a protective role against various diseases (Mahima et al., 2012).

The use of plant extracts in aquaculture has recently gained attention due to their beneficial properties, which can contribute to fish health management control (Reverter et al., 2014). Medicinal plants have immense potential in the management of fish health by modulating the immune system. Through their immunomodulatory activity, these plants have the capability to enhance fish immune responses, bolster disease resistance, and improve stress tolerance, thereby serving as valuable assets in aquaculture (Nipa et al., 2021). Furthermore, these plants synthesize secondary metabolites, such as terpenoids and flavonoids, which exhibit diverse chemical structures and biological activities, playing a vital role in their mechanism of action (Yeshi et al., 2022). Among the Asteraceae family, milk thistle (*Silybum marianum* (L.) Gaertn) is indeed an important medicinal plant species. Milk thistle is native to the Mediterranean region but is now cultivated worldwide due to its therapeutic properties. The plant has a long history of traditional use and has been extensively studied for its potential health benefits (Bhattacharya, 2020; Csupor et al., 2016; Surai, 2015). In addition to its liver-protective effects, milk thistle has also shown potential in other areas of health. Studies have suggested its anti-inflammatory properties may be beneficial for conditions such as diabetes, cancer, and cardiovascular diseases (Wahsha and Al-Jassabi, 2009). Moreover, milk thistle's antioxidant activity has been linked to its protective effects against oxidative stress and certain types of cellular damage (Deep et al., 2006). Aquaculture is an important industry that often relies on the use of veterinary drugs to prevent and treat diseases in fish and other farmed organisms. However, the use of these drugs in aquaculture can have potential negative effects on the environment and human health. To address these concerns and seek more sustainable alternatives, researchers have turned to natural products derived from plants and other flora sources for use in aquaculture practices (Tadese et al., 2022). One approach is the incorporation of natural products, such as those derived from flora origins, in aquaculture approaches (Mohamad Nek Rahimi et al., 2022). The present investigation was conducted to assess the hepatopancreatic protective properties of Milk thistle (*Silybum marianum*) seed extract against the cytotoxic effects induced by Supracide insecticide, known for its oxidative properties, in the fish species *Siganus rivulatus* (Forsskål & Niebuhr, 1775). The evaluation of Supracide-induced oxidative stress involved quantifying malondialdehyde (MDA) levels as a marker of lipid peroxidation, performing serum biochemical assays, and examining histopathological alterations in the hepatopancreas.

2. Materials and methods:

2.1. Fish samples

During the summer of 2018, a study was conducted at the Marine Science Station in Aqaba (located between the coordinates 29°27'20.9"N and 34°58'26.3"E). The study focused on male fish species. According to Khalaf and Disi's (1997) classification, the fish species known as Rivulated rabbitfish was identified as *Siganus rivulatus* (Forsskål & Niebuhr, 1775). Carefully selected fish samples were chosen from the aquaculture facility and transferred to the laboratory, where the temperature was maintained at 25 ± 3 °C. The fish were given a week to acclimate to these conditions. All the selected fish samples were of the same age, approximately six months old, with an average body weight of 70 ± 15 grams and a length of approximately 10 centimetres.

2.2. Plant samples:

Silybum marianum is a plant from the Asteraceae family and is also known as "ripe milk thistle". This plant is native to the Mediterranean and Middle Eastern regions. The ripe milk thistle (*Silybum marianum*) seeds were meticulously collected from locally cultivated plants in North Jordan, all of which were in the same growth stage and displayed robust physical characteristics. Per the classification by Webb et al. (1988), Milk thistle is identified as *Silybum marianum* (L.) Gaertn. The harvesting procedure adhered to the prescribed techniques documented by Curioni et al., (2002). To ensure optimal preservation and retain their freshness, the seed samples were packed in dark plastic bags and transported to the laboratory. Following transportation, the seeds underwent a 24-hour drying period at a temperature of 50˚C. Once completely dried, the samples were finely ground into a powder with particle sizes smaller than 5µm.

2.3. Metabolite determination:

Metabolite extraction, following De Vos et al. (2007) protocol, involved homogenizing and grinding dried seeds with a Retsch grinder (MM 400, Haan, Germany). Three replicated samples and three blank samples ensured precision and contamination prevention. Phenyl-$^{13}C_6$ salicylic acid served as an internal standard (IS). Seeds (50 mg ± 0.5) were weighed, extracted for 30 min in an ultrasonic bath (1.5 ml methanol/water, 75:25, v:v), and centrifuged for 20 min at 14,000 rpm. The supernatant, filtered through PTFE syringe filters (Ø 25 mm, 0.2 µm), underwent LC-MS analysis. Raw chromatographic data, aligned and corrected using MetAlign 3.0 (Lommen & Kools, 2012), and MSClust (Tikunov et al., 2012) for clustered mass signals, were processed using XcaliburTM software for molecular formulas. Metabolite identification utilized online libraries (Metlin, HMDB, Dictionary of Natural Products, and LIPID MAPS Structure Database) and literature, considering mono isotopic mass and fragmentation pattern.

2.4. Model of toxicity

In this study, Supracide (organophosphorous ≥ 95.0 %) was utilized as a representative oxidative agent. The Supracide insecticide used in the research was procured from Sigma.

2.5. Animals and ethics

In this research, the test fish were handled in strict accordance with the Global Guidelines for Animal Experimentation (1986). Every experimental protocol was thoroughly reviewed and approved by the animal welfare and ethics committees at the Oceanographic Research Centre, The University of Jordan, and Yarmouk University, Jordan. This ensured the appropriate care and welfare of the fish (session No. (4)/2015/2016, held on 7/28/2016).

2.6. LC_{50} determination

This study employed the up-and-down toxicity test method, initially introduced by Sunderam et al. (2004), to assess toxicity levels. This approach involves systematically adjusting the concentration of the toxic substance, either upward or downward in increments, until a clear pattern of responses is observed in the test organisms. The study spanned a single day, during which a functional solution of Supracide (40.03% w/v) was prepared to create specified toxin doses. Distinct quantities of the toxic substance (2.85, 1.12, 0.49, 0.2, 0.09, 0.04, 0.0175, 0.0075, and 0.0033 mg L^{-1}) were allocated to separate aquariums for the experiment, each with a volume of 60 liters. In each aquarium, ten fish, with an average weight of 70 grams and an average standard length of 10 centimeters, were housed. Throughout the 24-hour duration of the experiment, a meticulous record of the mortality rate and indicators of toxicity was consistently maintained and documented.

2.7. Fish bioassay and toxicity challenge

Forty fish were brought to the laboratory, where the water temperature was kept at 25 ± 3 °C. The fish were divided into four groups following the information in Table 1. The trials were conducted in glass aquariums containing 150 L of the specific test solution. The fish were allowed to acclimatize to the laboratory environment for seven days before the experiments began.

Table 1. Experimental design and conditions for the toxicity challenge experiment

Group	Description	Number of sacrificed fishes/time course
C	The control group did not receive any supplementation of crude extract or treatment with toxins.	Ten fish were sacrificed after 24 hrs (C24).
TC	The toxin control group was treated with Supracide (specific toxin) at a dose of 7.5 µg L^{-1}, based on the LC_{50} value.	Ten fish were sacrificed after 24 hrs (TC24).
SC	The control group for Milk thistle received a daily addition of 2.5g of the same per kg of aquatic creature mass, with this routine continued for a two-week period.	Ten fish were sacrificed after 24 hrs (SC).
ST	The fish were supplemented daily with 2.5g of Milk thistle per kilogram of fish body weight for 14 days, and after that, they were treated with Supracide at a dose of 7.5 µg L^{-1}.	Ten fish were sacrificed after 24 hrs (ST24).

Each fish was subjected to cardiac puncture to obtain blood samples using vials without anticoagulant. The collected blood was then centrifuged at 3000 X g for 30 minutes to separate the serum, which was later used for the enzyme assay. The tubes containing the serum were promptly sealed and stored at 4ºC for future use. Moreover, the hepatopancreas was immediately isolated and washed with phosphate-buffered saline at a pH of 7.2. A section of the isolated hepatopancreas was stored at -20ºC for biochemical tests, while another section was fixed in buffered formalin for histopathological analysis.

2.8. Biochemical assays

The level of malondialdehyde (MDA) in the hepatopancreas was determined following the protocol outlined by Wahsha et al. (2017). Furthermore, Cormay diagnostic kits were employed to measure the levels of lactate dehydrogenase (LDH), serum alanine transaminase (ALT), and total cholesterol (T.Ch).

2.9. Histopathological examination

To conduct the histopathological analysis, small 0.3 cm thick fragments of hepatopancreas tissues were fixed in 10% buffered formalin for 24 hours, following the method described by Al-Haj (2010). The fixed tissues were then gently washed under running tap water and dehydrated through increasing concentrations of alcohol. Subsequently, they were infiltrated with xylene and embedded in paraffin wax. Sections with a thickness of 6µm cut using a rotatory microtome, mounted with DPX and stained with Ehrlich Hematoxylin and Eosin (H&E), and the stained sections were examined using light microscopy.

2.10. Data processing and Statistical analysis.

In order to derive meaningful data from the raw chromatographic results, we employed a couple of specialized software tools. The task of spectral alignment and baseline correction was managed by MetAlign 3.0 whereas MSClust was used for the purpose of securing clustered mass signals, effectively representing reconstructed metabolites (Rizzato et al., 2017). XcaliburTM software (Thermo Scientific Inc.) was used to ascertain the molecular formulas. Further, we adhered to a set procedure for identifying metabolites, which involved predicting the most likely molecular formula according to the fragmentation pattern. We matched the mono-isotopic mass and mass spectra with published data and several online databases such as HMDB, Metlin, LIPID MAPS Structure Database, and the Dictionary of Natural Products. Sumner et al.'s (2007) method was adopted to designate the identification level. For the biochemical experiments, the statistical assessment was carried out using Sigma Stat Software version 3.5, and a significance threshold of $p < 0.05$ was set.

3. Results

3.1. Analysis of plant metabolites:

From the LC-MS chromatogram, a total of 126 secondary metabolites were detected. Out of these, 37 compounds were categorized as level 2 identifications, while the remaining compounds were classified as level 3 identifications based on Sumner et al.'s (2007) classification system. The primary constituents of the Milk thistle seed extract were found to be flavonoids and terpenoids, each accounting for approximately 22% of the total relative abundance. Additionally, glycosides comprised 14% of the identified compounds; fatty acids constituted 9%, and a diverse array of other compounds made up the remaining 33%. Notably, Table 2 showcases a selection of the most remarkable compounds among the 126 identified ones.

Table 2 Certain compounds of significance have been discovered in the seed extract of *Silybum marianum*

Formula	Compound	Biological/Pharmacological Activities	Reference
$C_{25}H_{22}O_{10}$	Silibinin (silymarin)	Antioxidant, Anti-inflammatory, Antiviral, Antitumor and Hepatoprotective.	Csupor et al., 2016.
$C_{15}H_{12}O_5$	Naringenin	Hepatoprotective, Anti-inflammatory, Anticancer, Antimutagenic, and Antimicrobial agent	Karim et al., 2018.
$C_{15}H_{12}O_6$	Eriodictyol	Antioxidant and Anti-inflammatory effects	Narvaez-Mastache et al., 2008.
$C_{15}H_{10}O_6$	Luteolin	Antioxidant, Antitumor, Anti-inflammatory, and Antiapoptotic efficacy	Zhang et al., 2011.
$C_{18}H_{18}O_6$	4'-Hydroxy-5,6,7-trimethoxyflavanone	Antimycobacterial activity	Suksamrarn et al., 2004.
$C_{25}H_{20}O_{10}$	2,3- Dehydrosilybin	Antioxidants	Reina and Martínez, 2015.
$C_{27}H_{48}O_{14}$	Naringin	Antioxidant, Lipid-lowering, Antimicrobial, Anti-inflammatory and Anticancer	Jeon et al., 2004.
$C_{28}H_{26}O_{16}$	Taxillusin	Antimicrobial activities	Fukunaga et al., 1989.
$C_{14}H_{18}O_9$	Vanillic acid 4-O-β-d-glucopyranoside	Antioxidants	Chemam et al., 2017.
$C_{16}H_{18}O_9$	Chlorogenic acid	Antioxidant and Anti-inflammatory activities	Farah et al., 2008.
$C_{17}H_{26}O_{10}$	Login	Cognitive enhancing and Free radical scavenging capacity	Lee et al. 2009.
$C_{18}H_{26}O_{11}$	Oleoside dimethyl ester	Antioxidant activity	Wang et al., 2010.
$C_{21}H_{32}O_{12}$	Darendoside B	Antioxidant activity	Pan et al., 2003.
$C_{17}H_{26}O_5$	Hymenolide	Phagostimulant activity	Juárez et al., 2014.
$C_{16}H_{32}O_2$	Palmitic acid	Antimicrobial activity	Huang et al., 2011.
$C_{18}H_{30}O_2$	Alpha-Linolenic acid	Neuroprotective and Anti-inflammatory	Nicolas et al., 2015.
$C_{18}H_{32}O_2$	Linoleic acid	Antibacterial activity	Zheng et al., 2005.
$C_{18}H_{34}O_3$	Ricinoleic acid	Antibacterial activity, Anti-inflammatory	Abdul et al., 2018.

3.2. LC_{50} determination

The fish were subjected to various concentrations of Supracide, including 2.85, 1.12, 0.49, 0.2, 0.09, 0.04, 0.0175, 0.0075, and 0.0033 mg L^{-1}, for duration of 24 hours. All groups, except for the control group, showed significant changes in behavior over the entire 24-hour test period, with the control group exhibiting no behavioral modifications and maintaining a 100% survival rate for all fish. These observed behavioral changes included loss of equilibrium, rapid and circular swimming, and dullness, surface swimmining, and increased opercular movement. The results indicated varying mortality rates among the fish, ranging from 0% to 100%. It was evident that the mortality rate was dependent on both the dosage and the duration of exposure. The LC_{50}-24h (lethal concentration at which 50% of the fish died after 24 hours) was estimated to be 7.5 μg L^{-1}.

3.3. Biochemical assays

The study aimed to understand the effects of Supracide on biochemical biomarker levels in *S. rivulatus* fish, and how Milk thistle seed extract might influence these effects. MDA levels were mainly analyzed in the fish's hepatopancreas (a digestive gland in some aquatic animals), and other blood serum biochemical markers were also measured. The data indicates significant differences in biomarker levels between the various groups, highlighting the potential impact of Supracide and the influence of Milk thistle seed extract on these biochemical parameters, as demonstrated in Table 3. Our results suggest that the organophosphorous insecticide has considerable effects on the fish's biochemical profile and the Milk thistle extract may have some mitigating effects.

Table 3. The results of the study evaluated the impact of Supracide on biochemical biomarker levels in *S. rivulatus* fish when subjected to bath administration of LC_{50} (7.5 µg L^{-1}), both with and without Milk thistle seed extract.

Group	C24	TC24	SC24	ST24
MDA+ (µmol/g)	4.2 ± 0.2	16.4 ± 0.8***	5.1 ± 0.2	5.7 ± 0.2
ALT++ (IU/ml)	11 ± 2	316 ± 2***	36 ± 1***	23 ± 3
LDH++ (IU/ml)	338 ± 9	12643 ± 45***	936 ± 17***	1455 ± 18***
T.Ch++ (IU/ml)	625 ± 12	30 ± 5***	726 ± 21***	253 ± 9***

The experimental groups were categorized as follows: C - Control group without extract or Supracide treatment, TC - Toxin Control group treated, SC - Milk thistle control group supplemented daily with 2.5g *S. marianum*/kg fish body weight for 14 days, and ST - Fish supplemented daily with 2.5 g Milk thistle/kg fish body wt for 14 days, followed by treatment with LC_{50} 7.5 µg (toxin) L^{-1}. The reported values represent the means of 3 replicates with standard deviation (SD).

+: The impact of Supracide (LC_{50} 7.5 µg L^{-1}) on MDA levels in fish hepatopancreas and++:The levels of blood serum biochemical markers. The results are expressed as means ± SD, with T representing time in hours. *** denotes statistical significance at $P < 0.05$, determined by an ANOVA test.Oxidative degradation of lipids (MDA levels)

The MDA levels in the fish hepatopancreas were significantly different among the groups ($p < 0.001$). The Toxin Control group (TC24) showed a substantially higher MDA level compared to the Control group (C24) and the Milk Thistle Control group (SC24). This indicates that exposure to the toxin (Supracide) led to increased oxidative stress and lipid peroxidation in the hepatopancreas of the fish. The Milk Thistle-supplemented group followed by toxin treatment (ST24) did not show a significant increase in MDA levels compared to the Control group, suggesting a potential protective effect of Milk Thistle extract.

3.3.1. Alanine transaminase (ALT)

ALT levels, an indicator of liver function, exhibited significant differences between the groups ($p < 0.001$). The Toxin Control group (TC24) had markedly elevated ALT levels compared to the other groups, indicating liver damage due to toxin exposure. The Milk Thistle Control group (SC24) and the Milk Thistle Toxin group (ST24) had ALT levels closer to the Control group (C24), implying that Milk Thistle supplementation might have a mitigating effect on toxin-induced liver damage.

3.3.2. Lactate dehydrogenase (LDH)

LDH levels, which reflect tissue damage, were significantly different among the groups ($p < 0.001$). The Toxin Control group (TC24) exhibited a substantial increase in LDH levels compared to the other groups, indicating tissue injury caused by the toxin. Both Milk Thistle-supplemented groups (SC24 and ST24) showed LDH levels closer to the Control group (C24), suggesting a potential protective role of Milk Thistle against toxin-induced tissue damage.

3.3.3. Total Cholesterol (T.Ch)

Total cholesterol levels also displayed significant differences between the groups ($p < 0.001$). The Toxin Control group (TC24) had remarkably reduced cholesterol levels compared to the other groups. This reduction could be due to the disruptive effects of the toxin on lipid metabolism. The Milk Thistle Control group (SC24) and the Milk Thistle Toxin group (ST24) had cholesterol levels closer to the Control group (C24), hinting at a possible protective influence of Milk Thistle on lipid homeostasis.

3.4. Histopathological changes in hepatopancreas

The control group's fish exhibited a typical histological structure in their hepatopancreas. The hepatocytes displayed central nuclei with a spherical shape, along with a significant presence of blood sinusoids (Figure 1). Melanomacrophage centers (MMC) were found in the hepatic parenchyma, usually near the hepatic arteries or bile ducts. In contrast, the liver sections of fish exposed to the LC_{50} concentration of Supracide for 24 hours displayed a range of histopathological changes. These changes included more severe damage characterized by dilation of intercellular spaces, blood congestion, and necrosis accompanied by cytoplasmic vacuolization (glycogen and lipid). Furthermore, there were some observed hepatic morphological alterations, albeit to a lesser extent, in the fish treated with the toxin and supplemented with Milk thistle (Figure 1).

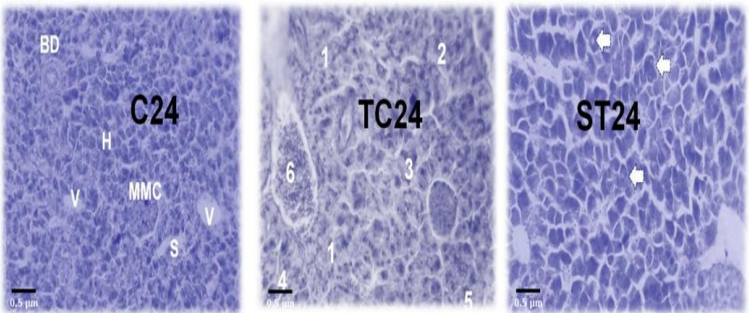

Figure1. Illustrative photomicrograph of hepatopancreas tissue slices derived from the following groups of fish: Control (C24), Toxic control (TC24), and toxin/Milk thistle pre-exposed (ST24) groups.C24: (H) Hepatocellular cells; (V) Hepatic vein; (BD) Bile duct; (MMC) Melanomacrophage clusters; (S) Sinusoidal cavity. TC24: (1) Localized necrosis and absence of nuclie; (2) Pyknotic nuclei; (3) Nuclier hypertrophy; (4) Cytoplasmic vacuolization; (5) Fatty Change; (6) Vascular congestion. ST24: Fish pre-exposed to toxin/Milk thistle (arrow) showcasing Cytoplasmic vacuolization. Stain used: H & E; Magnification at 40X.

4. Discussion

In the past few years, there has been a significant increase in the number of studies presenting compelling evidence on the connection between organophosphate pesticides, particularly Supracide, and oxidative stress induction in aquatic life (Sule et al., 2022; Özkan-Yılmaz et al., 2015). Despite a wealth of scientific data underscoring the harmful effects of organophosphates, their influence on Aquaculture has been given minimal consideration by researchers globally. Supracide (S-[(5-Methoxy-2-oxo-1,3,4-thiadiazol-3(2H)-yl)methyl] O,O-dimethyl phosphorodithioate), a potent organophosphate pesticide, sees broad application. Our study determined the Supracide concentration that caused mortality in 50% of the test fish (LC_{50}) to be 7.5 µg L^{-1} by employing an adjusted up and down toxicity test (Sunderam et al., 2004). It is noteworthy that this value diverges from previous findings on aquatic organisms such as Sheepshead minnow, rainbow trout, bluegill, and goldfish (Flaherty et al., 2009). Differences in LC_{50} values across various animal models can be traced back to elements such as species, age, and sex of the organisms involved (Ghosh and Saha, 2022).

In the present investigation, we documented signs of cellular harm following Supracide exposure, evaluated through particular biomarkers and histopathological specimen analysis. The main toxicity mechanism related to organophosphate pesticides is the suppression of acetylcholinesterase, a critical enzyme for neural operation (Fernandes et al., 2015; Lu et al., 2018; Sandoval-Herrera et al., 2019; Tsai and Lein, 2021). Latest studies imply that oxidative stress plays a pivotal role in organophosphates' toxic effects by boosting the generation of reactive oxygen species (ROS) and unsettling the equilibrium between ROS and antioxidant defense mechanisms (Martinez-Alvarez et al., 2005; Cortes-Iza and Rodriguez, 2018; and Sandoval-Herrera et al., 2019). In addition, research has suggested that lipid peroxidation (LPO) is a molecular mechanism involved in organophosphate toxicity and liver injury (Oruc, 2011, and Karami-Mohajeri et al., 2017).

Our study discovered a shift in the MDA (malondialdehyde) level in the liver and pancreas tissue of the fish used in the experiment following exposure to Supracide at the LC_{50} value. These outcomes corroborate prior research carried out by Modesto and Martinez, (2010) and Abhijith et al., (2016) and propose that reactive oxygen species (ROS) play a part in the onset of Supracide-induced damage. Several studies have reported that organophosphate pesticides could disturb antioxidant defense enzymes, leading to a surge in lipid peroxidation products by directly interacting with organic molecules in the cell membrane (Wu et al., 2011; Abhijith et al., 2016, and Yang et al., 2020). MDA, a lipid peroxidation byproduct, has been used as a biomarker for oxidative stress and as an indicator of the degree of lipid peroxidation (Tsikas, 2017, and Ito et al., 2019). In our investigation, we noticed an increase in MDA levels in the liver and pancreas tissue of *S. rivulatus* fish treated with the LC_{50} value of Supracide, suggesting that MDA levels could serve as an indicator of Supracide-induced damage.

Animal cells have various methods to neutralize oxidative stress's detrimental effects, either by repairing the inflicted damage or by inhibiting and neutralizing reactive oxygen species (ROS) via enzymatic and non-enzymatic antioxidant defense systems (Ponnampalam et al., 2022). Polyphenols, including flavonoids, are part of the non-enzymatic defense mechanism (Panche et al., 2016) and have demonstrated potential as therapeutic agents against a broad spectrum of ROS (Kumar and Pandey, 2013; Ullah et al., 2020; and Khan et al., 2021). Our results indicate that Supracide poisoning may incite the production of highly unstable free radicals capable of attacking lipids containing carbon-carbon double bonds, especially polyunsaturated fatty acids (PUFA). Past studies in our lab have underscored the impacts of milk thistle seed extracts on lipid peroxidation (Wahsha and Al-Jassabi, 2009) and antioxidant enzymes (Wahsha et al., 2012). Wilson Magdy et al (2016) showed that treatment with alpha-tocopherol (vitamin E) and ascorbic acid (vitamin C) post-Supracide administration could mitigate liver damage in rats. Karami-Mohajeri et al (2017) reported that sublethal Supracide doses could compromise the antioxidant enzymatic defense system and escalate lipid peroxide levels in the liver and pancreas of fish.

Biochemical markers are vital in the diagnosis of diseases in fish and for the detection of tissue impairment instigated by environmental toxins, functioning as sensitive detectors of metabolic perturbations in the organism (Bharti and Rasool, 2021). Enzymes such as ALT and LDH are often deployed in the identification of fish diseases, with their serum levels reflective of physiological changes or stress responses. These enzymes are valuable indicators of minor cellular disruptions (Ahmet Deveci et al., 2022).Our research demonstrated that the group of *S. rivulatus* fish exposed to Supracide exhibited a significant elevation in serum ALT and LDH activities compared to the control group. This observation indicates that severe stress conditions in fish lead to an augmented requirement for energy, driving the need for carbohydrates and other key compounds to uphold the glycolytic pathway and tricarboxylic acid cycle (Tiwari and Singh, 2004). Fish affected by toxicants adapt their metabolic processes to mitigate the stressors and sustain homeostasis (Petitjean et al., 2019). Prior research has shown that stress commonly results in enhanced aminotransferase activity, and specific studies have noted increased ALT activity, indicative of increased energy requirements due to tissue damage (Jee et al., 2005; Samanta et al., 2014). Additionally, ALT increase signifies liver tissue damage, caused by toxicant-induced harm to the liver, resulting in serum leakage of cellular enzymes. Hence, elevated enzyme activity is linked to liver damage inflicted by pesticides (Gowda et al., 2009; Vasantharaja et al., 2015; Xavier Martins et al., 2021).

LDH, a pivotal enzyme in fulfilling the energy needs of cells under varying oxygen conditions, can be used to signal the release of the enzyme from damaged cells, shifts in protein and carbohydrate metabolism, and cell leakage (Alarifi et al., 2012; Klein et al., 2020). A significant upsurge in LDH activity was recorded during Supracide exposure in our study, implying disruption in carbohydrate metabolism due to Supracide. Additionally, the notable rise in LDH activity could be associated with tissue harm inflicted by Supracide toxicity. Such alterations in LDH activity underscore the stress conditions experienced by the fish. Other organisms exposed to substances like carbamazepine, selenium, ibuprofen, clofibric acid, and

diclofenachave also demonstrated similar changes in LDH activity (Jos et al., 2003; Saravanan et al., 2011; Saravanan et al., 2012; Ramesh et al., 2014).Moreover, in our study, when fish were pre-exposed to Milk thistle seeds before Supracide exposure, an amplified serum LDH value was recorded, implying increased LDH activity. A more pronounced increase was observed in the group pre-treated with Milk thistle seeds than in the control group. These findings suggest that a 14-day pre-treatment with Milk thistle seeds offers significant recovery protection against Supracide toxicity.

In our experiment, serum T.Ch levels significantly decreased after Supracide exposure. Similar outcomes were reported in previous studies where various insecticides, such as dichlorvos, acephate, and cypermethrin, were used on different experimental animals (Ryhanen et al., 1984; Choudhari and Chakraharti, 1984; Shakoori et al., 1988). Lipids, vital components of animal cell plasma membranes, participate in numerous biological processes in the body (Muro et al., 2014).Earlier studies showed that Supracide could trigger the oxidative degradation of lipids through reactive oxygen species (ROS) action (Sule et al., 2022).Additionally, Supracide and other organophosphate insecticides might inhibit 3-hydroxy-3-methylglutaryl-CoA reductase, an essential enzyme for cholesterol synthesis (Ryhanen et al., 1984). The reduced serum total cholesterol levels could be due to the organophosphate-stimulated activation of the low-density lipoprotein (LDL) receptor, increasing the cholesterol clearance from the bloodstream (Ibrahim and El-Gamal, 2003).

Histological findings and biochemical data contribute to a thorough understanding of the death mechanisms in organisms exposed to toxic substances (Orrenius et al., 2011). As such, they are effective tools for assessing the health status of fish. The results of our study showed increased histopathological alterations in hepatopancreas tissue after Supracide exposure. However, pre-treatment with Milk thistle seed led to a remarkable decrease in these histopathological alterations. Similar observations were reported where Supracide exposure led to a notable rise in rat liver enzyme activities and morphological liver changes in carp exposed to Supracide (Asztalos et al., 1990; Altuntas et al., 2002; Karami-Mohajeri et al., 2017).

The phytochemical analysis of milk thistle seed extract revealed a remarkable array of bioactive compounds with diverse biological and pharmacological activities. Among the compounds identified, silibinin (silymarin) stood out for its numerous benefits. Csupor et al. (2016) reported silibinin to possess antioxidant, anti-inflammatory, antiviral, antitumor, and hepatoprotective properties, making it a potential candidate for combating oxidative stress, inflammation, viral infections, and even supporting liver health. Additionally, naringenin, as studied by Karim et al. (2018), demonstrated hepatoprotective, anti-inflammatory, anticancer, antimutagenic, and antimicrobial activities, indicating its potential in protecting the liver, combating inflammation, and acting as an agent against cancer and various microorganisms.

Other compounds found in milk thistle seed extract also exhibited promising attributes. Eriodictyol, as identified by Narvaez-Mastache et al. (2008), exhibited antioxidant and anti-inflammatory effects, making it valuable in neutralizing free radicals and reducing inflammation. Luteolin (Zhang et al., 2011) showed antioxidant, antitumor, anti-inflammatory, and antiapoptotic efficacy, suggesting its potential role in cellular protection, tumor inhibition, and antiapoptotic properties. Moreover, compounds like 4'-hydroxy-5,6,7-trimethoxyflavanone, 2,3-dehydrosilybin, and chlorogenic acid (Suksamrarn et al., 2004; Reina and Martínez, 2015; Farah et al., 2008) were found to possess antioxidant properties, which could contribute to their potential health benefits in combating oxidative stress-related disorders. The presence of other compounds, as reported in the table 2, further highlights the diverse pharmacological potential of milk thistle seed extract.

In summary, the results suggest that Supracide has detrimental effects on the biochemical biomarkers in *S. rivulatus* fish, leading to oxidative stress, liver damage, tissue injury, and disruption of lipid metabolism. Milk Thistle seed extract supplementation appears to provide some level of protection against these negative impacts, as indicated by the reduced levels of these biomarkers in the Milk Thistle-treated groups. The observed hepatoprotective effects may be attributed to the rich presence of active phytoconstituents found in the Milk thistle extract, including flavonoids, terpenoids, polyphenols, glycosides, and essential fatty acids. These findings highlight the potential benefits of Milk Thistle extract in mitigating the adverse impacts of the toxin on fish health and biochemistry of the fish hepatopancreas. However, further research is necessary to better understand the mechanisms underlying these effects and to validate the potential therapeutic role of Milk Thistle in such contexts.

References

Abdul WM, Hajrah NH, Sabir SM, Al-Garni SM, Sabir MJ, Kabli SA, Saini KS and Bora RS. 2018. Therapeutic role of *Ricinus communis L.* and its bioactive compounds in disease prevention and treatment. ASIAN PAC J TROP MED, **11(3):** 177-185.

Abhijith BD, Ramesh M and Poopal RK. 2016. Responses of metabolic and antioxidant enzymatic activities in gill, liver and plasma of Catla catla during methyl parathion exposure. J Basic Appl Zool, **77**, 31–40.

Ahmet Deveci H, Nur G, Deveci A, Kaya I, Mavioglu Kaya M, Kükürt A, Gelen V, Faruk Başer O and KarapehlivanM. 2022. An Overview of the Biochemical and Histopathological Effects of Insecticides. IntechOpen. doi: 10.5772/intechopen.100401

Alarifi S, Al-Doaiss A, Alkahtani S, Al-Farraj SA, Saad A, Al-Dahmash B, Al-Yahya H and Mubarak M. 2012. Blood chemical changes and renal histological alterations induced by gentamicin in rats, Saudi J Biol Sci, **19**: 103–110.
doi: 10.1016/j.sjbs.2011.11.002.

AL-Haj H. 2010. **Optical laboratory preparations**, Massira Press, Amman, Jordan, P238.

Altuntas I, Delibas N, Demirci M, Kilinc I and Tamer N. 2002. The effects of methidathion on lipid peroxidation and some liver enzymes: role of vitamins E and C, Arch Toxicol, **76**: 470–473, Doi:10.1007/s00204-002-0359-1.

Asztalos B, Nemcsok J, Benedeczky I, Gabrie R, Szabo A and Refaie OJ. 1990. The effects of pesticides on some biochemical parameters of carp (*Cyprinus carpio L.*)., Arch Environ Contam Toxicol, **19**: 275-82, https://doi.org/10.1007/BF01056097.

Bharti S and Rasool F. 2021. Analysis of the biochemical and histopathological impact of a mild dose of commercial malathion on Channa punctatus (Bloch) fish. Toxicol Rep, **25(8),** 443-455. doi: 10.1016/j.toxrep.2021.02.018.

Bhattacharya S, Milk thistle seeds in health. In: Preedy VR, Watson RR. (Eds.). **Nuts and Seeds in Health and Disease Prevention.** 2nd Ed., London, San Diego: Academic Press (an imprint of Elsevier Inc.); 2020, p. 429-438.
DOI: 10.1016/B978-0-12-818553-7.00030-9.

Chemam Y, Benayache S, Marchioni E, Zhao M, Mosset P and Benayache F. 2017. On-line screening, isolation and identification of antioxidant compounds of *Helianthemum ruficomum*. Molecules, **22**: 239.

Choudhari PD and Chakraharti CH. 1984. Effect of acephate (Orthene), an organophosphorus insecticide, on lipid metabolism in albino rats. Indian J Exp Biol, **22**: 45-49.

Cortés-Iza SC, Rodríguez AI. 2018. Oxidative Stress and Pesticide Disease: A Challenge for Toxicology. Rev. Fac. Med, https://doi.org/10.15446/revfacmed.v66n2.60783.

Csupor D, Csorba A and Hohmann J. 2016. Recent advances in the analysis of flavonolignans of *Silybum marianum*. J Pharm Biomed Anal. **130**: 301–317.

Curioni A, Garcia M, Alfonso W and Arizio O. 2002. Milk thistle harvest prediction through the external characteristics of the heads. Acta Hortic, **569**, 257–261.

Deep G, Agarwal R, Kroll DJ and Agarwal C. 2006. Silymarin and silibinin cause G1 and G2-M cell cycle arrest via distinct circuitries in human prostate cancer PC3 cells: a comparison of flavanone silibinin with flavanolignan mixture silymarin. Oncogene. 16;**25(7):**1053-69. doi: 10.1038/sj.onc.1209146.

De Vos RCH, Moco S, Lommen A, Keurentjes JJB, Bino RJ and Hall RD, 2007. Untargeted large-scale plant metabolomics using liquidchromatography coupled to mass spectrometry. Nat Protoc. **2(4),** 778–791.

Farah A, Monteiro M, Donangelo CM and Lafay S. 2008. Chlorogenic acids from green coffee extract are highly bioavailable in humans. J Nutr, 138(12): 2309-2315.

Fernandes LS, Emerick GL, Santos NA, de Paula ES, Barbosa FBF, Jr and Santos AC. 2015. In vitro study of the neuropathic potential of the organophosphorus compounds trichlorfon and acephate. Toxicol In Vitro, **29**, 522–528. 10.1016/j.tiv.2015.01.001

Flaherty C, Moore K and Hetrick J. 2009. Risks of Methidathion Use to Federally Threatened California Red-legged Frog - Pesticide Effects Determination. Environmental Fate and Effects Division Office of Pesticide Programs Washington, D.C. 20460.

FAO. 2020. The State of World Fisheries and Aquaculture 2020.Sustainability in action. Rome.
https://doi.org/10.4060/ca9229en.

Fukunaga T, Kajikawa I, Nishiya K, Takeya K and Itokawa H. 1989. Studies on the constituents of the Japanese mistletoe, *Viscum album* L. var. coloratum Ohwi grown on different host trees. Chem Pharm Bull. **37(5):** 1300–1303.

Ghosh D, and Saha SK. 2022. Determination of the Lethal Concentration 50% (LC_{50}) of Hexavalent Chromium in Nile Tilapia (Oreochromis niloticus). Advances in Zoology and Botany. **10(4),** 123-131.

Halliwell B and Gutteridge JM. 2015. **Free Radicals in Biology and Medicine**. Oxford University Press.

Huang CB, Alimova Y, Myers TM and Ebersole JL. 2011. Short- and medium-chain fatty acids exhibit antimicrobial activity for oral microorganisms. Arch Oral Biol. **56(7):** 650–654.

Lommen, A., and Kools, HJ, (2012). MetAlign 3.0: Performance enhancement by efficient use of advances in computer hardware. Metabolomics : Metabolomics. **8(4),** 719–726.

Ibrahim NA and El-Gamal BA. 2003. Effect of Diazinon, an Organophosphate Insecticide, on Plasma Lipid Constituents in Experimental Animals. J. Biochem. Mol. Biol**. 36(5),** 499-504.

International Guiding Principles for Biomedical Research Involving Animals issued by CIOMS. 1986. Veterinary Quarterly, **8**:4 350-352, DOI:10.1080/01652176.1986.9694068.

Ito F, Sono Y and Ito T. 2019. Measurement and Clinical Significance of Lipid Peroxidation as a Biomarker of Oxidative Stress: Oxidative Stress in Diabetes, Atherosclerosis, and Chronic Inflammation. Antioxidants. **8(3):** 72.

Jee JH, Masroor F and Kang JC. 2005. Responses of cypermethrin-induced stress in haematological parameters of Korean rockfish, Sebastes schlegeli (Hilgendorf). Aquac Res. **36(9):**898–905.

Gowda S, Desai PB, Hull VV, Math AA, Vernekar SN and Kulkarni SS. 2009. A review on laboratory liver function tests. Pan Afr Med J, 22;**3**:17.

Jeon SM, Park YB and Choi MS. 2004. Antihypercholesterolaemic property of naringin alters plasma and tissue lipids, cholesterol-regulating enzymes, fecal sterol and tissue morphology in rabbits.Clin Nutr, **23**: 1025-1034.

Jos A, Repetto D, Rios JC, Hazen MJ, Molero ML, Peso A, Salguero M, Ferna´ndez-Freire P, Pe´rez-Martı´n JM and Camea´n A. 2003. Ecotoxicological evaluation of carbamazepine using six different model systems with eighteen endpoints. Toxicol In Vitro, **17**, 525–532.

Juárez ZN, Fortuna AM, Sánchez-Arreola E, López-Olguín JF, Bach H and Hernández LR. 2014. Antifeedant and phagostimulant activity of extracts and pure compounds from *Hymenoxys robusta* on *Spodoptera exigua* (Lepidoptera: Noctuidae) Larvae. Nat Prod Commun, **9(7):** 895-8.

Karami-Mohajeri S, Ahmadipour A, Rahimi H and Abdollahi M. 2017. Adverse effects of organophosphorus pesticides on the liver: a brief summary of four decades of research. Arh Hig Rada Toksikol, **68**,261-275.

Karim N, Jia Z, Zheng X, Cui S and Chen W. 2018. A recent review of citrus flavanone naringenin on metabolic diseases and its potential sources for high yield-production. Trends Food Sci Technol, **79**: 35–54.

Khan J, Deb PK, Priya S, Medina KD, Devi R, Walode SG, and Rudrapal M. 2021. Dietary Flavonoids: Cardioprotective Potential with Antioxidant Effects and Their Pharmacokinetic, Toxicological and Therapeutic Concerns. Molecules. **26**, 4021. 10.3390/molecules26134021

Klein R, Nagy O, Tóthová C and Chovanová F. 2020. Clinical and Diagnostic Significance of Lactate Dehydrogenase and Its Isoenzymes in Animals. Vet Med Int. ID 5346483, https://doi.org/10.1155/2020/5346483

Kumar S and Pandey AK. 2013. Chemistry and biological activities of flavonoids: An overview. Scientific World Journal, 1, 16. doi: 10.1155/2013/162750.

Lee S, Najiah M, Wendy W and Nadirah M. 2009. Chemical composition and antimicrobial activity of the essential oil of *Syzygium aromaticum* flower bud (clove) against fish systemic bacteria isolated from aquaculture sites, Front Agric China, **3**: 332–336, https://doi.org/10.1007/s11703-009-0052-8.

Lu J, Zhang M, and Lu L. 2018. Tissue Metabolism, Hematotoxicity, and Hepatotoxicity of Trichlorfon in Carassius auratus gibelio After a Single Oral Administration. Front Physiol, 23, **9**: 551. doi: 10.3389/fphys.2018.00551.

Mahima A, Rahal R, Deb SK, Latheef H, Abdulsamad R, Tiwari AK, Verma A, Kumar K and Dhama. 2012. Immunomodulatory and therapeutic potentials of herbal, traditional / indigenous and ethnoveterinary medicines, Pak J Biol Sci, **15**: 754-774, DOI: 10.3923/pjbs.2012.754.774

Mali H, Shah C, Raghunandan B, Prajapati AS, Patel DH, Trivedi U and Subramanian R. 2023. Organophosphate pesticides an emerging environmental contaminant: Pollution, toxicity, bioremediation progress, and remaining challenges. J. Environ. Sci. **127**, 234-250.

Martemucci G, Costagliola C, Mariano M, D'andrea L, Napolitano P, D'Alessandro AG. 2022. Free Radical Properties, Source and Targets, Antioxidant Consumption and Health. Oxygen. **2(2):**48-78.

Martinez-Alvarez RM, Morales AE and Sanz A. 2005. Antioxidant Defenses in Fish: Biotic and Abiotic Factors. Rev Fish Biol Fish, **15**, 75–88. doi: 10.1007/s11160-005-7846-4.

Modesto KA and Martinez CB. 2010. Roundup causes oxidative stress in liver and inhibits acetylcholinesterase in muscle and brain of the fish Prochilodus lineatus. Chemosphere, **78**, 294–299.

Mohamad Nek Rahimi NN, Natrah I, Loh Y, Ervin Ranzil FK, Gina M, Lim HE, Lai S and Chong M. 2022. Phytocompounds as an Alternative Antimicrobial Approach in Aquaculture. Antibiotics. 11(4).

Muro E, Ekin Atilla-Gokcumen G, Eggert US and Bement W. 2014. Lipids in cell biology: how can we understand them better?. MBoC. DOI:10.1091/mbc.E13-09-0516.

Narvaez-Mastache JM, Novillo F and Delgado G. 2008. Antioxidant arylprenylcoumarin, flavan-3-ols and flavonoids from *Eysenhardtia subcoriacea*. Phytochemistry, **69**: 451–456.

Nicolas B, Robert HL, Miled B, Mark WD, Philip BG and Ann MM. 2015. Alpha-Linolenic Acid: An omega-3 fatty acid with neuroprotective properties ready for use in the stroke clinic. Biomed Res Int. https://doi.org/10.1155/2015/519830.

Nipa G, Shikta R and Anindita C. 2021. A Review on Medicinal Plants and Immune Status of Fish. Egypt J Aquat Biol Fish. **25(2),** 897 – 912.

Orrenius S, Nicotera P and Zhivotovsky B. 2011. Cell Death Mechanisms and Their Implications in Toxicology. Toxicological Toxicol. Sci. **119(1),** 3–19.

Oruc E. 2011. Effects of diazinon on antioxidant defense system and lipid peroxidation in the liver of *Cyprinus carpio* (L.). Environ. Toxicol, **26(6),** 571-8. doi: 10.1002/tox.20573.

Özkan-Yilmaz F, Hunt A, Gül Gündüz S, Berkoz M, Yalin S and Sahin, N, 2015. Effects of methidathion on antioxidant system and expression of heat shock protein 70 (HSP70) gene in the liver of *Oreochromis niloticus* L. 1758. Fresenius Environ Bull. 24, 2650-2658.

Pan J, Yuan C, Lin C, Jia Z and Zheng R. 2003. Pharmacological activities and mechanisms of natural phenylpropanoid glycosides. Pharmazie. **58**: 767–775.

Panche AN, Diwan AD and Chandra SR. 2016. Flavonoids: an overview. J Nutr Sci., 5, e47. doi: 10.1017/jns.2016.41.

Petitjean Q, Jean S, Gandar A, Côte J, Laffaille P and Jacquin L. 2019. Stress responses in fish: From molecular to evolutionary processes. Sci. Total Environ. 684,371 - 380. ff10.1016/j.scitotenv.2019.05.357ff.

Ponnampalam EN, Kiani A, Santhiravel S, Holman BWB, Lauridsen C and Dunshea FR. 2022. The Importance of Dietary Antioxidants on Oxidative Stress, Meat and Milk Production, and Their Preservative Aspects in Farm Animals: Antioxidant Action, Animal Health, and Product Quality—Invited Review. Animals. **12(23),** 3279.

Rad SM, Ray AK and Barghi S. 2022. Water Pollution and Agriculture Pesticide. Clean Technol. **4(4):**1088-1102.

Ramesh M, Sankaran M, Veera-Gowtham V and Poopal RK. 2014. Hematological, biochemical and enzymological responses in an Indian major carp *Labeo rohita* induced by sublethal concentration of waterborne selenite exposure. Chem Biol Interact. **207**: 67–73, http://dx.doi.org/10.1016/j.cbi.2013.10.018.

Reina M and Martínez A. 2015. Silybin and 2,3-Dehydrosilybin Flavonolignans as Free Radical Scavengers. J Phys Chem B, **119(35):** 11597–11606.

Reverter m, Tapissier-bontemps N, Lecchini D, Banaigs B and Sasal P. 2014. Use of plant extracts in fish aquaculture as an alternative to chemotherapy: Current status and future perspectives. Aquaculture. **433**, 50–61. 10.1016/j.aquaculture.2014.05.048. OK

Rizzato G, Scalabrin E, Radaelli M, Capodaglio G and Piccolo O. 2017., A new exploration of licorice metabolome. Food chemistry, **221**: 959–968.

Ryhanen R, Herranen J, Karhonen K, Penttila I, Popvilanpi M and Puhakainen E. 1984. Relationship between serum lipids, lipoproteins and pseudocholinesterase during organophosphate poisoning in rabbits. Int J Biochem, **16**: 687-690.

Samanta P, Pal S, Mukherjee AK and Ghosh AR. 2014. Evaluation of metabolic enzymes in response to Excel Mera 71, a glyphosate-based herbicide, and recovery pattern in freshwater teleostean fishes. Biomed Res Int, 425159. doi: 10.1155/2014/425159.

Sandoval-Herrera N, Mena F, Espinoza M and Romero A. 2019. Neurotoxicity of organophosphate pesticides could reduce the ability of fish to escape predation under low doses of exposure. Sci Rep, 19, **9(1):**10530. doi: 10.1038/s41598-019-46804-6.

Saravanan M, Karthika S, Malarvizhi A and Ramesh M. 2011. Ecotoxicological impacts of clofibric acid and diclofenac in common carp (*Cyprinus carpio*) fingerlings: hematological, biochemical, ionoregulatory and enzymological responses, J Hazard Mater, **195**: 188–194, doi: 10.1016/j.jhazmat.2011.08.029.

Saravanan M, Usha Devi K, Malarvizhi A and Ramesh M. 2012. Effects of Ibuprofen on hematological, biochemical and enzymological parameters of blood in an Indian major carp, *Cirrhinus mrigala*, Environ Toxicol Pharmacol, **34**: 14–22, http://dx.doi.org/10.1016/j.etap.2012.02.005.

Scalabrin E, Radaelli M, Rizzato G, Bogani P, Buiatti M, Gambaro A and Capodaglio G. 2015. Metabolomic analysis of wild and transgenic Nicotiana langsdorffii plants exposed to abiotic stresses: Unraveling metabolic responses. Anal Bioanal Chem. **407**: 6357-6368.

Shakoori AR, Ali SS and Saleem MA. 1988. Effects of six months feeding of cypermethrin on the blood and liver of albino rats. J Biochem Toxicol, **3**: 59-72.

Sies H and Jones DP. 2020. Reactive Oxygen Species (ROS) as Pleiotropic Physiological Signalling Agents. Nat Rev Mol Cell Biol. **21(7),** 363-383.

Song C, Sun C, Liu B and Xu P. 2023. Oxidative Stress in Aquatic Organisms. Antioxidants. **12(6):**1223.

Suksamrarn A, Chotipong A, Suavansri T, Boongird S, Timsuksai P, Vimuttipong S and Chuaynugul A, 2004. Antimycobacterial activity and cytotoxicity of flavonoids from the flowers of Chromolaena odorata. Arch Pharm Res. **27**: 507-11.

Sule RO, Condon L and Gomes AV. 2022. A Common Feature of Pesticides: Oxidative Stress-The Role of Oxidative Stress in Pesticide-Induced Toxicity. Oxid Med Cell Longev. **19**, 2022:5563759. doi: 10.1155/2022/5563759.

Sumner LW, Amberg A, Barrett D, Beale MH, Beger R, Daykin CA, Fan TWM, Fiehn O, Goodacre R, Griffin JL, Hankemeier T, Hardy N, Harnly J, Higashi R, Kopka J, Lane AN, Lindon JC, Marriott P, Nicholls AW, Reily MD, ThadenJJ and Viant MR. 2007. Proposed minimum reporting standards for chemical analysis. Metabolomics, **3**: 211–221. doi:10.1007/s11306-007-0082-2.

Sunderam RM, Patra RW, Julli M and Warne J. 2004. Use of the Up-and-Down Acute Toxicity Test Procedure to Generate LC50 Data for Fish. Bull Environ Contam Toxicol, **72**, 873–880.

Surai PF. 2015. Silymarin as a Natural Antioxidant: An Overview of the Current Evidence and Perspectives. Antioxidants. **5(4),** 43.

Tadese DA, Song C, Sun C, Liu B, Liu B, Zhou Q, Xu P, Ge X, Liu M, Xu X, Tamiru M, Zhou Z, Lakew A and Kevin NT. 2022. The role of currently used medicinal plants in aquaculture and their action mechanisms: A review. Rev Aquac. **14(2),** 816-847.

Trachootham D, Lu W, Ogasawara MA, Valle NR and Huang P. 2008. Redox regulation of cell survival. Antioxid Redox Signal, 10: 1343–1374, DOI: 10.1089/ars.2007.1957.

Tikunov YM, Laptenok S, Hall RD, Bovy A and De Vos RCH, 2012. MSClust: A tool for unsupervised mass spectra extraction of chromatography mass spectrometry ion-wise aligned data. Metabolomics. **8(4),** 714–718.

Tiwari S, and Singh A. 2004. Piscicidal activity of alcoholic extract of *Nerium indicum* leaf and their biochemical stress response on fish metabolism. Afr J Tradit Complement Altern Med, 1:15-29.

Tsai YH and Lein PJ. 2021. Mechanisms of organophosphate neurotoxicity. Curr Opin Toxicol, **26**, 49-60. doi: 10.1016/j.cotox.2021.04.002.

Tsikas D. 2017. Assessment of lipid peroxidation by measuring malondialdehyde (MDA) and relatives in biological samples: Analytical and biological challenges. Anal Biochem. 1, **524**:13-30.

Tudi M, Daniel Ruan H, Wang L, Lyu J, Sadler R, Connell D, Chu C and Phung DT. 2021. Agriculture Development, Pesticide Application and Its Impact on the Environment. International Int J Environ Res Public Health. **18(3):**1112.

Ullah A, Munir S, Badshah SL, Khan N, Ghani L, Poulson BG, Emwas AH and Jaremko M. 2020. Important Flavonoids and Their Role as a Therapeutic Agent. Molecules., **25(22),** 5243. doi: 10.3390/molecules25225243.

Vasantharaja D, Ramalingam V and Aadinaath Reddy G. 2015. Oral toxic exposure of titanium dioxide nanoparticles on serum biochemical changes in adult male Wistar rats. Nanomed J, **2(1):** 46-53.

Wahsha m, Al-Zibdah M, Al-Jawasreh R and Wahsheh H, 2023. Harnessing Garlic Extract and AI for Sustainable Disease Mitigation in Aquaculture. J Adv Zool. 44, S-5, 133-141.

Wahsha M and. Al-Jassabi S. 2009. The role of silymarin in the protection of mice liver damage dgainst microcystin- LR toxicity, Jordan J Biol Sci, **2**: 63-68.

Wahsha M, Al-Omari A, Hassan M, Abuadas FA, Ahmed ET, Mostafavi K, Moradi M and Ghotbi M. 2012. Protective action of flavonoids extracted from different Jordanian plants against oxidative stress, IJBPR, **3**: 450-456.

Wahsha M, Juhmani AS, Buosi A, Sfriso A and Sfriso A. 2017. Assess the environmental health status of macrophyte ecosystems using an oxidative stress biomarker. Case studies: The Gulf of Aqaba and the Lagoon of Venice. Energy Procedia, **125**, 19-26.

Wang HS, Gan DH, Zhang ZP and Pan YM. 2010. Antioxidant capacity of the extracts from pulp of *Osmanthus fragrans* and its components. LWT-Food Science and Technology. **43(2010),** 319–325.

Webb C,J, Sykes W,R and Garnock-Jones, P,J, 1988. **Flora of New Zealand Vol IV: Naturalised Pteridophytes, Gymnosperms, Dicotyledons. Christchurch, New Zealand: Botany Division**, Department of Scientific and Industrial Research.

Wilson Magdy B, El-sayed Mohamed F, Seleem Amin A and Sarhan Rana S. 2016. Ameliorative effect of antioxidants (vitamins C and E) against abamectin toxicity in liver, kidney and testis of male albino rats. J Basic Appl Zool. **77**, 69-82.

Wu H, Liu J, Zhang R, Zhang J, Guo Y and Ma E. 2011. Biochemical effects of acute phoxim administration on antioxidant system and acethylcholinesterase in *Oxya chinensis* (Thunberg) (Orthoptera: Acrididae). Pestic Biochem Physiol, **100**: 23-26.

Xavier Martins R, Vieira L, Ribeiro Souza J, Flor Silva M, Silva Muniz M, Souza T, Queiroga F, Ferreira Machado M, Silva B and Farias D. 2021. Exposure to 2,4-D herbicide induces hepatotoxicity in zebrafish larvae. Comp Biochem Physiol C Toxicol Pharmacol. **248**, 109110.

Yang C, Lim W and Song G. 2020. Mediation of oxidative stress toxicity induced by pyrethroid pesticides in fish. Comp Biochem Physiol C Toxicol Pharmacol, **234**, 108758.

Yeshi K, Crayn D, Ritmejerytė E and Wangchuk P. 2022. Plant Secondary Metabolites Produced in Response to Abiotic Stresses Has Potential Application in Pharmaceutical Product Development. Molecules. 5, **27(1),** 313.

Zhang BC, Zhang CW, Wang C, Pan DF, Xu TD and Li DY. 2016. Luteolin attenuates foam cell formation and apoptosis in Ox-LDL-stimulated macrophages by enhancing autophagy. Cell Physiol Biochem, **39**: 2065–2076.

Zheng CJ, Yoo JS, Lee TJ, Cho HY, Kim YH and Kim WG. 2005. Fatty acid synthesis is a target for antibacterial activity of unsaturated fatty acids. FEBS Letters, **579(23):** 5157–5162.

JJBS

Volume 17, Number 3,September 2024
ISSN 1995-6673
Pages 453 – 462
https://doi.org/10.54319/jjbs/170307

Jordan Journal of Biological Sciences

Anti Ovarian and Cervical Cancer Potential of *Tamarindus Indica* Leaf Ethanol Crude Extract and Its Bioactive Fraction, Apigenin

Shirisha Rao and Varalakshmi Kilingar Nadumane*

Department of Biotechnology, Center for Research in Pure and Applied Sciences, School of Sciences, Jain (Deemed to be University), Bangalore, 560027.

Received: July 7, 2023; Revised: November 14, 2023; Accepted: November 22, 2023

Abstract

Cervical and ovarian cancers account for the majority of deaths among women. Due to the failure of conventional therapies to completely cure these diseases, research has shifted focus to traditional and plant-based medicines. This study aimed to assess the potential anticancer activity of tamarind leaf extract on ovarian cancer PA-1 and cervical cancer HeLa cell lines. The extract was prepared using Soxhlet equipment with ethanol as the solvent and fractionated using Thin Layer Chromatography (TLC) under bioassay guidance. Anticancer activity was determined through *in vitro* tests, including MTT assay, fluorescence microscopy, trypan blue assay, LDH activity assay, caspase-9 activity assay, analysis of DNA fragmentation, Annexin V/PI staining and flow cytometry. Bioactive compound characterization was performed using gas chromatography-mass spectrometry (GC-MS) followed by NIST library search, to understand the underlying principles behind the anticancer attributes of tamarind leaf. The results revealed that treatment with tamarind leaf ethanol extract drastically reduced HeLa and PA-1 cell viabilities to 26.8% and 11.9%, respectively, after 72 hours. The yellow fraction (TLYF) of the extract was identified as the bioactive component through bioassay-guided fractionation. Trypan blue assay results showed cell concentrations reduced to 1.3×10^5 and 1.2×10^5 cells/mL compared to about 3.6×10^5 cells/mL in control HeLa and PA-1 cells. Cell cycle analysis demonstrated that TLYF reduced overall cell count, with a significant decrease in S and G2/M phases, and increased percentage of cells (50.9 and 18.8%) in early and late apoptotic stages as per annexin V/PI staining. Caspase assay confirmed apoptosis initiation through caspase-9 activation in cancer cells induced by TLYF. According to GC-MS data, apigenin, an anticancer compound reported in several fruits, was found in tamarind leaf. It can be assumed that apigenin in tamarind leaf might be the reason for its profound antiproliferative effects against cancer cells.

Keywords: Anticancer, apoptosis, caspase 9 activation, cell cycle, tamarind leaf, yellow fraction.

1. Introduction

Despite the availability of contemporary therapeutic options, cancer is one of the most feared diseases due to the high mortality rate linked with it (Jeong et al., 2009; Garg et al., 2015). Cervical cancer is the foremost reason for deaths due to cancer in several countries including India, sub-Saharan Africa, and Latin America (Sung et al., 2021; Arbyn et al., 2018). Inflammation is a key factor in the development of cancer, and the presence of an inflammatory response is a prominent characteristic of cancer (Hanahan and Weinberg, 2011). Research indicates that persistent inflammation can heighten the likelihood of cancer. Additionally, inflammation is significantly involved in the process leading to cervical cancer, besides the infection with human papilloma virus (HPV) (Wei et al., 2022). Chemotherapy plays a crucial role in the conventional treatment of cervical cancer and is usually given as an adjuvant therapy after surgery or in combination with radiotherapy. Cisplatin, a platinum-based drug, has been the most effective single-agent treatment for cervical cancer over the past thirty years (Tewari and Monk, 2005). Despite its initial effectiveness, patients often develop resistance to cisplatin during treatment. Therefore, it is vital to explore and create new and better therapies to address the issue of multidrug resistance in cancer cells, as this resistance significantly affects the success of chemotherapy. Recently, Complementary and Alternative Medicine (CAM) as therapeutic options are adopted more often to treat cancer, besides modern allopathic drugs and biological therapies in order to reduce the side effects of chemotherapy, which is known as integrative oncology. By all means, the less invasive therapeutic options with the use of natural compounds wherever possible are better to manage cancer ideally (Chizenga and Abrahamse, 2021). Therefore, during the past few decades, research on cutting-edge, better, and tumor-specific treatments has accelerated. Several nutritional and medicinal plants have so far contributed numerous anticancer compounds to this cause (Patel et al., 2010; Dev et al., 1999; Faridi et al., 2023).

The tamarind, or *Tamarindus indica* L., is an important dietary plant, with most of its parts, like the bark, leaves, seed pulp and seeds, having one or the other nutritional or medicinal property (Kumar and Bhattacharya, 2008). Its origins can be traced to the old tribal people who made decoctions of the components and utilised them as

* Corresponding author. e-mail: kn.varalakshmi@jainuniversity.ac.in; namavarapusiri@yahoo.com.

medicines. To treat wounds, the leaves and bark of tamarind tree was used in West and East Africa, as per a report (Havinga et al., 2010). Fruit and leaves possess laxative properties; dried seed paste was used to repair broken bones, and the bark, and leaf decoction was used to treat jaundice (El-Siddig et al., 2006; Vaidyanathan et al., 2013; Caluwe et al., 2010). According to certain reports, the tamarind tree's bark has analgesic, anti-inflammatory, and wound-healing qualities (Irvine et al., 1961; Morton, 1987).

Macerated fresh bark of tender twig was used in West Africa as a purgative and a remedy for stomach pain (Bhat et al., 1990). In a previous study, the anticancer potential of tamarind bark dichloromethane extract was reported on cervical and ovarian cancer cell lines, where cantharidin was identified as the bioactive component (Rao and Varalakshmi, 2016). The anti-inflammatory properties of the seeds, bark, leaves, and other parts of *T. indica* have been reported in traditional medicine and Ayurvedic medicine, and by some researchers (Havinga et al., 2010; Kuru, 2014). The anticancer activity of tamarind bark and seeds was also reported. However, the anticancer efficacy of the leaves of the tamarind plant has not been scientifically investigated, despite its anti-inflammatory property and the established causal relationship between inflammation and cancer. In this present study, due to the medicinal properties of tamarind leaves (along with their traditional use for treating inflammation, pain, and wounds), we focused on scientifically investigating and validating the anticancer efficacy of tamarind leaf ethanol extract, characterizing the bioactive principle, and evaluating its anticancer mechanism on in vitro ovarian and cervical cancer cell lines.

2. Materials and Methods

2.1. Cell Lines

The National Centre for Cell Sciences (NCCS) in Pune, India, provided the ovarian cancer (PA-1), and cervical cancer (HeLa) cell lines. The media used to culture HeLa cells was Dulbecco's Modified Essential Medium (DMEM from HIMEDIA, India), while Minimum Essential Medium with 10% foetal bovine serum was used to culture PA-1 cell line. Cell lines were used in the investigations of the study during the linear phase of growth, and were kept for up to passage 20. The anticancer experiments were conducted using both these cancer cell lines.

2.2. Lymphocyte isolation

Lymphocytes were extracted from the blood of five healthy individuals, both male and female, aged approximately 20 years. These individuals were visibly unaffected by pathogenic infections and had not undergone any medical treatments in the preceding six months. Blood collection process adhered to the ethical guidelines established by the Indian Council of Medical Research for research purposes (ICMR, 2006). The isolation process employed HiSep medium (HIMEDIA, India). The cells were then suspended in complete RPMI 1640 medium, which was enriched with 10% Fetal Bovine Serum (HIMEDIA, India) and 5 g ml−1 phytohemagglutinin (PHA). Subsequently, the lymphocytes were cultured at 37°C in a 5% CO2 humidified incubator. These lymphocytes served as normal control cells for evaluating the cytotoxicity of the plant extracts.

2.3. Crude Extract Preparation and Cytotoxicity Screening

Tamarind leaves were harvested in Bengaluru, inside the campus of Indian Institute of Science, and the plant sample was identified by Prof. Shivakumar Swamy, a Botanist and Adjunct Professor at Jain University, Bangalore. For future reference, the specimen samples of the tamarind plant were stored in the Jain University herbarium (voucher no. JUH-34). The leaves were dried under shade conditions. In order to isolate the metabolites from the leaf samples (50 gm), ethanol solvent was used and extracted in a Soxhlet apparatus (Hayashi et al., 1998). The extracted material was concentrated with the help of a rotary evaporator and was kept at 4ºC until further usage. Dimethyl sulphoxide (DMSO) was used to make the stock solution (at 1 mg/mL concentration), which was further diluted to the required quantities using phosphate buffered saline (PBS).

2.4. Assay of cytotoxicity (MTT)

The cytotoxic impact of tamarind leaf extract on cancer cell lines was evaluated using the MTT [3- (4,5-dimethylthiazol-2yl)-2,5-diphenyl tetrazolium bromide] test (Mosmann, 1983). In 96-well microplates, 2×10^4 cells per well were seeded and incubated for 24 hours at 37°C. From the stock solution (1000 µg/ml) of tamarind leaf ethanol extract serial dilutions were made, and the sample was added in various concentrations (1, 10, 50 and 100 µg/ml). Simultaneously, as a positive control the cancer drug, camptothecin was used at 5 and 10 µg/ml concentrations. The microplates were then incubated for an additional 24, 48, and 72 hours. 20 µl of MTT was added after the predetermined amount of incubation time and incubated for 3 hours in the dark. After three hours, 200 µl of DMSO was added to each well, and an ELISA plate reader (LISA Plus, Aspen Diagnostics, India) was used to measure the absorbance at 540 nm. Utilising the following formula, the % viability was calculated:

$$\text{Viability (\%)} = (\text{ODs}/\text{ OD}) \times 100$$

With, OD being Optical Density of the control, and ODs is the Optical Density of the sample.

2.5. Calculation of IC_{50} value

The IC_{50} values of the samples (tamarind leaf ethanol extract and its bioactive fraction) were determined from the dose response curves obtained after MTT results, through the application of the four parameter logistics (4PL) equation, a statistical model frequently employed for fitting sigmoidal curves (AAT Bioquest, Inc., 2023).

2.6. Thin Layer Chromatographic (TLC) separation of crude extract

Identification of the bioactive compound from the crude extract of tamarind leaf was done through bioassay guided fractionation using TLC sheets. Merck Specialties Private Limited in Mumbai provided the TLC plate (TLC Silica Gel 60 F 254). The optimal solvent combination was utilised to separate the fractions from tamarind leaf extract after trying various solvent combinations with various concentrations (Ciesla and Hajnos, 2010). By using preparative TLC, the fractions were collected, then dried

after being dissolved in methanol. The dried fractions underwent another MTT assay test for cytotoxicity, and the fraction showing maximum cytotoxicity was chosen for further studies.

2.7. Assessment of fragmentation of DNA

In 25cm^2 roux culture flasks, PA-1 and HeLa cells (2×10^4 cells/ml) were cultivated for 24 hours. The bioactive fraction from tamarind leaf (TLYF) was added at 10 µg/ml concentration, and afterwards the period of incubation was for 48 hours. Untreated cells were used as the negative controls. After 48 hours of treatment, cells were harvested by trypsinizing, followed by centrifuging, and the cells thus precipitated were lysed using a solution having 10mM Tris HCl, 10mM EDTA, and 0.5% Triton X-100. Afterwards, addition of 200 µg/ml of proteinase K and 200 µg/ml of RNAse was followed, to prevent contamination with RNA and proteins (DNA isolation kit, Bangalore Genei). The DNA was then precipitated by adding ice-cold ethanol and suspended in a Tris-EDTA solution. The DNA samples stained with ethidium bromide were loaded into the wells of 0.8% agarose gel, and electrophoresed at 50v, till the samples reached almost 3/4th of the gel. The samples were visualised using a UV Trans illuminator and were photographed (Lee and Shacter, 1999).

2.8. Cell count by trypan blue staining method

Using phosphate buffer (PBS), trypan blue stain was prepared (at 0.4% concentration). About 500 µl of this stain and 500 µl of PA-1 and HeLa cells were mixed thoroughly to avoid clump formation and allowed to stand for about 5 minutes. This sample (20µl) was loaded on the sample induction point on both sides of the chamber of a haemocytometer, and cells were counted with the help of a binocular microscope (Labomed, India).

2.9. Fluorescence Microscopy

TLYF (10µg/ml) was treated to the cancer cells, PA-1 and HeLa, for 24 hours along with the simultaneous maintenance of untreated controls. The control and treatment cells were collected separately and were stained using a 1:1 mixture of acridine orange (100µg/ml) and ethidium bromide (100µg/ml). The stained cells, after mounting on glass slides, were examined using a fluorescence microscope (Thermoscientific) (Roy et al., 2008).

2.10. Assay of Caspase 9 enzyme

Caspase 9 apoptosis assay kit (G-Biosciences, Missouri, USA) was used in accordance with the manufacturer's instructions to carry out the experiment. Along with untreated controls, cervical and ovarian cancer cells were given a 24 hour treatment with TLYF at a concentration of 5 µg/mL. Cells were harvested by trypsinization after 24 hours and then lysed with 50 µl of lysis buffer. To ensure that the cells were evenly suspended in PBS solution, the lysed cells were thawed and frozen thrice. Later, this solution was centrifuged, and the supernatant was collected. The lysate was mixed with 50 µl of 1M DTT (dithiothreitol)-containing caspase assay buffer. AFC conjugated substrate (5 µl) was added, and the mixture was incubated at 37 °C for 2 hours. Using an ELISA plate reader, absorbance was measured once in every 15 minutes, at 405 nm. We calculated the percentage caspase activity as per the formula given below:

OD_{405} control/sample – OD_{405} blank / OD_{405} blank X 100

2.11. Propidium iodide (PI) and Annexin V staining based analysis through Flow cytometry

The most popular method for detecting apoptosis using a flow cytometer is through annexin V combined with propidium iodide (PI) staining (Dicker et al., 2005). This assay can be used to determine the cell population going through apoptosis, necrosis, as well as the population of viable cells. HeLa cells were cultured in a roux flask (1×10^6 cells/mL), and 24 hours later were again incubated for 24 hours post treatment with the TLYF. Later, the trypsinized cells were collected, labelled with PI and Annexin V staining, and examined with the help of a flow cytometer.

2.12. Characterization through Gas chromatography and Mass Spectrometry

Tamarind leaf's bioactive fraction (TLYF) was analysed using GC-MS. Thermo GC - Trace Ultra ver. 5.0 and a Thermo MS DSQ II mass spectrometer were used for the GC-MS analysis. A non-polar DB 5 - MS Capillary Standard column with dimensions of 30 mm x 0.25 mm and a film of 0.25 µm thickness, was employed. The carrier gas, helium gas with 1 mL/min of flow rate was employed. The 70°C initial temperature of the oven was raised slowly to 260°C following a steady pace with 6°C increase per minute. After injecting 1 µl of the material onto the column, mass spectra with a mass range of 50-650amu were produced. The resulting mass spectra were analysed with the mass spectra obtained through the NIST collection, and the compounds' structure and molecular weight were established (Belayachi et al., 2014).

2.13. Statistical Analysis

Each experiment was performed three times. Standard error (SE) values were determined for the outcomes. The one-way analysis of variance (ANOVA), and Dunnett's multiple comparison tests were used to determine the statistical significance. The results deemed significant were with p values <0.05.

3. Results

3.1. Cytotoxicity of tamarind leaf ethanol extract

When we treated HeLa cells with the ethanol extract of tamarind leaf, a significant reduction in cancer cell viability was observed, following a time- and dosage-dependent pattern. At concentrations of 1, 10, 50, and 100 µg/ml, the cell viabilities were 71.4%, 61.9%, 48.8%, and 35.9% respectively after 24 hours. When the exposure duration was extended to 72 hours, the viabilities further decreased to 53.6%, 41.4%, 31.7%, and 26.8% respectively (Figure 1a). Similar trends were observed in PA-1 cells. At 1.0 µg/ml concentration of tamarind leaf ethanol extract, the viability was 65.5%, at 5 µg/ml it was 58.6%, at 10 µg/ml it was 53.4%, and at 15 µg/ml it was 50% after 24 hours. After 72 hours, viability decreased as the treatment concentration increased (Figure 1c). All these results were statistically significant according to ANOVA (p values < 0.05 and < 0.001).

3.2. Fractionation by TLC and bioassay

Due to the potent cytotoxicity of tamarind leaf extract against cancer cells, the crude ethanol extract was fractionated using thin-layer chromatography with different solvents. Using a solvent mixture of toluene:ethyl acetate: formic acid in the ratio 2.5:1:1 (v/v), seven distinct fractions were separated from the tamarind leaf ethanol extract when observed under UV light (Figure 1e). The yellow fraction (TLYF) exhibited the highest cytotoxicity against cervical cancer HeLa and ovarian cancer PA-1 cells. This TLYF fraction reduced HeLa cell viability to 84.0%, 69.0%, 51.1%, and 42.8% at concentrations of 1, 10, 50, and 100 µg/ml respectively after 24 hours of treatment (Figure 1a, 1c). A similar trend was observed in PA-1 cell line. At concentrations of 1.0, 2.5, 5.0, and 7.5 µg/ml, cell viabilities were 67.2%, 53.4%, 50%, and 41.3% respectively after 24 hours of incubation. The lowest viability (11.9%) was observed 72 hours after treatment with a 5 µg/ml concentration of TLYF. TLYF exhibited a superior antiproliferative effect on both HeLa and PA-1 cells, comparable to that of Camptothecin, the positive control (Figure 1b). Neither the crude extract nor the TLYF showed any cytotoxic effects on normal lymphocytes (Figure 1d). The IC_{50} value of TLYF was determined as 10.45 µg/mL for HeLa and 4.3 µg/mL for PA-1 cell lines after 72 hours, very much nearing to the IC_{50} value of camptothecin, which is 3.7 µg/mL for both the cell lines (Table 1).

Table 1. IC_{50} Value of Tamarind leaf yellow fraction on HeLa and PA-1 cells

Bioactive fraction	IC_{50} Values (µg/ml)					
	HeLa			PA-1		
	24 hr	48 hr	72 hr	24 hr	48 hr	72 hr
TLYF	40.46	93.85	10.45	4.33	4.31	4.3
Camptothecin	3.92	3.23	3.67	3.9	3.19	3.7

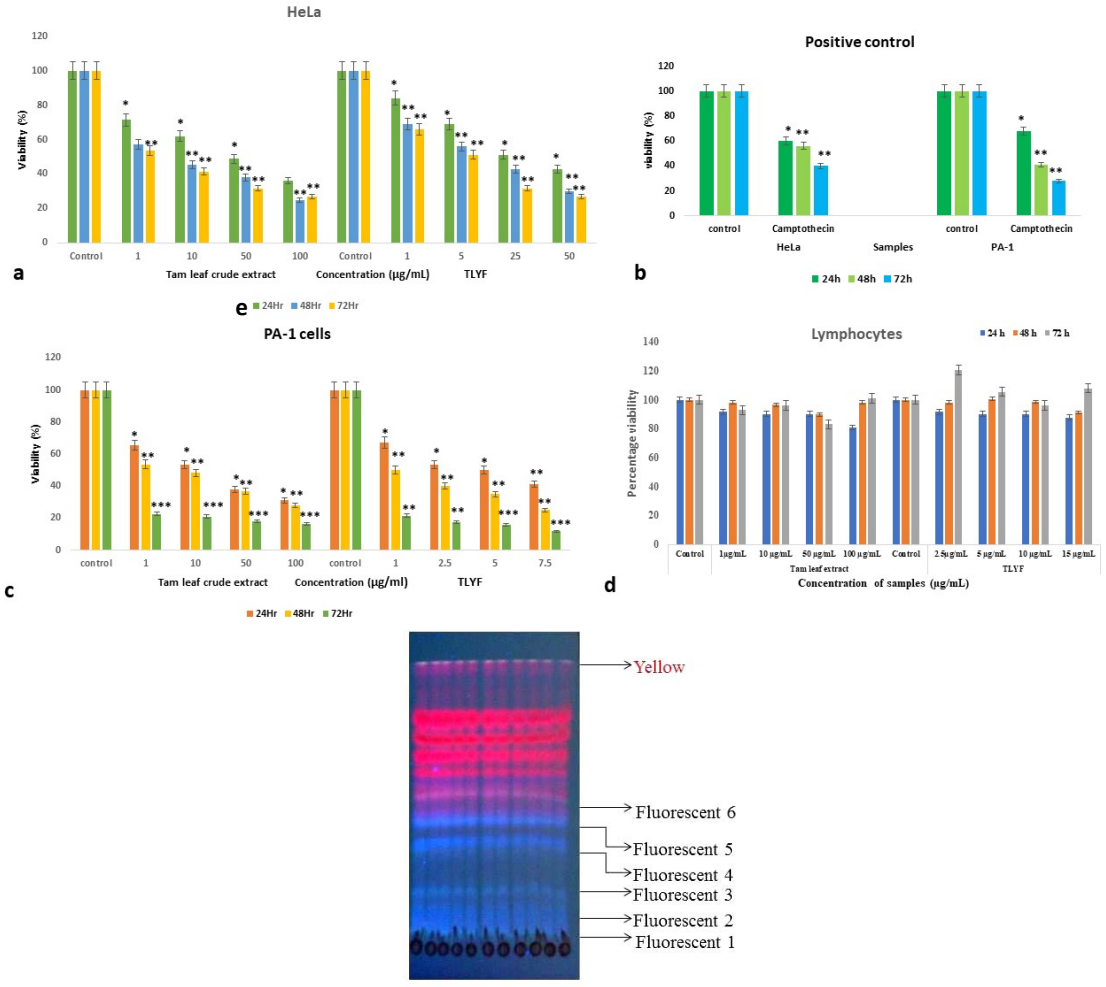

Figure 1: a) Effect of Tamarind leaf ethanol extract and TLYF on HeLa cells **b)** Effect of Camptothecin (10 µg/ml) on HeLa and PA-1 cells. **c)** Effect of Tamarind leaf ethanol extract and TLYF on PA-1 cell line. **d)** Effect of TL(et) and TLYF on lymphocytes. **e)** TLC chromatogram of tamarind leaf ethanol extract as observed under the UV light. Data represented as mean ± SE. Data were analyzed by one way ANOVA. * denotes significance at $p<0.05$, **denotes significance at $p<0.01$, *** significance at $p<0.001$

3.3. Cell Count Using Trypan Blue Dye Exclusion

Assessing total cell concentration through trypan blue staining is a traditional method wherein nonviable cells appear distinctly blue under the microscope. TLYF demonstrated effectiveness in reducing the viable cell count and viability of PA-1 and HeLa cancer cell lines. At

5 µg/ml of TLYF, the total cell count was 1.5×10^5 cells/mL for PA-1 and 1.6×10^5 cells/mL for HeLa, compared to the control counts of 3.6×10^5 cells/mL and 3.8×10^5 cells/mL respectively (Table 2). Similarly, at 10 µg/ml of TLYF, the total cell count was 1.2×10^5 cells/mL for PA-1 and 1.3×10^5 cells/mL for HeLa. These results were found to be statistically significant with $p<0.05$. The viable cell count decreased with increasing treatment concentrations.

Table 2. Total cell count of HeLa and PA-1 cell lines by trypan blue staining

Plant Extract	Concentration of the extract ((µg/ml)		Total Cell Count (cells/ml)		Percentage Viability of the cells (%)	
	HeLa	PA-1	HeLa	PA-1	HeLa	PA-1
Control	0.4% DMSO	0.4% DMSO	$3.8 \pm 0.5 \times10^5$	$3.6 \pm 0.45 \times10^5$	92.3	96.2
	5	5	$1.6 \pm 0.29 \times10^5$	$1.5 \pm 0.3 \times10^5$	43.5	49.6
TLYF	10	7.5	$1.3 \pm 0.27 \times10^5$	$1.2 \pm 0.28 \times10^5$	31.6	28.6

3.4. Fluorescence Microscopical observation

Because this particular fraction exhibited anti-proliferative effects in both cancer cell types, we aimed to investigate how it works by examining the appearance of cells under a fluorescence microscope. Our observations revealed that the treated cells underwent nuclear breakdown, unlike the control cells. The control cells emitted a vibrant green fluorescence, indicating that they were alive and had intact membranes, whereas the treated cells emitted a vivid orange fluorescence (Figure 3). These results have obviously proven that TLYF induced apoptotic changes in the cells.

3.5. Phytochemical screening

To identify the chemical groups in tamarind leaf crude extract and its active fraction TLYF, phytochemical screening was performed and the results are given in the Table 3. As we can see from the table, the yellow fraction from tamarind leaf indicated the presence of tannins and flavonoids.

Table 3. Phytochemical screening of the selected extracts and their bioactive fractions

TEST	TLE	TLYF
Alkaloids	+	-
Tannins	+	+
Flavonoids	+	+
Steroids	+	-
Terpenoid	+	-
Phenols	+	-
Glycosides	+	
Saponins	+	-

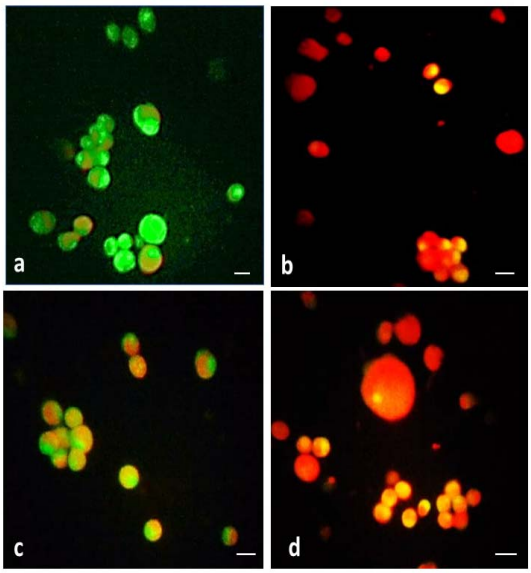

Figure 3: Fluorescence microscopic photographs of HeLa and PA-1 cells. **a**: untreated HeLa cells, **b**: TLYF treated HeLa cells, **c:** Control PA-1 cells, **b**: TLYF treated PA-1 cells. Scale bar: 20 µm. Magnification-100X.

3.6. Fragmentation of DNA Visualization by Agarose Gel

DNA fragmentation is a characteristic feature of cells undergoing apoptosis. The apoptotic potential of TLYF was evident from the DNA banding pattern observed during gel electrophoresis. Treated cells exhibited a smear of fragmented DNA when viewed under a UV transilluminator, whereas control cells showed intact DNA bands (Figure 4).

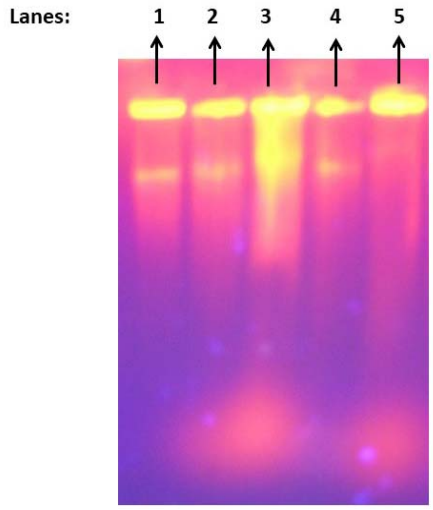

Figure 4: Analysis of DNA by gel electrophoresis in cancer cells treated with 5µg/ml of TLYF. **Lanes: 1 & 2**. DNA of untreated control HeLa cells, **3**. DNA of HeLa cells treated, **4**. DNA of untreated PA-1 cells. **5**. DNA of TLYF treated PA-1 cells.

3.7. LDH Release Assay

The release of LDH into the cytoplasm occurs as a consequence of damage due to apoptotic cell death or the cytotoxicity of the test compound. In cancer drug development and research, a test compound's activity can be determined by the LDH release assay in treated cancer cells, as it is a simple, reliable, and quick technique for estimating cell death. When HeLa cells were treated with TLYF at concentrations of 5 and 10 µg/mL, the percentage cytotoxicity was 39.5% and 53.7% respectively. Similarly, on PA-1 cells, the cytotoxicity percentages were 51.9% and 68.2% respectively (Figure 5). Thus, the bioactive fraction was responsible for membrane damage due to apoptosis or cytotoxicity in HeLa and PA-1 cancer cell lines.

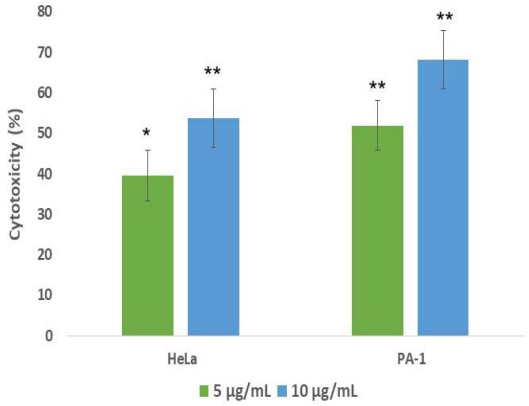

Figure 5: Percentage cytotoxicity as a measure of LDH release in PA-1 and HeLa cells treated with TLYF. Data was analyzed using one way ANOVA and *denotes significance at p<0.05, ** p<0.01.

3.8. Caspase 9 activity

The initiator caspase, caspase 9, can activate procaspases and induce apoptosis in living cells. Increased caspase 9 activity in any cell indicates that the cell is undergoing apoptosis. The initial caspase 9 activity in HeLa cells treated with TLYF was 89.9%, and in PA-1 cells it was 104.2% (Figure 6). After a 90-minute incubation period, caspase 9 activity increased to 146.3% in HeLa cells and 158.0% in PA-1 cells. Thus, there was a 56.4% increase in caspase 9 activity in HeLa cells and a 53.8% increase in PA-1 cells when comparing initial and final activity. These results were found to be statistically significant (p<0.05, p<0.01 and p<0.001 as per one-way ANOVA). Overall, a significant increase in caspase 9 activity was observed after TLYF treatment in cancer cells.

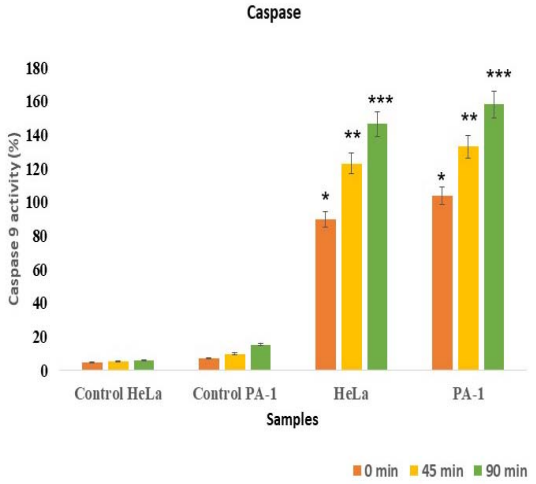

Figure 6: Activity of caspase- 9 (%) in the PA-1 and HeLa cells treated with TLYF. Data was analyzed by one way ANOVA. *Denotes significance with p<0.05, ** significance with p<0.01, *** significance with p<0.001.

3.9. Analysis of Cell cycle through Annexin V/ PI labelling and flow cytometry

The cancer cells become insensitive to normal cell signals, and hence avoid apoptosis and thereby proliferate faster. Therefore, quantitative measurement of the cell cycle has emerged as a key factor in identifying cell death. After Annexin V/PI labelling, we analysed the cell cycle stages of the TLYF treated PA-1 and HeLa cancer cells by flow cytometry, to ascertain the impact of the treatment on the cancer cells. Tamarind leaf yellow fraction was found to induce apoptosis in the cancer cells as shown by the cell populations in different quadrants. There were 18.84% of late apoptotic cells, 50.92% of early apoptotic cells and live cells were found to be 26.94%, while in untreated HeLa cell line, the percentage of viable cells were 95.97%, 2.53% early apoptotic cells, and a mere 0.61% cells were in late apoptotic phase (Figure 7). Thus, there was a clear indication of cells undergoing apoptosis by tamarind leaf fraction treatment.

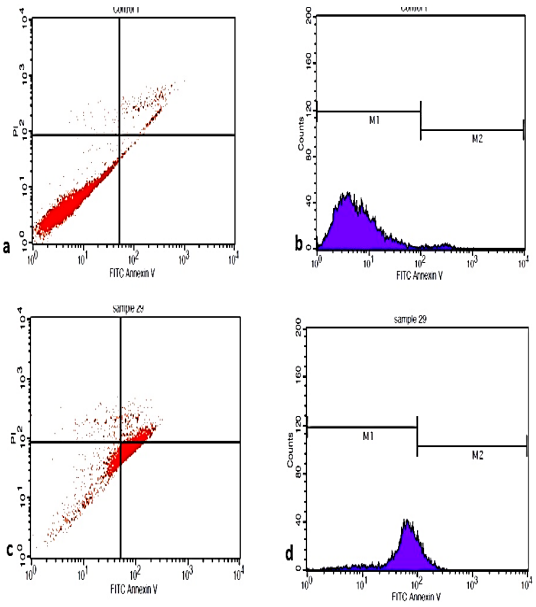

Figure 7: Annexin V/PI analysis of HeLa cells treated TLYF and control HeLa cells. **a) &b)** untreated control HeLa cells distributed in different phases (quadrants) of cell cycle, **c) & d)** treated HeLa cells distributed in different phases (quadrants) of cell cycle.

3.10. GC-MS analysis of TLYF

The potent anticancer activity of the bioactive fraction from tamarind leaf prompted us to further characterize the components underlying this activity through GC-MS analysis.

The GC-MS chromatogram of the tamarind leaf yellow fraction exhibited a major peak with 100% abundance at retention time (RT) 22.01 minutes (Figure 8a), indicating the presence of a compound with a mass-to-charge ratio (m/z value) of 74 (Figure 8b). The corresponding compound with a molecular weight of 270.2 was identified as Apigenin from the database (http://bioinf-data.charite.de/cancerresource), where it is listed as an anticancer compound. Apigenin, a flavonoid derived from edible plants, has been linked to various experimental and biological investigations suggesting its anticancer properties (Imran et al., 2020). We propose that apigenin could be the reason for the profound antitumor property of tamarind leaf ethanol extract, as it is documented in the literature for its anticancer activity (Luo et al., 2008). Notably, this is the first report of the presence of apigenin in tamarind leaf and its anticancer activity.

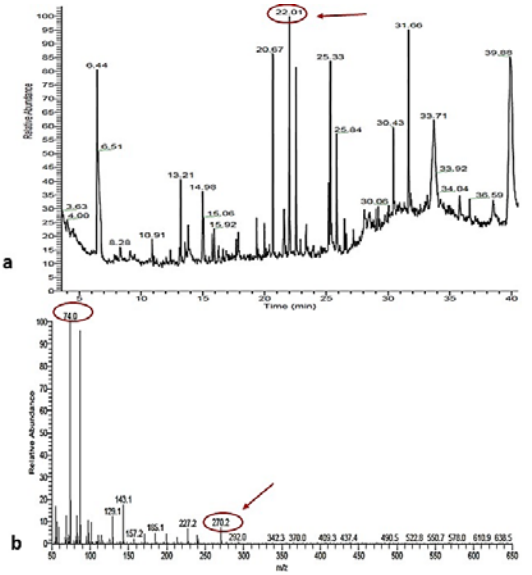

Figure 8: GC-MS depiction of TLYF **a**) The GC chromatogram **b)** Mass spectrum of the highest peak at 22.01 min. Arrow indicating a fragment ion having mol. wt. of 270.2 corresponding to apigenin.

4. Discussion

Cancer continues to dominate the diseases that cause significant morbidity and mortality, despite recent advancements in technologies for its detection and treatment. Among all the different types of cancers, ovarian and cervical cancers are the two most common cancers among women. Though surgery and other treatments are available, ovarian cancer has the highest mortality rate and the worst prognosis (Momenimovahed et al., 2019; Bray et al., 2018). Cervical cancer, the fourth most frequent female cancer globally, results in more than 300,000 deaths worldwide. Therapeutic approaches include surgery, radiotherapy, and/or chemotherapy either alone or in combination, all of which result in severe toxicity to the cells (Burmeister et al., 2022; Koppikar et al., 2010). Despite advancements in cancer diagnosis and treatment options, mortality rates due to cancer have not significantly declined. Synthetically prepared chemotherapeutic agents have a series of undesirable side effects on patients (Parveen and Nadumane, 2022). Recently, people are turning towards Complementary and Alternative Medicine more frequently for cancer treatment, alongside advanced allopathic drugs and other biological medicines, a practice known as integrative oncology. Less invasive therapeutic options using natural compounds wherever possible are ideal for managing cancer, with complementary and alternative medicines becoming the most sought-after treatment for ovarian and cervical cancers currently (Chizenga and Abrahamse, 2021; Adams and Jewell, 2007).

Different parts of the tamarind tree (*T. indica*) have traditionally been used for their high therapeutic properties, along with their nutritional components, attracting the attention of modern researchers (Kumar and Bhattacharya, 2008). Tamarind seeds are useful in treating bladder stones, boils, dysentery, ulcers, eye conditions, jaundice, chronic diarrhea, acne, and diabetes. Tamarind leaves can treat conjunctivitis, constipation, hemorrhoids, diarrhea, jaundice, boils, and liver disorders. When applied to boils, tamarind leaves reduce swelling and inflammation. Tamarind flowers are utilized as a pesticide and also used to cure eye conditions, jaundice, and bleeding piles. The bark is employed to treat ocular inflammations and digestive system conditions and has demonstrated anticancer potentials (Caluwe et al., 2010; Shirisha and Varalakshmi, 2016).

We hypothesized that tamarind leaves might possess anticancer potentials based on its reported therapeutic properties, anti-inflammatory action, and the known link between inflammation and cancer. Chronic inflammatory conditions are typically associated with a higher risk of developing cancer, as reported in several epidemiological studies. Cancer progression is often linked to inflammation, with both intrinsic and extrinsic types of inflammation leading to immunosuppression and creating a conducive environment for tumor development. Cancer-related inflammation cells are genetically stable, making them less prone to rapid drug resistance. Therefore, specifically targeting inflammation can be a viable strategy for cancer therapy or prevention (Singh et al., 2019; Coussens and Werb, 2002). We chose to investigate the leaves of the tamarind plant based on this idea, as numerous epidemiological findings point to the therapeutic benefits of dietary sources in cancer treatment, and tamarind leaves have been traditionally used in treating inflammations.

The potential anticancer efficacy of tamarind leaf was scientifically investigated in the current study. The ethanol extract of tamarind leaf was examined on the cervical cancer (HeLa) and ovarian cancer (PA-1) cell lines through the MTT assay. The results demonstrated a dose- and time-dependent decrease in cell density. Confirmation of this activity was obtained from trypan blue test results. Additionally, TLC was employed to guide the selection of the active component based on bioactivity. This method allowed the identification of the yellow fraction from tamarind leaf (TLYF) as having significant inhibitory effects on PA-1 and HeLa cancer cell lines. Viabilities decreased from 43% at 24 h to 27% at 72 h (in HeLa) and from 42% at 24 h to 11.9% (in PA-1) after 72 h of treatment. These effects were inversely proportional to treatment concentrations and duration of exposure, pointing to the antiproliferative property of the TLYF fraction. The IC_{50} value of TLYF was very low (0.1 µg/mL), within permissible limits for natural anticancer compounds suggested by the FDA. The TLYF fraction indicated the presence of both tannins and flavonoids through phytochemical screening.

Despite the enormous number of anticancer drugs developed and currently in use in clinical settings, they are not frequently chosen due to their impact on both tumor and healthy cells. Therefore, it is crucial to evaluate the safety of potential medicines before clinical trials in the development of anticancer drugs (Srivastava et al., 2005). In the current study, the safety evaluation of the tamarind leaf extract and the bioactive fraction TLYF was conducted on human peripheral lymphocytes. This choice is significant, as many anticancer drugs affect the survival of blood cells, leading to patients developing neutropenia and anemia after chemotherapy. Observations revealed that at all tested concentrations for 24, 48, and 72 hours, the percentage viability of lymphocytes remained above 90% and sometimes approached 100%, suggesting that this natural compound does not adversely affect blood cells. Consequently, we proceeded to analyze the mechanism of TLYF's anticancer activity on cervical and ovarian cancer cells using various *in vitro* assays.

Apoptotic cell death maintains tissue homeostasis and controls cell growth. Any deviation in the cell's ability to undergo apoptosis results in the formation of tumors. Hence, researchers in the field of anticancer drug development have been concentrating on identifying apoptotic inducers. In the current research, we aimed to investigate the apoptosis-inducing properties of TLYF on cancer cells. Apoptotic cells exhibit morphological and physiological changes such as cell shrinkage, the formation of apoptotic bodies, and chromatin condensation, observable directly under an inverted microscope or through staining for visualization under a fluorescence microscope (Loannou and Cheng, 1996). In this regard, when we treated the cancer cells with TLYF, we observed that the treated cells fluoresced bright orange, indicating apoptosis, while the untreated control cells fluoresced bright green, indicating viability, under fluorescence microscopy. Furthermore, we observed a significant increase of over 50% in caspase activity in PA-1 and HeLa cells treated with TLYF, clearly suggesting the apoptosis-inducing ability of this fraction. Caspases, members of the cysteine protease family, are well-known for their crucial role in apoptosis. Caspase 9, one of the most crucial apoptosis executors among various caspases, initiates and activates other apoptotic proteins. An increasing level of Caspase 9 indicates cell death.

Apoptosis in TLYF-treated cancer cells was also supported by the visualization of the DNA fragmentation pattern in agarose gel electrophoresis of DNA from treated cells. The DNA of TLYF-treated cells appeared as a smear upon gel electrophoresis, signifying a higher degree of apoptosis in these cancer cells (Mathi et al., 2014). Thus, there was strong evidence for the induction of apoptosis in cancer cells by TLYF. Moving forward, we estimated cell membrane damage through the LDH release assay. This assay, believed to be indicative of cytoplasmic release resulting from treatment with any cytotoxic compound, revealed that TLYF treatment caused the highest release of LDH compared to untreated control cells of both HeLa and PA-1.

Apart from inducing apoptosis, cell cycle progression is one of the effective mechanisms in cell proliferation. Blocking the cell cycle at various stages and inhibiting DNA replication were considered as some of the effects exerted by efficient or most successful anticancer drugs (Loniakan et al., 2023). In view of this we studied cell cycle phases of the cervical cancer cells by flow cytometry method following Annexin V and PI staining. The results have shown that TLYF treatment resulted in a significant decrease in S-phase cells along with a decline in the total cell population compared to the controls, indicating that it

had arrested the cell cycle at the G_0/G_1 phase. Thus, it can be interpreted that TLYF treatment resulted in direct cytotoxicity in the cells, as evidenced by the increased percentage of LDH release in the cells. Taken together, it appears that TLYF exerts its anticancer effects through inhibiting cell proliferation, initiating apoptosis, causing cell cycle arrest, and inducing direct cytotoxicity. This demonstrates its significant anticancer potential.

The characterization of TLYF was carried out by phytochemical analysis followed by LC-MS and GC-MS methods. The presence of flavonoids and tannins in the bioactive fraction of tamarind leaf was confirmed by phytochemical analysis of TLYF. In GC-MS results, it was observed that the mass-to-charge (m/z) ratio of the highest peak at the retention time (RT) 22.01 minutes of the LC-MS chromatogram indicated a compound with 100% relative abundance, having an m/z value of 74. The corresponding compound with a molecular weight of 270.2 was found to be apigenin during the library search. Apigenin, the flavonoid, was isolated from different sources, such as fruits and vegetables, and was reported to have anticancer activities (Luo et al., 2008). The identification of apigenin in tamarind leaf, as reported in this study, is the first of its kind according to our literature survey. Therefore, we assert that this compound is responsible for the appreciable anticancer activity observed *in vitro*.

5. Conclusion

In conclusion, the results of this study highlight the potential of dietary plants with medicinal significance, such as the tamarind leaf, to play a crucial role in anticancer drug discovery. Future research efforts should concentrate on the comprehensive chemical and structural characterization of the identified bioactive fraction, paving the way for subsequent clinical and drug development studies.

Declarations

Funding

Not applicable

Conflicts of interest/Competing interests

The authors disclose that they do not have any conflicts of interest.

Ethics approval

Not applicable

Consent to participate

Not applicable

Consent for publication

Not applicable

Availability of data and material

All the data generated or analysed during this study are included in this published article or available from the corresponding author upon reasonable request.

Code availability

Not applicable

Authors' contributions

SR and VKN contributed equally to the study conception and design. Material preparation, data collection, analysis was performed by SR. Supervision was by VKN. The initial write-up of the draft manuscript was by SR. The review and corrections for the previous version of the manuscript were carried out by VKN. All authors read and approved the final manuscript.

Acknowledgements

The authors express their deep gratitude and acknowledge the support by the management of Jain Group of Institutions for providing the infrastructural facilities to carry out the work and the Junior Research Fellowship offered to the author SR.

References

AAT Bioquest, Inc. 2023. Quest Graph™ Four Parameter Logistic (4PL) Curve Calculator. AAT Bioquest. https://www.aatbio.com/tools/four-parameter-logistic-4pl-curve-regression-online-calculator.

Belayachi L, Aceves-Luquero C, Merghoub N, Bakri Y, Fernández de Mattos S, Amzazi S and Villalonga P. 2014. *Retama monosperma* n-hexane extract induces cell cycle arrest and extrinsic pathway-dependent apoptosis in Jurkat cells. *BMC Complem Altern Medicine*, **14:** 1-12. doi: 10.1186/1472-6882-14-38.

Bhat RB, Eterjere EO and Oladipo VT. 1990. Ethnobotanical studies from Central Nigeria. *Econ Bot*, **44:**382–390. doi.org/10.1007/BF03183923.

Burmeister CA, Khan SF, Schäfer G, Mbatani N, Adams T, Moodley J and Prince S. 2022. Cervical cancer therapies: Current challenges and future perspectives. *Tumour Virus Res*, **13:**200238. doi: 10.1016/j.tvr.2022.200238.

Caluwe ED, Halamova K and Damme PV. 2010. *Tamarindus indica* L. – A review of traditional uses, phytochemistry and pharmacology. *Afrika Focus,* **23:** 53-83.

Chizenga EP and Abrahamse H. 2021. Biological Therapy with Complementary and Alternative Medicine in Innocuous Integrative Oncology: A Case of Cervical Cancer. *Pharmaceutics*, **13(5):** 626. doi: 10.3390/pharmaceutics13050626.

Ciesla UM and Hajnos MW. 2010. Application of thin-layer chromatography for the quality control and screening the free radical scav.ing activity of selected pharmaceutical preparations containing *Salvia officinalis* L. extract. *Acta Pol Pharm Drug Res*, **67:** 481-485. PMID: 20873415.

Coussens LM and Werb Z. 2002. Inflammation and cancer. *Nature*, **420:** 860–867. DOI: 10.1038/nature01322.

Dev S. 1999. Ancient-Modern Concordance in Ayurvedic Plants: Some Examples. *Environ Health Pers*, **107:** 783-789.

Dhasade V, Nirmal SA, Pal SC, Maiti PP and Mandal SC. 2015. Potential of Various Extracts of *Tamarindus indica* (Caesalpiniaceae) Leaves in the Treatment of Cancer. *Insight Cancer Research*, **1(1):** 1–6. doi: 10.5567/icr-ik.2015.1.6.

Diallo D, Sogn C, Samaké FB, Paulsen BS, Michaelsen TE and Keita A. 2002. Wound healing plants in Mali, the Bamako region. An ethnobotanical survey and complement fixation of water extracts from selected plants. *Pharm Biol*, **40:** 117–128. doi.org/10.1076/phbi.40.2.117.5846.

Dicker DT, Kim SH, Jin Z, Wafik S and El-Deiry. 2005. Heterogeneity in non-invasive detection of apoptosis among human tumor cell lines using annexin-V tagged with EGFP or Qdot-705. *Cancer Biol Ther*, **4:** 1014-1017. doi.org/10.4161/cbt.4.9.2150.

Dighe NS, Pattan SR, Nirmal SA, Kalkotwar RS, Gaware VM and Hole MB. 2009. Analgesic activity of *Tamarindus indica*. *Res J Pharmacogn Phytochem*, **1:** 69–71.

El-Siddig K, Gunasena HPM, Prasa BA, Pushpakumara DKNG, Ramana KVR, Vijayanand P and Williams JT. 2006. Tamarind – *Tamarindus indica* L. Fruits for the future. Southampton Centre for Underutilized Crops, Southampton, UK. pp.188.

Faridi UA, Zidan NS, Almutairi FM, Alalawy AI, Atteia HH, Al-Awthan YS, Akhtar MQ and Sakran MI. 2023. The Antioxidative, Anticancer and Hepatoprotective of Quercetin Nanoparticles In-vitro and In-vivo. *Jordan J Biol Sci*, **16(1):**117 – 123. https://doi.org/10.54319/jjbs/160114.

Garg M, Lata K and Satija S. 2015. Cytotoxic potential of few Indian fruit peels through 3-(4,5-dimethylthiazol-yl)-2,5-diphenyltetrazolium bromide assay on HepG2 cells. *Ind J Pharmacol*, **48:** 64-68.

Hartl A, Putscher J, Prehsler S, Buchmann C and Vogl CR. 2010. *Tamarindus indica* L. (Fabaceae): Patterns of use in traditional African medicine. *J Ethnopharmacol*, **127:** 573–588.

Hayashi Y, Nishikawa Y, Mori H, Tamura H, Matsushita Y and Matsu T. 1998. Antitumor Activity of (1 OE, 122)-9-Hydroxy- 10, 12-Octadecadienoic Acid from Rice Bran. *J Ferment Bioeng*, **86:** 149-153.

Hsia TC, Yu CC, Hsu SC, Tang NY, Lu HF, Huang YP, Wu SH, Lin JG and Chung JG. 2014. Cantharidin induces apoptosis of H460 human lung cancer cells through mitochondria-dependent pathways. *Int J Oncol,* **45(1):** 245-254.

Indian Council of Medical Research. 2006. Ethical Guidelines for Biomedical Research on Human Participants, New Delhi: Indian Council of Medical Research; 2006.

Imran M, Aslam Gondal T, Atif M, Shahbaz M, Qaisarani TB, Mughal MH, Salehi B, Martorell M and Sharifi-Rad J. 2020. Apigenin as an anticancer agent. *Phytotherapy Res*, **34(8):** 1812-1828. doi: org/10.1002/ptr.6647

Irvine FR. 1961. Woody Plants of Ghana. Oxford University Press, London.

Jeong CH, Bode AM, Pugliese A, Cho Y, Kim H, Shim J, et al. 2009. [6]-gingerol suppresses colon cancer growth by targeting leukotriene A4 hydrolase. *Cancer Res*, **69:** 5584-5591.

Lee YJ and Shacter E. 1999. Oxidative stress inhibits apoptosis in human lymphoma cells. *The J Biol Chem*, **9:** 19792-19798.

Liu D and Chen Z. 2009. The effects of cantharidin and cantharidin derivates on tumour cells. *Anticancer Agents Med Chem,* **9(4):** 392-396.

Loniakan S, Rafiee A and Monadi A. 2023. *Bacteroides fragilis* induce apoptosis and subG1/G1 arrest via caspase and Nrf2 signaling pathways in HT-29 cell line. *Jordan J Biol Sci*, **16(2):** 363 – 369. https://doi.org/10.54319/jjbs/160221

Mathi P, Nikhil K, Ambatipudi N, Roy P, Bokka VR and Botlagunta M. 2014. In-vitro and in-silico characterization of *Sophora interrupta* plant extract as an anticancer activity, *Bioinformation*. **10:**144–151. doi: 10.6026/97320630010144.

Meléndez PA and Capriles VA. 2006. Antibacterial properties of tropical plants from Puerto Rico. *Phytomedicine*, **13(4):** 272-276.

Morton J. 1987. Tamarind. In: Fruits of warm climates. Morton JF. (ed.), Miami, USA, pp. 115-121.

Mosmann T. 1983. Rapid calorimetric assay for cellular growth and survival: application to proliferation and cytotoxicity assays. *J Immunol Methods*, **65:** 55-63.

Parveen S and Nadumane VK. 2022. BAX and p53 over-expression mediated by the marine alga *Sargassum myriocystum* leads to MCF-7, HepG2 and HeLa cancer cells apoptosis and induces *in-ovo* anti-angiogenesis effects. *Jordan J Biol Sci*, **15(2)**: 275 – 287. doi.org/10.54319/jjbs/150216.

Patel B, Das S, Prakash R and Yasir M. 2010. Natural bioactive compound with anticancer potential. *Int J Adv Pharm Sci*, **1:** 32-41.

Rao S and Varalakshmi KN. 2016. *Tamarindus indica* Bark Extract and a Bioactive Fraction Induce Apoptosis in HeLa and PA-1 Cells. *Indian Journal of Pharmaceutical Sciences,* **78(6):**725-731.

Roy S, Besra SE, De T, Banerjee B, Mukherjee J and Vedasiromoni JR. 2008. Induction of apoptosis in human leukemic cell lines U937, K562 and HL-60 by *Litchi chinensis* leaf extract *via* activation of mitochondria mediated caspase cascades. *The Open Leukemia Journal*, **1:** 1-14.

Sakoff JA, Ackland SP, Baldwin ML, Kaene MA and McClusky A. 2002. Anticancer Activity and Protein Phosphatase 1 and 2A Inhibition of a New Generation of Cantharidin Analogues. *Invest New Drugs*, **20:** 1-11.

Siddhuraju P. 2007. Antioxidant activity of polyphenolic compounds extracted from defatted raw and dry heated *Tamarindus indica* seed coat. *LWT Food Sci Tech*, **40:** 982–990.

Singh N, Baby D, Rajguru JP, Patil PB, Thakkannavar SS and Pujari VB. 2019. Inflammation and cancer. *Ann Afr Med*, **18(3):**121-126. doi: 10.4103/aam.aam_56_18.

Vaidyanathan D, Salai Senthilkumar MS and Ghouse Basha M. 2013. Studies on ethnomedicinal plants used by malayali tribals in Kolli hills of Eastern ghats, Tamilnadu, India. *Plant Sci Res*, **3:** 29-45.

Yan X, Qi M, Li P, Zhan Y and Shao H. 2017. Apigenin in cancer therapy: anti-cancer effects and mechanisms of action. *Cell Biosci*, **7:**50. doi: 10.1186/s13578-017-0179-x. PMID: 29034071.

JJBS

Volume 17, Number 3,September 2024
ISSN 1995-6673
Pages 463 – 470
https://doi.org/10.54319/jjbs/170308

Jordan Journal of Biological Sciences

Antimicrobial, Antibiofilm and Antioxidant Properties of Algerian *Satureja graeca* L. Against Human Pathogens

Mouna Menakh [1,*], Saber Boutellaa [2], Amar Zellagui[3], Ozgur Ceylan [4], Mehmet Öztürk [5], Chawki Bensouici [6]

[1] Department of Nature and Life Sciences, University Center Abdehafid Boussouf, Mila, Algeria; [2] Laboratory of Natural Sciences and Materials (LSNM), Institute of Sciences and Technology, University Center AbdehafidBoussouf, Mila, Algeria ; [3] Laboratory of Bio-molecules and Plant Breeding, Department of Nature and Life Sciences, Faculty of Exact Sciences, Oum El Bouaghi University, Oum EL Bouaghi, Algeria; [4]Apiculture Program, Ali Kocman Vocational School, Mugla Sitki Kocman University, 48640, Ula, Mugla, Turkey; [5]Department of Chemistry, Faculty of Sciences, Muğla Sıtkı Koçman University, 48000 Mugla, Turkey; [6] Biotechnology Research Center, P.B E73/UV N°03 Ali Mendjeli Nouvelle Ville, 25000 Constantine, Algeria ;

Received: September 1, 2023; Revised: November 4, 2023; Accepted: November 29, 2023

Abstract

In this study, we evaluated the antimicrobial, antibiofilm and antioxidant properties, in addition to the chemical constituents of *Satureja graeca* L. ethyl acetate and *n*-butanol fractions using HPLC-DAD analysis, phenolic compound detection was established. Six in vitro assays (DPPH, ABTS, ß-carotene, $O_2^{\bullet-}$, CUPRAC, and Reducing power) were employed to assess the antioxidant capacities. In order to determine the minimum inhibitory concentrations (MIC) of both extracts against six bacterial strains and two fungi, the serial micro-dilution method was used. According to analysis, the extracts' main phenolic components were chlorogenic acid, rutin, ellagic acid, vanillin, and caffeic acid. Both fractions revealed high antioxidant capacities at different levels in all assays and they showed a strong antimicrobial activity against all tested strains as MIC came out to be 0.3–10 mg/ml. However, ethyl acetate fraction exerted important effect compared to that of *n*-butanol fraction on *Enterococcus faecalis* ATCC19433 (1.2 and 2.5 mg/mL), *Candida albicans* ATCC10239 (2.5 and 10 mg/mL) and *Candida tropicali*s RSKK 665 (2.5 and 5 mg/mL). Furthermore, ethyl acetate fraction showed a significant antibiofilm activity against *C. tropicalis* RSKK 665 (41.9%) and *C. albicans* ATCC 10239 (38.6%) at 2.5 mg/mL. These findings suggest that *Satureja graeca* L. can be used in food and may be a promising therapeutic agent for treating a wide range of disorders.

Keywords: Antibiofilm Activity; Microbial Inhibition; Antioxidant Properties; Phenolic profile; Greek Savory.

1. Introduction

The production of excessive free radicals in the human body, combined with the inadequacy of both endogenous and exogenous antioxidant systems, results in oxidative stress. This oxidative stress causes significant harm to cellular DNA, proteins, carbohydrates, and lipids (Sharifi-Rad *et al*., 2020). Antibiotic resistance and the ability of certain microorganisms to form biofilms pose a major threat to public health and are considered one of the most significant challenges of the 21st century (Júnior *et al*., 2018; Al-kafaween et al., 2020; Zullkiflee et al., 2023). The emergence of new pathogens, the reemergence of previously controlled ones, and the lack of effective treatments only compound the problem, making the discovery of new active molecules a continued necessity (Venkatesan, 2021).

The plant world offers a diverse array of molecules with a range of various pharmacological effects, especially phenolic substances, which have been investigated for their potential to combat diseases linked to oxidative stress and as alternatives to conventional antibiotics, which are becoming less effective (Danaei *et al*., 2021). The genus *Satureja*, part of the Lamiaceae family, the Nepetoideae subfamily, and the *Menteae* tribe, include around 200 species of fragrant plants and herbs native to the Mediterranean, Europe, Middle East, and western Asia. Algeria is home to 16 species of *Satureja*, which can be used as both a culinary and medicinal herb that can also be planted as a decorative plant. (Bensouici *et al*., 2013; Haouat *et al*., 2022). In Algeria and Morocco, *Satureja* is highly regarded for its ability to treat respiratory infections, coughs, and indigestion (Amiri, 2011). Recent studies have also shown that *Satureja* possesses vasodilatory, emmenagogue, antihyperlipidemic, bactericidal, fungicidal, antioxidant, antidiabetic characteristics (Seyedtaghiya et al., 2021).

This research is centered on a comprehensive analysis of the chemical profile and a thorough evaluation of biological properties of the ethyl acetate and *n*-butanol extracts derived from the aerial parts of *Satureja graeca* L. This particular species of *Satureja* is of significant medicinal and botanical interest in Algeria. The primary aim of this study is to uncover the therapeutic potential of these extracts, with a specific focus on their antioxidant

* Corresponding author. e-mail: m.menakh@centre-univ-mila.dz.

capabilities, antibacterial effects, and antibiofilm properties.

2. Material and Methods

2.1. Plant material

Satureja graeca L. aerial components were gathered in March 2020 in Mila, North Eastern Algeria (36°30'25.55"N Latitude and 6°21'43.70"E Longitude, at a height of 240 m), during the floral stage. At the Life Science and Nature Department of the University of Larbi Ben Mhidi Oum El Bouaghi in Algeria, a sample was kept in the herbarium of the Biomolecules and Plant Breeding Laboratory.

2.2. Preparation of extracts

The aerial portions of *S. graeca* L. (50 g) were pulverized and macerated for three cycles of 24 hours each with 80% ethanol and water at room temperature. The resultant hydroalcoholic extract was concentrated under decreased pressure (40°C) and twice filtered through ordinary filter paper to remove ethanol. After that, it was fractionated using progressively polar solvents. Before usage, the fractions were kept at 4°C.

2.3. Phytochemical analysis

2.3.1. Total phenolics and flavonoids quantification

The content of total soluble phenolics in the ethyle acetate (EtOAc) and butanolic extracts (*n*-but) from the aerial portions of *S. graeca* L. was evaluated using the Folin reagent by colorimetry (Singleton *et al*., 1965). 500 µL of each extract, diluted to a dose of 0.25 mg/mL, 2500 µL of F.C. reagent, diluted a tenth in water, and 2000 µL of sodium carbonate (20 g/l) made up the reaction mixture. The absorbance at 760 nm was determined after 90 minutes. The procedure utilizing aluminum trichloride was used to determine the flavonoid content of both extracts (Miliauskas et al., 2004). A 2% methanolic solution of $AlCl_3$ was combined with one milliliter of each extract (250 µg/mL) in methanol, and after incubating at room temperature for 10 minutes, the absorbance was measured at 430 nm. The total phenolics and flavonoids were expressed in µg of GA equivalent and µg of quercetin equivalent per milligram of extract, respectively, using gallic acid and quercetin as reference standards to generate calibration curves.

2.3.2. HPLC-DAD screening of phenolics

To analyze ethyle acetate and butanolic extracts as well as 27 standard phenolics, we used a Shimadzu reverse stationary phase HPLC system which is controlled by LC-solution and includes a Shimadzu model LC-20AT solvent supply unit. 35°C was chosen as the column temperature. Aqueous acetic acid 0.1% (A) and methanol served as the mobile phases for the chromatographic separation, which was carried out on an Inertsil ODS-3 guard column (4 µm, 4.0 mm x 150 mm) column (B). Elution was done in gradients ranging from 2% to 100%. Sample stock solutions were created in methanol at a concentration of 8mg.mL^{-1} and filtered through an Agilent 0.45 µm filter. 20 µL of fluid was injected. A diode array detector (DAD) operating at a wavelength of 254 nm was used to find the phenolics. The results were presented as micrograms per gram of dry weight, and their characterization was based on a comparison of the retention times (Tel-Çayan *et al*., 2015).

2.4. Antioxidant activity

Using a microplate reader (Perkin Elmer, Enspire), all experiments were carried out in 96-well microplates. The tests used to define the results were CUPRAC and Reducing power assays, where $A_{0.5}$ refers to the dose indicating 0.5 absorbance, and DPPH, ABTS, $O_2^{\bullet -}$ and ß-Carotene-linoleic acid, where IC_{50} refers to sample dose giving 50% activity.

2.4.1. DPPH assay

According to BLOIS (1958), diphenyl-picrylhydrazyl (DPPH) free radicals were used to measure the antiradical effect of ethyl acetate and *n*-butanol fractions. 160 µL of 0.1mM DPPH methanolic solution was added with triplicate samples (40 µL of 6.25-200 µg.mL^{-1}). A blank (methanol) was used as a reference during a half-hour incubation period at 25°C to quantify the mixture's absorbance. The following equation was employed to compute the proportion of DPPH scavenger activity:

$$\%I = [(A_1 - A_2)/A_1] \times 100$$

Where; A_1 and A_2 are respectively absorbencies of negative control and sample.

2.4.2. ABTS Cation Assay

To create the ABTS cation radical, A 7 mM ABTS solution in water received the addition of 2.45 mM potassium persulfate, which was then kept for 12 hours at room temperature. Later, using H_2O, the solution's absorption was brought to 0.700±0.020 at 734 nm. 40 µL of each sample and standard was diluted in triplicate with 160 µL of this solution in each well. As typical antioxidants, BHT and BHA were utilized, while methanol served as a blank. The absorbance was measured at 734 nm after ten minutes of incubation at 25°C. Using the DPPH formula the inhibition % was then determined (Re *et al*., 1999).

2.4.3. β-Carotene assay

According to Marco (1968), 25 µL of linoleic acid were combined with 0.5 mg of *β*-carotene in 1 mL of chloroform, and 200 µL of Tween 40 were used to emulsify the mixture. Chloroform was evaporated at 40°C, and the rest was recovered using 100 mL of purified water that had been infused with oxygen. With oxygenated water, the absorbance was changed to (0.8 - 0.9) at 470 nm. 40 µL of samples at concentrations ranging from 6.25 to 200 µg/mL were added to 160 µL of this solution. *β* -carotene bleaching percentage was calculated after two hours of incubation at 50 °C using an absorbance measurement at 470 nm and the result was calculated as follows:

$$R = (ln\ a_1/a_2)/t$$

a_1 and a_2 were the relative absorbencies at the beginning of the reaction (t0) and 120 minutes afterward (t120). Antioxidant capacity was computed using the following formula:

$$A\% = [(R_{control} - R_{sample})/ R_{control}] \times 100$$

2.4.4. Superoxide anion assay

The alkaline DMSO technique, with minor modifications, was used to test $O_2^{\bullet -}$ scavenging activity

(Kunchandy and Rao, 1990). This process depends on the synthesis of alkaline DMSO while changing the yellow color of Nitroblue tetrazolium (NBT) into formazan (blue hue). Following the addition of 30 µL of NBT (1 mg/mL in distilled water), 40 µL of each extract was combined with 130 µL of alkaline DMSO (created by dissolving 20 mg of NaOH in 100 mL of DMSO to create $O_2^{\bullet-}$). Tannic acid and α-tocopherol served as benchmarks. Following 10 min of incubation at ambient temperature, the absorbance was recorded at 560 nm, and the ratio of $O_2^{\bullet-}$ blockage was calculated employing the DPPH formula.

2.4.5. Reducing power assay

Using Oyaizu (1986) method of Fe^{3+} to Fe^{2+} reductive capability, the extracts' reductive capacities were evaluated. 50 µL of potassium ferricyanide (1%) (1 g of $K_3Fe(CN)_6$ in 100 mL H_2O) and 40 µL of phosphate buffer (pH 6.6) were added to 10 µL of each sample (1.562-50 µg/mL), followed by a 20 min incubation period at 50°C for the combination. Then, 10 µl of ferric chloride $FeCl_3$ (0.1%), 40 µl of water, and 50 µl of trichloroacetic acid (TCA) (10%) were added to the mixture. On a blank surface (methanol), at 700 nm, absorption was determined.

2.4.6. Cupric reducing capacity (CUPRAC)

A mixture consisting of 60 µL of ammonium acetate buffer (pH 7.0), 50 µL of 10 mM ($Cu Cl_2$, $2H_2O$), and 50 µL of 7.5 mM neocuproin was prepared. To this mixture, 40 µL of sample solutions with 6.25-200 µg/mL concentrations were then supplemented (Apak et al., 2008). After one hour of incubation, the intensity of absorption at 450 nm was obtained and contrasted with a blank solution. BHT and BHA were common antioxidants employed in this assay.

2.5. Antimicrobial activity

According to the micro-dilution method of Rota *et al*., (2004), minimal inhibitory concentration (MIC) and minimal bactericide concentration (MBC) of the extracts, which reflect the lowest concentration that gave no observable growth, were determined. *E. foecalis* ATCC19433, *L. monocytogenes* ATCC7644, *S. aureus* ATCC 25923, and *S. aureus* MU40 have been chosen as positive Gram bacteria. *C. violaceum* CV 026 and *P. fluorescens* RSKK240 have been chosen as negative Gram bacteria. All mentioned bacterial strains were put to grow in nutrient broth and incubated at 37°C for 24 h excepted *P. fluorescens* RSKK240, *L. monocytogenes* ATCC7644 and Fungi (30°C for 24-48 h). Afterwards, inocula 5×10^5 colony-forming units (CFU)/mL were prepared. The test medium was Mueller Hinton Broth (MHB) from Biolife in Milan, Italy. Each extract was produced in five final doses (0.625–10) mg/mL in DMSO solution. 10 µL of cell suspension were added to each well of a 96-well microplate containing 170 uL of sterile MHB. Then, 20 uL of sample were added in duplicate at various concentrations. Three wells were reserved for negative controls (media, media + bacteria and media + bacteria + DMSO). For 24 hours, microplates with inoculums were incubated at 37°C.

2.6. Antibiofilm activity

We tested the impact of extracts in different concentrations ranging from the minimum inhibitory concentration (MIC) to one-fourth MIC on the biofilm formation ability of both bacteria and yeasts using polystyrene microplates (Ceylan and Ugur, 2015). The microorganisms were cultured overnight in 5 ml of Tryptone-Soy Broth (TSB) supplemented with glucose (1%). The microbial suspension was then diluted (5×10^5 CFU ml^{-1}), and each well received 100 µL along with 100 µL of each extract at various concentrations (MIC, MIC/2, and MIC/4) or 100 µL of the control (culture medium). Each well was rinsed with water after being incubated for 48 h at 37°C to get rid of any planktonic bacteria. The remaining bacteria were then dyed for 10 minutes at 25°C with a 0.1% crystal violet solution. To remove the crystal violet solution (which had not particularly colored the attached bacteria), the wells were washed once more. To remove any extra liquid, the microplates were flipped and firmly tapped on absorbent paper. They were then allowed to air dry. The wells containing Gram-negative and Gram-positive bacteria, respectively, received 200 l each of 95% ethanol and 33% glacial acetic acid, and the plates were automatically shaken. Spots of the biofilm dissolved at room temperature. Finally, a microplate reader was used to detect the absorbance at a wavelength of 550 nm. The biofilm formation inhibition percentages were calculated using the next equation:

$$I\% = [(Ab_{control} - Ab_{sample}) / Ab_{control}] \times 100$$

2.7. Statistical analysis

All results and findings were obtained in triplicate and reported as mean ± S.D. The data were processed by SPSS V.16. One-way analysis of variance (ANOVA) and Tukey Post Hoc test were performed to establish the differences among the means. P values < 0.05 were considered to be significant. The IC_{50} values (50% inhibition concentration) for the antioxidant activity were calculated by the linear regression method from the curve [% inhibition = f (concentrations)].

3. Results

3.1. Total phenolics and flavonoid contents

Total phenolics and flavonoid contents of ethyl acetate (EtOAc) and butanolic extracts (*n*-but) from aerial parts of *S.graeca* L. are presented in Table 1. A great richness of both extracts in total phenols was noted. However, EtOAc extract had the highest content significantly (268.4 ±1.9 µg EAG/mg E) compared to that of *n*-but extract ($P < 0.05$). In contrast, the latter contained more flavonoids (37.6 ± 0.2 EQ/mg E) than EtOAc extract (20.9 ± 0.2 EQ/mg extract) ($P < 0.05$).

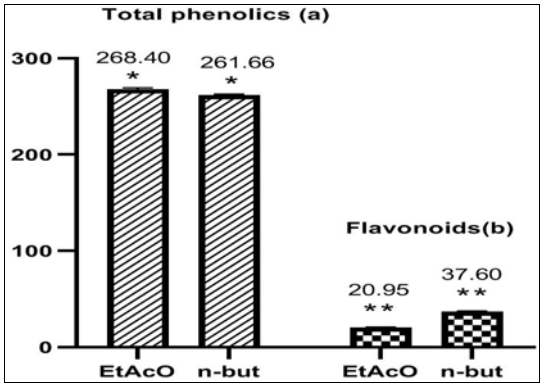

Figure 1. Total phenolics and flavonoids contents in *S. graeca* L. extracts

Results are expressed as means ± standard deviation of three measurements.

(a) Microgram of Gallic Acid Equivalent per milligram of extract,(b) Microgram of Quercetin Equivalent per milligram of extract. ***P<0.001, ** P <0.01 and * P <0.05 compared between means.

3.2. Compounds identified by HPLC-DAD

The results of HPLC analysis are given in Table 1. Only five minor compounds were identified in EtOAc fraction: chlorogenic acid (4.8µg/g), caffeic acid (1.4µg/g), vanillin (1.3µg/g), protocatechuic acid (0.8µg/g) and 4-hydroxybenzoic acid (0.2 µg/g). The majority of the detected peaks were not identified due to the absence of suitable standards (Figure 1). For *n*-but fraction, nine compounds were identified: Rutin (41.6 µg/g), chlorogenic acid (41.1 µg/g), ellagic acid (3.3 µg/g), 2,4-dihydroxybenzoic acid (0.3 µg/g), Coumarin (0.3 µg/g), p-coumaric acid (0.2 µg/g), ferulic acid (0.1 µg/g), trans-cinnamic acid (0.2 µg/g) Quercetin (0.2 µg/g) and Rosmarinic acid (0.1 µg/g).

Table 1. Bioactive phenolics obtained from of *S. graeca* L. extracts.

N°	Compounds	Rt (min)	EtOAc (µg/g)	*n*-but (µg/g)
1	Protocatechuic acid	14.0	0.8	-
2	4-hydroxybenzoic acid	19.5	0.2	-
3	Caffeic acid	24.1	1.4	-
4	Vanillin	24.8	1.3	-
5	2,4,-dihydroxybenzoic acid	25.2	-	0.3
6	Chlorogenic acid	27.3	4.8	41.1
7	*p*-coumaric acid	29.8	-	0.2
8	Ferrulic acid	31.0	-	0.1
9	Coumarin	32.5	-	0.2
10	Rutin	34.2	-	41.6
11	Ellagic acid	38.1	-	3.3
12	*trans*-cinnamic acid	43.2	-	0.2
13	Quercetin	44.0	-	0.2
14	Rosmarinic acid	45.3	-	0.1

(-): not detected

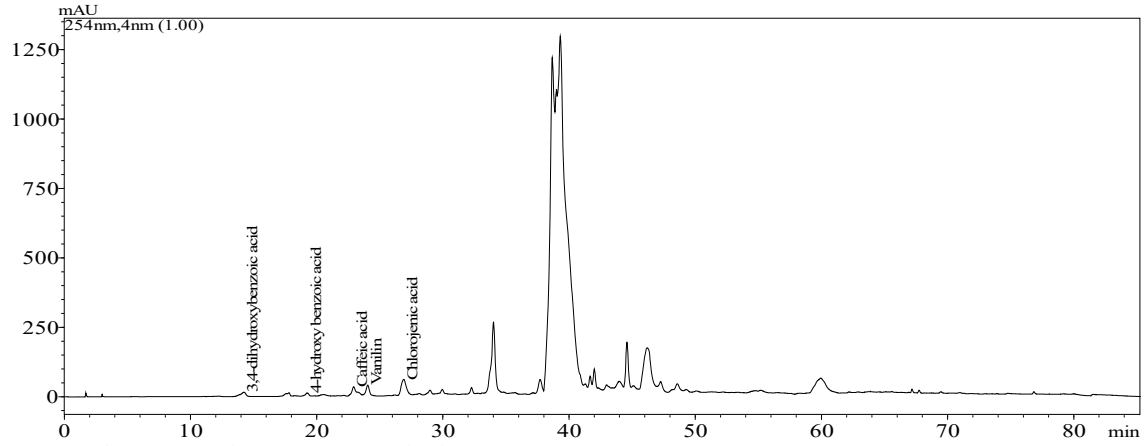

Figure 2. Chromatogram of *S. graeca* L. EtOAc fraction at 254 nm.

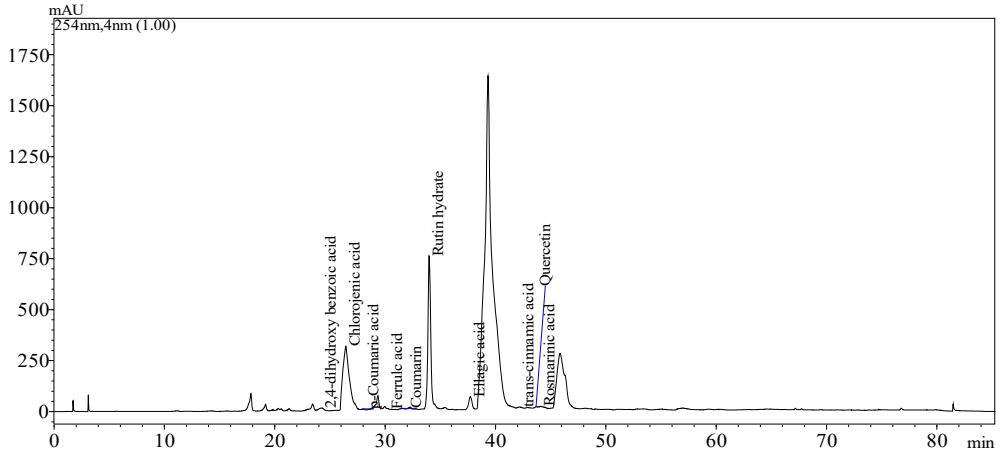

Figure 3. Chromatogram of *S. graeca* L. *n*-but t fraction at 254 nm.

3.3. Antioxidant activity

Results of antioxidant activities are represented as percentage inhibition for each concentration as well as 50% radical scavenging concentration (IC_{50}) values for the DPPH, ABTS, $O_2^{\bullet-}$ and β-Carotene tests, and $A_{0.5}$ values, which correspond to the concentrations indicating 0.5 absorbance for CUPRAC and reducing power (RP) tests. According to data mentioned in Tables 2 and 3, and based on the values of CI_{50} and $A_{0.5}$, we have found that both extracts exhibited a very significant activity in comparison to standard antioxidants, as we have recorded CI_{50} values very near to those of BHA in the ABTS and β-carotene tests (P <0.05), significantly better than those of BHT in DPPH (CI_{50}: 10.6 ± 0.4 µg/mL and 11.4 ± 0.5 µg/mL) and CUPRAC ($A_{0.5}$: 4.4 ± 0.4 µg/mL and 6.2 ± 0.3 µg/mL) tests (P <0.01) and significantly better than that of α-tocopherol in the RP test ($A_{0.5}$: 6.9 ± 0.6 µg/mL and 11.5 ± 0.7 µg/mL) for EtOAc and *n*-but, respectively (P<0.001).

Table 2. Antioxidant activity of *S. graeca* L. extracts by DPPH•, $ABTS^{\bullet+}$, $O_2^{\bullet-}$, *β*-carotene, inhibition % at minimum concentration and IC_{50}.

	DPPH• assay		$ABTS^{\bullet+}$ assay		*β*-carotene-linoleic acid assay		$O_2^{\bullet-}$ assay	
	Inhibition (%) at 6.2µg/mL	IC_{50} µg/mL	Inhibition (%) at 6.2µg/mL	IC_{50} µg/mL	Inhibition (%) at 6.2µg/mL	IC_{50} µg/mL	Inhibition (%) at 6.2µg/mL	IC_{50} µg/mL
EtOAc	28.9±0.1*	10.6 ±0.4**	89.5±0.3*	3.3±0.1*	66.4±2.5*	2.4±0.1*	82.8±0.4	1.2±0.1*
n-but	26.5±1.3*	11.4 ±0.5**	65.2±1.8	4.6±0.3*	61.1±0.4*	2.6±0.1*	78.1±1.4	7.3±0.2***
BHA	54.3±1.6**	5.7 ±0.4***	93.5±0.1*	1.8±0.1*	90.1±0.6**	0.9±0.1*	nt	nt
BHT	22.2±1.3*	13.0 ±0.4**	78.5±3.4*	1.2±0.3**	86.1±1.0**	1.0±0.1*	nt	nt
Tannic ac	nt	nt	nt	nt	Nt	nt	78.8±0.9	1.6±0.1*
α-Tocopherol	nt	nt	nt	nt	Nt	nt	64.9±1.0*	3.1±0.4*

Results are expressed as means ± standard deviation of three measurements

(-) : no inhibition; nt : not tested. ***P<0.001, ** P <0.01 and * P <0.05 compared between means.

Table 3. Antioxidant activity of *S. graeca* L. extracts py CUPRAC, Ferric reducing power, inhibition % at minimum concentration and $A_{0.5}$.

	CUPRAC		Ferric reducing power	
	Inhibition (%) at 6.2µg/mL	$A_{0.50}$ µg/mL	Inhibition (%) at 1.5µg/mL	$A_{0.50}$ µg/mL
EtOAc	0.6±0.1**	4.4±0.4**	0.3±0.00***	6.9±0.6***
n-but	0.5±0.1**	6.1±0.3**	0.3±0.01***	11.4±0.7***
BHA	0.8±0.1**	3.6±0.1**	0.1±0.01***	8.4±0.6***
BHT	0.3±0.2**	9.6±0.8**	0.1±0.00***	>50***
Tannic ac	nt	nt	Nt	5.3±0.9***
α-Tocopherol	nt	nt	Nt	34.9±2.3***
Ascorbic ac	nt	nt	0.1±0.00***	6.7±1.1***

Results are expressed as means ± standard deviation of three measurements

(-) : no inhibition; nt : not tested. ***P<0.001, ** P <0.01 and * P <0.05 compared between means.

3.4. Antimicrobial and Antibiofilm activities

Antimicrobial activity of both *S. graeca* L. extracts against 9 reference microbial strains tested in this study was qualitatively evaluated by the minimum inhibitory concentrations (MICs) and results were represented in Table 4. Our data showed that EtOAc fraction of *S. graeca* L. possesses a strong effect and a wide range of action covering Gram positive, Gram negative bacteria and *Candida* genus, as MIC came out to be 0.3–10 mg/ml (mean range). *n*-but fraction had the same antibacterial

effect (MIC) against *S.aureus* ATCC25923 (0.6 mg/ml), *L. monocytogenes* ATCC7644 (1.2 mg/ml) and *P. fluorescens* RSKK240 (0.3 mg/ml). However, EtOAc fraction exerted a significant effect compared to that of *n*-but on *E. faecalis* ATCC19433 (1.2 and 2.5 mg/mL), *C. albicans* ATCC10239 (2.5 and 10 mg/mL) and *C. tropicalis* RSKK 665 (2.5 and 5 mg/mL).

Results of antibiofilm activity presented in Table 4 as inhibition percentages showed that EtOAc extract exerted a moderate effect of inhibition of the biofilm formed by only three strains: *L. monocytogenes* (23.4%), *C. albicans* (38.6%) and *C. tropicalis* (42.1%). However, there was no effect with the *n*-but fraction against the biofilm produced by the major strains examined.

Table 4. Antimicrobial and antibiofilm activities of *S. graeca* L. extracts values.

Strains		*n*-but				EtOAc			
		MIC	% inhibition on biofilm formation			MIC	% inhibition on biofilm formation		
		mg/mL	MIC	MIC/2	MIC/4	Mg/mL	MIC	MIC/2	MIC/4
Gram-Positive bacteria	*S.aureus* MU40	0.62	-	-	-	0.6	-	-	-
	E. foecalis ATCC19433	2.5	-	-	-	1.2	-	-	-
	L. monocytogenes ATCC7644	1.2	-	-	-	1.2	23.4±0.4	18.7±0.8	12.4±1.2
	B. subtilis ATCC6633	10	nt	nt	nt	5	nt	Nt	nt
	S.aureus ATCC25923	> 10	-	-	-	5	-	-	-
Gram-Negative bacteria	*C. violaceum* CV 026	1.2	-	-	-	1.2	-	-	-
	P. fluorescens RSKK240	0.3	-	-	-	0.3	-	-	-
Fungi	*C. albicans ATCC 10239*	10	19.3±3.2*	-	-	2.5	38.6±2.2*	16.9±2.7*	-
	C. tropicalis RSKK 665	5	-	-	-	2.5	42.1.±0.2	-	-

Results are expressed as means ± standard deviation of three measurements.

MIC: minimal inhibitory concentration (mg. mL^{-1})

(-): no inhibition; nt : not tested. * P <0.05 compared between means.

4. Discussion

Infectious diseases brought on by bacteria, viruses, and fungi continue to pose a significant threat to public health (Al-kafaween *et al*., 2020; Shidiki and Vyas, 2022). Finding alternate methods to combat bacterial infection has become urgently necessary due to the rise in multidrug-resistant pathogenic microorganisms (Zullkiflee *et al*., 2023).

In the current study, rutin, ellagic acid, vanillin, caffeic and chlorogenic acids, were shown to be the major phenolic components in *Satureja graeca* L. extracts. According to several studies, phenolic chemicals are commonly found in species of *Satureja*. For example, *p*-coumaric, ferulic, caffeic and protocatechuic acids have been detected in ethyle acetate and *n*-butanol extracts of *S. montana* L. which are analyzed qualitatively by HPLC-DAD, as well as in the methanolic extract of *S. montana* subsp. *Kitaibelii* of Serbia (López-Cobo *et al*., 2015). HPLC analysis of *S. hortensis* (Georgia) ethanol extract confirmed the presence of several phenolic compounds such as caffeic, *p*-coumaric acids, rutin, hesperidin and 7-glucoside (Boroja *et al*., 2018).

Antioxidant activity can be determined using a variety of techniques. Depending on the test employed, the chemical structure of extracts, which sometimes consists of several of compounds mixed together with different functional groups, polarity, and chemical behaviors, may produce dispersed results (Boutellaa *et al*., 2019; Menakh *et al*., 2020). Therefore, it would be more beneficial and even required to utilize a method that involves many tests to estimate the antioxidant capability of extracts. In this investigation, six methods were used to evaluate in *vitro* antioxidant activity of ethyl acetate (AcOEt) and *n*-butanol (*n*-but) fractions of *S. graeca* L. based on different mechanisms of action such as radical scavenging properties ($DPPH^{\bullet}$, $ABTS^{\bullet+}$ and $O_2^{\bullet-}$), ability to prevent lipid peroxidation (*β*-carotene) and ability to reduce copper and ferric ions (CUPRAC and RP). Our findings consistently demonstrated that both the AcOEt and *n*-but extracts exhibited similar antioxidant activities across most of these tests. Notably, the AcOEt extract displayed a slightly higher level of activity compared to the *n*-but extract. This observation underscores the robust antioxidant potential of both extracts.

Additionally, our analysis of the extracts' composition revealed high and closely matched contents of total phenolic compounds and flavonoids in both fractions. These results suggest that the extracts' antioxidant activities can be attributed to their rich content of these bioactive compounds, further supporting their potential utility in medicinal and therapeutic applications.

Our antioxidant properties investigation of *S.graeca* L. extracts are consistent with those reported by previous studies for aqueous and ethanolic extracts of *S. hispidula* (Algeria), for wild and cultivated *S. bachtiarica* (Iran), for methanolic extract of *S. rechingeri* (Iran) depending on the phenological stage and for *S. montana* (Serbia) who have all found similar relationships between these species' total phenolic compound concentration and antioxidant capacity (Alizadeh, 2015; Veličković *et al*., 2018; Haouat *et al*., 2022). Thus, HPLC analyses have proven a diversity of phenolic compounds in both extracts. The presence of Chlorogenic acid and Rutin at high concentrations and Ellagic acid in *n*-but extract, on one hand, and the presence of Caffeic acid, Vanillin and Protocatechuic acids in AcOEt extract could be the reason for their most powerful antioxidant potential. Moreover, the proportion of

unidentified compounds in both fractions is generally non-negligible.

The creation of bioactive secondary metabolites, which leads to the discovery of antibiotics, has attracted the attention of researchers who have been mining the understudied sources to find novel secondary metabolites that are of considerable interest in the present (Abdolhosseini *et al*., 2019; Abdel-Mawgoud *et al*., 2019). Our funding demonstrated that *S. graeca* L. extracts possess a strong antimicrobial activity because they are abundant in phenolic and flavonoid chemicals, which can be used as an alternative to antibiotics. Besides, chlorogenic acid and rutin, known for their antimicrobial potential, were detected as major phenolic compounds, which could explain the observed effect (Kabir *et al*., 2014; Stojković *et al*., 2013). According to the literature review, there was no work on the antimicrobial activity of *S. graeca* L. extracts. Previous studies have examined the antimicrobial properties of extracts from other species within the *Satureja* genus. For instance, research on *S. kitaibelii* explored the antimicrobial potential of chloroform, ethyl acetate, and *n*-butanol extracts. The results indicated that the ethyl acetate extract exhibited the highest activity, with a minimum inhibitory concentration (MIC) of 10 mg/ml against *P. aeruginosa* and *S. aureus*, while the chloroform extract was particularly effective against *P. aeruginosa*. However, the *n*-butanol extract showed weaker activity with an MIC of 50 mg/ml against *S. aureus* (López-Cobo *et al*., 2015). In another study, aqueous and EtOH extracts of *S. boissieri* (Turkey), rich in hesperidin and ac rosmarinique, showed weak activity against *S. aureus* and *P. aeruginosa*, and were not effective against *C. albicans (Aras et al*., 2018). Our results are similar with those of previous funding who reported a strong antimicrobial activity of *S. kitaibelii* MeOH extract from Serbia against *S. aureus* (0.6 mg/mL), *L. monocytogenes* (1.25 mg/mL), *P. aeruginosa* (1.2 mg/mL) and *C. albicans* (0.6 mg/mL) (Stanojković *et al*., 2013) . Moreover, with MICs varying from 0.02 to 0.4 mg/mL, the antibacterial activity of *S. hortensis* (Turkey) extracts in EtOH, MeOH, and dichloromethane was significant against *S. aureus*, *E. faecalis*, *P. aeruginosa*, and *C. albicans* (Sharifi *et al*., 2018).

Bacterial survival in challenging environments is supported by biofilms, which are essential cell colonies that bind to biotic or abiotic environments and produce an extracellular matrix. Different degrees of biofilm formation are capable of occurring in both Gram-positive and Gram-negative bacteria (Al-kafaween *et al*., 2020; Seyedtaghiya *et al*., 2021).

The results of the current study's evaluation of the antibiofilm qualities of *S. graeca* L. extracts revealed that AcOEt extract reduced the development of biofilms at concentrations lower than MIC. This finding holds significant promise for the potential application of S. graeca L. extracts in combating biofilm-related issues, a subject for which data have been notably scarce in the existing literature. Currently, there is a dearth of data on the antibiofilm activity of S. graeca L. extracts, making our study one of the pioneering works in this regard. While previous research has focused on related species like *S. hortensis* and its essential oil (Seyedtaghiya et al., 2021; Sharifi et al., 2018), few studies have specifically delved into the antibiofilm qualities of *S. graeca* L. extracts. The antibiofilm effects of the plant extract may be caused by a reduction in structure development, such as a decrease in exopolysaccharide production, or an alteration in the transcription of genes linked to biofilms (Swamy *et al*., 2016).

In summary, our research not only highlights the promising antibiofilm properties of *S. graeca* L. extracts but also underscores the need for more extensive studies to elucidate the mechanisms underlying these properties and their suitability for practical applications in areas such as medicine, agriculture, and biotechnology.

5. Conclusion

In conclusion, our study has revealed that *Satureja graeca* extracts, characterized by their rich composition of phenolic compounds and flavonoids, have the potential to serve as a valuable source of bioactive phenolic compounds. These compounds hold promise in the fields of medicine and therapy due to their demonstrated antioxidant and antimicrobial properties. Furthermore, this research has contributed to a deeper understanding of the antibiofilm properties of *Satureja graeca* L. extracts, showing their effectiveness in inhibiting biofilm formation by bacterial and yeast species. This discovery is particularly significant, as biofilm inhibition has wide-ranging implications in various industries, including healthcare and agriculture. While our findings are promising, it is important to note that further research is necessary to validate the applicability of these extracts, both as feed additives and in clinical settings. Future in vivo studies are warranted to confirm the efficacy and safety of these extracts for potential use in practical applications.

Disclosure statement

The authors report no conflicts of interest.

Acknowledgements

This study was supported by the Ministry of Higher Education and Scientific Research of Algeria.

References

Abdel-Mawgoud M, Khedr F G and Mohammed E I. 2019.Phenolic Compounds, Antioxidant and Antibacterial Activities of *Rhus flexicaulis* Baker. *Jordan J Biol Sci*., **12(1):** 17–21.

Abdolhosseini M, Zamani HA and Salehzadeh A. 2019. Synergistic antimicrobial potential of ciprofloxacin with silver nanoparticles conjugated to thiosemicarbazide against ciprofloxacin resistant Pseudomonas aeruginosa by attenuation of MexA-B efflux pump genes. *Biologia.,* **74** : 1191–1196.

Alizadeh A. 2015. Essential oil composition, phenolic content, antioxidant, and antimicrobial activity of cultivated *Satureja rechingeri* Jamzad at different phenological stages. *Z Naturforsch*., **70(1)**: 51–58.

Al-kafaween MA, Hilmi ABM, Jaffar N, Al-Jamal HAN, Zahri MK and Jibril FI. 2020. Antibacterial and Antibiofilm activities of Malaysian Trigona honey against Pseudomonas aeruginosa ATCC 10145 and Streptococcus pyogenes ATCC 19615. *Jordan J Biol Sci*., **13(1)**: 69–76.

Amiri H. 2011. The *in vitro* antioxidative properties of the essential oils and methanol extracts of *Satureja macrosiphonia* Bornm. *Nat Prod Res.,* **25(3)**: 232–243.

Apak R, Güçlü K, Özyürek M and Çelik SE. 2008. Mechanism of antioxidant capacity assays and the CUPRAC (cupric ion reducing antioxidant capacity) assay. *Microchim Acta* .,**160(4)**:413–419.

Aras A, Bursal E, Alan Y, Turkan F, Alkan H and Kılıç Ö. 2018. Polyphenolic Content, Antioxidant Potential and Antimicrobial Activity of *Satureja boissieri*. *Iran J Chem Chem Eng*., **37(6)**: 209–219.

Bensouici C, Benmerache A, Chibani S, Kabouche CS, Abuhamdah S and Semra Z. 2013. Antibacterial activity and chemical composition of the essential oil of *satureja calamintha* ssp. sylvatica from Jijel, Algeria. *Der Pharm Lett*., **5(2)**: 224–227.

BLOIS MS .1958. Antioxidant Determinations by the Use of a Stable Free Radical. Nature., **181(4617)**:1199–1200.

Boroja T, Katanić J, Rosić G, Selaković D, Joksimović J, Mišić D and Mihailović V .2018. Summer savory (*Satureja hortensis* L.) extract: Phytochemical profile and modulation of cisplatin-induced liver, renal and testicular toxicity. *Food Chem Toxicol*., **118**: 252–263.

Boutellaa S, Zellagui A, Öztürk M, Bensouici C, Ölmez ÖT, Menakh M and Duru M E .2019. HPLC-DAD profiling and antioxidant activity of the butanol extract from aerial parts of Algerian *Crithmum maritimum* L. *Acta Sci Nat*., **6(1)**: 8–16.

Ceylan O and Ugur A .2015. Chemical composition and anti-biofilm activity of *Thymus sipyleus* BOISS. subsp. sipyleus Boiss. var. davisianus Ronniger essential oil. *Arch Pharm Res*., **38(6)**: 957–965.

Danaei M, Motaghi MM, Naghmachi M, Frazane A and Moravej R. 2021. Green synthesis of silver nanoparticles (AgNPs) by filamentous algae extract: comprehensive evaluation of antimicrobial and anti-biofilm effects against nosocomial pathogens. *Biologia*., **76(10)**: 3057–3069.

Haouat A, Rechek H, Pinto DCGA, Cardoso SM, Válega MSGA, Boudjerda M and Mekkiou R. 2022. Metabolite Profiling, Antioxidant and Key Enzymes Linked to Hyperglycemia Inhibitory Activities of *Satureja hispidula*: An Underexplored Species from Algeria. *Molecules*.**,27(24):**8657.

Júnior S D da C, Santos JVde O, Campos LA de A, Pereira MA, Magalhães NSS and Cavalcanti IMF. 2018. Antibacterial and antibiofilm activities of quercetin against clinical isolates of *Staphyloccocus aureus* and *Staphylococcus saprophyticus* with resistance profile. *Inter J Env Agr Biotech*., **3(5)**: 1948–1958.

Kabir F, Katayama S, Tanji N and Nakamura S. 2014. Antimicrobial effects of chlorogenic acid and related compounds. *J Korean Soc App Biol Chem*., **57(3)**: 359–365.

Kunchandy E and Rao MNA. 1990. Oxygen radical scavenging activity of curcumin. *Inter J Pharm*., **58(3)**: 237–240.

López-Cobo A, Gómez-Caravaca AM, Švarc-Gajić J, Segura-Carretero A and Fernández-Gutiérrez A .2015. Determination of phenolic compounds and antioxidant activity of a Mediterranean plant: The case of *Satureja montana* subsp. kitaibelii. *J Func Foods*., **18**: 1167–1178.

Marco G J .1968. A rapid method for evaluation of antioxidants. *J Am Oil Chem Soc*., **45(9)**: 594–598.

Menakh M, Mahdi D, Boutellaa S, Zellagui A, Lahouel M and Bensouici C .2020. antioxidant activity and protective effect of *Hertia cheiriefolia* L. *n*-butanol extract against liver and heart mitochondrial oxidative stress in rat. *Acta Sci Nat*., **7(1)**: 33–45.

Miliauskas G, Venskutonis P R and Van Beek TA .2004. Screening of radical scavenging activity of some medicinal and aromatic plant extracts. Food Chem., **85(2)**: 231–237.

Oyaizu M .1986. Studies on Products of Browning Reaction. *Jap J of Nutr*., **44(6):** 307–315.

Re R, Pellegrini N, Proteggente A, Pannala A, Yang M and Rice-Evans C. 1999. Antioxidant activity aplying an improved ABTS radical cation decolorization assay. *Free Radic Biol Med*., 26(9):1231–1237.

Rota C, Carraminana JJ, Burillo J and Herrera A .2004. *In vitro* antimicrobial activity of essential oils from aromatic plants against selected foodborne pathogens. *J of Food Prot*., **67(6)**:1252-1256.

Seyedtaghiya MH, Fasaei BN and Peighambari SM .2021. Antimicrobial and antibiofilm effects of *Satureja hortensis* essential oil against *Escherichia coli* and *Salmonella* isolated from poultry. *Iran J Microbiolo*., **13(1)**: 5485–5495.

Sharifi-Rad M, Anil Kumar NV, Zucca P, Varoni EM, Dini L, Panzarini E and Sharifi-Rad J .2020. Lifestyle, Oxidative Stress, and Antioxidants: Back and Forth in the Pathophysiology of Chronic Diseases. *Front Physiol*., **11**: 694.

Sharifi A, Mohammadzadeh A, Zahraei Salehi T and Mahmoodi P .2018. Antibacterial, antibiofilm and antiquorum sensing effects of T*hymus daenensis* and *Satureja hortensis* essential oils against *Staphylococcus aureus* isolates. *J App Microbiol*., **124(2)**: 379–388.

Shidiki A and Vyas A .2022. Evaluation of Antibacterial Potential of *Syzygium cumini* against Methicillin-Resistant *Staphylococcus aureus* and Macrolide-Lincosamide-Streptogramin B Strains of *Staphylococcus aureus* and Its Liquid Chromatography Mass Spectroscopy Analysis. *Biomed Biotechnol Res J*., **6(1)**: 66-72.

Singleton VL, Joseph A and Rossi J .1965. Colorimetry of Total Phenolics with Phosphomolybdic-Phosphotungstic Acid Reagents. *Amer J Enol Viticult*., **16(3)**: 144–158.

Stanojković T, Kolundžija B, Ćirić A, Soković M, nikolić D and Kundaković T .2013. Cytotoxicity and antimicrobial activity of *Satureja kitaibelii* wierzb. Ex heuff (Lamiaceae). *Dig J Nanomater Biostruct*., **8(2)**: 845–854.

Stojković D, Petrović J, Soković M, Glamočlija J, Kukić-Marković J and Petrović S .2013. *In situ* antioxidant and antimicrobial activities of naturally occurring caffeic acid, *p*-coumaric acid and rutin, using food systems. *J Sci Food Agricul*., **93(13)**: 3205–3208.

Swamy MK, Akhtar MS and Sinniah UR .2016. Antimicrobial Properties of Plant Essential Oils against Human Pathogens and Their Mode of Action: An Updated Review. *Evid Based Complement Alternat Med*., 2016, 3012462.

Tel-Çayan G, Öztürk M, Duru ME, Rehman MU, Adhikari A, Türkoglu A and Choudhary MI .2015. Phytochemical investigation, antioxidant and anticholinesterase activities of *Ganoderma adspersum*. *Indus Crops and Prod*., **76**: 749–754.

Veličković V, Mašković JM and Mašković PZ .2018. Analytical Control and Antioxidative Activity of Different Teas in Serbia. *Der Chem Sin*., **9(1)**: 599–604.

Venkatesan P .2021. Re-emergence of infectious diseases associated with the past. *The Lancet Microbe*., **2(4)**: e140.

Zullkiflee N, Hashim F, Taha H and Usman A. 2023. Antifungal and Antiamoebic Activities, Cytotoxicity, and Toxicity of Aqueous and Ethanolic Extracts of Propolis Produced by Brunei Stingless Bees. *Jordan J Biol Sci*., **16(2)**: 259–266.

JJBS

Volume 17, Number 3,September 2024
ISSN 1995-6673
Pages 471 – 480
https://doi.org/10.54319/jjbs/170309

Jordan Journal of Biological Sciences

The Evaluation of the Antifungal activity of Chitosan Nanomolecules laden with *Trichoderma harzianum* Extract on *Fusarium oxysporum* f.sp. *lycopersici*

Rasha Khalid Hussein AL-Masoudi*, Neamat J. AL Judy

Department of Biology, College of Science, Baghdad University, Baghdad, Iraq.

Received: December 26, 2023; Revised: February 16, 2024; Accepted: February 22, 2024

Abstract

The economic repercussions of Fusarium wilt on global tomato crops underscore the disease's paramount importance. And by employing non-toxic, environmentally friendly ingredients that align with sustainable practices and emphasize biosafety considerations, green synthesis, an emerging field in nanobiotechnology, presents financial and ecological benefits surpassing customary chemical and physical approaches. The main objective of the present investigation is to formulate chitosan nanomolecules laden with *Trichoderma harzianum* extract and characterize them. Additionally, the study aimed to investigate the antifungal effectiveness of these chitosan nanomolecules towards *Fusarium oxysporum* f.sp. *lycopersici*. Employing the ionic gelation technique and tripolyphosphate (TPP), chitosan nanomolecules laden with *T. harzianum* extract were synthesized. Subsequent characterization involved UV-vis, FTIR, AFM, SEM, XRD, and EDX techniques to demonstrate the effectiveness of the biochemical transformation. In addition, the antifungal efficacy of bio-manufactured chitosan nanomolecules has been assessed against five strongly virulent isolates from *F. oxysporum* f.sp. *lycopersici*. The study revealed the highest inhibition rates of growth for all isolates to be 100% at a 1 mg/ml concentration of CNPs. In contrast, the minimal inhibitory level rates at 0.125 mg/ml of CNPs were 32.75, 32.83, 32.85, 36.92, and 41.17%, consecutively. This investigation's findings have revealed a recently discovered biological pathway to biosynthesize chitosan nanomolecules in an environmentally friendly way by using *T. harzianum*. The confirmed antifungal efficacy of the synthesized CNPs towards *F. oxysporum* suggests their potential as alternatives to or reducers of widespread fungicide use, applicable across various technical and agricultural domains.

Keywords: Chitosan nanomolecules, Fusarium wilt, Ionic gelation, Tomato plant

1. Introduction

One of the globally significant and extensively consumed vegetables, particularly in Iraq, is the tomato (*Lycopersicon esculentum* Mill) (Al-dobaissi, and Al-masoudi, 2021). The soil fungus Fusarium is a facultative parasitizer that favors parasitizing live tissues over saprophytic ones. Although it can be found in various kinds of soils, sandy soils are thought to be the best for its development. When there is no host present, it can live in the soil for ten to fifteen years (Hashim *et al.,* 2023). *F. oxysporum* f. sp. *lycopersici* pathogenicity first targets the roots. After that, the vascular fabric colonizes and results in severe necrosis, aerial chlorosis, and wilting. Certain species yield poisons, such as fusaric acid, which first infects the floral tissue during anthesis and then spreads across the inflorescence's central axis, harming and contaminating grains (Fradi, 2022).

The successful cultivation of tomatoes faces various challenges, among which Fusarium wilt stands out as a noteworthy concern, attributed to *Fusarium oxysporum* f. sp. *lycopersici*. In the context of diseases and crop productivity losses, fungi exert a more pronounced influence compared to other plant parasites (Juber, 2012). Chemical fungicides can eliminate plant pathogenic fungi; however, their excessive use gives rise to multiple adverse effects (Abdullah *etal*., 2019). These include the degradation of soil quality, disturbance of the natural balance of flora and fauna, escalation of infection resistance, and contamination of the surrounding environment (Fradi, 2022). As one of the world's most sustainable control methods, biological control is strongly advised and supported (Jasim *et al*., 2022).

Fusarium crown and root rot disease may be suppressed by biological control agents (Abed *et al*., 2021). A common presence in soil, root, and foliar ecosystems, *Trichoderma harzianum* Rifai is a potentially useful tool for biological control; it can effectively combat numerous soil-borne pathogenic fungi, including strains of *Fusarium* (Kareem and Al-Araji, 2021). By competing with pathogens for resources, colonizing root surfaces, mycoparasitism, and other strategies, *T. harzianum* can directly provide biocontrol. Consequently, to improve crops and biocontrol soil-borne fungal infections, *T. harzianum* has become one of the most extensively used beneficial fungi (Esmael *et al*.,2021).

Nanotechnology has become a vital technology across many disciplines due to recent advancements in the production of diverse nano molecules that vary in

* Corresponding author. e-mail: rasha.khalid@sc.uobaghdad.edu.iq.

dimension, form, and action. In contrast to bulky substances, nanoparticles possess a higher specified external space as well as a greater reaction efficacy and, therefore have been demonstrated to affect a variety of live cells, including fungal cells. Green synthesis of nanomolecules has various advantages over physical and chemical techniques (Zhao *etal*., 2023). For the synthesis of nanoparticles in a variety of applications, chitosan has frequently been a preferred solution; it is a naturally occurring polysaccharide biopolymer, and the most well-known form is an amino polysaccharide derived cellular walls for insects, crustaceans, and fungal (Mustafa and Al –Ogaidi, 2023).

The use of Nano natural polymers is becoming more and more popular as a means of phytopathogenic fungi; this could provide a safe alternative to chemical fungicides and reduce the toxicity of metal nanoparticles (MNPs) (Medda *et al*., 2015). Out of all known nano-polymers, chitosan nanoparticles (CNPs) are drawing considerable attention for their application as the antifungals of choice for various pathogenic fungi. This interest is attributed to their unique characteristics, including non-toxicity, efficiency, biodegradability, high permeability, and broad-spectrum mycotoxic towards diverse phytopathogenic fungi (Oh *etal*., 2019). The primary objective of the current study has been to synthesize and characterize chitosan nanoparticles laden by using *T. harzianum* extract. Furthermore, the study aimed to assess the mycotoxic efficiency of these nanoparticles towards *F. oxysporum* f.sp. *lycopersici.*

2. Materials and methods

2.1. Fungal pathogen isolation, identification

The present investigation focused on *F. oxysporum* f.sp. *lycopersici* which leads to Fusarium wilt disease. This fungus has been isolated from infected tomato plants between August and December 2022, and in January 2023 sourced from fields and greenhouses in Al-Rashidiya, Al-Zaafaraniya, Al-Mahmoudiya, Al-Nahrawan, Al-Taji, Al-Swayrah, and Karbala, Iraq. The symptoms that appeared on the shoots and roots of the infected plants in a field included yellowing and drooping leaves, the death of some branches, reddish-brown streaks that appeared in the vascular tissues of the stem when sliced with a knife, and finally, the death of the plants. Collected samples were individually sealed in plastic bags with the name of the location and the date of collection recorded on each bag. The pathogens were isolated and then identified from infected samples in the lab. Five parts of each infected plant (two for the root and three for the stem) were subjected to surface sterilization with a 1% hypochlorite solution, and subsequently cultured in Petri dishes with sterilized Potato Dextrose Agar (PDA), with a 5-day incubation period at 25 ± 2 °C. After obtaining pure cultures on the PDA medium using a single-spore method, they were stored at 4 °C until required (Farahani *etal.*, 2020). According to the morphology of the colony, conidiophores, and spore forms were used to identify *Fusarium* isolates in the lab. All fungal isolates were cultivated and preserved on autoclaved PDA and incubated for five days at 25±2 °C (Awad *et al*., 2020). Moreover, slant cultures were created, and all were kept in a refrigerator at 4 °C (Hussain e*t al*., 2022). The molecular and morphological characterization of isolates had been addressed in another accepted research done by the same researchers. The selection of five pathogenic isolates of *F. oxysporum* has been based on pathogenicity tests, prioritizing those exhibiting the highest severity.

2.2. Preparation of T.harzianum Crude Extract

T.harzianum isolate was obtained from the Department of Agricultural Research in Baghdad and was diagnosed morphologically, and its diagnosis was also confirmed by molecular methods. For the preparation of *T. harzianum* extract, a 10 mm diameter mycelial agar disc has been taken from the mature layer of a 120-hour-old *T. harzianum* culture on Potato Dextrose Agar (PDA). This disc has been subsequently transferred to a 500 ml flask containing 300 ml of autoclaved Potato Dextrose Broth (PDB). The flask was then subjected to a ten-day incubation period at 27±2˚C on a shaker incubator operating at 150 rpm. Following incubation, the fungal cultures underwent centrifugation at standard measures, and the resulting extract was concentrated using a rotary evaporator (Mahdavi *etal*., 2013).

2.3. Preparation of Chitosan/T. harzianum Nanoparticles

Using the same procedures mentioned in the references (El Naggar *etal*., 2022), the formulation of the chitosan-*T. harzianum* adduct involved the following procedures: Chitosan and 5% of *T. harzianum* extract were combined in equimolar ratios, and the calculated amount of water was removed. An intensification reaction has been conducted using a Dean-Stark (Clevenger) device using xylene. The chitosan amide product underwent repeated washing with methanol, ethanol, and warm distilled water. Afterward, the material was dried using a 50°C temperature, resulting in the production of a chitosan amide derivative.

The Chitosan NPs laden with *T. harzianum* extract were obtained using the ionic gelation pathway following the procedure outlined below (A 1% w/v), acetic acid solution has been employed to dissolve 5 mg/ml of the Chitosan-*T. harzianum* extract until the solution achieved transparency. Subsequently, a solution of Tri polyphosphate has been incrementally added to the Chitosan-*T. harzianum* extract solution in a 1:2.5 (w/w%) ratio, with constant mixing at room temperature for six hours. The resulting nanoparticles underwent separation; multiple wishing, removal of the supernatant layer, re-suspension of the precipitate in water, and subsequent drying (Agarwal etal., 2018).

2.4. Characterization of CNPs laden T. harzianum extract

CNPs loaden *T. harzianum* extract has been characterized using UV-visible spectrum, FTIR, XRD, AFM, EDX, and SEM.

2.4.1. UV-Visible Absorption Spectroscopy

The absorbance spectrum of the chitosan nanoparticles (CNPs) incorporating *T. harzianum* extract has been determined utilizing UV-VIS double-beam spectrophotometers, covering a 200 to 800 nm range, to measure the absorption (Oh *et al*.,2019).

2.4.2. Fourier Transform Infrared (FTIR) Test:

Analyzing the functional groups present on the chitosan nanoparticles (CNPs) laden with *T. harzianum* extract and the extract itself has been accomplished through Shimadzu Fourier Transform Infrared Spectroscopy (FTIR). Spectra have been scanned with a resolution of 4 cm^{-1} within the range of 400–4000 cm^{-1}. Standard sample preparation methods were employed, involving the dispersion of samples on a microscope slide (Dheeb *et al*., 2015).

2.4.3. Atomic Force Microscopy (AFM)

The shape of the nanoparticles' top layer has been seen using Atomic Force Microscopy (AFM) in Contact mode under ambient atmospheric conditions. The analysis has been conducted following established methodologies and procedures (Thomas *etal.,* 2017).

2.4.4. X-ray diffraction (XRD)

A thin layer of nanoparticles dispersed in a homogeneous water medium has been deposited onto a glass slide and allowed to undergo drying. Subsequently, an X-ray diffractometer, configured in 2θ/θ scanning mode with operational parameters set at 40 kV voltage, 30 mA current, and Cu K (α) radiation (λ = 1.540), has been employed to generate an XRD pattern (23). Data acquisition occurred with a step size of 0.0200 degrees over the 2θ range from 10 to 80 degrees. The analysis of Chitosan nanoparticles (CNPs) involved the interpretation of the XRD results using the JCPDS reference. The application of the Scherer equation facilitated the determination of particle sizes in the produced samples (Dheeb *etal.*, 2023).

2.4.5. Analysis of Scanning Electron Microscopy (SEM

Analyzing the top layer of the synthesized nanoparticles has been conducted using Scanning Electron Microscopy (SEM). A Brucker SEM instrument has been employed for the characterization of the morphology of CNPs laden with *T. harzianum* extract. Sample preparation adhered to established procedures (Abed *et al.*, 2021).

2.4.6. Energy Dispersive X-ray (EDX)

EDX test has been conducted utilizing EDX devices, which are employed in conjunction with a Scanning Electron Microscope (SEM) operating in transmission mode (Khan *et al.***,** 2019).

2.5. Antifungal Activity of Chitosan NPs Laden T. harzianum Extract.

The test has been designed to explore the in vitro antifungal efficiency of CNPs-laden *T. harzianum* extract towards *F. oxysporum* f.sp. *lycopersici*. The test has been performed in Petri dishes comprising sterilized Potato Dextrose Agar (PDA). Specific quantities of CNPs-laden *T. harzianum* extract were dissolved in deionized distilled water under aseptic conditions with stirring for 90 minutes. After adding the nanomaterial to PDA, the ultimate concentrations were achieved (0.125, 0.25, 0.5, and 1 mg/ml). To concoct the inoculum of the fungus, *F.oxysporum* mycelium has been transferred onto PDA plates extracted from a single colony (Huang *et al.*, 2021). A fungal disc with a diameter of 5 mm has been obtained from the pure and active growth periphery placed in the middle of the plates. Daily check-ups were conducted on the inoculated plates till the CNP-free control treatment reaches the margins of the plates. The antifungal efficacy has been compared with that of the commercial Topsin fungicide (with the active ingredient Thiophanate Methyl at 70%) regarding the mycelial outgrowth of *F. oxysporum* under identical conditions. Three replicates were conducted for each concentration with an additional three replicates for both the positive and negative control treatments. The inhibition of fungal growth has been evaluated using the formula below:

"Percentage inhibition of radial growth (PIRG) (٪) = [(A1-A2)/A1] × 100٪ "

A1 denotes the *F. oxysporum* radial growth in the control plate, and A2 denotes the *F. oxysporum* radial growth in the treatment plate (EL Sayed *et al*., 2023).

2.6. Statistical Analysis:

For the evaluation of the effect of different elements on this investigation's variables, the SAS software has been used (SAS, 2018). In the present investigation, the ANOVA test known as the least significant difference (LSD) has been employed to compare the means.

3. Results and Discussion

3.1. Morphological Identification of Fusarium isolates

Pathogenic *Fusarium* isolates were purified and identified using morphological and microscopic characteristics. The morphological characteristics of *Fusarium* isolates were observed on PDA media, such as cottony mycelium growth and changing color according to age, from a colony with pinkish violet colors to white, and cream-colored colonies. Characteristics of *F. oxysporum* observed under a microscope revealed that macroconidia have sickle-shaped, three to five septate, and basal cells with a foot shape. Microconidia are oval to reniform, without septa, in addition to the chlamydospores, as seen in culture. These features matched with *F. oxysporum* and were in concord to (Fradi, 2022).

3.2. The Synthesized CNPs' Primary disclosure

The present investigation focuses on a new fabrication of Chitosan NPs from chitosan solution utilizing *T. harzianum* extracts. No previous study on the application of the fungus *T. harzianum* for the transformation of chitosan polymers into nanoforms. As a result, the present investigation employs *T. harzianum* extract to establish a new methodology for the eco-friendly manufacturing method of CNPs. This process offers several advantages compared to the standard biosynthesis techniques (Abdulbaqi *et al.,* 2018).

3.3. Characterization of CNPs Laden with T.harzianum Extract

3.3.1. UV-Vis Spectroscopy

The UV-Vis spectrum depicted in Figure 1 for the *T. harzianum* extract reveals a singular peak at 254 nm, exhibiting an absorbance of 0.843. This peak is attributed to the π–π* and n–π* transitions within the characteristic category of organic compounds in the fungal extract. The presence of this broad peak is solid evidence affirming the efficacy of the fungal extraction method (Salih *et al*.,

2022).According to Figure 2, the spectrum of UV-Vis for CNPs laden with *T. harzianum* extract showed a characteristic peak at 297 nm with an absorbance of 0.72. The observed shift in UV-Vis spectrum stands as substantial evidence of the chemical reaction; consequently, this technique provides robust confirmation of the formation of a new material (Dheeb *etal*., 2019).

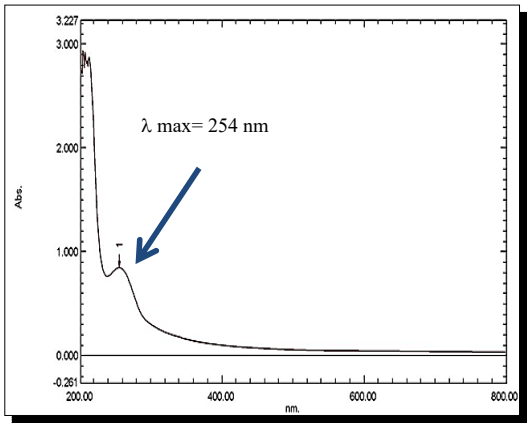

Figure1. UV-visible spectroscopy of *T.harazanium* extract with a peak at 254 nm ,and analyzed through a UV/VIS'S spectra range of 200–800 nm

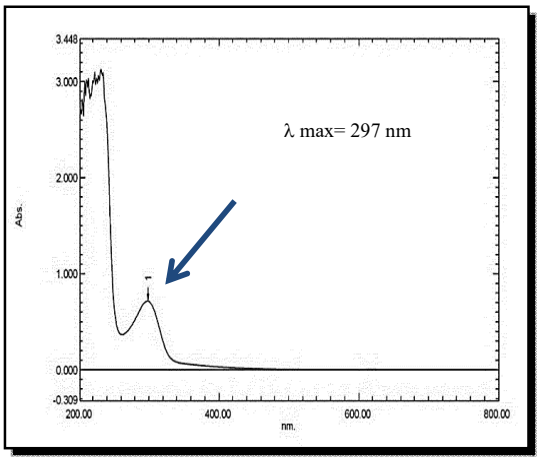

Figure2. UV- visible spectroscopy of CNPs laden with *T.harazanium* extract with a peak at 297 nm, ,and analyzed through a UV/VIS'S spectra range of 200–800 nm

3.3.2. Fourier Transform Infrared (FTIR) Analysis:

The FTIR spectrum presented in Figure 3 for the *T. harzianum* extract reveals characteristic peaks corresponding to the functional groups of the organic compounds within the extract. The peak observed at 3390.86 cm^{-1} is attributed to the OH group's stretching vibration in cis-aconitic anhydride, butyn-1-ol, 2-pyrrolidine thione, and decanoic acid, as indicated by the GC-MS results. The peak at 2939.52 cm^{-1} corresponds to the stretching vibration of aliphatic C-H in the compounds. The presence of carboxylic acid is indicated by the peak at 2322.29 cm^{-1}, associated with the stretching vibration of C=O. The peak at 1608.63 cm^{-1} is attributed to the C=C cyclic alkene. Additionally, the peak at 1402.25 cm^{-1} is associated with the stretching vibration of S=O, indicative of Sulfonyl chloride. Peaks observed at 1327.03 and 1247.94 cm^{-1} are attributed to the stretching of C-N, signifying aromatic amines. The C-O stretching of primary alcohol may be responsible for the peak at 1064.71 cm^{-1}. Peaks at 927.76, 860.24, 817.82, and 775.38 cm^{-1} are assigned to the N-H wagging of amine compounds' stretching vibration. Lastly, the C-Br group's stretching vibration in alkyl halide compounds is identified as the origin of the peaks at 617.22 and 551.64 cm^{-1}.

The FTIR spectrum depicted in Figure 4 for Chitosan nanoparticles (CNPs) laden with *T. harzianum* extract exhibits characteristic peaks. The initial peak, identified at 3437.15 cm^{-1}, corresponds to the vibratory stretching of the OH bond of alcohol. Subsequently, the second peaks observed at 2924.09 and 2854.65 cm^{-1} are attributed to the stretching vibrations of aliphatic C–H group'. Peaks at 1788.01 and 1714.72 cm^{-1} are associated with the presence of the C=O stretching in conjugated acid halide and unsaturated ester. The absorption peak at 1651.07 cm^{-1} is linked to the C=C stretching of the alkene group. The peak at 1381.03 cm^{-1} is attributed to the wagging of CH3. The presence of the (C-O-C) bridge's anti-symmetric stretching is denoted by the peak at 1143.79 cm^{-1}, while the stretching vibration associated with the C–O group is indicated by the peak at 958.62 cm^{-1}. The stretching vibrations of the C-Cl group in alkyl halide compounds contribute to the peaks observed at 837.11, 623.01, and 511.14 cm^{-1}.

Demchenko *et al.* (2020) reported that the variable position chemical groups showed successful loading meaning the successful loading process of *T. harazanium* into chitosan/TPP and the formation of CSNPs loaded with *T. harazanium*. These results were confirmed by Alqaysi *etal* (2016), who demonstrated that shifted peaks indicate the formation of a new compound and thus changes in the functional groups of bioactive molecules suggested that they were related to the formation of *T. harazanium*-loaded CSNPs.

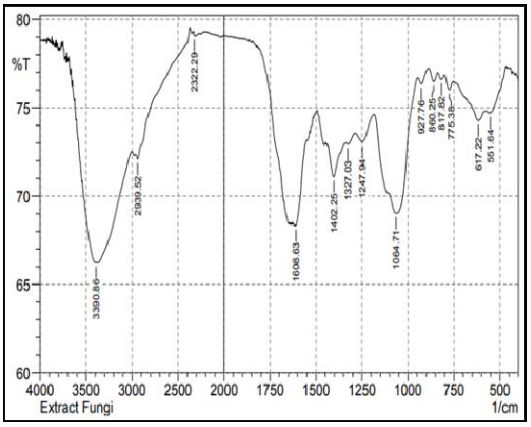

Figure 3: FTIR spectrum showed functional group of *T.harazanium* extract, spectra have been scanned with a resolution of 4 cm^{-1} within the range of 400–4000 cm^{-1}.

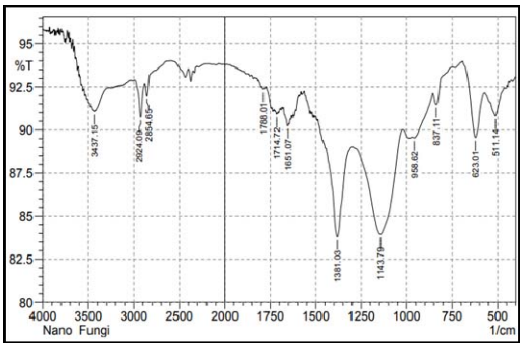

Figure 4: FTIR spectrum showed functional group of CNPs loaded with *T.harazanium* extract, spectra have been scanned with a resolution of 4 cm^{-1} within the range of 400–4000 cm^{-1}.

3.3.3. X-ray diffraction (XRD)

The XRD pattern is thought to be the distinctive mark of periodical atomic structures in any particular material. XRD analysis is a quick procedure that is mostly utilized in the discipline of material science, in the stage of determining the crystalline structure; moreover; it can provide data about the measurement of unit cells. The XRD of CNPs laden with *T. harzianum* extract in Figure 5 showed the characteristic peaks of nanochitosan at 11.625, 19.225, 22.975, 25.225, 33.525, and 38.975 degrees.

Furthermore, the measurement showed other peaks that could be attributed to the compounds of *T. harzianum* extract at 14.825, 29.375, 29.775, 35.375, 42.475, 46.925, 47.875, and 31.875 degrees. Depending on the Scherrer equation, the particle size has been calculated and found in the range 8.12-42.80 nm with a typical particle size of 22.68 nm, as illustrated in Table 1. These findings were consistent with those of Thamilarasan *et al*. (2018), who discovered that the pure chitosan diffraction peak, which had previously been discovered at 20.20°, had moved to a lower value of 19.85°. This migration may have been caused by the interaction between CS-NPs and TPP as well as the crystalline structure of CS-NPs. The patterns' variations may be related to changes in the crystal lattice's molecular arrangement (Morsy, 2019). The presence of both Nano chitosan and fungi extract peaks is solid evidence for the success of the reaction between the two starting materials.

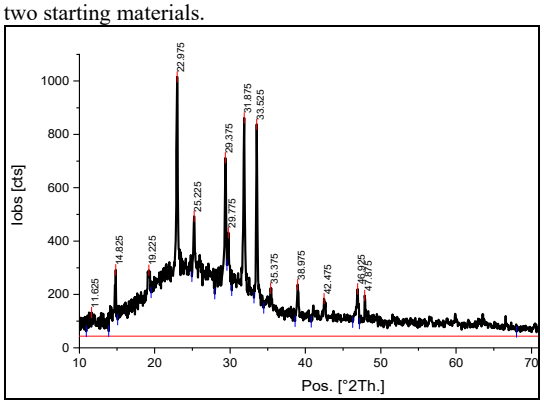

Figure 5. XRD of CNPs loaded with *T.harazanium* extract showed the five characteristic peaks of nanochitosan and eight characteristic peaks of fungal extract, X-ray diffractometer, configured in 2θ/θ scanning mode with operational parameters set at 40 kV voltage, 30 mA current, and Cu K (α) radiation (λ = 1.540)

Table 1. XRD data, particle size, and average particle size of CNPs laden with *T.harzianum*

Peak position (degree)	Assignment	Height (Counts)	FWHM (degree)	Particle size (nm)	Average particle size (nm)
11.625	*CS	88.8945	0.56161	14.86	22.68
14.825	*FE	248.7567	0.2338	35.82	
19.225	CS	247.5352	1.03677	8.12	
22.975	CS	972.4502	0.26067	32.51	
25.225	CS	449.5584	0.79469	10.71	
29.375	FE	668.5985	0.28233	30.40	
29.775	FE	388.5954	0.6	14.32	
31.875	FE	818.4524	0.2631	32.82	
33.525	CS	794.59	0.20264	42.80	
35.375	FE	179.8877	1.82232	4.78	
38.975	CS	193.8549	0.39316	22.40	
42.475	FE	140.4034	0.65992	13.50	
46.925	FE	177.4748	0.44537	20.33	
47.875	FE	152.693	0.26553	34.22	

* CS refer to Nano chitosan *FE refer to Fungal extract

3.3.4. Energy Dispersive X-ray (EDX)

The EDX accounted for CNP load with *T. harzianum* extract (Figure 6) and showed five main peaks at 0.277, 0.432, 0.525, 1.041, and 3.312 KeV which attributed to the carbon, nitrogen, oxygen, sodium, and potassium, consecutively. The presence of these elements could be considered additional evidence for the formation of CNPs laden with *T. harzianum*. Furthermore, the EDX measurement showed one additional peak of Au (used in the sample preparation) at 2.250 keV.

The constituent parts of CNPs were examined using an electron microscope in conjunction with an EDXS study. When an electron beam from a scanning electron microscope (SEM) strikes an element's inner orbit, another electron from an outer orbit moves into the vacancy to fill it. This process results in the liberation of an energy variation that is specific to that element and manifests as an X-ray. Furthermore, there is a direct correlation between the particle's amount of the element and the intensity of the particular X-ray. Nonetheless, the analysis gives a positive result of the native chitosan's different elemental compositions, assuring the consistency and sustainment of CNPs throughout the biological conversion procedure (Thamilarasan *et al*. 2018). The outcomes concur with those of Raza and Anwar (2017), who verified the existence of CSNPs on the treated fabric using scanning electron microscopy outfitted with EDX. Furthermore, the Energy Dispersive X-ray Spectroscopy (EDX) spectrum of CS10 has four types of elements: C, O, N, and Br, according to Dheeb *et al*.(2022).

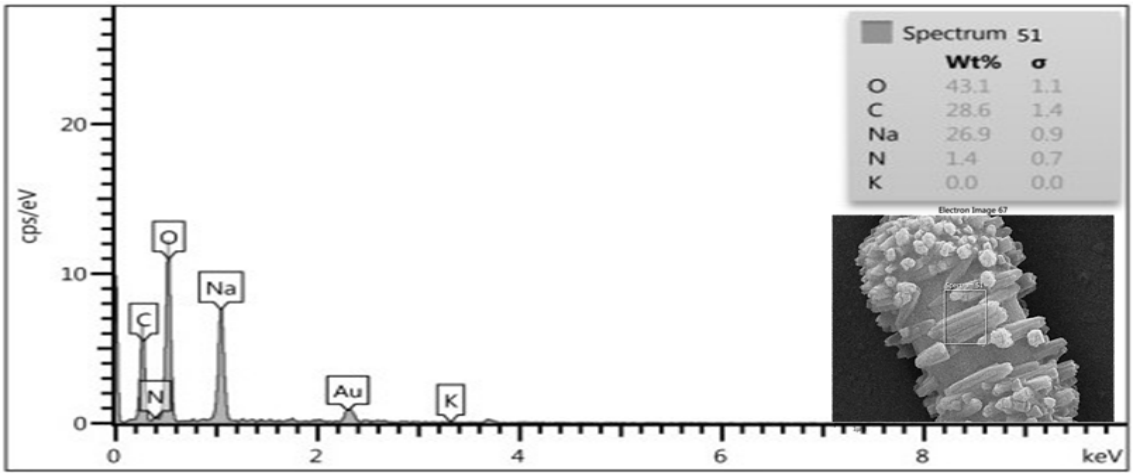

Figure 6.Spectrum of elemental analysis of CNPs loaded *T.harazanium* showed five main peaks by EDX, EDX analysis was performed via EDX Oxford instruments INCA 350 with Si detector 10mm2 area, resolution at Mn 133eV

3.3.5. Atomic Force Microscopy (AFM)

The Atomic Force Microscopy (AFM) investigation for Chitosan nanoparticles (CNPs) laden with *T. harzianum* extract, as depicted in Figure 7, establishes the presence of homogenous sphere-like structures with a medium diameter of 33.62 nm, aligning with the dimensions derived from XRD outcomes. These observations affirm the existence of nano chitosan, attesting to its preferred structural configuration. Additionally, the analysis conclusively demonstrates that the surfaces exhibit nano chitosan characteristics, as portrayed in Figure 8, providing substantiation of the encapsulation with the fungal extract. This finding agrees with (Du *et al*., 2008); they showed that the biosynthesized chitosan nanoparticles were homogenous particles with an average size of 30–98 nm.

Global statistics				
Mean	*****	2469	33.62	1146
Min	*****	123.0	7.748	1100
Max	*****	119670	329.9	2365

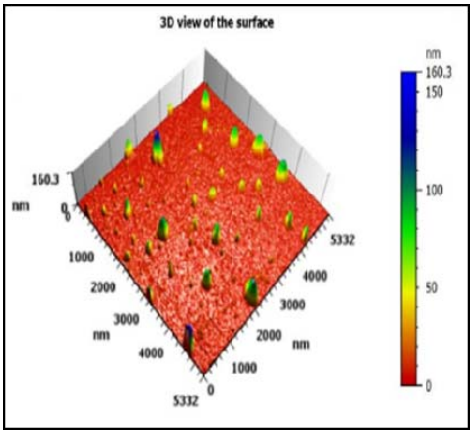

Figure7.Granularity distribution chart of CNPs loaden with T.harazanium extract based on particles size with a medium diameter of 33.62 nm surface morphology of the nanoparticles was visualized by Atomic Force Microscope Contact mode, under normal atmospheric conditions

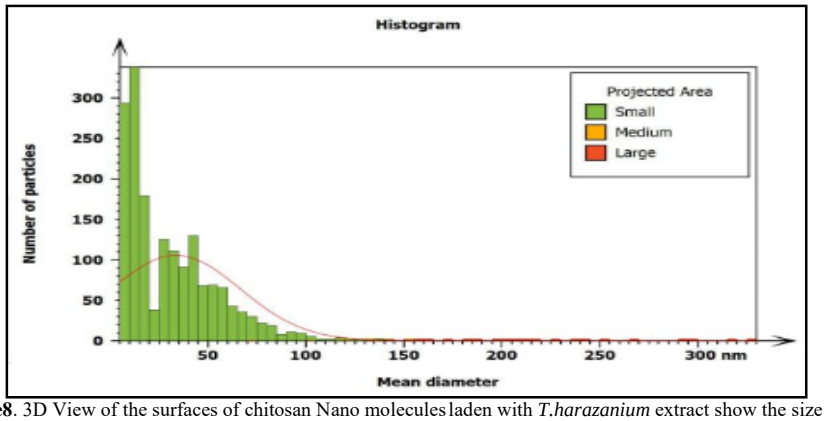

Figure8. 3D View of the surfaces of chitosan Nano molecules laden with *T.harazanium* extract show the size of particles

3.3.6. Analysis of Scanning Electron Microscopy

The exceptional dispersion and intricate morphology of Chitosan nanoparticles (CNPs), resulting in an increased exposed surface area, are discernible in the three-dimensional scanning electron microscopy (3D SEM) image. This observation further substantiates the suitability of CNPs for adsorption purposes. The analysis revealed a distinctive geometric structure for the CNPs laden with *T. harzianum* extract composite, illustrating the presence of uniformly shaped spherical structures with diameters ranging from 17.86 to 31.26 nm, indicative of Nano chitosan and affirming the success of encapsulation (refer to Figure 9). These porosity and aggregated CNPs have been identified as crucial characteristics for the manufacturing of innovative CNPs to enhance their efficacy as biologically synthesized nanomaterials in the applications of agriculture. The porous nature of these CNPs facilitates the effective adsorption of harmful chemicals and the suppression of pathogens. Notably, high-porosity nanoparticles exhibit greater specific external area and heightened reaction activity compared to lower-porosity bulk materials (Khan, 2019). The ratio of TPP to chitosan determines the size of the nanoparticles. To create nanoparticles, TPP, a positive charge ion, combines with the chitosan's negatively altered amino group. Previous studies indicate that altering the chitosan to stabilizer ratio can change the size and surface of chitosan nanoparticles (Deshaies *et al.,* 2022)

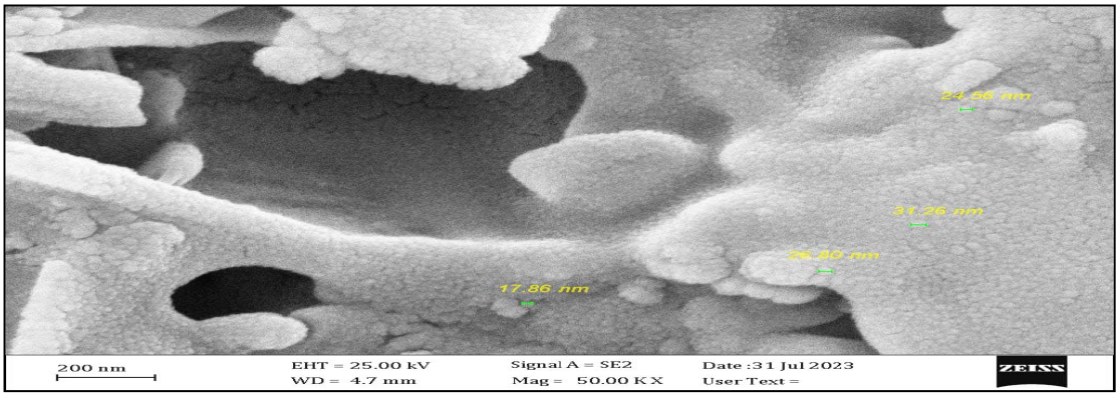

Figure 9. Image from Scanning Electron Microscopy showed the shape and size of chitosan nanomolecules laden *T. harazanium* extract , illustrating the presence of uniformly shaped spherical structures with diameters ranging from 17.86 to 31.26 nm

3.4. Antifungal Activity of CNPs Laden T. harzianum Extract

Utilizing Chitosan nanoparticles (CNPs) as a biodegradable polymer, the in vitro antifungal efficacy of CNPs laden with *T. harzianum* extract demonstrated significant inhibition of *F. oxysporum* f.sp. *lycopersci* growth in the PDA medium. The reaction occurring in the cationic amino groups of CNPs and fungal cellular constituents together suggests inherent antifungal properties (Deshaies *etal*., 2022). Each experiment has been conducted in a PDA medium with varying CNP concentrations ranging from 0.125 to 1 mg/ml, at room temperature for 168 hours. Figure 10 and Table 2 illustrate the impact of CNPs laden with *T. harzianum* extract on the mycelium radial growth for five isolates of *F. oxysporum* f.sp.*lycopersci.* The results indicate that elevating CNPs concentration correlates with increased inhibition percentages for all isolates (Huang, 2021). The highest inhibition rates of mycelium radial growth for all isolates were observed at 100% for a CNPs amount of 1 mg/ml, while the minimum inhibition rates for the five isolates were 32.75, 32.83, 32.85, 36.92, and 41.17% at a CNPs concentration of 0.125 mg/ml, consecutively. In comparison, the recommended dosage of Topsin fungicide (positive control) resulted in nearly 100% inhibition of fungal growth.

The concentration of chitosan directly correlates with the level of fungicidal effectiveness; previous research has shown that chitosan derivatives inhibit the growth of several plant-pathogenic fungi (Abdulateef *et al*., 2023). These results were similar to those found by Du *et al.* (2008) who reported that nano-chitosan was effective and gave promising antifungal activity at a lower concentration of 1000 ppm against *F. solani* and *F. oxysporum*, with a fungal growth inhibition rate of 41.48 and 30.37%, respectively. These results were also consistent with those found by Boruah and Dutta (2021), who mentioned that CNPs synthesized using *T. asperellum* were effective in inhibiting the growth of *F. oxysporum* and other soil-borne pathogenic fungi.

The ability of nano chitosan may be directly related to the activity of enzymes (catalase and peroxidase), which control the balance of reactive oxygen species (ROS) for plant resistance, and this led to a significant reduction in disease severity (Dheeb *et al.* 2015). Plant pathogenic fungi have varying levels of tolerance to chitosan nanoparticles (Al-Sarraj, 2024; Kaur *et al*., 2012; El-Mohamedy *et al.,* 2014).

It is crucial to note that variations in experimental conditions and fungal types may contribute to discrepancies between the findings of the present investigation *F. oxysporum* f.sp. *lycopersci* has been effectively inhibited by CNPs, suggesting potential strategies to impede sporogenesis, spore germination, and mycelia development. Three proposed mechanisms elucidate chitosan's inhibitory action. First, chitosan primarily targets the fungal cell membrane, increasing permeability and leading to the leakage of cellular contents, ultimately inducing cell death. The modification of membrane permeability and its interaction with the

fungal cell membrane may underlie chitosan's inhibitory effect.

In the second strategy, chitosan's chelating action binds trace elements, preventing their utilization for fungal development. Lastly, the positive charge of chitosan facilitates interaction with the negatively charged phospholipid elements of the fungal cell membrane, potentially disrupting proteins or DNA within fungi, and hindering the synthesis of necessary proteins and enzymes by preventing mRNA synthesis (AL Karagholy 2017).

Table2. The Impact of Chitosan Nanoparticles Laden with *T. harzianum* Extract on the Growth Inhibition Percentage of the Investigated Isolates.

CNPs laden *T.harzianum* extract conc.(mg/ml)	Mean ±SE of Inhibition Percentage of fungal growth (%)				
	*F.oxysprum*3	*F.oxysprum*5	*F.oxysprum*9	*F.oxysprum*17	*F.oxysprum*20
C: 0.125	41.17 ±2.07 d	32.75 ±1.97 d	32.85 ±2.19 d	32.83 ±1.87 d	36.92 ±1.69 d
C: 0.25	58.82 ±2.65 c	58.62 ±2.61 c	61.42 ±3.08 c	58.2 ±2.05 c	64.61 ±2.97 c
C: 0.5	75.0 ±3.96 b	74.13 ±3.56 b	74.28 ±4.05 b	76.11 ±3.54 b	78.46 ±3.55 b
C: 1	100 ±0.00 a	100 ±0.00 a	100 ±0.00 a	100 ±0.00 a	100 ±0.00 a
Control Topsin (+ve)	100 ±0.00 a	100 ±0.00 a	100 ±0.00 a	100 ±0.00 a	100 ±0.00 a
Control(- ve)	68 ±3.72 e	58 ±2.96 e	70 ±3.05 e	67 ±3.56 e	65 ±3.61 e
LSD value	8.77 **	8.65 **	9.02 **	8.61 **	8.69 **

** (P≤0.01).

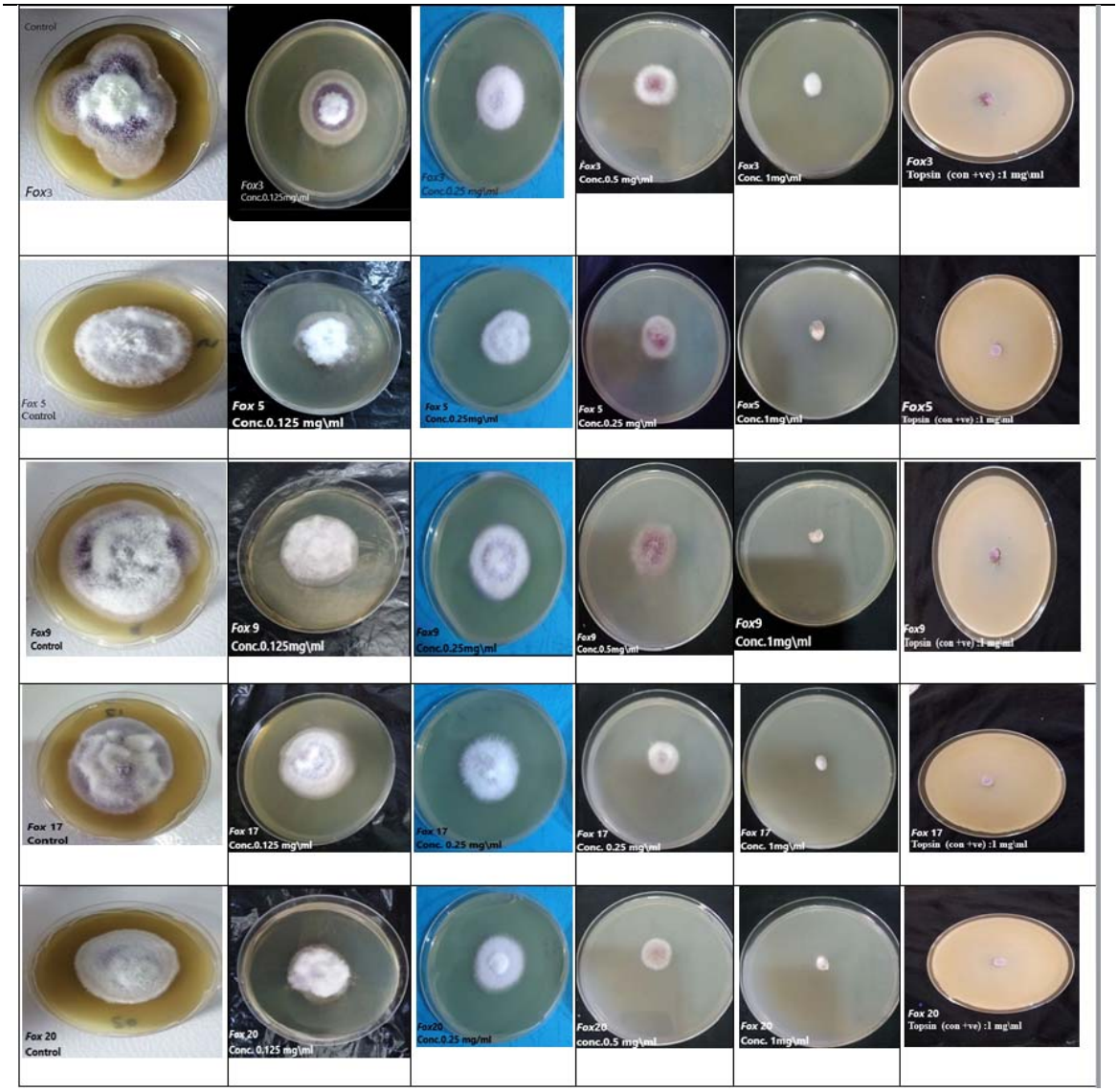

Figure10. Antifungal activity of Chitosan nanoparticles loaded with *T.harazanium* extract against *F.oxysporum* f.sp.*lycopersci*

4. Conclusions

The present investigation introduces a new eco-friendly method employing *T. harzianum* extract for the eco-friendly manufacturing of CNPs. The comprehensive characterization for the CNPs substantiates the efficacy and suitability of *T. harzianum* extract as a bio-transforming agent. The demonstrated antifungal efficacy of the synthesized CNPs towards *F. oxysporum* underscores their potential as alternatives to or mitigators of the widespread use of chemical fungicides. Moreover, their versatility extends to diverse applications in both technical and agricultural domains.

References

Abdulbaqi N J , Dheeb, B I and Irshad R. 2018. Expression of biotransformation and antioxidant Genes in the Liver of Albino Mice after exposure to aflatoxin B1 and an Antioxidant Sourced from Turmeric (Curcuma longa). *Jordan J Biol Sci*., **11(2) :** 89 – 93.

Abdullah HI, Hammadi SY, Hussein AS, Dheeb BI .2019. Investigation of genetic diversity and relationships among the clinical candida species using random amplified polymorphic DNA (RAPD) analysis. *Research J of Biotech.*, **14(1):**6–13.

Abed FD, Saadedin S MK and Shareef HK. 2021. Molecular deduction of *Aspergillus flavus* isolated from wheat grains in Karbala city. *Iraqi J of Biotech.* ,**20(1):**46-53.

Abed SM, Farhan MG, Madhloom NK, DheebDI. 2022 .Magnetic Field Exposure to Clinical Isolates of Acinitobacter baumanii. *Biomed .Pharmacol. J*., **15(4):**5-17

Agarwal MK, ShrivastavN, PandeyS, Das R and Gaur P. 2018. Preparation of chitosan nanoparticles and their In-vitro characterization. *Int. J. Life Sci. Scienti. Res.* **4(2):**1713–1720.

AL Karagholy K A .2017. Chitosan and keratin hydrolysate treatment of archived newsprint. *Ibn AL-Haitham J. for Pure and Appl. Sci.* , **23(1):** 180–188.

Aldobaissi IAM and Almasoudi RKH. 2021. Study of fruits morphological features for 33 species belong to Cruciferae family in Iraq . *Iraqi J. Agric. Sci.* , **52(4):** 1039–1049.

Alqaysi S,Aldeen AS and Alwan AH. 2016 .Molecular identification of rhizosphere *Trichoderma* spp. and their antagonistic impact against some plant pathogenic fungi. *Baghdad Sci. J.,* **13 (1):** 53-65.

Awad FM, Al-Samarrai AHM, Dheeb BI. 2020 .Study of the inhibitory effects of rheum ribes extracts on a pathogenic fungi and cancer cell line. *Plant Archives*, **20(1):** 3161–3168.

Abdulateef S M, Ibraheem S, Hussein H S, Dheeb BI, Khashman BM, Ahmed DM, Abu-Elteen KH . 2024. MMP-1 and MMP-7 expression is influenced by ginsenosides in mice exposed to aflatoxin B1: in vivo study. *Jordan J. of Pharm. Sci*., **17 (1):** 135-1139.

Al-Sarraj BM, Massadeh MI, Dheeb BI. 2024. Bacteriological and Molecular Detection of Fluoroquinolone Resistance in *Escherichia coli* Isolated from Women Patients with urinary Tract Infections. *farmacia*., **27(4):**840-842.

Boruah S and Dutta P. 2021. Fungus mediated biogenic synthesis and characterizat- upon of chitosan nanoparticles and its combine effect with *Trichoderma asperellum* against *Fusarium oxysporum, Scleroium rolfsii* and *Rhizoctonia solani*. *Indian Phytopath.,* **74(1):**81–93

Demchenko V, Riabov S, Sinelnikov S, Radchenko O, Kobylinskyi S and Rybalchenko N. 2020.Novel approach to synthesis of silver nanoparticles in interpolyelectrolyte complexes based on pectin, chitosan, starch and their derivatives. *Carbohydr Polym*. **242**:116431.

Deshaies M, Lamari N, Ng CKY, Ward P and Doohan FM. 2022. The impact of chitosan on the early metabolomics response of wheat to infection by *Fusarium graminearum*. *BMC Plant Biol.* , **73(22):** 1–17.

Dheeb B I, Abdulla S N, Shanter ALQaysi, S A, Al-Sarraj B M and Farhan M S. 2023. Extraction of *Klebsiella pneumoniae* and *Candida albicans* biofilm and studying their cytotoxic effects on human lymphocytes. *Jordan J Biol Sci.*,., **16(4):** 717 – 726.

Dheeb B I, Al-Mudallal N H, Salman Z A and Ali M. 2015. The Inhibitory Effects of Human, Camel and Cow's Milk against Some Pathogenic Fungi in Iraq. *Jordan J Biol Sci.,* **8(2):** 89 – 93.

Dheeb BI, Hashim SS, Hussein HS, Hamada TA.2022. Study of TGF- β Immune Marker Expression in Mice Exposed to Candida Spp. *AIP Conf. Proc.,* Vol (**2394):1**.

Du W L, Xu Z R,Han XY, Xu Y L and Miao Z G .2008. Preparation, characterization and adsorption properties of chitosan nanoparticles for eosin Y as a model anionic dye. *J. of Haz.Mat.* , **153(2):** 152–156.

El Naggar N E, Saber WIA , Zweil A M and Bashir SI. 2022. An innovative green synthesis approach of chitosan nanoparticles and their inhibitory activity against phytopathogenic *Botrytis cinerea* on strawberry leaves. *Sci. Rep.,***12(1):**3515.

EL Sayed ME, Yomna S E and Mohamed MA M. 2023. Biocontrol of *Fusarium equiseti* using chitosan nanoparticles combined with *Trichoderma longibrachiatum* and *Penicillium polonicum. Fungal Biol and Biotech.*, **10(5)** : 1-8

El-Mohamedy RS, Abdel-Kareem F, Jaboun-Khiareddine H and Daami-Remadi M. 2014. Chitosan and *Trichoderma harzianum* as fungicide alternatives for controlling Fusarium crown and root rot of tomato. *Tunisian J. of Plant Pro..,* **9(1):** 31-43.

Esmael Majed R,Ali Hadwan H, Adel Abed H, Mansor Hamza M,Faris Hasen O and Hmood Ali E. 2021. Estimate different bioagent as A biofertilizer with two level from chemical fertilizer on wheat crop improvement. *Iraqi J. of Sci*., ***58*(4B):**2035–2040.

Farahani-Kofoet RD, Witzel K, Graefe J, Grosch R and Zrenner R. 2020. Species-specific impact of *Fusarium* infection on the root and shoot characteristics of asparagus. *Pathogens.*, **9(6) :** 1 - 20.

Fradi A J .2022.The Effective concentration of the crude extract of *Mentha picata* and *Eucalyptus* against the growth of *Fusarium oxysporum*. *Ibn Al-Haitham J.For Pure and Appl. Sci.* , **35(4):** 1-8.

Hashim S S, Mahmood Z F, Abdulateef S F, Dheeb B I. 2023. Evaluation Cytotoxicity Effects of *Centaurea Cineraria* Extracts Against some of Cancer Cell Lines. *Biomed .Pharmacol. J.,* **16(1):**3-17 .

Huang X, You Z, Luo Y, Yang C, Ren J, Liu Y, Wei G, Dong P and Ren M. 2021.Antifungal activity of chitosan against *Phytophthora infestans*, the pathogen of potato late blight. *Inter.J. of Biol. Macro*.,**166(1)**: 1365-1376

Hussain AF, Sulaiman GM, Dheeb BI , Hashim AJ. 2018. Histopathological changes and expression of transforming growth factor beta (TGF-β3) in mice exposed to gliotoxin. *J. of K S U Sci*., **27(12):** 193–197.12.

Jasim SF, Abdulbaqi NJ, Al-Zubaidi LA and Jasim AD. 2022.Evaluation of atmospheric cold plasma technique activity on phenylpropanoids gene expression and essential oil contents and different traits of *Ocimum basilicum* L. *Baghdad Sci. J.,* **19(5):**966–975

Juber KS. 2012. Evaluating the virulence of some pathogenic isolates for three *Fusarium* species in Date- palm and their control. *Iraqi J. Agric. Sci.*, **43(2):**7-17.

Kareem H J and Al-Araji A M. 2021. Evaluation of *Trichoderma Harzianum* Biological control Against *Fusarium oxysporum* F. Sp. *Melongenae*. *Iraqi J. of Sci.*, ., **58(4B):** 2051–2060.

Kaur P, Thakur R and Choudhary A. 2012. An in-vitro study of antifungal activity of silver/chitosan nanoformulations against important seed borne pathogens. *Int. J of Sci. & Techn. Res*., **1(6):** 83-86.

Khan, I., Saeed, K. & Khan, I. (2019).Nanoparticles: Properties, applications and toxicities. *Arabian J. of Chem* **., 12(7) :** 908-931

Mahdavi V, Saber M, Dastjerdi HR. And Mehrvar A. 2013.Susceptibility of the Hymenopteran Parasitoid, Habrobracon hebetor (Say) (Braconidae) to the Entomopathogenic Fungi Beauveria bassiana Vuillemin and Metarhizium anisopliae Sorokin. *Jordan J Biol Sci.,* **6 (1)**: 17-20

Medda S, Hajra A, Dey U, Bose P and Mondal N K. 2015. Biosynthesis of silver nanoparticles from Aloe vera leaf extract and antifungal activity against *Rhizopus* sp. and *Aspergillus* sp. *Appl. Nanosci.*, **5(7):** 875-880.

Morsy M, Mostafa K, Amyn H, El-EbissyA A H, Salah A M and Youssef M A. 2019. Synthesis and characterization of freeze dryer chitosan nano particles as multi-functional eco-friendly finish for fabricating easy care and antibacterial cotton textiles. *Egypt. J.of Chem.* **, 62(7):** 1277-1293.

Mustafa HNand Al –OgaidiI. 2023. Efficacy of zinc sulfide – chitosan nanoparticles against bacterial diabetic wound infction . *Iraqi J. Agric. Sci.*, **54(1):**1–17.

Oh J W, Chun S C and Chandrasekaran M. 2019.Preparation and in vitro characterization of chitosan nanoparticles and their broadspectrum antifungal action compared to antibacterial activities against phytopathogens of tomato. *Agronomy*., **9(1):** 21-31.

Rabea EI, Badawy M E I, Steurbaut Wand Stevens CV. 2009. In-vitro assessment of N-(benzyl) chitosan derivatives against some plant pathogenic bacteria and fungi. *Eur. Polym. J.*. , 45**(1):** 237–245.

Raza Z A and Anwar F. 2017. Fabrication of chitosan nanoparticles and multi-response optimization in their application on cotton fabric by using a Taguchi approach. *NanoStru.s and Nano-Obj.*, **10**: 80–90.

Salih, II, Seddiq SH, Hashim SS, Dheeb BI . 2022.Application of Omics and Proteomics in Fungi. *AIP Con.Proc.,* Vol. **(2394):1.**

SAS 2018. **Statistical Analysis System, User's Guide. Statistical**. Version 9.6th ed. SAS. Inst. Inc. Cary. N.C. USA,

Thamilarasan V, Sethuraman V, Gopinath K, Balalakshmi C, Govindarajan M, MothanaR A, Siddiqui N A, Khaled J M and Benelli G. 2018. Single step fabrication of chitosan nanocrystals using Penaeus semisulcatus: potential as new insecticides, antimicrobials and plant growth promoters. *J of Clus. Sci.* , **29(2):** 375-384.

Thomas S, Thomas R, Zachariah AK and Mishra RK.2017. Spectroscopic Methods for Nanomaterials Characterization.In: Dutta A (Eds.), **Fourier Transforms Infrared Spectroscopy**. Elsevier Publishers, pp. 73-93.

Zhao X H, Li N N, Xu J, Dong X Y, Li S and Zang S Q. 2023. Pseudorotaxane ligand-induced formation of copper (I) iodide cluster based assembly materials: from zero to three dimensional. *Chin. J of Chem*., **41(16):** 1943-1949.

JJBS

Volume 17, Number 3,September 2024
ISSN 1995-6673
Pages 481 – 486
https://doi.org/10.54319/jjbs/170310

Jordan Journal of Biological Sciences

Evaluation of Liver Antioxidants in an induced Oxidative Stress in Albino Rat Model

Mohammad Abu-Lubad[1,*], Yaseen T. Al Qaisi[2], Ahmad Z. Alsarayreh[2], Mathhar Ahmad Abu Murad[3], Hussam Alshraideh[4]

[1]*Department of Microbiology and Pathology, Faculty of Medicine, Mutah University, Jordan;* [2]*Department of Biological Sciences, Faculty of Science, Mutah University, Al-Karak, Jordan;* [3]*Department of Microbiology and Pathology, Faculty of Medicine, Mutah University, Al-Karak, Jordan;* [4]*Department of Industrial Engineering, College of Engineering, American University of Sharjah, Sharjah, United Arab of Emirates*

Received: December 16, 2023; Revised: February 5, 2024; Accepted: February 23, 2024

Abstract

Background: Oxidative stress is a state of persistent imbalance between reactive oxygen species generation and ability of cellular antioxidant system to deactivate them.

Objectives: The present case-control study aimed to evaluate antioxidants of liver in an induced oxidative stress by lipopolysaccharide (LPS) in an albino rat model at different time intervals (6 and 72 hours) and the correlations between the studied antioxidant indicators.

Materials and methods: Ninety albino rats (male and female) were divided into two groups: 30 rats (control group) and 60 rats (test group)) were injected intraperitoneally (i. p) with saline and 60 rats (test group) injected i. p with 100 µg/kg of LPS. Rats were sacrificed at intervals of 6 and 72 hours for evaluatingTumor necrosis factor α) TNF-α) , Myeloperoxidase (MPO), caspase-3, Cyclooxygenase-2 (COX-2), Interleukin-6 (IL-6), Malondialdehyde (MDA), Catalase, Glutathione peroxidase (GPx), Glutathione reductase (GR) and superoxide dismutase (SOD)in liver tissues using ELISA technique.

Results: Our results revealed significant elevation in TNFα, MPO, Caspase-3, COX-2, IL-6 and MDA levels, a significant reduction in catalase level and insignificant decrease in GPx, GR and SOD levels in both time intervals compared to the controls. There was significant difference in the indicator levels after 6 hours compared to 72 hour intervals, but it was insignificant for MPO, Caspase-3, GPx, GR and SOD. There were positively significant correlations for all indicators at 6 and 72-hours intervals except for MDA with GPx, GR and SOD, for MDA with catalase, GPx, GR and SOD. They were negatively significant at 6 and 72-hours intervals respectively; also, correlations were insignificant between catalase and GR after 6-hours interval and between TNFα and catalase, MDA and MPO, IL-6 and MPO, GPx and SOD after 72-hours interval.

Conclusion: The levels of the studied indicators were increased in LPS-induced oxidative stress up to 72 hours except for GPx, GR and SOD; catalase was decreased significantly at both time intervals. Upon comparing 6-hours to 72-hours intervals, significant difference was detected in all indicators except for MPO, Caspase-3, GPx, GR and SOD. Correlations between indicators were positively and negatively significant except at 6-hours interval for catalase and GR, at 72-hours interval for TNFα and catalase, MDA and MPO, IL-6 and MPO, GPx and SOD after 72-hours interval, correlations were insignificant.

Keywords: Oxidative stress, TNF-α, Lipopolysaccharide, COX-2, Caspase-3, Glutathione peroxidase.

1. Introduction

Lipopolysaccharide (LPS) is a thermostable endotoxin,glycolipid component found in the outer membrane of Gram-negative bacteriasuch as *Salmonella* and *Escherichia* species (Kabanov and Prokhorenko 2010). The toxic proinflammatory properties of LPS are due to its lipid content (Milicaj et al. 2021), and the serological specificity is attributed to its distal polysaccharide and core oligosaccharide. The toxic effect of LPS is mediated by signaling pathway employing Toll-like receptors that stimulate NF-kβ translocation to nucleus (Di Gioia and Zanoni 2015)and enhance cytokines transcription such as TNFα and IL-6, which leads to inflammatory responses causing oxidative stress (Gutsmann et al. 2007).

Tumor necrosis factor α (TNFα) is a cytokine that has different effects on various types of cells secreted by macrophages in response to inflammatory agents and septic shock; it is involved in the pathogenesis of inflammatory and autoimmune diseases (Chen and

* Corresponding author. e-mail: Abu_lubbad@mutah.edu.jo

** **Abbreviations**: Cyclooxygenase-2 (COX-2), Glutathione peroxidase (GPx), Glutathione reductase (GR), Lipopolysaccharide (LPS), Malondialdehyde (MDA), Nuclear factor kappa-light-chain-enhancer of activated B cells (NF-kβ), Phosphate buffered saline (PBS), Superoxide dismutase (SOD), Tumor necrosis factor α (TNFα)

Oppenheim 2016). The expression of cyclooxygenase-2 (COX-2) is especially enhanced in damaged hepatocytes and Kupffer cells mainly during antigen induced inflammation by inflammatory cytokines under effect of stimuli such as pro-inflammatory IL-1b and TNFα resulting in increased production of prostanoids at the inflammation site (Tunctan 2020). Interlukin-6 (IL-6) is induced by infection and damage of tissues. Physiologically, serum concentration of IL-6 is very low, but it is rapidly elevated in cases of trauma, infection and injury, and it is considered as an early indicator of inflammation and a predictor of disease activity (Yang et al. 2016).

Myeloperoxidase (MPO) is a heme peroxidase enzyme; it catalyzes a reaction to produce hypochlorous acid that reacts with nucleic acids, proteins and lipids causing dangerous cellular effects and leads to inflammatory conditions such as the atherosclerotic changes (Aratani 2018). Caspase 3 is one of the pro-apoptotic caspases, contributed to signal transduction for programmed cell death. It induces apoptosis by activating caspase-activated DNase and DNA fragmentation (Kroemer 2016).Malondialdehyde (MDA) is produced endogenously from polyunsaturated fatty acids oxidation. Free MDA can be scavenged by protein and nucleic acids because it reacts with their functional groups. The level of oxidative stress cannot be reflected correctly by measuring the amount of free MDA; its toxicity is contributed to its ability to do cross linkage leading to mutagenesis(Ho et al. 2013).

Reactive oxygen species (ROS), the main oxidants are partially reduced oxygen metabolites that have strong oxidizing abilities. They are deleterious to cells at high concentrations because they can oxidize lipids and protein cellular components. Besides the damage of DNA, the prolonged production of ROS is considered a risk leading to the progression of the inflammatory processes. Their role in inducing inflammation has been excessively studied in experimental models (Pizzino et al. 2017). To avoid the harmful effects of oxidants, there are groups of antioxidants that can scavenge for removing ROS, including superoxide dismutase (SOD), catalase and glutathione peroxidase (GPx) (Handy and Loscalzo 2012).

Superoxide dismutase (SOD) is a metalloenzyme that catalyzes superoxide radical dismutation into hydrogen peroxide and molecular oxygen to protect cells from damage that results from accumulation of ROS (Singh et al. 2017). Catalase is a cytoplasmic antioxidant enzyme that can detoxify H_2O_2 to oxygen and water to maintain the homeostasis of cellular redox. It was reported to be an important enzyme associated with mutagenesis and inflammatorydisorders; also, it is related to oxidative stress states(Zhang et al. 2015).

Glutathione peroxidase (GPx) is an antioxidant selenoenzyme; it catalyzes the reduction of H_2O_2 to water and destroy fatty acid hydroperoxidesfor mitigating their toxicity. It acts in association with SOD and catalase as an antioxidant enzyme system to minimize ROS and their toxicity(Zhao et al. 2019).Glutathione reductase (GR), homodimeric flavoprotein cytosolic and mitochondrial enzyme that catalyzes glutathione disulfide (GSSG) reduction utilizing NADPH as the reducing cofactor to sustaincellular redox homeostasis(Iozef et al. 2000).

The aim of the present study is to assess the antioxidants of hepatic tissues in an induced oxidative stress by LPSin an experimental rat model at different time intervals (6 and 72 hours), and the correlation between the studied antioxidant indicators. This study is considered as an extension of a previous one titled "Time-dependent expression patterns of inflammatory markers in rat model of lipopolysaccharide-induced acute systemic inflammation" *Medical Science*, 2021, 25(118), 3336-3344 (Albataineh et al. 2021).

2. Materials and Methodology

2.1. Design of the study

Ninety albino rats, age-matched with weight range of 200-250 gm were divided into 30and 60 rats as control and test sets, respectively; then, each set was subdivided into two subgroups each including 15 and 30 rats, respectively. A standard diet was fed to the animals; they were housed in the animal house. The rats were given a light/dark cycle of 12:12 hours and free access to get water and food during the full time of the experiment. Each rat of the two subgroups of the controls were injected once with normal saline intraperitoneally. Teeling et al. [2020] was followed for suspending LPS (*Salmonella abortusequi* derivative) (L5886, Sigma, Poole, UK) in normal saline (Teeling et al. 2010). Each rat of the two test subgroups was injected once with LPS (100 µg/kg body weight) intraperitoneally.Later, one subgroup of both the controls and the test were sacrificed at 6 hours and the second control and test subgroups were sacrificed at 72 hours of the challenge to obtain their livers for the biochemical analyses of the required parameters in the tissues. The procedure of Aksoy et al. [2014] was used to prepare tissues for biochemical analyses(Aksoy et al. 2014).

2.2. Ethical considerations

The Ethics Committee of Faculty of Medicine, Mutah University had approved the study (reference no. 1302023).

2.3. Biochemical analyses

Engvall et al. [1971] method was used to analyze all studied oxidative indicators(Aksoy et al. 2014). The used kits for the biochemical analyses were purchased from ELK Biotechnology CO.,Ltd, China. About 100 mg of liver tissues were rinsed with 1X PBS (Phosphate buffered saline); then, homogenizedin 1 ml of 1XPBS and stored at -20ºC overnight. After performing two freeze-thaw cycles to break the cell membranes, the homogenates were centrifuged at 5000 x g for 5 min at 4°C. The supernatant was withdrawn, divided into aliquots, and stored at -80°C till the assay time.

2.4. Statistical analyses

SPSS Software version 25 was used to analyze the data statistically, and expressed as mean±SD. *t*-test was applied for comparing between groups. Spearman's correlation coefficient (*r*) was used to study the correlation between the numerical data. *P*value <0.05 was considered statistically significant.

3. Results

Table 1 shows mean±SD of all studied indicators after 6 hours of LPS challenge, and the results revealed statistically significant increase in TNFα, MPO, Caspase-3, COX-2, IL-6 and MDA levels. A statistically significant decrease in the level of catalase, on the other hand, there was statistically insignificant decrease in the levels of GPx, GR and SOD when the test group was compared to the controls.

Table 1. Comparison between the levels of the studied oxidative stress and antioxidant indicators expressed as mean±SDin the test group versus the controls after 6 hours of the challenge with LPS

Parameters	Control group (no. 15)	Test group (no. 30)	*P* value
TNF-α (ng/ml)	28.6 ±1.1	82.8±7.61	0.006
MPO (ng/ml)	3.64±0.70	7.82±0.90	0.025
Caspase-3 (U/g)	19.88±.1.72	37.20±2.10	0.001
COX-2 (ng/ml)	25.46±1.65	51.43±4.21	0.001
IL-6 (pg/ml)	89.40±2.95	156±6.44	0.033
MDA (nmol/g)	8.28±0.52	14.31±0.83	0.011
Catalase (U/g)	0.307±0.073	0.179±0.042	0.005
GPx (U/g)	45.58±1.66	39.27±1.34	0.420
GR (U/g)	67.39±7.35	59.23±6.92	0.322
SOD (U/g)	196.63±10.72	187±13.79	0.215

t-test was applied, *P* value <0.05 (significant).

By comparing mean±SD of all antioxidant indicators in the test group compared to the controls after 72 hours of the LPS administration, our findings showed statistically significant increase in the levels of TNFα, MPO, Caspase-3, COX-2, IL-6 and MDA. In addition, there was a statistically significant decrease on the level of catalase, and a statistically insignificant decrease in the levels of GPx, GR and SOD when the test group was compared to the controls. (Table 2)

Table 2. Comparison between the levels of the studied oxidative stress and antioxidant indicatorsas mean±SD in the test group versus the controls after 72 hours of the challenge with LPS

Parameters	Control group (no. 15)	Test group (no. 30)	*P* value
TNF-α (ng/ml)	26.3 ±1.12	94.6±7.73	0.012
MPO (ng/ml)	4.02±0.72	9.11±1.22	0.001
Caspase-3 (U/g)	18.96±.0.81	41.38±1.02	0.017
COX-2 (ng/ml)	28.03±1.52	61.98±4.35	0.005
IL-6 (pg/ml)	86.52±6.88	198.26±10.21	0.005
MDA (nmol/g)	9.215±0.66	17.47±0.92	0.001
Catalase (U/g)	0.295±0.079	0.133±0.091	0.000
GPx(U/g)	45.82±6.35	34.31±1.03	0.339
GR (U/g)	67.31±4.41	64.27±5.34	0.441
SOD (U/ml)	197.63±10.81	176.71±13.95	0.266

t-test was applied, *P* value <0.05 (significant).

In table 3, the comparison was between the antioxidant indicators in both test subgroups after 6 and 72 hours of LPS injection. Also, the results in the present study elucidate statistically significant increase in the levels of TNF-α, COX-2, IL-6, MDA, and there is low catalase activity, which could contribute to more oxidative stress. There was, however, insignificant difference in the levels of MPO, Caspase-3, GPx, GR and SOD in the test subgroup after 72 hours of the challenge when compared to the test subgroup after 6 hours.

Table 3. Comparison between the levels of the studied oxidative stress and antioxidant indicators expressed as mean±SD in the two test subgroups after 6 and 72 hours of the challenge with LPS

Parameters	6 hours test subgroup (no. 30)	72 hours test subgroup (no. 30)	*P* value
TNF-α (ng/ml)	82.8±7.61	94.6±7.73	0.037
MPO (ng/ml)	7.82±0.90	9.11±1.22	0.147
Caspase-3 (U/g)	37.20±2.10	41.38±1.02	0.332
COX-2 (ng/ml)	51.43±4.21	61.98±4.35	0.001
IL-6 (pg/ml)	156±6.44	198.26±10.21	0.005
MDA (nmol/g)	14.31±0.83	17.47±0.92	0.042
Catalase (U/g)	0.179±0.042	0.133±0.091	0.005
GPx (U/g)	39.27±1.34	34.31±1.03	0.115
GR (U/g)	59.23±6.92	55.27±5.34	0.247
SOD (U/ml)	187±13.79	176.71±13.95	0.062

t-test was applied, *P* value <0.05 (significant).

The correlation analysis was performed for all the studied mediators at a 6-hours interval. The values of Pearson's coefficient (r^2) were positive and statistically significant among the indicators, except the correlations between MDA on one hand and catalase, GPx, Gr and SOD on the other hand, they were negative, however, these correlations were statistically significant. The highest negative correlation was between MDA and SOD (r^2=-0.822), while the lowest positive one was between GPx and GR (r^2=0.322); on the other hand, the only insignificant correlation was between catalase and GR (r^2=0.282) (table 4).

Pearson's coefficient values (r^2) for the correlations between the studied indicators at a 72-hours interval were positive and statistically significant in the range of 0.376-0.774 except the correlations between MDA on the one hand and catalase, GPx, Gr and SOD on the other hand, which were negative and statistically significant. The highest correlation was between MPO and catalase (r^2=0.774), while the lowest one was between MDA and IL-6 (r^2=0.376); the insignificant correlations were between TNFα and Catalase, MDA and MPO, IL-6 and MPO, GPx and SOD (r^2=0.301, 0.288, 0.337 and 0.341, respectively) (table 5).

Table 4. The correlations between the studied oxidative stress and antioxidant indicators after 6 hours of the challenge with LPS [Pearson Correlation (r^2)]

	TNFα	MPO	Caspase	COX 2	IL-6	MDA	Catalase	GPx	GR	SOD
TNFα	1	0.544**	0.612**	0.733**	0.512**	0.549**	0.522*	0.612**	0.533*	0.667**
MPO	0.544**	1	0.679**	0.529*	0.702**	0.423*	0.549**	0.606*	0.552**	0.693**
Caspase	0.612**	0.679**	1	0.452*	0.647**	0.463*	0.395**	0.537**	0.507**	0.445**
COX-2	0.733**	0.529*	0.452*	1	0.558**	0.557**	0.628**	0.537*	0.665**	0.455**
IL-6	0.512**	0.702**	0.647**	0.558**	1	0.560**	0.680*	0.379*	0.669**	0.477*
MDA	0.549**	0.423*	0.463*	0.557**	0.560**	1	- 0.643**	- 0.559**	- 0.359*	- 0.822**
Catalase	0.522*	0.549**	0.395**	0.628**	0.680*	- 0.643**	1	0.469**	0.282***	0.441*
GPx	0.612**	0.606*	0.537**	0.537*	0.379*	- 0.559**	0.469**	1	0.322*	0.433**
GR	0.533*	0.552**	0.507**	0.665**	0.669**	- 0.359*	0.282***	0.322*	1	0.429**
SOD	0.667**	0.693**	0.445**	0.455**	0.477*	-0.822**	0.441*	0.433**	0.429**	1

** Correlation is significant at the 0.01 level (2-tailed); * Correlation is significant at the 0.05 level (2-tailed); ***insignificant correlation

Table 5. The correlations between the studied oxidative stress and antioxidant indicators after72 hours of the challenge with LPS [Pearson Correlation (r^2)]

	TNFα	MPO	Caspase	COX 2	IL-6	MDA	Catalase	GPx	GR	SOD
TNFα	1	0.616**	0.414*	0.403**	0.469**	0.482**	0.301***	0.726**	0.592**	0.417**
MPO	0.616**	1	0.455**	0.556*	0.337***	0.288***	0.774**	0.552**	0.479*	0.653**
Caspase	0.414*	0.455**	1	0.524**	0.643**	0.538**	0.558**	0.395**	0.686**	0.534**
COX-2	0.403**	0.556*	0.524**	1	0.567**	0.605**	0.723**	0.495**	0.510**	0.539**
IL-6	0.469**	0.337***	0.643**	0.567**	1	0.376**	0.666**	0.564**	0.644**	0.670**
MDA	0.482**	0.288***	0.538**	0.605**	0.376**	1	- 0.532**	- 0.561**	- 0.597**	- 0.652**
Catalase	0.301***	0.774**	0.558**	0.723**	0.666**	- 0.532**	1	0.545**	0.602**	0.602**
GPx	0.726**	0.552**	0.395**	0.495**	0.564**	- 0.561**	0.545**	1	0.453**	0.341***
GR	0.592**	0.479*	0.686**	0.510**	0.644**	- 0.597**	0.602**	0.453**	1	0.753**
SOD	0.417**	0.653**	0.534**	0.539**	0.670**	- 0.652**	0.602**	0.341***	0.753**	1

** Correlation is significant at the 0.01 level (2-tailed); * Correlation is significant at the 0.05 level (2-tailed); ***insignificant correlation

4. Discussion

Oxidative stress is attributed to the imbalance between excessive accumulation of ROS intracellularly and the inability of the antioxidants to detoxify them. Physiologically, ROS can play several roles such as cell signaling. When the production of ROS is exceeding the normal physiological limit, it can cause harmful effects on cellular components such as nucleic acids, proteins and lipids of the cells (Pizzino et al. 2017).Antioxidants are stable molecules having scavenging properties to terminate the chain reaction of free radicals before damaging the cellular vital molecules (Khallouki et al. 2022).

In the present study, LPS was used for the induction of oxidative stress in the experimental rat model and the changes in antioxidant indicators were studied after 6 and 72 hours-interval of the challenge. Upon comparing the levels of the indicators in the test group versus the controls, our results after 6 hours of the challenge revealed significant elevation in the levels of TNFα, MPO, Caspase-3, COX-2, IL-6 and MDA; the level of catalase showed a significant reduction, and the decrease in the levels of GPx, GR and SOD was insignificant. In a study conducted to explore the link between oxidative stress mediated by thyroid dysfunctioninduction and TNFα, the estimated oxidative stress indicators showed significant increase in TNFα and MDA levels in the rats under effect of oxidative stress status (Hazzaa et al. 2013). Another study revealed significant increase in the levels of TNFα and caspase-3 in the test group compared to the controls. Their obtained results were based on the proven link between the deficiency of TNFα and the prevention of oxidative stress in mice (Wang et al. 2017). In addition, Awooda et al. [2014] stated that TNFα and MDA levels were higher in brain tissues of rats due to oxidative stress induced by transient cerebral ischemia which showed an association between TNF-α and oxidative stress biomarkers (Awooda et al. 2014). Francéset al, demonstrated the contribution of TNF-α and the resulting oxidative stress in hepatic tissues in streptozotocin-induced diabetes in experimental animal models (Frances et al. 2013). Additionally, both TNF-α and MDA levels are significantly elevated in an induced sepsis and its associated oxidative stress (Erbaş and Taşkıran 2014). In a Turkish study, the animal model was under ischemic-induced oxidative stress status mediated through TNF-α;

the results showed significant higher levels of TNF-α. On the other hand, there was significant reduction in the activities of catalase and SOD (Akbulut et al. 2005).

When metabolic syndrome and ulcerative colitis were induced chemically in experimental rat model, the oxidative status in both situations was associated with rise of MPO, SOD, catalase and GPx levels in the test group when compared to the control group (Garagiola et al. 2016, Geetha et al. 2017). In addition, in rheumatoid arthritis patients, there was elevation of MPO level that was contributed to the inflammatory disorder and its associated oxidative stress status (Stamp et al. 2012). In another animal model study, liver and kidney were subjected to toxicity by carbon tetrachloride; the results of studying the oxidative stress status and antioxidants levels showed significant higher SOD and MDA, lower GPx and catalase in the test group versus the controls (Balahoroğlu et al. 2008). Chlorpyrifos, the pesticide, was used for inducing oxidative stress in rat model; then, the oxidative indicators were studied. The findings showed significant rise in TNF-α and caspase-3 levels, decrease in SOD, catalase and GPx in chlorpyrifos-treated rats after 14 consecutive days of exposure compared to the control group of rats (Owumi and Dim 2019).

Sulindac sulfide, the chemo-preventive agent, its effect was studies in several dying cell lines; it can generate an oxidative stress status leading to the initiation of an increase in the synthesis and activity of COX-2 (Sun et al. 2009). In a streptozotocin-induced diabetic retinopathy, the increase of oxidative stress is apparent through elevating the levels of MDA and IL-6, but catalase is reduced in the test group when compared to the controls. Additionally, IL-6 can reduce the oxidative stress in β cells of islets of Langerhans (Robinson et al. 2020). Furthermore, the generated and accumulated ROS in the diaphragm muscle in mice is associated with over-expression of circulating IL-6. The use of antioxidants for protecting mitochondria is capable of reducing IL-6 and oxidative stress in sepsis-induced state in a rat model (Lowes et al. 2013). Mostly, our obtained results were in accordance with those reported in some of the above- mentioned studies and yet disagree with others. These could be attributed to the difference in the type of animal model, the average of their weights, the different conditions in the animal house where the animals were kept, and the sample size.

In the present study, all antioxidant indicators in the test group were compared to the control group after 72 hours of the LPS injection intraperitoneally. Our results showed elevation in the levels of TNFα, MPO, Caspase-3, COX-2, IL-6 and MDA, a decrease in catalase level, and both situations were statistically significant, while there was insignificant reduction in the levels of GPx, GR and SOD. Halawa et al. [2018] studied the enhancement of oxidative stress and apoptosis in the testicular tissues of rats by LPS intraperitoneal administration (Halawa et al. 2018).The indicators of oxidative stress, antioxidants and caspase-3were investigated after 6 and 72 hours of the challenge; their results identified a slight insignificant and significant reduction in SOD levels after 6 hours and 72 hours of the LPS-treated group, respectively, compared to the controls. In both time intervals, there was significant reduction in catalase, and the level of MDA was increased significantly but without significant difference between 6 and 72 hours. In addition, the increase in the concentration of caspase-3 was higher after 6 hours than the controls with more increase after 72 hours; the difference in both comparisons was statistically significant, proving that it was time-dependent. Those results are in agreement with the obtained ones in the present study, especially the designation of the study to be time-dependent in investigating the oxidative status and the antioxidants after 6 and 72 hours-time intervals of LPS challenge.

Concerning the correlation analysis for all oxidative mediators at a 6 and 72-hours interval of LPS injection, Spearman's correlation coefficient was significant positively among all indicators. Moreover, there was a negative and statistically significant correlation between MDA and four of the indicators (catalase, GPx, GR and SOD). On the other hand, there were insignificant correlations between catalase and GR after 6-hours of the challenge, while the insignificant correlations after 72-hours of LPS injection were between TNFα and Catalase, MDA and MPO, IL-6 and MPO, GPx and SOD. Noeman et al. [2011] found negative significant and negative insignificant correlations between MDA and GPx on one hand and between MDA and catalase on the other hand, respectively, in hepatic tissues (Noeman et al. 2011).

5. Conclusion

In the present study, LPS was used to induce oxidative stress in rat model; the oxidative status results were in significant differences in the levels of TNFα, MPO, Caspase-3, COX-2, IL-6 MDA and catalase, and insignificant differences for GPx, GR and SOD after both intervals (6 and 72-hours). Levels of indicators showed significant differences when 6-hours interval were compared to 72-hours interval except for MPO, Caspase-3, GPx, GR and SOD. There were positive and negative significant correlations between the studied indicators except for catalase and GR, on the one hand, and for TNFα and catalase, MDA and MPO, IL-6 and MPO, GPx and SOD, on the other hand, after 6 and 72 hours of the challenge.

Funding

This project is funded by the Deanship of Scientific Research at Mutah University under the project number 773/2023

Conflict of Interest

The authors declare that there are no conflicts of interests.

References

Akbulut G, Dilek ON, Kahraman A, Köken T, Serteser M.2005. The correlation between renal tissue oxidative stress parameters and TNF-alpha levels in an experimental model of ischemia-reperfusion injury in mice. Ulus Travma Acil Cerrahi Derg. 2005 Jan;**11(1)**:11-6.

Aksoy AN, Toker A, Celık M, Aksoy M, Halıcı Z, Aksoy H. 2014. The effect of progesterone on systemic inflammation and oxidative stress in the rat model of sepsis. Indian J Pharmacol **46**: 622.

Albataineh EM, Abdulrahman S, Hussain SSF, Abd El Kareem HM, Mahgoub SS. 2021. Time-dependent expression patterns of inflammatory markers in rat model of lipopolysaccharide-induced acute systemic inflammation. Med Sci **25**: 3336-3344.

Aratani Y. 2018. Myeloperoxidase: Its role for host defense, inflammation, and neutrophil function. Arch Biochem Biophys **640**: 47-52.

Awooda HA, Sharara GM, Mahmoud SA. 2014. Tumor Necrosis Factor-α in Rats Following Transient Focal Cerebral Ischemia Reperfusion and Its Relation to Oxidative Stress. Int J Clin Exp Neu **2**: 24-28.

Balahoroğlu R, Dülger H, Özbek H, Bayram İ, Şekeroğlu MR. 2008. Protective effects of antioxidants on the experimental liver and kidney toxicity in mice. Eur J Gen Med. **5**: 157-164.

Chen X, Oppenheim JJ. 2016. Paradoxical effects of targeting TNF signalling in the treatment of autoimmunity. Nat Rev Rheumatol **12**: 625-626.

Di Gioia M, Zanoni I. 2015. Toll-like receptor co-receptors as master regulators of the immune response. Mol Immunol **63**: 143-152.

Erbaş O, Taşkıran D. 2014. Sepsis-induced changes in behavioral stereotypy in rats; involvement of tumor necrosis factor-alpha, oxidative stress, and dopamine turnover. Journal of Surgical Research **186**: 262-268.

Frances DEA, Ingaramo PI, Ronco MT, Carnovale CE. 2013. Diabetes, an inflammatory process: oxidative stress and TNF-alpha involved in hepatic complication. J Biomed Sci Eng, 2013, **6**, 645-653

Garagiola ML, Tarán M, Scribano MP, Balceda A, García E, Fonseca I, Moya M, Baez MC. 2016. Myeloperoxidase as an indicator of oxidative stress in metabolic syndrome. ev Argent Cardiol **84**: 514-518.

Geetha P, Kumar BL, Indra U, Sheetal P. 2017. Role of antioxidant and myeloperoxidase levels in 7, 12-dimethylbenz [a] anthracene induced experimental rat model: Evidence for oxidative damage in active ulcerative colitis. Int J Pharm Pharm Sci **9**: 282-286.

Gutsmann T, Schromm AB, Brandenburg K. 2007. The physicochemistry of endotoxins in relation to bioactivity. Int J Med Microbiol **297**: 341-352.

Halawa AA, El-Adl MA, Hamed MF, Balboula AZ, Elmetwally MA. 2018. Lipopolysaccharide prompts oxidative stress and apoptosis in rats' testicular tissue. J Vet Healthc **1**: 20-31.

Handy DE, Loscalzo J. 2012. Redox regulation of mitochondrial function. Antioxid Redox Signal **16**: 1323-1367.

Hazzaa S, Badr E, Abdou A. 2013. The link between oxidative stress response and tumor necrosis factor-alpha (TNF-alpha) in hepatic tissue of rats with induced thyroid dysfunction. J Afr Assoc Physiol Sci **1**: 47-54.

Ho E, Galougahi KK, Liu C-C, Bhindi R, Figtree GA. 2013. Biological markers of oxidative stress: applications to cardiovascular research and practice. Redox Biol **1**: 483-491.

Iozef R, Becker K, Boehme CC, Schirmer RH, Werner D. 2000. Assembly and functional expression of murine glutathione reductase cDNA: a sequence missing in expressed sequence tag libraries. Biochim Biophys Acta Mol Basis Dis **1500**: 137-141.

Kabanov D, Prokhorenko I. 2010. Structural analysis of lipopolysaccharides from Gram-negative bacteria. Biochem (Mosc)**75**: 383-404.

Khallouki F, Saber S, Bouddine T, Hajji L, Elbouhali B, Silvente-Poirot S, Poirot M. 2022. In vitro and In vivo oxidation and cleavage products of tocols: From chemical tuners to "VitaminEome" therapeutics. A narrative review. Food Biosci **49**: 101839.

Kroemer G. 2016. Dying cell recognition shapes the pathophysiology of cell death. Cell Death Differ **23**: 913-914.

Lowes D, Webster N, Murphy M, Galley H. 2013. Antioxidants that protect mitochondria reduce interleukin-6 and oxidative stress, improve mitochondrial function, and reduce biochemical markers of organ dysfunction in a rat model of acute sepsis. Br J Anaesth **110**: 472-480.

Milicaj J, Castro CD, Jaunbocus N, Taylor EA. 2021. Extraction of ADP-heptose and Kdo2-lipid A from E. coli deficient in the heptosyltransferase I gene. Appl Sci **11**: 8314.

Noeman SA, Hamooda HE, Baalash AA. 2011. Biochemical study of oxidative stress markers in the liver, kidney and heart of high fat diet induced obesity in rats. Diabetol Metab Syndr **3**: 1-8.

Owumi SE, Dim UJ. 2019. Manganese suppresses oxidative stress, inflammation and caspase-3 activation in rats exposed to chlorpyrifos. Toxicol Rep **6**: 202-209.

Pizzino G, Irrera N, Cucinotta M, Pallio G, Mannino F, Arcoraci V, Squadrito F, Altavilla D, Bitto A. 2017. Oxidative stress: harms and benefits for human health. Oxid Med Cell Longev 2017.

Robinson R, Srinivasan M, Shanmugam A, Ward A, Ganapathy V, Bloom J, Sharma A, Sharma S. 2020. Interleukin-6 trans-signaling inhibition prevents oxidative stress in a mouse model of early diabetic retinopathy. Redox biology **34**: 101574.

Singh N, Gupta VK, Kumar A, Sharma B. 2017. Synergistic effects of heavy metals and pesticides in living systems. Front Chem **5**: 70.

Stamp LK, Khalilova I, Tarr JM, Senthilmohan R, Turner R, Haigh RC, Winyard PG, Kettle AJ. 2012. Myeloperoxidase and oxidative stress in rheumatoid arthritis. Rheumatology (Oxford) **51**: 1796-1803.

Sun Y, Chen J, Rigas B. 2009. Chemopreventive agents induce oxidative stress in cancer cells leading to COX-2 overexpression and COX-2-independent cell death. Carcinogenesis **30**: 93-100.

Teeling J, Cunningham C, Newman TA, Perry V. 2010. The effect of non-steroidal anti-inflammatory agents on behavioural changes and cytokine production following systemic inflammation: Implications for a role of COX-1. Brain Behav Immun **24**: 409-419.

Tunctan B. 2020. **CYP-derived eicosanoids in inflammatory diseases.** Pages 106424.

Wang H, Li J, Gai Z, Kullak-Ublick GA, Liu Z. 2017. TNF-α deficiency prevents renal inflammation and oxidative stress in obese mice. Kidney Blood Press Res **2**: 416-427.

Yang R, Masters AR, Fortner KA, Champagne DP, Yanguas-Casás N, Silberger DJ, Weaver CT, Haynes L, Rincon M. 2016. IL-6 promotes the differentiation of a subset of naive CD8+ T cells into IL-21–producing B helper CD8+ T cells. J. Exp. Med **213**: 2281-2291.

Zhang F, Ren T, Wu J. 2015. TGF-β1 induces apoptosis of bone marrow-derived mesenchymal stem cells via regulation of mitochondrial reactive oxygen species production. Exp Ther Med **10**: 1224-1228.

Zhao L, Zong W, Zhang H, Liu R. 2019. Kidney toxicity and response of selenium containing protein-glutathione peroxidase (Gpx3) to CdTe QDs on different levels. Toxicol Sci **168**: 201-208.

JJBS

Volume 17, Number 3,September 2024
ISSN 1995-6673
Pages 487 – 494
https://doi.org/10.54319/jjbs/170311

Jordan Journal of Biological Sciences

Prevalence of Anemia Among Patients with Subclinical and Clinical Hypothyroidism in Jordan

Nada H. Al-Madanat[1,2], Manal A. Abbas [1,*]

[1] Faculty of Allied Medical Sciences, Al-Ahliyya Amman University, 19328 Amman, Jordan; [2] Precision Medical Labs, Jordan

Received: October 13, 2023; Revised: February 16, 2024; Accepted: March 13, 2024

Abstract

Malabsorption of iron and/or vitamin B_{12} and low thyroid hormone levels may cause anemia in patients with hypothyroidism. This cross-sectional study investigates anemia prevalence, types, and potential causes in 69 patients with hypothyroidism. The control group consisted of 31 healthy volunteers. Diagnostic assessments for hypothyroidism and anemia, in addition to participant-completed questionnaires, were conducted. Females with hypothyroidism exhibited a higher anemia prevalence (12:1 ratio) than males. Among L-thyroxine-treated patients, 22.8% had anemia compared to 11.5% in the untreated subclinical group with hypothyroidism ($p>0.05$). Females under L-thyroxine therapy had significantly lower hemoglobin level than females in the control group ($p=0.0001$). Also, L-thyroxine-treated females had lower ferritin level compared to the untreated females with hypothyroidism ($p=0.026$) and females in the control group ($p=0.007$) while having higher red blood cell distribution width (RDW) compared to the untreated females ($p=0.012$) and the control group females ($p=0.0001$). No significant differences in hemoglobin, ferritin, or RDW were found between males with hypothyroidism and the control group. Also, no significant differences were found among patients with hypothyroidism and the control group in Vitamin B_{12} level. Blood film examination revealed that normochromic normocytic anemia was present in 53.8% of anemic cases with hypothyroidism while hypochromic microcytic anemia was evident in 46.2% of cases. None of the anemic patients had macrocytic anemia. Ferritin level correlated negatively with RDW in patients with hypothyroidism treated with L-thyroxine ($r =-0.517$, $p <0.01$). In conclusion, screening and treating anemia in patients with hypothyroidism is recommended. Treatment with L-thyroxine alone may not be sufficient to prevent anemia in hypothyroidism.

Keywords: Anemia, Hashimoto, ferritin, hypothyroidism, L-thyroxine, red blood cell distribution width.

1. Introduction

According to a recent report, anemia in Eastern Mediterranean Region ranged between 22.6% - 63% amongst pregnant women, 27% - 69.6% amongst women of reproductive age, and 23.8% - 83.5% among children under the age of five (Abdo et al., 2019). Several factors contribute to the high prevalence of anemia in developing countries including the economic situation, health-care costs and poor dietary habits (Abu-Baker et al., 2021). Hypothyroidism is a common endocrine condition characterized by decreased thyroid hormone production. Most cases of primary hypothyroidism are caused by auto-immune thyroiditis (Hashimoto's thyroiditis), idiopathic atrophy, or earlier treatment of hyperthyroidism with radioactive iodine or surgery (Gittoes et al., 1997). Based on large number of studies, anemia is a common, although often underestimated, clinical condition accompanying thyroid diseases (Antonijević et al., 1999; Peraka et al., 2019; Shah et al., 2020).

In addition to the direct impact of low thyroid hormone on erythropoiesis, people with hypothyroidism may be more susceptible to anemia due to other conditions like heavy menstrual bleeding or difficulty absorbing vital nutrients like iron, Vitamin B_{12} and folate (Yadav et al., 2019). The severity of anemia in hypothyroidism was related to the degree of hypothyroidism (Yadav et al., 2019).

In hypothyroidism, anemia may manifest as normocytic, microcytic, or macrocytic (Antonijević et al., 1999). Microcytic anemia is typically attributed to iron malabsorption and iron loss through conditions like hypermenorrhea or menorrhagia, both of which are clinical manifestations associated with a deficiency in thyroid hormones (Szczepanek-Parulska et al., 2017). On the other hand, malabsorption of Vitamin B_{12}, folic acid and pernicious anemia are common causes of macrocytic anemia. Pernicious anemia occurs 20 times more frequently in individuals with hypothyroidism compared to the general population (Antonijević et al., 1999; Lippi et al., 2008). Normocytic anemia emerges due to the deficiency of thyroid hormones without accompanying nutritional deficits (Antonijević et al., 1999; Yadav et al., 2019).

Elevated rates of anemia in patients with hypothyroidism were documented in poor countries such as India and Bangladesh (Peraka et al., 2019; Shah et al., 2020). In contrast, no such association between anemia and hypothyroidism was identified in certain developed

* Corresponding author. e-mail: m.abbas@ammanu.edu.jo.

nations like the Netherlands (Du Puy et al., 2022). Given the scarcity of prior research on the prevalence of anemia among individuals with hypothyroidism in Jordan, this study was undertaken to explore its occurrence and identify its specific types. Identifying the type and cause of anemia will facilitate the implementation of appropriate treatments, supplements, and interventions.

2. Material and Method

2.1. Participants and ethical consideration

This cross-sectional study included 69 Jordanian adults with hypothyroidism of both sexes; thirty-four of them were untreated, newly diagnosed cases, and thirty-five patients were under L-thyroxine hormone replacement therapy. A 31 healthy, age-matched control subjects were included in the study. Exclusion criteria were: medical history of anemia of any type diagnosed before the diagnosis of hypothyroidism including pernicious anemia, pregnancy, cancer, thyroidectomy, radioactive iodine treatment, celiac disease, renal disease or any platelet dysfunction. The study was approved by the research ethical committee at Al-Ahliyya Amman University (ethical approval number IRB: AAU/1/10/2021-2022). Blood was collected after signing an informed consent form by participants. Also, a questionnaire was filled by each of them. The questionnaire included information about age, sex, body mass index (BMI), smoking, presence of chronic or autoimmune diseases, thyroidectomy, iron intake, vitamin intake, red meat intake, blood transfusion, COVID-19 infection and vaccination, menstrual cycle irregularities and bleeding extent, symptoms of hypothyroidism and medications.

2.2. Blood collection and processing

Two milliliters of blood were collected in EDTA tubes for complete blood count (CBC) and blood film testing. Plain; anticoagulant-free, tubes were used to collect 5 ml blood from participants between 10 am – 12 pm. After clot formation, blood samples were centrifuged at 5000 rpm for 7 minutes. The serum was then separated and assayed for Vitamin B_{12}, ferritin, thyroid peroxidase antibody (TPO), thyroid stimulating hormone (TSH), free tri-iodothyronine (FT_3) and free thyroxine (FT_4) testing within 2 hours of blood collection.

Kits for Vitamin B_{12}, TSH, TPO, FT_3 and FT_4 were purchased from Roche Diagnostics, USA and analyzed with Cobas e_{411} – Roche while ferritin was analyzed using (Cobas C_{311}) – Roche. For CBC Sysmex (XS-500i) analyzer. Blood film was stained with Wright's stain.

The precision assessment of the TPO assay involved the utilization of commercially available quality control material (Elecsys PreciControl ThyroAB) within two concentration ranges (level 1 and 2). BioRad standards were employed for Vitamin B_{12}, TSH, FT_3, and FT_4 assays. According to product information, the specificity of Roche Diagnostics' Elecsys was determined to be 95%, 99%, 99.5%, and 99.5% for Vitamin B_{12}, TSH, FT_4, and FT_3 tests, respectively. The sensitivity of Roche Diagnostics' Elecsys for the Vitamin B_{12} assay was established at 225 pg/mL. Additionally, the functional sensitivity values for TSH, FT_4, and FT_3 were measured at 0.014 µIU/mL, 0.2 pmol/L, and 0.15 pmol/L, respectively.

2.3. Statistical analysis

For statistical analysis, the Statistical Package for the Social Sciences (SPSS) version 26.0 (Chicago, IL, USA) was used. Normality of the distribution of variables was checked using the Kolmogorov-Smirnov and Shapiro-Wilk test. The difference in means for the 3 groups (newly diagnosed, untreated cases with hypothyroidism, L-thyroxine-treated cases of hypothyroidism and control) was carried out using one-way analysis of variance (ANOVA) for normally distributed variables followed by Tukey's post-hoc test. For variables which were not normally distributed, independent-sample Kruskal-Wallis test was used. Spearman's correlation coefficient was obtained after 2-tailed bivariate correlation analysis was performed. An on-line version of Fisher's Exact test (https://www.socscistatistics.com/tests/fisher/default2.aspx) was used to compare the symptoms of anemia and hypothyroidism in the treated and untreated groups. In all tests, a $p<0.05$ was considered significant.

3. Results

3.1. Demographic and clinical characteristics of the study's population

A total of 100 participants were recruited voluntarily in the study including newly diagnosed, untreated cases of hypothyroidism (n = 34), patients with hypothyroidism under L-thyroxine therapy (n = 35), and healthy controls (n = 31). About 82.4% of the untreated group had subclinical hypothyroidism while overt hypothyroidism was present in 17.6% of them.

The demographic and clinical data of the 3 studied groups is illustrated in Table 1**.** The age of the studied subjects ranged from 18-45 years with an average age of 33.4, 35.2 and 34.6 years for untreated, L-thyroxine-treated patients with hypothyroidism and healthy controls, respectively. No significant difference in age and gender was found between different groups (Table 1). Also, no significant differences in BMI, smoking, COVID-19 previous infection or vaccination were encountered. None of the participants had autoimmune disease or any other hormonal imbalance. Chronic diseases were present in 5.7% of the untreated group and 22.8% of the L-thyroxine-treated group but not in the healthy control group (Table 1).

In the untreated group, all females experienced regular menstrual cycles, with 34.7% of them reporting heavy bleeding. Conversely, among L-thyroxine-treated females with hypothyroidism, 79.3% had regular periods, and 24.1% experienced heavy bleeding. In the control group, all females had regular periods, and only 4.3% of them reported heavy bleeding. A significant difference in the regularity of menstrual period was found between the 3 studied groups (Table 1).

Table 1. Demographic and clinical data of untreated cases of hypothyroidism, treated patients with hypothyroidism, and control subjects. Data is represented as number (%).

	Variable	Untreated cases of hypothyroidism Number (%)	Cases of hypothyroidism under L-thyroxine treatment Number (%)	Control Number (%)	*p* value*
Number of participants		34	35	31	
Age (Years)	Average	33.4	35.2	34.6	0.474
	Range	19-45	21-45	18-45	
Gender	Male	11 (32.3)	6 (17.1)	9 (29.0)	0.342
	Female	23 (67.6)	29 (82.8)	22 (70.9)	
Chronic diseases	Present	2 (5.7)	8 (22.8)	-	0.005
	Absent	32 (94.1)	27 (77.1)	31 (100)	
Smoking	Cigarettes	6 (17.6)	5 (14.2)	3 (9.6)	0.462
	Hookah	11 (32.3)	13 (37.1)	6 (19.3)	
	Both	1 (2.9)	2 (5.7)	1 (3.2)	
	Stopped smoking	1 (2.9)	-	-	
	Not smoker	15 (44.1)	15 (42.8)	21 (67.7)	
Previous confirmed	Yes	29 (85.2)	29 (82.8)	23 (74.1)	0.532
COVID-19 infection	No	5 (14.7)	6 (17.1)	8 (25.8)	
Received COVID-19 Vaccine	1 dose	-	1 (2.8)	-	0.395
	2 doses	25 (73.5)	28 (80)	27 (87.0)	
	3 doses	9 (26.4)	6 (17.1)	4 (12.9)	
	None	-	-	-	
Vitamins intake	Vitamin B_{12}	9 (26.4)	12 (34.2)	12 (38.7)	0.878
	Vitamin D_3	22 (64.0)	27 (77.1)	14 (45.1)	0.017
	Iron	5 (14.7)	11 (31.4)	0	0.01
	Multivitamins	6 (17.6)	6 (17.1)	6 (19.3)	0.836
No meat intake (Vegetarians)		2 (5.9)	2 (5.7)	2 (6.4)	0.543
Autoimmune disease	Yes	-	-	-	---
	No	34 (100)	35 (100)	31 (100)	
Imbalance in other hormones	Yes	-	-	-	---
	No	34 (100)	35 (100)	31 (100)	
Regular period	Yes	23 (100)	23 (79.3)	22 (100)	0.006
(Females only)	No	-	6 (20.6)	-	
		*(out of 23)	*(out of 29)	*(out of 22)	
Period bleeding	Light	-	1 (3.4)	-	0.095
(Females only)	Medium	15 (65.2)	21 (72.1)	21 (95.5)	
	Heavy	8 (34.7)	7 (24.1)	1 (4.5)	
		*(out of 23)	*(out of 29)	*(out of 22)	
Relatives having hypothyroidism	Yes	27 (79.4)	31 (88.5)	1 (3.2)	0.0001
	No	7 (20.5)	4 (11.4)	30 (96.7)	
Type of medication	L-thyroxine	0	35 (100)	0	0.0001
Blood transfusion	Yes	0	0	0	
	No	34 (100)	35 (100)	31 (100)	
BMI	18.5-24.0	9 (26.4)	10 (28.5)	8 (25.8)	0.341
	24.5-30	14 (41.1)	18 (51.4)	15 (48.3)	
	> 30	10 (29.4)	6 (17.1)	6 (19.3)	
	NA	1 (2.9)	1 (2.8)	2 (6.4)	

Chronic diseases include: Hyper/hypotension, diabetes, hyperlipidemia, colon diseases, cancers, splenomegaly and platelets disorders.

* P value is based on chi square test results. $P<0.05$ was considered significant.

3.2. Comparison of thyroid function tests between different groups

The untreated group with hypothyroidism had higher TSH level compared to the control group (p=0.0001) and the treated group (p=0.0001) (Table 2). TSH level was within the normal range in 85.7% of the L-thyroxine-treated patients with hypothyroidism. No significant difference in TSH level between control and L-thyroxine-treated group was found (Table 2).

Both untreated and L-thyroxine-treated groups with hypothyroidism had significantly higher TPO levels compared to the control group (p=0.0001). No significant difference between untreated and L-thyroxine-treated groups in TPO level was found. High TPO levels (>16 IU/ml) were present in 70.6% of the untreated and 57.1% of L-thyroxine-treated cases with hypothyroidism with no significant difference between treated and untreated groups (p>0.05).

Patients in the treated group, receiving L-thyroxine hormone replacement therapy, had higher FT_4 levels compared to the control group (p=0.01) and untreated group (p=0.0001). No significant difference between the untreated and the control group in FT_4 level was found. On the other hand, a significantly lower FT_3 level was reported in the treated group compared to the control group (p=0.028).

Table 2. Laboratory characteristics of the study groups. Values are the mean±SD

Parameter	Normal range	Newly diagnosed, untreated group (n=34)	L-thyroxine-treated group (n=35)	Control group (n=31)	*p* value
Hb (g/dL)	Male: (13.8-18.0)	15.6±1.26	15.0± 1.16	15.6 ±1.05	0.564
	Female: (12.0-16.0)	13.0±1.41	12.2 ± 1.15	13.8±0.81	0.0001
Hct (%)	Male: (42.0-45.0)	46.7±4.23	44.4± 3.14	46.4±2.84	0.479
	Female: (37.0-47.0)	39.8±3.67	37.8 ± 3.06	43.1±3.24	0.0001
RBC (x10^12/L)	Male: (4.70-6.10)	5.23±0.37	5.06± 0.60	5.21±0.28	0.534
	Female: (4.20-5.40)	4.71±0.32	4.44± 0.35	4.80±0.28	0.001
RDW (%)	Male: (11.8-14.5)	13.9±0.74	14.0± 0.57	14.2±0.72	0.711
	Female: (12.2-16.1)	14.0±0.81	15.0± 1.35	13.7 ±0.84	0.0001
MCV (fL)	(76.0-99.0)	86.4±7.51	86.0 ± 6.44	87.5±4.74	0.601
MCH (pg)	(27.0-31.0)	28.8±2.56	28.2 ± 2.68	29.2±1.55	0.409
MCHC (g/dL)	(32.0-36.0)	32.7±1.41	32.7 ± 1.23	33.4±1.23	0.108
WBCs (x10^9/L)	(4.0-11.0)	7.45±2.00	7.03± 1.79	6.73±1.17	0.210
Neutrophils (%)	(2.0-7.0)	56.9±10.3	57.8 ± 8.14	56.8±7.38	0.921
Lymphocytes (%)	(1.0-3.0)	35.5±9.34	34.7 7.26	35.0±7.00	0.983
Monocytes (%)	(0.20-1.0)	6.5±1.88	6.45 1.88	6.90±1.59	0.702
Eosinophils (%)	(0.02-0.50)	1.02±0.1	1.02 0.16	1.16±0.72	0.712
Platelets (x10^3/µL)	(150-450)	281.6 ±64.5	281.8 ± 70.2	262.4 ±57.8	0.389
Ferritin (ng/ml)	Male: (30-400)	131.1±62.0	111.3 ± 61.3	123.2 ±53.1	0.719
	Female: (15-150)	83.6 ±104.3	41.1 ± 42.6	61.3 ±25.6	0.014
Vitamin B_{12} (pg/mL)	(200-1000)	284.3 ±162.4	291.4 ±149	352.3 ±93.9	0.104
TSH (uIU/ml)	(0.27-4.20)	18.4 ±37.6	3.39 ± 9.34	2.03 ±0.68	0.0001
FT_3 (pg/mL)	(2.0-4.4)	2.73 ±0.62	2.60 ± 0.50	2.83 ±0.38	0.037
FT_4 (ng/ml)	(0.93-1.71)	1.20 ±0.33	1.44 ± 0.23	1.26 ±0.16	0.0001
TPO (IU/ml)	(1.0-16.0)	185.3 ±188.7	250.4 ± 265	10.94 ±6.71	0.0001

SD: Standard deviation.

P values are based on ANOVA test for normally distributed variables and Kruskal-Wallis test for variables that are not distributed normally.

3.3. Comparison of hematological parameters between different groups

3.3.1. Hemoglobin (Hb) level

In females, the Hb level was significantly lower in the L-thyroxine-treated group, but not in the untreated group, compared to the control group (p=0.0001). On the other hand, no significant difference in Hb level between males with hypothyroidism, including treated and untreated groups, and the control group was observed (Table 2).

Females with hypothyroidism exhibited a higher anemia prevalence than males (12:1 ratio). No significant difference in the prevalence of anemia between treated and untreated cases of hypothyroidism was found (p>0.05). Within the L-thyroxine-treated group, anemia was present in 22.8% of cases (7 females and 1 male): 5 cases had mild anemia while 3 cases had moderate anemia. None of the patients had severe anemia. In the untreated group with overt hypothyroidism, 2 patients out of 8 (25%) had

anemia: 1 case of mild and 1 case of moderate anemia. In patients with subclinical hypothyroidism, 3 females out of 26 cases (11.5%) had anemia: 1 case was mild and 2 cases were moderate anemias. On the other hand, none of the control group had anemia.

3.3.2. Hematocrit (Hct)

L-thyroxine-treated females had lower Hct level compared to females in the control group (p=0.0001), while no significant difference was observed between untreated females and females in the control group. Also, no significant difference between males in different groups was found (Table 2).

3.3.3. Red blood cell (RBC) count

L-thyroxine-treated females had lower RBC count compared to the control females (p=0.001) and untreated females (p=0.016). No significant difference in RBC count between males in different groups was found (Table 2).

3.3.4. Red blood cell distribution width (RDW)

In females, the L-thyroxine-treated group had significantly higher RDW levels compared to the untreated female group (p=0.012) and control group (p=0.0001). No significant difference in RDW between males in different groups was found (Table 2).

3.3.5. RBC indices

No significant difference was found in mean corpuscular volume (MCV), mean corpuscular hemoglobin (MCH) and mean corpuscular hemoglobin concentration (MCHC) between L-thyroxine-treated, untreated patients with hypothyroidism and control subjects according to the data set in Table 2.

3.3.6. Blood film

Blood film examination revealed that normochromic normocytic anemia was present in 53.8% of anemic cases with hypothyroidism while hypochromic microcytic anemia was evident in 46.2% of cases.

3.3.7. Ferritin levels

Low ferritin level was present in 37.1% of the L-thyroxine-treated group and 5.9 % in the untreated group with hypothyroidism with significant difference between the two groups (p=0.0027). Based on the questionnaire, 14.7% and 31.4% of the untreated and treated patients with hypothyroidism, respectively, are taking iron supplementation (Table 1). In females, the L-thyroxine-treated group had significantly lower ferritin level compared to the untreated (p=0.026) and control groups (p=0.007). No significant difference was detected between the 3 male groups in ferritin level (Table 2).

3.3.8. Vitamin B_{12}

No significant difference was found between the three studied groups in Vitamin B_{12}level (Table 2).

3.4. Correlation between ferritin and different Lab parameters in patients with hypothyroidism treated with L-thyroxine

No correlation was found between the duration of treatment with L-thyroxine and Hb or ferritin levels ($p>0.05$). On the other hand, a positive correlation was found between ferritin level and FT_4 ($r =0.362$, $p <0.05$), Hb ($r =0.637$, $p <0.01$), Hct ($r =0.601$, $p <0.01$), MCH ($r = 0.488$, $p < 0.01$) and MCV ($r = 0.555$, $p < 0.01$). Also, a negative correlation between ferritin and RDW ($r =-0.517$, $p <0.01$) was found in patients with hypothyroidism treated with L-thyroxine (Table 3).

Table 3. Correlation between ferritin and different Lab parameters in patients with hypothyroidism treated with L-thyroxine

		VitaminB12	Ferritin	TSH	TPO	T3	T4	Hb	Hct	RBC	RDW	MCH	MCHC	MCV
VitaminB12	Correlation Coefficient	1.0001	-.288	-.101	.095	-.074	-.147	-.196	-.169	-.004	.368*	-.334*	-.260	-.280
	Sig. (2-tailed)	.	.094	.564	.588	.673	.399	.259	.331	.982	.030	.050	.132	.103
Ferritin	Correlation Coefficient	-.288	1.0001	-.189	-.138	.221	.362*	.637**	.601**	.085	-.517**	.488**	.257	.555**
	Sig. (2-tailed)	.094	.	.278	.431	.202	.033	.0001	.0001	.625	.001	.003	.136	.001
TSH	Correlation Coefficient	-.101	-.189	1.0001	.097	-.152	-.529**	-.209	-.215	-.171	.160	.107	-.073	.150
	Sig. (2-tailed)	.564	.278	.	.581	.382	.001	.229	.216	.325	.358	.541	.677	.390
TPO	Correlation Coefficient	.095	-.138	.097	1.0001	.250	-.074	.114	.125	.074	.088	.121	.021	.100
	Sig. (2-tailed)	.588	.431	.581	.	.147	.674	.514	.476	.673	.617	.488	.904	.567
FT3	Correlation Coefficient	-.074	.221	-.152	.250	1.0001	.391*	.239	.321	.165	-.067	.043	-.080	.180
	Sig. (2-tailed)	.673	.202	.382	.147	.	.020	.166	.060	.342	.700	.807	.647	.299
FT4	Correlation Coefficient	-.147	.362*	-.529**	-.074	.391*	1.0001	.322	.377*	.176	-.293	.084	-.138	.158
	Sig. (2-tailed)	.399	.033	.001	.674	.020	.	.059	.025	.312	.088	.630	.429	.365
Hb	Correlation Coefficient	-.196	.637**	-.209	.114	.239	.322	1.0001	.936**	.509**	-.604**	.462**	.464**	.380*
	Sig. (2-tailed)	.259	.0001	.229	.514	.166	.059	.	.0001	.002	.0001	.005	.005	.024
Hct	Correlation Coefficient	-.169	.601**	-.215	.125	.321	.377*	.936**	1.0001	.607**	-.437**	.307	.229	.349*
	Sig. (2-tailed)	.331	.0001	.216	.476	.060	.025	.0001	.	.0001	.009	.073	.187	.040
RBC	Correlation Coefficient	-.004	.085	-.171	.074	.165	.176	.509**	.607**	1.0001	.062	-.400*	-.039	-.426*
	Sig. (2-tailed)	.982	.625	.325	.673	.342	.312	.002	.0001	.	.723	.017	.825	.011
RDW	Correlation Coefficient	.368*	-.517**	.160	.088	-.067	-.293	-.604**	-.437**	.062	1.0001	-.715**	-.661**	-.548**
	Sig. (2-tailed)	.030	.001	.358	.617	.700	.088	.0001	.009	.723	.	.0001	.0001	.001
MCH	Correlation Coefficient	-.334*	.488**	.107	.121	.043	.084	.462**	.307	-.400*	-.715**	1.0001	.623**	.870**
	Sig. (2-tailed)	.050	.003	.541	.488	.807	.630	.005	.073	.017	.0001	.	.0001	.0001
MCHC	Correlation Coefficient	-.260	.257	-.073	.021	-.080	-.138	.464**	.229	-.039	-.661**	.623**	1.0001	.311
	Sig. (2-tailed)	.132	.136	.677	.904	.647	.429	.005	.187	.825	.0001	.0001	.	.069
MCV	Correlation Coefficient	-.280	.555**	.150	.100	.180	.158	.380*	.349*	-.426*	-.548**	.870**	.311	1.0001
	Sig. (2-tailed)	.103	.001	.390	.567	.299	.365	.024	.040	.011	.001	.0001	.069	.

*. Correlation is significant at the 0.05 level (2-tailed). **. Correlation is significant at the 0.01 level (2-tailed).

3.5. Symptoms of anemia in hypothyroidism groups.

Based on the gathered information from the questionnaire, 79.60% of the patients in the untreated group had no symptoms of anemia, while all L-thyroxine-treated patients had at least one symptom of anemia. About 8.80% of the untreated group and 33.6% of the treated group complained from weakness and tiredness which was statisticaly significant between the two groups ($p<0.05$), whereas 5.80% of the untreated group presented with palpitation, compared to 23.5% in the treated group, and it was significant between the two groups ($p<0.05$). A significant difference was present in hair loss between untreated and treated group ($p<0.05$) in which 23.0% of patients in the treated group had hair loss compared to 0% in the untreated group. Also, 2.90% of the untreated group had shortness of breath compared to 4.70% in the treated group. Also, 2.90% had pallor in the untreated group compared to 15.20% in the treated group which was significant between the two groups ($p<0.05$).

4. Discussion

Routine monitoring for anemia is imperative in individuals with hypothyroidism, as it is frequently observed in such cases (Shah et al., 2020). In light of the limited clinical manifestations of anemia in subclinical hypothyroidism, it is advised to conduct regular investigations for early detection and management as recommended earlier (Anand et al., 2018). This aligns with our findings, indicating that 79.60% of newly diagnosed, untreated cases of hypothyroidism displayed no symptoms of anemia.

In the current investigation, anemia was present in 11.5% of Jordanian patients with subclinical hypothyroidism, 25% of patients with overt untreated hypothyroidism and 22.8% among L-thyroxine-treated patients. In different countries, prevalence rates of hypothyroidism-associated anemia varied. In India, anemia was prevalent in 26.6% of patients with subclinical hypothyroidism and 73.2% of patients with overt hypothyroidism (Peraka et al., 2019). In another study in India, anemia was found in 69% of the overt group and 56% of the subclinical group with hypothyroidism (Anand et al., 2018). In Bangladesh, anemia was present in 21- 60 % of patients with hypothyroidism (Shah et al., 2020). On the other hand, no baseline associations were found between TSH and Hb levels or the presence of anemia in patients with hypothyroidism in Netherlands (Du Puy et al., 2022).A simple explanation for the contradicting findings between different studies is that it is expected that the prevalence of anemia among patients with

hypothyroidism is higher in poorer countries since it is related to the prevalence of anemia in the general population. Based on WHO reports, anemia prevalence is higher in poor countries and can reach 33% of the general population (WHO, 2017). According to a study conducted in India, anemia was present in 86.6% of the hypothyroid group and 33% in the euthyroid control group (Aparajita et al., 2022). It is important to highlight that our study excluded all cases of anemia diagnosed before the onset of hypothyroidism. Therefore, our findings reflect cases of hypothyroidism-associated anemia only.

It has been suggested that thyroid hormones promote erythropoiesis by increasing erythropoietin gene expression (Golde et al., 1977). In the current study, some patients under L-thyroxine therapy had anemia despite high FT_4 levels compared to the control group. In a recently published study, L-thyroxine treatment failed to rise Hb levels in persons aged 65 years and older with subclinical hypothyroidism (Du Puy et al., 2022). In another study, treatment with L-thyroxine plus iron was superior to treatment with L-thyroxine alone or iron alone in increasing Hb levels (Ravanbod et al., 2013). Therefore, identifying the precise nutritional deficiency in individuals with hypothyroidism is essential for the appropriate treatment of anemia.

In the current investigation, blood film examination demonstrated that 53.8% of anemic cases were normocytic normochromic. This type of anemia emerges due to the deficiency of thyroid hormones without accompanying nutritional deficits (Antonijević et al., 1999; Yadav et al., 2019). On the other hand, 46.2% of anemia cases were diagnosed as iron deficiency anemia. Anisopoikilocytosis was commonly seen. This may explain the higher RDW levels in L-thyroxine-treated patients, with lower ferritin and Hb levels, compared to the control group. These findings agree with previous studies reporting a statistically significant higher RDW value in patients with hypothyroidism (Aparajita et al., 2022). Therefore, checking RDW and RBC morphology in blood film, rather than relying solely on MCV, is essential in such cases to diagnose hypothyroidism-associated anemia.

To be diagnosed with iron deficiency anemia, the patient must have Hb levels of less than 12 g/dL in females, ferritin levels of less than 30 g/L and/or two of the appearance characteristic of iron deficiency anemia (e.g. microcytosis, hypochromia, anisocytosis, poikilocytosis) (WHO, 2007). Depending on our findings, low ferritin levels in anemic group, anisopoikilocytosis in the peripheral blood film and significantly higher RDW in L-thyroxine-treated hypothyroid group existed, confirming the diagnosis of iron deficiency anemia.

In the current investigation only mild or moderate anemia were reported. According to the questionnaire, 14.7% of untreated patients and 31.4% of treated patients with hypothyroidism reported taking iron supplementation. This could potentially reduce the severity of anemia in anemic patients with hypothyroidism.

Multiple studies have indicated that ferritin levels in individuals with hypothyroidism are lower compared to those in healthy individuals (Tripathi et al., 2019; Zwirska-Korczala et al., 1990). In our study, 37.1% of females in the L-thyroxine-treated group exhibited low ferritin levels, contrasting with the 0% observed in the females in the control group. A potential contributor to anemia in hypothyroidism is excessive bleeding in female patients. This may elucidate why L-thyroxine-treated females, in contrast to males with hypothyroidism, demonstrated lower hemoglobin and ferritin levels compared to the control group. Approximately 34.7% of untreated females and 24.1% of treated females experienced heavy bleeding, contrasting with only 4.5% in the control group. This finding aligns with prior research, suggesting an elevated risk of blood loss associated with menorrhagia in women with hypothyroidism, which was accused of iron deficiency in hypothyroidism (Christ-Crain et al., 2003; Peraka et al., 2019).

Our study did not identify any significant differences in Vitamin B_{12} levels between individuals with hypothyroidism and the control group. These results contrast with a study that reported a notable decrease in Vitamin B_{12} levels in patients with hypothyroidism compared to individuals without the condition (Tripathi et al., 2019). One potential explanation for our findings is that 26.4% of the untreated group and 34.2% of the L-thyroxine-treated group were supplementing with Vitamin B_{12}, reducing the likelihood of Vitamin B_{12} deficiency. It has been proposed that celiac disease may contribute to Vitamin B_{12} deficiency in patients with hypothyroidism (Aon et al., 2022). However, individuals with celiac disease were excluded from our study. This might clarify our observation that macrocytic anemia was not reported in patients with hypothyroidism. In a previous investigation, Vitamin B_{12} deficiency anemia was reported in 9% of patients with hypothyroidism and this percent was equal to the prevalence of macrocytic anemia in the general population (Mehmet et al., 2012).

5. Conclusion

The results of this study revealed a significant prevalence of anemia among individuals with hypothyroidism in Jordan, especially among females. The identified types of anemia included normochromic normocytic anemia and hypochromic microcytic anemia, with no instances of macrocytic anemia observed in patients with hypothyroidism. RDW emerged as a vital hematological parameter indicating the degree of erythrocyte anisocytosis, and its correlation with ferritin levels, reflecting the iron deficiency status, underscores its importance.

The present findings suggest that it is crucial to screen for anemia in hypothyroidism and to initiate timely and appropriate treatment before the condition deteriorates. Additionally, it is worth noting that relying solely on L-thyroxine treatment may not be sufficient to prevent anemia in hypothyroidism, especially in females with menorrhagia.

Conflict of interest statement

All the authors declare that they have no conflict of interest in this work.

References

Abdo N, Douglas S, Batieha A, Khader Y, Jaddou H, Al-Khatib S, El-Khatib M, AbuZaid H, Ajlouni K. 2019. The prevalence and determinants of anemia in jordan. *EMHJ*. **25**(5):341-349.

Abu-Baker NN, Eyadat AM, Khamaiseh AM. 2021. The impact of nutrition education on knowledge, attitude, and practice regarding iron deficiency anemia among female adolescent students in jordan. *Heliyon*. **7**(2):e06348.

Anand R, Mishra AK, Mahdi AA, Verma SP, Gupta KK. 2018. A study of prevalence and pattern of anemia in primary hypothyroidism. *IJMEDPH*. **7**(2):153-160.

Antonijević N, Nesović M, Trbojević B, Milosević R. 1999. Anemia in hypothyroidism. *Medicinski pregled*. **52**(3-5):136-40.

Aon M, Taha S, Mahfouz K, Ibrahim MM, Aoun AH. 2022. Vitamin b12 (cobalamin) deficiency in overt and subclinical primary hypothyroidism. *Clin Med Insights: Endocrinol Diabetes*. **15**:11795514221086634.

Aparajita S, Manas T, Santasmita P. 2022. Red blood cell indices and hypothyroidism. JK Science: *J Med Educ Res*. **24**(3):177-182.

Christ-Crain M, Meier C, Huber P, Zulewski H, Staub J-J, Muller B. 2003. Effect of restoration of euthyroidism on peripheral blood cells and erythropoietin in women with subclinical hypothyroidism. *Hormones* (Athens). 2:237-242.

Du Puy RS, Poortvliet RK, Mooijaart SP, Stott DJ, Quinn T, Sattar N, Westendorp RG, Kearney PM, McCarthy VJ, Byrne S. 2022. No effect of levothyroxine on hemoglobin in older adults with subclinical hypothyroidism: Pooled results from 2 randomized controlled trials. *J Clin Endocrinol Metab*. **107**(6):e2339-e2347.

Gittoes NJ, McCabe CJ, Verhaeg J, Sheppard MC, Franklyn JA. 1997. Thyroid hormone and estrogen receptor expression in normal pituitary and nonfunctioning tumors of the anterior pituitary. *J Clin Endocrinol Metabol*. **82**(6):1960-1967.

Golde D, Bersch N, Chopra I, Cline M. 1977. Thyroid hormones stimulate erythropoiesis in vitro. *Br J Haematol*. **37**(2):173-177.

Lippi G, Montagnana M, Salvagno GL, Guidi GC, Targher G. 2008. Prevalence of folic Acid and vitamin B12 deficiencies in patients with thyroid disorders. *AJMS*, **336**(1):50-2.

Mehmet E, Aybike K, Ganidagli S, Mustafa K. 2012. Characteristics of anemia in subclinical and overt hypothyroid patients. *Endocr J*. **59**(3):213-220.

Peraka SA, Karre S, Ravuri S, Shanmugam CK. 2019. To evaluate prevalence of anaemia in hypothyroid patients. *J Diagn Pathol Oncol*. **4**(2):110-113.

Ravanbod M, Asadipooya K, Kalantarhormozi M, Nabipour I, Omrani GR. 2013. Treatment of iron-deficiency anemia in patients with subclinical hypothyroidism. *Am J med.***126**(5):420-424.

Shah MS, Begum M, Akter MD, Rahman AA, Uddin MF, Rahman MJ. 2020. Anaemia in hypothyroidism. *Bangladesh Med Res Counc Bull*. **46**(1):55-60.

Szczepanek-Parulska E, Hernik A, Ruchała M. 2017. Anemia in thyroid diseases. *Pol Arch InternMed.*, **127**(5):352-60.

Tripathi P, Saxena N, Verma MK, Singh AN. 2019. Association of vitamin b12, folate and ferritin with thyroid hormones in hypothyroidism. *AIMDR*. **5**(1):1.

WHO. 2017. Nutritional anaemias: Tools for effective prevention and control.

WHO C. 2007. Assessing the iron status of populations. Geneva. World Health Organization.

Yadav RK, Ahmad M, Mathur MK, Dhingra V. 2019. Study of prevalence and types of anemia in primary hypothyroidism. *IMSEAR*. **6**(5):1574.

Zwirska-Korczala K, Buntner B, Sobieraj H, Ostrowska Z, Kniazewski B, Swietochowska E. 1990. Serum ferritin, iron and transferrin in women with thyrotoxic graves' disease before and after methimazole treatment. *Acta Physiologica Polonica*. **41**(7):163-168.

JJBS

Volume 17, Number 3,September 2024
ISSN 1995-6673
Pages 495 – 505
https://doi.org/10.54319/jjbs/170312

Jordan Journal of Biological Sciences

Biological Diversity of Seawater Microalgae Isolated from Ujung Genteng Sukabumi and Their Novel Genomic DNA Isolation Technique

Miftahul Huda Fendiyanto[1,*], Ence Darmo Jaya Supena[1,2], Iin Eka Sari[2], Mentari Putri Pratami[1], Rizky Dwi Satrio[1], Isna Arofatun Nikmah[1]

[1]*Study Program of Biology, Faculty of Military Mathematics and Natural Sciences, Indonesia Defense University. Kampus Universitas Pertahanan Sentul Bogor, Kawasan IPSC, 16810, West Java, Indonesia;* [2]*Department of Biology, Faculty of Mathematics and Natural Sciences, Bogor Agricultural University. Kampus IPB Darmaga Bogor 16680, West Java, Indonesia*

Received: December 17, 2023; Revised: March 9, 2024; Accepted: March 14, 2024

Abstract.

The Ujung Genteng Beach, located in Sukabumi, is renowned for its extensive seagrass beds and functions as an intertidal area. However, there has been limited scientific investigation into the diversity of microalgae in this ecosystem. This research aimed to identify the diversity of microalgae sourced from the seawater of Ujung Genteng Beach based on morphological characteristics and optimize DNA isolation and amplification techniques. Sampling was conducted three times at predetermined research locations. Morphological identification was performed using a binocular microscope, while DNA isolation and amplification were performed using CTAB methods with modification. The number of species found at Ujung Genteng Beach, Sukabumi is 47 species, 12 of which are often found at the three research locations both morning and afternoon, namely Navicula sp., Frustulia sp., Diploneis parma, Nitzschia sp., Achnanthidium sp., Amphora sp., Oscillatoria teneuis, Achanthes sp., Planothidium sp., Uronema sp., Zygnema sp., and Flagillaria sp.Based on the gel image, genomic DNA of seawater microalgae was successfully isolated, despite the relatively low purity and concentration. Analysis of diversity index and species diversity revealed variations in species abundance and diversity among different locations, particularly in seawater microalgae found within distinct zones: 0-2 meters from the low tide line (location I), seawater within seagrass areas located 2-5 meters away (location II), and seawater near the open sea, situated 5-10 meters away (location III).Therefore, the diversity of microalgae at all sampling locations was in the medium category and the uniformity index between species was low.

Keywords: DNA Isolation, Genomic, Microalgae, Seawater, Ujung Genteng Sukabumi

1. Introduction

Indonesia has an area of around 7.81 million km2, of which 5.9 million km2 is sea with a coastline of 108,920 km. This fact makes Indonesia one of the largest marine mega biodiversity areas in the world, one of which is microalgae (Setiawan 2018). Microalgae are microscopic microscopic plants (between 3-30 µm in diameter) which are included in the algae class and live as colonies or single cells in all fresh and marine waters (Amini and Susilowati 2010; Fendiyanto et al. 2023). The habitat of microalgae is that it occupies damp places such as rocks, tree trunks, cliffs, and is able to live in hot springs (Gusrianto 2012). Microalgae have an important role as primary producers of oxygen produced from the photosynthesis process (Waluyo 2004). Economically, microalgae are widely used as raw materials for the production of medicines, cosmetics, bioremediation and bioenergy (Purbani et al. 2019; Pratami et al. 2022).

Microalgae identification is divided into two ways, namely morphological identification which is used to determine the type of microalgae species, and molecular identification which is used to support the morphological identification. Microalgae are a very heterogeneous group of organisms with different characteristics, including differences in cell tissue type, cell size, cell morphology, and cell color (Mercer and Armenta 2011; Fendiyanto et al. 2023). Based on the research results of Suharno and Lantang (2012) who have observed the morphology of the microalgae found in Manokwari and Sorong Sea Waters, West Papua, it is dominated by the types Diatoma sp., Euglena sp., Lyngbya sp., Navicula sp., Proboschia sp., Spirogyra sp., Nitzschia sp., Bacteriastrum sp., Peridinium sp., and Rhisosolenia sp. Other morphological identification results were shown by the identification of 21 genera of microalgae in Tanah Merah Bay, Jayapura (Sujarta et al. 2011).

Molecular identification is needed to strengthen morphological data which has limited characters and tends to be influenced by the environment. Identification based on molecular characters is obtained from DNA sequences taken from nucleus, chloroplasts and mitochondria (Suparman 2012; Pratami et al. 2023). Molecular identification in plants including microalgae is also widely

* Corresponding author. e-mail: miftahul.fendiyanto@idu.ac.id.

studied based on RNA through gene expression analysis (Satrio et al. 2019; Fendiyanto et al. 2021; Fendiyanto et al. 2023) and/or molecular dynamics i.e., metabolomic approaches (Fendiyanto et al. 2020; Fendiyanto et al. 2021). Based on the research results of Purbani et al. (2019) showed that 14 isolates of marine microalgae from Tambrauw, West Papua which were traced using the NCBI website generally had a homology percentage of 98-99% to the closest type strain. A similarity value of 95-100% can be stated as the same species (Henry et al. 2000). Another study revealed that a total of 1,293 representative sequences of seawater microalgae from Kuwaiti waters could be classified into different eukaryotic taxa. The results showed that the microalgae communities in Kuwait waters were diverse and varied significantly between different ones during winter and summer (Kumar et al. 2021).

Ujung Genteng is a coastal area on the southern coast of West Java which is included in the Pangumbahan Beach area, Ciracap District, Sukabumi Regency (Ruswandi 2014). Ujung Genteng is one of the beaches in Sukabumi with the highest seagrass cover, namely around 10-15%. The results of the identification of the Directorate General of Aquaculture in collaboration with the Mina Bisnis Science and Technology Clinic Ujung Genteng Sukabumi Regency show the diversity of seagrass from the type Enhalus sp. and Thalasia sp. generally grows on coral flats at Ujung Genteng Beach. Seagrass beds are one of the energy sources in food webs in aquatic ecosystems (Paramasivam et al. 2015). Apart from that, Ujung Genteng also includes an intertidal zone which is a tidal zone where there are various types of living biota, one of which is microalgae (Widiansyah et al. 2016). Therefore, this research aimed to identify the diversity of microalgae originating from sea water based on morphological characteristics and Bulk DNA isolation optimation of seawater-microalgae.

2. Materials and Methods

2.1. Sample collection

Microalgae sampling and aquatic environmental parameters were determined based on the conditions of the research area as a whole (Evita et al. 2021).

Figure 1 The research location was at Ujung Genteng Beach, Sukabumi. The research location is marked with a red location symbol (https://www.google.com/maps/)

The sampling location was divided into three locations, namely the first location with a distance of 0-<2 m from the low tide line, the second location (seagrass area) with a distance of 2-<5 m, and the third location with a distance of 5-10 m which is connected to the open sea. Sampling was carried out at low tide (Rachmawan et al. 2021). Sample analysis was carried out at the Plant Physiology and Molecular Biology Laboratory, Department of Biology IPB Dramaga Bogor. The study area of this research was Ujung Genteng Beach, Sukabumi, Indonesia (7°17'42.1"S 106°25'32.7"E [-7.295038, 106.425741]) (Figure 1). The sampling was conducted from January to June 2022. Sampling was performed using a purposive sampling method (Fendiyanto et al. 2023) at low tide at Ujung Genteng Beach, Sukabumi for one day at intervals, namely in the morning (09.00 to 10.00 West Indonesian Time/WIT) and in the afternoon (12.00 to 13.00 WIT) (Rizqina et al. 2017).

Sampling was carried out vertically by filtering 10 liters of water using a plankton net, then the net that had been sunk to a depth of 1 m was pulled from above the surface and left for 5 minutes at the three predetermined sampling locations. Water samples were taken and put into 35 ml sample bottles and labeled with the name, location and date of sampling (Fachrul 2012, Evita et al. 2021). The sampling point was created by drawing a straight line from the lowest low tide point (05.00 to 11.00 WIT), with a distance of 10 m towards the sea and divided into three sampling locations. Sampling was carried out 3 times at each location (Erlangga et al. 2022; Fendiyanto et al. 2023). A total of 18 microalgae samples were obtained, then 1.5 ml of 4% formalin and 2 to 4 drops of betadine were added to keep the chlorophyll from being damaged. Next, the samples were taken to the Plant Physiology and Molecular Biology Laboratory, Department of Biology IPB. Apart from seawater sampling, environmental data collection was also carried out once in the morning and afternoon, namely pH, light intensity, water temperature, air humidity and wind speed. This data measurement is to describe the physico-chemical environmental conditions that support the growth of microalgae.

2.2. Morphological characterization

Identification of microalgae morphology was carried out by observation using a binocular microscope. Observation of microalgae was carried out by dripping water samples on an object glass, then covering it with a cover glass and observing under a binocular microscope connected to an Olympus CX33 camera and personal computer with the IndomicroView application starting from 4x objective lens magnification to 100x magnification (100x magnification using immersion oil). Observation of each sample using a microscope was carried out one repetition. Microalgae that are found and often appear on the microscope are documented and given the name and sampling location to facilitate identification of microalgae from the three sampling locations. The shape or architecture of the cells is observed by observing the morphological characters, namely round, elongated, irregular, in colonies or single, and slimy or not (Fendiyanto et al. 2023). Identification was carried out by referring to the identification book entitled "The Freshwater Algae" (Prescott 1978) and the book

"Introduction to the Algae Structure and Reproduction second edition" (Bold and Wynne 1985).

2.3. Biological data analysis

The morphological characteristic data obtained was analyzed descriptively to find out a complete description of each type. Quantitative data was processed using the R program version 4.0.4. Diversity parameter values include index values for species richness, abundance, diversity and evenness (Fendiyanto et al. 2023). the Menhinick index (MeI), the Margalef index (MaI), Rarefaction (Ra), the Shannon-Wiener Index (H'), Simpson Index (D), and Pilou evenness (J) were performed in this study (Magurran 1988; Boontawee et al. 1995; Odum 1996; Fendiyanto et al. 2023).

$$\text{MeI} = \frac{n}{\sqrt{N}} \qquad \text{MaI} = \frac{n-1}{lnN}$$

where n is the number of species and N is the number of individuals:

$$Ra = \sum 1 - \left[\frac{(\frac{\mathbf{N-Ni}}{\mathbf{n}})}{(\frac{\mathbf{N}}{\mathbf{n}})}\right]$$

where N is the total number of individuals in the new rarefied taxa, and Ni is the total number of individuals in each original

$$\text{H'} = -\sum\left(\frac{ni}{N}\, x\, ln\frac{ni}{N}\right) \qquad \text{D} = \frac{N(N-1)}{\sum ni(ni-1)}$$

where ni is the number of individuals of each species i and N is the total number of individuals

$$\text{J} = \frac{H'}{\ln S}$$

where H' is the true diversity value (Shannon-Wiener Index) and S is the number of species

2.4. DNA isolation and amplification

DNA isolation was carried out using the method of Sambrook et al. (1989) which has been modified following Fendiyanto et al. (2019a), namely by preparing a water sample then placing it in a 15 ml tube, then centrifuging at a speed of 4,000 rpm, temperature 4 ℃, for 5 minutes. After that, the supernatant was discarded and repeated 3 times so that the volume of each sample became 45 ml. The initial stage was the destruction of cell membranes and walls using liquid nitrogen. The powder obtained was added with 3 ml of CTAB buffer, stirred and added 60 µl of β Mercaptoethanol; after that it was vortexed until evenly mixed (Fendiyanto et al. 2019b). The mixture was incubated in a water bath at a temperature of 65℃ for 30 minutes, which served to optimize the work of the extraction buffer added to the sample (Cheng et al. 2003), then turned over every 10 minutes to make it homogeneous.

In the next stage, 30 µl of polyvilpyrrolidone was added and incubated again for 30 minutes, turned over until homogeneous every 10 minutes, then incubated at -20 ℃ for 5 minutes. A total of 3 ml of Chloroform Isoamylalcohol was added and turned over until homogeneous for 10 minutes. The mixture was centrifuged at 3600 rpm, temperature 4 ℃, for 20 minutes. The supernatant was transferred to a 15 ml tube and labeled, 3 ml of isopropanol was added, stirred back and forth, incubated at -20 ℃ for 24 hours. Precipitation is carried out with the aim of precipitating DNA (Syafaruddin and Santoso 2011). After 24 hours, the mixture was centrifuged at 4,000 rpm, temperature 10 ℃, for 30 minutes. The supernatant was discarded, and the pellet was dried in an incubator for 60 -120 minutes. The pellet was added with 20 µl free nucleic water and then vortexed and spundown. The results of the genomic DNA are viewed using a spectrophotometer or electrophoresis to determine the purity and concentration of the genomic DNA. A total of 1 µl of DNA was diluted with 199 µl of ddH_2O, then read on a spectrophotometer with a wavelength of 260 nm and 280 nm for proteins. Amplification of DNA fragments was carried out using 4 pairs of primers (18_KWT_F and 18_KWT_R, 18_ss5_F and 18_ss3_R, 16_Stiller_PS_F and 16_Stiller_U_R, 16_Stiller_PS_R and 16_Stiller_U_F) on a thermocycler machine (Stiller 2005; Table 1). PCR analysis was carried out with a total of 15 µl reactions containing 1 ng template DNA, DreamTaq Green PCR Master Mix (2x), 10 pmol forward primer, 10 pmol reserve primer, ddH_2O. The mixture is homogenized then put into a thermocycler machine.

The PCR reaction goes through the following stages, namely initial denaturation at 95ºC for 3 minutes, then denaturation at 95ºC for 30 seconds, annealing at 51ºC for 30 seconds, and existence at 72ºC for 1 minute followed by final existence at 72ºC for 10 minutes and cooling at 4ºC for 3 minutes. The amplification results were visualized using horizontal electrophoresis with a 1% (w/v) agarose gel in 1x TAE buffer. A total of 5 µl of loading dye and 10 µl of genomic DNA were inserted into the wells of a 1% agarose gel. Electrophoresis was carried out for 30 minutes at 100 Volts with 1X TAE buffer as running buffer. Gel soaked in a solution of Ethidium Bromide (EtBr). The gel can be visualized by placing the gel on a UV illuminator to see whether there are bands of genomic DNA. Fragment size is determined by comparing it to the 1 kb Ladder standard.Genetic diversity in PCR products is determined based on whether DNA bands appear or not. DNA bands resulting from PCR are measured based on the ladder used, namely 1 kb DNA ladder. In addition, this research will be continued by future researchers with metagenomic analysis using 18S rDNA primers.

Table 1. Primers used in DNA amplification of seawater microalgae at Ujung Genteng Beach (Stiller 2005; Khaw et al. 2020; Kumar et al. 2021)

No	Primer	Sekuen (5'-3')
1	18_KWT_F	GCG GTA ATT CCA GCT CCA A
	18_KWT_R	AAT CCR AGA ATT TCA CCT CT
2	18_ss5_F	GGT GAT CCT GCC AGT AGT CAT
	18_ss3_R	ATG CTT G GAT CCT TCC GCA
3	16_Stiller_PS_F	GGT TCA CCT ACG GAA ACC
	16_ Stiller_U_R	GGG ATT AGA TAC CCC WGT AGT CCT
4	16_ Stiller_U_F	ACG GYT ACC TTG TTA CGA CTT
	16_ Stiller_PS_R	GAG AGT TTG ATC CTG GTC AG
		CCC TAA TCT ATG GGG WCA TCA GGA

3. Results

3.1. Aquatic Environmental Parameters

Ujung Genteng Beach is at coordinates 07°22'55.7"S and 106°24'24.0"E. The results of absolute measurements of aquatic environmental parameters are presented (Table 2).

Table 2. Water environmental parameters at Ujung Genteng Beach, Sukabumi at the time of sampling

Abiotic Parameters	Condition	
	Morning	Midday
Temperature (ºC)	29.2	30.0
Humidity (%)	77.0	73.6
Wind velocity (m/s)	1.2	1.1
Light intensity (lux)	10,430.0	11,370.0
Water pH	7.7	7.9

The water temperature in the morning and afternoon in Ujung Genteng is 29,2-30,0 ºC. This shows that it is still suitable for the growth of microalgae because the optimum water temperature for microalgae growth is around 20-30 ºC (Nybakken 1982; Barten et al. 2020). The high and low water temperature is influenced by the intensity of incoming light and the depth of the water, and can directly influence and control the rate of metabolic processes in microalgae cells (Rianto et al. 2008).

The light intensity at Ujung Genteng Beach ranges from 10.430-11.370 lux. Light greatly influences photosynthesis in microalgae. High light intensity can make the rate of photosynthesis in algae also high and vice versa. Microalgae can be distributed based on the influence of light intensity and temperature. The higher the light intensity (range 2,500-8,000 lux) and water temperature (25-32 ºC), the higher the photosynthesis process of microalgae so that the types of microalgae can be diverse (Novasaraseta et al. 2018). Light intensity that is too high (>11,700 lux) will affect the increase in water temperature so that microalgae have problems in growth (Prasetyo et al. 2018). Based on this phenomenon, high light intensity (10,430-11,370 lux) at Ujung Genteng Beach can affect microalgae cell population density. Each type of microalgae has a different tolerance to variations in light intensity (Huang et al. 2011).The presence of seagrass and microalgae in an ecosystem can also cause competition, because they require the same nutrients to live, which can reduce the diversity (number of species) of microalgae on Ujung Genteng Beach (Roem et al. 2017).

The results of measuring the pH of sea water at Ujung Genteng Beach in the morning and afternoon were 7.7-7.9. This pH value is included in the optimum pH for microalgae growth which ranges from 7.0 to 8.5 (Pescod 1971; Filali et al. 2021). The pH value is a description of the intensity of acidity and alkalinity of water which can influence water biochemical processes, such as nitrification. Water with a pH value of less than 4 is very acidic water. This condition can cause death to aquatic organisms. Meanwhile, waters with a pH value of more than 9.5 are very alkaline waters and can reduce the productivity of aquatic organisms because they are toxic, causing an increase in ammonia content (Siregar 2009).

3.2. Diversity of seawater microalgae

The results of morphological identification of all seawater samples from Ujung Genteng Beach, Sukabumi showed 47 species of microalgae covering six classes, namely the Bacillariophyceae, Chlorophyceae, Cyanophyceae, Dinophyceae, Chrysophyceae, and Euglenida classes (Figure 2). Location II in the research results graph shows that the diversity of species found is less than in locations I and III, in fact some species found in locations I and III were not found in location II. The presence of microalgae often becomes a competitor for seagrass that lives in the same ecosystem, causing several species not to be found at location II due to competition in obtaining nutrients and placement of growth locations (Riniatsih et al. 2017).

Species abundance of classes Bacillariophyceae in all locations is relatively high among other classes. Species abundance of class Bacillariophyceae in Location III is higher than location I and II. Location I had high species number of class Chlorophyceae while Location II had the lowest number of species in class Chlorophyceae, Cyanophyceae, Dinophyceae, Chrysophyceae, and Euglenida. In addition, Location III has highest species abundance in class Bacillariophyceae, Cyanophyceae, Dinophyceae, and Euglenida (Figure 2).

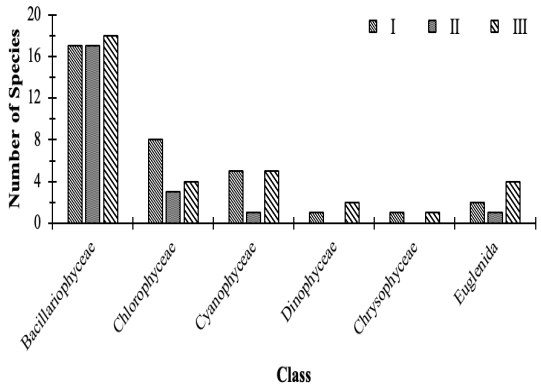

Figure 2. Diversity of microalgae at Ujung Genteng Beach, Sukabumi

The most common species found from the three sampling locations in both morning and afternoon conditions were from the Bacillariophyceae Class with 12 species, namely *Navicula* sp., *Frustulia* sp., *Diploneis parma*, *Nitzschia* sp., *Achnanthidium* sp., *Amphora* sp., *Oscillatoria teneuis*, *Achanthes* sp., *Planothidium* sp., *Uronema* sp., *Zygnema* sp., and *Flagillaria* sp. (Figure 3). According to Arinardi et al. (1997), the Bacillariophyceae class includes microalgae that are widely distributed and are able to adapt to the environment and have high tolerance. This is in accordance with the statement that the microalgae found in marine waters are generally of the diatom type (Bacillariophyceae) followed by the Dinophyceae class and blue algae (Cyanophyceae) (Nontji 1984). Diatoms will dominate waters when light intensity is high and temperatures are low (Welch 1980).

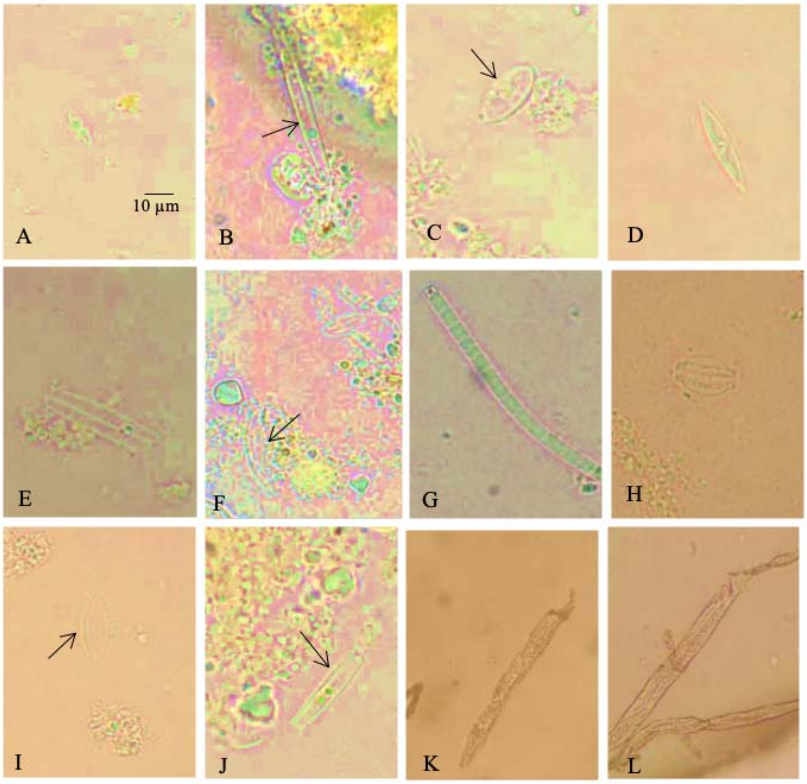

Figure 3. Microgae species that are often found on Ujung Genteng Beach, Sukabumi: A. *Navicula* sp.; B. *Frustulia* sp.; C. *Diploneis parma*; D. *Nitzschia* sp.; E. *Achnanthidium* sp.; F. *Amphora* sp.; G. *Oscillatoria teneuis*; H. *Achanthes* sp.; I. *Planothidium* sp.; J. *Flagillaria* sp.; K. *Uronema* sp.; and L. *Zygnema* sp.. The scale lines in image A apply to images A-L with 100x magnification.

Location I, both in the morning and afternoon, found microalgae consisting of the classes Bacillariophyceae (17 species), Chlorophyceae (8 species), Cyanophyceae (5 species), Euglenida (2 species), while only 1 species was found in the Dinophyceae and Chrysophyceae classes. In location II, during the morning and afternoon, the microalgae found were in the classes Bacillariophyceae (17 species), Chlorophyceae (3 species), Cyanophyceae and Euglenida (1 species), while Dinophyceae and Chrysophyceae did not find any type of microalgae. The microalgae found at location III in both morning and afternoon conditions included the Bacillariophyceae class (18 species), Cyanophyceae (5 species), Chlorophyceae and Euglenida (4 species), Dinophyceae (2 species), while for the Chrysophyceae class only 1 species was found. The diversity of microalgae at Ujung Genteng Beach depicted in the graph shows that the eight classes of microalgae that were identified can be found from the three research locations (Table 3, Figure 4).

Table 3. Types of microalgae found at Ujung Genteng Beach, Sukabumi

No.	Microalgae	Location					
		I		II		III	
		M	D	M	D	M	D
	Class Bacillariophyceae						
1.	*Naviculla* sp.	+	+	-	+	+	+
2.	*Pinnularia gibba*	-	+	-	-	+	-
3.	*Pinnularia braunii*	+	-	-	+	-	-
4.	*Pinnularia legume*	-	-	+	-	-	+
5.	*Frustulia* sp.	+	+	-	+	-	+
6.	*Diploneis parma*	+	-	-	+	+	+
7.	*Nitzschia* sp.	+	+	+	+	+	+
8.	*Cymbella turgida*	-	-	+	-	-	-
9.	*Cymbella tumida*	-	-	-	+	-	-
10.	*Epithemia alpestris*	-	+	+	+	-	+
11.	*Rhoicospenia* sp.	-	-	+	-	+	+
12.	*Flagillaria* sp.	-	+	-	+	+	-
13.	*Fragillaria vaucheriae*	+	-	-	-	+	+
14.	*Synedra ulna*	-	+	-	-	+	-
15.	*Achnanthidium* sp.	+	-	-	+	+	+
16.	*Brachysira* sp.	+	-	+	+	+	+
17.	*Rhopalodia gibberula*	-	-	+	-	-	-
18.	*Amphora* sp.	+	+	-	+	+	-
19.	*Melosira varians*	+	-	-	-	-	-
20.	*Planothidium* sp.	-	+	-	+	+	+
21.	*Achanthes* sp.	-	+	+	-	+	+
22.	*Craticula* sp.	-	-	-	-	+	+
23.	*Humidophila* sp.	-	+	-	-	+	-
	ClassChlorophyceae						
24.	*Tetrahedron obesum*	+	-	-	-	-	-
25.	*Tetrahedron minimum*	+	-	-	-	-	-
26.	*Sachroederia setigera*	-	+	+	-	+	-
27.	*Uronema* sp.	-	+	+	+	-	+
28.	*Zygnema* sp.	-	+	-	+	-	+
29.	*Pleurotaenium* sp.	+	-	-	-	-	+
30.	*Ulothrix* sp.	-	+	-	-	-	-
31.	*Protococcus viridis*	-	+	-	-	-	-
	ClassCyanophyceae						
32.	*Chroococcus linnclius*	+	-	-	-	-	-
33.	*Chroococcus disperses*	-	-	-	-	+	-
34.	*Oscillatoria teneuis*	+	+	+	-	+	+
35.	*Rhabdoderma lineare*	-	+	-	-	+	-
36.	*Aphanocapsa gravillei*	-	+	-	-	-	-
37.	*Schizothrix tinctoria*	-	+	-	-	-	+
38.	*Microcystis* sp.	-	-	-	-	-	+
	Class Dinophyceae						
39.	*Glenodinium palustre*	-	-	-	-	-	+
40.	*Gymnodium coudata*	-	+	-	-	-	-
41.	*Ceratium hirundinella*	-	-	-	-	+	-
	ClassEuglenida						
42.	*Trachelomonas superba*	-	+	-	-	-	+
43.	*Trachelomonas rotunda*	-	-	-	-	+	+
44.	*Trachelomonas abrupta*	-	-	-	-	-	+
45.	*Trachelomonas kelloggiii*	-	-	+	-	-	+
46.	*Trachelomonas volvocina*	+	-	-	-	-	-
	ClassChrysophyceae						
47.	*Dinobryon tabellaria*	+	+	-	-	+	-
	Total	17	23	12	14	22	24

+ = found; - = not found

Location I = sea water which is 0- <2 m from the low tide line, location II = sea water in the seagrass area which is 2- < 5 m away, location III = sea water which is close to the open sea, 5-10 m away m. M = conditions in the morning; D = conditions during the day.

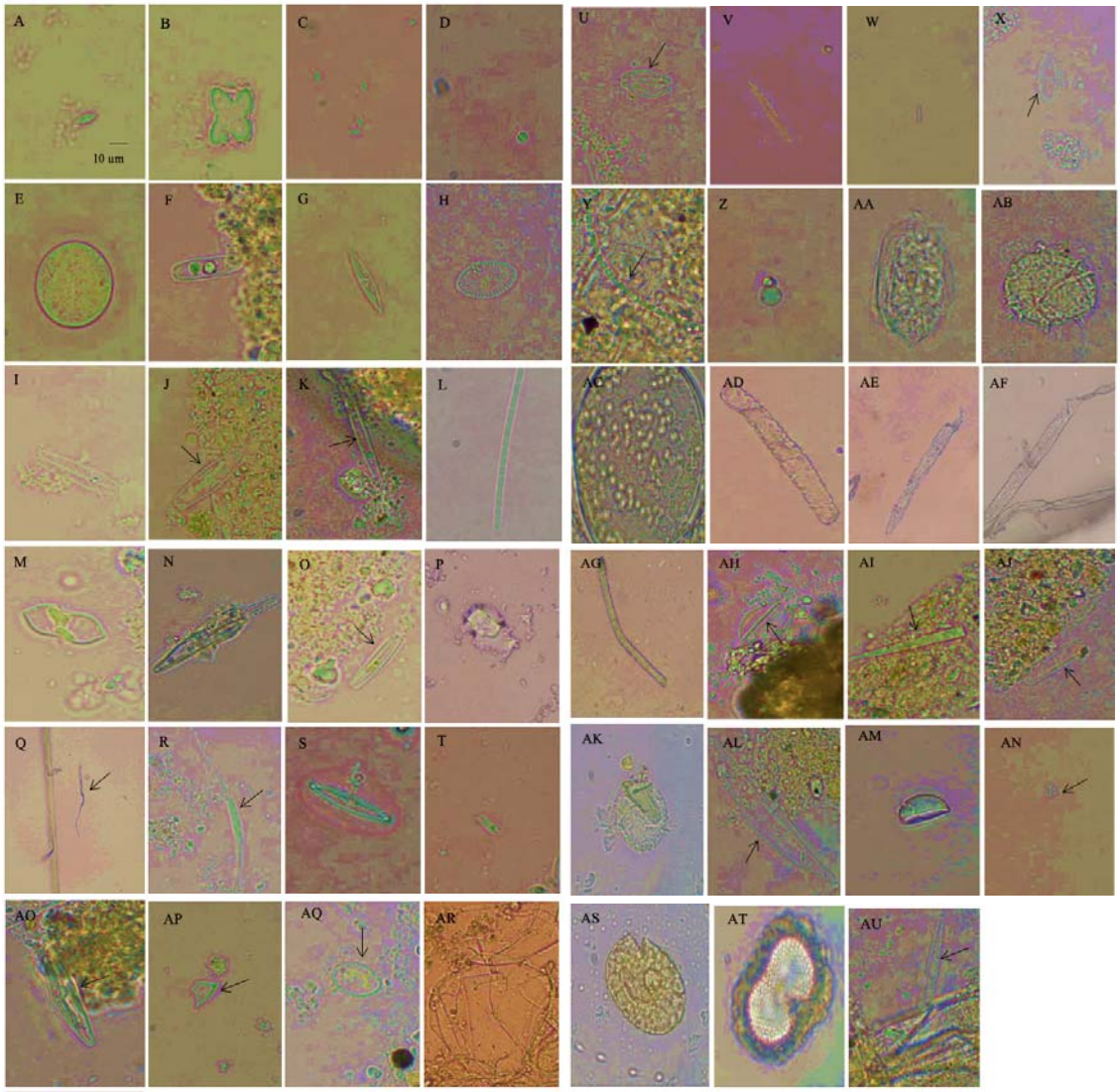

Figure 4. Microalgae species found from the three research locations on Ujung Genteng Beach during the morning and day: A. *Tetrahedron obesum*; B. *Minimum tetrahedron*; C. *Dinobryon Tabellaria*; D. *Chroococcus linnchius*; E. *Trachelomonas volvocina*; F. *Navicula* sp.; G. *Nitzschia* sp.; H. *Diploneis parma*; I. *Achnanthidium* sp. J. *Brachysira* sp.; K. *Frustulia* sp.; L. *Oscillatoria teneuis*; M. *Pinnularia braunii*; N. *Amphora* sp.; O. *Flagillaria* sp.; P. *Melosira variance*; Q. *Pleurotaenium* sp.; R. *Sachroederia setigera*; S. *Pinnularia gibba*; T. *Humidophila* sp.; U. *Achanthes* sp.; V. *Synedra ulna*; W. *Rhabdoderma lineare*; X. *Planothidium* sp.; Y. *Schizothrix tinctoria*; Z. *Protococcus viridis*; AA. *Gymnodium coudata*; AB. T*rachelomonas superba*; AC. *Aphanocapsa gravillii*; AD. *Epithemia alpestris*; A.E. *Uronema* sp.; AF. *Zygnema* sp.; AG. *Ulothrix* sp.; AH. *Rhopalodia gibberula*; A.I. *Rhoicospenia* sp.; A.J. *Pinnularia legume*; AK. *Trachelomonas kelloggii*; AL. *Cymbella turgida*; A.M. *Cymbella tumida;* AN. *Chroococcus disperses*; AO. *Craticula* sp.; AP. *Ceratium hirundinella*; I. *Trachelomonasrotunda*; AR. *Glenodinium palustre*; US. *Trachelomonas abrupta*; AT. *Microcystis* sp.; AU. *Flagillaria vaucheriae*. The scale lines in image A apply to image A-AU at 100x magnification.

3.3. Microalgae Diversity Index

Analysis of microalgae diversity parameters is based on the values of species richness, abundance, diversity and uniformity. Species richness and abundance can be tested using the rarefaction method, Menhinick index (MeI) and Margalef index (MaI), which indicates the richness and abundance of Ujung Genteng seawater microalgae species. The highest Ra value is found at location II in the morning conditions at 2.96, which means that the species at that location are unique and the majority can only be found at that location. Locations I and III have high wealth values, while the lowest wealth is in location II during the day. The greater the value of the Menhinick index (MeI) and Margalef index (MaI), the greater the value of microalgae species richness (Boontawee et al. 1995).

Microalgae diversity can also be tested with two types of indices, namely the Shannon-Wiener Index (H') and the Simpson Index (D). Based on testing these two types of index, the microalgae community as a whole has a diversity index (H') value of around 1.0<H'<3.3 (Table 4). This diversity index value shows that the abundance of microalgae types on Ujung Genteng Beach is moderate and indicates that the waters have a stable, balanced ecosystem. This refers to the diversity index criteria: H'<1: Low community stability, 1.0<H'<3.3: Medium community stability, H'>3: High community stability (Odum 1998).

Table 4. Parameter values for diversity and uniformity of microalgae from three research locations on Ujung Genteng Beach

Location	SR	MeI	MaI	SA	Ra	H'	D	J	E_{a-b}
Conditions in the morning									
Location I	17	3,57	4,75	29	2,80	2,60	0,90	0,32	0,14
Location II	12	3,33	4,29	13	2,96	2,46	0,91	0,37	0,21
Location III	22	3,28	5,51	45	2,87	2,90	0,93	0,30	0,12
Conditions during the day									
Location I	23	3,35	5,71	47	2,83	2,85	0,92	0,29	0,11
Location II	14	2,60	3,86	29	2,82	2,50	0,90	0,34	0,18
Location III	24	3,27	5,77	54	2,87	2,97	0,94	0,30	0,11

Note: SR: *Species richness*; MeI: Menhinick's index; MaI: Margalef's index; SA: *Species abundance*; Ra: *Rarefaction*; H': Shannon-Wiener Index; D: Simpson's Index; J: *Pilou evenness*; $E_{a:b}$: *Hill's ratios*.

The species uniformity value shows the inverse value of the diversity index value (both in the Shannon-Wiener Index and Simpson Index). In this study, two types of uniformity index were used, namely Pilou (J) and Hill ratio (Ea:b). Locations I and III during the day have low Pilou and Hill's ratio uniformity values, while location II in the morning has high Pilou and Hill's ratio uniformity values. The uniformity index value (J') can describe the distribution and number of microalgae in Ujung Genteng which has a low uniformity value, namely 0.29 -0.37, which means that the distribution of individuals for each type is not the same, with a tendency to be dominated by certain types (Odum 1993). The uniformity value category ranges from 0 to 1 (Odum 1993). This is reinforced by the statement that if the uniformity is close to zero, it means that the uniformity between species in the community is low and, conversely, if the uniformity is close to one, it can be said that the uniformity between species is even or the same (Pirzan et al. 2008).

3.4. Genomic DNA Isolation and DNA Quantity Measurement

The DNA isolation results showed poor results because the average of the seven samples showed low DNA concentration values. Likewise, from the DNA purity value, none of the samples showed good quality purity because the absorbance value was below 1.8 or above 2.0. Good quality DNA purity will have an A260/A280 ratio of between 1.8-2.0 (Maftuchah et al. 2014). The range of values in the results of this study indicates that the amount of DNA in the sample is less than the amount of protein, or indicates that the DNA isolation results are still contaminated with RNA and protein (Murtiyaningsih 2017).

The results of analysis of the quality of genomic DNA in 7 samples of seawater microalgae using PCR and electrophoresis methods using four pairs of primers (18_KWT_F and 18_KWT_R, 18_ss5_F and 18_ss3_R, 16_Stiller_PS_F and 16_Stiller_U_R, 16_Stiller_PS_R and 16_Stiller _U_F) are presented (Figure 5, Figure 6) . It can be seen that the DNA bands amplified by the KWT primer and SS primer have a size of 250 bp (Figure 5). Samples I1-6 of genomic DNA in each primer pair did not show any bands. The shape of the band pattern that appears indicates the presence of primary dimers. Primary dimers are potential byproducts in polymerase chain reactions consisting of two primary molecules that stick together due to complementary base sequences in the primer. The reason the 6 seawater microalgae samples did not contain bands was because the DNA concentration in the isolated samples was very low and the DNA purity was not good. However, for sample I7 of seawater microalgae (Figure 6) with a low concentration and DNA purity with a ratio of A260/A280 nm, namely 1.40-1.75, the PCR process was successful in proving the appearance of a band measuring > 250 bp by amplification using the KWT primer. Whether or not bands appear in DNA PCR electrophoresis can be influenced by differences in the primers used as well as the concentration and purity ratio of the DNA (Dzikrina et al. 2022).

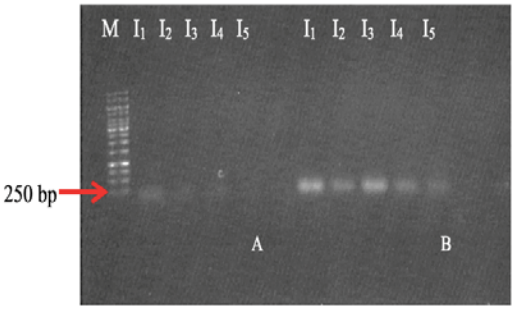

Figure 5. Gel image of Microalgae genomic DNA amplification in Ujung Genteng, M= marker 1 kb; I1-5= Genomic DNA of Ujung Genteng seawater microalgae; A= KWT primer; B= SS primer.

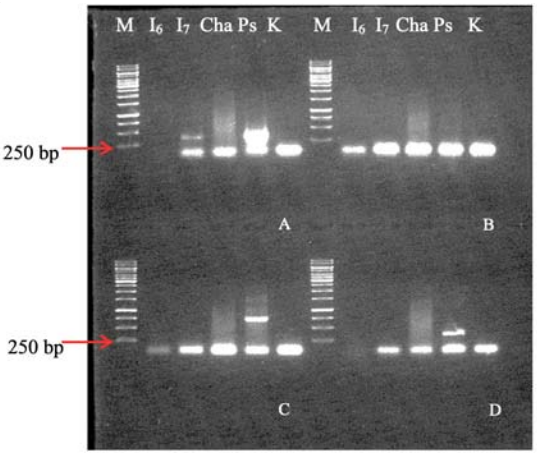

Figure 6. Gel image of amplification of genome DNA electrophoresis of seawater microalgae and microalgae culture, M= marker 1 kb; I6-7= Genomic DNA of Ujung Genteng seawater microalgae; A= KWT primer; B= SS primer, C= PS_F,U_R primer; D= PS_R,U_F primer; Cha, Ps= microalgae culture, and K= positive control.

This research also conducted experiments on microalgae culture, with the results obtained available in Figure 6. Culture of the microalgae Cha (*Chaetosceros* sp.) and Ps (*Porphyridium* sp.) on primer KWT, primer PS_F,U_R, and primer PS_R,U_F showed quite good results because thick DNA bands appeared with band sizes ranging from 250-1000 bp. Seawater microalgae samples showed that many genomic DNA samples could not be amplified properly (Figure 5, Figure 6). Poor amplification results can be caused by mismatched primers, efficiency and optimization of the PCR process. Primers that are not specific or appropriate can cause amplification of other

regions in the genome that are not targeted or, conversely, no regions of the genome are amplified (Azizah 2009).

Primers PS_F,U_R and PS_R,U_F are primers specifically designed for phytoplankton. 18S rDNA primers can target all phototrophic eukaryotes with coverage that can span the entire diversity (Stiller 2005). The KWT_R primer and KWT_F primer were used in several studies to see the abundance of Chlorophyta and other types of algae (Kumar et al. 2021). Likewise, the primer pair ss5 and ss3, these primers showed the highest universality among 18S rDNA primer sets in sequencing microalgae. However, these primers are group specific and are not suitable for determining precise identity and phylogenetic alimony because the resulting DNA sequences are short (Moro et al. 2009).

PCR optimization needs to be carried out to produce the desired characteristics which are related to the DNA denaturation and annealing temperature in the PCR machine. A low denaturation temperature can cause the double-stranded DNA to not open so that primer attachment does not occur. The process of attaching a primer to an open DNA strand requires an optimum temperature because a temperature that is too high can cause amplification to not occur because the primer does not stick or, conversely, a temperature that is too low causes the primer to stick to the other side of the genome which is not the homologous side. This causes the amplification of many non-specific regions in the genome. The annealing temperature is determined based on the primer. There are several factors that greatly influence the success of the electrophoresis process. These factors include the size of the DNA molecule, agarose gel concentration, voltage, the presence of DNA dye, and the composition of the electrophoresis buffer (Sinaga et al. 2017).

4. Discussion

Several types of microalgae found at Ujung Genteng Beach such as *Navicula* sp. and *Oscillatoria* sp. can be an alternative source of lipid production as renewable biodiesel raw material. The average lipid content of microalgae cells varies between 1-70% but can reach 90% dry weight under certain conditions (Spolaore et al. 2006). Microalgae have the potential to be used as biodiesel as an alternative renewable energy because they contain lipids that are suitable for esterification or transesterification (Umdu et al. 2009). *Oscillatoria* sp. can produce lipid extraction, namely 18.16%, while *Navicula* sp. (a type of diatom) can produce up to 60% of the cellular mass as triglycerides (TAG), which will be converted easily into biodiesel through a transesterification reaction (Lebeau and Robert 2003).

At all sampling locations, Bacillariophyceae class microalgae were found. This is in accordance with the statement that the phytoplankton found in marine waters are generally of the diatom type (Bacillariophyceae) followed by Dinophyceae and blue algae (Cyanophyceae) (Nontji 1984). The Bacillariophyceae class of microalgae is a type of microalgae that is widely distributed and is able to adapt to environmental conditions and utilize nutrients optimally for its growth. The form of adaptation of the Bacillariohyceae class is by utilizing the frustule structure on its body to float on the surface of the water. This aims to get sunlight to carry out photosynthesis (Sachlan 1982; Duxbury et al. 2002). The Chlorophyceae class was also found in all three research locations. The Chlorophyceae class is microalgae that has a high abundance in both marine and fresh waters and lives in solitary or colony form.

Types of microalgae from the Dinophyceae class were only found in location I and location III. The Dinophyceae class has chlorophyll a and chlorophyll c in their bodies (Bold and Wyne 1985), and reproduces by self-division. The difference between this type of microalgae and diatoms is that their bodies have flagella. The Cyanophyceae class is a type of microalgae that is prokaryotic and has the form of single cells, colonies or filaments. The process of nitrogen fixation can occur in microalgae in the form of colonies or filaments, so it can cause an explosion in microalgae populations in both marine and fresh water (Sachlan 1982). According to sampling results at location II, very few types of this class were found, namely only 1 type (*Oscillatoria teneuis*). The Chrysophyceae class is often known as golden algae because the carotene and xanthophyll pigments contained in their chloroplasts are greater in quantity than the chlorophyll pigments. Based on sampling results at Ujung Genteng Beach, Sukabumi, microalgae of the Chrysophyceae class were found in locations I and III. This shows that microalgae belonging to the Cyanophyceae and Chrysophyceae classes can be found in all waters including the sea (Luttge 1976).

Another type of microalgae found at Ujung Genteng Beach is the Euglenida class. This class is a type of microalgae that is very rarely found in the three research locations. The number of microalgae species on Ujung Genteng Beach during the day is greater than in the morning. According to the sampling results of the three research locations, the microalgae species found during the day are location I (23 species), location II (14 species), and location III (24 species); the microalgae species found in the morning are location I (17 species), location II (12 species), and location III (22 species).

5. Conclusion

The number of species found at Ujung Genteng Beach, Sukabumi is 47 species, 12 of which are often found at the three research locations both morning and afternoon, namely *Navicula* sp., *Frustulia* sp., *Diploneis parma*, *Nitzschia* sp., *Achnanthidium* sp., *Amphora* sp., *Oscillatoria teneuis*, *Achanthes* sp., *Planothidium* sp., *Uronema* sp., *Zygnema* sp., and *Flagillaria* sp. The diversity of microalgae at all sampling locations was in the medium category and the uniformity index between species was low. Examination of diversity indices and species diversity indicated differences in species abundance and diversity across various sites, specifically in seawater microalgae inhabiting distinct zones: within the ranges of 0-2 meters from the low tide line (location I), in seawater within seagrass areas situated 2-5 meters away (location II), and in seawater close to the open sea, approximately 5-10 meters away (location III). All DNA sample of the Ujung Genteng seawater microalgae genome that was successfully well amplified as evidenced by the appearance of a thick band pattern measuring 250 bp using KWT and SS specific primers.

Acknowledgements

This research was fully supported by Ministry of Defense, the Republic of Indonesia, through Dr.Mentari Putri Pratami, S.Si., M.Sifiscal year 2021-2022 through LPPM grant, particularly the Republic of Indonesia Defense University (RIDU) Funding.We thank Laboratory of Plant Physiology and Molecular Biology, Biology Department, IPB University for supporting identification of microalgae.

References

Amini S and Susilowati R. 2010. Biodiesel production from *Botrycoccus braunii* microalgae. *Squalen.*,**5(1)**: 23-32.

Arinardi OH, Trimaningsih SH, and Riyono. 1997. **Range of Abundance and Composition of Predominant Plankton in Eastern Indonesia.**Lembaga Ilmu Pengetahuan Indonesia, Jakarta.

Azizah A. 2009. **Comparison of DNA Amplification Band Patterns in Normal and Abnormal Leaves, Flowers of Palm Oil.**IPB University Pr, Bogor.

Barten RJP, Wijffels RH, Barbosa MJ. 2020. Bioprospecting and characterization of temperature tolerant microalgae from Bonaire. *Algal Res.*,**50**: 102008. DOI: 10.1016/j.algal.2020.102008.

Bold HC and Wynne MJ. 1985. **Introduction to the Algae Structure and Reproduction** Second edition. Prentice-Hall Inc, New Jersey.

Boontawee B, Phengkhlai C, and Kaosaard A. 1995. **Monitoring and Measuring Forest Biodiversity in Thailand. In Boyle TJB, Boontawee B. Measuring and Monitoring Biodiversity in Tropical and Temperate Forest**. Cifor, Bogor.

Cheng YJ, Guo WW, Yi HL, Pang XM, and Deng X. 2003. An efficient protocol for genomic DNA extraction from citrus species. *Plant MolBiol Rep.*,**21**: 177a-177g.

Duxbury. 2002. **Fundamentals of Oceanography 4th ed Chapter Select**. McGraw-Hill, Boston.

Dzikrina H, Sari DP, Faridah N, Saidah SS, Alifah SAN, and Kusumawaty D. 2022. DNA markers: Halal testing on processed meat foods using multiplex PCR (Polymerase Chain Reaction) primers.*JBios Logos.*,**12(1)**: 1-8.

Erlangga, Andika Y, Imanullah, Imamshadiqin, and Syahrin A. Identification of potential marine microalgae as biodiesel raw materials in Banda Sakti District, Lhokseumawe City.*J Ilmu Tek Kelaut Trop.*,**14(1)**: 147-160.

Evita INM, Hariyati R, and Hidayat JW. 2021. Abundance and diversity of plankton as a bioindicator of water quality in the waters of Sayung Beach, Demak Regency, Central Java.*Bioma.,* **23(1)**: 25-32.

Fachrul MF. 2012. **Bioecological Sampling Methods.**Bumi Aksara, Jakarta.

Fendiyanto MH, Satrio RD, Suharsono, Tjahjoleksono A and Miftahudin. 2019a. Correlation among Snpb11 markers, root growth, and physiological characters of upland rice under aluminum stress. *Biodiversitas.*, **20(5)**: 1243-1254. DOI: 10.13057/biodiv/d200514.

Fendiyanto MH, Satrio RD, Suharsono, Tjahjoleksono A, Hanarida I and Miftahudin. 2019b. QTL for aluminum tolerance on rice chromosome 3 based on root length characters. *SABRAO J Breed Genet.,***51(4)**: 451-469.

Fendiyanto MH, Satrio RD and Darmadi D. 2020. Metabolic profiling and pathway analysis in red arillus of Salacca sumatrana demonstrate significant pyruvate, sulfur, and fatty acid metabolisms. *Biodiversitas.,***21(9)**: 4361-4368. DOI: 10.13057/biodiv/d210955.

Fendiyanto MH, Satrio RD, Widana IDKK, Pratami MP, Nikmah IA and Darmadi D. 2021. Differential hierarchical metabolites expression of red/white Salacca sumatrana arillus and its molecular docking studies. *Biodiversitas.*, **22(2)**: 1014-1024. DOI: 10.13057/biodiv/d220258.

Fendiyanto MH, Pratami MP, Satrio RD , Nikmah IA, Sari NIP, Awwanah M, Farah N, Nurhadiyanta N. 2021. Analysis of *Superoxide Dismutase (OsSOD)* Gene Expression Using qRT-PCR, Its Morphophysiological Characters, and Path Analysis in Rice Variety IR64 Under Aluminum Stress. *Inter J Agric Biol.*, **26(4)**: 546-554. Doi: 10.17957/IJAB/15.1866

Fendiyanto MH, Pratami MP, Satrio RD , Nikmah IA, Sari NIP, Awwanah M, Farah N, Nurhadiyanta N. 2023. Species diversity of freshwater microalgae in dramaga, bogor based on morpho-ecological identification between low and high light intensity environment. *Jordan J Biol Sci.*, **16 (1)**: 27-34. Doi: 10.54319/jjbs/160105

Fendiyanto MH, Hastilestari BR, Maysha DJ. 2023. *LCYB* Gene Expression and Morphophysiological Traits of Musa acuminata Cultivars. *SABRAO J Breed Genet.,***55(6)**: 1984-1993.

Filali R, Tian H, Micheils E, Taidi B. 2021. Evaluation of the growth performance of microalgae based onfine pH changes. *Austin JBiotech Bioeng.*, **8(1)**: 102008. Doi: 10.1016/j.algal.2020.102008

Gusrianto D. 2012. **Mikroalga pada Sumber Air Panas Sapan Maluluang Kabupaten Solok Selatan**. Universitas Andalas Pr, Padang.

Henry T, Iwen PC, and Hinrichs SH. 2000. Identification of *Aspergillus* spesies using internal transcribed spacer regions 1 and 2. *J Clinical Microbiol.,***38(4)**: 1510-1515.

Huang WW, Dong BZ, Caidan ZP, and Duan SS. 2011. Growth effect on mixed culture of Dunaliella salina and Phaeodactylum trucornutum under different inoculation densities and nitrogen concentrations. *African JBiotechnol.,***10 (1):** 13164 -13174.

Khaw YS, Khong N, Shaharuddin NA, and Yusoff F. 2020. A simple 18S rDNA approach for the identification of cultured eukaryotic microalgae with an emphasis on primers. 1:1-47. *J Microbiol Methods.*,**5(172)**:105890. Doi: 10.1016/j.mimet.2020.105890.

Kumar V, Momin S, Kumar VV, Ahmed J, Musallam L, and Shajan AB. 2021. Distribution and diversity of eukaryotic microalgae in Kuwait waters assessed using 18S rRNA gene sequencing. *PLoS ONE.*,**16(4)**: e0250645. Doi: 10.1371/journal.pone.0250645.

Lebeau T and Robert JM. 2003. Diatom cultivation and biotechnologically relevant products. Part II: current and putative products. *ApplMicrobiolBiotechnol.,***60**: 624-632.

Luttge U and Pitman MG. 1976. **Transport in Plants II: Part A cells**. Springer-Verlag, Berlin.

Maftuchah, Winaya A, and Zainudin A. 2014. **Molecular Biology Analysis Techniques.**Deepublish, Yogyakarta.

Magurran AE. 1988. **Ecological Diversity and Its Measurement**. Princeton University Pr, New Jersey.

Mercer P and Armenta RE. 2011. Developments in oil extraction from microalgae. *European J Lipid SciTechnol.,***113 (5)**: 539-547.

Moro CV, Crouzet O, Rasconi S, Thouvenot A, Coffe G, Batisson I, andBohatier J. 2009. New design strategy for development of specific primer sets for PCR-based detection of Chlorophyceae and Bacillariophyceae in environmental samples. *Appl Environ Microbiol.*,**75**: 5729–5733.

Murtiyaningsih H. 2017. Isolation of genomic DNA and identification of genetic relationships in pineapple using RAPD (Random Amplified Polymorphic DNA).*Agritrop.*,**15(1)**: 83 – 93.

Nybakken JW. 1982. **Marine Biology, An Ecologycal Approach.** Harper and Row Publisher, New York.

Nontji A. 1984. **Phytoplankton Biomass and Productivity in Jakarta Bay Waters and Their Relation to Environmental Factors.**IPB University, Bogor.

Novasaraseta N, Abidin Z, and Junaedi E. 2018. Phytoplankton diversity in Situ Balong Kambang, Pasawahan Village, Kuningan Regency.*J Pendidikan Biol.*,**10(1)**: 33-41.

Odum EP. 1993. **Dasar –Dasar Ekologi Ed III. Terjemahan: Samingan T**. Gadjah Mada University Pr, Yogyakarta.

Paramasivam K, Venkataraman K, Venkatraman C, Rajkumar R, and Shrinivaasu S. 2015. Diversity and distribution of sea grass associated macrofauna in Gulf of Mannar Biosphere Reserve, Southern India. *Marine Faunal Divers*.,**1(1)**: 137-158.

Pescod MB. 1971. **Water Supply and Waste Water Disposal in Developing Countries**. Asian Institute of Technology, Bangkok.

Pirzan, Andi M, andPetrus RPM. 2008. The relationship between phytoplankton uniformity and water quality on Bauluang Island, Akalar Regency, South Sulawesi.*Biodiversitas.*,**9(3)**: 217-221.

Prasetyo LD, Supriyantini E, andSedjati S. 2022. Growth of the microalgae *Chaetoceros calcitrans* in cultivation with different light intensities.*Buletin Oseanografi Marina*.,**11(1)**: 59-70.

Pratami MP, Fendiyanto MH, Satrio RD , Nikmah IA, Awwanah M, Farah N, Sari NIP,Nurhadiyanta N. 2022. In-silico Genome Editing Identification and Functional Protein Change of *Chlamydomonas reinhardtii* Acetyl-CoA Carboxylase (CrACCase). *Jordan J Biol Sci.*, **15 (3):** 431-440. Doi: 10.54319/jjbs/150312

Prescott GW. 1978. **How to Know the Freshwater Algae**. 3rd edition. Brown Company, Lowa.

Purbani DC, Ambarwati W, Kusuma AB, andHerliany NE. 2019. Identification of marine microalgae from Tambrauw, West Papua.*J Ilmu TekKelautan Trop.*,**11(3)**: 777-790.

Rachmawan EW, Suryono CA, andRiniatsih I. 2021. Perbandingan tutupan antar lamun, makroalga, dan epifit di Perairan Paciran Lamongan. *JMarine Res.*,**10(4)**: 509-514.

Rianto R, Ariyani A, Widyawan A, Hendrayanti D, Wardhana W, and Prihantini BW. 2008. **Biodiversitas Cyanobacteria dari Beberapa Danau di Kawasan Jakarta-Depok-Bogor.** Universitas Indonesia Pr, Depok.

Ritniasih I, Munasik M, Suryono CA, Azizah R, Hartati R, Pribadi R, andSubayigo S. 2017. Composition of associated macroalgae in the seagrass ecosystem of Tumpul Lunik Island, Rimau Balak Island and South Kandang Balak Island, South Lampung Waters.*J Kelautan Trop.*,**20(2)**: 124-130.

Rizqina C, Sulardiono B, andDjunaedi A. 2017. The relationship between nitrate and phosphate content and phytoplankton abundance in the waters of Pari Island, Seribu Islands.*J Maquares.*,**6(1)**: 43-50.

Roem M, Wiharyanto D, and Darnawati D. 2017. Association of macroalgae with seagrass in Panjang Island waters.*J Borneo Saintek.*,**1(1)**: 50-62.

Ruswandi A. 2014. **The Ups and Downs of the Life of the Ujung Genteng Fisherman Community.**Universitas Pendidikan Indonesia, Bandung.

Sachlan M. 1982. **Planktonologi.** Universitas Diponegoro, Semarang.

Sambrook J, Fritsch EF, Maniatis T. 1989. **Molecular Cloning: A Laboratory Manualsecond edition.** Cold Spring Harbor Lab, New York.

Satrio RD, Fendiyanto MH, Suharsono, Supena EDJ and Miftahudin. 2019. Identification of drought-responsive regulatory genes by hierarchical selection of expressed sequence tags and their expression under drought stress in rice. *Intl J Agric Biol.*,**22(6)**: 1524-1532.DOI: 10.17957/IJAB/15.1230.

Setiawan R, Atmowidi T, Widayati KA, andPurwati P. 2018. Habitat preferences of *Ophiuroidea* species in the intertidal zone of Pancur Beach, Alas Purwo National Park.*JKelautan.*,**11(2)**: 151-166.

Siregar MH. 2009. **Study of Plankton Diversity in the Upper Asahan Porsea River.**Universitas Sumatera Utara, Medan.

Spolaore P, Joannis-Cassan C, Duran E, and Isambert A. 2006. Commercial applications of microalgae. *J BiosciBioeng.*,**101**: 87-96.

Stiller JW and Clanahan AM. 2005. Phyto-specific 16S rDNA PCR primers for recovering algal and plant sequences from mixed samples. *Mol EcoNotes.*,**5**: 1-3.

Suharno andLantang D. 2012. The fertility status of marine waters is seen from the diversity of plankton in the Bird's Head area, West Papua.*JBiol Papua.,* **4(2)**: 75-82.

Sujarta P, Ohee H, and Rahareng E. 2011. Study of the diversity of plankton and fish in the waters of Tanah Merah Bay, Depapre District, Jayapura Regency, Papua.*JBiolPapua.*,**3(2)**: 67-73.

Suparman 2012. Molecular markers in the identification and analysis of plant relationships and their implications for genetics courses.*JBioedukasi.*,**1(1)**: 59-68.

Syafaruddin andSantoso TJ. 2011. Optimization of efficient and effective DNA isolation and purification techniques in Kemiri Sunan (*Reutalis trisperma*).*JLittri.*,**17(1)**: 11-17.

Umdu ES, Tuncer M, andSeker E. 2009. Transesterifikasi lipid mikroalga Nannochloropsis oculata menjadi biodiesel pada katalis CaO dan MgO yang didukung Al2O3. *Tek Sumber Daya Hayati.*,**100(11)**: 2828-2831.

Waluyo. 2004. **Mikrobiologi Umum**. Universitas Muhammadiyah, Malang.

Welch EB. 1980. **Ecological Effect of Waste Water.** Cambridge Univ Press, Cambridge.

Widiansyah AT, Munzil M, and Indriwati SE. 2016. Inventory of Arthropod and Echinodermata types in the tidal zone of rocky substrate type at Gatra Beach, Malang Regency. *J Pendidikan: Teori, Penelitian, Pengembangan.*,**1(7)**: 1417-1420.

JJBS

Volume 17, Number 3,September 2024
ISSN 1995-6673
Pages 507 – 512
https://doi.org/10.54319/jjbs/170313

Jordan Journal of Biological Sciences

Chiliadenus montanus (Vahl.) Brullo which grows wild in the Jordanian environment shows distinguished Terpinen-4-ol levels and antibacterial powers

Reham W. Tahtamouni[1,*], Rida A. Shibli[2], Tamara S. Al- Qudah[3], Hanan Azzam[3] and Sobhia Saifan[4]

[1]*Department of Social and Applied Sciences, Princess Alia University College, Al-Balqa Applied University, Amman, Jordan.*[2]*Department of Horticulture and Crop Sciences, Faculty of Agriculture, The University of Jordan, Amman, Jordan.* [3]*Hamdi Mango Center for Scientific Research (HMCSR), University of Jordan, Amman, Jordan,*[4] *Faculty of Agricultural Technology, Al Ahliyya Amman University, Amman, Jordan* .

Received: October 26, 2023; Revised: March 11, 2024; Accepted: March 19, 2024

Abstract

Chiliadenus montanus(Vahl.) Brullo is a wild herb that grows in narrow parts of Jordan and is locally named Hneedeh. Despite being used for treating mild abdominal and respiratory ailments, Hneedeh is still locally known on a very small scale, and its healing capabilities are still waiting for a solid scientific justification. No previous studies were made to explore the antibacterial potential of Jordanian Hneedeh as well as its chemical composition despite being researched by scientists from neighboring countries. For this reason, this research aimed to unveil the active compounds behind the medicinal properties of wild *C. montanus* collected from Garissa-Jordan by analyzing the essential oil using the GC MS system. Also, the antibacterial activity was explored in two extracts (methanolic and ethanolic) collected from the succulent branches of *C. montanus* was examined using Microdilution and Disc Diffusion Assays. Data revealed the presence of 23 compounds grouped into eight classes and oxygenated monoterpenes were the predominant class (40.36%).Terpinen-4-ol, which is known for its super curative antibacterial and antitumoral powers, was indicated to be the major chemical compound in the essential oil of Hneedeh as it comprised (23.3%) of the essential oil, which disagreed with other previous studies made on the same plants growing in neighboring counties. Moreover, both extract types restricted growth in most tested bacterial types. The results recorded in the Microdilution Assay showed that the inhibitory effect of both extract types was stronger thanthose obtained in the antibiotic treatment (control) in *E. coli* and *Staphylococcus aureus*. Meanwhile, both methanolic and ethanolic extracts were as effective as the antibiotic when administrated to *Bacillus subtilis and Salmonella* sp. at similar minimal inhibition concentration (MIC) values. Moreover, Disc Diffusion Assay showed that both extract types could prevent the development of six bacteria types while no effect was recorded in *Klebsiella pneumoniae*. However, *E coli* bacteria was the most affected strain. The presence of the oxygenated monoterpenes, especially Terpinen-4-ol at premium levels, might be the causal agent behind the remarkable antibacterial powers of *C. montanus* extract. To our knowledge, this is the first time that *C. montanus*which grows wild in the village of Ghareesa is reported to containTerpinen-4-ol as the main active ingredient, which is unlike results reported in other studies conducted on similar plant species growing in other countries.

Keywords: Antibacterial activity, *Chiliadenus montanus,*Garisa, Jordan, oxygenated monoterpenes, Terpinen-4-ol.

1. Introduction

Controlling ailments worldwide is threatened nowadays by the antimicrobial resistance phenomenon which would put the whole of humanity under serious challenge with microbes(WHO, 2019). Unfortunately, earnest actions towards such a global threat have not been taken yet, although the World Health Organization (WHO) has announced most antibiotics are useless due to antimicrobial resistance (Masi et al., 2021).Finding alternative weapons against microorganisms is a priority to overcome the growing resistance to antibiotics (Tahtamouni et al., 2018).

Herbal medicine is mostly practiced by people in developing countries as they have found in plants an effective, natural, safe, and cheap source to cure diseases. Numerous plants have been documented to exhibit medicinal properties effective against various types of microorganisms. (Jaganthan et al., 2015). So, plant extracts can be used as natural antibiotics against pathogens that might in some cases outperform synthetic ones (Masi et al., 2021).

Many endemic plants in Jordan were screened for their healing properties. Abu Odeh et al. (2023) have listed many examples of medicinal plants that are endemic to the Jordanian environment and were researched by Jordanian scientists for their healing properties such as *Ocimum*

* Corresponding author. e-mail: rehwtt@bau.edu.jo.

basilicum (Hudaib et al,. 2008), *(Achillea santolina* L. and *Origanum syriacum* L. (Oran and Al-Eisawi, 2015), *Salvia ceratophylla* L. (Abu-Darwish et al., 2020) and *Viscum cruciatum* Sieb (Abo-Elghiet et al., 2022), and many more, but many of Jordan's medicinal plants are still veiled.

Ghareesa is an ancient village located in the Jordanian governorate of Zarqa, Al-Hashimiya District where 52% of the Jordanian industry is located and concentrated like the oil refinery, the Al-Hussein thermal station, multiple iron factories, along with the existence of the Khirbet Al-Samra station for the processing of household sewage. Consequently, Ghareesa suffers from air pollution due to emissions of air pollutants from these factories, such as sulfur dioxide, hydrogen sulfide, and carbon monoxide(Saffarinia and Odat, 2008).Air pollution, climate change, and excessive collection have put the unique plant biodiversity of Garissa under threat of extinction.

Chiliadenus montanus (Vahl.) Brullo is a type of healing herb that is classified under the Asteraceae family. This shrublet grows wild along the southern edge of the Mediterranean, especially in Egypt, Sinai, and Jordan (Bengtson and. Anderberg, 2018). In Jordan, it is commonly known as (Hneedeh). This plant grows wild in Garissa, especially on hillsides, rocky valleys, and roadsides. Recently, this plant was put under the microscope by scientists from nearby countries, especially Egypt, for its remarkable healing properties, as it was found to possess antioxidant, antidiabetic and anti-obesity powers(Hegazy et al., 2014; Helal et al., 2015) besides its curative potential against Alzheimer's disease and tumors (Ahmad et al., 2018; Elhadyet al., 2020). In Jordan, this valuable medicinal plant is not well-researched yet. However, according to the findings of Eissa et al. (2014), the essential oil derived from *C. montanus* aerial parts collected from Sinai, Egypt, contained cis-verbenol as its primary component. Cis-Verbenol has been reported for its anti-inflammatory and anti-ischemic characteristics, as well as its ability to promote healthier neuronal growth (Nadeem et al., 2022).

Disc diffusion and Microdilution assays were routinely used in testing the antimicrobial powers of plant extracts in many research studies. The official method employed in numerous clinical microbiology laboratories is Disk Diffusion Assay, which was developed in 1940 (Heatley, 1944), where discs of agar are treated with the tested microorganism, then filter paper discs with a desired concentration of the tested extract are positioned on the agar surface before being kept under appropriate circumstances, and the diameters of the regions where growth inhibition takes place were evaluated(Balouiri et al., 2016).

Microdilution Assay is also considered very suitable in antimicrobial research, as it was described to allow the estimation of the concentration of the antimicrobial agent which was found to stop the growth of the microbes (Balouiri et al., 2016).

The GC/MS was commonly utilized for characterizing and uncovering new compounds and metabolites, and it was reported to be an exceptional and potent technology as it has offered a distinct chance to analyze novel compounds (Al-Rubaye et al., 2017).

So, based on the lack of information about *C. montanus* which grows in the Jordanian environment and is used by limited local people without solid scientific proof, the purpose of our study was to determine the active components of the extract of *C. montanus* (Vahl.) Brullo growing wild in Garissa, Jordan, using GC/MS technique ,and to assess the extract's antimicrobial efficacy against specific bacterial strains using Disc diffusion and Microdilution assays. The results of this study might encourage other research work toward the conservation and development of this neglected plant.

2. Materials and Methods

2.1. Extraction and identification of active ingredients

The areal branches of *C. montanus* (Vahl.) Brullo were taken from a single shrublet growing wild in Ghareesa, Zarka- Jordan(32°10'13.0"N; 36°04'30.8"E) in March 2019(Figure 1). Extraction and identification of the active ingredients were performed according to Abu Rjai et al. (2020) where plant material was hydro-distilled to extract oil by Clevenger apparatus. The weight of the collected oil served as a benchmark for determining the proportionate amount of oil obtained from the dried plant material (w/w %).Next, the aliquot of oil-diluted samples(1 µl) was injected into the GC-MS system utilizing an automated injection device. The GC-MS was performed using a modified Chrompack CP3800 GC/MS/MS-200 (Satum, Netherlands) which was outfitted with a split- splitless injector and DB-5 capillary column (5 % diphenyl 95 % dimethyl polysiloxane, 30 m×0.25 mm ID, 0.25 µm film thickness)(Abu Rjai et al. 2020). The linear temperature program was utilized, with the injector temperature set at 250° and a split ratio of 1:30, starting with a column temperature of 60° for 1 minute then was gradually increased to 250° at a rate of 3°/min and maintained at 250° for 2 minutes, resulting in a total runtime of approximately 66 minutes(Abu Rjai et al. 2020). Helium was the carrier gas, and the ions were scanned according to the protocol established by Abuja et al. (2020), with a DB-5 column utilized in GC-MS. The oil components were calculated by identifying peaks through the linear retention index (Arithmetic-Kovats index), and subsequently separated by GC-MS based on retention times and n-alkanes retention time references according to Van Den Dool Equation (1963).The computer software libraries NIST, WILEY, and ADAMS were utilized to separate the essential oil components (Abuja et al., 2020). Different oils of eugenol, linalool, and eucalyptol were analyzed to confirm their constituents. Standards were acquired from (Sigma-Aldrich) and employed to determine the oil components using identical chromatography (GC) parameters, while the chemical constituents of the oil were identified through utilization of GC-FID analysis using an FID detector and a split less injector in a thermos quest gas chromatograph and a column of HP-5 (Abu Rjai et al., 2020). The standard curve was formulated, and the quantities of the compounds were determined by calculating the area under each peak.

Figure 1. *C. montanus* (Vahl.) Brullo was collected from Ghaeesa, Zarka- Jordan (32°10'13.0"N; 36°04'30.8"E) in March 2019.

2.2. Antibacterial Activity

For studying the antibacterial activity of *C. montanus* (Vahl.) Brullo, samples of the aerial components were subjected to drying in the oven at a temperature of 45°C.beforegrounded into fine powder. Subsequently, samples of the powder derived from plant material were treated with either ethanol or methanol in a 1:10 ratio. The resulting extracts underwent filtration and evaporation until they reached a state of dryness, after which they were dissolved in DMSO. The Disc diffusion and Microdilution techniques were employed to assess the antibacterial activity of every extract type. Seven bacterial strains were tested (*Bacillus subtilis* ATCC 6633, *Staphylococcus aureus* ATCC 25923, *Staphylococcus epidermidis* ATCC 12228, *Klebsiella pneumoniae* ATCC 31488, *Esherichia coli, Salmonella* sp., and *Erwinia carotovora*).

The Microdilution Method was used to find the minimum inhibitory concentration (MIC) based on guidelines set by the National Committee for Clinical Laboratory Standards(NCCLS 1997). To achieve this, methanolic and ethanolic extracts were diluted in a serial manner, with each dilution being doubled, using Muller Hinton and potato dextrose broth. As a control, the eleventh well contained nutrient broth plus Tetracycline (10 mg/mL). The resulting concentrations from both extracts were between 50 mg/mL to 0.098 mg/ ml. After incubating for 24 hours at 37 °C in a plate shaker incubator the results for (MIC) were recorded.

In the Disc Diffusion Assay, discs with a diameter of 6.0 mm were placed on Muller Hinton agar plates from Mast Group Ltd. U.K. A volume of 100 µL of each bacterial type fixed to 0.5 McFarland (Karlsmose, 2010) was streaked on the discs. Subsequently, 10 mg of both methanolic and ethanolic extracts were applied to each disc. Tetracycline antibiotic at a level of 10 mg/mL served as the reference standard. The zone of inhibition was recorded after 24hrs. of being kept at 37°C to determine antibacterial activity.

Treatments in the Disc Diffusion Assay were randomized completely and were repeated 5 times. Data of the inhibition zones were analyzed according to (ANOVA) using SPSS (17), and means were compared using Tukey's HSD test at a significance level of 0.05.

3. Results and Discussion

3.1. Chemical composition of the essential oil

Results obtained in (Figure 2, Table 1) illustrated that (23) compounds were identified in the extracted essential oil of *C. montanus* (Vahl.) Brullo aerial parts. The identified compounds were grouped into eight classes where oxygenated monoterpenes were the predominant class as they comprised (40.36%) (Table 1). The major chemical compound identified in the extract was Terpinen-4-ol as it comprised (23.3%) of the essential oil (Table 1). Our results matched the findings of Eissa et al. (2014) as they reported that oxygenated monoterpenes were the main class detected in the oil extracted from *C. montanus* growing wild in Sinai- Egypt. On the other hand, our data contrasted with Eissa et al. (2014) results when they reported Cis-Verbenol as the major compound of the essential oil of Hneedeh of Egypt. According to our results,Terpinen-4-ol was the major component (23.3%) of the essential oil extracted from *C. montanus*aerial parts collected from Ghareesa- Jordan. No Terpinen-4-ol was found in Eissa et al. (2014) results, as they reported cis-verbenol (22.2%) as the main constituent of the oil extracted from Hneedeh fresh branches collected from Sinai, Egypt. Such variation might be attributed to the different nature of climate, rainfall, soil, and time of collection. To our knowledge, this is the first time that Terpinen-4-ol has been announced as the major active ingredient in *C. montanus*. In another study, Terpinen-4-ol was detected as the major compound (42%) in the essential oil *Melaleuca alternifolia* (Tea Tree), a tree that was reported in many research articles for its super curative antibacterial, anti-inflammatory, and antitumoral powers (Hart et al., 2000). Recently, Terpinen-4-ol attracted the attention of scientists as it was found to stop the development of many tumors such as melanoma (Calcabrini et al., 2004), lung cancer (Wu et al., 2012), leukemia, (Banjerdpongchai et al., 2013), and colorectal cancer(Nakayama et al., 2017). Moreover, Terpinen-4-ol is extensively utilized in the food sector to prevent staling as it forms a microbial biofilm in food products instead of using salt to prevent food spoilage (Yong et al., 2022). Our results indicated that *C. montanus* can be used as a natural source of Terpinen-4-ol, and this plant might become easily a potential bioreactor for the production of Terpinen-4-ol if introduced to means of plant biotechnology.

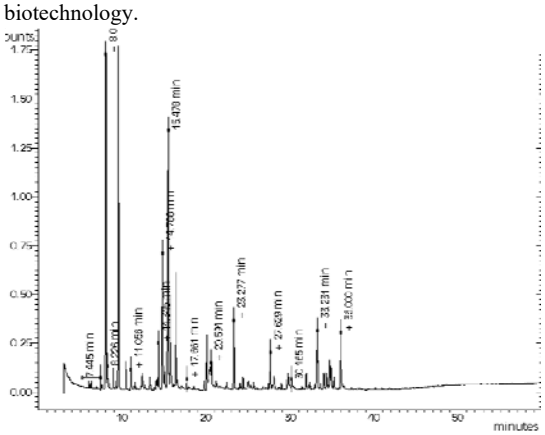

Figure2. Essential oil components of *C. montanus* as obtained by GC-MS chromatography.

Table 1. Components of essential oil extracted from *C. montanus* aerial parts.

NO.	Compound name	KI lit.	Content%	Classification group name
1.	Unknown	-	12.7	-
2.	2,5,5-trimethyl-3,6-heptadien-2-ol (Yomogi alcohol)	988	1.43	Monoterpenes alcohol
3.	α-Terpinene	1014	0.70	Monoterpenes hydrocarbons
4.	Eucalyptol (1,8Cineol)	1026	12.4	Oxygenated monoterpenes
5.	γ-Terpinene	1054	1.04	Monoterpenes hydrocarbons
6.	Unknown	1024	1.3	Monoterpenes hydrocarbons
7.	Trans-Sabinene hydrate	1098	1.51	Monoterpenes hydrocarbons
8.	Terpineol	1130	1.26	Oxygenated monoterpenes
9.	Neroloxide	1154	2.14	Oxygenated monoterpenes
10.	Lavandulol	1165	9.29	Monoterpenes alcohol
11.	Terpinen-4-ol	1174	23.3	Oxygenated monoterpenes
12.	Trans-Piperitol	1208	4.75	Monoterpenes alcohol
13.	Bornyl acetate	1287	2.4	Miscellaneous
14.	Chrysanthemumic acid	1296	3.82	Bronsted acid
15.	Neryl acetate	1359	2.9	Monoterpenes ester
16.	Unknown	-	0.53	-
17.	2-(2-butynyl)-cyclohexanone		1.78	Miscellaneous
18.	Germacerene D	1249	0.53	Oxygenated monoterpenes
19.	Delta cadinene	1522	1.78	Sesquiterpenes hydrocarbons
20.	Palustrol	1567	1.2	sesquiterpenes alcohol
21.	B-oplopenone	1607	0.73	Oxygenated monoterpenes
22.	Unknown	-	0.62	-
23.	Murrola-4,10(14) -dien-1-beta-ol	1630	1.73	sesquiterpenes hydrocarbons
24.	α-cadinol	1652	2.5	Sesquiterpenoid alcohol
25.	Torreyol	1645	1.12	Phenolic compound
26.	Apiol	1677	3.4	Phenolic compound

3.2. Antibacterial activity of C. montanus extract

3.2.1. Microdilution Assay

Obtained data showed that extract of *C. montanus* has inhibited growth in most selected types of bacteria (Table 2). Moreover, our results indicated that the growth inactivation effect of both extracts (methanolic and ethanolic) against some bacteria strains was auspicious as it was stronger than the results obtained in the control treatment (Tetracycline) (Table 2). For example, both methanolic or ethanolic extracts at a level of (0.39 mg/mL) were able to stop growth in *E. coli* bacteria, while Tetracycline concentration needed to be increased four times that of *C. montanus* extract (1.56 mg/mL) to stop *E. coli* growth (Table 2). This trend was also recorded in *Staphylococcus aureus* bacteria, while the effect of both extract types on the growth of *Bacillus subtilis* was similar to those obtained in the control (Table 2). On the other hand, higher levels of both extract types were needed to inhibit the growth of *Staphylococcus epidermidis, Erwinia carotovora, and Salmonella* sp. compared to the control, while both extract types were not able to prevent the development of *Klebsiella pneumoniae* at all levels (Table 2). Meanwhile, data indicated that the inhibitory effect of the methanolic extract of *C. montanus* was stronger than that obtained when ethanolic extract was administrated to *Staphylococcus epidermidis, Erwinia carotovora* and *Salmonella* sp. (Table 2). Extract type was reported in many research articles to affect extract efficiency against microbes. Eloff (1998) reported that the superiority of methanolic extract might be due to its polarity as it is higher than that in ethanol which would permit more active compounds to dissolve in the extract.

Table 2. Minimal Inhibition Concentration (MIC) of the extracts of *Chiliadenus montanus* (Vahl.) Brullo against selected strains of bacteria.

Bacteria strain	Methanolic extract (mg/mL)	Ethanolic extract (mg/mL)	Tetracycline (control: mg/mL)
E. coli	0.39	0.39	1.56
Staphylococcus aureus	0.78	0.78	1.56
Staphylococcus epidermidis	3.12	6.24	1.56
Klebsiella pneumoniae	-	-	3.12
Bacillus subtilis	1.56	1.56	1.56
Erwinia carotovora	6.24	12.48	3.12
Salmonella sp.	1.56	3.12	1.56

3.2.2. Disc Diffusion Assay:

Disc Diffusion Assay test revealed that both extract types of *Chiliadenus montanus* (Vahl.) Brullo were able to inhibit growth in six bacteria strains while no effect was recorded in *Klebsiella pneumoniae* (Table 3).The inhibitory power of the methanolic extract against the development of *E. coli* bacteria was more effective than the antibiotic (control) as it was able to record an inhibition zone diameter of (28.0 mm) compared to (24.0 mm) obtained in the control (Table 3). Meanwhile, administration of methanolic extract to *Staphylococcus aureus* was as efficient as the control as it recorded an inhibition zone diameter of (24.0 mm) (Table 3). Growth of the rest of the bacteria strains was inhibited in response to exposure of the methanolic extract but to a lesser extent than those recorded in the control treatment (Table 3). Moreover, growth was inhibited in most bacteria strains when treated with the ethanolic extract, while no effect was recorded in *Klebsiella pneumoniae* and *Erwinia carotovora* (Table 3). However, it was noticed from the results that methanolic extract was more effective than ethanolic extract which would confirm the findings recorded earlier in the microdilution assay experiment.

Our results showed that both extract types of *Chiliadenus montanus* (Vahl.) Brullo has promising antibacterial powers against the tested strains, which could be attributed to the presence of high amounts of oxygenated monoterpenes (40.36%) (Table 1). The oxygenated monoterpenes were reported to possess variable antibacterial powers depending on bacteria strain (Kotan et al., 2007). Moreover, our data revealed that Terpinen-4-ol was the major compound in the extract (23.3%) (Table 1). This oxygenated monoterpene was repeatedly reported in many research articles for its antibacterial, antifungal, antiviral, and anticancer potentials (Barra et al., 2007; Cha et al., 2007; Shapira et al., 2016). Zhang et al. (2018) explained the mechanism by which Terpinen-4-ol attacks bacteria, as they found that Terpinen-4-ol was able to damage cell membranes and to affect negatively the synthesis of protein and DNA in *Streptococcus agalactiae* bacteria. Additionally, Bordini et al. (2018) investigated the effect of Terpinen-4-ol on bacteria at the gene level, as they reported that Terpinen-4-ol was able to modulate the production of the gbpA and slpA genes which are responsible for the adherence and biofilm development in *Streptococcus mutans* and *Lactobacillus acidophilus*.

Table 3. Inhibition zone diameters (mm) recorded in Disc Diffusion Assay of the extracts of *Chiliadenus montanus* (Vahl.) Brullo against selected strains of bacteria.

Bacteria strain	Methanolic extract	Ethanolic extract
Tetracycline (control)	24.0± 1.04 ab	20.0± 1.09 a
E. coli	28.0± 2.28 a	22.0± 2.42 a
Staphylococcus aureus	24.0± 1.67 ab	21.0± 1.97 a
Staphylococcus epidermidis	12.0± 1.54 cd	4.0± 0.89 c
Klebsiella pneumoniae	0.0± 0.0 e	0.0± 0.0 d
Bacillus subtilis	18.0± 1.97 b	15.0± 1.45 ab
Erwinia carotovora	8.0± 0.84 d	0.0± 0.0 d
Salmonella sp.	15.0± 1.97 bc	10.0± 1.37 b

* Means that have different letters were found to be significantly different based on Tukey's HSD test at a probability level of 0.05. Means within each column were analyzed separately.

4. Conclusions

From our data, it might be concluded that the oxygenated monoterpenes which were found at premium levels in the essential oil of *C. montanus* in addition to their high content of Terpinen-4-ol (57.7% of total oxygenated monoterpenes) might have contributed to the distinguished antibacterial powers of the extracts. More attention should be paid to this valuable threatened plant, and more research needs to be done to improve the production of these curative active ingredients from *C. montanus* (Vahl.) Brullo growing wild in the Jordanian environment.

References

Abo-Elghiet F, Ibrahim MH, El Hassab MA, Bader A, Abdallah QM and Temraz A. 2022. LC/MS analysis of *Viscum cruciatum* Sieber ex Boiss. extract with antiproliferative activity against MCF-7 cell line via G0/G1 cell cycle arrest: an in-silico and in vitro study. *J. Ethnopharmacol*, **295:**1-14

Abu-Odeh A, Fino L, Al-Absi G, Alnatour D, Al-Darraji M, Shehadeh M, and Suaifane G. 2023. Medicinal plants of Jordan: Scoping review. *Heliyon*,**9(6):** 1-19.

Abu-Darwish MS, Cabral C, Ali Z, Wang M, Khan SI., Jacob MR, Jain SK, Tekwani BL and Khan IA. 2020.*Salvia ceratophylla* L. from South of Jordan: new insights on chemical composition and biological activities. *Nat. Prod. Bioprosp*,**5(10):**307–316.

Aburjai T A, Mansi K, Azzam H, Alqudah D A, Alshaer W, and Abuirjei M. 2020. Chemical Compositions and Anticancer Potential of Essential Oil from Greenhouse-cultivated *Ocimum basilicum* Leaves. *Indian Journal of Pharmaceutical Sciences*, **82(1):** 179-184.

Adams RP and Sparkman OD. 2007. Review of Identification of Essential Oil Components by Gas Chromatography/Mass Spectrometry. *J Am Soc Mass Spectrum,***18**:803-806.

Ahmed H H, Booles H F, Khalil W K, El Ashmaoui HM and Othman S M. 2013. Possible therapeutic role of *Jasonia Candicans* and *Jasonia Montana* extracts in the regression of Alzheimer's Disease in the experimental model. *American Journal of Biochemistry & Biotechnology*, **9(2):** 144.

Alnweiri K H. 2021. Endophytic fungi: A new strategy to conserve medicinal plants in Jordan. *Microbial Biosystems*, **5(2):** 20-28.

Balouiri M, Sadiki M, Ibnsouda S K.2016. Methods for in vitro evaluating antimicrobialactivity: A review. *Journal of Pharmaceutical Analysis*, **6 (2)**: 71–79

Banjerdpongchai R and KhawO P. 2013. Terpinen-4-ol induces autophagic and apoptotic cell death in human leukemic HL-60 cells. *Asian Pacific Journal of Cancer Prevention*, **14(12):**7537-7542.

Barra A, CoroneoV, DessiS, Cabras P and Angioni A. 2007. Characterization of the volatile constituents in the essential oil of Pistacia lentiscus L. from different origins and its antifungal and antioxidant activity. *Journal of agricultural and food chemistry*, **55(17):** 7093-7098.

Bengtson A and Anderberg A A. 2018. Species diversification in the Mediterranean genus Chiliadenus (Inuleae-Asteraceae). *Plant Systematics and Evolution*, **304(7):** 853-860.

Bordini E A F, TononC C, FrancisconiR S, Magalhães F AC, HuachoP MM, Bedran T L, and Spolidorio D P. 2018. Antimicrobial effects of terpinen-4-ol against oral pathogens and its capacity for the modulation of gene expression. *Biofouling*, **34(7):** 815-825.

Calcabrini A, StringaroA, Toccacieli L, Meschini S, Marra M, ColoneM and MondelloF. 2004. Terpinen-4-ol, the main component of *Melaleuca alternifolia* (tea tree) oil inhibits the in vitro growth of human melanoma cells. *Journal of Investigative Dermatology*, **122(2):** 349-360.

Cha J D, JeongMR, Jeong S I, Moon S E, Kil B S, YunS I and Song Y H. 2007. Chemical composition and antimicrobial activity of the essential oil of *Cryptomeria japonica*. *Phytotherapy Research*, **21(3):** 295-299.

Eissa TF, González-Burgos E, Carretero M E and Gómez-Serranillos M P. 2013. Phenolic composition and evaluation of antioxidant and cytoprotective activity of *Chiliadenus montanus*. *Records of Natural Products*, **7(3):** 184.

Eissa T F, González-Burgos E, Carretero M E and Gómez-Serranillos M P. 2014. Compositional analysis and in vitro protective activity against oxidative stress of essential oils from Egyptian plants used in traditional medicine. *Natural product communications*, **9(9):** 1377-1382.

Elhady SS, Eltamany E E, Shaaban AE, Bagalagel A A, Muhammad Y A, El-Sayed NM and Ahmed S A 2020. Jaceidin flavonoid isolated from *Chiliadenus montanus* attenuates tumor progression in mice via VEGF inhibition: In Vivo and in silico studies. *Plants*, **9(8):** 1031.

Eloff J N. 1998. Which extractant should be used for the screening and isolation of antimicrobial components from plants? *Journal of Ethnopharmacology*, **60(1):** 1-8.

Hammerschmidt F J, Clark A M, Soliman, F M, El-Kashoury E S A, Abd El-Kawy M M and El-Fishawy A M. 1993. Chemical composition and antimicrobial activity of essential oils of *Jasonia candicans* and *J. montana*. *Planta medica*, **59(1):** 68-70.

Hart P H, Brand C, Carson C F, Riley TV, Prager R H and Finlay-JonesJ J. 2000. Terpinen-4-ol, the main component of the essential oil of *Melaleuca alternifolia* (tea tree oil), suppresses inflammatory mediator production by activated human monocytes. *Inflammation Research*, **49(11):** 619-626.

Heatley N G. 1944. A method for the assay of penicillin, *Biochem. J*. **38,** 61-65

Hegazy M E F, Matsuda H, Nakamura S, Hussein T A, Yoshikawa M and Paré P W. 2014. Chemical constituents and their antibacterial and antifungal activity from the Egyptian herbal medicine *Chiliadenus montanus*. *Phytochemistry*, **103:** 154-161.

Helal E G, Abou-Aouf N and Khattab A L. 2015. A possible hypoglycemic and antioxidant effect of herbal mixture extraction in diabetic rats. *The Egyptian Journal of Hospital Medicine*, **58(1):** 109-119.

Hudaib M, Mohammad M, Bustanji Y, Tayyem R, Yousef M, Abuirjeie M and Aburjai T. 2008. Ethnopharmacological survey of medicinal plants in Jordan, Mujib nature reserve and surrounding area. *J. Ethnopharmacol*,**120(1):**63–71.

Jaganthan R, Nagarajan R and Vadivel B.2015. Antimicrobial activity and preliminary phytochemical screening of flower extracts from *Azima tetracantha* (L.). *Eur J Pharm Med Res*, **2 (6):** 195-7.

Karlsmose S. 2010. **Laboratory Protocol:Susceptibility testing of Enterobacteriaceae using disk diffusion**. WHO Global Foodborne Infections Network. Protocol, (2010GFNLAB002).

KotanR, Kordali S and Cakir A. 2007. Screening of antibacterial activities of twenty-one oxygenated monoterpenes. *Zeitschrift für Naturforschung C*, **62(7):** 507-513.

Masi M, Roscetto E, Cimmino A, Catania MR, Surico G and Evidente A. 2021. Farnesane-Type Sesquiterpenoids with Antibiotic Activity from *Chiliadenus lopadusanus*. *Antibiotics*, **10(2):** 148.

Moustafa A, Fahmy D M, Zaghloul M S and El-Azeem S A A. 2017. Autecology of *Chiliadenus montanus* as a threatened plant species growing in Saint Katherine protectorate, South Sinai, Egypt. *J. Global Agric. Ecol*, **7(4):** 145-163.

Nadeem A, Ahmed B, Shahzad H, Imran Mand Craker E. 2022.*Artemisia rutifolia* Mewah extracts: Phytochemical profiling, Gc-Ms analyses, anti-bacterial and antioxidant activity. *International Journal for Biology, Pharmacy and Allied SciencesIJBPAS*,**11(5):**2397-2422

Nakayama K, Murata S, Ito H, Iwasaki K, Villareal M O, Zheng Y W and Ohkohchi N. 2017. Terpinen-4-ol inhibits colorectal cancer growth via reactive oxygen species. *Oncology letters*, **14(2):** 2015-2024.

National Committee for Clinical Laboratory Standards (NCCLS). 1997**. Performance standards for antimicrobial disk susceptibility tests. Approved standar**d.Wayne, USA

Oran S A and Al-Eisawi D M. 1998. Checklist of medicinal plants in Jordan. *Dirasat*, **25(2):** 84-112.

Oran S, Al-Eisawi D. 2015. Ethnobotanical survey of the medicinal plants in the central mountains (North-South) in Jordan. *J. Biodivers. Environ. Sci*,**6 (3):**381–400.

Al-RubayeA F, Hameed I H and Kadhim M J. 2017. A Review: Uses of Gas Chromatography-Mass Spectrometry (GC-MS)Technique for Analysis of Bioactive Natural Compounds of Some Plants. *International Journal of Toxicological and Pharmacological Research*,**9(1):** 81-85

Saffarinia G and Odat S. 2008.Time Series Analysis of Air Pollution in Al-Hashimeya Town Zarqa, Jordan.*Jordan Journal of Earth and Environmental Sciences,***1(2):** 63- 72.

Shapira S, Pleban S, Kazanov D, Tirosh P and Arber N. 2016. Terpinen-4-ol: A novel and promising therapeutic agent for human gastrointestinal cancers. *PLoS One*, **11(6):** e0156540.

TahtamouniR W. 2018. Investigating the Antibacterial Potential of Ethanolic and Methanolic Extracts of the *Schinus molle* L Tree. *Jordan Journal of Biological Sciences*, **11(5):** 527-531

Van Den DoolH and Kratz, P. D. 1963. A generalization of the retention index system including linear temperature programmed gas-liquid partition chromatography. *Journal of Chromatography*,**2:** 463-471

World Health Organization (WHO).2019. **Antimicrobial Resistance. No Time to Wait: Securing the Future from Drug-ResistantInfections.** Report to the Secretary-General of the United Nations. Available online: https://www.who.int/antimicrobialresistance/interagency-coordination-group/IACG_final_report_EN.pdf.ua=1 (accessed on 19 February 2021).

Wu C S, Chen Y J, Chen J J, Shieh J J, Huang C H, Lin P S and Lin C C. 2012. Terpinen-4-ol induces apoptosis in human nonsmall cell lung cancer in vitro and in vivo. *Evidence-Based Complementary and Alternative Medicine*, DOI: 10.1155/2012/818261

Yong Y, Fang B, Huang Y, Li J, Yu T, Wu L, Hu C, Liu X, Yu Z, Ma X, Gooneratne R, Li S, Abd El-Aty AM and Ju X. 2022. Tea tree oil Terpinen-4-ol protects gut barrier integrity by upregulation of tight junction proteins via the ERK1/2-signaling pathway. *Front. Nutr*, **8:** 1-14

Zhang Y, Feng R, LiL, Zhou X, Li Z, JiaR and Yin Z. 2018. The antibacterial mechanism of terpinen-4-ol against Streptococcus agalactiae. *Current Microbiology*, **75(9):** 1214-1220.

JJBS

Volume 17, Number 3,September 2024
ISSN 1995-6673
Pages 513 – 522
https://doi.org/10.54319/jjbs/170314

Jordan Journal of Biological Sciences

Genetic diversity of Bottle gourd (*Lagenaria siceraria* (Molina) Standl.) landraces in Jordan assessed by Agro-morphological traits and Inter Simple Sequence Repeat markers

Wesam Al Khateeb[1*], Azhar Ananzeh[1], Muhammad Alu'datt[2], Mohammad Brake[3]

[1]*Department of Biological Sciences, Faculty of Science, Yarmouk University, Irbid, Jordan;*[2]*Department of Food Science & Nutrition, College of Life Sciences, Kuwait University, P.O. Box. 5969, Safat 13060, Kuwait;*[3]*Science Department, Faculty of Science, Jerash University, Jerash, Jordan*

Received: October 5, 2023; Revised: March 4, 2024; Accepted: March 21, 2024

Abstract

Bottle gourd (*Lagenaria siceraria* (Molina) Standl.) is an important crop in Jordan, but it remains under-researched. The primary aim of this study was to evaluate the genetic variability existing among different bottle gourd landraces in Jordan using Agro-morphological traits and molecular markers. Bottle gourd landraces were collected from various locations in Jordan; phenotypic differences and genetic variation using ISSR were studied between collected landraces. Results show that phenotypic coefficients of variance were larger than their genotypic coefficients of variance for all characters, demonstrating that the environment had an impact on these features. High genetic advance was found for plant length, number of leaves, leaf width and seed area; this could be explained by additive gene action. High heritability >60% estimates were observed. Principal component analysis identified two principal components responsible for 69.6% of total variation. Plant height showed positive association with number of tendrils, number of leaves and leaf length. 246 amplified markers were obtained using 24 ISSR primers, 135 of which were polymorphic. Genetic distance varied between 0.78 to 0.92 based on molecular analysis and ranged from 0.42 to 0.91 for agro-morphological data. Dendrograms constructed based on morphological and ISSR data clustered landraces to six and five main groups, respectively. The results of this work could be used in future bottle gourd breeding programs.

Keywords: Bottle gourd, genetic diversity, landrace, agro-morphological traits, ISSR.

1. Introduction

Bottle gourd (*Lagenaria siceraria* (Molina) Standl.), a member of the family Cucurbitaceae, having chromosome number 2n = 22, is a climbing, monoecious plant, with large white flowers, hairy stems, and long forked tendrils. Its fruits are fleshy and vary in shape and size. As archaeological evidence indicates that bottle gourd is one of the earliest plant species that have been cultivated for human uses (more than 10,000 years ago). Bottle gourd is grown worldwide for its fruit and for its medicinal value because it has essential constituents that are required for human health (Xu et al., 2011). Bottle gourd fruits were used traditionally as a cardio-protective, to promote diuresis, and to counteract poisoning (Prajapati et al., 2010). The ethanolic extract of this fruit was shown to be an effective antioxidant, hepatoprotective and cardiotonic agent (Deshpande et al., 2008). In addition to its nutritional and medicinal values, it has traditional and decorational uses (Mladenović et al., 2012). Bottle gourd seeds are also a valuable source of amino acids and essential oil (Ogunbusola et al., 2010). Another recent and useful agronomic application of bottle gourd is that it has been shown that bottle gourd rootstock is tolerant to low soil temperature stress and soil-borne diseases (Mashilo et al., 2016).

Landraces are defined as cultivar with unique characteristics and historical background, genetically diverse, having high adaptation potential, and with minimum genetic improvement (Villa et al., 2005). These landraces can adapt to shifting environmental conditions and modifying agricultural practices due to the genetic diversity inherent within their genome (Azeez et al., 2018).

Molecular markers are now being utilized in a variety of plant biodiversity studies. There are various molecular markers that can be used for genetic studies such as Simple Sequence Repeat (SSR), Random Amplified Polymorphic DNA (RAPD), Amplified Fragment Length Polymorphisms (AFLP) and Inter Simple Sequence

* Corresponding author. e-mail: wesamkh@yu.edu.jo.

Repeat (ISSR) (Idrees and Irshad, 2014). Molecular markers techniques are not influenced by environmental factors, stable across different developmental stages, and result in a powerful data regarding genetic distance and genetic similarity (Mashilo et al., 2016).

ISSR has the advantage of not requiring sequence knowledge neither for primer construction nor genome sequence information. It causes multi-loci and highly polymorphic patterns and is randomly distributed throughout the genome (Jabbarzadeh et al., 2010). ISSR markers have been demonstrated to have advantages over other genetic markers, including being ubiquitous, inexpensive, quick, simple to use, highly reproducible, and polymorphous (Mohammadabadi et al., 2017). ISSR method has been used in genetic diversity studies in various crops, including strawberry, potato, rice and others (Tahir and Karim, 2011; Brake et al., 2021).

The objective of this study was to assess the biodiversity status of bottle gourd landraces collected from different regions of Jordan using molecular and agro-morphological markers.

2. Materials and Methods

2.1. Plant materials

Nineteen *Lagenaria siceraria* landraces were used in this study. Eleven landraces were collected from different regions in Jordan, and eight samples were provided by the National Agriculture Research Centre (NARC) (Table 1). Landraces seeds were grown in the field at Yarmouk University/ Irbid during the period of February – August, 2020 under rainfed conditions. The study site has silty clay soil texture. Three replications were used with 15 seeds in each replicate. Field was kept free of weeds and diseases during the experiment.

Table 1: Bottle gourd landraces and description of collection sites

Number #	Sample code	Location	Altitude	Longitude	Latitude
1	4414	Irbid	620	N 35.85	E 32.55
2	4451	Irbid	620	N 35.85	E 32.55
3	4514	Irbid	620	N 35.85	E 32.55
4	4515	Irbid	620	N 35.85	E 32.55
5	4517	Irbid	620	N 35.85	E 32.55
6	4597	Irbid	620	N 35.85	E 32.55
7	-	Ibbin	1141	N 32.37	E 35.82
8	4460	Balqa'	546	N 35.75	E 23.12
9	851	Balqa'	546	N 35.75	E 23.12
10	-	Madaba	709	N 31.42	E 35.47
11	-	Al-Karak	930	N 31.10	E 35.42
12	-	Aqaba	6	N29.30	E 35.00
13	-	Sal	574	N 32.34	E 35.54
14	-	Al-mazar	1264	N 35.65	E 31.82
15	-	Samaalrousan	350	N 31.55	E 35.55
16	-	Kufrjayez	508	N 23.37	E 35.49
17	-	Baytyafa	632	N 32.52	E 35.78
18	-	Deirabe said	508	N 23.30	E 35.41
19	-	Enbeh	541	N 31.96	E 35.93

2.2. Agro-morphological traits analysis

Seeds of each landrace were planted at a depth of 25 mm, spaced 60-70 cm between plants. A completely randomized design was laid out with three replicates. For agro-morphological traits assessment, several traits were measured including; seed length, seed width, seed area, plant length, leaf length and width, number of leaves, number of tendrils, length of tendrils.

2.3. ISSR analysis

Young bottle gourd leaves were collected from all landraces and DNA was extracted using CTAB method (Doyle, 1991). A total of 24 ISSR primers (University of British Columbia, Canada) were used (Table 6). DNA amplification was performed in Genepro (model- TC-E-96G) thermal cycler. PCR reactions were carried out in a final volume of 25 µl containing30 ng of genomic DNA, 12.5 µl of 1X master mix,1.5µLof each primer and 9 µl free nuclease water. The PCR program consists of an initial denaturation step of 94ºC for 5 min, followed by 40 cycles of 240 s denaturation at 94ºC, 300 s annealing at 50ºC, and 60 s extension at 72ºCwith final extension step at 72ºC for 5 min. Amplified products of ISSR were separated by electrophoresis using 1.25% agarose gel stained with ethedium bromide and visualized using gel documentation system (Alpha DigiDoc System, USA).

2.4. Statistical analysis

The whole experiment was repeated two times. The collected data were processed using one-way analysis of variance (ANOVA). Investigation of multi-character variation was conducted by Cluster Analysis and Principal Component Analysis (PCA). Dendrogram for molecular and agro-morphological

data was drown using NTSYS pc (2.20) Software. ImageJ software was used to measure seeds length, width and area for each landrace. The DNA profile was scored from the resulting gels. Clear bands were considered as a separate marker and scored as either present (1) or absent (0) across all landraces. Primer efficiency and primer discrimination were calculated by dividing the number of markers for each primer by the total number of markers and by dividing the number of polymorphic markers by the total number of polymorphic markers, respectively (Khierallah et al., 2011). DNA fragment size was estimated using the relative migration distance of DNA ladder.

3. Results

3.1. Agro-morphological characterization

Table 2 displays the mean and standard error of studied landraces morphological characteristics. The quantitative features examined showed significant differences (P< 0.05) among landraces, demonstrating the presence of morphological variations. For example, sample number 8 collected from Balqa', showed the longest plant length (2.05 m), highest number of tendrils (11) and highest number of leaves (14). On the other hand, sample number 15 collected from Samaalrousan, showed the shortest plant length (0.35 m),samples 14 and 19 showed the lowest number of tendrils, and samples 1 and 19 showed the lowest number of leaves.

Table 2: Mean and standard error for quantitative traits of 19 bottle gourd landraces.

Sample number	Plant length (m)	Number of tendrils	Tendril length (cm)	Number of leaves	Leaf width (cm)	Leaf length (cm)	Distance between tips of cotyledons (cm)	Petiole length (cm)	Seed length (cm)	Seed width (cm)	Seed area (cm^2)
					Mean ± SE						
1	1.08±0.04	4±0.9	21±1.1	6±1.0	9.75±1.2	8.5±1.5	12.5±1.1	5.5±0.2	1.6±0.0473	0.75±0.01	1.11±0.03
2	1.3±0.02	8±0.7	15±0.9	11±0.8	13±1.1	10.5±0.8	15±0.9	5±0.4	1.8±0.11	0.7±0.01	1.21±0.02
3	2.2±0.08	9±0.5	22±1.2	13±0.9	14.5±1.2	14.5±1.1	14±1.2	6±0.4	1.8±0.05	0.78±0.01	1.23±0.01
4	1.65±0.05	6.5±0.5	36±1.0	11±1.1	15±1.5	11±0.4	15±1.1	7.5±0.5	1.9±0.08	0.7±0.02	1.30±0.05
5	1.07±0.08	4.33±0.5	25.3±1.3	7±0.5	9.75±0.6	7.9±0.3	12.8±1.4	5.6±0.4	1.6±0.03	0.8±0.02	1.26±0.05
6	1.25±0.29	8±0.6	25.5±0.5	10.5±1.1	11.5±0.5	11.5±0.5	14.5±1.5	7±0.3	1.6±0.05	0.57±o.o3	0.91±0.02
7	0.97±0.01	4.66±0.6	28.3±1.3	8±1.1	8.6±0.8	7.6±0.8	12.3±1.7	5±0.2	1.7±0.02	0.65±0.02	1±0.01
8	2.05±0.04	11±0.9	29±1.2	14±0.8	12.5±0.9	11±0.9	14±0.9	5±0.3	1.8±0.05	0.69±0.01	1±0.09
9	1.11±0.09	6.66±0.8	12±1.4	9±0.8	9.33±0.6	8.3±0.7	15.6±1.8	4.75±0.2	1.7±0.02	0.76±0.02	1.1±0.03
10	0.82±0.1	4.5±0.6	23.3±1.0	8±0.7	8.33±0.6	7.4±0.6	16.25±0.9	4.8±0.4	1.6±0.04	0.65±0.01	0.94±0.05
11	0.79±0.02	5±0.5	22±0.5	8±0.5	9.25±0.5	8.5±0.5	14±1.1	6.3±0.4	1.5±0.08	0.86±0.01	1.1±0.06
12	1.97	9±0.8	19±0.8	13±0.8	12.5±0.7	10.5±0.8	15±1.3	7±0.5	1.6±0.08	0.74±0.02	1.2±0.05
13	0.51±0.09	4.75±0.5	28.3±1.6	7.75±1.3	10±0.3	8.5±0.4	11±0.8	6±0.4	1.6±0.06	0.63±0.02	0.95±0.02
14	0.91±0.06	3±0.4	22±0.5	6.3±0.6	10.1±0.6	9.2±0.4	14.3±0.8	6.8±0.4	1.6±0.02	0.79±0.03	1.0±0.04
15	0.35±0.06	5±0.3	23.5±0.5	7.5±0.5	9.25±0.2	7.75±0.3	14±1.0	3.75±0.25	1.6±0.04	0.67±0.01	0.94±0.01
16	0.91±0.06	3.66±0.3	27.2±1.8	6.4±0.8	8.8±1.0	7.7±0.5	12.4±0.8	5±0.3	1.5±0.06	0.65±0.03	0.88±0.04
17	0.64±0.03	8±0.4	21±1.1	11±0.7	9±0.8	9.5±0.4	14±1.1	5±0.5	1.9±0.05	0.79±0.02	1.36±0.06
18	1.2± 0.07	8.5±0.5	19.5±1.5	19±0.5	16.5±0.5	12.5±0.5	13.3±1.2	5.5±0.7	1.5±0.03	0.67±0.03	0.87±0.03
19	1.65±	3±0.5	23.5±1.4	6±0.5	9.16±0.7	8.8±0.3	13.5±0.6	4.8±0.2	1.7±0.06	0.70±0.01	1.0±0.03

3.2. Genetic parameters of agro-morphological traits

Estimates of genetic advance (GA) and genetic advance as a percentage of the mean (GAM), genotypic variance (Vg) and phenotypic variance (Vp), genotypic coefficient of variation (GCV), phenotypic coefficient of variation (PCV), broad sense heritability (H2), and genetic advance (GA) are presented in Table3. High phenotypic and genotypic variances were observed for tendril length (33.3 and 15.2, respectively). On the other hand, small genotypic and phenotypic variances were observed for seed width (0.006 and 0.007) and seed length (0.01 and 0.02).

In general, the relative coefficients values indicate the level of variability existing in a population. Genotypic and phenotypic coefficients of variation are straightforward measures of variability. Low magnitude of genotypic as well as phenotypic coefficient of variation were observed for number of tendrils (1.48 and 2.02, respectively). Moderate GCV and PCV were observed for leaf width (16.4 and 21.0), leaf length (14.1 and 18.6), petiole length (12.7 and 18.9), seed width (10.6 and 11.4) and seed area (13.2 and 14.9).

Broad sense heritability (H^2) ranged from 41.98% to 85.7%, for distance between cotyledons and seed width, respectively. Genetic advance is an increase in a plant's mean genotypic value relative to its parent population, the highest value of GA was observed for tendril length (5.42) and the lowest (0.05) for distance between cotyledons. The highest genetic advance as per cent of the mean (GAM) (47%) was recorded for plant length, and the lowest percent was observed (2%) for tendrils number (Table 3).

Table 3: Estimates of genetic parameters for 11 quantitative traits in different bottle gourd landraces.

	Plant length	Number of tendrils	Tendril length	Number of leaves	Leaf width	Leaf length	Distance between cotyledons	Petiole length	Seed length	Seed width	Seed area
Between groups	0.38	11.0	63.7	23.9	11.0	6.76	5.77	2.15	0.05	0.01	0.07
Within group	0.05	2.07	18.2	3.26	2.08	1.30	5.60	0.62	0.009	0.001	0.006
Mean	1.19	116.6	23.3	9.60	10.9	9.53	13.9	5.6	1.70	0.73	1.089
Vg	0.11	2.99	15.2	6.89	3.17	1.81	0.06	0.51	0.01	0.006	0.02
Vp	0.16	5.05	33.3	10.1	5.25	3.13	5.67	1.13	0.02	0.007	0.03
GCV	27.6	1.48	16.7	27.3	16.4	14.1	1.70	12.7	6.69	10.6	13.2
PCV	33.4	2.02	24.7	33.2	21.0	18.6	17.2	18.9	8.70	11.4	14.9
H^2	67.9	59.1	45.5	67.9	60.4	58.1	41.98	45.02	59.0	85.7	77.5
GA	0.56	2.87	5.42	4.46	2.85	2.12	0.05	0.99	0.1	0.15	0.26
GAM (GA %)	47	2	23	46	26	22	36	17	5	20	24

3.3. Principle component analysis

Principal component analysis was used to detect the most significant variables in the data set. It measures the importance and contribution of particular trait relative to the total variability. Table 4 displays the eigen values and principal components (PCs) for quantitative qualities. For 19 landraces, the first two principal components (PCs) with eigenvalues greater than one explained 69.6% of the variation in various agro-morphological parameters. Other PCs had eigenvalues less than 1. The first principal component (PC1) accounted for 50.8% of total variation. Quantitative traits that contributed more positively toPC1 included plant height, number of tendrils, number of leaves, leaf width, leaf length, distance between tips of cotyledons, petiole length, seed length, seed width, seed area, whereas tendril length was negatively associated with PC1. Principal component 2 (PC2) showed 18.8% of the total agromorphological variability. Plant height, number of tendrils, number of leaves, leaf width, leaf length, distance between tips of cotyledons, petiole length, seed length, seed width, seed area contributed positively to PC2, whereas tendril length was negatively associated with PC2 (Figure 1). Plotting the link between 19 bottle gourd landraces using the first two PCs (Figure 2). This distinction between the landraces was made on the basis of significant morphological variations.

Table 4: Eigen value and percent of total variation for the principal component axes.

	PC1	PC2
% of variance	50.753	18.822
Eigenvalue	5.583	2.070
Cumulative %	50.753	69.575

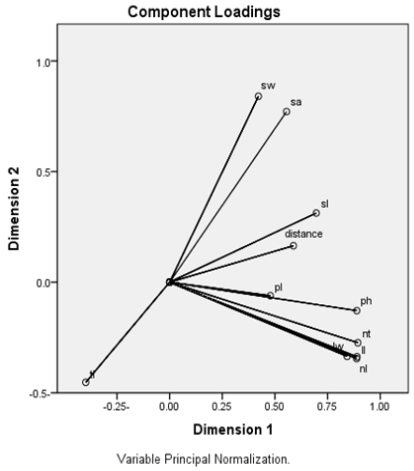

Figure 1: Scattered diagrams of first two principal components showing the contribution of various traits in the separation of various *Lagenaria siceraria* landraces from Jordan. (sw:seed width; sa: seed area; sl:seed length; distance:distance between cotyledons; pl:petiole length; ph:plant length; nt:number of tendrils; ll:leaf length; lw:leaf width; nl:number of leaves; tl:tendril length).

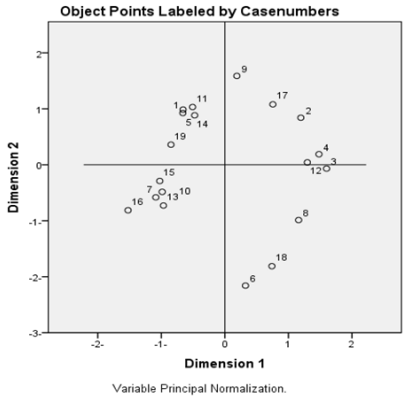

Figure 2: Scattered diagram of first two principal components based on mean values of 19 quantitative traits in *Lagenaria siceraria* of bottle gourd from Jordan.

3.4. Correlation analysis of agro-morphological traits

Correlation assesses the degree of association between variables. The results of correlation analysis (Table 5) in the present study showed a positive strong correlation between plant length and number of tendrils (r=0.86), number of leaves (r=0.67) and leaf length (r=0.74). On the contrary, tendril length had negative correlation with distance between tips of cotyledons (r=-0.36) and number of leaves (-0.12). Furthermore, a positive correlation was observed between number of leaves with leaf length and width(r=0.79) (r=0.83) respectively. In addition, a positive correlation between plant length with seed length (r=0.56), seed width (r=0.10) and seed area (r=0.48) was observed.

Table 5: Correlation coefficients among morphological traits in bottle gourd landraces.

	Number of tendrils	Tendril length	Number of leaves	Leaf width	Leaf length	Distance between the tips of cotyledons	Petiole length	Seed length	Seed width	Seed area
Plant length	0.86	0.07	0.68	0.65	0.74	0.20	0.28	0.56	0.10	0.48
Number of tendrils		-0.14	0.86	0.66	0.75	0.33	0.13	0.45	-0.07	0.28
Tendril length			-0.12	0.05	0.07	-0.36	0.29	0.02	-0.19	0.09
Number of leaves				0.83	0.79	0.23	0.17	0.21	-0.11	0.08
Leaf width					0.88	0.17	0.43	0.25	0.01	0.16
Leaf length						0.19	0.42	0.34	0.08	0.21
Distance between the tips of cotyledons							0.09	0.27	0.06	0.28
Petiole length								0.04	0.22	0.25
Seed length									0.15	0.71
Seed width										0.78

3.5. Dendrogram for agro-morphological traits

The collected landraces were clustered into six main groups as shown in agro-morphological traits Dendrogram(Figure 3). The first group comprises 4414-Irbid, Ibbin, 4517-Irbid, Al-karak, Samaalrousan, Bayt yafa, 4597-Irbid, 4515-Irbid, Madaba, 851-Balqaa'. The second group includes 4451-Irbid only. Two landraces (Aqaba and 4460-Balqaa') were grouped in group 3. Group4 includes Al-mazar, Enbeh and Kufrjayez, while group 5 includes 4514-Irbid only, and finally group six contains landrace collected from Deirabe said region.

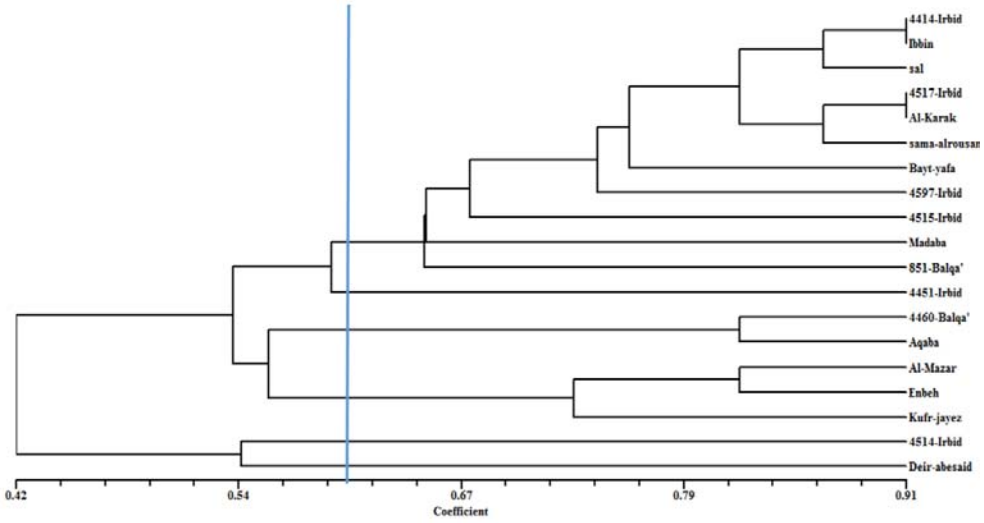

Figure 3: Dendrogram constructed from Agro-morphological data.

3.6. ISSR analysis

The selected primers and the maximum number of reproducible polymorphic bands produced by each primer, % Primer efficiency, number of Polymorphic bands, number of unique bands, % of polymorphism, %Discrimination power and PIC are listed in Table 6. A total of 246 markers were produced by 24 primers, of which 135 were polymorphic. The efficiency of ISSR primers has been tested in producing polymorphic DNA bands in the bottle gourd genome, the highest primer efficiency was 8.53 for UBC-857 and the lowest was 0.81 for UBC-845, and the average primer efficiency for all primers was 4.43%. A 100% polymorphism was found for UBC-825, and 0%was observed for UBC-812, UBC-864 and UBC-844. The average percentage of polymorphic markers for all primers in the examined 19 landraces was 54%.

The discrimination power ranged from 0% (for UBC-864, UBC-812 and UBC-841) to 12.5% (for UBC-856 and UBC-857). Primers UBC-823, UBC-843, UBC-856, UBC-860, UBC-828 and UBC-815 were able to generate 2, 1, 1,1,1,1 unique bands, respectively.

For cluster analysis, Jaccard similarity coefficients were used. Dendrogram was formed using Unweighted Pair-Group method (UPGMA) by SAHN clustering function of NTSYS software. The dendrogram's similarity coefficient ranged from 0.74 to 0.92. (Figure 4). Five main groups of the investigated landraces were identified: Group 1 comprises 4414-Irbid, 4451-Irbid, 4514-Irbid, 4517-Irbid, 4597-Irbid, Ibbin, 4460-Balqaa' and 851-Balqaa'. Eight landraces were found in group 2; Al-Karak, Aqaba, Samaalrousan, Kufrjayez, Baytyafa, Enbeh, Sal, Al-Mazar. Group 3 comprises 4515-Irbid only, group 4 contains only Madaba, and finally group 5 contains deirabesaid only.

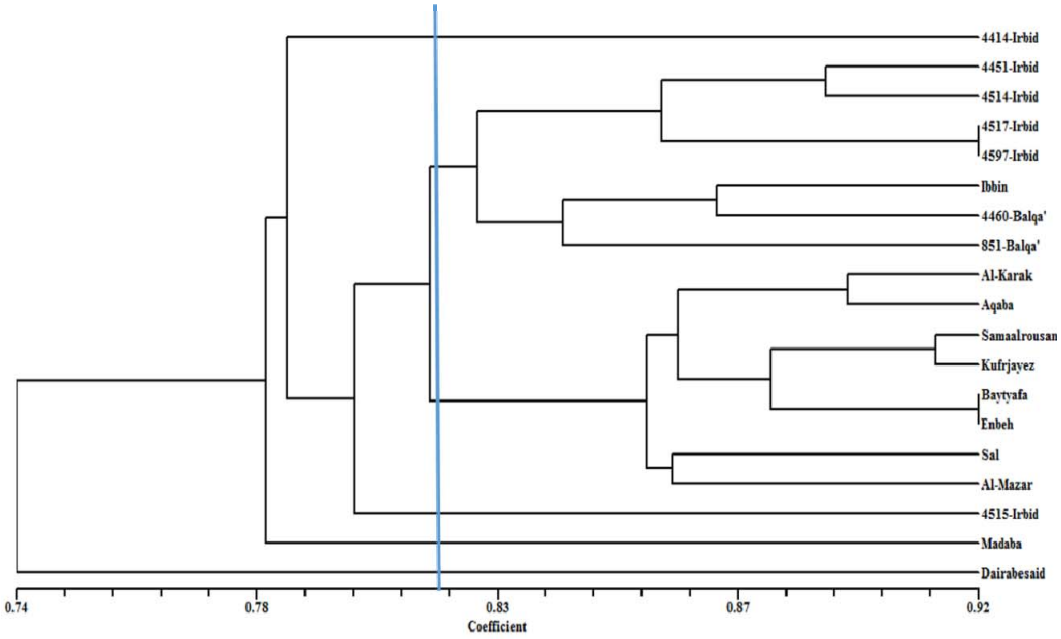

Figure 4: Dendrogram estimating the genetic distance among 19 bottle gourd landraces based on ISSR data.

Table 6: Primer name, total number of markers generated, % Primer efficiency, number of Polymorphic bands, number of unique bands, % of polymorphism, %Discrimination power and PIC.

Primer name	Total number of bands	%Primer efficiency	Polymorphic band	Unique band	% Polymorphism	% Discrimination power	Polymorphic Information Content (PIC)
UBC-807	14	5.69	8		57.14	5.92	0.26
UBC-823	11	4.47	8	2	72.72	5.92	0.61
UBC-826	11	4.47	6		54.54	4.44	0.34
UBC-843	6	2.43	4	1	66.66	2.96	0.68
UBC-848	11	4.47	7		63.63	5.18	0.35
UBC-856	19	7.72	17	1	89.47	12.5	0.77
UBC-880	13	5.28	2		15.38	1.48	0.15
UBC-900	7	2.84	5	1	71.42	3.70	0.44
UBC-812	13	5.28	0		0	0	0.00
UBC-860	6	2.43	2	1	33.33	1.48	0.31
UBC-864	8	3.25	0		0	0	0.00
UBC-810	11	4.47	5		45.54	3.70	0.21
UBC-868	16	6.50	5		31.25	3.07	0.11
UBC-834	15	6.09	4		26.66	2.96	0.16
UBC-855	14	5.69	11		78.57	8.14	0.45
UBC-825	8	3.25	8		100	5.92	0.75
UBC-828	9	3.65	5	1	55.55	3.70	0.52
UBC-815	11	4.47	9	1	81.81	6.66	0.81
UBC-835	5	2.03	4		80	2.96	0.26
UBC-841	6	2.43	0		0	0	0.00
UBC-845	2	0.81	1		50	0.74	0.30
UBC-844	9	3.65	7		87.5	5.18	0.39
UBC-857	21	8.53	17		80.95	12.5	0.40
Total	246		135				
Avg.		4.43			54.00		

4. Discussion

Statistical analysis results (ANOVA) revealed significant differences between the tested landraces for all morphological characteristics, demonstrating the considerable variability among landraces. Similarly, variations in morphological characters have been reported in Turkish bottle gourd landraces. *Lagenaria siceraria* was found in 162 accessions, all of which were gathered from Turkey's Mediterranean coast. These accessions varied greatly in several morphological characteristics, particularly in fruit size and form (Yetişir et al., 2008). One of the major factors that influence the phenotypic characteristics in organisms is the environmental influence. According to Parsaeian et al.(2011), there is a high degree of variability in the phenotypic traits of 27 accession of sesame (*Sesamum indicum* L.) that were collected from different regions of Iran along with six exotic genotypes from Asian countries. They explained that this high degree of variability is caused by the effect of different environmental aspects on phenotypic features and the complex genetic structure of many morpho-physiological traits.

According to the current study, for each of the investigated features, phenotypic variance (Vp) and phenotypic coefficient of variance (PCV) were greater than their associated genotypic variance (Vg) and genotypic coefficient of variance (GCV).This suggests that there was significant interaction between the environment and these characters' expressions, which was greatly influenced by the surrounding conditions. Similarly, Konate et al., (2016) reported that rice (*Oryza sativa* L.) phenotypic coefficients of variance were higher than genotypic coefficients of variance in all the studied characters, which indicates environmental influence on traits expression. This, however, contrasts Malek et al(2014) study, they studied

genetic diversity among 27 soybean genotypes and found small differences between phenotypic and genotypic coefficients of variation (PCV and GCV) for most characters, which shows less environmental effect on these features' manifestation. In genetic studies of quantitative features, one of the most crucial roles of heritability estimation is its ability to forecast the accuracy of phenotypic value as a breeder's guide (Singh et al., 2011). In this study, high heritability values (>60%) for seed width, seed area, plant length, number of leaves and leaf width were observed. High heritability in morphological features suggests that these characters could be easily improved through selection (Rashid et al., 2017). Low heritability values, however, were found for the length of the tendrils, the number of tendrils, the length of the tendrils, the length of the leaves, the length of the petioles, and the length of the seeds. These characters with low value of heritability are of little importance in selection strategies because their most variations are non-transmissible (Singh et al., 2011).

According to Ajayi et al., (2014), genetic advance as a percentage of mean is divided into three categories: low(10%), moderate(10%–20%), and high (>20%). High genetic advance as percentage of mean was observed for plant height, tendril length, number of leaves, leaf width, leaf length and distance between tips of cotyledons, whereas number of tendrils, and seed length showed low genetic advance as percentage of mean and moderate genetic advance for petiole length and seed width.

Characters with high heritability coupled with high genetic advance as a percent of mean (GA %) resulted from additive gene action could be used in further improvement programs due to their performance and simple phenotypic selection (Reddy et al., 2013). In the current study, high heritability values coupled with high genetic advance were recorded for plant height, number of leaves, leaf width and seed area. Similar findings were reported by Kumar et al. (2016) where high heritability coupled with high genetic advance as percent of mean recorded for almost all of the characters they studied.

In this study, no strong association was observed between geographical origin of bottle gourd landraces and phenotypic traits, except for one group of landraces;Kufrjayez, Al-mazar and Enbeh were in one cluster, and they belong to one geographical area (Irbid governorate). All the other landraces were clustered according to morphological traits rather than to geographical distribution. This is in agreement with the results of Pandey et al. (2015) who found that clustering of sesame genotypes based on their morphological traits did not reflect their geographical origin. In plant breeding, correlation assists in the choice of characters whose selection would result in the improving of any character such as yield (Joshi, 2005). In this study, a positive strong correlation between plant length and number of tendrils (r=0.86), number of leaves (r=0.67) and leaf length (r=0.74) was found. This indicates that plant length is a helpful characteristic to bottle gourd breeders because it is associated with a high number of tendrils and high number of leaves. Similarly, research has indicated that one of the most crucial qualities taken into account in the development of high yield variants in plant breeding projects is plant length (Ahmad et al., 2015). On the contrary, tendril length had negative correlation with distance between tips of cotyledons (r=-0.36) and number of leaves (-0.12). Moreover, there was a positive correlation between number of leaves with leaf length and width. Leaf area is considered as an important parameter in determining plant growth and it has an important role in yield and productivity (Hashimoto et al., 2023). Tendrils are considered as specialized stem, leaf or petiole with a threadlike shape that plants used for climbing, support and attachment; high number of tendrils led to an improvement in standing ability of crops (Liou and Ruan, 2011).

ISSR and other molecular markers are powerful tools for genetic characterization of bottle gourd (Decker-Walter et al., 2001; Abdinet al., 2014). In this study, the average percentage of polymorphic markers for all primers in the examined 19 landraces is 54%, which indicated a high level of genetic variation among landraces. Similar findings were reported by Yuan et al.(2015) who examined the genetic variety of 48 Okra (*Abelmoschus escullentus* L.) genotypes using morphological features and ISSR markers. Their study found that the average polymorphism was 54.55%. The greatest similarity coefficient between the landraces Enbeh and Baytyafa was 0.92; this shows a significant degree of resemblance between them and suggests that they may have common ancestor. Landraces 4515-Irbid and Dairabe said showed the lowest similarity coefficient values (0.68), indicating that they are distinct from one another due to the diverse morphological characteristics and different geographic origins or ancestors. Based on ISSR marker analysis, the studied landraces cluster into various groups, indicating that they are genetically distinct. Landraces placed in the same groups represent a close genetic similarity. There was no clear association between genetic divergence and geographical origins in the same cluster. One explanation for this could be the limited number of ISSR markers used. Izadpanah et al. (2015) reported similar findings, no correlation between Saffron's(*Crocus sativus L.*) diversity pattern and its geographic origins. In the present study, no full agreement was observed between molecular and agro-morphological analysis except for 8 landraces which grouped similarly in both dendograms; namely, Al-mazar, Enbeh and Kufrjayez were found in one group in both dendograms, and 851-Balqaa', Ibbin and 4414-Irbid in another group in both dendograms also. Finally, deirabesaid was found in a distinct group in both dendograms, which is in agreement with studies of Greene et al. (2004), Yuan et al., (2015) and Guliyev et al., (2018) who used morphological and molecular markers in red clover (*Trifolium pratense* L.), okra (*Abelmoschus escullentus* L.) and melon (*Cucumismelo* L.); they

found that there is no association between molecular and morphological analysis in terms of clustering. Garciaet al. (2008) found that there is no correlation between morphological and RAPD methods in many strawberry varieties cultivated in Argentina. Moreover, Ristiet al. (2013) investigated the genetic diversity of maize landraces using 15 morphological features, 7 RAPD primers, and 10 SSR primer pairs, and they found that no significant associations between any two types of markers were detected. Syed (2016) proposed two explanations for the weak correlation between DNA fingerprinting markers and morphological characters. The first one is the possibility that a few alleles may be responsible for morphological characteristics and that their genotypes may not be correlated with the overall marker scores for these lines. Also, molecular markers study relatively most of the genome, which is wider than the morphological markers only.

In conclusion, ISSR markers were significantly valuable for genetic diversity analysis at the molecular level in bottle gourd landraces. They showed high discrimination power, and were able to differentiate between bottle gourd landraces with high efficacy and accuracy**.** The findings imply that there is significant genetic diversity at both the agromorphological and molecular levels. This shows the possibility of such landraces in bottle gourd breeding initiatives. Despite this, ISSR markers did not completely match agro-morphological data. Only 8 landraces were grouped similarly in both dendograms. Neither molecular nor agro-morphological diversity was associated with geographical distribution of landraces in Jordan.

5. Conflict of Interest

The authors declare that there are no conflicts of interest.

Acknowledgment

This study was supported by Deanship of Graduate Studies and Scientific Research at Yarmouk University as M.Sc. thesis for AA.

References

Ahmad F, Hanafi MM, Hakim MA, Rafii MY, Arolu IW and Abdullah SNA. 2015. Genetic Divergence and Heritability of 42 Coloured Upland Rice Genotypes (*Oryza sativa*) as Revealed by Microsatellites Marker and Agro-Morphological Traits. *PLoS ONE*., **10(9)**:1-18.

Ajayi, AT, Adekola MO, Taiwo BH and Azuh VO. 2014. Character expression and differences in yield potential of ten genotypes of cowpea (Vigna unguiculata L. Walp). *Int. J. Plant Res.,***4(3)**: 63-71.

Azeez, M.A., Adubi AO and Durodola FA. 2018. Landraces and Crop Genetic Improvement. In Rediscovery of Landraces as a Resource for the Future. *IntechOpen.,* 1-18.

Bhawan, Abdin MZ, Arya L, Saha D, Sureja AK, Pandey C and Verma M. 2014. Population structure and genetic diversity in bottle gourd [*Lagenaria siceraria* (Mol. Standl.] germplasm from India assessed by ISSR markers. *Plant Syst. Evol*., **300(4)**: 767-773.

Brake, M., Moath A. Al-Gharaibeh , Hassan R. Hamasha, Nuha S. Al Sakarneh , Ibrahim A. Alshomali, Hussein M. Migdadi , Muien M. Qaryouti , Nizar J. Haddad. 2021. Assessment of genetic variability among Jordanian tomato landrace using inter-simple sequence repeats markers. *Jordan J. Biol. Sci.,***14**: 91 – 95

Doyle J. 1991. DNA protocols for plants. In Molecular techniques in taxonomy. **Springer,** 283-293

Decker-Walters, D., Staub J, Lopez-Sese A and Nakata E. 2001. Diversity in landraces and cultivars of bottle gourd (*Lagenaria siceraria*; Cucurbitaceae) as assessed by random amplified polymorphic DNA. *J Genet Resour*., **48(4)**: 369-380.

Deshpande, J.R., Choudhari AA, Mishra MR, Meghre VS, Wadodkar SG and Dorle AK. 2008. Beneficial effects of *Lagenaria siceraria* (Mol.) Standley fruit epicarp in animal models. *J. Exp. Biol.*, **48(2)**: 234-242.

Garcia, M.G., Ontivero M, Diaz Ricci JC and Castagnaro A. 2008. Morphological traits and high resolution RAPD markers for the identification of the main strawberry varieties cultivated in Argentina. *Plant Breed.,***121(1)**: 76-80.

Greene, S.L., Gritsenko M and Vandemark G. 2004. Relating Morphologic and RAPD marker varlation to collection site environment in wild populations of Red Clover (*Trifolium pratense* L.). *J Genet Resour.,* **51(6)**: 643-653.

Guliyev, N., Sharifova S, Ojaghi J, Abbasov M and Akparov Z. 2018. Genetic diversity among melon (*Cucumis melo* L.) accessions revealed by morphological traits and ISSR markers. Turkish JAF Sci. Tech.,**42(6)**:393-401.

Hashimoto, N., Saito Y, Yamamoto S, Ishibashi T, Ito R, Maki M, Homma K. 2023. Relationship between Leaf Area Index and Yield Components in Farmers' Paddy Fields. *Agric. Eng., 5*: 1754-1765

Idrees, M, and Irshad M. 2014. Moleculars markers in plants for analysis of genetic diversity: a review. *EAR.,***2(1)**: 1513-1540.

Izadpanah, F.A., Kalantari SA, Hassani MEB, Naghavi MRC and Shokrpoura M. 2015. Molecular and morphological variation in some Iranian saffron (*Crocus sativus* L.) accessions. *Genetika.,* **47(2)**:711-722.

Jabbarzadeh, Z., Khosh-Khui M, Salehi H and Saberivand A. 2010. Inter simple sequence repeat (ISSR) markers as reproducible and specific tools for genetic diversity analysis of rose species. *Afr. J. Biotechnol.,* **9(37)**: 6091-6095.

Joshi, BK. 2005. Correlation, regression and path coefficient analyses for some yield components in common and Tartary buckwheat in Nepal. *Fagopyrum.,***22**:77-82.

Khierallah, H., Bader S, BaumM and Hamwieh A. 2011. Genetic Diversity of Iraqi Date Palms Revealed By Microsatellite Polymorphism. *(JASHS*.,**136(4)**: 282-287.

Konate, A.K., Zongo A, Kam H, Sanni A and Audebert A. 2016. Genetic variability and correlation analysis of rice (*Oryza sativa* L.) inbred lines based on agro-morphological traits. *Afr. J. Agric. Res.*,**11(35)**: 3340-3346.

Kumar, L. 2016. Genetic Diversity, Heritability and Agro-morphological Characterization in Bottle gourd [*Lagenaria siceraria* (Mol.) Standl.]. *IJCMAS.,***6**: 264-271

Liou, NS and Ruan GW. 2011. The mechanical properties of tendril of climbing plant. *Biol. Syst.,***(2)**: 101-104.

Malek, M.A., Rafii MY, Afroz SS, Nath UK and Mondal M. 2014. Morphological characterization and assessment of genetic variability, character association, and divergence in soybean mutants. *Sci. World J*., **14**:1-12.

Mashilo, J., Shimelis H and Odindo A. 2016. Genetic diversity of bottle gourd (*Lagenaria siceraria* (Molina) Standl.) landraces of South Africa assessed by morphological traits and simple sequence repeat markers. *S. Afr. j. plant soil.,***33(2)**: 113-124.

Mladenović, E., Berenji J, Ognjanov V, Ljubojević M and Čukanović J. 2012. Genetic variability of bottle gourd *Lagenaria siceraria* (Mol.) Standley and its morphological characterization by multivariate analysis. *Arch. Biol. Sci.,***64(2)**: 573-583.

Mohammadabadi, M.R., Esfandyarpoor E and Mousapour A. 2017. Using inter simple sequence repeat multi-loci markers for studying genetic diversity in Kermani sheep. *Int. J. Dev. Res*., **5(2)**:1-4.

Ogunbusola, M., T. Fagbemi., O. Osundahunsi (2010). Amino acid composition of *Lagenariasiceraria* seed flour and protein fractions. *J Food Sci Technol*., **47(6)**: 656–661.

Prajapati R.P., Kalariya M, Parmar S, Sheth N. 2010. Phytochemical and pharmacological review of *Lagenaria sicereria*. *J Ayurveda Integr Med.,* **1**:266–272.

Parsaeian, M., Mirlohi A and Saeidi G. 2011. Study of genetic variation in sesame (*Sesamum indicum* L.) using agro-morphological traits and ISSR markers. *Russ. J. Genet.,***47(3)**.

Pandey, S.K., Das A, Rai P and Dasgupta T. 2015. Morphological and genetic diversity assessment of sesame (*Sesamum indicum* L.) accessions differing in origin. *Physiol Mol Biol Plants.,* **21(4)**: 519-529.

Rashid, M.M., Nuruzzaman M, Hassan L and Begum SN. 2017. Genetic variability analysis for various yield attributing traits in rice genotypes. *J. Bangladesh Agric. Univ.,* **15(1)**:15-19.

Reddy, M.P., Reddy BN, Arsul BT and Maheshwari JJ. 2013. Genetic variability, heritability and genetic advance of growth and yield components of linseed (*Linum usitatissimum* L.). *IJCMAS.,***2**: 231-237.

Ristić, D., Babić V, Anđelković V, Vančetović J, Mladenović-Drinić S and Ignjatović-micić D. 2013. Genetic diversity in maize dent landraces assessed by morphological and molecular markers. *Genetika.,***45(3)**: 811-824.

Singh, T., Bhat MM and Khan MA. 2011. Critical analysis of correlation and heritability phenomenon in the silkworm, Bombyxmori (Lepidoptera: bombycidae). *Adv Biosci Biotechnol*., **2(05)**: 347-353.

Syed, N.2016. A comparative study between molecular and agro-morphological methods for describing genetic relationships in Tunisian Faba bean populations. *J. New Sci.,***27(8)**:1513-1518.

Tahir, N and Karim H. 2011. Determination of Genetic Relationship among Some Varieties of Chickpea (Cicer arietinum L) in Sulaimani by RAPD and ISSR Markers. *JJBS* **4**: 77 – 86

Villa, T.C.C., Maxted N, Scholten M, Ford-Lloyd B. 2005. Defining and identifying crop landraces. *Plant Genet. Res.,***3(3)**: 373-384.

Xu, P., Wu X, Luo J, Wang B, Liu Y, Ehlers JD, Wang S, Lu Z and Li G. 2011. Partial sequencing of the bottle gourd genome reveals markers useful for phylogenetic analysis and breeding. *BMC genomics*., **12**:467.

Yetişir, H., Şakar M and SerçeS. 2008. Collection and morphological characterization of *Lagenaria siceraria* germplasm from the Mediterranean region of Turkey. *Genet. Resour. Crop Evol.,***55(8)**:1257-1266.

Yuan, C.Y., Wang P, Chen PP, Xiao WJ, Zhang C, Hu S, Zhou P, Chang HP, He Z, Hu R, LuXT, Ye JZ and Guo XH. 2015. Genetic diversity revealed by morphological traits and ISSR markers in 48 Okras (*Abelmoschusescullentus* L.). *Physiol Mol Biol Plants.,***21(3)**, 359-364.

JJBS

Volume 17, Number 3,September 2024
ISSN 1995-6673
Pages 523 – 529
https://doi.org/10.54319/jjbs/170315

Jordan Journal of Biological Sciences

Diagnostic Screening for Microdeletion Frequency in the AZF-region of Y- Chromosome among the Emirati Infertile Males

Ferdos Ebrahim and Ihsan Ali Mahasneh*, PhD, Professor

Department of Applied Biology-Biotechnology Program, Faculty of Science, University of Sharjah, UAE.

Received: October 5, 2023; Revised: February 5, 2024; Accepted: March 21, 2024

Abstract

A total of 154 Emirati infertile patients were included in this study of which a cohort of 18 infertile males undergoing fertility counseling were recruited from Dubai Fertility Center (DFC) and University Hospital of Sharjah (UHS), in addition to136 azoospermic Emirati infertile patients who performed AZF-deletion screening as counselled and recorded by DFC during the period of January 2011 and January 2021. Diagnostic screening was conducted to investigate the frequency of microdeletion in the Azoospermia Factor (AZFa, AZFb, AZFc, AZFd) gene cluster of the Y-chromosome among Emirati infertile male patients using the Sequences-Tagged-Sites (STS)-Multiplex PCR diagnostic technology. The frequency of the AZF microdeletions was 2.2% as detected in three patients with azoospermia (n= 3/136). There were two complete deletions in the AZFc region as shown by deletion of the two STS; SY254 (380 bp) and SY255 (124 bp). Our findings are similar to those reported in regional and global range, which appeared to vary across genealogical-lineages in different geographical landscape. This article is the first to profile AZF microdeletions in Emirati Azospermic males, offering valuable insights into male infertility genomics worldwide. The novelty and importance of the findings are especially relevant for improved healthcare and male infertility in Gulf countries due to shared tribal genetic lineage. This highlights the importance of the screening for the AZF-deletion for male infertility diagnosis for better management and treatments in the fertility clinics and hospitals in the UAE.

Keywords AZF microdeletion, Y-chromosome microdeletion, azoospermia, spermatogenesis, male-infertility, Emirati-males

1. Introduction

Recently, there has been worldwide growing interest on diagnostic screening of the microdeletions on the AZF region within the human Y chromosome (Yq11.23), which have been used as genetic marker, playing a fundamental role in male infertility. The AZF region, as coding for testes-specific functions, is divided into four subsidiary subregions, namely AZFa, AZFb, AZFc, and AZFd, all of which are associated in different stages of spermatogenesis process. This makes the human Y chromosome essential in reproductive biology ensuring continuity of human species. More importantly, the problem relies on the susceptibility of the AZF region to microdeletions leading to severe male infertility. The genomic structure of AZF region consists of palindromic and ampliconic sequences with high degree of homology, which make the region unstable, inducing breakage or stalling of the replication fork or even DNA double-strand break (DSB) (Xu and Pang, 2022). Such processes also involve activation of different types of repair mechanisms as Non-Allelic Homologous Recombination (NAHR) and Non-Homologous End Joining (NHEJ), which by their activation AZF microdeletions are promoted (Chang *et al.,* 2017; Cejka and Symington, 2021; Witherspoon *et al.,* 2021). Accordingly, microdeletions within the AZF gene cluster, recognized as the most common structural chromosomal abnormality, primarily cause a severe reduction in sperm quantity (azoospermia) rather than other sperm deformities (Witherspoon *et al.,* 2021; Rabinowitz *et al.,* 2021). In fact, a major challenge upon the infertility clinical practices is that the infertile males with AZF microdeletions usually appear phenotypically normal; for this reason, implementing of AZF screening is crucial in diagnosis and treatment of male infertility.

Moreover, the Emirati population is characterized by unique homogeneity with a highly conserved gene pool, owing to the high rates of consanguineous and endogamous unions (Al-Gazali and Hamamy, 2014; Elliott *et al.,* 2022). In a previous study, we reported the chromosomal abnormalities and clinical conditions associated with male infertility among Emiratis (Ebrahim and Mahasneh, 2022). However, to date and in comparison with other parts of the world, the microdeletion on the AZF gene cluster among Emirati infertile males has not been studied before. Therefore, the aim of this study was to investigate and genetically screen for the frequency of the microdeletions in the gene cluster AZFa, AZFb, AZFc and AZFd within the infertile male patients of the Emiratis. The utilization of the latest powerful technology of STS Multiplex-PCR analysis provides a novel approach to screen for most vulnerable sites of the AZF subregions using the international standard of the World Health organization and as reported worldwide by several researchers according to the recommendations of European

* Corresponding author. e-mail: imahasneh@sharjah.ac.ae.

Academy of Andrology/European Molecular Genetics Quality Network (EAA/EMQN) (WHO, 2021; Krausz *et al.,* 2023). Here, we present, for the first time, the microdeletion profiling of the AZF gene cluster among Emirati infertile males with a comparative discussion in comparison with other regional and global infertile male populations.

2. Materials and Methods

2.1. Subjects and Ethics

A total of 154 Emirati infertile patients were recruited in this study, compromising of a cohort of 136 male patients with azoospermia who performed AZF-deletion screening as counselled and recorded by DFC during the period of January 2011 and January 2021 in addition to 18 infertile males undergoing fertility counseling between April 2021 and January 2022 recruited from DFC and UHS. These are:

I. Dubai Fertility Center (DFC), Dubai, UAE:

Out of cohort of 18, 15 patients were recruited from DFC, of which 11 patients were azoospermic (61.1%; n=11/18;), four patients were non-azoospermic that involved three cases of severe oligoasthenoteratozoospermia (OAT) (16.6%; n= 3/18), and one case of asthenoteratozoospermia (5.5%; n=1/18). Furthermore, due to difficulty in blood collection and to obtain a clear picture of type and frequency of AZF deletion among Emiratis, we extended our study to cover the recorded data of the patients that referred to DFC for counseling as a 10-years retrospective cross-sectional study which included 136 patients. This part of the study was approved by Postgraduate committee of University of Sharjah (session 9; dated 3/2/2020), University Student and Resident Research Committee, Dubai Health Authority (Reference USRRC09-29/PG/2020) and Dubai Scientific Research Ethics Committee, Dubai Health Authority (Reference DSREC-SR-09/2020_03).

II. Sharjah Fertility Center in University Hospital of Sharjah (UHS), Sharjah, UAE:

Out of cohort of 18, three patients (non-azoospermic) were recruited from Sharjah Fertility Center in UHS, of which two cases showed severe oligozoospermia (11.1%; n=2/18), and one case showed oligozoospermia (5.5%; n=1/18). This part of the study was approved by Postgraduate committee of University of Sharjah (session 9; dated 3/2/2020) and University Hospital of Sharjah (Reference UHS-HERC-072-16092021).

2.2. DNA Extraction

Peripheral blood was collected from the 18 participants according to venipuncture method and transferred in cool packs within couple of hours to Molecular Biology Laboratory in University of Sharjah. Genomic DNA was extracted from blood lymphocytes using the DNeasy Blood & Tissue kit according to manufacturer's instructions. The purity and quantity of the eluted gDNA were estimated using NanoDrop™ One Microvolume UV-Vis spectrophotometer.

2.3. Diagnostic AZF Microdeletion Screening Protocol

Genomic DNA of each sample was screened for AZF microdeletions using 20 set of STS markers (table 1) as provided by the latest adapted method of Y Chromosome Deletion Detection system, version 2.0 kit (MD1531 Promega, USA), according the manufacturer's recommendation and EAA/EMQN (Krausz et al., 2023).

Amplification condition was based on the following program: 94 °C for 2 minutes, then 94°C for 1 minute (denaturation phase), 57°C for 30 seconds (annealing phase), 72°C for 1 minute (35cycles) (extension phase) followed by a final extension 72 °C for 5 minutes for multiplex master mix A, B, C and E, whereas for the multiplex master mix D, the annealing temperature was reduced to 56°C for 30 second. The generated electrophoretic bands were analyzed using Gel Doc EZ Imager and Image-Lab software (BIO-RAD, USA).

Table 1. The 20 set of STS markers used to screen for Y chromosome microdeletions as provided by Promega kit.

No.	region	STS	Locus	Size of Product (bp)
1.	AZFa	SY81	DYS271	209
		SY182	KAL-Y	125
		SY86	DYS148	232
		SY84	DYS273	177
2.	AZFb	SY121	DYS212	190
		SY124	DYS215	109
		SY127	DYS218	274
		SY128	DYS219	228
		SY130	DYS221	173
		SY133	DYS223	177
		SY134	DYS224	303
3.	AZFc	SY157	DYS240	290
		SY208	DAZ	140
		SY242	DAZ	233
		SY254	DAZ	380
		SY255	DAZ	124
4.	AZFd	SY145	DYF51S1	143
		SY152	DYS236	125
5.	SRY	SY14	SRY	400

2.4. Retrospective Cross Sectional Chart Review for AZF deletion

Retrospective cross sectional chart review for the 10-year period of study (2011–2021) was conducted depending on the medical reports of 136 Emirati infertile male patients who were azoospermic and conducted AZF deletion screening between January 2011 and January 2021 in DFC.

3. Results

3.1. Demographics and Characteristics of the Male Patients

The age of the 18 patients ranged from 24 to 52 years old, with an average of 32.2 years old and a median of 32 years, whereas the age of the 136 patients ranged from 24 to 66 years old with average of 38.0 years old and median of 37 years. All of the patients were of Emirati nationals from different geographical cities across the UAE.

3.2. Diagnostic Screening of the AZF-region among Emirati Infertile Male Patients

The frequency of AZF deletion was 2.2% (n=3) among the group of 136 azoospermic male patients of which complete AZFc deletion accounted for all deletions 100% (n=3/3). The deleted sequences and their size on the AZFc subregion were: SY254 (380bp) and SY255 (124 bp). The hormonal profiling and histological finding of the three unrelated azoospermic males with complete AZFc deletion and normal karyotype are given in Table 2. On the other hand, the cohort of 18 samples with normal karyotype had no AZF deletion as the tested Multiplex-PCR results are shown in Figure 1, 2 and 3.

Table 2. The hormonal profiling and histological finding of the three unrelated azoospermic patients with complete AZFc deletion as recorded by DFC.

Patient #	Testosterone (350.0-865.0) ng/dl	(LH) (1.7-8.6) mIU/ml	(FSH) (1.5-12.4) mIU/ml	Histological findings
#1	467.7	4.7	11.57	Varicocele
#2	346.7	6.2	16.47	Sertoli Cell Only syndrome and Varicocele
#3	538.6	10.7	17.22	Sertoli Cell Only syndrome

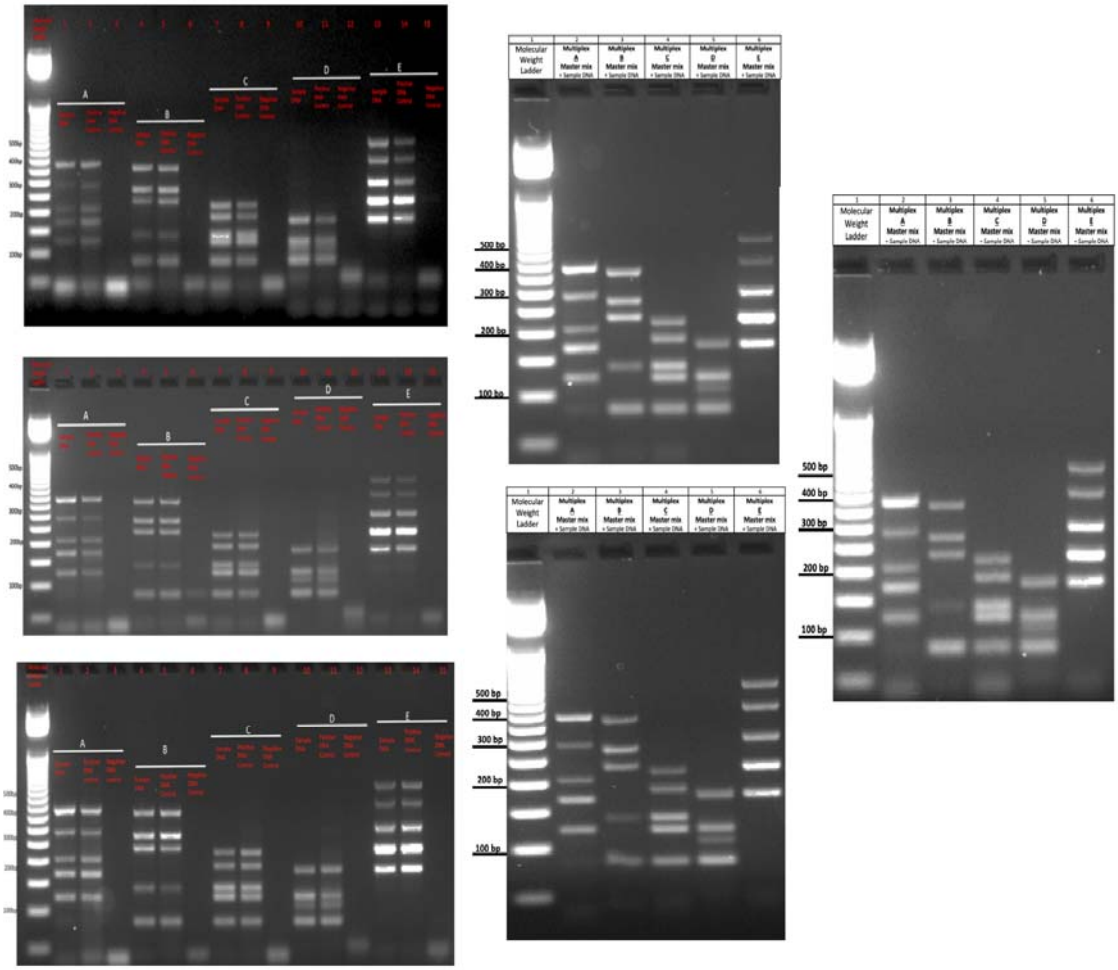

Figure 1. Diagnostic screening for the Y-chromosome showing no deletions in six selected tested patients with azoospermia. Lanes 1, 4, 7, 10 and 13 show the sample DNA with multiplex master mix; Lanes 2, 5, 8, 11 and 14 show the positive control (fertile male genomic DNA provided by Promega kit) with the multiplex master mix; Lanes 3, 6, 9, 12 and 15 shows the negative control (no DNA) with multiplex master mix.

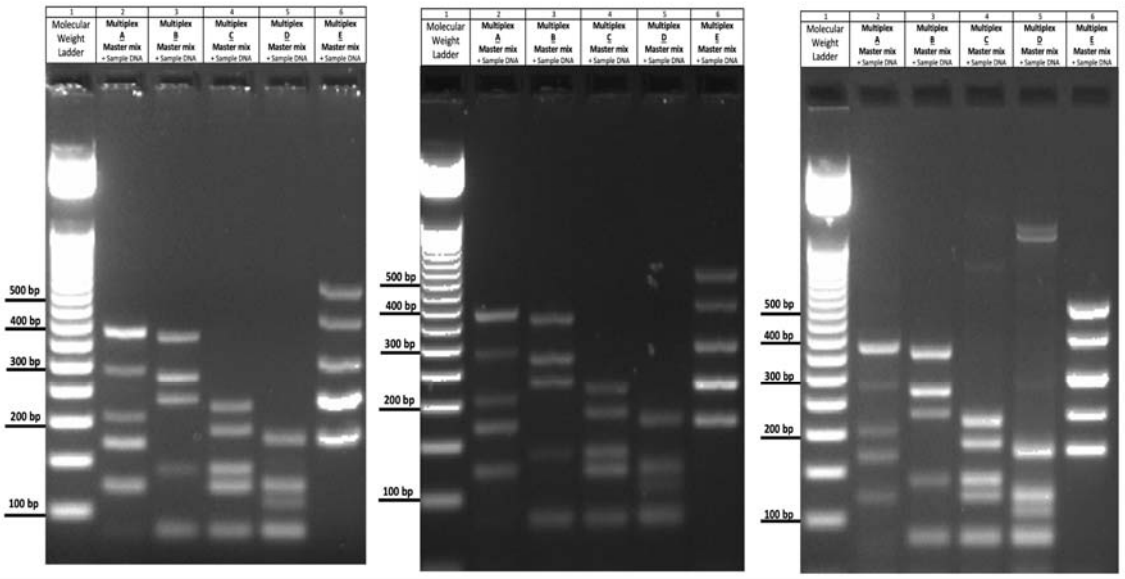

(2.1) (2.2) (2.3)

Figure 2. Diagnostic screening for the Y-chromosome showing no deletions in three selected tested patients with severe OAT (2.1)(2.2) and asthenoteratozoospermia (2.3).

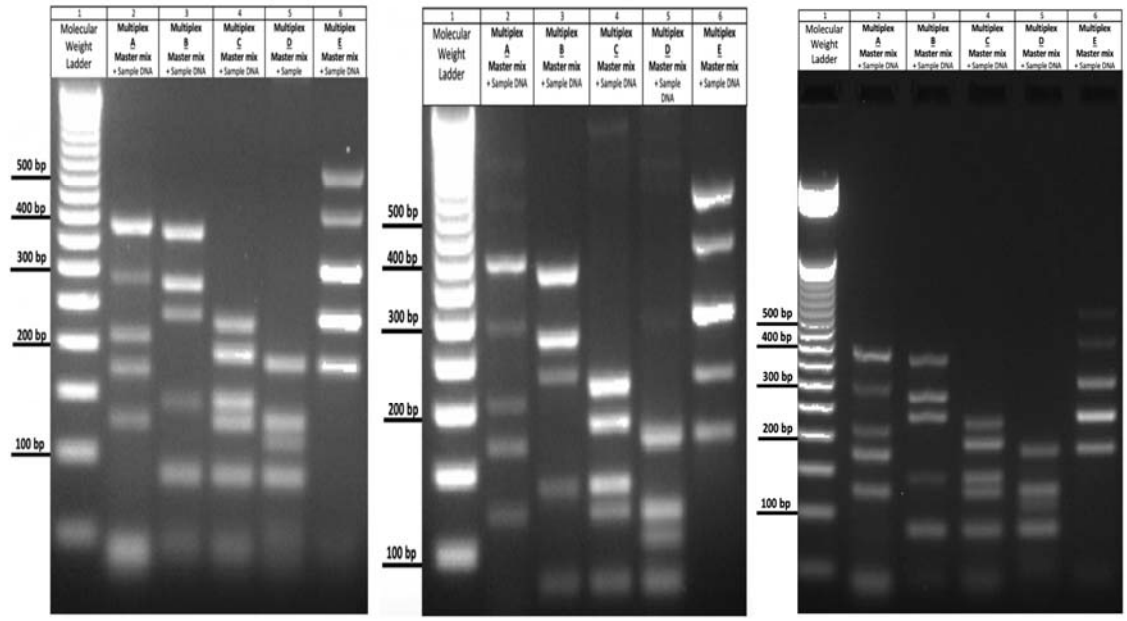

(3.1) (3.2) (3.3)

Figure 3. Diagnostic screening for the Y-chromosome showing no deletions three tested patients with severe oligozoospermia (3.1)(3.2) and oligozoospermia (3.3).

4. Discussion

4.1. Diagnostic Screening of AZF microdeletions among Emirati Infertile Male Patients

The novelty and importance of the article relies on being the first study to determine the profiling of the AZF microdeletions among Emirati Azospermic males which, therefore, underlines its significance not only across Emirates but worldwide on understanding the genomics of male infertility for a better healthcare treatment and management in the fertility clinics and hospitals. Besides, understanding infertility genetics is crucial for tailored treatments and better outcomes in fertility clinics. Our results reveal that the frequency (2.2%) of AZF microdeletions among Emirati azoospermic males is in consistence with several reported studies among Arab and non-Arab populations as it falls within the global range (Table 3). The variation among different studies is explained due to several factors such as influence of Y-haplogroups and genealogical-lineages, geographical

location, selection of inclusion criteria, protocol inconsistency and possible methodological errors. Our results showed that the AZFc microdeletion was the only type of deletion. In fact, AZFc deletion is reported as most frequent type among the AZF deletions as per different reported studies (Lahoz Alonso *et al.,* 2023; Arumugam *et al.* 2021; Akbarzadeh Khiavi *et al.,* 2020; Batiha *et al.,* 2018; Chabchoub *et al.,* 2019). This has been explained due to the genetic makeup of the AZFc region, making it more prone to deletions comparing to the rest of AZF regions (Witherspoon *et al.*, 2021; Xu and Pang, 2022).

Table 3. Comparison of frequency of AZF microdeletions among selected Arabic and global populations.

No	Population block landscape	Population	AZF microdeletions frequency (%)	Reference
1.	Gulf Council Arabs gene pool	United Arab Emirates	2.2%	The present study
		Saudi Arabia	2.27%	(Beg *et al.,* 2019)
		Qatar	1.11%	(Arafa *et al.,* 2018)
		Kuwait	2.6%	(Mohammed *et al.,* 2007)
2.	Fertile crescent Arabs gene pool	Jordan	4.93%	(Batiha *et al.,* 2018)
		Iraq	61.33%	(Al-Qaisi *et al.,* 2020)
		Iraq	47.8%	(Al-Janabi *et al.,* 2020)
		Lebanon	2.5%	(Degheili *et al.,* 2022)
		Syria	28.4%	(Al-Achkar *et al.,* 2013)
3.	North Africa Arabs gene pool	Tunisia	9.5%	(Chabchoub *et al.,* 2019)
		Morocco	9%	(Rochdi *et al.,* 2023)
		Sudan	58.8%	(Elsaid *et al.,* 2021)
		Algeria	1.3%	(Chellat *et al.,* 2013)
4.	Asia gene pool	India	2%	(Arumugam *et al.,* 2021)
		Iranian Azeri Turkish	32.05%	(Akbarzadeh Khiavi *et al.,* 2020)
		Turkey	5.5%	(Yavas *et al.,* 2023)
		Japan	6.79%	(Iijima *et al.,* 2020)
		Korea	14.1%	(Lee *et al.,* 2024)
		Bengal	16.1%	(Dutta *et al.,* 2022)
		China	3.31%	(Chen *et al.,* 2023)
		Mongolia	2.66%	(Damdinsuren *et al.,* 2022
5.	Europe gene pool	United Kingdom	4%	(Johnson *et al.,* 2019)
		Portugal	4.6%	(Pinho *et al.,* 2020)
		Spain	3.88%	(Lahoz Alonso *et al.,* 2023)

4.2. AZF Microdeletions among Emirati Infertile Males in Comparison with the that of the Gulf Cooperation Council (GCC) Arab Populations

Our study represents the most recent investigation on AZF deletion in the GCC region. The present findings have significant importance for the males in the Gulf countries as populations belongs more or less to close tribal genetic lineage. For instance, our results align with the reported data from other GCC populations such as Saudi Arabia, Qatar and Kuwait, which have high possibility in sharing gene pools with Emirati population. The range of the AZF microdeletions among males of GCC populations varies between minimum of 1.11% for Qatar to the maximum of 2.6% for Kuwait (Table 3 ; block 1). Additionally, to our knowledge, the most recent GCC study conducted by Beg *et al.* (2019), reported two cases (2.27%) of AZF microdeletions concerning AZFb+c deletions among a cohort of 88 infertile males in Western Saudi Arabia.

4.3. AZF Microdeletions among Emirati Infertile Males in Comparison with the that of the Fertile Arab Crescent Countries Populations

The range of the AZF microdeletions among males of Fertile Crescent Arab populations varies between minimum of 2.5% for Lebanon to the maximum of 61.33% for Iraq (Table 3; block 2). Batiha *et al.* (2018) presented frequency of 4.93% for the AZF microdeletions among 142 Jordanian azoospermic males, as the most frequent deletion was AZFc deletions (4.2%), followed by the AZFa deletions (2.1%) and then AZFb deletions (1.4%). On the other hand, Al-Janabi *et al.* (2020) reported higher frequency (47.8%) upon screening of 90 Iraqi infertile males in which AZFb microdeletion was most common (33.3%) followed by AZFc microdeletions (23%).

4.4. AZF Microdeletions among Emirati males in Comparison with the that of the African-Arab Populations

The range of the AZF microdeletions among males of African Arab populations varies between minimum of 1.3% for Algeria to the maximum of 58.8% for Sudan

(Table 3; block 3). Chabchoub *et al.* (2019) presented 9.5% of Tunisian infertile males with AZF microdeletions of which AZFc deletion was most common followed by AZFbc deletion and AZFb deletion.

4.5. AZF Microdeletions among Emirati Infertile Males in Comparison with the that of the Asian Populations

The range of the AZF microdeletions among males of Asian populations varies between minimum of 2% for India to the maximum of 32.05% for Iranian Azeri Turkish cohort (Table 3; block 4). Akbarzadeh Khiavi *et al.* (2020) reported frequency of 32.05% for AZF microdeletions among 100 Iranian Azeri Turkish infertile males as AZFc deletion was identified as most common deletion. On the other hand, Arumugam *et al.* (2021) conducted cross sectional study including 100 Indian infertile males, of which two cases (2%) were detected with AZF microdeletions concerning AZFc deletion only.

4.6. AZF Microdeletions among Emirati Infertile Males in Comparison with that of the European Populations

The range of the AZF microdeletions among males of European Populations varies between minimum of 3.88% for Spain to the maximum of 4.6% for Portugal (Table 3; block 5). Lahoz Alonso *et al.* (2023) reported frequency of 3.88% for AZF microdeletions among 644 Spanish infertile men of which AZFc deletion was identified as most common deletion.

5. Conclusions

In conclusion, this study sheds light on the frequency and profile of AZF microdeletions among Emirati infertile males, providing crucial insights into the genetic basis of male infertility in the region. The frequency of AZF microdeletions among Emirati infertile males falls within the regional and the global ranges as identification of only complete AZFc deletions underscores the necessity for comprehensive genetic screening in male infertility diagnostics. Comprehensive understanding of infertility genetics is crucial for improving outcomes of the patients. Therefore, according to the importance of our results in the Emirati healthcare services and clinical practice, we strongly recommend implementing the AZF diagnostic screening for the early prognosis, diagnosis, and treatment of male infertility.

Acknowledgments

The authors would like to acknowledge the funding support from College of Graduate of University of Sharjah along with sincere appreciation to the Faculty of Dubai Fertility Center and University Hospital of Sharjah.

References

Akbarzadeh Khiavi M, Jalili A, Safary A, Gharedaghchi Z, Mirinezhad S K, Mehdizadeh A and Rahmani S A. 2020. Karyotypic abnormalities and molecular analysis of Y chromosome microdeletion in Iranian Azeri Turkish population infertile men. *Sys. Biol. Rep. Med.*, ***66*(2):**140-146.

Al-Achkar W, Wafa A and Moassass F. 2013. Cytogenetic abnormalities and Y-chromosome microdeletions in infertile Syrian males. *Biomed Rep.*, **1(2):**275–279.

Al-Gazali LI, and Hamamy H. 2014. Consanguinity and dysmorphology in Arabs. *Hum. Her.*, **77(1-4):**93-107.

Al-Janabi A M, Rahim AI, Faris S A, Al-Khafaji S M and Jawad D. 2020. Prevalence of Y chromosome microdeletion in azoospermic infertile males of Iraqi population. *J. Gen.*, **99(0):**18.

Al-Qaisi M N, Al-Ouqaili M T and Al-Hadithi D T. 2020. Molecular analysis for azoospermia factor microdeletions in the Y chromosome for azoospermic and severe oligospermic infertile Iraqi patients. *Sys. Rev. Phar.*, **11(8):**562-570.

Arafa M M, Majzoub A, AlSaid S S, ElAnsari W, Al Ansari A, Elbardisi Y and Elbardisi HT. 2018. Chromosomal abnormalities in infertile men with azoospermia and severe oligozoospermia in Qatar and their association with sperm retrieval intracytoplasmic sperm injection outcomes. *Ar. J. Urol.*, **16(1):**132-139.

Arumugam M, Shetty D P, Kadandale J S and Kumari S N. 2021. Y chromosome microdeletion and cytogenetic findings in male infertility: A cross-sectional descriptive study. *Inter. J. Rep. BioMed.*, **19(2):**147–156.

Batiha O, Haifawi S, Al-Smadi M, Burghel G J, Naber Z, Elbetieha A M, Bodoor K, Al Sumadi A, Swaidat S, Jarun Y and Abdelnour A. 2018. Molecular analysis of CAG repeat length of the androgen receptor gene and Y chromosome microdeletions among Jordanian azoospermic infertile males. *Androl.*, ***23*(18):**10594.

Beg M A, Nieschlag E, Abdel-Meguid T A, Alam Q, Abdelsalam A, Haque A, Mosli H A, Bajouh O S, Abuzenadah A M and Al-Qahtani M. 2019. Genetic investigations on causes of male infertility in Western Saudi Arabia. *Androl.*, **51(6):**e13272.

Cejka P and Symington L S. 2021. DNA End Resection: Mechanism and Control. *Ann. Rev. Gen.*, **55:**285-307.

Chabchoub I, Kdous M, Zhioua F, Gaied A and Merdassi G. 2019. Y chromosome microdeletions screening in Tunisian infertile men. *Annal. de Biol. Clin.*, **77(5):**517-523.

Chang H H Y, Pannunzio N R, Adachi N and Lieber M R. 2017. Non-homologous DNA end joining and alternative pathways to double-strand break repair. *Nat. Rev. Mol. Cell Biol.*, **18(8):**495-506.

Chellat D, Rezgoune M L, McElreavey K, Kherouatou N, Benbouhadja S, Douadi H, Cherifa B, Abadi N and Satta D. 2013. First study of microdeletions in the y chromosome of algerian infertile men with idiopathic oligo- or azoospermia. *Urol. Inter.*, **90(4):**455-9.

Chen D, Fan G, Zhu X, Chen Q, Chen X, Gao F, Guo Z, Luo P and Gao Y. 2023. Y chromosome microdeletions in Chinese men with infertility: prevalence, phenotypes, and intracytoplasmic sperm injection outcomes. *Rep. Biol. and Endoc.*, ***21*(1):** 116

Degheili J A, Yacoubian A A, Dargham R H A and Bachir B G. 2022. Prevalence of Y-chromosomal microdeletions and karyotype abnormalities in a cohort of Lebanese infertile men. *Urol. Annal.*, **14(1):**48-52.

Dutta S, Paladhi P, Pal S, Bose G, Ghosh P, Chattopadhyay R, Chakravarty B and Ghosh S. 2021. Prevalence of Y chromosome microdeletion in azoospermia factor subregions among infertile men from West Bengal, India. *Mol. Gen. and Geno. Med.*, **9(10):**e1769.

Ebrahim F and Mahasneh I A. 2022. Chromosomal abnormalities and clinical conditions associated with the male infertility among Emirati: 10-year retrospective research study. *Adv. Biomed. Heal. Sci.*, **1(4):** 228-236.

Elliott K S, Haber M, Daggag H, Busby G B, Sarwar R, Kennet D, Petraglia M, Petherbridge L J, Yavari P, Heard-Bey F U, Shobi B, Ghulam T, Haj D, Al Tikriti A, Mohammad A, Antony S, Alyileili M, Alaydaroos S, Lau E, … Barakat M T. 2022. Fine-Scale Genetic Structure in the United Arab Emirates Reflects Endogamous and Consanguineous Culture, Population History, and Geography. *Mol. Biol. Evol..*, **39(3):**msac039.

Elsaid H O A, Gadkareim T, Abobakr T, Mubarak E, Abdelrhem M A, Abu D, Alhassan E A and Abushama H. 2021. Detection of AZF microdeletions and reproductive hormonal profile analysis of infertile sudanese men pursuing assisted reproductive approaches. *BMC Urol.*, **21(1):**69.

Iijima M, Shigehara K, Igarashi H, Kyono K, Suzuki Y, Tsuji Y, Kobori Y, Kobayashi H and Mizokami A, 2020. Y chromosome microdeletion screening using a new molecular diagnostic method in 1030 Japanese males with infertility. *As. J. Androl.*, ***22*(4):** 368-37

Johnson M, Raheem A, de Luca F, Hallerstrom M, Zainal Y, Poselay S, Mohammadi B, Moubasher A, Johnson T F, Muneer A, Sangster P and Ralph D J. 2019. An analysis of the frequency of Y-chromosome microdeletions and the determination of a threshold sperm concentration for genetic testing in infertile men. *BJU Inter.*, **123(2):**367-372.

Krausz C, Navarro-Costa P, Wilke M and Tüttelmann F. 2023. EAA/EMQN best practice guidelines for molecular diagnosis of Y-chromosomal microdeletions: State of the art 2023. *Androl.*, **2023:**1-18.

Lahoz Alonso R, Sienes Bailo P, César Márquez M Á, Sánchez Torres J C, Albericio Portero J I, Sánchez Parrilla M, Suárez Broto M Á, Rello Varas L and Izquierdo Álvarez S. 2023. AZF gene microdeletions in azoospermic–oligozoospermic males. *Med. Clin..*, **160(4):**151-155.

Lee T H, Song S H, Kim D K, Shim SH, Jeong D and Kim D S. 2024. An analysis of Y-chromosome microdeletion in infertile Korean men with severe oligozoospermia or azoospermia. *Inves. Clin. Urol.*, **65(1):** 77–83.

Mohammed F, Al-Yatama F, Al-Bader M, Tayel S M, Gouda S and Naguib K K. 2007. Primary male infertility in Kuwait: A cytogenetic and molecular study of 289 infertile Kuwaiti patients. *Androl.*, **39(3):**87-92.

Pinho A, Barros A and Fernandes S. 2020. Clinical and molecular characterization of Y microdeletions and X-linked CNV67 implications in male fertility: a 20-year experience. *Androl.*, **8(2):**307-314.

Rabinowitz M J, Huffman P J, Haney N M and Kohn T P. 2021. Y-chromosome microdeletions: A review of prevalence, screening, and clinical considerations. *Appl. Clin. Gen.*, **14:** 51–59.

Rochdi C, Bellajdel I, El Moudane A, El Assri S, Mamri S, Taheri H, Saadi H, Barki, A, Mimouni A and Choukri M. 2023. Hormonal, clinical, and genetic profile of infertile patients with azoospermia in Morocco. *Pan Afr. Med. J.*, ***45*:**119.

WHO. 2021. World Health Organization. WHO laboratory manual for the examination and processing of human semen. 6th ed. World Health Organization, Department of Reproductive Health and Research. Geneva, Switzerland. *WHO Press*.

Witherspoon L, Dergham A and Flannigan R. 2021. Y-microdeletions: A review of the genetic basis for this common cause of male infertility. In *Transl. Androl. and Urol.*, **10(3):**1383-1390.

Xu Y and Pang Q. 2022. Repetitive DNA Sequences in the Human Y Chromosome and Male Infertility. In *Fron. Cell Devel. Biol.*, **10:**831338.

Yavas C, Dogan M, Recep E R Ö Z. and Canat H L. 2023. Evaluation of Y Chromosome Microdeletion and Chromosome Analysis Results in Infertile Male Patients. *Konuralp Med. J.*, ***15*(3):** 383-389.

JJBS

Volume 17, Number 3,September 2024
ISSN 1995-6673
Pages 531 – 540
https://doi.org/10.54319/jjbs/170316

Jordan Journal of Biological Sciences

Production, Characterization and Enhancement of Biopolymer Levan from *Lactobacillus fermentum* SHN1

Hiba A. Jasim[1], Safaa A. A. S. Al-Qaysi[2,*] , Nadhem H. Haydar[1]

[1]*Department of Biotechnology, College of Science, University of Baghdad, Baghdad. Iraq;*[2]*Department of Biology, College of Science (for Women), University of Baghdad, Baghdad. Iraq*

Received: January 12, 2024; Revised: March 22, 2024; Accepted: March 31, 2024

Abstract

Levan is a highly water-soluble biopolymer that has extensive applications in the pharmaceutical, personal care, food, and industrial fields. *Lactobacillus fermentum* SHN1 was isolated from milk and dairy products as an exopolysaccharide (levan) producer and identified according to morphological, biochemical tests and using the *16S rRNA* gene sequencing. The sequence alignment in the gene bank indicated that the isolate has a high percentage of similarity (100%) to the recovered sequence of *Lactobacillus fermentum* isolate. The produced biopolymer was characterized as levan by FTIR, ^{1}H-NMR, and ^{13}C-NMR spectroscopy. The effect of various nutritional and physical factors including pH, carbon source, sucrose concentration, nitrogen source, inoculum size, and incubation period, on the synthesis of levan by *L. fermentum* SHN1 was studied. The findings indicated that the optimal carbon source for the production of levan was 100 g/L sucrose, yielded of 25.95 g/L. Additionally, a combination of peptone + yeast extract at a ratio of 2:0.5 was identified as the most effective nitrogen source for levan production, giving in a yield of 24.21 g/L. *L. fermentum* SHN1 produces the greatest quantity of levan, 23.89 g/L, under a pH of 6.5 and an inoculum size of 1%, resulting in a yield of 25 g/L. The most favorable period for incubation was 48 hours, resulting in a production yield of 24.87 g/L.

Keywords: Biopolymer, Exopolysaccharides, *Lactobacillus fermentum*, Levan

1. Introduction

Levan is known as β -2, 6-linked fructose homopolymer; it has existed in many plants and microbial products. Levan generated by bacteria is considerably larger than that of plants, with numerous branches and molecular weights ranging from 2 to 100 million Daltons (Keith *et al*., 1991; Arvidson *et al*., 2006). Levan is a unique microbial exo-polysaccharide that has numerous industrial applications (Panteli´c *et al*., 2020; Lonˇcarevi´c *et al*., 2019). It is a water-soluble biopolymer consisting of fructose monomeric units that repeat, with a terminal group consisting of D-glucosyl residue. Levan possesses a number of advantageous qualities, including flexibility, biodegradability, biocompatibility, antibacterial activity, antioxidant activity, stimulation the immune system and the anti-inflammatory effects (Srikanth *et al*., 2015a; Costa e*t al*., 2021).

Levan is produced by the extracellular enzyme levansucrase (EC 2.4.1.10) in response to the presence of sucrose as a carbon source (substrate). This enzyme degrades sucrose, constructing levan polymer from the fructose residues (Poli *et al*., 2009). The unique levan polymer is distinguished by its viscosity, capacity to dissolve in water, resistance to acid, alkali and heat, as well as its biological properties and capacity for film formation (Bekers *et al*., 2005). Numerous bacterial species possess the capacity to produce levan, such as *Zymomonas, Azotobacter, Mycobacterium, Erwinia, Corynebacterium, Pseudomonas*, *Bacillus, Brachybacterium phenoliresistens, Bacillus subtilis Lactobacillus, Bacillus amyloliquefaciens and* others (Poli *et al*., 2009; Teixeira *et al*., 2010; Al-Halbosiy *et al*., 2018; Ngampuak *et al*., 2023; Al- Mousawi and Abd- Aljabar, 2018; Sánchez-León et *al*., 2023). In recent decades, wide ranges of microbial extracellular polymers (EPSs) have been identified and thoroughly studied, including their composition, structure, manufacturing, and functional capacities. The heightened fascination with microbial-produced polysaccharides stems from the increasing need for natural polymers in various fields such as food, medicine, and industry in recent times (Costerton *et al*., 1987; Mohammed *et al*., 2021).

Compared to levan produced from plants, microbial levan offers a wider range of applications. It is utilized in food, medicine, aquaculture, and personal care applications (Owner *et al*., 2016).

The objective of this study was the isolation and characterization of a newly bacterial isolate from natural milk and dairy products. The selected *L. fermentum* SHN1 was tested for the production of levan at the production medium, the effect of optimal conditions, carbon sources, nitrogen sources, initial pH, sucrose concentration, inoculum size and incubation time. FTIR, ^{1}H-NMR and ^{13}C-NMR analyses were conducted for levan identification and characterization.

* Corresponding author. e-mail: Safaaa_bio@csw.uobaghdad.edu.iq.

2. Material and methods

2.1. Isolation of the bacterial isolates

A total of 115 samples from different natural milk and dairy products were collected from local markets in Baghdad province, Iraq. A small amount of each sample was suspended in 10 ml of sterile distilled water. One milliliter from the homogenized suspension was added to 9 ml of sterilized De Man Rogosa-Sharp-broth (MRS broth) (HIMEDIA, INDIA) and incubated anaerobically (via candle jar) for 24hr at 37°C. After incubation, the suspension was serially diluted in a sterile normal saline (NaCl) 0.85% from 10^{-1} to 10^{-5} and streaked on MRS agar plates in duplicates. The plates were incubated anaerobically for 48hr at 37°C. The process was carried out several times to obtain single colonies. Then, the purified colonies were sub-cultured on MRS slants and stored at 4°C as stock cultures. The pure isolates were initially tested for their Gram staining, cell morphology, oxidase and catalase reaction (Ahmed, 2013; Al-Maliki, 2020; Mohsin *et al*., 2020).

2.2. Detection of levan production

2.3. Primary screening of levan production on solid media

The isolated bacterial colonies were transferred to a modified levan screening solid medium composed of g/L: 5.5 K_2HPO_4, 0.2 $MgSO_4.7H_2O$, 100 Sucrose, 2 Peptone, 0.5 yeast extract, and 15 agar-agar (Abou-Taleb *et al*., 2015).

The cultured plates were kept anaerobically at 37°C for 48 hr and the isolates with a slimy mucoid appearance were identified as levan producer (Nasir *et al*., 2015).

2.4. Secondary screening of levan production in liquid media

The selected bacterial colonies recorded as levan producer were grown on levan screening broth as previously mentioned (without using agar agar) and incubated anaerobically at 37°C in a shaker incubator for 48 hr. For levan recovery, the broth was centrifuged at 10000 rpm for 10 minutes, and twice the volume of chilled absolute ethanol was added to the supernatant. The mixture was cooled at 4°C for 48 hr., and the precipitated levan polymer was collected using a cooling centrifuge at 8000 rpm for 10 min. The pellet was collected and dried at 50°C for 2-3 days to estimate levan dry weight (Semjonovs *et al*., 2016).

2.5. Molecular identification (genotypic identification)

The most productive isolate was identified by 16s rRNA gene sequencing. Genomic DNA was extracted from the bacterial growth according to the protocol of ABIO. The 16s rRNA from the genome was amplified by the use of the universal bacterial primer (27F: 5-GAGAGTTTGATCCTGGCTAG-3 and 1492R: 5-CTACGGCTACCTTGTTACGA-3. PCR products were sent to Macrogen Corporation in Korea for Sanger sequencing utilizing an automated DNA sequencer (ABI3730XL). The resulting sequences were compared using Basic Local Alignment Search Tool (BLAST) network services at the gene bank databases of the National Center for Biotechnology Information (NCBI) and the accession number was obtained. The Phylogenetic tree was constructed through the alignment of nucleotide sequences using the neighbor-joining algorithm in MEGA 11 software.

2.6. Determination the optimum conditions for levan production

For levan production, various parameters were studied to standardize the fermentation conditions. In each experiment, levan dry weight was determined.

2.6.1. Effect of pH

In order to evaluate the impact of pH values on levan production, the pH of the media was adjusted to various levels (4, 5, 6, 6.5, 7, and 8).

2.6.2. Effect of Carbon source

This experiment was carried out by using different carbon sources which include: Sucrose, fructose, maltose, lactose, glucose and mannose used as alternatives.

2.6.3. Effect of sucrose concentration

To determine the effect of sucrose concentration on levan production, the experiment achieved using six different concentrations of sucrose were used (25, 50, 75, 100, 125, 150) g/L.

2.6.4. Effect of Nitrogen source

The experiment was conducted through the use of six organic and inorganic sources of nitrogen (peptone, yeast extract, KNO_3, NH_4Cl and (peptone + yeast extract together) to investigate their impact on levan production.

2.6.5. Effect of inoculum size

Production of levan by the selected isolate was determined by inoculating the culture medium with 7 different inoculum size (0.5, 1, 2, 4, 8, 10, 15, 20) % of inoculum ($1.5x10^8$ CFU/ml, OD600 = 0.5).

2.6.6. Effect of incubation time

The incubation period required for levan production was evaluated. The selected isolate was incubated anaerobically at 37°C for 12, 24, 36, 48, 60, 72 and 96 hr. separately. Post fermentation, the culture was centrifuged (10000 rpm for 20 min), and the pellets were washed twice with distilled water then dried at 40 °C to determine the biomass (cell dry weight).

2.7. Production and purification of levan

Levan production was carried out by culturing the selected isolate in 250 ml Erlenmeyer flasks containing fifty milliliter of the media used for levan production (5.5 K_2HPO_4, 0.2 $MgSO_4.7H_2O$, 100 Sucrose, 2 Peptone, 0.5 yeast extract) gram per liter which autoclaved and then inoculated with 1% ($1.5x10^8$ CFU/ml, OD_{600} = 0.5 on McFarland) of the bacterial inoculum. The flasks were incubated at 37°C for 48hr in a shaker incubator at 120 rpm with N_2 gas flashing to obtain anaerobic conditions.

The culture was centrifuged at 10000 rpm for 10 min to remove the bacterial cells. The supernatant containing levan was collected and mixed with twice the volume of absolute iced ethanol, then cooled at 4°C for 48 hrs. The precipitated levan polymer was collected using a cooling centrifuge at 8000 rpm and dried at 50°C for 2-3 days. After that, dialysis technique was used for the partial purification process. The collected levan pellet was dissolved in a minimum amount of demineralized water,

then dialyzed using a membrane with a cutoff of 10 Kilo Dalton (KD) against deionized water (dH_2O) for a duration of 3 days, with daily water replacement. After that, levan was collected by precipitation using double volume of chilled absolute ethanol. The precipitated polymer was dried in an oven at 50°C for2-3 days to determine the levan dry weight for further analysis (Zhang *et al*., 2014)

2.8. Characterization of levan

2.8.1. Fourier Transform-Infrared spectroscopy (FTIR):

The functional groups present in the partially purified levan polymer were analyzed using Shimadzue FTIR spectrophotometer (Shimadzu- Japan) using KBr pellets. The spectrum was recorded at a wave range of (4000 to 400) cm^{-1}. Furthermore, the FTIR spectra of the standard levan from *Erwinia herbicola* sigma- Aldrich were applied to compare the spectra of the current study with standard levan.

2.8.2. Nuclear Magnetic Resonance (NMR)

The spectra of ^{1}H and ^{13}C NMR were measured and recorded using UXNMR, a Bruker instrument. Levan was solubilized in dimethyl sulfoxide (DMSO) for both analyses. The ^{1}H NMR spectrum was conducted at a frequency of 400 MHz, whereas the ^{13}C NMR spectrum was conducted at a frequency of 100 MHz. The chemical changes were determined and reported in parts per million (ppm). Also, ^{1}H and ^{13}C NMR spectra of the standard levan from *E. herbicola* sigma- Aldrich were detected for comparison.

2.9. Statistical analysis

The effect of different parameters on levan production were tested statistically using *T-test*, one-way ANOVA and Tukey's test to assess the data's significance at $p < 0.05$. The average mean values were reported along with standard deviation. The softwares used for the analysis are (R Studio and the figures by Origin software).

3. Results and discussion

3.1. Isolation of Lactobacillus Isolates:

A total number of 27 isolates (23%) have been collected from various sources of dairy products (yogurt, cheese, butter, labneh, milk, cream, and whey) from local markets were belong to the genus *Lactobacillus*. All of these isolates were gram-positive, cocci, organized singly, pairs or short chains, non-motile, oxidase and catalase negative (Jameel and Haider, 2021; Jeyagowri *et al*., 2023). These isolates were identified using morphological, microscopical, and biochemical tests. Their morphological characteristics showed that they belong to the genus *Lactobacillus* by their small (2-5mm), creamy, smooth round, little sticks colonies and opaque without pigment on MRS agar as shown in Figure (1) (Taye *et al*., 2021; Hussein and Luti, 2023).

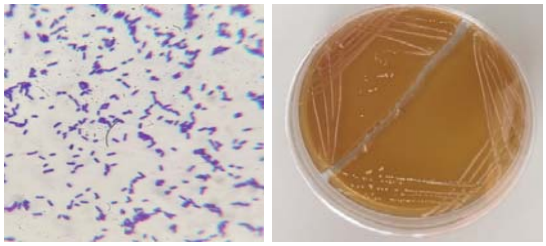

A B

Figure 1: Cells and colony morphology of *Lactobacillus spp*. A- Bacterial cells under a microscope using oil emersion lens (100×) B- Colonies growing on MRS agar.

3.2. Primary screening on solid media

Levan production had been determined in all 27 isolates of *Lactobacillus* spp. The identification and evaluation of levan production were documented based on the observation of mucoid and viscous colonies on the surface of the levan screening medium. The data presented in Table (1) indicated that 15 isolates only had a viscous mucoid appearance which were subsequently employed in a secondary screening process.

The screening for levan was conducted using sucrose-rich media as a substrate which induces the enzymatic activity of levansucrase enzyme (also known as fructosyltransferase) (Nasir *et al*., 2015). Its main function is to facilitate the development of ß-(2,6)-levan by breaking down sucrose into its constituent fructose and glucose units. Furthermore, it participates in the synthesis of fructooligosaccharides (FOS) (Vieira *et al*., 2021). Moreover, the morphological findings indicated a viscous and mucoid appearance, consistent with (Nasir *et al*., 2015; Alshammery and Alaubydi, 2020; Hamada *et al*., 2022). The identification of EPS in lactic acid bacteria is accomplished through the observation of the slimy and mucoid characteristics of the colonies on a solid medium (Tsveteslava and Ivanov, 2016; Chun-lei *et al*., 2014). In their study, Ahmed *et al*. (2022) successfully isolated a strain capable of making levan, which was identified as *Lactobacillus reutri*. They noticed that when sucrose was present, the colonies exhibited a slimy mucoid look, indicating the formation of extracellular polymeric substances (EPS) from sucrose. Also, Mamay *et al*. (2015) observed that the presence of levan was identified based on the slimy appearance of the colonies on solid media.

Table 1: Primary screening for levan synthesis by *Lactobacillus* spp. isolates on solid medium

No.	Bacterial isolates	mucoid growth	No. of isolates
1	Lactobacillus spp.	+++	LA3
2	Lactobacillus spp.	+	LA6
3	Lactobacillus spp.	-	LA8
4	Lactobacillus spp.	-	LA12
5	Lactobacillus spp.	-	LA13
6	Lactobacillus spp.	-	LA14
7	Lactobacillus spp.	-	LA15
8	Lactobacillus spp.	-	LA17
9	Lactobacillus spp.	++	LA19
10	Lactobacillus spp.	+	LA20
11	Lactobacillus spp.	+	LA21
12	Lactobacillus spp.	-	LA22
13	Lactobacillus spp.	-	LA26
14	Lactobacillus spp.	-	LA27
15	Lactobacillus spp.	-	LA29
16	Lactobacillus spp.	+++	LA30
17	Lactobacillus spp.	+++	LA31
18	Lactobacillus spp.	-	LA32
19	Lactobacillus spp.	+	LA33
20	Lactobacillus spp.	+	LA34
21	Lactobacillus spp.	++	LA35
22	Lactobacillus spp.	-	LA36
23	Lactobacillus spp.	+	LA37
24	Lactobacillus spp.	++	LA38
25	Lactobacillus spp.	+++	LA39
26	Lactobacillus spp.	+	|LA40
27	Lactobacillus spp.	++	LA41

+++: high levan production, ++: moderate levan production, +: weak levan production, - : no levan production

3.3. Secondary screening on liquid media

Based on the results of primary screening, levan concentration was estimated. The results presented in Table 2 showed that the isolate *Lactobacillus* spp. (LA31) had the highest productivity of levan, with an average concentration of approximately 23 g/L (dry weight). The remaining isolates had concentrations ranging from 8.85 g/L to 17.6 g/L. Therefore, the isolate (LA31) was selected for the remaining experiments in the current study.

Table 2: Secondary screening for levan production by *Lactobacillus spp*. isolates in liquid medium

Bacterial isolates	Levan dry weight Average g/L
Lactobacillus spp. (LA3)	8.85
Lactobacillus spp. (LA30)	11.5
Lactobacillus spp. (LA31)	23
Lactobacillus spp. (LA35)	17.6
Lactobacillus spp. (LA38)	10.4
Lactobacillus spp. (LA39)	13.25

3.4. Molecular identification of Lactobacillus spp. (LA31) by 16s rRNA:

According to the findings of *16S rRNA* gene sequence analysis, the isolate LA31was identified as *L. fermentum* SHN1 (new scientific name, *Limosilactobacillus fermentum*). The nucleotide sequence was submitted and deposited at GenBank under the accession number OQ588768. The neighbor-joining method was employed to conduct a phylogenetic study of *L. fermentum* SHN1 (accession number OQ588768). The results revealed a substantial level of similarity and close clustering with other *L. fermentum* strains retrieved from the NCBI GenBank database (Figure 2).

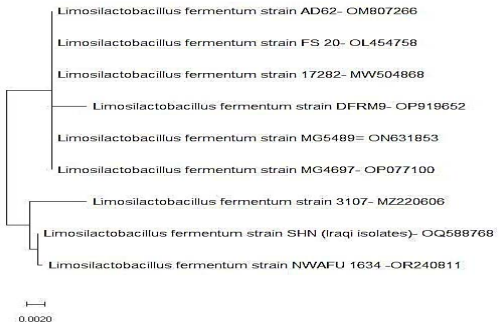

Figure 2: Phylogenetic tree represents the relationship between the sequence of the 16S rRNA gene of *L. fermentum* SHN1 and the related isolates. The phylogenetic tree was created with MEGA11 using neighbor-joining method.

3.5. Determination of the optimal conditions for levan production

3.5.1. The effect of pH on levan production

The experiment involved testing several pH values (4, 5, 6, 6.5, 7, and 8) to determine the optimal pH for levan synthesis. The production of Levan by *L. fermentum* SHN1 demonstrated a gradual and consistent rise with an increase in pH values from 6 to 6.5 (Figure 3). *L. fermentum* SHN1 exhibited its maximum levan production of 23.89 g/L at a pH of 6.5. Belghith *et al*. (2012) deduced that the enzyme levansucrase exhibited its optimal activity at a pH of 6.5; this finding could potentially account for the observed increase in levan production. Abou-taleb *et al*. (2015) also found that the maximum quantity of levan produced by *Bacillus lentus* V8 strain on a sucrose supplemented medium occurred at a pH of 6.5. The findings obtained from our work are in consistence with those of Khassaf *et al*. (2019) who reported that the optimum pH for levan production by *Bacillus subtilis* was 6.5.

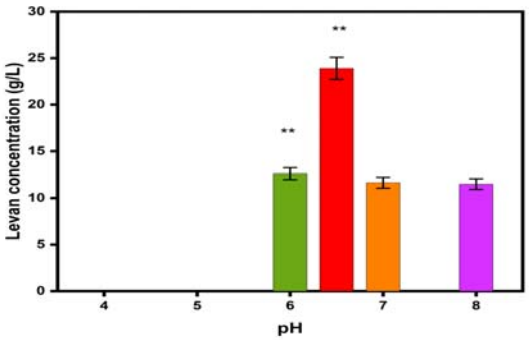

Figure 3: The effect of initial pH values on levan production by *L. fermentum* SHN1 isolate. The experiment was repeated as triplicate and the values are represented as mean ± SD at (*$P \leq 0.05$), (**$P \leq 0.01$) and (***$P \leq 0.001$).

The effect of carbon sources on levan production

To find out the optimal carbon source for levan yield enhancement, five different carbon sources (fructose, maltose, lactose, mannose, glucose, and sucrose) were employed. Based on the results, sucrose was shown to be the most effective carbon source for levan production by *L. fermentum* SHN1 resulting in a yield of 24.4 g/L. In comparison, mannose, fructose, maltose, glucose, and lactose yielded (2.1, 3.9, 5.1, 9, 11) g/L, respectively (Figure 4). Using fructose as the exclusive carbon source leads to a reduction in levan synthesis. According to reports, the production of levan declined when fructose was utilized instead of sucrose in the productive medium. These findings suggest that sucrose is the most effective stimulant and material for the enzyme levansucrase (Van Hijum *et al*., 2006; Al-qaysi *et al*., 2016; Moussa *et al*., 2017). Other bacterial species that demonstrate similar results regarding sucrose as the most favorable carbon source include, *B. licheniformis* (Dahech *et al*., 2012), *B. lentus* (Abou-Taleb *et al*., 2014) and *Z. mobilis* (Senthilkumar and Gunasekaran, 2005).

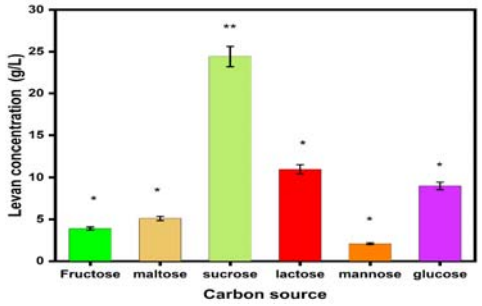

Figure 4: The effect of different types of carbon sources on levan production by *L. fermentum* SHN1 isolate. The experiment was repeated as triplicate and the values are represented as mean ± SD at (*$P \leq 0.05$), (**$P \leq 0.01$) and (***$P \leq 0.001$).

The effect of sucrose concentration

The amount of levan produced by *L. fermentum* SHN1 was affected by using different concentrations of sucrose. The findings indicated that the maximum concentration of levan (25.95 g/L) was identified at 100 g/L. Further increase in sucrose concentration led to an extreme decrease in the yield of the produced levan (Figure 5). It has been determined that the concentration of sucrose is the most significant factor influencing levan molecular weight (Wu *et al*., 2013). *Leuconostoc mesensteroides* produced a similar result, with the maximum levan yield at 10% sucrose content (Khudair *et al*., 2018). Also, Chidambaram *et al*. (2019) reported that levan production by *B. subtilis* was optimized at a sucrose concentration of 100 g/ L. On the other hand, Aramsangtienchai *et al*. (2020) reported that levan production by *Tanticharoenia sakaeratensis* increased steadily from 2.1 g/ L to 24.7 g g/ L as the sucrose concentration increased from 50 g/ L to 200 g g/ L.

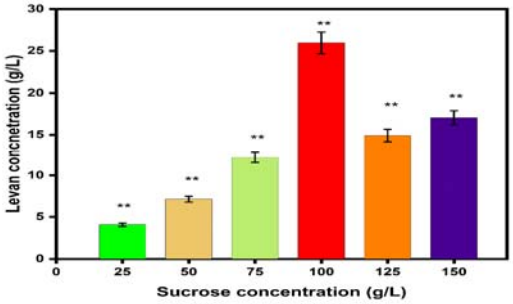

Figure 5: The effect of different concentrations of sucrose on levan production by *L. fermentum* SHN1 isolate. The experiment was repeated as triplicate and the values are represented as mean ± SD at (*$P \leq 0.05$), (**$P \leq 0.01$) and (***$P \leq 0.001$).

The effect of nitrogen sources on levan production

A total of six nitrogen sources, namely peptone, yeast extract, casein, KNO3, NH4Cl, and a combination of peptone and yeast extract, were used in order to determine the optimal nitrogen source for levan synthesis. As illustrated in Figure (6), a combination of peptone + yeast extract at a ratio (2:0.5) was the optimal nitrogen source for levan synthesis, resulting in a yield of 24.21g/L. The data presented in Figure 6 clearly demonstrate that the nitrogen sources have a significant impact on the synthesis of levan by *L. fermentum* SHN1 strain. The highest levan dry weight was achieved when (peptone+ yeast extract) was used as a nitrogen source, while the lowest levan dry weight (6.1 g/L) was obtained when yeast extract was used alone. Lactic acid bacteria (LAB) are highly specialized microbes that grow on complicated organic substances. These bacteria need carbohydrates, nucleotides, amino acids, peptides, vitamins and minerals for their growth because of the absence of specific metabolic pathways.

For example, in the absence of exogenous amino acids, LAB cannot grow at the expense of mineral nitrogen (Morishita *et al*., 1981). To meet their nutritional requirements in complex growth media, expensive and undefined compounds such as peptone, meat extract, and yeast extract are typically added (De Man *et al*., 1960). In line with our discoveries, de Oliveira *et al*. (2007) confirmed that yeast extract played a crucial role in the formation of levan. The combination of yeast extract with KH_2PO_4 and yeast extract with $MgSO_4$ was found to have a substantial impact on levan production. Additionally, Silbir *et al*. (2014) discovered that yeast extract produced the greatest amount of levan in comparison to other nitrogen sources. The greatest EPS production by two strains of *Lactobacillus plantarum* isolated from cow milk was obtained when yeast extract used as a N_2 source. This effect is explained by the composition of yeast extract which includes amino acids, peptides, carbohydrates, and salts (Imran *et al*., 2016).

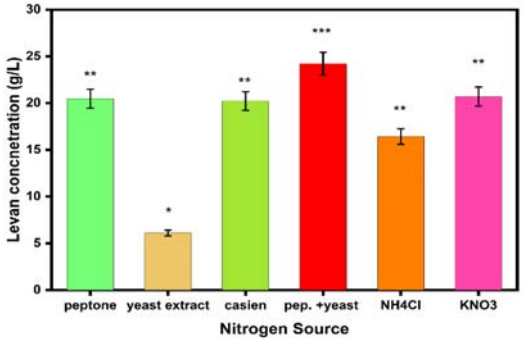

Figure 6: The effect of different types of nitrogen sources on levan production by *L. fermentum* SHN1 isolate. The experiment was repeated as triplicate and the values are represented as mean ± SD at (*$P \leq 0.05$), (**$P \leq 0.01$) and (***$P \leq 0.001$).

The effect of inoculum size

The impact of various inoculum volumes on the production of levan was examined and illustrated in Figure (7). *L. fermentum* SHN1 was incubated with various inoculum sizes (0.5, 1, 2, 4, 8, 10, 15, 20) % of inoculum (1.5x10 ^{8} CFU/ml, OD600 = 0.5). The findings indicated that an inoculum volume of 1% was the optimal for levan production, resulting in a yield of 25 g/L. On the other hand, using of 2% inoculum size resulted in a reduced levan dry weight to 17.52 g/L.

The reduction in the production of levan could be associated with the elevation in cell growth in the production media, which resulted in the consumption of nutrients in a short period of time that leading to a quick consumption of carbohydrates and decreased levan production. The findings were consistent with those of Khassaf *et al*. (2019) who reported that the greatest quantity of levan was generated when an inoculum volume of 1% was employed. In addition, Küçükaşik *et al*. (2011) employed a 1% inoculum size to achieve the maximum levan synthesis from molasses by *Halomonas* spp. However, the current study differs from what some other researchers found when using of 5% inoculum size for levan production (Dahech *et al*. 2014). This could be attributed to variations in the growth rate among various isolates. Additionally, the isolate employed in this study is regionally isolated, which means that its development and production may differ from that of strains and isolates that are universal.

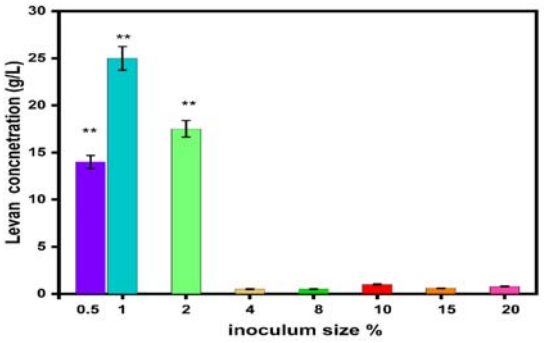

Figure 7: The effect of inoculum size on levan production by *L. fermentum* SHN1 isolate. The experiment was repeated as triplicate and the values are represented as mean ± SD at (*$P \leq 0.05$), (**$P \leq 0.01$) and (***$P \leq 0.001$).

3.5.2. The effect of the incubation period

Production of levan was estimated at various incubation periods (12, 24, 36, 48, 60, 72 and 96 hr.). The maximum levan level produced by *L. fermentum* SHN1 was 24.87 g/L and biomass of 8.25 g/L was achieved after 48hr of incubation (Figure 8).

The findings align with previous studies that have reported the highest yield of levan synthesis by *L. reuteri* FW2 was after incubation for 48 hours (Ahmed *et al.*, 2022). Based on another investigation, *Z. mobilis* achieved the maximum levan production after 42 hours of incubation (Silbir *et al.*, 2014). Sims *et al*. (2011) conducted a separate investigation and found that the highest amount of levan produced by the gut bacteria *L. reuteri* 100–23 was achieved after a period of 96 hr. of incubation. Under optimal conditions, the probiotic *Bacillus tequilensis*-GM produces 2.8 g/L of levan following 72 hr. of incubation (Abid *et al.*, 2019).

The isolate *L. fermentum* SHN1, isolated in this work, exhibits a significant capacity to produce abundant quantities of levan in a shorter incubation period compared to prior research. Consequently, it holds great potential for commercial applications.

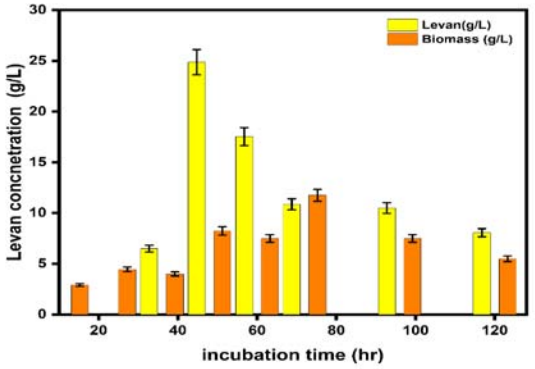

Figure 8: The effect of different incubation periods on levan production by *L. fermentum* SHN1 isolate. The experiment was repeated as triplicate and the values are represented as mean ± SD at (*$P < 0.05$), (**$P < 0.001$) and (***$P < 0.0001$).

3.6. Characterization of levan

3.6.1. Fourier Transform-Infrared spectroscopy (FTIR):

The Fourier Transform Infrared (FTIR) spectrum of *L. fermentum* SHN1 levan exhibited multiple distinct peaks that are indicative of its unique properties (Figure 9). The distinctive peak corresponding to the stretching of the O-H bond of polysaccharide was observed at about 3406.05 cm^{-1}. A medium C-H stretching vibration has been detected at 2935.46 cm^{-1}and C=O stretching was detected at 1650.95 cm^{-1}(Salman *et al.*, 2019). The peaks between 1126 and 900 cm^{-1} correspond to the characteristic features of polysaccharides (Kadhum and Haydar, 2020; Sánchez-León et *al*., 2023).

The observed three peaks at 1128.28 cm^{-1}, 1060.78 cm^{-1}, and 1014.49 cm^{-1} correspond to the ring vibration of C-OH groups and the glycosidic linkage C-O-C stretching vibration (Srikanth *et al.*, 2015b). The stretching vibration of the presence of C-H and the band at 1650.95 cm^{-1} were attributed to the bounding of water (Xu *et al.*, 2016). In addition, the presence of the furanoid ring and the bending vibration of D-type C-H in furanose were indicated by

peaks in the range of 927-810 cm-1, which are characteristic of carbohydrates (Ahuja *et al.*, 2013). As summarized in Table 3, the data revealed that the polymer synthesized by *L. fermentum* SHN1 was levan.

The FTIR spectrum obtained in this work from *L. fermentum* SHN1 is in agreement with the FTIR spectra of levan produced by *Pantoea agglomerans* ZMR7 (Al-Qaysi *et al.*, 2021), *Brachybacterium phenoliresistens* (Moussa *et al.*, 2017), and is similar to the standard levan from *E. herbicola* (Figure10).

Table 3. The comparison of FTIR values of levan produced by *L. fermentum SHN1* with other bacteria

Chemical groups	*E. herbicola* Standard levan (cm^{-1})	*B. phenoliresistens* Levan (cm^{-1})	*P. agglomerans* Levan (cm^{-1})	*L. fermentum* SHN1 Levan (cm^{-1}) this study
O-H	3429.20	3394.1	3417.68	3406.05
C-H	2927.74	2932.23	2935.66	2935.46
C=O	1637.45	1647.88	1639.49	1650.95
References		(Moussa et al., 2017)	(Al-Qaysi et al., 2021)	

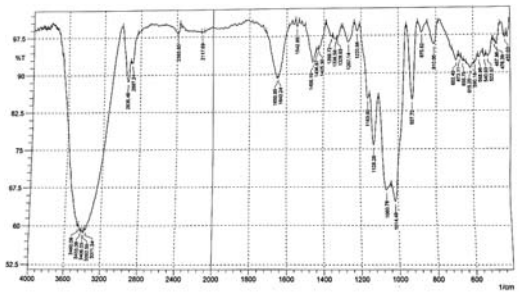

Figure 9: FT-IR spectrum of the levan obtained from *L. fermentum* SHN1 isolate.

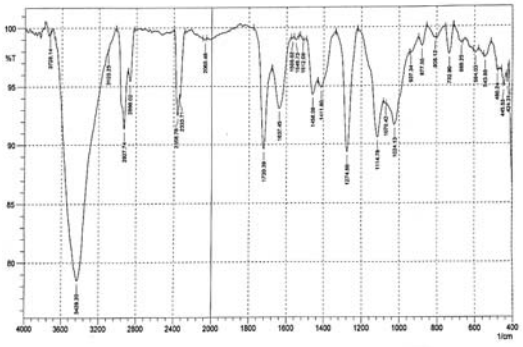

Figure 10: FT-IR spectrum of the Standard levan obtained from *E. herbicola.*

3.6.2. Nuclear Magnetic Resonance (NMR)

The ^{1}H-NMR spectra of levan exopolysaccharide produced by *L. fermentum* SHN1 displayed distinct signals that are indicative of levan. The proton signals were detected within the chemical shift range of 3.27 to 5.16 ppm (Figure11). The spectrum revealed that the isolated molecule exhibits proton signals that cannot be interchanged and correlated to the resonance of the standard levan from *E. herbicola* (Figure12). In addition, the composition of the produced levan by *L. fermentum* SHN1 was verified by using ^{13}C-NMR spectroscopy analysis as shown in Table 4. The ^{13}C NMR spectra exhibited six prominent resonances at 61.04, 104.68, 76.39, 75.75, 80.65, and 63.37, which were designated, in that order, for the C1 through C6 atoms comprising the structure of levan (Figure 13). Significantly, the ^{13}C NMR spectrum of EPS S81 displayed a signal at 63.2 ppm (C-6) that was displaced towards the lower end of the spectrum. This signal verified the existence of a β-(2 → 6) linkage, thereby establishing the structure as levan rather than inulin (Xu *et al.*, 2016; Taylan *et al.*, 2019). The signal alterations observed were consistent with those of other levans generated by different bacteria, including *Bacillus subtilis* MTCC441 (Veerapandian *et al.*, 2023), *P. agglomerans* ZMR7 levan (Al-Qaysi *et al.*, 2021), *B. phenoliresistens* (Moussa *et al.*, 2017) and *E.herbicola* (Figure 14).

Table 4: Comparison of ^{13}C NMR values of *L. fermentum* SHN1, and other bacteria

Carbon atom	Standard levan from *E. herbicola*	*B. phenoliresistens levan*	*P. agglomerans* levan	*L. fermentum* SHN1 *levan* this study
C-1	60.98	59.073	60.58	61.04
C-2	104.68	103.834	104.38	104.68
C-3	75.69	7.0217	75.83	76.39
C-4	76.30	74.183	76.74	75.75
C-5	80.62	82.253	80.35	80.65
C-6	63.37	62.007	63.15	63.37
Reference		(Moussa *et al.*, 2017)	(Al-Qaysi *et al.*, 2021)	

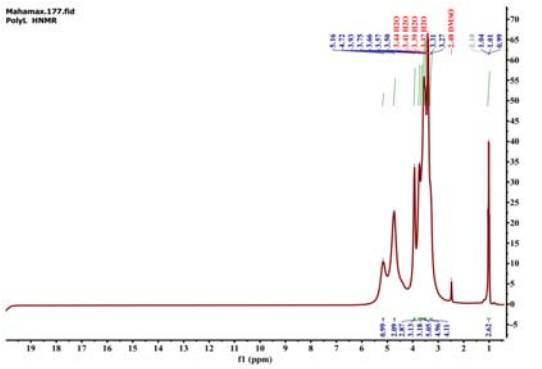

Figure 11: ^{1}HNMR spectrum for levan obtained from *L. fermentum* SHN1 isolate.

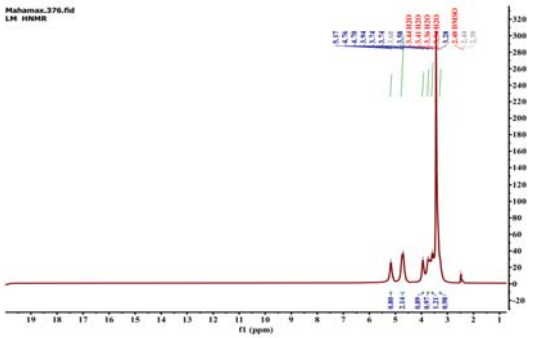

Figure 12: [1]HNMR spectrum for standard levan obtained from *Erwinia herbicola.*

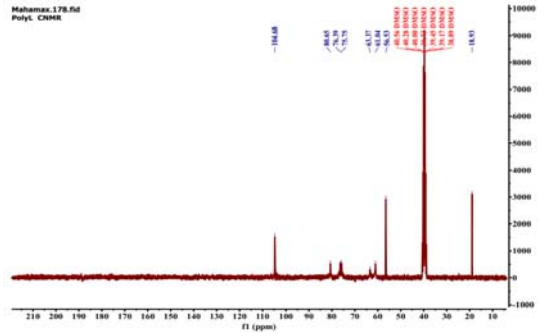

Figure 13:[13]C NMR spectrum for levan obtained from *L. fermentum* SHN1 isolate.

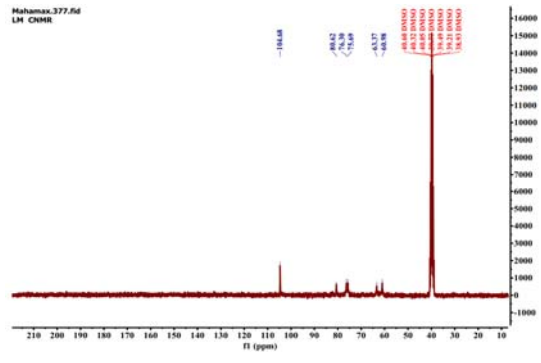

Figure 14: [13]C NMR spectrum for standard levan obtained from *Erwinia herbicola*

4. Conclusion

Based on previous findings, a novel levan (EPS) producing isolate of *L. fermentum* SHN1was isolated from milk and dairy products. This isolate was identified using phenotypic characteristic and *16S rRNA* gene sequencing. The production of levan was enhanced using optimized conditions (pH, carbon source, sucrose concentration, nitrogen source, inoculum size and incubation time). The partially purified biopolymer was characterized by FTIR and NMR. These analyses confirmed the presence of the functional groups within the levan structure and the similarity with the standard levan.

Acknowledgements

This work was supported by the Department of Biotechnology, College of Science, University of Baghdad (Baghdad, Iraq).

References

Abid Y, Azabou S, Casillo A, Gharsallah H, Jemil N, Lanzetta R, Attia H and Corsaro M M. 2019. Isolation and structural characterization of levan produced by probiotic *Bacillus tequilensis*-GM from Tunisian fermented goat milk. *Int J Biol Macromol*.,**133:**786–794. Doi:https://doi.org/10.1016/j.ijbiomac.2019.04.130.

Abou-Taleb K, Abdel-Monem M, Yassin M and Draz A. 2015. Production, purification and characterization of Levan polymer from *Bacillus lentus* V8 strain. *Brit Microbiol Res J*., **5(1)**: 22-32.doi: https://doi.org/10.9734/BMRJ/2015/12448

Abou-Taleb KA, Abdel-Monem MO, Yassin MH and Draz AA. 2014. Nutritional factors affecting levan production by *Bacillus sp.* V8 strain isolated from rhizosphere bean (Vicea faba) plant. *J Agric Technol*., **10**: 899–914.

Ahmad AA. 2013. In vitro screening of *Lactobacillus* species from homemade yoghurt for antagonistic effects against common bacterial pathogens. *JJBS*., **6(3)**: 211 – 216.

Doi: http://dx.doi.org/10.12816/0001535

Ahmad W, Nasir A, Sattar F *et al.* 2022. Production of bimodal molecular weight levan by a *Lactobacillus reuteri* isolate from fish gut. *Folia Microbiol*., **67**: 21–31. Doi: http://dx.doi.org/10.1007/s12223-021-00913-w

Ahuja M, Singh S and Kumar A. 2013. International journal of biological macromolecules evaluation of carboxymethyl gellan gum as a mucoadhesive polymer. *Int J Biol Macromol.,* **53**: 114-121.doi: https://doi.org/10.1016/j.ijbiomac.2012.10.033

Al- Mousawi BNE and Abd- Aljabar EK. 2018. Study of the effect of wheat germ extract on the production of exopolysaccharides from the bioenhancers. *Iraqi J Agric Sci.*, **44 (1)** :55-63. Doi: http://dx.doi.org/10.36103/ijas.v49i1.207

Al-Halbosiy MM, Thabit ZA, Al-Qaysi SA-DAS and Moussa TA. 2018. Biological activity of levan produced from rhizospheric soil bacterium *Brachybacterium phenoliresistens* KX139300. *Baghdad Sci J.*, **15(3)**: 0238. doi: https://doi.org/10.21123/bsj.2018.15.3.0238

Al-Maliki AA. 2020. Production, characterization and assessment of biological activity of lipopeptide produced by clinical *Lactobacillus plantarum*. PhD thesis, College of science, University of Baghdad, Iraq.

Al-Qaysi SAS, Thabit ZA and Kadhem SB. 2016. Levan production using *Pseudomonas brassicacearum* isolated from rhizosphere soil of Cowpea farm in Iraq. *Iraqi J Biotech*., **15**: 83-96. Doi: http://dx.doi.org/10.13140/RG.2.2.31042.84167

Al-Qaysi SAS, Al-Haideri H, Al-Shimmary SM, Abdulhameed JM, Alajrawy OI, Al-Halbosiy MM, Moussa TAA and Farahat MG.2021. Bioactive levan-type exopolysaccharide produced by *Pantoea agglomerans* ZMR7: Characterization and optimization for enhanced production. *J Microbiol Biotechnol*., **31(5)**:696-704. Doi: http://dx.doi.org/10.4014/jmb.2101.01025

Alshammery RM and Alaubydi MA. 2020. Extraction and partial purification of exo-polysaccharide from *Lactobacillus rhamnosus* isolated from vaginal specimens. *Iraqi J Sci.*, **61 (4)**: 754-764. Doi: http://dx.doi.org/10.24996/ijs.2020.61.4.7

Aramsangtienchai P, Kongmon T, Pechroj S, Srisook K. 2020. Enhanced production and immunomodulatory activity of levan

from the acetic acid bacterium, *Tanticharoenia sakaeratensis*, *Int J Biol Macromol*., **163**: 574-581.
Doi: https://doi.org/10.1016/j.ijbiomac.2020.07.001

Arvidson SA, Rinehart BT and Gadala-Maria F. 2006. Concentration regimes of solutions of levan polysaccharide from *Bacillus sp. Carbohydr Polym*, **65**:144-149.
Doi: http://dx.doi.org/10.1016/j.carbpol.2005.12.039

Bekers M, Upite D, Kaminska E, Laukevics J, Grube M, Vigants A and Linde R. 2005. Stability of levan produced by *Zymomonas mobilis*. *Process Biochem*., **40**: 1535–1539. Doi: http://dx.doi.org/10.1016/j.procbio.2004.01.052

Belghith KS, Dahech I, Belghith H and Mejdoub H. 2012. Microbial production of levansucrase for synthesis of fructooligosaccharides and levan. *Int Biol Macromol*., **50(2):** 451-458. Doi: http://dx.doi.org/10.1016/j.ijbiomac.2011.12.033

Chidambaram SCA, Veerapandian B, Sarwareddy KK, Mani KP, Shanmugam SR and Venkatachalam P. 2019. Studies on solvent precipitation of levan synthesized using *Bacillus subtilis* MTCC 441. *Heliyon.*, **5 (9)**.

Doi: http://dx.doi.org/10.1016/j.heliyon.2019.e02414

Costa GT, Vasconcelos QD and Aragão GF. 2021. Fructooligosaccharides on inflammation, immunomodulation, oxidative stress, and gut immune response: A systematic review. *Nutr Rev*., **80(4)**: 709–722.
Doi: http://dx.doi.org/10.1093/nutrit/nuab115

Chun-lei Z, Jia-qi L, Hai- tao G, Jie W and Ri-hua X. 2014. Selection of exopolysaccharide - producing lactic acid bacteria isolates from Inner Mongolian traditional yoghurt. *Mljekarstvo*., **64 (4)**: 254-260.

Doi: http://dx.doi.org/10.15567/mljekarstvo.2014.0404

Costerton JW, Cheng KJ, Geesey GG, Ladd TI, Nickel JC, Dasgupta M and Marrie TJ. 1987. Bacterial biofilms in nature and disease. *Annu Rev Microbiol*., **41**: 435-464.
Doi: http://dx.doi.org/10.1146/annurev.mi.41.100187.002251

Dahech I, Belghith KS, Belghith H and Mejdoub H. 2012. Partial purification of a *Bacillus licheniformis* levansucrase producing levan with antitumor activity, *Int J Biol Macromol*., **51**: 329–335. Doi: http://dx.doi.org/10.1016/j.ijbiomac.2012.04.030

Dahech I, Bredai R and Srih K. 2014. Optimization of levan production from *Bacillus licheniformis* using response surface methodology. *Biochem*., **8(4)**: 115-119.

De Man JC, Rogosa M and Sharpe ME. 1960. A medium for the cultivation of Lactobacilli. *J Appl Bacteriol*., **23**: 130 – 135. Doi: http://dx.doi.org/10.1111/j.1365-2672.1960.tb00188.x

De Oliveira MR, da Silva RSSF, Buzato JB and Celligoi MAP C. 2007. Study of levan production by *Zymomonas mobilis* using regional low-cost carbohydrate sources. *Biochem Eng J.*, **37(2)**, 177–183. Doi: http://dx.doi.org/10.1016/j.bej.2007.04.009

Hamada MA, Hassan RA, Abdou AM, Elsaba YM, Aloufi AS, Sonbol H and Korany SM. 2022. Bio_fabricated levan polymer from *Bacillus subtilis* MZ292983.1 with antibacterial, antibiofilm, and burn healing properties. *Appl Sci*.,**12**: 6413.

doi: http://dx.doi.org/10.3390/app12136413

Hussein NA and Luti KJK. 2023. In vitro antimicrobial activity of *Lactobacillus Parabuchneri* Nu14 as a probiotic. *Iraqi J Agric Sci.*, **54(6):**1647–1658. https://doi.org/10.36103/ijas.v54i6.1864

Imran MYM, Reehana N, Jayaraj KA, Ahamed AAP, Dhanasekaran D, Thajuddin N, Alharbi NS and Muralitharan G. 2016. Statistical optimization of exopolysaccharide production by *Lactobacillus plantarum* NTMI05 and NTMI20. *Int J Biol Macromol*., **93**: 731–745.
Doi: https://doi.org/10.3390/chemengineering5030039

Jeyagowri N, Ranadheera CS, Manap MY, Gamage A, Merah O and Madhujith T. 2023. Phenotypic characterisation and molecular identification of potentially probiotic *Lactobacillus* sp. isolated from fermented rice. *Fermentation*., **9 (9): 807**.
Doi: http://dx.doi.org/10.3390/fermentation9090807

Jameel AA and Haider NH. 2021. Determination of the optimum conditions for biosurfactant production by local isolate of *Lactobacillus plantarum* and evaluate its antimicrobial activity. *Iraqi J Agric Sci.,* **52(1):**170-188.

Kadhum MKH and Haydar NH. 2020. Production and characterization of biosurfactant (Glycolipid) From *Lactobacillus helviticus* M5 and evaluate its antimicrobial and antiadhesive activity. *Iraqi J Agric Sci.*, **51(6):**1543-1558.
Doi: http://dx.doi.org/10.36103/ijas.v51i6.1182

Keith J, Wiley B, Ball D, Arcidiacono S, Zorfass D, Mayer J and Kaplan D. 1991. Continuous culture system for production of biopolymer levan using *Erwinia herbicola*. *Biotechno Bioeng*, **38**:557-560. Doi: https://doi.org/10.1002/bit.260380515

Khassaf WH, Niamah AK and Al-Manhel AJA. 2019. Study of the optimal conditions of levan production from a local isolate of *Bacillus subtilis* subsp. *subtilis* w36. *Basrah J Agric Sci.*, **32(2)**: 213–222.
https://doi.org/10.37077/25200860.2019.211.

Khudair AY, Salman JA and Ajah HA. 2018. Production of levan from locally *Leuconostoc mesensteroides* isolates. *J Pharm Sci. & Res*., **10(12):** 3372-3378.

Küçükaşik F, Kazak H, Güney D, Finore I, Poli A, Yenigün O, Nicolaus B and Öner E T. 2011. Molasses as fermentation substrate for levan production by *Halomonas sp*. *Appl Microbiol Biot.,* **89(6):** 1729-1740.
Doi: http://dx.doi.org/10.1007/s00253-010-3055-8

Lonˇcarevi´c B, Ljeˇsevi´c M, Markovi´c M, Anđelkovi´c I, Gojgi´c-Cvijovi´c G, Jakovljevi´c D and Beˇskoski V. 2019. Microbial levan and pullulan as potential protective agents for reducing adverse effects of copper on Daphnia magna and Vibrio fischeri. *Ecotoxicol Environ Saf*., **181**:187–193.
https://doi.org/10.1016/j. ecoenv.2019.06.002.

Mamay A, Wahyuningrum D and Hertadi R. 2015. Isolation and characterization of levan from moderate halophilic bacteria *Bacillus licheniformis* BK AG21. *Procedia Chem*, **16**: 292-298.
Doi: http://dx.doi.org/10.1016/j.proche.2015.12.055

Mohammed MJ, Mahdi MS, Jameel AH and Thalj KM. 2021. The Role of *Lactobacillus casei* and *Lactobacillus acidophillus* to Decrease the Biological Effects of Potassium Bromate in Rats. *Iraqi J of Agric Sci.*, **52(1)**:70-78. Doi: http://dx.doi.org/10.36103/ijas.v52i1.1237

Mohsin YMB, Hasan AM, Dari WA, Bataah EH and Mohammed MJ. 2020. Natural products of *Lactococcus* overcome nosocomial infection in some of Baghdad hospitals in Iraq. *Baghdad Sci J*., **17**(1(Suppl.)): 0227.
Doi: http://dx.doi.org/10.21123/bsj.2020.17.1(Suppl.).0227

Morishita T, Deguchi Y and Yajima M. 1981. Multiple nutritional requirements of lactobacilli: genetic lesions affecting amino acid biosynthetic pathways. *J Bacteriol*., **148(1):** 64–71. Doi: http://dx.doi.org/10.1128/JB.148.1.64-71.1981

Moussa TAA, Al-Qaysi SAS, Thabit ZA and Kadhem SB. 2017. Microbial levan from *Brachybacterium phenoliresistens*: Characterization and enhancement of production, *Process Biochem.*, **57**: 9-15. https://doi.org/10.1016/j.procbio.2017.03.008.

Nasir DQ, Wahyuningrum D and Hertad R. 2015. Screening and characterization of levan secreted by halophilic bacterium of *Halomonas* and *Chromohalobacter* genuses originated from bledug kuwu mud crater. *Procedia Chem.*, **16**: 272-278.
Doi: http://dx.doi.org/10.1016/j.proche.2015.12.050

Owner ET, Hernandez L and Combie J. 2016.Review of levan polysaccharide: from a century of past experiences to future prospects. *Biotechnol Adv*., **34**: 827- 844.

Doi: http://dx.doi.org/10.1016/j.biotechadv.2016.05.002

Ngampuak V, Thongmee A, Pongpoungphet N, Wongwailikhit K and Kanchanaphum P. 2023. Probiotic Properties of Exopolysaccharide-Producing Bacteria from Natto. Int J Food Sci., **2023**(1): 3298723.
doi: https://doi.org/10.1155/2023/3298723

Panteli´c I, Luki´c, M, Gojgi´c-Cvijovi´c G, Jakovljevi´c D, Nikoli´c I, Lunter D J, Daniels R and Savi´c S. 2020. *Bacillus licheniformis* levan as a functional biopolymer in topical drug dosage forms: from basic colloidal considerations to actual pharmaceutical application. *Eur J Pharm Sci.*, **142**. Doi: http://dx.doi.org/10.1016/j.ejps.2019.105109

Poli A, Kazak H, Gürleyendag B, Tommonaro G, Pieretti G, Öner ET and Nicolaus B. 2009. High level synthesis of Levan by a novel *Halomonas* species growing on defined media. *Carbohydr Polym*.,**78**: 651–657.
Doi: http://dx.doi.org/10.1016/j.carbpol.2009.05.031

Salman JAS, Ajah HA and Khudair AY. 2019. Analysis and characterization of purified levan from *Leuconostoc mesenteroides* ssp. cremoris and its effects on *Candida albicans* virulence factors. JJBS., **12(2):** 243 – 249.

Sánchez-León E, Huang-Lin E, Amils R and Abrusci C. 2023. Production and characterization of an exopolysaccharide *by Bacillus amyloliquefaciens*: biotechnological applications. *Polym*., **15(6):** 1550.
https://doi.org/10.3390/polym15061550

Semjonovs P, Shakirova L, Treimane R, Shvirksts K, Auzina L, Cleenwerck I and Zikmanis P. 2016. Production of extracellular fructans by *Gluconobacter nephelii* P1464. Lett. *Appl Microbiol*., **62 (2)**: 145–152. Doi: http://dx.doi.org/10.1111/lam.12521

Senthilkumar V and Gunasekaran P. 2005. Influence of fermentation conditions on levan production by *Zymomonas mobilis* CT2. *Indian J Biotechnol*., **4**: 491–496.

Silbir S, Dagbagli S, Yegin S, Baysal T and Goksungur Y. 2014. Levan production by *Zymomonas mobilis* in batch and continuous fermentation systems. *Carbohydr Polym.*, **99**: 454–461.doi: http://dx.doi.org/10.1016/j.carbpol.2013.08.031

Sims IM, Frese SA and Walter J. 2011. Structure and functions of exopolysaccharide produced by gut commensal *Lactobacillus reuteri* 100–23. *ISME J*., **5 (7):**1115–1124. Doi: http://dx.doi.org/10.1038/ismej.2010.201

Srikanth R, Siddartha G, Sundhar Reddy CHSS, Harish BS, Janaki Ramaiah M and Uppuluri KB. 2015a. Antioxidant and anti-inflammatory levan produced from *Acetobacter xylinum* NCIM2526 and its statistical optimization. *Carbohydr Polym*., **123**: 8-16. doi: https://doi.org/10.1016/j.carbpol.2014.12.079

Srikanth R, Reddy,CHSSS, Siddartha G, Ramaiah MJ and Uppuluri KB. 2015b. Review on production, characterization and applications of microbial levan. *Carbohydr Polym*.,**120**: 102–114. https://doi.org/10.1016/j.carbpol.2014.12.003.

Taye Y, Degu T, Fesseha H, Mathewos M. 2021. Isolation and identification of lactic acid bacteria from cow milk and milk products. *The Scientific World Journal*, **2021(1)**:4697445. https://doi.org/10.1155/2021/4697445

Taylan O, Yilmaz MT, Dertli E. 2019. Partial characterization of a levan type exopolysaccharide (EPS) produced by *Leuconostoc mesenteroides* showing immunostimulatory and antioxidant activities. *Int J Biol Macromol.,***136 (1):** 436-444. Doi: http://dx.doi.org/10.1016/j.ijbiomac.2019.06.078

Teixeira LC, Peixoto RS, Cury JC, Sul WJ, Pellizari VH, Tiedje J and Rosado AS. 2010. Bacterial diversity in rhizosphere soil from Antarctic vascular plants of Admiralty Bay, maritime Antarctica. *ISME J.,***4 (8)** :989–1001.
Doi: http://dx.doi.org/10.1038/ismej.2010.35

Tsveteslava II and Ivanov R. 2016. Exopolysaccharides from Lactic Acid Bacteria as Corrosion Inhibitors. *J Life Sci*., **3 (1)**: 940-945.doi: http://dx.doi.org/10.1515/asn-2016-0008

Van Hijum SAFT, Kralj S, Ozimek LK, Dijkhuizen L and van Geel-Schutten IGH. 2006. Structure-function relationships of glucansucrase and fructansucrase enzymes from lactic acid bacteria. *Microbiol Mol Bio Rev*., **70 (1)**: 157–176.doi: https://doi.org/10.1128%2FMMBR.70.1.157-176.2006

Veerapandian B, Shanmugam SR, Sivaraman S, Sriariyanun M, Karuppiah S and Venkatachalam P.2023. Production and characterization of microbial levan using sugarcane *(Saccharum* spp.) juice and chicken feather peptone as a low-cost alternate medium. *Heliyon*., **9(6)**. doi: https://doi.org/10.1016/j.heliyon.2023.e17424

Vieira AM, Zahed F, Crispim AC, de Souza Bento E, França RFO, Pinheiro IO, Pardo LA and Carvalho BM. 2021. Production of Levan from *Bacillus subtilis* Var. Natto and Apoptotic Effect on SH-SY5Y Neuroblastoma Cells. *Carbohydr Polym*., **273 (2)**:118613. Doi: http://dx.doi.org/10.1016/j.carbpol.2021.118613

Wu FC, Chou SZ and Shih IL. 2013. Factors affecting the production and molecular weight of levan of *Bacillus subtilis* natto in batch and fed - batch culture in fermenter. *J Taiwan Inst Chem Eng.*, **44 (6)**: 846-853.
Doi: http://dx.doi.org/10.1016/j.jtice.2013.03.009

Xu X, Gao C, Liu Z, Wu J, Han J, Yan M and Wu Z. 2016. Characterization of the levan produced by *Paenibacillus bovis sp*. nov BD3526 and its immunological activity. *Carbohydr Polym*., **144**: 178-186.
Doi: http://dx.doi.org/10.1016/j.carbpol.2016.02.049

Zhang T, Li R, Qian H, Mu W, Miao M and Jiang B. 2014. Biosynthesis of levan by levansucrase from *Bacillus methylotrophicus* SK 21.002. *Carbohydr Polym*., **101**: 975-981. Doi: http://dx.doi.org/10.1016/j.carbpol.2013.10.045

JJBS

Volume 17, Number 3,September 2024
ISSN 1995-6673
Pages 541 – 548
https://doi.org/10.54319/jjbs/170317

Jordan Journal of Biological Sciences

Antiproliferative Effect of *Entada rheedii* Crude Lectin Extract on Human Colorectal Cancer Cells

Amruta Sridhara, Dhrithi J. Mallur and Reshma S.V.*

Department of Biotechnology, PES University, 100 Feet Ring Road, Banashankari III Stage, Bengaluru, Karnataka, India 560085

Received: March 23, 2023; Revised: March 11, 2024; Accepted: April 1, 2024

Abstract

Several studies have proved that leguminous lectins are often explored as a potential anti-cancer agent owing to their substantial anti-cancer properties which include inhibition of cell adhesion, proliferation and colony formation. This group of carbohydrate-binding proteins is seen to cause agglutination and an increase in cancer cell cytotoxicity. The study aims to isolate and purify the lectin present in *Entada rheedii*, a tropical legume and analyse its significance as a potential antiproliferative agent against human colorectal cancer cells. Previously published work confirmed the lactose, galactose and cellobiose specificity of the lectin, and this lectin was isolated, purified and separated by sodium dodecyl sulphate polyacrylamide gel electrophoresis. Cytotoxic assay was performed to investigate the extent of its strength as an antiproliferative protein. The purified lectin agglutinates processed chicken RBCs with a maximum hemagglutination Unit of 32. The lectin was observed to be stable when stored at 0-4°C. The antiproliferative activity of lectin from *Entada rheedii* was confirmed against human colorectal carcinoma cells HCT 116 with IC_{50} values of 188.72 µg/mL.

Keywords: Antiproliferative, Cancer, *Entada rheedii,* Lectin

1. Introduction

Cancer treatment is a complex field, involving considerations such as specificity, selectivity, toxicity and mechanisms of action in the development of effective anticancer drugs. Some natural compounds or phytocompounds have shown potential in preclinical studies. Some typical examples include taxol analogs, vinca alkaloids such as vincristine, vinblastine, and podophyllotoxin analogs (Choudari *et al.,* 2020).

Lectins are defined as a class of proteins that selectively bind to carbohydrates. These phytocompounds show a high affinity towards glycoproteins, glycolipids and polysaccharides. They are oligomeric in nature, with each lectin presenting at least 2 carbohydrate binding sites. Lectin-carbohydrate interaction resembles antigen-antibody interaction through a non-catalytic, reversible and highly selective domain (Law & Strijdom, 1977; Kasapoğlu & Dere, 2022). All legume lectins share homologies with significant conserved regions of the protein subunits. The 3D structures of all legume lectins exhibit similarities in carbohydrate binding, ligand binding and allosterically interactive sites. Specifically, lectins being metallo-proteins, the 3D structures of leguminous lectins show remarkable similarity in binding to metal ions (Sharon & Lis, 1990).

Lectins are abundant in cotyledons of mature seeds of most legumes. Legume lectins, being ubiquitously available, include the largest and the best characterized family of lectins. Lectins in legumes play a major role in plant immunity against phytopathogens acting as pattern recognition receptors and also have the ability to influence the production of various interleukins mentioned in Tamilarasan *et al*. (2021) and De Mejía & Prisecaru (2005).

A major advantage of dietary lectins is their resistance to gastrointestinal digestion, owing to their compact globular structure (De Mejía & Prisecaru, 2005). This structure protects ingested lectins from protease denaturation, allowing them to retain their structure and activity post ingestion (Kelsall *et al*., 2002). As an added domestic advantage, most plant lectins can retain a significant amount of activity when subjected to gentle cooking methods (Ryder *et al*., 1992).

A unique property of lectins is their ability to agglutinate or clump together certain cells. This agglutination is evident when lectins are tested against red blood cells (RBCs). Specific sugar residues on the outer membrane of erythrocytes have a high affinity for the lectin and cause the surrounding cells to clump together. This property of lectins is used in human blood typing experiments described by Gorakshakar & Ghosh (2016).

Previous research on various legume lectins has demonstrated their ability to induce antiproliferative

* Corresponding author. e-mail: reshma@pes.edu.

**Abbreviations:E. rheedii - Entada rheedii; PBS - Phosphate Buffer Saline; rpm - Rotations per minute; RBC - Red Blood Cells; EDTA - Ethylenediaminetetraacetic acid; HU - Hemagglutination Unit; PEG - Polyethylene glycol; ACR - Alkaline copper reagent; FCR - Folin–Ciocalteu reagent; SDS - Sodium dodecyl sulphate; APS - Ammonium persulphate; SDS-PAGE - Sodium dodecyl sulfate polyacrylamide gel electrophoresis; MTT - 3-(4,5-dimethylthiazol-2-yl)-2,5-diphenyl-2H-tetrazolium bromide; HCT 116 - Human colorectal cancer cells; EAC - Ehrlich ascites carcinoma; PHA - Phytohemagglutinin ; WGA - Wheat germ agglutinin

activities in selected cell lines such as HeLa, A549 (Naik & Kumar, 2020) and EAC (Kabir *et al.,* 2021). The induction of apoptosis through type-II programmed cell death in transformed cells is one of the most common abilities of lectins. For example, soybean lectin has been shown to induce autophagy and DNA damage in HeLa cells by generating reactive oxygen species which have a cytotoxic effect on cells (Yau *et al*., 2015). This tumor specificity of the lectins depends on the type and abundance of carbohydrate moieties expressed on the tumor cells, allowing them to be classified as biomarkers by specifically binding to tumor-associated carbohydrates (Maaroof *et al*., 2018).

Numerous reports highlight a prevailing trend whereby transformed cells exhibit greater susceptibility to lectin agglutination than their normal cell counterparts. In addition, transformed cells tend to show increased sensitivity to the toxic effects of lectins, a contrast to the relatively reduced impact observed on normal cells (Burger *et al*., 1969).

In cases involving lectins such as concanavalin A, phytohemagglutinin (PHA), abrin and ricin, their efficacy has been observed in specific tumor systems. Within these systems, the inhibition of tumor growth can be attributed to the greater toxicity of the lectins to tumor cells compared to their effect on normal cells.

It is proposed that the difference in surface membrane structure between normal and transformed cells contributes to the different toxic effects of plant lectins on healthy and cancerous cells.
It is also proposed that the difference in surface membrane structure between normal and transformed cells contributes to the different toxic effects of plant lectins on healthy and cancerous cells (Esumi-Kurisi *et al*., 1983).

In their work, Esumi-Kurisi *et al.* suggested that wheat germ agglutinin (WGA) operates *in vivo* by facilitating the proximity of tumor cells and macrophages, achieved by linking the N-acetyl glucosamine groups present on their respective glycoproteins. Notably, this interaction does not extend to normal cells, which lack this particular recognition by macrophages, leading to reduced activity of WGA against them.

Entada rheedii is a tropical liana belonging to the family of Fabaceae, a medicinally relevant subset of African and Indian subcontinental flora (Gurib-Fakim *et al.,* 2013). It is large in size with a hard seed coat containing large cotyledons with ample amounts of proteins. It has been well established to have medicinal, anti-cancer (Li *et al*., 2014), (Panda *et al*., 2014), (Thies *et al*., 2008) anti-bacterial (Carvalho *et al*., 2015; Li *et al*., 2014) and anti-fungal properties (Sitohy *et al.*, 2007; Phadungsil & Grams, 2021). Traditional medicine, supported by recent scientific studies, shows a wide range of drugs extracted from *Entada rheedii* including treatment for mumps (Shivanna & Rajakumar, 2011) and remedies for diarrhoea (Okba *et al.,* 2013). Entadamine from crude extracts showed pronounced activity against protozoan diseases such as trypanosomiasis and leishmaniasis (Okba *et al*., 2013).

Prior studies (Naik & Kumar, 2020) on the lectin in *Entada rheedii* revealed the presence of a 19.333 kDa protein that specifically binds to lactose, galactose and cellobiose. This *Entada rheedii* lectin was further examined for its stability in varying temperatures, pH and in the presence of metal ions. The protein band of interest, as previously analyzed by Naik *et al*., (2020) confirmed that lectin from *E. rheedii* appeared as a single band with an approximate molecular weight of 20 kD with and without β-mercaptoethanol and was monomeric in nature. The study also included *in vitro* cytotoxicity and morphological analysis of *Entada rheedii* lectin on lung cancer cell line A549, HeLa. Tha results from MTT assay performed on these cell lines showed an IC_{50} value of 28 µg/mL confirming the induced apoptotic activity of *Entada rheedii* lectin (Naik & Kumar, 2020).

This *Entada rheedii* lectin was further investigated for its stability at different temperatures, pH and in the presence of metal ions. The protein band of interest, as previously analysed by Naik & Kumar et al. (2020) confirmed that the lectin from *E. rheedii* appeared as a single band with an approximate molecular weight of 20 kD with and without β-mercaptoethanol and was monomeric in nature.

Further work by Naik & Kumar (2020) demonstrated that when normal cells (African Green Monkey Normal Kidney Cells (Vero) were exposed to different concentrations of Entadin lectin and assessed by the dose-dependent MTT assay, cell viability was largely unaffected. This observation supports the notion that Entadin lectin has a preferential effect on cancer cells without inducing notable toxicity towards normal cells.

The present study focuses on the characterization and evaluation of the anti-cancer properties of the lectin extracted from *Entada rheedii* seeds. Drawing upon insights and findings from previously published research, our primary objective is to investigate the effects of lectins from *Entada rheedii* on the Human colon cancer cell line HCT 116.

2. Materials and Methods

2.1. Extraction of total protein

Seeds of *Entada rheedii* were sustainably harvested from fallen pods from Puttur, Dakshina Kannada District of Karnataka and were identified and confirmed by the taxonomist at The University of Trans-Disciplinary Health Sciences and Technology (TDU, Bangalore). The hard testa was cracked open and the inner contents were crushed to a coarse powder and were stored in an air-tight container at 4 °C. 5 g of seed powder was homogenized thoroughly for 10 minutes with 0.15M phosphate buffer saline of pH 7.2 using a mortar and pestle and stored overnight at 4°C followed by centrifugation at 7200 rpm for 20 minutes. The pellet was washed using 0.15 M PBS and centrifuged again. The supernatants were pooled and filtered using Whatman Filter Paper (Grade 1, 125 mm). Hemagglutination assay was performed to confirm the presence of lectin in the supernatant (Naik & Kumar, 2020).

2.2. Hemagglutination assay

Gorakshakar & Ghosh (2016) describe an efficient method to analyse a sample for the presence of lectins. Following their method, upon addition of the sample and the RBC suspension to a 96-well, V-bottom microtiter plate, the formation of mesh-like structures indicates that specific binding has taken place, and the sample is positive for lectins, whereas the formation of dots indicates the

unbound RBCs have settled at the bottom of the well and the sample is considered negative for lectin content.

Hemagglutination tests were routinely carried out at each step to check the presence and concentration of lectins. Fresh chicken blood was obtained from a local butcher shop and mixed with 0.01M ethylenediaminetetraacetic acid (EDTA). The mixture was centrifuged at 2500 rpm for 10 minutes to remove the EDTA, and the pellet was washed and centrifuged twice with 1 M PBS to prepare a 4% RBC (Adamová *et al*., 2014).

Hemagglutination assays were performed in a 96-well, U-bottom microtitre plate. 25 µl of 1 M PBS was added to all the wells and a two-fold dilution of the sample was performed with 25 µl of the sample. An equal amount of 4% RBC solution was added to all wells, and the plate was incubated for 30 minutes at room temperature. The Hemagglutination Unit (HU) of the sample was calculated based on the number of meshes formed, and results were analysed in triplicates as described by Grimes *et al., (*2002) in their published protocols.

2.3. Salting out of total protein content

The total protein content in the crude extract was subjected to ammonium sulphate precipitation. Salt saturation was gradually increased from 0% to 30%, 30% to 50% and 50% to 80% with two-hour incubation periods and constant stirring for each saturation increase. After each round of precipitation, the solution was centrifuged at 7200 rpm for 20 minutes. The supernatants were used for the next round of precipitation, and the pellets were resuspended in 2 mL of 0.15 M PBS buffer. The pellets of 30%, 50% and 80% saturation were tested for the presence of lectins by hemagglutination.

The pellets showing hemagglutination activity were pooled together and passed through a 10 mL desalting column (Genei Laboratories Private Limited) which was equilibrated with 2-bed volumes of 0.15 M PBS buffer. The pooled pellets were added to the column and incubated for 1 hour at 4°C. The desalted protein was eluted out with 2 more bed volumes of 0.15 M PBS buffer and collected as 1 mL fractions. Each fraction was tested for the presence of lectin by hemagglutination assay.

2.4. PEG assisted-osmosis driven protein concentration

The fractions collected from the desalting column were tested for their hemagglutination activity using 4% chicken blood. The fractions forming meshes were pooled together and concentrated by osmotically removing excess buffer in the solution. The fractions showing positive hemagglutination results were pooled together and placed in a 17 cm cellulose membrane (HiMedia Dialysis Tubing Size 1 with a molecular weight cut off of 14 kDa) ensuring no leaks (Goldring & Dean Goldring, 2019). This was subjected to dialysis for 3 hours at room temperature using 0.15 M PBS to eliminate any residual salt content. The membrane was then laid on a bed of polyethylene glycol (PEG) 6000 until the solution reduced by four times the original volume. The concentrated protein was checked for lectin content by hemagglutination with 4% RBC.

2.5. Quantification of protein

The amount of protein in crude extract and PEG concentrated protein was estimated by following the standard procedure of Lowry's Assay (Lowry *et al*., 1951).

2.6. Molecular Mass Separation of Proteins

Proteins present in the concentrated fraction were electrophoretically separated on a discontinuous vertical gel using the Biorad Mini-PROTEAN® Electrophoresis System and stained in Coomassie brilliant blue G-250 overnight. Post destaining, the gel was visualised using the Biorad GelDoc Go System. Himedia Prestained Protein Ladder (MBT092).

2.7. In vitro cytotoxicity test by MTT (3-(4, 5-dimethylthiazol-2)-2, 5-diphenyltetrazolium bromide) analysis

MTT (Liu *et al*., 1997) analysis of concentrated *Entada rheedii* protein extract was performed. HCT 116 cells were obtained and subcultured from the National Centre for Cell Science Cell Repository, Pune, India. Cultured cells were dislodged by trypsin and centrifuged at 300 g. A solution of 10,000 cells per 200 µl of cell suspension was made. 200 µl of cell suspension was added to all the wells of a 96-well microtitre plate and incubated at 37°C at 5% CO_2 for 24 hours. After aspirating the spent medium, 200 µl of prepared sample concentrations were added (undiluted, 21.5625 µg/mL, 43.125 µg/mL, 86.25 µg/mL, 172.5 µg/mL, 345 µg/mL) to the wells and incubated again at 37°C for another 24 hours. The medium was removed and 200 µl of 10% MTT was added to each well and incubated at similar conditions for 3 hours. The culture media was completely removed and 100 µl of DMSO was added and kept on a gyratory shaker to solubilize the crystals. Absorbance was read using a microplate reader set to 570 nm and percent growth inhibition and IC_{50} values were calculated by plotting protein concentrations represented on the X-axis and the variance in percent cell viability represented on the Y axis. The plot was then fitted to a straight line from which the IC_{50} value was obtained from the equation (1) and (2) ("Science Gateway," n.d.)

$$Y = a*X + b \quad (1)$$

$$IC_{50} = (0.5 - b)\ a. \quad (2)$$

In Y = a*X + b, a is the slope, representing the rate of change, and b is the y-intercept, indicating the value when X is zero.

The treated cells were imaged using XDFL series biological microscope, Sunny Instruments, China.

3. Results

3.1. Purification of E. rheedii proteins

The *E. rheedii* protein was isolated and purified from a 50% ammonium sulfate saturated crude extract yielding a final concentration of 686.948 µg/mL post PEG assisted-osmosis driven protein concentration which is soluble in 0.15 M PBS. Presence of lectins was confirmed by assessing its hemagglutination activity against 4% RBCs.

3.2. Hemagglutination activity

The purified protein showed hemagglutination activity against 4% chicken erythrocytes. The lectins present in total proteins showed mesh formation when administered as crude extract and after every step of purification (Figure

1). Similar results were observed in earlier studies done on lectins present in *E. rheedii* (Naik & Kumar, 2020).

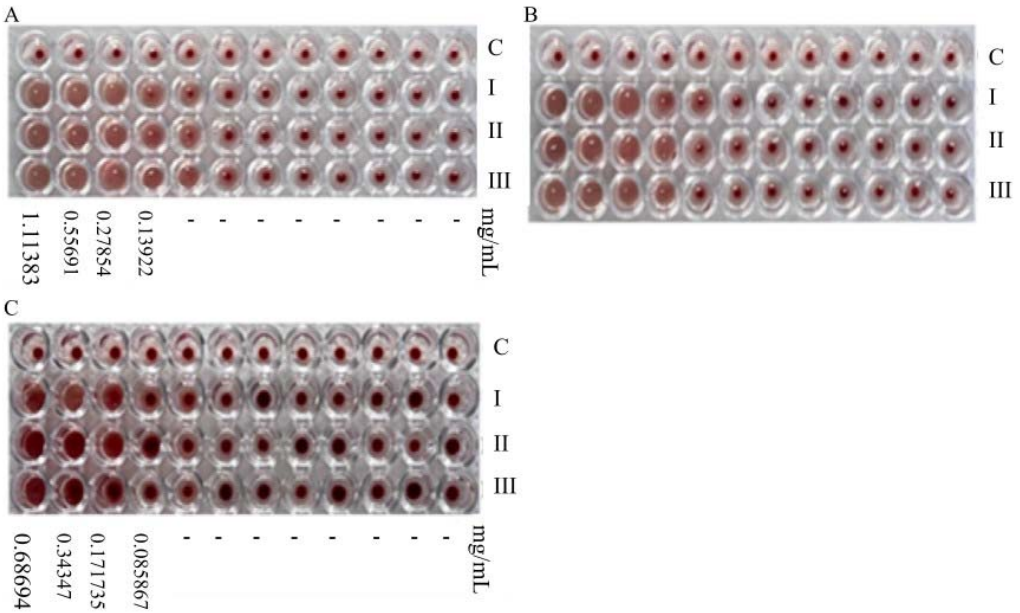

Figure 1. Hemagglutination of Chicken red blood cells by *E. rheedii* lectin shown in triplicates as in I, II, III for each image (A, B, C). (A) Hemagglutination activity of crude extract of *E. rheedii* indicating hemagglutination unit of 32 with a serially diluted concentration of 0.13922 mg/mL. (B) Hemagglutination activity of 50% ammonium sulphate saturated crude extract indicating hemagglutination unit of 16. (C) Hemagglutination activity of concentrated purified protein from *E. rheedii* indicating hemagglutination unit of 8 and a serially diluted concentration of 0.085 mg/mL.

3.3. Molecular mass separation

The high-resolution separation of mixtures of protein was performed on crude extract by SDS-PAGE (Figure:2).

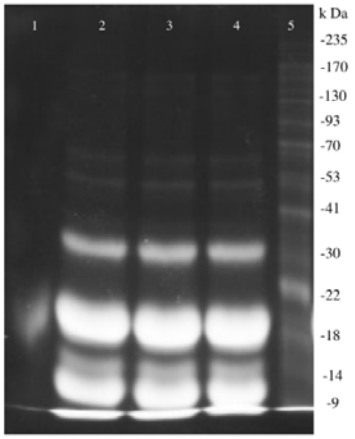

Figure 2. Molecular weight based separation of *Entada rheedii* crude extract shown in triplicates. Lane 1 - Protein Marker Lactoglobulin (18.4 kDa). Lane 2, 3, 4 - *E. rheedii* crude extract (19.33 kDa). Lane 5 - Protein Ladder.

3.4. In vitro cytotoxicity of crude extract of lectins from E. rheedii on HCT 116

MTT assay for lectins from *E. rheedii* was performed on HCT 116 cancer cells. The dosage dependent assay administered the lectins present in purified proteins in the concentrations of 345 µg/mL, 172.5 µg/mL, 86.25 µg/mL, 43.125 µg/mL, 21.5625 µg/mL and 686.948 µg/mL.

The assay showed a reduction in cell viability after incubating the cells for 24 hours and the IC_{50} was found to be 188.72 g/mL (Table 1 and Figure 3). There is an observed appearance of apoptotic bodies upon administration of the sample (Figure 4).

Table 1. MTT assay results

HCT 116 cells vs *E.rheedii* Lectin	Blank	Untreated	Test concentration µg/mL				
			21.5625	43.125	86.25	172.5	345
Trial 1	0.002	1.554	1.589	1.046	0.888	1.022	0.022
Trial 2	0.002	1.501	1.518	1.36	1.196	1.021	0.019
Trial 3	0.002	1.518	1.4	1.627	1.176	1.089	0.019
Mean Absorbance	0.002	1.524	1.502	1.344	1.087	1.044	0.02
Mean OD-Mean Blank		1.5223	1.5003	1.3423	1.0847	1.042	0.018
Standard deviation		0.0271	0.0955	0.2908	0.1723	0.0390	0.0017
Standard error		0.0156	0.0551	0.1679	0.0995	0.0225	0.0010
% Standard error		1.0263	3.6207	11.0293	6.5361	1.4781	0.0657
% Viability		100	98.5500	88.1800	71.250	68.450	1.1800

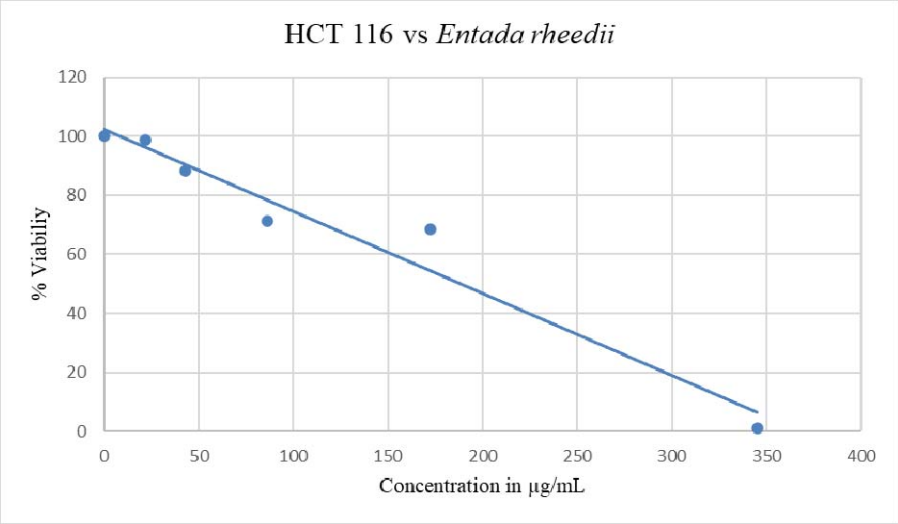

Figure 3. Effect of lectin on cell survival on HCT 116 human colorectal cancer cells. MTT assay. The Y-Axis represents the % cell viability and the X-axis represents the administered dosage in increasing concentrations ranging between 0 to 345*µ*g/mL. The scatter plot also depicts a trend line showing the cytotoxic nature upon administration of *E.rheedii* crude lectin extract.

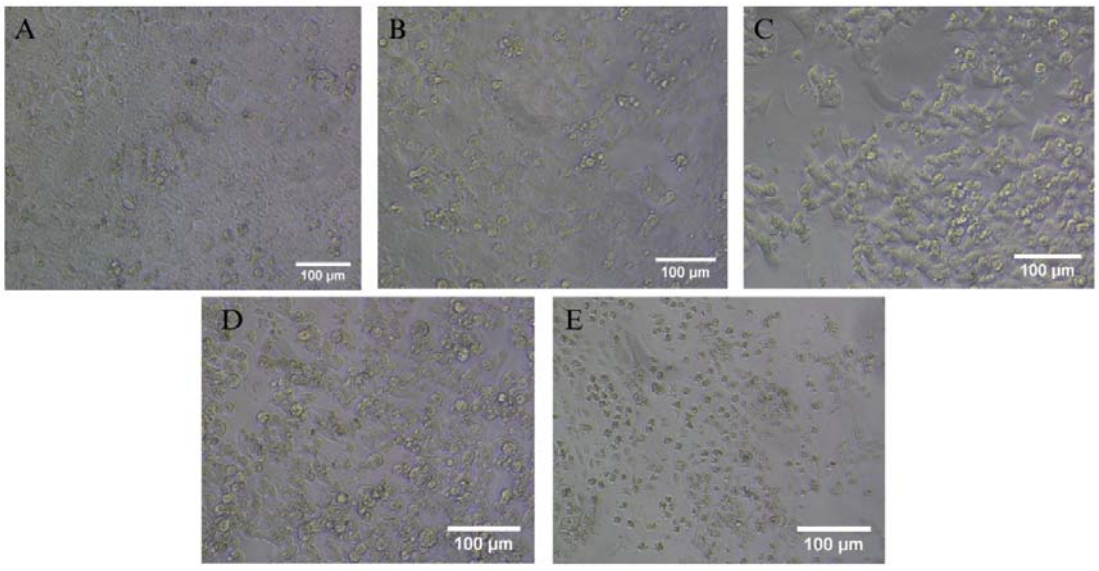

Figure 4. Cytotoxic effect of different concentration of lectin extract of *E. rheedii* administered on HCT 116 - Human colorectal cancer cells: (A). 21.56 µg/mL, (B). 43.12 µg/mL, (C). 86.25 µg/mL, (D). 172.5 µg/mL and (E). 345 µg/mL.

4. Discussion

With increasing occurrences of cancer, there is a dire need for safe alternative therapies; either from nutritional changes or lifestyle changes with the former being a more promising section that allows exploration in the field of medicaments from nature. Extensive review of literature indicated that different seed and plant contents of *E. rheedii* possess medicinally active principles.

In the present study, lectin from seed proteins were purified by ammonium sulphate protein precipitation, desalting and dialysis, followed by PEG assisted-osmosis driven protein concentration yielding a pure and concentrated form.

On account of the above-mentioned "requirement of changes" in nutritional habits as a cancer preventive/treatment measurement, legume lectins included as a part of the diet as a nutritional therapy may possibly prove helpful in detecting, targeting and applying its antiproliferative abilities onto cancers particularly occurring in the course of the digestive system. Since lectins surpass the digestive system without loss of activity or any structural degradation, *E. rheedii,* if included in the diet, upon reaching the colon may provide a fixed and more targeted delivery of the Entadin lectin and may help induce its therapeutic features by acting on the surrounding colorectal cancer cells.

Lectins, including soybean lectins, have been shown to have anti-inflammatory and antioxidant properties, which are associated with chemopreventive effects in colorectal cancer. Lectin-binding patterns in tumors have been strongly linked to their biological behaviour in this type of cancer. Soybean bioactive proteins and peptides, such as lectins, have been studied for their antioxidant and anti-inflammatory properties in relation to colorectal cancer prevention. Research has demonstrated that soybean lectins can boost the immune response, exert chemopreventive effects, and affect protein kinases in cell-based assays by inducing cytotoxic activity, apoptosis, reducing cell proliferation, arresting the cell cycle through the caspase cascade, inhibiting telomerase activity and angiogenesis (Chakrabarti *et al*., 2014, Chen & Hsieh, 2018, Pan *et al*., 2011).

Chemoprevention aims to reduce the risk of cancer by understanding it as a complex, multistep process at the molecular and cellular level. It uses protective compounds to stop or reverse the development of cancerous cells (Greenwald *et al*., 1995). Similarly, from comparative decipherment, it can be hypothesized that bioactive proteins, specifically lectins from *E. rheedii,* being a natural dietary compound, may also exhibit similar chemopreventive properties which can be attributed to its proven anti-inflammatory and antioxidant properties as shown by Okba *et al.,* (2013) and Nzowa *et al.,* (2010).

Performing a cell viability assay, such as an MTT dosage-dependent assay, can help to strengthen the hypothesis that including lectins from *E. rheedii* in the diet can effectively and directly impact colon cancer cells. This would also associate the relevance of utilizing *E. rheedii* lectins as a potential anti-cancer molecule against HCT 116.

A frequently observed glycosylation abnormality in colon cancer and precancerous conditions is the elevated presence of the disaccharide molecule composed of galactose and N-acetylgalactosamine connected by a beta-1,3 glycosidic linkage, within the mucosal layer (Evans *et al*., 2002; Greenwald *et al*., 1995). Further, from earlier studies of Nadia *et al.,* 2011 (Arndt *et al*., 2011) and Naik *et al.,* 2020 (Naik & Kumar, 2020), it is understood that there is overexpression of lactose and galactose moieties on the altered cell surface of HCT 116. In parallel, it is also known that lectin from *E. rheedii* shows carbohydrate specificity towards lactose and galactose. This may possibly be beneficial, as the key aspect of lectins to be able to promote its antiproliferative activity lies in the binding of lectins onto the specific carbohydrates present on the cell surface.

The glyco-biological profile of HCT116 and other colorectal cancer cells reveals the overexpression of Lewis Antigens (LeX and LeA) as glyco-epitopes (Shimizu *et al*., 2023). These LeX and LeA as well as their respective sialylated derivatives play a vital role in cancer cell adhesion, tumour formation and malignant transformation (Durrant *et al*., 2012). Lewis Antigens are well known to bind to selectins (or cell surface C-type Lectins). This leads to another strong hypothesis that the *Entada rheedii* lectin has the potential to selectively target Lewis Antigen expressing colorectal cancer cells (such as HCT116), providing another epitope for targeted induction of necrosis or apoptosis.

MTT analysis conducted on HCT 116 cells exposed to *Entada rheedii* lectin gave an IC_{50} value of 188.72µg/mL. The results showed that a concentration of 345µg/mL of *Entada rheedii* lectin must be used to reduce the viability of colorectal cancer cells to 1.18%. This can be seen in the increase in the number of apoptotic bodies constricted cell shape and darker appearance with increase in concentration (Figure 4). Studies done on *Entada rheedii* by Naik *et al*. (2020) solidifies the theory of *Entada rheedii* lectin being apoptotic in nature towards cervical cancer cells and lung cancer cell lines. HCT 116 cells clearly express Neu5Acα6Gal glycosyl and sometimes mannose complexes.

Other lectins and plant phytocompounds have been studied for their reaction with HCT 116 cells. Lectins from *Eclipta alba* and *Origanum vulgare* all show a similar range of IC_{50} values of 160 µg/mL, 256 µg/mL, 179 ± 0.81 µg/mL and 140.77 ± 2.13µg/mL respectively (Kabir *et al*., 2021), (Nelson *et al*., 2020) and (Jovankić *et al*., 2022). The diethyl ether lectin extract from the plant *Utrica urens* subjected to MTT analysis gave an IC_{50} value of 41.21µg/mL for HCT116 cells (Gaafar *et al*., 2020). Similarly, the *B. papyrifera* lectin showed cytotoxicity towards HCT116 cells with an IC_{50} value of 71.50 ± 9.24 µg/mL (Kumar *et al*., 2014). *Entada rheedii* lectin also falls in the same range with an IC_{50} value of 188.72µg/mL. As a potential drug, it is necessary to consider the toxic effects lectins have on the human body. As previously stated, the toxicity of *Entada rheedii* lectin on normal, non-cancerous African Green Monkey Normal Kidney Cells was analysed by MTT assay in the paper Naik *et al*., 2020 and shown to have no significant effect on the cell viability. The garlic lectin showed cytotoxicity towards U937 and HL60 cells but not towards human leukocytes (Karasaki *et al.,* 2001). Numerous lectins have shown their selective cytotoxicity to cancer cells, but *Entada rheedii* lectins's toxicity towards normal human colon cells needs to be further evaluated.

Through MTT Analysis, cytotoxicity and anti-cancer activity of Entadin has been established against Human colorectal cancer cells, Lung cancer and Cervical cancer cells (Naik *et al.,* 2020). This concludes that *Entada rheedii* can be a potential anti-cancer medicament for more than one cancer type. Being a natural phytocompound, ingestion of Entadin as a prepared colorectal cancer drug should aid in easy drug delivery to the affected colon. More research is needed to understand the anti-tumour pathway induced by Entadin, but this potential should be recognized in future studies.

5. Conclusion

E.rheedii lectins showed significant hemagglutinating activity against chicken erythrocytes. A 0.15 M phosphate buffer saline was used, which is a novel method for the extraction of proteins. The study introduced desalting and PEG-assisted osmosis-driven protein concentration techniques. The carbohydrate binding protein was stable when stored at 0-4 ºC for up to three weeks. This was confirmed by weekly hemagglutination. This study revealed the antiproliferative effect of *E. rheedii* lectins on the HCT 116 cell line, with an IC_{50} value of 188.72 µg/mL, indicating significant therapeutic promise. Moreover, the study successfully isolated, purified, and confirmed the stability of lectin extracts, thereby affirming their potential as effective therapeutic agents targeting transformed colon cells.

Acknowledgment

The authors profoundly thank PES University for the financial support provided as a University internal grant for the investigation.

Conflict of interest

This study was equally contributed to by all authors, and they declare that they have no conflict of interests.

References

Adamová, L., Malinovská, L., & Wimmerová, M. (2014). New sensitive detection method for lectin hemagglutination using microscopy. Microsc. Res. Tech., **77(10),** 841–849.

Arndt, N. X., Tiralongo, J., Madge, P. D., von Itzstein, M., & Day, C. J. (2011). Differential carbohydrate binding and cell surface glycosylation of human cancer cell lines. J. Cell. Biochem., **112(9),** 2230–2240.

Burger, M. M. (1969). A difference in the architecture of the surface membrane of normal and virally transformed cells. Proc. Natl. Acad. Sci. U.S.A., 62(3), 994–1001. https://doi.org/10.1073/pnas.62.3.994

Chakrabarti, S., Jahandideh, F., & Wu, J. (2014). Food-derived bioactive peptides on inflammation and oxidative stress. Biomed. Res. Int., 2014, 608979.

Chen, S., & Hsieh, C. (2018). Chemoprevention by means of soy proteins and peptides – current status and future approaches: a review. Int. J. Food Sci. Technol., **54(5),** 1460–1466.

https://doi.org/10.1111/ijfs.14053

Choudhari, A. S., Mandave, P. C., Deshpande, M., Ranjekar, P., & Prakash, O. (2020). Phytochemicals in cancer treatment: From preclinical studies to clinical practice. Front. Pharmacol., 10. https://doi.org/10.3389/fphar.2019.01614

De Mejía, E. G., & Prisecaru, V. I. (2005). Lectins as bioactive plant proteins: a potential in cancer treatment. Crit. Rev. Food Sci. Nutr., **45(6),** 425–445.

Durrant, L. G., Noble, P., & Spendlove, I. (2012). Immunology in the clinic review series; focus on cancer: glycolipids as targets for tumour immunotherapy. Clin. Exp. Immunol., **167(2),** 206–215.

Evans, R. C., Fear, S., Ashby, D., Hackett, A., Williams, E., Van Der Vliet, M., Dunstan, F. D. J., & Rhodes, J. M. (2002). Diet and colorectal cancer: an investigation of the lectin/galactose hypothesis. Gastroenterology, **122(7),** 1784–1792.

Esumi-Kurisu, M., Iwata-Dohi, N., Mizuno, D., & Yamazaki, M. (2008, March 17). Inhibition of murine tumor development by the lectin wheat germ agglutinin. Gann (Japanese Journal of Cancer Research).https://www.jstage.jst.go.jp/article/cancersci1959/74/3/74_3_398/_article/-char/ja/

Gaafar, A. A., Ali, S. I., Kutkat, O., Kandeil, A. M., & El-Hallouty, S. M. (2020). Bioactive ingredients and anti-influenza (H5N1), anticancer, and antioxidant properties of Urtica urens L. Jordan J. Biol. Sci., 13.

Goldring, J. P. D., & Dean Goldring, J. P. (2019). Concentrating proteins by salt, polyethylene glycol, solvent, SDS precipitation, three-phase partitioning, dialysis, centrifugation, ultrafiltration, lyophilization, affinity chromatography, immunoprecipitation or increased temperature for protein isolation, drug interaction, and proteomic and peptidomic evaluation. In **Methods in Molecular Biology** (pp. 41–59). https://doi.org/10.1007/978-1-4939-8793-1_4

Gorakshakar, A. C., & Ghosh, K. (2016). Use of lectins in immunohematology. Asian J. Transfus. Sci., 10(1), 12.

Greenwald, P., Kelloff, G. J., Boone, C. W., & McDonald, S. S. (1995). Genetic and cellular changes in colorectal cancer: proposed targets of chemopreventive agents. Cancer Epidemiol. Biomarkers Prev., **4(7),** 691–702.

Grimes, S. E. (2002). A basic laboratory manual for the small-scale production and testing of I-2 Newcastle disease vaccine (RAP publication 2002/22). FAO Regional Office for Asia and the Pacific (RAP), Senior Animal Production and Health Officer and Secretary of APHCA. ISBN 974-7946-26-2, https://www.fao.org/4/ac802e/ac802e0d.htm#bm13

Gurib-Fakim, A. (2013). African flora as potential sources of medicinal plants: towards the chemotherapy of major parasitic and other infectious diseases: a review. Jordan J. Biol. Sci., 6(2).

How to calculate IC50 (no date) Star Republic: Guide for Biologists.https://www.sciencegateway.org/protocols/cellbio/drug/hcic50.htm (Accessed: December 2022).

Govindaraj, S., & Ranjithakumari, B. D. (2013). Composition and larvicidal activity of Artemisia vulgaris L. stem essential oil against Aedes aegypti. Jordan J. Biol. Sci., **6(1),** 11-16.

Jovankić, J., Nikodijević, D., Blagojević, S., Radenković, N., Jakovljević, D., Grbović, F., & Cvetković, D. (2022). The biological activity of Ocimum minimum L. flowers on redox status parameters in HCT-116 colorectal carcinoma cells. Kragujevac J. Sci., (Issue 44), 155-168. https://doi.org/10.5937/kgjsci2244155j

Kabir, S. R., Islam, J., Ahamed, M. S., & Alam, M. T. (2021). Asparagus racemosus and Geodorum densiflorum lectins induce apoptosis in cancer cells by altering proteins and genes expression. Int. J. Biol. Macromol., 191, 646–656.

Karasaki, Y., Tsukamoto, S., Mizusaki, K., Sugiura, T., & Gotoh, S. (2001). A garlic lectin exerted an antitumor activity and induced apoptosis in human tumor cells. Food Res. Int., **34(1),** 7-13.

Kasapoğlu, T., & Dere, E. (2022). Roles of plant and fungal lectins in cancer diagnosis and treatment: a scoping review. Uluslararası Bilim Teknol. Tasarım Derg., **3(1),** 28–55.

Kelsall, A., FitzGerald, A. J., Howard, C. V., Evans, R. C., Singh, R., Rhodes, J. M., & Goodlad, R. A. (2002). Dietary lectins can stimulate pancreatic growth in the rat. Int. J. Exp. Pathol., **83(4),** 203–208.

Kumar, N., Naveen & Ramakrishnaiah, H. V., Krishna & Radhika, And. (2014). Cytotoxic activity of Broussonetia papyrifera (L.) vent on MCF-7, HeLa and HepG2 cell lines. Int. J. Pharm. Pharm. Sci., 6.

Law, I. J., & Strijdom, B. W. (1977). Some observations on plant lectins and Rhizobium specificity. Soil Biol. Biochem., **9(2),** 79–84. https://doi.org/10.1016/0038-0717(77)90041-4

Li, M., Li, C., Ma, C., Li, H., Zuo, H., Weng, S., Chen, X., Zeng, D., He, J., & Xu, X. (2014). Identification of a C-type lectin with antiviral and antibacterial activity from pacific white shrimp Litopenaeus vannamei. Dev. Comp. Immunol., **46(2)**, 231–240.

Liu, Y., Peterson, D. A., Kimura, H., & Schubert, D. (1997). Mechanism of cellular 3-(4,5-dimethylthiazol-2-yl)-2,5-diphenyltetrazolium bromide (MTT) reduction. J. Neurochem., 69(2). https://doi.org/10.1046/j.1471-4159.1997.69020581.x

Lowry, O. H., Rosebrough, N. J., Farr, A. L., & Randall, R. J. (1951). Protein measurement with the Folin phenol reagent. J. Biol. Chem., **193(1),** 265–275.

Maaroof, M. N., & Mahmood, A. E. (2019). Determination of the immunogenic and hematologic effects of titanium nanoparticles manufactured from Aspergillus flavus in vivo. Jordan J. Biol. Sci., 12(2).

Naik, S., & Kumar, S. (2020). Biochemical characterization of lactose-binding entadin lectin from Entada rheedii seeds with cytotoxic activity against cancer cell lines. ACS Omega, **5(27),** 16430–16439. https://doi.org/10.1021/acsomega.0c00577

Nelson, V. K., Sahoo, N. K., Sahu, M., Sudhan, H. H., Pullaiah, C. P., & Muralikrishna, K. S. (2020). In vitro anticancer activity of Eclipta alba whole plant extract on colon cancer cell HCT-116. BMC Complement. Med. Ther., **20(1),** 355.

Nzowa, L. K., Teponno, R. B., Tapondjou, L. A., Verotta, L., Liao, Z., Graham, D., Zink, M.-C., & Barboni, L. (2013). Two new tryptophan derivatives from the seed kernels of Entada rheedei: Effects on cell viability and HIV infectivity. Fitoterapia, **87**, 37–42.

Okba, M. M., Soliman, F. M., Deeb, K., & MF, Y. (2013). Botanical study, DNA fingerprinting, nutritional values and certain proximates of Entada rheedii Spreng. Int. J. Pharm. Pharm. Sci., **5(3),** 311–329.

Panda, P. K., Mukhopadhyay, S., Behera, B., Bhol, C. S., Dey, S., Das, D. N., Sinha, N., Bissoyi, A., Pramanik, K., Maiti, T. K., & Bhutia, S. K. (2014). Antitumor effect of soybean lectin mediated through reactive oxygen species-dependent pathway. Life Sci., **111(1-2),** 27–35.

Pan, M.-H., Lai, C.-S., Wu, J.-C., & Ho, C.-T. (2011). Molecular mechanisms for chemoprevention of colorectal cancer by natural dietary compounds. Mol. Nutr. Food Res., **55(1),** 32–45.

Phadungsil, W., & Grams, R. (2021). Agglutination activity of Fasciola gigantica DM9-1, a mannose-binding lectin. Korean J. Parasitol., **59(2),** 173–178. https://doi.org/10.3347/kjp.2021.59.2.173

Ryder, S. D., Smith, J. A., & Rhodes, J. M. (1992). Peanut lectin: A mitogen for normal human colonic epithelium and human HT29 colorectal cancer cells. J. Natl. Cancer Inst., 84(18), 1410–1416.

Sharon, N., & Lis, H. (1990). Legume lectins—a large family of homologous proteins. FASEB J., **4(14),** 3198–3208. https://doi.org/10.1096/fasebj.4.14.2227211

Shimizu, Y., Tamiya-Koizumi, K., Tsutsumi, T., Kyogashima, M., Kannagi, R., Iwaki, S., Aoyama, M., & Tokumura, A. (2023). Hypoxia increases cellular levels of phosphatidic acid and lysophospholipids in undifferentiated Caco-2 cells. Lipids. https://doi.org/10.1002/lipd.12366

Shivanna, M. B., & Rajakumar, N. (2011). Traditional medico-botanical knowledge of local communities in Hosanagara Taluk of Shimoga District in Karnataka, India. J. Herbs Spices Med. Plants, **17(3),** 291–317. https://doi.org/10.1080/10496475.2011.602617

Sitohy, M., Doheim, M., & Badr, H. (2007). Isolation and characterization of a lectin with antifungal activity from Egyptian Pisum sativum seeds. Food Chem., **104(3),** 971–979. https://doi.org/10.1016/j.foodchem.2007.01.026

Tamilarasan, K., Annapoorani, A., Manikandan, R., & Janarthanan, S. (2021). Isolation, characterization of galactose-specific lectin from Odoiporus longicollis and its antibacterial and anticancer activities. Int. J. Biol. Macromol., **183**, 1119–1135.

Thies, A., Dautel, P., Meyer, A., Pfüller, U., & Schumacher, U. (2008). Low-dose mistletoe lectin-I reduces melanoma growth and spread in a scid mouse xenograft model. Br. J. Cancer, **98(1),** 106–112. https://doi.org/10.1038/sj.bjc.6604106

Yau, T., Dan, X., Ng, C., & Ng, T. (2015). Lectins with potential for anti-cancer therapy. Molecules, **20(3),** 3791–3810. https://doi.org/10.3390/molecules20033791

JJBS

Volume 17, Number 3,September 2024
ISSN 1995-6673
Pages 549 – 554
https://doi.org/10.54319/jjbs/170318

Jordan Journal of Biological Sciences

The significance of FEV1 and FEV1/FVC in COPD diagnosis

Arwa I Rawashdeh*

Department of Biochemistry and physiology, Faculty of Medicine, Mutah University, Jordan

Received: March 2, 2024; Revised: March 31, 2024; Accepted: April 13, 2024

Abstract

Objectives: The forced expiratory volume in the first second (FEV1) and FEV1/FVC ratio alone is limited in its ability to expose COPD's complexity. Given the heterogeneity of the affected population, the use of additional pulmonary function tests (PFTs) in the routine clinical evaluation of COPD patients may be beneficial.

Methods: A total of 598 male individuals aged 25-80+ years were recruited for this study. Spirometry testing was conducted using the SPIROVIT SP-1G2 device manufactured by SCHILLER Switzerland, in accordance with the American Thoracic Society criteria for spirometry. High-intensity interval training (HIIT) was used to evaluate the impact of exercise on respiratory function and dyspnea experienced by COPD patients.

Results: Participants in this study were defined as Non-smoker and healthy if they reported never smoking and did not have asthma, bronchitis, angina pectoris, myocardial infarction, or stroke. FEV1% predicted and FVC% predicted were calculated using the Norwegian equation developed by Langhammer and co-workers. Independent samples T-tests were employed to examine the statistical significance of group differences. The mean and the 5% percentile of FEV1/FVC% were compared with the expected mean and lower limit of normal (LLN) using an equation developed by Enright and co-workers. The statistical analyses were performed using SPSS 16.0 for Windows (SPSS Inc, Chicago, Illinois, USA).

The study results indicated that there was a continuous increase in chances of any respiratory symptom as FEV1/FVC ratios increased and FEV1 in men ≤ 50, reaching a minimum of 0.85 and 0.90, respectively, in all participant characteristics. This would suggest a higher optimal threshold associated with respiratory symptoms than the commonly used threshold of 0.70. Conversely, the chances of any respiratory symptom continued to decrease with lower FEV1/FVC ratios and FEV1 in men >50 and reached a minimum of 0.66 and 0.75, respectively, in all participant characteristics, suggesting a lower optimal threshold associated with respiratory symptoms than the commonly used threshold of 0.70.

Conclusion: Incorporating additional PFTs beyond FEV1 and FEV1/FVC is crucial for a comprehensive evaluation of COPD patients and can lead to more personalized and targeted care.

Keywords: COPD, FEV1, FV1/FVC, GOLD Threshold

1. Introduction

The Global Initiative for Obstructive Lung Diseases (GOLD) recommends using a fixed ratio of FEV1/FVC < 0.70 to diagnose chronic airflow limitation (Cui *et al*., 2019). However, the suggested cut-off limits for this ratio range between 0.60 and 0.75, with many researchers stating that the fixed threshold of 0.70 is based on expert opinion rather than population-based evidence (Cui *et al*., 2019).

The underlying assumption is that this limit is a clinically useful marker of increased morbidity and mortality. There is a lack of population-based evidence to support that the exact threshold < 0.70 for the FEV1/FVC ratio is the most discriminative limit for prediction of morbidity and mortality (Johannessen *et al*., 2005b).

There are limitations to the use of FEV1 alone as a diagnostic tool for COPD (Maldonado-Franco *et al*., 2023). One such limitation is over-diagnosis in older patients as a result of using a fixed FEV1/FVC ratio as a diagnostic cutoff, as their measured FEV1/FVC values may be within the normal range for their age and health status (Vaz Fragoso *et al*., 2016). Conversely, using the fixed FEV1/FVC ratio may result in underestimating the presence of COPD in younger patients, as their measured values may fall within the normal range despite having the disease (Torén *et al*., 2021).

FEV1 measurement alone as a diagnostic tool for COPD also has limitations, including its insensitivity to early-stage COPD. Because small airway narrowing is not yet extensive in early-state COPD, FEV1 measurement may not be an accurate marker of airway obstruction (Kakavas *et al*., 2021). Additionally, FEV1 measurement only provides information on the first second of forced exhalation, during which small airways experience substantial distending forces, meaning that small airway obstruction may not be noted unless extensive narrowing is present (Medbø and Melbye, 2007).

Pulmonary function tests (PFTs) are important tools for COPD phenotyping and individualized care. These tests can provide additional information beyond FEV1 measurement and help guide treatment decisions (Bestall *et al*., 1999).

* Corresponding author. e-mail: drarwa@mutah.edu.jo.

Examples of PFTs that contribute to COPD phenotyping and individualized care include diffusion capacity measurements (DLCO), which can help assess the extent of gas exchange abnormalities in COPD patients and guide treatment decisions and field and cardiopulmonary exercise testing (Haynes *et al*., 2023). These tests provide dynamic physiological information and can reveal abnormalities in patients who present with normal spirometry but report respiratory discomfort when engaged in various activities. They can also assess exercise capacity and peak oxygen uptake, which correlates with survival in COPD patients (Bhatt et al., 2019; Bhatt *et al*., 2014).

Another such example is a forced oscillation technique, which measures respiratory impedance and can provide information about airway resistance and lung mechanics. It can be useful in assessing small airway dysfunction in COPD patients. Other PFTs that may contribute to COPD phenotyping and individualized care include lung volume measurements, airway resistance measurements, and bronchodilator responsiveness testing (Lange *et al*., 2016).

Pulmonary function tests (PFTs) can provide a more comprehensive evaluation of COPD patients beyond FEV1 and FEV1/FVC ratio measurement, allowing for a better understanding of the underlying pathophysiological processes and functional profiles. These tests can also help tailor medical management for the specific needs of each patient, thereby optimizing patient care and improving clinical outcomes (Pierson, 2006).

This paper discusses the limitations of the fixed ratio approach for diagnosing chronic airflow limitation (CAL) and the need for alternative thresholds. We are concerned about over-diagnosis and misclassification, particularly in older and younger adult males, where both old individuals with normal lung function but lower FEV1/FVC ratio and FEV1 and young individuals with lung disease and higher FEV1 and FEV1/FVC ratio may be included in the CAL category.

Also, this paper highlights the ongoing debate between the fixed ratio approach and the lower limit of normal (LLN) approach for defining CAL, with the LLN approach considering significant deviation from normality using equations based on different populations.

2. Methods

2.1. Sample size

A total of 598 male individuals were recruited for the purpose of this study.

2.2. Study population

Subjects aged 25-80+ years were recruited. After a thorough explanation of the experiment, each participant provided informed consent. The subjects were asked to fill out questionnaires about their medical history to ensure they had no serious conditions and were a good fit for our study.

2.3. Protocol

We used High-intensity interval training (HIIT) to evaluate the impact of exercise on respiratory function and dyspnea in patients with COPD. All the participants were instructed to perform six cycles of high intensity rebounding for 90 seconds, followed by 60 seconds of recovery (Rawashdeh and Alnawaiseh, 2018a).

2.4. Examinations

Spirometry testing was conducted using the SPIROVIT SP-1G2 device manufactured by SCHILLER Switzerland, in accordance with the spirometry criteria established by the American Thoracic Society (Rawashdeh and Alnawaiseh, 2018b).

The participants were seated, wearing a nose clip, and instructed to exhale for at least six seconds, or as long as possible. They were also asked to take a complete inspiration before inserting the provided mouthpiece. It was necessary to exhale at least three times. The difference in FEV1 and FVC between the best and next best should not be larger than 5% or 200 ml (Medbø and Melbye, 2007).

2.5. Statistical analysis

Using a variety of factors, including sex, age, smoking behaviors, and reported lung and cardiovascular disease, our study utilized the following methods to analyze spirometric results and symptoms:

- Participants were considered healthy non-smokers if they had never smoked and had never had asthma, bronchitis, angina pectoris, myocardial infarction, or stroke.
- FEV1% predicted and FVC% predicted were calculated using the Norwegian equation developed by Langhammer and co-workers (Langhammer *et al*., 2001).
- Independent samples T-tests were conducted to see if there were statistically significant differences between groups.
- The mean and the 5% percentile of FEV1/FVC% were compared with the expected mean and lower limit of normal (LLN) using an equation developed by Enright and co-workers (Enright *et al*., 1993).
- The statistical analyses were performed using SPSS 16.0 for Windows (SPSS Inc, Chicago, Illinois, USA).
- The Ethics Committee/ Mutah University/School of medicine/ Al-Karak, Jordan approved this study, and all participants provided written informed consent.

3. Results

Spirometry was performed in 598 individuals, and the results were analyzed. In men aged 50 or younger. Regardless of age, smoking status, or disease, the predicted mean FEV1% was less than 90% and the predicted FVC% was greater than 90% for all age groups. However, the FEV1/FVC ratio was less than 85%, which decreased significantly with increasing age, regardless of smoking behaviors and any kind of disease (P=0.001 in Table 1).

In men older than 50, the predicted FEV1% was less than 75%, and the predicted FVC% was greater than 75%, which decreased significantly with increasing age (P=0.001 in Table 1). Moreover, the FEV1/FVC ratio was less than 66%, which decreased significantly with increasing age, regardless of smoking behaviors and any kind of disease (P=0.001 in Table 1).

Individuals who reported chronic pulmonary disease had significantly lower lung function measures than those not reporting pulmonary or cardiovascular disease

(P=0.001, Table 1). Furthermore, there was a strong association between reports of cardiovascular illness and decreased lung function in men (P=0.001 in Table 1).

Table 1. Results from spirometric test on 598men, by age, smoking status, reported diseases, and healthy men who never smoked.

Age group	FEV1 % Predicted Mean	FVC % Predicted Mean	FEV1/FVC % Mean
Mean	78.81	82.84	72.84
25-35	88.7	92	84.8
36-40	87.7	91.6	82.8
41-50	85.1	90.2	82.3
51-60	74.7	79.1	65.98
61-70	73.5	78.5	65.50
71-80	72	75.5	64.6
80+	70	73	63.9
Smoking behaviors			
Never Smoked	88	93	78
Ex-Smoker	77	78	72
Flow –Smoker	70.3	75	66
Revealed cardiovascular illness			
Myocardial infarction	78	79	72.5
Angina pectoris	76	80	71.2
Revealed Pulmonary illness			
Asthma	69	71.1	67.4
Chronic Bronchitis	68	74	67.5
Non-smoker and healthy	89	92	77

Of the 598men, 30.86% were aged 50 or younger, while 68.99% were older than 50. Asthma and bronchitis have been recorded. 5% and 3% of men, respectively, while cardiovascular diseases were reported by 3.59% for myocardial infarction and 2% for angina pectoris. The percentage of Never Smoked was 41.75%, former smokers were 3.67%, and flow smokers were 15%. Non-smoker and healthy accounted for 26.35% of the total population (Table 2).

Table 2. Characteristics of the participants in the study

Age (years)	%
25-35	11.6
36-40	12
41-50	7.26
51-60	15.56
61-70	30.63
71-80	8.8
80+	14
Smoking behaviors	
Never Smoked	41.75
Former smokers	3.67
Flow smokers	15
Pack-Years smoked	
<10	12
10-19	11
20-29	13
30+	14
Revealed cardiovascular illness	
Myocardial infarction	3.59
Angina pectoris	2
Revealed Pulmonary illness	
Asthma	5
Chronic bronchitis	3
Non-smoker and healthy	26.53

In Table 3, regardless of smoking behaviors or pulmonary and cardiovascular disease, the incidence of FEV1/FVC ratios <70% and FEV1 <80% increases with age. The frequency is around three times higher among men over 50 years of age who currently smoke than men aged 50 or younger (81.5% and 26%, respectively) (p=0.001) who currently smoke. In Never Smoked over 50 years of age, the incidence of FEV1/FVC ratio <70% and FEV1<80% is five times higher than those aged 50 or younger (53% and 10%, respectively) (p=0.001). The frequency of FEV1/FVC ratio <70% and FEV1<80% among Non-smoker and healthy over 50 years of age is around five times higher than in Non-smoker and healthy aged 50 or younger (54.5% and 12%, respectively) (p=0.001).

Table 3. The percentage of FEV1/FVC 70% and FEV1 80% across all groups, based on age, smoking behaviors, reported disease, and healthy nonsmokers.

Age group	Non-smoker and healthy	Never Smoked	Flow smokers	Pulmonary disease	Cardiovascular disease
25-35	5	3	23	13	11
36-40	11	9	25	14	12
41-50	20	18	30	15	13
51-60	40	38	72	15	15
61-70	48	41	80	16	15
71-80	60	60	86	18	16
80+	70	73	88	20	17

Using FEV1/FVC < 66% and FEV1 < 75% to diagnose COPD in individuals over 50 years of age can significantly reduce the prevalence of COPD. Specifically, the prevalence of COPD would decrease from 81.5% to 40.75% in flow smokers, from 54.5% to 27.25% in Non-smoker and healthy, from 53% to 30.5% in Never Smoked

s, from 17% to 12% in pulmonary disease, and from 15.75% to 11% in cardiovascular disease (P = 0.001-0.005 in Tables 3 and 4). These findings suggest that using a lower threshold for the FEV1/FVC ratio may be more appropriate for diagnosing COPD in older individuals, as the FEV1/FVC ratio declines with age.

Table 4. Percentage (%) of FEV1/FVC< 66 % and FEV1 < 75 by age, smoking behaviors, reported sickness and for the Non-smoker and healthy among men > 50 years.

Age group	Non-smoker and healthy	Never Smoked	Flow smokers	Pulmonary disease	Cardiovascular disease
51-60	20	25	36	11	10
61-70	24	27	40	12	11
71-80	30	33	43	13	11
80+	35	37	44	14	12

While utilizing FEV1/FVC < 85% and FEV1 < 90% to analyze COPD in people under 50 years old, the commonness of COPD would increment from 26% to 36% in flow smokers, from 14% to 22% in pneumonic illness, and from 12%to 22.6% in cardiovascular sickness s(P = 0.001-0.004) (Tables 4 and 5). However, there would be no change in the prevalence of COPD in healthy smokers or Never Smoked. These findings suggest that using a lower threshold for the FEV1/FVC ratio may not be appropriate for diagnosing COPD in younger individuals.

Table 5. Percentage (%) of FEV1/FVC< 85% and FEV1 <90% in men 50 years of age by age, smoking behaviors, reported disease, and for the healthy never smoker.

Age group	Non-smoker and healthy	Never Smoked	Flow smokers	Pulmonary disease	Cardiovascular disease
25-35	7	3	35	20	20
36-40	10	9	36	22	22
41-50	20	18	37	25	26

Table 6 provides evidence supporting the use of a lower threshold in men older than 50 and a higher threshold in men aged 50 or younger for defining COPD. Specifically, the odds for any respiratory symptom, such as dyspnea, decreased with a lower threshold FEV1<75% and FEV1/FVC<66% in men older than 50. Conversely, the odds for any respiratory symptom, such as dyspnea, increased with higher FEV1<85% and FEV1/FVC<95% in men ≤ 50.

Table 6. Observed dyspnea by age group, smoking behaviors, and illnesses.

Age group (years)	Dyspnea Non-smoker and healthy	Dyspnea in Never Smoked	Dyspnea flow smokers	Dyspnea in pulmonary disease	Dyspnea in cardiovascular disease
25-35	5	2	33	22	20
36-40	11	8	35	24	23
41-50	19	17	37	26	25
51-60	22	27	38	12	10
61-70	26	29	42	13	11
71-80	32	35	45	15	12
80+	37	39	46	17	13

Numbers given in %.

4. Discussion

The ongoing investigation discovered that lung capability measures; for example, FEV1% predicted and FVC% predicted are affected by both increasing age and a smoking behavior. This suggests that these factors can contribute to decreased lung function over time. The use of percentages to calculate the predicted values allowed for a more accurate comparison of lung function across different individuals and groups (Table 1) (Medbø and Melbye, 2007).

Moreover, the study found that individuals who reported chronic pulmonary or cardiovascular disease had significantly lower lung function measures compared to those who reported neither pulmonary nor cardiovascular disease (Enright *et al*., 1993, Ramalho *et al*., 2021). This suggests that chronic pulmonary and cardiovascular disease can significantly impact lung function, regardless of age or other factors. Table 1's presentation of these findings enabled for a clear and concise comparison of lung function measures across different groups.

These findings underscore the importance of maintaining healthy lung function through lifestyle choices and disease management. By understanding the factors that can contribute to decreased lung function, individuals can take steps to protect their respiratory health and prevent the development of chronic pulmonary disease (Rawashdeh and Alnawaiseh, 2018a, 2018b).

The study also revealed a significant drop in the FEV1/FVC ratio after the age of 50, and FEV1/FVC<70% and FEV1<80 was more common in older men than those aged 25–50 years (Table 3). The relative increase in frequency in all age groups was markedly higher among flow smokers than Non-smoker and healthy, indicating that smoking has a significant impact on the FEV1/FVC ratio and FEV1, as well as reported pulmonary and cardiovascular disease. However, it is uncertain whether the increase in incidence among healthy smokers with age represents an increase in COPD prevalence or simply the natural aging process (Johannessen *et al*., 2005b; Light and George, 1983).

According to our study, being a smoker is the most significant risk factor for developing COPD. Flow smokers

were significantly more likely to have FEV1/FVC < 70% and FEV1 < 80 than Non-smoker and healthy or Never Smoked s in all age groups (Table 3). Furthermore, a fifty percent decline in lung function can be explained in part by structural changes in the airways that occur with age, such as alveolar dilatation and loss of supporting tissue in the peripheral airways known as "senile emphysema" (Lundbäck *et al*., 2003a, Schneider *et al*., 2021).

Another characteristic of normal aging is muscle atrophy and decreased physical endurance (Hayes *et al*., 2023). Furthermore, the elderly have co-morbidities that might affect lung function, particularly pulmonary and cardiovascular illness, which are known to be related with lower spirometry values, including, in severe cases, the FEV1/FVC ratio and FEV1 (Lundbäck *et al*., 2003b)

Our study provides evidence supporting the use of a lower threshold in men older than 50 and a higher threshold in men aged 50 or younger for defining COPD. Specifically, the odds for any respiratory symptom, such as dyspnea, decreased with a lower threshold FEV1<75% and FEV1/FVC<66% in men older than 50 (Tables 4 and 6). Conversely, the odds for any respiratory symptom, such as dyspnea, increased with higher FEV1<85% and FEV1/FVC<95% in men aged 50 and younger (Tables 5 and 6)

There has been criticism of the use of the fixed ratio approach for diagnosing COPD due to concerns about overdiagnosis and misclassification. Specifically, over-diagnosis may occur in men older than 50, leading to the inclusion of individuals with normal lung function but lower FEV1 and FEV1/FVC ratios. This is because the fifth percentile for the ratio falls below 0.70 near age 45, which means that older patients may be misdiagnosed with airway obstruction if their FEV1/FVC falls below 0.70(Enright *et al*., 1993). Estimates of COPD over-diagnosis due to the fixed ratio ranged from 4.6% to 42.7% in different studies (Ekström *et al*., 2019).

Misclassification in men aged 50 and younger can occur due to the possibility that they are experiencing structural changes in the lungs and their increased respiratory morbidity and mortality is being classified as normal due to higher FEV1 and FEV1/FVC ratios. This is because FEV1 declines more rapidly than FVC with aging, leading to age-dependent decline in FEV1/FVC in healthy, non-smoking, elderly (Lundbäck *et al*., 2003a).

Our study highlights the limitations of using FEV1 and FEV1/FVC ratio alone for diagnosing COPD, as well as the need for additional pulmonary function tests to complement these measurements to provide a more comprehensive assessment of COPD patients. The ongoing debate between using a fixed ratio approach or the lower limit of normal (LLN) approach for defining CAL is discussed in several studies. The LLN approach takes into account reference equations developed from different normal populations and considers significant deviation from normality (Ekström *et al*., 2019; Lundbäck *et al*., 2003b).

In contrast, the fixed ratio approach assumes a certain airflow limitation is normal regardless of age, gender, or body size (Ekberg-Aronsson *et al*., 2005). The flow study suggests that the LLN approach may be more in line with statistical theory and should be further evaluated.

5. Conclusion

Our study highlights the need for further research to evaluate alternative thresholds, such as the LLN approach, for defining CAL and to investigate the clinical implications of different FEV1/FVC ratios and FEV1 in terms of respiratory morbidity and mortality. Incorporating additional PFTs beyond FEV1 and FEV1/FVC is crucial for a comprehensive evaluation of COPD patients and can lead to more personalized and targeted care.

Acknowledgement

The author would like to thank Prof. Sameeh Al-Sarayreh, Prof. Yousef Al-Saraireh and Prof. Jehad Al-Shuneigat for their help and support throughout this research study.

References

Bestall JC, Paul E, Garrod R, Garnham R, Jones P and Wedzicha JA. 1999. Usefulness of the Medical Research Council (MRC) dyspnoea scale as a measure of disability in patients with chronic obstructive pulmonary disease. *Thorax*., **54(7)**:581-586.

Bhatt SP, Balte PP, Schwartz JE, Cassano PA, Couper D, Jacobs DR Jr, Kalhan R, O'Connor GT, Yende S, Sanders JL, Umans JG, Dransfield MT, Chaves PH, White WB and Oelsner EC. 2019. Discriminative Accuracy of FEV1:FVC Thresholds for COPD-Related Hospitalization and Mortality. *JAMA*., **321(24)**: 2438-2447.

Bhatt SP, Washko GR, Dransfield MT, Sieren JC, Newell JD Jr and Hoffman EA. 2014. Comparison of spirometric thresholds in diagnosing smoking-related airflow obstruction:

authors' response. *Thorax*., **69(12)**:1147-1148.

Cui Y, Dai Z, Luo L, Chen P and Chen Y. 2019. Classification and treatment of chronic obstructive pulmonary disease outpatients in China according to the Global Initiative for Chronic Obstructive Lung Disease (GOLD) 2017: Comparison with GOLD 2014. *J Thorac Dis*., **11(4)**:1303-1315.

Ekberg-Aronsson M, Pehrsson K, Nilsson JA, Nilsson PM and Löfdahl CG. 2005. Mortality in GOLD stages of COPD and its dependence on symptoms of chronic bronchitis. *Respir Res*., **6(1)**:1-9.

Ekström MP, Blomberg A, Bergström G, Brandberg J, Caidahl K, Engström G, Engvall J, Eriksson M, Gränsbo K, Hansen T, Jernberg T, Nilsson L, Nilsson U, Olin AC, Persson L, Rosengren A, Sandelin M, Sköld M, Sundström J, Swahn E, Söderberg S, Tanash HA, Torén K, Östgren CJ and Lindberg E. 2019. The association of body mass index, weight gain and centralobesity with activity-related breathlessness: the Swedish Cardiopulmonary Bioimage Study. *Thorax*., **74(10)**: 958-964.

Enright PL, Kronmal RA, Higgins M, Schenker M and Haponik EF. 1993. Spirometry reference values for women and men 65 to 85 years of age. Cardiovascular health study. *Am Rev Respir Dis*., **147(1)**: 125-133.

Hayes EJ, Stevenson E, Sayer AA, Granic A and Hurst C. 2023. Recovery from Resistance Exercise in Older Adults: A Systematic Scoping Review. *Sports Med Open*., **9(1)**:51.

Haynes JM, Kaminsky DAand Ruppel GL. 2023. The Role of Pulmonary Function Testing in the Diagnosis and Management of COPD. *Respir Care*., **68(7)**:889-913.

Johannessen A, Omenaas ER, Bakke PS and Gulsvik A. 2005a. Implications of reversibility testing on prevalence and risk factors for chronic obstructive pulmonary disease: a community study. *Thorax*., **60(10)**: 842-847.

Johannessen A, Omenaas E, Bakke P and Gulsvik A. 2005b. Incidence of GOLD-defined chronic obstructive pulmonary disease in a general adult population. *Int J Tuberc Lung Dis*., **9(8)**: 926-932.

Kakavas S, Kotsiou OS, Perlikos F, Mermiri M, Mavrovounis G, Gourgoulianis K and Pantazopoulos I. 2021. Pulmonary function testing in COPD: looking beyond the curtain of FEV1. *NPJ Prim Care Respir Med*., **31(1)**: 1-11.

Lange P, Halpin DM, O'Donnell DE and MacNee W. 2016. Diagnosis, assessment, and phenotyping of COPD: beyond FEV. *Int J Chron Obstruct Pulmon Dis*., **19(11)**: 3-12.

Light RW and George RB. 1983. Serial pulmonary function in patients with acute heart failure. *Arch Intern Med*., **143(3)**: 429-433.

Langhammer A, Johnsen R, Gulsvik A, Holmen TL and Bjermer L. 2001. Forced spirometry reference values for Norwegian adults: the bronchial obstruction in Nord-Trondelag study. *Eur Respir J*., **18(5)**: 770-779.

Lundbäck B, Gulsvik A, Albers M, Bakke P, Rönmark E, van den Boom G, Brøgger J, Larsson LG, Welle I, van Weel C and Omenaas E. 2003a. Epidemiological aspects and early detection of chronic obstructive airway diseases in the elderly. *Eur Respir JSuppl*., **40**: 3s-9s.

Lundbäck B, Lindberg A, Lindström M, Rönmark E, Jonsson AC, Jönsson E, Larsson LG, Andersson S, Sandström T and Larsson K. 2003b. Not 15 but 50% of smokers develop COPD?-Report from the Obstructive Lung Disease in Northern Sweden Studies. *Respir Med*., **97(2)**: 115-122.

Maldonado-Franco A, Giraldo-Cadavid LF, Tuta-Quintero E, Bastidas Goyes AR and Botero-Rosas DA. 2023. The Challenges of Spirometric Diagnosis of COPD. *Can Respir J*.,**29**: 1-12.

Medbø A and Melbye H. 2007. Lung function testing in the elderly-Can we still use FEV1/FVC<70% as a criterion of COPD. *Respir Med*., **101(6)**: 1097-1105.

Pierson DJ. 2006. Clinical practice guidelines for chronic obstructive pulmonary disease: a review and comparison of current resources. *Respir Care*., **51(3)**: 277-288.

Ramalho SHR and Shah AM. 2021. Lung function and cardiovascular disease: A link. *Trends Cardiovasc Med*., **31(2)**:93-98.

Rawashdeh A and Alnawaiseh N. 2018a. Effects of cigarette smoking and age on pulmonary function tests in ≥ 40 years old adults in Jordan. *Biomed Pharmacol*., **11(2)**:789-793.

Rawashdeh A and Alnawaiseh N. 2018b. The effect of high-intensity aerobic exercise on the pulmonary function among inactive male individuals. *Biomed Pharmacol*., **11(2)**:735-741.

Schneider JL, Rowe JH, Garcia-de-Alba C, Kim CF, Sharpe AH and Haigis MC. 2021. The aging lung: Physiology, disease, and immunity. *Cell*.,**184(8)**:1990-2019.

Torén K, Schiöler L, Lindberg A, Andersson A, Behndig AF, Bergström G, Blomberg A, Caidahl K, Engvall JE, Eriksson MJ, Hamrefors V, Janson C, Kylhammar D, Lindberg E, Lindén A, Malinovschi A, Lennart Persson H, Sandelin M, Eriksson Ström J, Tanash H, Vikgren J, Johan Östgren C, Wollmer P and Sköld CM. 2021. The ratio FEV_1 /FVC and its association to respiratory symptoms-A Swedish general population study. *Clin Physiol Funct Imaging*., **41(2)**:181-191.

Vaz Fragoso CA, McAvay G, Van Ness PH, Casaburi R, Jensen RL, MacIntyre N, Yaggi HK, Gill TM and Concato J. 2016. Phenotype of Spirometric Impairment in an Aging Population. *Am J Respir Crit Care Med*., **193(7)**: 727-735.

JJBS

Volume 17, Number 3,September 2024
ISSN 1995-6673
Pages 555 – 560
https://doi.org/10.54319/jjbs/170319

Jordan Journal of Biological Sciences

Assessment of Hepato-Renal Functions and Markers of Oxidative Stress in Animals Exposed to Ionic Contrast Media

Amaka Okonkwo[1], Ngozi Rosemary Njeze[2], Kenechukwu Chibuike Onyekwelu[1,*], Chigozie Peace Okorie[1], Nonso Collins Ejiofor[1], Joy Ebele Ikekpeazu[1]

[1]*Department of Medical Biochemistry, Faculty of Basic Medical Sciences, College of Medicine, University of Nigeria Enugu Campus, Nigeria;*[2]*Department of Radiation Medicine, University of Nigeria Medical School, Ituku Ozalla Enugu*

Received: October 8, 2023; Revised: March 20, 2024; Accepted: April 13, 2024

Abstract

The increase in imaging technologies as well as many disease conditions requiring contrast media for diagnosis makes it important to investigate the effect of contrast media on hepato-renal function and its relation to oxidant and antioxidant status. To achieve this, twenty-five male albino rats were divided into 5 groups and administered with different doses of contrast agents (urografin and iohexol). After 48 hours of administration, 5 ml of blood samples was collected for the assessment of renal function, hepatic function and oxidative stress. The liver and kidneys were also excised for histological analysis. The result showed a significant increase (p=0.003) in the mean serum creatinine and urea in animals treated with either iohexol or urografin at different doses compared to the control. There was a significant increase (p=0.003) in serum malondialdehyde (MDA) level in contrast media group when compared with the control but serum total antioxidant status (TAS) level decreased in the groups administered with contrast media though the difference was not significant (p=0.003). Groups injected with iohexol showed no obvious histopathological alteration in both renal and hepatic tissues. In the groups treated with urografin, especially in higher dose, inflammatory cellular infiltration was observed at the peri-glomerular region and within the medulla in the kidney, while in the liver the portal tract appeared enlarged with infiltration of inflammatory cells. The result suggests that both iohexol and urografin are risk factors of kidney and liver damage as a result of increase in the pro-oxidant MDA and marked histomorphological alteration.

Keywords: Hepatic Function, Iohexol, Oxidative Stress, Renal Function, Serum Creatinine, Urografin.

1. Introduction

Technological advancements have led to the development of sophisticated imaging techniques used in the diagnosis of various human diseases. Such imaging techniques include computed tomography (CT), magnetic resonance imaging (MRI), digital subtraction angiography (DSA) and others which make use of contrast media/materials/agents that are introduced into the patient to aid image resolution by contrasting the selected areas of the body from surrounding tissue.[1] Contrast material can be administered orally, rectally or intravenously. Iodine-based contrast media are classified as high osmolality contrast media and low osmolality contrast media and are intravenously administered.[2]

Humans are exposed to many endogenous and xenobiotic substances that could have detrimental pathological outcomes if left un-modified and excreted.[3]When contrast materials are introduced intravenously, they move into the extracellular space through the vascular compartment and get eliminated by glomerular filtration. This may lead to dysfunction of the kidney, most especially in individuals with pre-existing health conditions like diabetes mellitus and renal impairment.[4] Apart from the kidney, the liver also plays an important role in the metabolism and biotransformation of these contrast materials. The detoxification of xenobiotics in the body is an important process in the maintenance of homeostasis, and any change in the homeostatic state could result to an imbalance in the dynamic equilibrium of metabolism leading to oxidative stress because of generation of reactive oxygen species (ROS) and liver dysfunction.[5-8]

To counter the damaging effects of reactive oxygen species, the body is endowed with antioxidant defence system that is made up of enzymes like glutathioneperoxidase (GPX), superoxide dismutase (SOD) and catalase, vitamins like vitamin E, C and A, and minerals like selenium, zinc, copper, and manganese which are produced either endogenously or received from exogenous sources. All of these play crucial roles in maintaining homeostasis.[9-12]

Creatinine, urea, serum electrolytes and uric acid are makers of renal function test[13], while markers of hepatic function test involve serum measurements of liver-derived enzymes like alanine aminotransferase (ALT), aspartate aminotransferase(AST), alkaline phosphatase and other non-enzymatic proteins.[14]Adverse reactions to intravenously administered contrast agents have been extensively investigated in humans and in animal models using mainly serum creatinine as a biomarker.[15-17] In

* Corresponding author. e-mail: kenechukwu.onyekwelu@unn.edu.ng.

humans, the use of contrast media may lead to contrast-induced nephrotoxicity (CIN) which is characterized by an increase in serum creatinine level within 24–72 hours following administration.[18-19]In addition to co-morbidities such as peripheral vascular disease, hypertension and anaemia[20], advanced congestive heart failure, diabetes mellitus and pre-existing renal impairment are some of the risk factors for contrast-induced nephrotoxicity.[21-22]Oxidative stress is one of the several mechanisms underlying CIN which result in the hypoxia of medulla and subsequent tubular damage.[23] Hypoxia may lead to the formation of reactive oxygen species which have been implicated in the toxicity of contrast agents.[24-25]

With the increase in disease conditions requiring contrast media for diagnosis, there is need to investigate the impact of contrast media using other markers of renal function apart from creatinine and markers of hepatic function among the exposed patients and also look at the level and effect of ROS generated in the course of using such contrast agents.

2. Materials and Methods

2.1. Experimental animals and groupings

Twenty-five (25) adult male albino rats weighing between 180-250g were procured for this study. The animals were acclimatized for 7 days under standard environmental conditions (temperature and humidity) and were given free access to rat chow and clean water *ad libitum*. The rats were randomly divided into 5 groups of 5 animals each. Group 1 (the control group) received l ml/kg body weight (bw) of physiological saline, group 2 and 3 received 1 and 3 ml/kg body weight of urografin, respectively, while group 4 and 5 received 1 and 3ml/kg body weight of iohexol, respectively. Animals were placed in individual metabolic cages and were deprived of water 24 hours before the administration of contrast media.

2.2. Collection of blood samples and processing

Exactly 48 hours after urografin and iohexol administration, 5 ml of blood samples was collected from the animals by retro-orbital bleeding under mild anesthesia (diethylether). Blood samples were collected using plain and EDTA tubes. Samples in the plain tubes were allowed to clot and centrifuged to get the serum which was stored at 4 °C until used. The liver and the kidney of all the rats were excised for histological investigations.

2.3. Biochemical analysis

Serum creatinine and urea levels were measured for the evaluation of renal function.

Creatinine level was determined as described by Mitchell (1973)[26], while the enzymatic method as described by Machado and Horizonte (1958)[27] was used for urea determination.

Levels of aminotransferase (ALT) and aspartate aminotransferase (AST) were measured for the evaluation of hepatic function. Alanine aminotransferase and aspartate aminotransferase levels were determined according to the method described by Reitman and Frankel (1975)[28].

Total antioxidant status (TAS) and malondialdehyde (MDA) were also measured to evaluate the level of oxidative stress. Based on the trolox equivalent antioxidant capacity method of Miller et al. (1993)[29] for quantitative assessment of *in vivo* antioxidant status, serum total antioxidant status (TAS) was determined using commercial Randox kit. The method of Ohkawa et al.(1979)[30] was used in the determination of malondialdehyde level. Using this method, 0.5 ml of plasma and 2.5 ml of 10% trichloroacetic acid were mixed and incubated for 15 min at 90°C. After cooling, the mixture was centrifuged at 3000 rpm for 10 min, 2 ml of the supernatant was added to 1 ml of 0.675% TBA solution in a test tube, sealed and incubated for 15 min at 90°C and then allowed to cool to room temperature. MDA level was measured spectrophotometrically at 532 nm wavelength.

2.4. Histological analyses

Liver and kidney of each rat were removed and, after histological processing, stained with ematoxylin and eosin. Stained sections were examined under light microscopy with different magnification, and the photograph of each of the slides was taken.

2.5. Statistical analysis

IBM SPSS 20.0 for windows was adopted for statistical analysis. Data were expressed as the mean ± SD. One-way analysis of variance (ANOVA) was used for comparisons of group data. Ducan multiple range test was used as a post-hoc test to determine where the exact difference lies, and p value $\leq$ 0.05 were considered as statistically significant.

2.6. Ethical Considerations

This study was carried out in accordance with the ethical standards of the University of Nigeria ethics committee on animal experimentation.

3. Results

3.1. Assessment of the effect of urografin and iohexol on renal function

The result of effect of urografin and iohexol on renal function is shown in table 1. It is shown that the mean creatinine and urea levels was significantly lower in the control groups compared to groups administered with contrast media, but there were no significant differences between groups with different doses of contrast media.

Table 1. Serum creatinine and urea values following administration of graded doses of urografin and iohexol

Groups	Creatinine (mg/dL)	Urea (mg/dL)
Group 1 (control)	2.46±0.36^{a}	67.27±8.56^{a}
Group 2 (1ml/kg bw of Urografin)	3.26±0.35^{b}	83.94±2.75^{b}
Group 3(3ml/kg bw of Urografin)	3.21±0.41^{b}	84.72±2.23^{b}
Group 4(1ml/kg bw of Iohexol)	3.20±0.18^{b}	81.24±4.49^{b}
Group 5(3ml/kg bw of Iohexol)	3.50±0.43^{b}	82.99±6.78^{b}

No significant difference exists between any groups with similar superscript in each row, and there is a significant difference if there is no similar superscript (p=0.003).

3.2. Assessment of the effect of urografin and iohexol on hepatic function

The serum ALT level of the animals in group 5 and group 3 that were treated with 3ml/kg of iohexol and 3ml/kg of urografin, respectively, were significantly higher (p=0.003) than the serum ALT levels of animals in group 2 and the control group, but there was no significant difference between the ALT level of animals in group 4 (iohexol 1ml/kg) and the other groups (Table 2).

Table 2.Serum ALT and AST values following administration of graded doses of urografin and iohexol

Groups	ALT (IU/L)	AST (IU/L)
Group 1 (control)	4.48±0.44[a]	13.80±5.29[a]
Group 2 (1ml/kg bw of Urografin)	4.60±0.60[a]	15.60±3.13[a]
Group 3(3ml/kg bw of Urografin)	6.28±1.38[b]	16.50±1.91[a]
Group 4(1ml/kg bw of Iohexol)	5.47±1.09[ab]	14.00±2.55[a]
Group 5(3ml/kg bw of Iohexol)	6.21±1.12[b]	13.75±1.80[a]

No significant difference exists between any groups with similar superscript in each row, and there is a significant difference if there is no similar superscript (p=0.003).

3.3. Assessment of effect of urografin and iohexol on oxidative stress

No significant difference was observed in the mean TAS level between the groups though the mean TAS level were found to be higher in the control group when compared with groups administered with contrast media (Table 3).

Table 3. Serum TAS and MDA values following administration of graded doses of urografin and iohexol

Groups	TAS (mg/dL)	MDA (mg/dL)
Group 1 (control)	2.43±0.28[a]	4.26±0.72[a]
Group 2 (1ml/kg bw of Urografin)	2.43±0.28[a]	4.98±0.80[a]
Group 3 (3ml/kg bw of Urografin)	1.99±0.35[a]	5.31±0.58[a]
Group 4 (1ml/kg bw of Iohexol)	1.80±0.31[a]	5.42±0.87[ab]
Group 5 (3ml/kg bw of Iohexol)	1.98±0.59[a]	6.50±0.99[b]

No significant difference exists between any groups with similar superscript in each row, and there is a significant difference if there is no similar superscript (p=0.003).

3.4. Histopathological examination of liver tissues

Histopathological examination of liver tissues of the control group showed normal histo-architecture of the hepatic tissue. The central vein (Cv), portal tract (Pt), and sinusoidal spaces (S) flanked by plates of hepatocytes (H) appear normal (figure 1). Those treated with iohexol (groups 4 and 5) showed no obvious histoarchitectural disruption with intact portal tract (Pt), hepatocytes (H), sinusoidal spaces (S) and central veins (Cv) (figure 2).

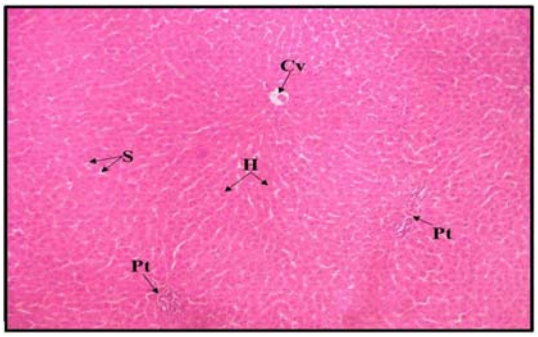

Figure 1: Photomicrograph of liver tissue section from control group 1 showing normal histo-architecture of the hepatic tissue.

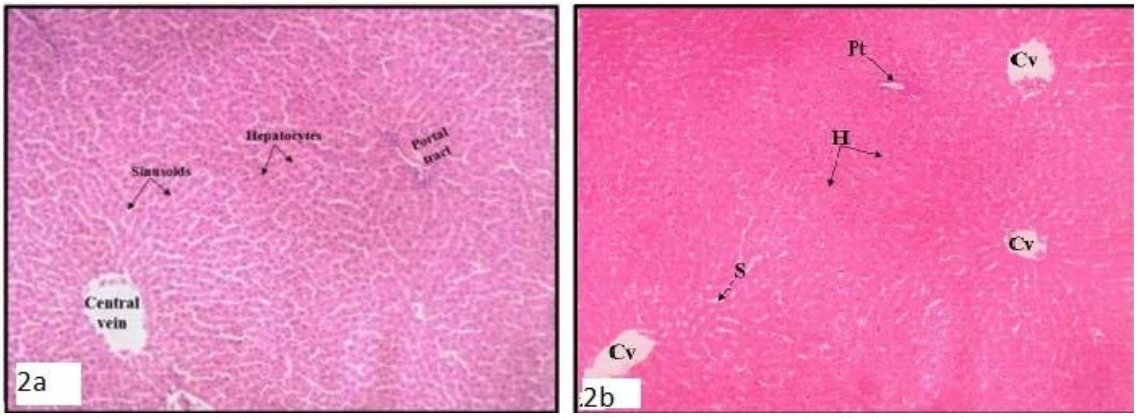

Figure 2: Photomicrograph of liver tissue section from rat treated with 1ml/kg body weight (2a) and 3ml/kg body weight of iohexol (2b) showing no obvious histo-architectural disruption with intact portal tract (Pt), hepatocytes (H), sinusoidal spaces (S) and central veins (Cv).

However, the photomicrograph of liver tissue of rats treated with 1ml/kg body weight of urografin (Group 2) showed intact tissue parenchyma, but the portal tracts (Pt) appeared mildly enlarged with infiltration of inflammatory cells (figure 3a) while the photomicrograph of liver tissue of rat treated with 3ml/kg body weight of urografin (Group 3) showed marked inflammatory cellular infiltration (black arrows) along the interlobular septa and portal tracts with damage of limiting plate. However, most hepatocytes at midzonal and centrilobular regions appeared intact (figure 3b).

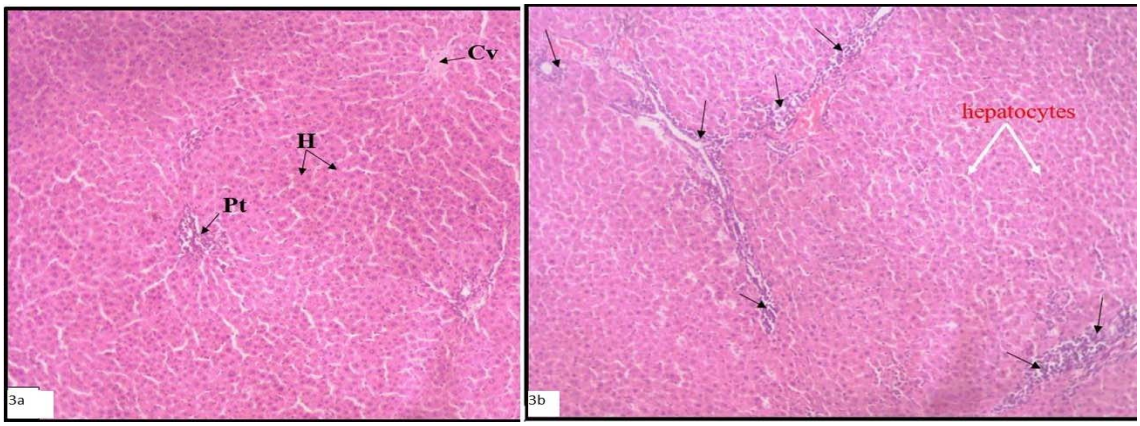

Figure 3: Photomicrograph of liver tissue section from rats treated with 1ml/kg body weight (3a) showing intact tissue parenchyma, but the portal tracts (Pt) appearing mildly enlarged with infiltration of inflammatory cells and 3ml/kg body weight of urografin (3b) showing marked inflammatory cellular infiltration (black arrows) along the interlobular septa.

3.5. Histopathological examination of kidney tissue

The histological examination of kidney tissues of the control group (figure 4), the group treated with 1ml/kg body weight of urografin and the groups treated 1ml/kg and 3ml/kg body weight of iohexol (figure 5), respectively, showed normal histoarchitecture of the cortical and medullary portions of the renal tissue with no obvious histopathological change.

However, the glomeruli of those treated with 3ml/kg body weight of urografin appeared to be shrunken with corresponding increase in bowman's capsular space. Inflammatory cellular infiltration was also observed at the peri-glomerular regions and within the medulla (figure 6).

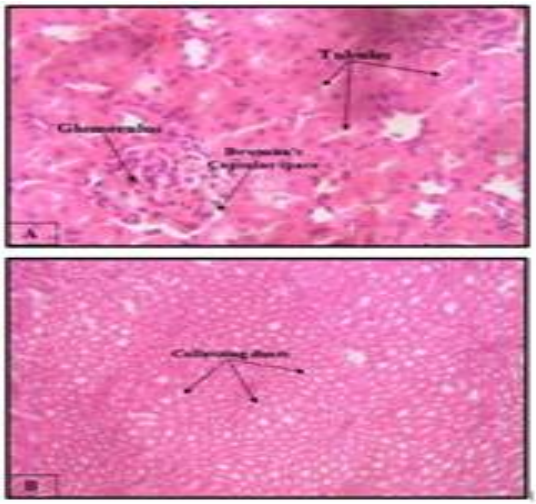

Figure 4: Photomicrograph showing the cortical (A) and medullary (B) portions of kidney tissue from control group 1 showing normal histoarchitecture of the cortical and medullary portions of the renal tissue.

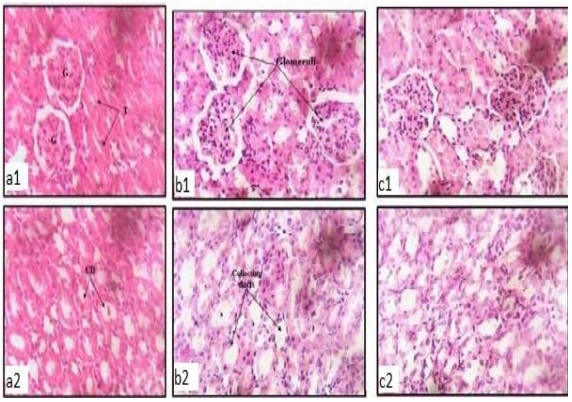

Figure 5: Photomicrograph showing the cortical (a1) and medullary (a2) portions of kidney tissue of rat treated with 1ml/kg body weight of urografin; cortical (b1) and medullary (b2) portions of kidney tissue of rat treated with 1ml/kg body weight of Iohexol; cortical (c1) and medullary (c2) portions of kidney tissue of rat treated with 3ml/kg body weight of Iohexol showing normal histoarchitecture of the cortical and medullary portions of the renal tissue.

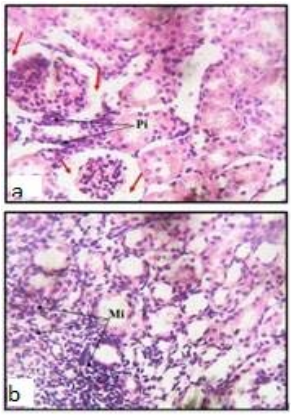

Figure 6: Photomicrograph showing the cortical (a) and medullary (b) portions of kidney tissue of rat treated with 3ml/kg body weight of urografin showing shrunken glomeruli with corresponding increase in bowman's capsular space.

4. Discussion

In the assessment of effect of urografin and iohexol on renal function, the mean serum creatinine level was highest in group 5 (3.50±0.43) that was treated with 3ml/kg of iohexol, followed by group 2 (3.26±0.35) that was treated with 1ml/kg of urografin, while the lowestvalue was observed in group 4 (3.20±0.18) that was exposed to 1ml/kg of urografin. The mean serum urea level was highest in group 3 (84.72±2.23) that was treated with 3ml/kg of urografin, followed by group 2 (83.94±2.75) that was treated with 1ml/kg of urografin while the least value was observed in group 4 (81.24±4.49) that was exposed to 1ml/kg of iohexol.

All rats in the contrast media groups treated with either urografin or iohexol at different doses exhibited a significant increase in serum creatinine and urea when compared with the control group. Variation in serum creatinine urea levels after contrast media administration has been interpreted as an indication of nephrotoxicity.[31] A study done by Choi et al. (2001)[32] reported an increased serum urea levels after administration of contrast agents in dogs with normal renal function.

In the assessment of effect of urografin and iohexol on hepatic function, the animals administered with 3ml/kg urografin (group 3) exhibited an increase in serum AST when compared with control group and other contrast media groups. However, no significant difference in the mean AST level was observed between the groups (Table 2). Elevations in serum enzyme levels (aspartate aminotransferase, alanine aminotransferase and alkaline phosphatase) are indicators of hepatotoxicity; a dysfunction, damage or injury of the liver that is associated with an overload of xenobiotics or drugs.[33-34] Hepatic function test may not be able to reveal detectable toxicity of contrast materials unless the liver is severely affected. Billström et al. (1987)[35] observed a slight increase in serum values of liver enzymes following administration of contrast agents particularly in patients with impaired hepatic function.

Total antioxidant status (TAS) measures the overall antioxidant status of the body.[36] Oxidative stress occurs in response to the oxidative damage caused when the body's scavenging and antioxidant activities cannot withstand the oxidants produced by a harmful stimulant[37] (in this case the contrast agents). Malondialdehyde (MDA) is a stable end product of lipid peroxidation, and its level is used as a marker of oxidative stress and of antioxidant status.[38]Table 3 also showed an increase in serum malondialdehyde (MDA) in all the groups injected with contrast media when compared with those of the animals in the control group. However, only the MDA level of animals in group 5 (treated with 3ml/kg of iohexol) were significantly increased when compared to those of the animals in the control group and in other groups. The increase in MDA and decrease in TAS values following administration of graded doses of contrast agents suggest that contrast agents play an important role in oxidative stress.

The liver and the kidney are the organs that play an important role in the metabolism, biotransformation and excretion of foreign compound which makes them highly susceptible to their adverse and toxic effects leading to hepatotoxicity and nephrotoxicity which refers to liver or kidney dysfunction, injury or damage that is associated with an overload of drugs or other foreign compounds. The histo-architectural disruption observed mainly in the liver and kidney of animals administered with urografin (especially high dose) could be attributed to the toxic effect of urografin on the organs. Iodine-based contrast media are classified as high osmolality contrast media (HOCM) and low osmolality contrast media (LOCM). Low osmolality contrast media (iohexol) are less nephrotoxic and hepatotoxic than high osmolality contrast media (urografin).[39]

5. Conclusions

Both iohexol and urografin are risk factors of kidney and liver damage as a result of increase in the pro-oxidant MDA and marked histomorphological alteration. However, the histopathological analsysis showed that it is safer and more reliable to use iohexol (a low osmolality contrast media) especially a lower dose.

Financial support and sponsorship

None.

Conflict of interest

We have no conflict of interests to declare.

References

Caschera L, Lazzara A, Piergallini L, Ricci D, Tuscano B, Vanzulli A (2016). Contrast agents in diagnostic imaging: present and future. *Pharmacol. Res.,* **110**: 65-75.

Davenport MS, Wang CL, Bashir MR, Neville AM, Paulson EK (2012). Rate of contrast material extravasations and allergic-like reactions: effect of extrinsic warming of low-osmolality iodinated CT contrast material to 37°C. *Radiology,* **262(2)**: 475-84.

Petriello MC, Hoffman JB, Morris AJ, Hennig B (2017). Emerging roles of xenobiotic detoxification enzymes in metabolic diseases. *Rev Environ Health*., **32(1-2)**: 105-110.

Andreucci M, Solomon R, Tasanarong A (2014). Side effects of radiographic contrast media: pathogenesis, risk factors, and prevention. *Biomed Res Int*., 741018.

Pandit A, sachdeva T, bafna P (2012) Drug-induced hepatotoxicity: a review. *J. Appl. Pharm. Sci.,* **2**: 233–243.

Upadhyay G, kumar A Singh MP (2007). Effect of silymarin on pyrogallol and rifampicin induced hepatotoxicity in mouse. *Eur. J. Pharmacol*., **565(1-3):** 190-201

Upadhyay G, Singh AK, Kumar A, Prakash O, Singh MP (2008). Resveratrol modulates pyrogallol-induced changes in hepatic toxicity markers, xenobiotic metabolizing enzymes and oxidative stress. *Eur J. of Pharmacol.,* **596 (1–3)**: 146–152.

Ufelle S, Onyekwelu K, Chinweoke A, Ibegbu D, Okoli U, Ikekpeazu J (2020). Assessment of hepatic functions, hematopoietic cytokines and haematological parameters in people occupationally exposed to volatile petroleum hydrocarbons. *Arch Environ Occup Health.,* **76(8):** 567-571.

Adwas AA, Elsayed ASI, Azab AE, Fawzi AQ (2019). Oxidative stress and antioxidant mechanisms in human body. *J. Appl. Biotechnol. Bioeng.,* **6(1)**: 43-47.

Deepali P, Supriya K, Neeta B, Meena K, Aditi M, Yashwant I, Varsha D (2013). Antioxidant defence system. *Oral and Maxillofacial Pathology Journal*, **4(1)**: 309-315.

Nwokolo LN, Onyekwelu KC, Ene MC, Adilieje CM, Ezechukwu IN, Ezeh RC (2019). In vitro antioxidant and free radical scavenging potential of methanolic extracts of uvariachamae leaves and roots. *Int. J. Pharm. Pharm. Sci.,* **11(1)**: 67-71.

Ikekpeazu JE, Ikekpeazi JA, Eke CN, Ogbu IS, Onyekwelu KC, Orji OC, Ibegbu MD, Eze AA (2016). Oxidative stress/lipid peroxidation and antioxidant enzymes in apparently healthy individuals involved in physical exercise. *Asian J. Med. Sci*., **7(6)**: 16-19.

Gowda S, Desai PB, Kulkarni SS, Hull VV, Math AA, Vernekar SN (2010). Markers of renal function tests. *N. Am. J. Med. Sci.,* **2(4):** 170-173.

Targher G, Byrne CD (2015). Circulating markers of liver function and cardiovascular disease risk. *Arterioscler. Thromb Vasc. Biol.,* **35(11)**: 2290-2296.

Weisbord SD, Mor MK, Resnick AL, Hartwig KC, Palevsky PM, Fine MJ (2008). Incidence and outcomes of contrast induced AKI following computed tomography. *Clin J. Am. Soc. Nephrol.,* **3(5)**: 1274–1281.

Bruce RJ, Djamali A, Shinki K, Michel SJ, Fine JP, Pozniak MA (2009). Background fluctuation of kidney function versus contrast-induced nephrotoxicity. *Am. J. Roentgenol.,* **192(3)**: 711–718.

Kirberger RM, Cassel N, Carstens A, Goddard A (2012). The effects of repeated intravenous iohexol administration on renal function in healthy beagles – a preliminary report. *Acta Vet. Scand.,* **54:** 47.

Widmark JM (2007). **Imaging-related medications: A class overview**. *Proceedings (Baylor University Medical Center)* 20, 408–417.

Barrett BJ, Katzberg RW, Thomsen HS, Chen N, Sahani D, Soulez G, Heiken JP, Lepanto L, Ni ZH, Ni ZH, Nelson R (2006). Contrast-induced nephropathy in patients with chronic kidney disease undergoing computed tomography: A double-blind comparison of iodixanol and iopamidol. *Invest. Radiol.,* **41**: 815–821.

Al-Ghonaim M, Pannu N (2006). Prevention and treatment of contrast-induced nephropathy. *Tech.Vasc. Interv. Radiol.,* **9**: 42–49.

Detrenis S, Meschi M, Savazzi G (2007). Contrast nephropathy: Isosmolar and low-osmolar contrast media. *J. Am. Coll. Cardiol.,* **49**: 922.

Nguyen SA, Suranyi P, Ravenel JG, Randall PK, Romano PB, Strom KA, Costello P, Schoepf UJ (2008). Iso-osmolality versus low-osmolality iodinated contrast medium at intravenous contrast-enhanced CT: Effect on kidney function. *Radiology,* **248**: 97–105.

Wong PC, Li Z, Guo J, Zhang A (2012). Pathophysiology of contrast-induced nephropathy. *Int. J. Cardiol.,* **158(2)**: 186-192.

Giaccia AJ, Simon M, Johnson R (2004). The biology of hypoxia: the role of oxygen sensing in development, normal function, and disease. *Genes Dev*. **18(18)**: 2183–2194.

Heyman SN, Rosen S, Khamaisi M, Idée JM, Rosenberger C (2010). Reactive oxygen species and the pathogenesis of radiocontrast-induced nephropathy. *Invest. Radiol.,* **45(4):** 188–195.

Mitchell RJ (1973). Improved method for specific determination of creatinine in serum and urine. *Clin. Chem.,* **19**: 408–410.

Machado M, Horizonte B (1958). Simple and rapid method for determination of urea by urease. *Rev. Assoc. Med. Bras*., **4**:364–367.

Reitman S, Frankel S (1957). A colorimetric method for the determination of serum glutamic oxalacetic and Glutamic pyruvic transaminases. *Am. J. Clin. Pathol.* **28(1)**: 56–63.

Miller NJ, Rice-Evans C, Davies MJ (1993). A new method for measuring antioxidant activity. *Biochem. Soc. Trans.,* **21 (2)**: 95S.

Ohkawa H, Ohishi N, Yaji, K (1979). Assay for lipid peroxides in animal tissues by thiobarbituric acid reaction. *Anal Biochem*., **95(2)**: 351-358.

Newhouse JH, Kho D, Rao QA, Starren J (2008). Frequency of serum creatinine changes in the absence of iodinated contrast material: implications for studies of contrast nephrotoxicity. *Am. J. Roentgenol.,* **191(2)**: 376–382.

Choi J, Lee H, Chang D, Lee K, Eom K, Lee Y, Choi M, Yoon J (2001). Effect of dopamine excretory urographic image quality and the prevention of contrast-induced nephropathy in dogs. *J. Vet. Med. Sci.,* **62**: 383–388.

Rosalski SB, Mcintyre N (1999). **Biochemical investigations in the management of liver disease**. In: Bircher J, Benhamou JP, McIntyre N, Rizetto M, Rodes J, eds. Oxford handbook of clinical hepatology. 2nd ed. Oxford, England: Oxford University Press. 1999. 504.

Navarro VJ, Senior JR (2006). Drug-related hepatotoxicity. *N. Engl. J. Med.,* **354**: 731-739.

Billström A, Hietala SO, Wirell S (1987). Effects of metrizoate and iohexol on the liver at visceral angiography. *Acta Radiol.,* **28(6)**: 707-710.

Erel O (2004). A novel automated direct measurement method for total antioxidant capacity using a new generation, more stable ABTS radical cation. *Clin. Biochem.,* **37**: 277–285.

Durackova Z (2010). Some current insights into oxidative stress. *Physiol. Res.,* **59**: 459–469.

Gaweł S, Wardas M, Niedworok E, Wardas P (2004). Malondialdehyde (MDA) as a lipid peroxidation marker. *Wiad. Lek*., **57(9-10)**: 453-455.

Gleeson TG, Bulugahapitiya S (2004). Contrast-inducednephropathy. *Am. J. Roentgenol.,* **183(6)**: 1673–1689.

JJBS

Volume 17, Number 3,September 2024
ISSN 1995-6673
Pages 561 – 573
https://doi.org/10.54319/jjbs/170320

Jordan Journal of Biological Sciences

Oat Crown Rust in Jordan: A Comprehensive Survey and Analysis

Mohammad Asad Ibrahim [1], Kholoud M. Alananbeh [1,*] , Yahia Othman[2], Muhannad Massadeh[3], Riyadh Muhaidat[4]

[1]Department of Plant Protection, School of Agriculture, The University of Jordan, Amman 11942, Jordan; [2]Department of Horticulture and Crop Science, The University of Jordan, Amman 11942, Jordan; [3]Department of Biology and Biotechnology, Faculty of Science, The Hashemite University, Zarqa P.O. Box 11315, Jordan, 4Department of Biological Sciences, Faculty of Science, Yarmouk University, Irbid P.O. Box 21163, Jordan. First and second authors contributed equally to this work.

Received: January 21, 2024; Revised: March 19, 2024; Accepted: April 23, 2024

Abstract

This research aimed to study the ecological context of *Puccinia coronata* f. sp. *avenae* (Pca), a pathogen affecting oats, in Jordan. The region is identified as a natural habitat for various wild oat species and the Rhamnaceae family, serving as an alternative host for Pca. The prolonged coexistence of the pathogen, wild oats (*Avena* spp.), and *Rhamnus* creates a scenario conducive to natural selection for long-term resistance. Although oats are not a major crop in Jordan, studying this disease is still significant. The survey spans were between 2018 and 2023, focusing on the upper and lower regions of Jordan Valley. The survey involved collecting, coding, preserving, and morphologically identifying Pca-infected leaves, wild oats, and *Rhamnus* specimens. Results indicated the majority of Pca isolates were from wild oats, particularly in the northern region. Wild oat samples mainly belonged to *A. sterilis*. *Rhamnus* spp. specimens, identified primarily as *Rh. lycioides* with subspecies *graecae* and *lycioides* and few *Rh. punctata*showed no roleasan alternative host of Pca infection. The research provides a foundation for future investigations, emphasizing race characterization and evaluating wild oat accessions for potential resistant genes against Pca.

Keywords: *Avenasterilis*,*Avena barbata*, *Rhamus* spp., wild oat, buckthorn.

1. Introduction

Oats (*Avena* spp.), comprising numerous species within the genus *Avena*, have gained prominence as a cultivated crop across various countries globally, assuming a progressively essential role in human and animal diets. Notably, oats stand as the sixth most consequential cereal crop internationally, a distinction underscored by statistical data from 2021 (Statista, 2021). Demonstrating an array of health benefits contributing to its growing popularity (Clemens and Klinken, 2014), oat consumption has risen to prominence.

Among the Mediterranean countries, Jordan emerges as a native habitat for several wild oat species (El-Shatnawi and Ghosheh, 1999), although oat cultivation remains infrequent. However, the prevalence of wild oat species, particularly as a favorable grazing option for diverse livestock classes, holds promise (Carson, 2008).

The cultivation of oats faces a multitude of diseases that significantly impede yield and quality, with crown rust disease being a notable example (Leonard, 2002). Generally, crown rust is a fungal disease affecting several Poaceae plant species, attributed to *Puccinia coronata*. In the context of oats (*Avenae* spp.), the special form of this pathogenic agent (also called *forma specialis,* biological race, or morphotype) is recognized as *P.coronata* f. sp. *avenae* (Pca), a polycyclic heteroecious fungus. The impact of crown rust, Pca, extends to compromising both the quantity and quality of seeds, casting its prevalence across cultivated oat areas (Leonard, 2002; Simons, 1985). Evidencing a successful interaction, symptoms are discernable as pustules full of clusters of uredospore. Subsequently, the uredial phase converts into the overwintering teliospores, distinguished by their black color, and these endure on straw or host plants of the buckthorn genus (Rhamnaceae) until the following spring (Nazareno *et al.*, 2018; Simons, 1985).

Favorable conditions for the proliferation of crown rust predominantly encompass oat plantation regions characterized by moderate to high temperatures (20-25°C), complemented by abundant dew or elevated relative humidity (RH %). The conjunction of temperature and aerial moisture (including rainy or foggy circumstances) exerts the most substantial influence on the incidence and dispersal of crown rust. Notably, cultivated and wild oats thriving in arid environments typically remain unscathed by crown rust infection due to the scarcity of the requisite RH % (Carson, 2011; USDA-ARS, 2017). Instances of heightened incidence and spread correlate with rainy and warm conditions warm droughty and fog-laden nights. Conversely, moderate infection is associated with extreme instances of either factor, such as exceedingly dry warmth,

* Corresponding author. e-mail: k.alananbeh@ju.edu.jo.

adverse hot and dry conditions can delay infection (Soovali and Koppel, 2003).

Genetic resistance via breeding constitutes the most dependable strategy for disease management. The race-specific seedling resistance was characterized by a hypersensitive response, discernible as flecks on leaves devoid of pustules (Murphy, 1935). However, managing disease through resistance genes in cultivated oats confronts challenges engendered by the rapid evolution of Pca, which facilitates the consistent breakdown of resistance genes (Carson, 2011; Leonard, 2002). The pressure of selection hastens this process, consequently limiting the longevity of a resistance (Carson, 2010). For instance, while *Pc38* and *Pc39* conferred resistance in Canada for several years, by 1990, most races had developed virulence against these genes. Furthermore, new races weakened *Pc91*, *Pc94*, and *Pc96* (Chong *et al.*, 2008). Recent endeavors focusing on genetic resistance underscore the significance of resistant genes in wild oats, thus highlighting the pursuit of cultivars capable of withstanding or tolerating crown rust and other consequential diseases.

In addition to *Avena* spp., Jordan has been reported as a native habitat of the Rhamnaceae family, the alternative host of *P. coronata* (Al Eisawi, 1996; Oran, 2014). In general, alternative host has a vital role in regenerating new races and creating virulence diversity of rust diseases due to its role in sexual reproduction (Jin, 2011; Mehmood *et al.*, 2020), and scarcely mutation has a role in the emergence of new races (Chen *et al.*, 2017). Regarding oat crown rust, *Rhamnus* spp. is responsible for the regeneration of *Pca* races (Wahl *et al.*, 1960). Even among the same aecial cluster, genetic diversity from one cup to another exists (Berlin *et al.*, 2017). However, the long-lasting coexistence of the pathogen, wild oat (such as *A. sterilis* in the Middle East) and the alternative host *Rhamnus* creates natural selection toward long-term resistance (Wahl, 1958).

The causal pathogen and its alternative host trace their origins to the Mediterranean, including the Levant region (Clegg and Allard, 1972; Wahl, 1970). Consequently, despite oats not being a staple and cultivated crop in Jordan, studying this disease is important. The Levant has been identified as a prolific source of Pc genes, with over 25 Pc genes predominantly identified in *A. sterilis* (Simons, 1978). The present study endeavors to comprehensively survey diverse locations in Jordan for *P. coronata* f. sp. *avenae* (Pca) infections, and wild oats and buckthorn distributions. This research serves as fundamental for future investigation on race characterization and evaluation of wild oat accessions against Pca races for identifying potential resistant genes.

2. Materials and Methods

2.1. Surveys

2.1.1. Puccinia coronata f.sp. avenae

Collection

The present study aims to comprehensively investigate the distribution of the crown rust pathogen, *P. coronata* f. sp. *avenae* (Pca), across various regions of Jordan, encompassing the North, Mid, and Southern geographical zones. Notably, our surveys emphasized Northern Jordan, following the approach outlined by (Leonard *et al.*, 2004). In addition, differential lines, including susceptible cultivars, recognized for their distinct interactions with the pathogen, were cultivated in three strategically chosen locations with different environmental conditions, namely the Jubiha station (32°00'40.4"N 35°52'19.5" E), Agricultural Research Center, The University of Jordan (32°05'05.0"N 35°35'44.2" E), and Marow station, Bani Kananah (32°36'26.7"N 35°54'04.9" E), in the year 2022, as trap crops. The choice of these locations aimed to capture variations in environmental factors influencing Pca distribution. Furthermore, our investigation also encompassed previously collected isolates spanning the years 2018 to 2020. To ensure accurate tracking of collection sites, precise GPS coordinates, including longitude and latitude, were recorded for each sampling location. During the survey, plant leaves infected with Pca pustules, from oat (*Avena* spp.), were collected and subjected to careful preservation techniques. Specifically, the collected infected leaves were carefully placed in paper bags to facilitate air drying. The desiccation process took place over (3-4) days at room temperature or using a desiccator, ensuring the preservation of the fungal pustules.

Isolate coding

Each Pca isolate collected during our survey was assigned a unique accession code based on the year of collection, thereby facilitating subsequent data management and analysis. As an illustrative example, accession codes may follow the format "Pca2020JOR-01," signifying the pathogen's isolation in Jordan during the year 2020.

Preservation of Pca pustules

Discernible single pustules were selectively excised from the infected plant material and preserved in two distinct manners: (i) living pustules: these pustules were carefully dried and stored in 2 ml test tubes. Subsequently, they were preserved in an ultra-freezer at a temperature of -80°C. This preservation method will allow for the long-term viability of the pathogen, facilitating further race identification through the utilization of differential lines; and (ii) dead pustules in which the selected pustules were immersed in 95% alcohol for one day, followed by thorough drying. This preservation technique ensures the inactivation of the pathogen while retaining its morphological characteristics, thus enabling detailed microscopic examination and future molecular analysis.

Morphological identification and characterization of Pca isolates

Different *Pca* sample isolates were used to describe the morphology for characterization and taxonomy identification purposes. For light macro- and microscopic characterization, isolates were prepared as follows: infected leaves with pustules of both telia and uredia were examined using a stereo microscope (LB-321, Labomed), while spores themselves were scratched and located on a glass slide and then inspected using a light microscope (Microstar 410, Cambridge Instruments). For scanning electron microscope (SEM) micrographing: *Pca* samples of uredia and telia were scratched to obtainuredospore and teliospores (some samples have both). Spores were located

on aluminum stubs and then coated by platin using Emltech K550X sputter coater. Finally, surface micrographs were taken for these processed samples by using SEM at Hamdi Mango Centre (Inspect F50 - FEI Company). Identification of rust species was done using identification key. This key is based initially on the infected host plant which was *Avena* sp. Different details of morphological characteristics of uredium, telium, uredospore, and teliospore were investigated and ensured, relying on those in (Cummins, 2013; Grove, 1913). Additionally, and as observational data, the same keys and characteristics were followed to identify samples of oats with an infection on the stem (which are commonly supposed to be *P graminis* f.sp *avenae* based on the infected part, color and pustule shape), and compared with those findings of *Pca* (Appendix 1).

2.1.2. Wild oat survey (Avena spp.)

Collection and coding of wild oat genotypes

In our investigation, wild oats (*Avena* spp.) were collected from diverse environments, including roadsides and natural habitats, across Jordan mainly in 2021and some in 2022. Each collected specimen was coded to facilitate accurate tracking and documentation based on the collection year, adhering to a standardized nomenclature format, exemplified as "WO2021JOR-01." The comprehensive collection endeavor aimed to encompass unique wild oat genotypes, each representative of distinct ecological niches and geographical locations within the country. A minimum distance of two kilometers was maintained between the different locations where wild oat plants were collected. Seeds from each location were collected randomly from mature parent plants exhibiting typical wild oat characteristics. Location coordinates were collected for each sampling site. This geospatial data will serve as valuable metadata for subsequent analyses, aiding in the elucidation of the genetic and ecological factors shaping the wild oat populations in Jordan.

Seed selection and genotype purity assurance

To ensure the genetic purity of each collected wild oat genotype, a rigorous selection process was implemented. From each collection, a single seed was randomly chosen and subjected to an increase in the greenhouse to guarantee the preservation of its inherent genetic constitution. This approach serves to maintain the integrity of each genotype and minimize genetic variation within collected samples.

Morphological identification and taxonomy

Given the potential presence of multiple oat species within each collection, a comprehensive morphological identification process was undertaken for the entire seed collection. Until species-level identification is achieved, the collected wild oats were designated as "*Avena* sp.". Then, species of samples were identified using the weighted key with “the most important diagnostic characteristics only” by Baum (1977) and, in some cases shifting to another detailed key known as the unweighted key in cases that characteristic is not clear enough to be identified or more comparative characteristics need to be taken in consideration. Also, another key of Loskutov (2007) was used for certainty (Appendix 2).

2.1.3. Buckthorn survey (Rhamnus spp.)

Collection

A survey of buckthorn (*Rhamnus* spp.) populations across diverse regions of Jordan was conducted in 2022-2023. Various regions, including North, South, East, and West, were systematically explored to provide a comprehensive overview of buckthorn distribution and prevalence. Our survey efforts prioritized areas in proximity to wild oat (*Avena* spp.) habitats, as these locations are of particular interest in the context of crown rust epidemiology. GPS coordinates, encompassing longitude and latitude, were recorded for each sampling site. Each collected specimen was coded to facilitate accurate tracking and documentation based on the year of collection, adhering to a standardized nomenclature format, exemplified as "Rh2022JOR-01." Leaf samples from 1-3 different distant plants from the same location were collected.

Morphological identification

The collected *Rhamnus* buckthorn specimens underwent a morphological identification process up to the genus, species, and subspecies level. This process depends on botanical characteristics related to the description of the *Rhamnus* genus, which was described as follows: deciduous (mostly) or evergreen plants, shrubs, or small trees, with grey to brown stem color, branch is alternate or opposite. The leaf's shape is oblong (mostly), oboval or linear, greenish-yellow or green, alternate or opposite. The blade is undivided with serrate or entire margins. Some plants may have two different types of leaf according to leaf apex: one emarginate to obcordate (dimorphic leaf), and the other is obovate. Flowers are yellowish green, single or in-groups, with berry-like fruits and (2-4) drupes. Stems are with or without spines. Habitats are mountainsides, rocky lands, and poor deserts (Nguyen, 2007). A key characteristic was designated to identify collected samples to species level (of the four *Rhamnus* species referred by (Taifour and El-Oqlah, 2016), and to subspecies level (if was of *Rh. lycioides)*. This key originated from those keys and characteristics mentionedby (Davis, 1970; Muschler, 1912; Tutin, 1986) (Appendix 3).

Sample processing for further analysis

In the context of crown rust research, sampled *Rhamnus* plants were examined for the presence of crown rust pustules on leaves. Additionally, leaves were excised and placed immediately in vials containing silica gel. Silica gel serves as a desiccant, effectively drying out the leaves and preventing degradation of DNA. Preserved samples will be used as a genetic source for future genetic diversity studies of buckthorn.

2.2. Statistical analysis

Plants and disease locations were mapped using ArcGIS ArcMap (Version 10.2 for Windows; ESRI, Redlands, CA). Excel from Microsoft Office 2016 was employed to compile summaries detailing the number of surveyed locations and samples collected for *P. coronata*, *Avena* spp., and *Rhamnus* spp.

3. Results

3.1. Surveys

3.1.1. Puccinia coronata f.sp. avenae

A total of 1600single pustule isolates (spi) of *P. coronata* f.sp *avenae* (Pca) were collected from 135 locations over the period spanning 2018 to 2023, except 2019 (Table 1). The majority of these isolates were collected from wild oats, whereas only 196 samples originated from differential oat cultivars, as delineated in Table 1. Notably, the majority of spi were retrieved from the northern region, particularly in Irbid, where the count exceeded one thousand spi (Figure 1A, 1D).

Morphological Identification of Pca

The identification of rust species and determination of biological race were executed employing the taxonomic key outlined by Cummins (2013). In general, all isolates obtained from oat sources were conclusively identified as belonging to the genus *Puccinia*, a classification supported by the distinct characteristics observed in the teliospores. Specifically, these teliospores exhibited pedicellate structures, comprised of two cells, each possessing a single germ pore, and featured echinulate uredospore (Figure 2,3).

Further refinement of the identification process, conducted at the species and special form levels, involved a meticulous examination of teliospores isolated from oat plants. This inspection led to the clear identification of *P. coronata avenae* (Pca) and *P. graminis avenae* (Pga) based on the discernible morphological features described in the taxonomic key. Notably, the teliospores of Pca were distinguished by their coverage of spore cells and digitated tip appearance, as illustrated in Figure (3). In contrast, the teliospores of Pga were characterized by their exposed spore cell configuration, and the tip is without digitations, exemplified in Figure 2. Many morphological features examined exhibited similarities with the descriptions provided by Cummins (2013) and Grove (1913) as cataloged in Appendix 1.

3.1.2. Wild oat survey (Avena spp.)

A comprehensive survey of *Avena* species was conducted in this study, encompassing approximately 264 samples sourced from 184 distinct and documented locations (Figure 1B, 1D). For about 56% of the samples collected from Irbid governorate, the identification of wild oat samples revealed two species, mainly *A. sterilis,* with 90% and 10% *A. barbata* (Table 2, Figure 4, Figure 5). Common characteristics shared by both species and primary characteristics for *A. sterilis* and *A. barbarata* are presented in Appendix 2.

Table 1. Survey summary of *P. coronata*. f.sp *avenae* across governates during 2018-2023.

Source	Governate								Total
	Ajloun	Al-Balqa	Al-Mafraq	Al-Zarqa	Amman	Irbid	Jerash	Madaba	
Differentials	0	96	0	0	0	100	0	0	196
Wild oat	115	47	205	31	9	988	57	30	1482
Total	115	143	205	31	9	1088	57	30	1678
Year									
2018		2020		2021		2022		2023	
Locations	Samples	Locations	Samples	Locations	Samples	Locations	Samples	Locations	Samples
15	60	13	48	14	199	16	292	77	1079
Total locations = 135			Total samples = 1678						

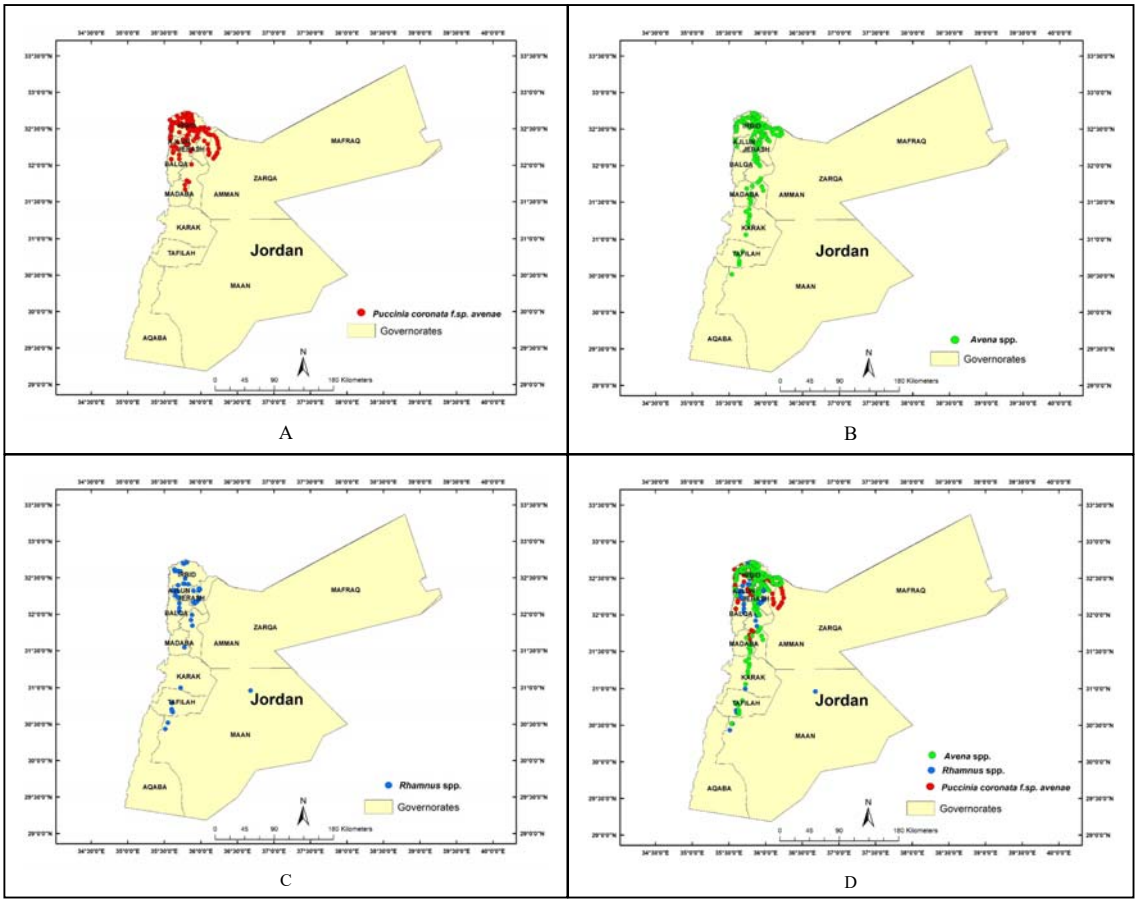

Figure 1. The survey locations conducted for oat crown rust, wild oats, and buckthorn. Sub-figures include: A) A four-year survey overview for oat crown rust (Pca), B) Wild oat (*Avena* spp.) survey conducted in 2021, C) A survey map highlighting locations of buckthorn (*Rhamnus* spp.) in 2022-2023, and D) Combined survey locations for *Rhamnus* spp., *Avena* spp., and oat crown rust (Pca) depicted in a single map.

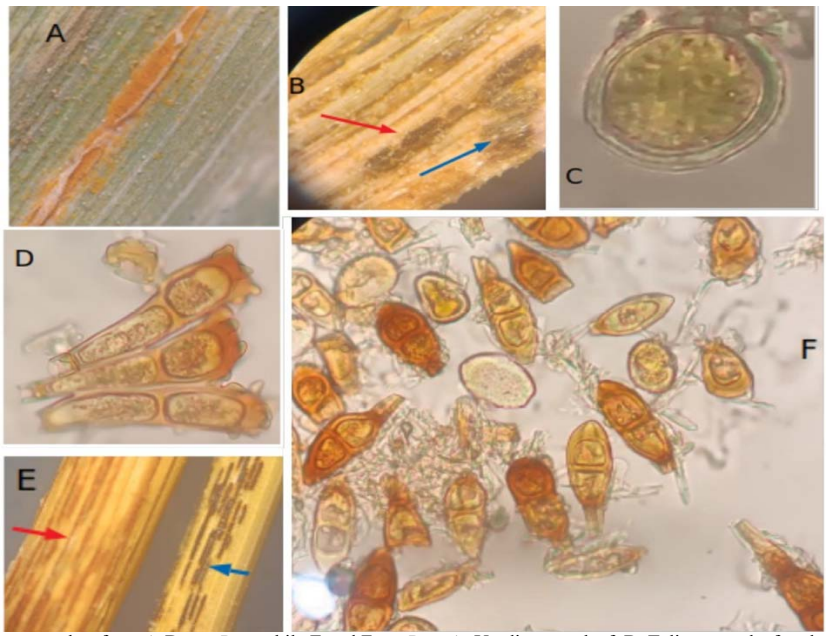

Figure 2. Rust on oat samples, from A-D, are *Pca*, while E and F are *Pga*. A: Urediaon oat leaf, B: Telia on oat leaf, red arrow refers to ruptured pustule while blue arrow refers to unruptured one, C: uredospore, D: teliospores (D is zoomed), E: Uredia (red arrow), telia (blue arrow) both on oat culm, F: both uredospores and teliospores, C, D, F were further inspected under 600x, while A, B and E were inspected under 10x.

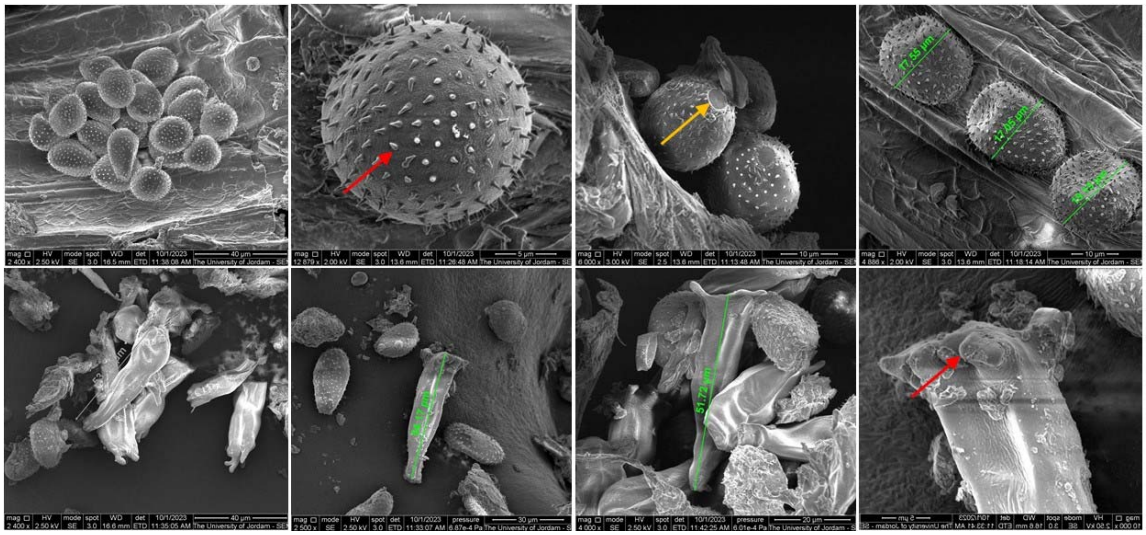

Figure 3. SEM micrographs of *Pca* spores. Upper: uredospores; the red arrow refers to the short spines (echinula), while the yellow arrow refers to the germ pore. Lower part: teliospore, red arrow refers to the digital projections.

Table 2. Survey of wild oat *Avena* spp. collected from different locations in 2021.

Governate	no. of location	no. of samples		
		sterilis	*barbata*	Total
Ajloun	4	7	0	7
Al-Balqa	5	9	0	9
Al-Karak	10	16	4	20
Al-Mafraq	15	13	2	15
Al-Tafilah	8	10	4	14
Amman	11	13	2	15
Irbid	104	139	7	146
Jerash	20	24	2	26
Madaba	7	10	2	12
Total	184	241	23	264

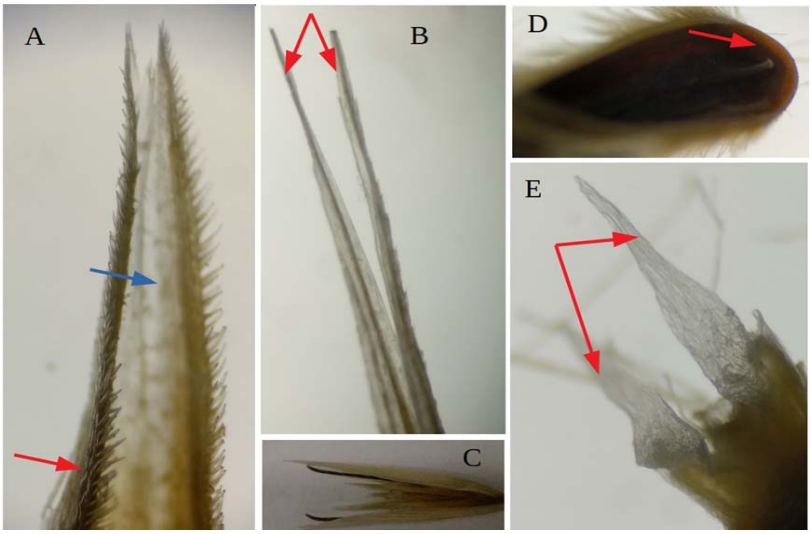

Figure 4. *A. sterilis*, an example of a sample identified according to morphological profile, A: Palea keel with 2 cilia rows (red arrow), palea vestiture with prickles (blue arrow), B: lemma tips are bisubulate, red arrows refer to the subules, C: disarticulation: all florets (here 4 florets) disarticulate as one unit (only the most lower floret disarticulated), spikelet has three florets, glumes are nearly equal, number of glume nerves is 10 nerves, awns inserted in the lower one-third of the lemma (not figured here), D: the shape of primary floret abscission scar is oval, and periphery ring (callus, the shiny part of abscission scar) confined to about (1/3-1/4) of scar, E: lodicule of fatua-type, (no side lobe present).

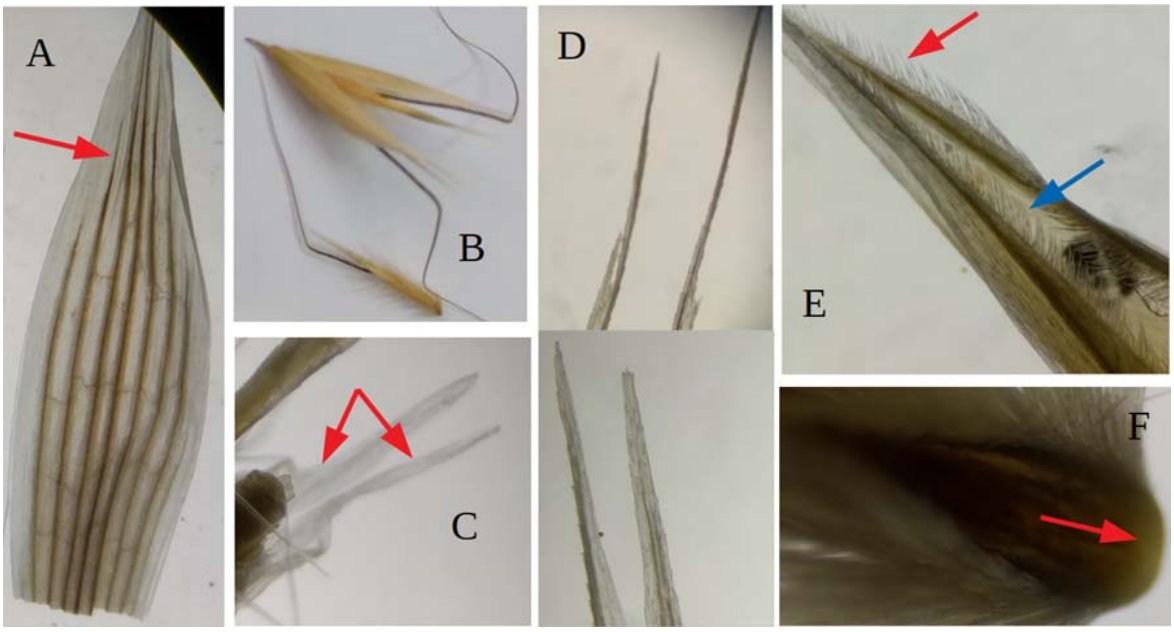

Figure 5. *A. barbata*, A: spikelet glume with 9 nerves (two of them are very short), B: disarticulation: all florets (two florets here) disarticulate, spikelet with nearly equal glumes, awns inserted in the lower (1/3) of lemma, C: two lodicules of fatua-type, red arrows refer to the lodicule arms, D: two types of lemma tips the upper one is biaristulate, the lower one is bisubulate, E: palea keel with one cilia row (red arrow), vestiture of palea back is glabrous (blue arrow), F: the primary floret abscission scar is oval, and ring confined to about (1/3) of scar periphery.

3.1.3. Buckthorn survey (Rhamnus spp.)

This investigation involved the systematic survey of *Rhamnus* plant samples, totaling 102 specimens collected from 46 diverse locations (Table 3). Most of *Rhamnus* plants were concentrated in northern governorates (Figure 1C, 1D). Morphological characteristics were accurately examined to determine their classification within the *Rhamnus* genus. All surveyed plants exhibited spinescent features, characterized by spiny stems, and displayed deciduous leaves (Figure 6). Additionally, a predominant majority of the surveyed plants exhibited an obovate leaf morphology (Appendix 3). The most common *Rhamnus* species was *Rh. lycioides*. Details of the identified species and subspecies are provided in Appendix 3.

In the context of *Rhamnus* potential role as alternative hosts, the surveyed *Rhamnus* plants underwent a thorough screening process. However, none of the examined plants demonstrated any signs of infection by *P. coronata avenae* (Pca). Thus, none exhibited the sexual phase of Pca (aecial stage) throughout the entire collection period. This discerning observation contributes valuable insights into the distribution and host association of Pca, elucidating the absence of its aecial stage on the examined buckthorn plants.

Table 3. Survey of *Rhamnus* spp. from different locations in Jordan during 2022-2023.

Governate	no. of samples	no. of location	Rh. *punctata*	subsp *graecae*	subsp *lycioides*
Ajloun	21	*10*	*0*	10	0
Al-Balqa	8	3	0	3	0
Al-Karak	3	1	0	1	0
Al-Mafraq	2	2	0	2	0
Al-Tafilah	13	4	0	4	0
Amman	7	3	0	3	0
Irbid	22	12	2	8	2
Jerash	9	4	0	4	0
Maan	7	3	0	3	0
Madaba	3	1	0	1	0
Total	102	46	2	42	2

Figure 6.*Rhamnus* in Jordan, at left *R. lycioides* subsp. *lycioides* at right *R. lycioides* subsp. *graeca*. Red arrows refer to the spiny stem; blue arrows refer to the two types of leaf, the obovate and the emarginate-obovate.

4. Discussion

This research represents the first survey in Jordan to investigate the presence of oat crown rust on its primary host, wild oat, as well as its alternative host, buckthorn. In the current investigation, *P. coronata avenae* (Pca) samples, were collected from wild oats over four years from diverse locations and governorates in Jordan. These collected samples underwent thorough processing and preservation for subsequent in-depth analyses.

Conducting a comprehensive Pca survey involved exploring various regions with distinct environmental conditions, even within the same governorate, to ensure a broader spectrum of variability and diversity among Pca isolates (Ali *et al.*, 2021; Lyon and Broders, 2017). Nevertheless, this study showed a concentration of Pca samples in the northern part of Jordan. This region, characterized by prolonged intermediate temperatures and moderated extremes in temperature and humidity, provides optimal conditions for Pca infection. The Northern regions of Jordan exhibit a high prevalence and diversity of host plants, which could be attributed to specific soil characteristics. Additionally, the proximity of the northern region to other Mediterranean countries, which also harbor both Pca and alternative hosts, contributes to the observed distribution patterns.

The assessment of Pca infection revealed a significant variation in disease incidence from one year to another, with most isolates being collected in 2023. This underscores the pronounced influence of environmental conditions on the epidemic status of the disease (Ali *et al.*, 2023). Our geographic regions are characterized by well-documented weather and climatic fluctuations, both seasonally and daily. The persistent presence of this disease has the potential to drive the evolution of Pca genotypes, giving rise to diverse and novel races; such cases were referred to by (Moreau *et al.*, 2023). To investigate deeper into the molecular aspects of this evolutionary process, additional studies are required, specifically focusing on genetic variation analyses among Pca populations in Jordan.

The consistent annual occurrence of natural *P. coronata avenae* (Pca) infection on oats over four years prompted our investigation into the potential involvement of nearby alternative hosts (Zhao *et al.*, 2016). Concurrent surveys of buckthorns, oat, and crown rust indicated their proximity, coupled with the known limited dispersal capability of Pca basidiospores. Despite these observations, screening results revealed no substantiating evidence that the surveyed *Rhamnus* plants function as alternative hosts for Pca in Jordan. While studies often highlight the windborne transmission capacity of uredospore across countries and continents (Berlin *et al.*, 2017; Moreau *et al.*, 2023), our findings did not align with this expectation. Given these results, further investigation, potentially employing more recent methodologies such as multiplex PCR, may be warranted to explore the possible association of Pca with *Rhamnus* in the region.

This study involved the random collection of wild oat plants from various locations, followed by morphological identification at the species level, which is valid and still used (Jabar and Yahya, 2019; Belsariya *et al.*, 2023; Singh *et al.*, 2019). The identification process relied primarily on the keys provided by (Baum, 1977). However, due to the difficult nature of wild oat taxonomy, a combination of keys, sometimes necessitating shifts, was employed to enhance accuracy. The results indicated that the surveyed wild oat samples belonged to two species: *A. sterilis* and *A. barbata;* those two species have been recorded in Jordan by many authors (Loskutov and Rines, 2011; Taifour and Oqlah 2016). *A. sterilis* was more abundant than *A. barbata* by tenfold (Table 2), aligning with previous findings that highlight the superior distribution and multiplication success of *A. sterilis* compared to *A. barbata* (Baum *et al*., 1972).

Taxonomy and classification complexities were evident, with variations among authors regarding species/subspecies designations. The morphological keys, while valuable, were not always straightforward, and differences existed between different keys (Leggett, 1992). *A. barbata* posed more significant identification challenges than *A. sterilis*, with potential confusion arising from similar species such as *A. wiestii*, *A. hirtula*, *A. damacina*, *A. fatua*, and *A. longiglumis* (Loskutov and Rines, 2011). However, the study observed few samples resembling *A. barbata*-like characteristics (all florets disarticulated at maturity) (Table 3).

This study highlighted limitations in morphological identification, showcasing unique cases not covered by existing keys (Kumar *et al.*, 2023). These cases included features such as aristulate-subulate lemma tips, palea backs with long hairs, *A. barbata* with a ring confined to 1/6 of the scar, *A. sterilis* glumes with 12 nerves, and *A. barbata* with fewer than nine nerves. Additionally, the study introduced extra morphological details not previously mentioned in the literature, such as two types of cilia rows (short and long), the fusion of the two subules, and subules with toothed tips. The presence of unique traits not addressed by traditional morphological keys suggests the potential existence of unidentified subspecies or even new species. For that, further studies, including molecular techniques, may be essential in resolving these cases, considering the inheritability of these distinctive traits and the possibility of uncovering previously unrecognized taxa based in the term of phenotype stability (Devi *et al*., 2023).

In this investigation, *P. graminis avenae* (Pga) was incorporated into the study alongside *P. coronata avenae* (Pca) as observational data. This inclusion was motivated by the frequent co-occurrence and potential overlap of both infections, complicating their differentiation (Cabral et al. 2014). Challenges in distinguishing the two species arose from the possibility of late-stage infection on various plant parts, the resemblance in coloration, particularly in the telial stage, and the general similarity in the shape of uredospores as mentioned in (Cummins, 2013). Therefore, a comprehensive characterization of both rust species was conducted at macro- and microscopic levels, including a comparative description. The applied key in this study facilitated differentiation, commencing with the host plant genus. Rust infections within the *Avena* genus were found to be limited to Pga and Pca. Distinguishing between Pga and Pca teliospores was achieved through simple microscopic observation. The later teliospores of Pca exhibited digitate projections, imparting a crown-like appearance to the apical part, while Pga teliospores lacked such digitations. Most characteristics of Pca and Pga aligned with descriptions provided by (Cummins, 2013; Grove, 1913). Additionally, the study introduced supplementary descriptions, including the darker color of Pca apex compared to other teliospore parts, the tapering nature of some Pga apex toward one side in many instances, the notably long pedicel of Pga teliospores, potentially exceeding the combined length of both teliospore and pedicel cells, the relatively shorter echinula of Pca uredospores compared to Pga's (though not quantitatively measured), the generally more globose shape of Pca uredospore s in contrast to the more ellipsoid shape of Pga's, and the relatively thinner cell wall of Pca uredospore's compared to Pga's (with "relatively" indicating the mean cell wall thickness relative to the entire cell).

Irrespective of whether *Rhamnus* species documented in Jordan were previously recognized in the literature as hosts for the sexual stage or not, the current study spanned two years to thoroughly survey this plant. The investigation involved concurrent inspection and random collection of *Rhamnus* plant samples at each visited location for subsequent analyses. Samples were grouped based on morphological similarities, followed by detailed morphological identification. Categorization revealed distinct morphological differences among samples. Consequently, a comprehensive morphological characterization was conducted using keys and traits outlined in the methodology section. Results showed two *Rhamnus* species, one of which has two subspecies; these species had been previously reported in Jordan by Taifour and El-Oqlah (2016).

P. coronata avenae (Pca) presence on *Rhamnus* was assessed through visual observation of leaves. Results showed no discernible evidence supporting their role as alternative hosts for Pca. While further extensive observations and investigations may be necessary, it is noteworthy that both the identified species in this study and those mentioned in prior literature, such as *Rh. diperma* and *Rh. alaternous*, have not been documented as alternative hosts, except for one case reported in Tunisia (Hemmami *et al.*, 2006). It is important to emphasize that the pictures of plants shown in the figures in that research do not align with the morphology of *Rh. lycioides* leaves. In general, such negative interactions of Pca and alternative hosts were found by others (Dietz, 1926).

5. Conclusions

This research represents the first survey in Jordan to investigate the presence of oat crown rust on its primary host, wild oat, as well as its alternative host, buckthorn. In summary, a thorough investigation was conducted on *P. coronata* f.sp. *avenae* (Pca), comprising the collection and morphological identification of 1600 single pustule isolates (spi) throughout 2018 to 2023. All of these isolates were retrieved from wild oats, particularly in the northern region, notably Irbid. Additionally, a comprehensive survey of *Avena* species identified *A. sterilis* as the predominant species in the Irbid governorate. Moreover, the survey of *Rhamnus* species revealed significant concentrations in northern governorates, with 102 specimens collected from 46 locations. Morphological examination facilitated accurate classification within the *Rhamnus* genus, predominantly identifying *Rh. lycioides*. Despite the potential role of *Rhamnus* as alternative hosts, none of the surveyed plants showed signs of infection by Pca, indicating the absence of its aecial stage throughout the collection period. These findings shed light on the distribution and host association of Pca, providing valuable insights into its ecological dynamics.

Acknowledgments

The authors express their gratitude to the Deanship of Scientific Research at the University of Jordan for the financial support provided through grants numbered 2323 and 1942, which facilitated the procurement of materials and conducted the survey during the years 2018-2020, respectively. Additionally, appreciation is extended to Abdul Hameed Shoman Foundation for their support, grant number 3/2019, which enabled the continuation of the survey from 2021 to 2022. Special thanks are also extended to Muslim B. Alananbeh and Farah Al-Amir for their assistance in collecting *Rhamnus* spp. Furthermore, the authors would like to acknowledge Khalaf Al-Enezi for his contribution to the measurement of selected isolates of oat rust uredospores and teliospores.

References

Al Eisawi D. 1996. Vegetation of Jordan. Regional Office for Science and Technology for the Arab States/UNESCO e Cairo Office, Cairo.

Ali Y, Iqbal S, Aatif HM, Naveed K, Khan AA, Ijaz M, Raza A. 2023. Predicting stripe rust severity in wheat using meteorological data with environmental response modeling. *J King Saud Univ Sci*., **35(4)**: 102591.

Ali Y, Khan AA, Ijaz M, Aatif HM, Rahim A, Ahmad S, Rafiq M. 2021. Characterization of environmental conditions conducive for leaf rust and genetic diversity on wheat crosses based upon physiomorphic traits. *Pakistan J Phytopathol*., **33(1)**: 125-136.

Baum BR, Fleischmann G, Martens JW, Rajhathy T, Thomas H. 1972. Notes on the habitat and distribution of *Avena* species in the Mediterranean and Middle East. *Canad J Bot*, **50 (6):** 1385-1397.

Baum BR. 1977. Oats: wild and cultivated. a monograph of the genus *Avena* L. (Poaceae). Ottawa, Canada: Minister of Supply and Services, 108-114.

Belsariya N, Sahu M, Kak A, Roy S. 2023. Morphological characterization using nonmetric variables in exotic oat (*Avena* sp.) accessions. https://doi.org/10.21203/rs.3.rs-2633376/v1 (Under review).

Berlin A, Samils B, Andersson B. 2017. Multiple genotypes within aecial clusters in *Puccinia graminis* and *Puccinia coronata*: improved understanding of the biology of cereal rust fungi. *Fung Biol Biotechnol*., 4(1): 1-7.

Cabral AL, Gnanesh BN, Mitchell Fetch J, McCartney C, Fetch T, Park RF., Menzies JG, McCallum B., Nanaiah GK, Goyal, A. 2014. Oat fungal diseases and the application of molecular marker technology for their control. In *Future challenges in crop protection against fungal pathogens* (pp. 343-358). New York, NY: Springer New York.

Carson ML. 2008. Virulence frequencies in oat crown rust in the United States from 2001 through 2005. *Plant Dis*., **92(3)**: 379-384.

Carson ML. 2010. Additional sources of broad-spectrum resistance to *Puccinia coronata* f. sp. *avenae* from Canadian accessions of *Avena barbata*. *Plant Dis*., **94(12):** 1405-1410.

Carson ML. 2011. Virulence in oat crown rust (*Puccinia coronata* f. sp. *avenae*) in the United States from 2006 through 2009. *Plant Dis*., **95(12):** 1528-1534.

Chen J, Upadhyaya NM, Ortiz D, Sperschneider J, LiF, Bouton C, Dodds PN. 2017. Loss of AvrSr50 by somatic exchange in stem rust leads to virulence for Sr50 resistance in wheat. *Science*, **358(6370)**: 1607-1610.

Chong J, Gruenke J, Dueck R, Mayert W, Woods S. 2008. Virulence of oat crown rust (*Puccinia coronata* f. sp. *avenae*) in Canada during 2002–2006. *Canad J Plant Pathol*., **30(1):** 115-123.

Clegg MT and Allard RW. 1972. Patterns of genetic differentiation in the slender wild oat species *Avenabarbata*. *Proc Nation Acad Sci USA*, **69(7):** 1820-1824.

Clemens GV and Klinken BJ. 2014. The future of oats in the food and health continuum. *Brit J Nut.*, **112**: S75–S79.

Cummins GB. 2013. The rust fungi of cereals, grasses, and bamboos. Springer Science & Business Media.

Davis PH. 1970. Flora of Turkey and the East Aegean Islands, Volume 2. Edinburgh: Edinburgh University Press, pp. 527.

Devi R, Sood VK, Arora A. 2023. Stability analysis for seed yield and related traits of oat (*Avena sativa* L.) under varied conditions of North-Western Himalayas. *Inter J Env Clim Change*, **13(11):** 2409-2418.

Dietz, SM. 1926. The alternate hosts of crown rust, *Puccinia coronata* Corda*. J Agric Res*., **33:** 953–970.

El-Shatnawi MKJ and Ghosheh HZ. 1999. The influence of sowing rate on the production and growth of wild oat (*Avena fatua*) in the depleted semi-arid rangelands of Jordan. *AfriJ Range For Sci*., **16(2-3):** 96-100. DOI: 10.2989/10220119909485723.

Grove WB. 1913. The British rust fungi (Uredinales): Their Biology and Classification. University Press.

Hemmami I, Allagui MB, Chakroun M, Gazzah ME. 2006. *Rhamnus lycioides* in Tunisia is a new aecial host of oat crown rust. *Europ J Plant Pathol*., **115:** 357-361.

Jabar A and Yahya AA. 2019. Using morphological and chemical characteristics of grains for identification and taxonomy of some oat cultivars (*Avena sativa* L.). *Mesop J Agricul*., **45(1):** 229-242.

Jin Y. 2011. Role of *Berberis* spp. as alternate hosts in generating new races of *Puccinia graminis* and *P. striiformis*. *Euphytica*, **179(1)**: 105-108.

Kumar R, Varghese S, Jayaswal D, Jayaswall K, Yadav K, Mishra G, Kumar S. 2023. Agro-morphological and genetic variability analysis in oat germplasms with special emphasis on food and feed. *Plos One*, **18(2):** e0280450.

Leggett JM. 1992. Classification and speciation in *Avena*. *Oat Sci Technol*., **33**: 29-52.

Leonard KJ, Anikster Y, Manisterski J. 2004. Patterns of virulence in natural populations of *Puccinia coronata* on wild oat in Israel and in agricultural populations on cultivated oat in the United States. *Phytopathology*, **94(5):** 505-514.

Leonard KJ. 2002. Oat lines with effective adult plant resistance to crown rust. *Plant Dis*., **86(6)**: 593-598.

Loskutov IG, and Rines HW. 2011. Avena. Wild crop relatives: genomic and breeding resources: cereals, 109-183.

Loskutov IG. 2007. Oats (*Avena* L.) distribution, taxonomy, evolution and breeding value. Saint-Petersburg: SSC RF VIR Publishing.

Lyon B and Broders K. 2017. Impact of climate change and race evolution on the epidemiology and ecology of stripe rust in central and eastern USA and Canada. *Canad J Plant Pathol*., **39(4)**: 385-392.

Mehmood S, Sajid M, Zhao J, Huang L, Kang Z. 2020. Alternate hosts of *Puccinia striiformis* f. sp. *tritici* and their role. *Pathogens*, **9(6)**: 434.

Moreau ELP, Riddle JM, Nazareno ES, Kianian SF. 2023. Three decades of rust surveys in the United States reveal drastic virulence changes in oat crown rust. *Plant Dis*. DOI: 10.1094/PDIS-09-23-1956-RE.

Murphy HC. 1935. Physiologic specialization in *Puccinia coronata avenae*. Bull. US Depart. *Agriculture*, **433:** 1–48.

Muschler R. 1912. A Manual Flora of Egypt, Volume 1. Berlin: R. Friedlaender & Sohn, Karlstrasse, pp. 618.

Nazareno ES, Li F, Smith M, Park RF, Kianian SF, Figueroa MP. 2018. *Puccinia coronata* f. sp. *avenae*: a threat to global oat production. *Mol. Plant Pathol*., **19(5)**: 1047-1060.

Nguyen, M. L. 2007. Flora of China. Vol. 12, Hippocastanaceae through Theaceae. Edited by Wu Zhengyi, Raven Peter H., Hong Deyuan. Beijing: Science Press; St. Louis: Missouri Botanical Garden Press, 139-162.

Oran SA. 2014. A list of flowering wild plants in Tafila Province, Jordan. *Inter J Biodiv Conserv*., **6(1):**, 28-40.

Simons MD. 1978. Oats: a standardized system of nomenclature for genes and chromosomes and catalog of genes governing characters (No. 509). Department of Agriculture, Science and Education Administration.

Simons MD. 1985. Crown rust. In: The Cereal Rusts, Vol. II, Diseases, Distribution, Epidemiology and Control. A.P. Roelfs and W.R. Bushnell, Eds.; Academic Press: Orlando, FL, pp. 131-172.

Singh A, Chaudhary M, Chaudhary NK, Chiranjeev N. 2019. Stability analysis for morphological characters in oats (*Avena sativa* L.). *Int J Chem*., **7(5)**: 3172-3178.

Soovali P and Koppel M. 2003. Genetic control of oat rust diseases. *Agron Res*., **1(2):** 245-251.

Statista. 2021. Grain production worldwide by type, 2020/21. Available at: https://www.statista.com/statistics/263977/world-grain-production-by-type/

Taifour H and El-Oqlah, A. 2016. The plants of Jordan, an annotated checklist. Kew Publishing Royal Botanic Gardens, U.K., Kew.

Tutin TG. 1968. Flora Europaea: Rosaceae to Umbelliferae, Ed.; Cambridge Univ. Press, Volume 2, pp. 244.

USDA-ARS CDL. 2017. Oat crown rust. USDA-ARS Cereal Disease Laboratory. Available at: https://www.ars.usda.gov/midwest-area/stpaul/cereal-disease-lab/docs/cereal-rusts/oat-crown-rust/

Wahl I. 1958. Studies on crown rust and stem rust on oats in Israel. *Bull Res Counc Isr Sect. D*, **6(3)**.

Wahl I. 1970. Prevalence and geographic distribution of resistance to crown rust in *Avena sterilis*. *Phytopathology*, **60(5):** 746-749.

Wahl L, Dinoor A, Halperin J, Schreiter S. 1960. The effect of *Rhamnus palaestina* on the origin and persistence of oat crown rust races. *Phytopathology*, **50(7)**: 562-567.

Zhao J, Wang M, Chen X, Kang Z. 2016. Role of alternate hosts in epidemiology and pathogen variation of cereal rusts. *Ann RevPhytopathology*, **54:** 207-228.

Appendix 1. Characterization of *Pca* in comparison to *Pga.*

Characteristic	*Pca*	*Pga*	Main possible similarity
Macroscopic characterization			
Uredium and telium location	Mostly the infected part of host is the leaf, uredia are on both sides of leaf (amphigenous) but mainly on upper side (epiphylous), telia are hypophyllous	The infected part of the host is mainly the culm and sheath, beginning on parts near soil. Both types of pustules are amphigenous	In a few cases, both may infect most plant parts especially in advanced infection and late in the season
Uredium and telium color	Uredium with orange color	Uredium with brown to brick color	Both have black telium
Uredium shape, size, and arrangement	In general, smaller, oblong, and less elongated, arranged irregularly or in rows	In general, bigger, linear, and more elongated, arranged in rows	Both pustules are pulverate (have a powdery nature)
Telia shape, size, and arrangement	In general, smaller, (appear as tiny dots), oblong to a linear pustule, arranged irregularly, teliaremain with epidermis for long time (rigid)	In general, bigger, elongated pustule, telia became naked soonly so consider as pulverate, arranged in rows,	
Microscopic characterization			
Apical of the teliospore upper cell	Nearly curved to flat apix, with crown-shaped digital projections, apical and projections are darker in colors than other parts	Apix tapered toward one side, curved to ovate (candle flame-shape) or nearly circular and always without digital projections	
Number of projections on the upper cell tip of teliospore and its length	(2-7) but five is the most frequent, projections are darker than other parts of teliospore diam= (2.5-7) µm	No projections	
Teliospore shape	Wedge-shaped (width decrease gradually toward the pedicel)	Shape is the same (not decreased) along the two cells and there is clear difference in width with pedicel	
Teliospore cells	Covered cells, both cells are with nearly equal length	In exposed cells, the lower cell in most cases, is longer than the upper one	Both are 2-celled spore
Teliospore pedicel	Pedicel is shorter	Pedicel is longer and, in some spores, may has length more than the sum of both spore cells length	Both are pedicelated
Teliospore colour	In general, darker	In general, lighter	Both may have colourless teliospore
Uredospore ornamentations	Echinula are relatively shorter = (0.7-1) µm	Echinula are longer (not measured)	Both are echinulated
Uredospore general shape	Most of spores are nearly globose, (some ovate or irregular)	Most of spores are ellipsoid (some are ovate or oblong)	Both are unicellular
Uredospore cell wall thickness	Relatively thinner	Relatively thicker	
Uredospore dimensions as an average	(17.5-19.15) x (19.5-22) µm	(22-43) x (16-22) µm	
Teliospore dimensions as an average	(34-54) x (10-14) µm	(35-60) x (12-22)µm	
Dimensions of uredospore germ pore	3-4 µm	Not measured	
Presence of paraphyses			No paraphyses found

Appendix 2

Common and specific characteristics for *Avena* spp. collected in this study.

a. Common characteristics shared by both species include:

- Annual lifespan, with none of the samples identified as perennial.
- Erect or erect-geniculate culms.
- Green coloration in early stages, with no glaucous samples.
- Plant height ranges from 70 to 150 cm.
- Mostly equilateral or slightly flagged panicles.
- Glumes are either equal or nearly so in length.
- Awn insertion is approximately at the lower third of the lemma back.
- Lemma are distinct from glumes and possess a tough texture.
- The lemma back, under awn insertion, is densely covered with microhairs, and none were found to be
- glabrous.
- Scar shapes mostly oval with some being elliptic or nearly round.
- Lodicules of fatua-type and consistently devoid of hairs.
- Periphery ring confined to 1/3-1/4 of the scar in *A. sterilis* or 1/5-1/2 in *A. barbata.*
-

b. Primary characteristics for *Avena sterilis*:

- Disarticulation at maturity occurs solely on the lowermost floret.
- Most of samples have bisubulate lemma tips, few have bidenticulate or
- bimucronate lemma tips.
- Mostly, palea keels bears more than one cilia rows (2-3).
- Palea back with prickles.
- The number of florets per spikelet ranges from 2 to 5, with 9 to 11 glume nerves.

a. Primary characteristics for *Avena barbata*:

- All spikelet florets disarticulated at maturity.
- Most lemma tips are biaristulate and the less exhibit bisubulate lemma tips, some samples have
- Bothtypes.
- Mostly, palea keels bears 1 cilia row and palea back is glabrous.
- Arista in biaristulated lemma tips is never longer than 5 mm.
- Lodicule length rarely falls below 8 mm.
- The number of florets per spikelet ranges from 2 to 3, with 9 to 11 glume nerves, some are with 7 to
- 9nerves.

Appendix 3. Key to identify *Rhamnus* species in Jordan (*Rh. lycioides, Rh. disperma, Rh. punctata* and *Rh. alaternus*):

0….. Plants are with soft stipules, stipules are not persistent (mostly absent) winter buds covered with scales, stipules are subulate.

Rhamnus. spp.

1….. Plants leaves are evergreen:

2….. Plants without spines

Rh. alaternus (leaves are entire, shiny, and leathery).

2….. Plants with spiny stems.

Rh. lycioides.

1….. Plants leaves are deciduous:

3….. Plant leaf margins with small teeth (serrate).

Rh. lycioides (leaf is flat, branch is direct).

3….. Plant leaf entire, with smooth margins:

4….. Plant leaf margins are revolute, leaf densely pubescent below.

Rh. punctata (branch is direct, lateral veins are conspicuous, glabrous fruits).

4….. Plants branches are tortuous, bark always with ash-colour.

Rh. disperma (2-seeded drupes,much spiny plant, plant habitat of rocky-desert type).

Key to identify the *Rh. lycioides* subspecies:

1….. leaf is linear or linear-spatulate, lateral veins are invisible on upper side, mature drupe is black.

Rh. lycioides subsp. *lycioides*

1….. leaf is obovate or obovate-elliptical:

2….. Plant is evergreen leaves; lateral veins are conspicuous.

Rh. lycioides subsp. *oleoides*

2….. Plant is decidiuos leaves, lateral veins are inconspicuous.

Rh. lycioides subsp. *graecus*.

JJBS

Volume 17, Number 3,September 2024
ISSN 1995-6673
Pages 575 – 581
https://doi.org/10.54319/jjbs/170321

Jordan Journal of Biological Sciences

The Effect of Stressful Conditions on Biochemical and Hematological Parameters Among University Students

Rahaf. M. Al-Zubaidi[1] , Husni. S. Farah[1,*] , Khaled. A. Ahmed[1] , Esam. Y. Qnais[2] , Sana. M. Audeh[3], Mahmoud .S. Abu-Samak[4]

[1] *Department of Medical Laboratory Sciences, Faculty of Allied Medical Sciences, Al-Ahliyya Amman University, 19328, Amman, Jordan.* [2] *Department of Biology and Biotechnology, Faculty of Science, The Hashemite University, Zarqa, Jordan,* [3]*Abdali Hospital, Cardiology Department, Amman, 11191, Jordan,* [4]*Department of Clinical Pharmacy and Therapeutics, Faculty of Pharmacy, Applied Science Private University, Amman, Jordan*

Received: August 3, 2023; Revised: October 9, 2023; Accepted: October 26, 2023

Abstract

University students are more susceptible to stress and other mental health problems, which can have a negative impact on their health and academic performance. The main objective of the present study was to explore the influence of exam stress on various biochemical and hematological parameters among university students. The study involved 100 undergraduate students (n=100) aged between 18 and 35. Blood samples were collected from each student three times. The first sample was taken one week before the exam, the second on the day of the exam, and the third 10 days after the exam. Various tests were carried out to evaluate the impact of academic stress on different parameters, such as Glutamate oxaloacetate transaminase (GOT), Glutamate pyruvate transaminase (GPT), glucose, iron, magnesium, sodium, potassium, thyroid-stimulating hormone (TSH), cortisol, insulin, complete blood count, and blood pressure. Blood samples obtained during exams indicated a substantial decrease in the levels of liver enzymes (GOT, GPT), serum magnesium, insulin, and white blood cell count as compared to pre-post examination findings ($P<0.001$). A significant increase was recorded in electrolyte levels (sodium and potassium; $P<0.001$), blood pressure (systolic and diastolic; $P<0.001$), glucose level ($P<0.001$), Hormones level (TSH; $P<0.001$, cortisol; $P<0.001$), and platelet counts ($P<0.002$). The study has revealed that exam stress can significantly impact certain blood test results, leading to physical changes that could affect a student's academic performance. This study is significant because it explores the impact of stress on tests that have not been previously examined

Keywords: Stress, hematological parameters, biochemical parameters, Examination period, university students.

1. Introduction

Stress is a chain of events that commences with a stressor stimulus and culminates in a hypothalamus-triggered reaction in the brain, which prompts physiological responses throughout the body's systems (Colon-Emeri *et al.*, 2023). It is a process of perceiving and coping with external events, not just a stimulus or a response (Beer *et al.*, 2021). The impact of a stressor on an individual can also be quite variable, ranging from minor to life-threatening (Stewart *et al.*, 2019). Academic stress is a common occurrence in the daily lives of students and is a significant issue in our society (Wu *et al.*, 2020). A student may be worried for a variety of reasons or stressors, including academic overloads, insufficient study time, a heavy workload each semester, a lack of enthusiasm, and high family expectations all contribute to moderate stress among students (Wuthrich *et al.*, 2020; Karaman *et al.*, 2019).

Stress has been reported to cause a variety of symptoms and illnesses, depending on the reasons and degree of stress (Effati-Daryani *et al.*, 2020). According to physiological studies, any type of stress has a major influence on the hematogenic and endocrine systems (Burtkhanovich and Khasanov, 2023; Alhmoud *et al.*, 2021**)**. During the examination period, psychological stress can affect students in various ways and disrupt their body's balance, leading to changes in blood pressure levels. This can result in an increase in both systolic and diastolic blood pressure (Stock *et al.*, 2020). Previous studies have examined whether stress due to the examination is enough to alter certain hematological parameters. (Alhmoud *et al.*, 2021, Dawson *et al.*, 2020). The increase in platelet count may cause health problems, from bleeding problems to the formation of various clots, and the reduction in white blood cells (WBCs) can impact the effectiveness of the immune system. A recent study has shown that the stress of exams can impact specific blood parameters, including neutrophils, platelet counts, packed cell volume (PCV), and MCV (Seiler *et al.*, 2020). These parameters were found to be elevated, while lymphocyte counts were found to decrease. However, there were no significant changes observed in hemoglobin, red blood cells, or other indicators (Alhmoud *et al.*, 2021).

* Corresponding author. e-mail: h.farah@ammanu.edu.jo.

Academic examination stress is reported to decrease immune functioning; students showed increased salivary cortisol concentrations and reported greater acute perceived stress during the examination period compared to the non-examination period (Seiler *et al.*, 2020). Previous investigation has provided new insight into the complex relationship between examination stress, cortisol, and immune functioning (Concerto *et al.*, 2017). Individual exam performance is influenced by a variety of changeable and non-modifiable factors, including pre-examination anxiety (Alsulami *et al.*, 2018).

During exams, the body experiences heightened stress levels that trigger the release of adrenaline and corticosteroids. These hormones can affect insulin production, increase glucagon levels, and prompt the liver to release more glucose (Hinds and Edwin, 2022). Changes in hormonal homeostasis, activation of lipoperoxidation processes with the development of oxidative stress, and the disintegration of antioxidant protection factors are typical for academic stress in students (Al Qteishat *et al.*, 2021). Growth hormone levels increase concurrently, decreasing the insulin responsiveness of body tissues (such as muscle and fat). More glucose is consequently available in the bloodstream. Low insulin results in decreased Na/K ATPase activity, reduced sodium reabsorption, and increased sodium ion exhalation from the distal convoluted tubules (Onyango, 2018)**.** It is possible that an increase in AST and ALT levels after an exam is due to the dietary habits commonly adopted by students during this period (Maradi and Usha, 2019). The purpose of this study was to explore how exam stress affects the health of undergraduate students. Specifically, it aims to identify physiological markers that are influenced by short-term stress and could impact academic performance. Managing stress effectively can help minimize negative effects on overall health.

2. Materials and Methods

2.1. Study population

The current study was conducted to examine the changes in the biochemical and hematological characteristics due to exams at Al-Ahliyya Amman University's, Department of Medical Laboratory Sciences, Faculty of Allied Medical Sciences. A total of 100 undergraduate students (n=100) aged between 18 and 35 participated in this study. All students were subjected to a preliminary medical examination. Students with blood hypertension, renal or liver problems, any endocrine disorder, such as diabetes mellitus or thyroid abnormalities, students with any autoimmune disease, and smokers were all disqualified from the study.

2.2. Ethical consideration

The ethical approval for this study was obtained from the Al-Ahliyya Amman University, Faculty of Allied Medical Sciences. Informed written consent was taken from each participant prior to the commencement of the study to explain the benefits and/or any risks related to participation in the study.

2.3. Procedure

A total of 100 students (n=100) underwent intravenous blood collection three times, with 5 ml collected from their median antecubital vein on each occasion. The collection was carried out in the morning, specifically between 8 and 9 am. The first sample was collected a week before the test, the second on the day of the exam, and the third 10 days after the exam. The blood was distributed into two types of blood collecting tubes, vacutainers containing EDTA and heparin-containing tubes, and subjected to centrifugation at 3500 rpm for 5 minutes.

The serum was separated and divided into two Eppendorf tubes. One tube was stored at -20°C as a backup, and the other was used for biochemical analysis. The samples collected in EDTA were used for hematological parameter analysis. Participants were informed of the study's objective and procedure and signed a consent form before blood collection.

The liver enzyme (aspartate aminotransferase (AST) and alanine aminotransferase (ALT)), as well as other parameters such as magnesium and glucose, were analyzed on Human Fully Automatic Biochemistry analyzers (HumaStar 200, Germany). Serum samples were tested in duplicate for cortisol, insulin and TSH levels using commercially available ELISA kits (Ray Biotech) in a single batch. A blood count was performed on an automated hematology analyzer (Sysmex XP-300). Blood pressures were measured in the supine position using the Beurer BM 26 device after a 10-minute rest interval. To ensure the reliability of the data, participants were advised to fast, particularly when measuring the glucose levels in their samples.

2.4. Statistical Analysis

All data were analyzed by the SPSS software (V.28 Inc., Chicago, USA) and the figures were created by Microsoft Excel 2019. Kolmogorov-Smirnov test was used for variables distribution. Normally distributed numerical variables of all data are expressed as mean ± standard deviation (SD). One-way analysis of variance (ANOVA) was used for comparison of biochemical and hematological parameters before, during, and after examination with Bonferroni post hoc test for multiple comparisons between the readings. Nominal variables were presented as frequency and percentage (%) and a comparison between studied groups was performed using the *Chi*-square test. The significance of the difference was considered at $p<0.05$.

3. Results

Table 1 displays the mean, standard deviation (SD), and P-value for the hematological and biochemical parameters. It summarizes the fundamental features of the study sample a week before the exam (pre-exam), during the exam day, and 10 days after the exam.

Table 1. Comparison of hematological and biochemical parameters before, during, and after the examination (Paired Samples Test).

Parameters	N=100 Student			P-value
	Before	During	After	
Liver enzyme				
GOT (UI/L)	24.20±5.33	16.77±4.05	21.53±5.07	<0.001
GPT (UI/L)	27.70±10.93	15.60±7.84	21.63±7.79	<0.001
Serum electrolyte				
Magnesium (mg/dl)	2.07±0.36	1.22±0.43	2.24±0.37	<0.001
Iron (µg/dl)	88.82±21.97	88.83±28.50	92.91±36.66	0.828
Sodium (mEq/l)	132.65±2.44	145.25±2.29	137.11±2.54	<0.001
Potassium (mEq/l)	3.98±0.46	4.95±0.38	4.15±0.48	<0.001
Blood pressure				
SBP (mm Hg)	103.23±7.15	119.60±7.01	101.60±7.91	<0.001
DBP (mm Hg)	74.47±5.10	79.63±4.30	73.93±3.44	<0.001
Hematological parameters				
WBCs (*10^3/ml)	7.79±0.98	6.33±1.18	7.55±1.24	<0.001
Platelets (*10^3/ml)	294.40±57.57	351.20±69.34	300.60±67.74	<0.002
Neutrophil (%)	58.93±8.08	59.14±10.87	58.73±9.22	0.986
Lymphocytes (%)	34.27±7.64	33.61±10.21	34.24±8.72	0.948
Hormones				
TSH (µIU/ml)	1.61±0.95	2.45±0.96	1.12±0.46	<0.001
Cortisol (µg/dl)	9.60±3.17	15.90±4.76	9.70±4.08	< 0.001
Insulin µU/ml	7.87±.640	5.50±.925	6.25±1.38	<0.001
Blood sugar				
Glucose mg/dl	93.12±2.85	105.12±2.90	94.12±2.03	<0.001

SBP: Systolic blood pressure. DBP: Diastolic blood pressure. * Significant differences at p-value <0.05.

The findings presented in Figures 1 and 2 indicate a significant difference (P < 0.001) between the GOT and GPT levels prior to the exam (24.20 5.33 U/L and 27.70 10.93 U/L, respectively), during the exam period (16.774.05U/L and 15.607.84 U/L, respectively), and after a 10-day after the exam period (21.53 ± 5.07 U/L and 21.63 ± 7.79 U/L, respectively).

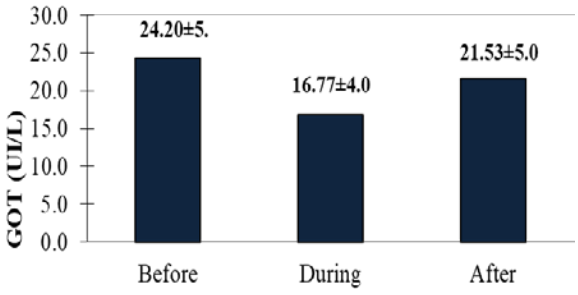

Figure 1. The mean levels of serum GOT of the students before, during, and after the examination period. Statistically difference (P<0.001) was observed between the level of GOT during the exam and that before and after on the other hand.

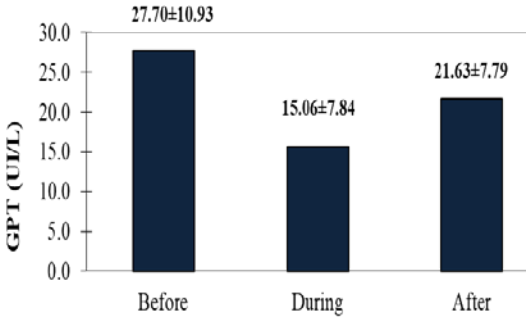

Figure 2. The mean levels of serum GPT of the students before, during, and after the examination period. Statistically difference (p<0.001) was observed between the level of GOT during the exam and that before and after on the other hand.

In the course of the present study, magnesium levels were significantly reduced (p,<0.001) during the exam period (1.22±0.43 mg/dl) compared to that before (2.07±0.36 mg/dl) and after the exam period (2.24±0.37 mg/dl) after the exam (Figure 3 and table 1). There was a statically difference between the levels of magnesium before the exam period and after the exam period (Figure 3 and Table 1).

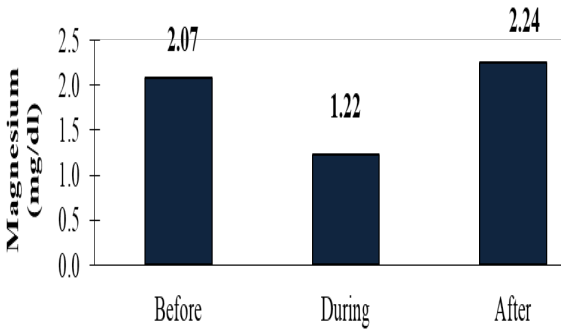

Figure 3. The mean levels of serum magnesium of the students before, during and after the examination period**.**

According to the current data (Table 1), the mean sodium levels before the exam period (132.65±2.44 mEq/l), during the exam period (145.25 ±2.29 mEq/l), and after 10 days of the exam period (137.11 ± 2.54 mEq/l) were significantly different (P< 0.001). The level of sodium significantly increased during the exam period compared to that before and after the exam period (P <0.001). As indicated in (Table 1&2) there was no significant difference in serum potassium levels before and after the exam, despite the serum potassium level on exam day (4.95±0.38) being much higher (P< 0.001) than that levels before the exam (3.98±0.46) and after the exam (4.15±0.48).

During the exam, there was a significant increase in both systolic and diastolic blood pressure levels (P <0.001), with measurements of 119.60±7.01 mmHg and 79.63±4.30 mmHg respectively. Prior to the exam, these levels were 103.23±7.15mmHg and 74.47±5.10mmHg respectively. However, after the exam period, the levels returned to similar values of 101.60±7.91mmHg and 73.93±3.44 mmHg respectively, as illustrated in Figure 4.

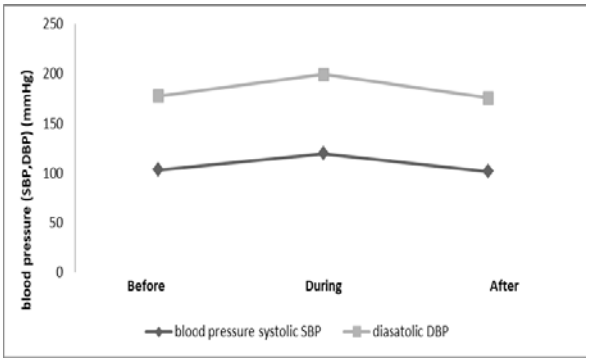

Figure 4. The mean levels of systolic and diastolic blood pressure for the students before, during, and after the examination period. A statistical difference (p<0.001) was observed in the systolic and diastolic blood pressure during the exam compared to the levels before and after the exam..

The count of white blood cells (WBC) was higher before (6.33±1.18) and after (7.55±1.24) the exam compared to during the exam (7.79±1.98), with a significant difference (P<0.001).. There was a significant increase in platelet count (P<0.001) during the exam period (351.20±69.34) compared to that before the exam (294.40±57.57) and after the exam (300.60±67.74). The platelet count before and after the exam remained the same with no significant difference (P<0.002),

The present study revealed a significant increase (P<0.001) in glucose level during the exam (105.125±2.9 mg/dl) compared to that before (93.125±2.85 mg/dl and after (94.125±2.031 mg/dl) the exam period. However, there were no significant changes (P=1.00) in glucose levels before and after the exam period (Table 2). Figure 5 reveals a significant rise (P< 0.001) in cortisol levels during exam periods (15.9±4.76 µg/dl) as compared with that before the exam period (9.6±3.17 µg/dl).

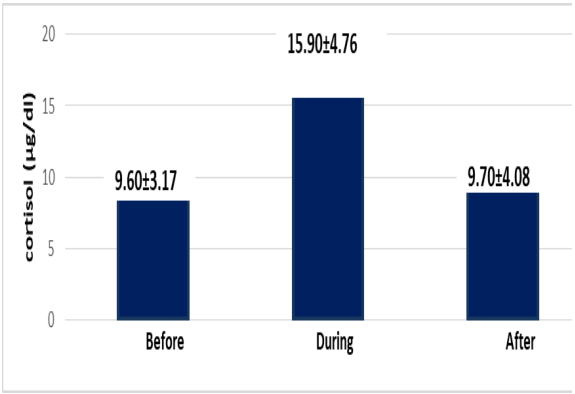

Figure 5. The mean level of cortisol before, during ,and after the examination period.

A substantial decrease (P<0.001) in insulin levels during the exam period (5.50±0.925 µU) in comparison to before (7.87±0.64 µU) and after the exam (6.25±1.38 µU) as indicated in Table 1. A significant difference (P <0.001) was observed between insulin levels before and during the exam, and a significant difference (P < 0.015) was also noted between insulin levels before and after the exam, as shown in Table 2.

Table 1 shows the thyroid stimulating hormone (TSH) level before (1.61±0.95 pg/ml), during (2.45±0.96pg/ml), and after the exam period (1.12±0.46 pg./ml). The levels of TSH during the exam were significantly higher (P<0.001) than the levels before and after the exam, there was no significant difference (P=0.075) between the levels before and after the exam (Table 2)**.**

Table 2. Bonferroni post-hoc analysis of the difference between (Magnesium, Sodium, potassium , SBP, DBP, glucose, cortisol, and insulin) of the students before, during and after the examination period.

Dependent Variable		Period	p-value
Magnesium (mg/dl))	Before	During	<0.001
		After	0.264
	During	Before	<0.001
		After	<0.001
	After	Before	0.264
		During	<0.001
Sodium (mEq/l)	Before	During	<0.001
		After	<0.001
	During	Before	<0.001
		After	<0.001
	After	Before	<0.001
		During	<0.001
Potassium (mEq/l)	Before	During	<0.001
		After	0.355
	During	Before	<0.001
		After	<0.001
	After	Before	0.355
		During	<0.001
SBP(mm Hg)	Before	During	<0.001
		After	1.000
	During	Before	<0.001
		After	<0.001
	After	Before	1.000
		During	<0.001
DBP (mm Hg)	Before	During	<0.001
		After	1.000
	During	Before	<0.001
		After	<0.001
	After	Before	1.000
		During	<0.001
Glucose (mg/dL)	Before	During	<0.001
		After	1.00
	During	Before	<0.001
		After	<0.001
	After	Before	1.00
		During	<0.001
Cortisol	Before	During	<0.001
		After	1.00
	During	Before	<0.001
		After	<0.001
	After	Before	1.00
		During	<0.001
Insulin	Before	During	<0.001
		After	<0.015
	During	Before	<0.001
		After	0.483
	After	Before	0.015
		During	0.483
TSH (pg/ml)	Before	During	<0.001
		After	0.075
	During	Before	<0.001
		After	<0.001
	After	Before	0.075
		During	<0.001

*Significant differences at p-value <0.05

4. Discussion

University students often experience academic-related stress, which can have negative effects on their mental and physical health and lead to academic difficulties (Lassiter *et al.*, 2022). Regularly conducting biochemical and hematological examinations is crucial in monitoring physiological changes that occur during exam periods. This study involved tests that had not been previously examined, including liver enzymes, thyroid hormone, and magnesium levels, alongside other tests that had been antecedently studied. The levels of liver enzymes (GOT, GPT) were significantly decreased during the examination period. Our results are consistent with the study that found lower levels of GOT and GPT before exams compared to that after the exam period (Maradi and Usha, 2019). It's likely that the significant decrease in liver enzymes during stressful situations is caused by an overabundance of cortisol hormone **(**Edoardo *et al.*, 2005).

The findings of the current study observed a significant reduction in serum magnesium levels during the examination period when compared to that before and after the examination period ($P < 0.001$). However, there was no statistically significant difference between magnesium levels before and after the exam ($P= 0.264$). This decrease is likely due to increased urinary magnesium excretion during the examination period, as previously reported (Lopresti *et al.*, 2020). Another study found that a stimulus-induced rise in cortisol levels results in a fall in magnesium levels, creating a shortage that increases the body's susceptibility to stress (Pickering *et al.*, 2020).

Recent research indicates that academic stress can activate the release of adrenaline and corticosteroids in the body, leading to negative effects on insulin levels and the function of the Na/K ATPase pump. This pump system is essential for maintaining the balance of sodium and potassium in the body, and when its function is compromised, more sodium ions are excreted while potassium ions flow out of the cell (Maradi and Usha., 2019). The current study's results support the observation that potassium levels tend to increase during exam periods (Maradi and Usha., 2019).

It has been observed in this study that blood pressure tends to increase during times of exams. However, there was no significant change in systolic and diastolic blood pressure before and after the exam ($P=1.000$). Our findings are in line with the recent report that has demonstrated an increase in blood pressure during exam periods (Singh *et al.*, 2022). Stress triggers the hypothalamus to stimulate the adrenal glands to release epinephrine and cortisol, which in turn elevates heart rate, blood pressure, and metabolic rate (Hinds and Edwin, 2022). According to previous reports, individuals who experience the greatest rise in blood pressure or heart rate in reaction to sudden stress are more likely to develop future health problems (Kivimäki and Andrew , Turner *et al.*, 2020).

There was a reduction in the count of white blood cells during the examination period in comparison to the count before the exams. However, the count of white blood cells returned to its pre-examination phase level after the exams were over. Catecholamines have the ability to lower the activity of specific white blood cells which can lead to a weakened immune system. This effect is most prominent in individuals who experience significant stress reactions

such as an increase in heart rate and blood pressure (Sharma *et al.*, 2022). Conversely, individuals with no significant changes in heart rate and blood pressure did not experience any changes in white blood cell activity. This finding is similar to a report that demonstrated a decrease in the total leucocyte count during examination periods (Dhabhar *et al.*, 1996).

There was a significant increase in platelet count ($P<0.001$) during the exam period compared to that before the exam and after the exam. The platelet count before and after the exam remained the same with no significant difference ($P=1.000$), which is consistent with the findings of the previous investigation (Engler *et al.*, 2004). It was found that platelet count increased significantly during the examination period and remained elevated for three days after the end of the exam period (Alhmoud *et al.*, 2021). However, in the current study, platelet count returned to normal within ten days after the examination period ended. This suggests that platelets remained elevated for no more than ten days after the examinations.

During exam periods, the stress hormone cortisol was found to be elevated, which directly affects glucose levels in the bloodstream by triggering glucose synthesis through gluconeogenesis (Maduka *et al.*, 2015). This study confirms the previous report of a significant increase in cortisol levels during exam weeks compared to non-exam weeks (Glaser *et al.*, 1994). A study revealed that glucose levels tend to be higher during exams compared to before and after the exams. This is due to an increase in cortisol levels and a decrease in insulin levels (Chan *et al.*, 2020). Stress hormones such as cortisol can hinder the proper functioning of insulin-producing cells in the pancreas, resulting in decreased insulin production and reduced insulin levels (Rahman *et al.*, 2021). According to a report, patients who experience persistent stress states may develop type II diabetes due to stress-induced hyperglycemia and other mechanisms causing insulin resistance at the tissue level (Sharma *et al.*, 2022). This study examined the impact of exam stress on thyroid gland function by measuring TSH hormone levels. The findings showed a significant increase in TSH levels during the exam period compared to before and after. Our findings are consistent with those of a recent study that found a rise in TSH levels during stress (Hettiarachchi *et al.*, 2014). On the other hand, there is a conflicting study that associates insulin resistance and problems with regulating blood sugar with hypothyroidism and it has indicated that cortisol may decrease the level of TSH in the bloodstream (Gierach *et al.*, 2014).

5. Conclusion

This study investigated the impact of exam stress on various biochemical and hematological tests, which affects a significant number of students. The study examined previously untested factors and found that these changes could have an adverse effect on students' academic performance. However, the study did not investigate the potential impact of other hormones, and thus more studies are necessary to gain a complete understanding.

Conflict of Interest

The authors declare no conflict of interest.

Authors' Declaration

The authors of this article, affirm that the work presented herein is entirely original. Any responsibility for claims related to the content of this article will rest solely upon us.

Acknowledgments

The authors express their gratitude for the financial support given by Al-Ahliyya Amman University in Jordan. They also thank every member of the university, especially Dr. Talal Al-Qaisi and Walaa Hamdan, for their continuous inspiration and support throughout the entire study.

References

Alhmoud J F, Husni SF and Talal Q. 2021.The Changes in Some Hematological Parameters among University Students Due to Stressful Conditions During and after Examinations Period.Indian Journal of Forensic Medicine & Toxicology. **15**: 1181-1186.

Al Qteishat A, Gabriyanchik MA and Bokov DO. 2021. Changes in parameters of biochemical and oxidative stress in university students during and after examinations. Cell Stress and Chaperones. 26: 811–817.

Alsulami S, Zaid A, Mohammed SB, Fahad A, Amr A, Abdulkarim A, Meshary A and Mohammed A. 2018. Perception of academic stress among health science preparatory program students in two Saudi universities. Advances in medical education and practice 159-164.

Burtkhanovich KB. 2023. Structural and Functional Features of the Thymus Under Some Impacts. American Journal of Pediatric Medicine and Health Science. **1**: 81-87.

Chan, MZ and Isra T. 2020. Blood Glucose Levels in Students with Stress. Stress. 5: 10.

Colon EK, Schmader, HJ, Miriam M and Heather W. 2023. "Ageing and physical resilience after health stressors." Stress Health. **2**:1-7

Concerto C, Dhaval P, Carmenrita I, Eileen C, Maria RM, Antonio B, Rocco Z, Eugenio A, and Fortunato B. 2017. Academic stress disrupts cortical plasticity in graduate students." Stress. **20**: 212-216.

Dawson AF, William WB, Joanna A, Bella D, James ND, Karen H, Sophie A, Tom BM, Peter BJ and Julieta G. Mindfulness-based interventions for university students: A systematic review and meta-analysis of randomized controlled trials. 2020.Applied Psychology: Health and Well-Being. **12**: 384-410.

Dhabhar FS, Andrew HM, Bruce SM, and Robert LS. 1996. Stress-induced changes in blood leukocyte distribution. Role of adrenal steroid hormones. Journal of Immunology. 157: 1638-1644.

Edoardo GG, Roberto T and Vincenzo S. 2005. Liver enzyme alteration: a guide for clinicians. CMAJ. **172**: 367–379.

Effati DF, Somayeh Z, Azam M, Elnaz H, Sakineh GY and Mojgan M. 2020. Depression, stress, anxiety and their predictors in Iranian pregnant women during the outbreak of COVID-19. BMC psychology **8**: 1-10.

Engler H, Lutz D, Sabine H, Susanne K, J. Ross S, Konr S, and Volker Stefanski. 2004. Effects of social stress on blood leukocyte distribution: the role of α-and β-adrenergic mechanisms. Journal of neuroimmunology. **156**: 153-162.

Gierach M, Joanna G and Roman . 2014. Insulin resistance and thyroid disorders." Endokrynologia Polska. **65**: 70-76.

Glaser RD, Pearl JK, Kiecolt G, and William BM. 1994. Plasma cortisol levels and reactivation of latent Epstein-Barr virus in response to examination stress. Psychoneuroendocrinology. **19**: 765-772.

Hettiarachchi M, Chathuranga LF, Priyanka G, Prasanjanie J and Dasun Maduranga. 2014. How does the quality of life and the underlying biochemical indicators correlate with the performance in academic examinations in a group of medical students of Sri Lanka?. Medical Education Online **19**: 227-72.

Hinds JA, and Edwin RS. (2022. The role of the hypothalamus–pituitary–adrenal (HPA) axis in test-induced anxiety: assessments, physiological responses, and molecular details Stresses. **2**: 146-155.

Karaman, MA., Eunice L, Javier CV and Joshua CW. 2019. Predictors of academic stress among college students. Journal of College Counseling. **22**: 41-55.

Kivimäki M and Andrew S. 2018. Effects of stress on the development and progression of cardiovascular disease. Nature Reviews Cardiology **15**: 215-229.

Lassiter JW, Amanda LC, Carrie WL and Brendan D. 2022. The Impact of Academic Disruption on Stress Among College Athletes. Journal of Issues in Intercollegiate Athletics. **15**:149-167.

Lopresti AL 2020.The effects of psychological and environmental stress on micronutrient concentrations in the body: a review of the evidence. Advances in Nutrition. **11**: 103-112.

Maduka IC, Emeka EN and Silas AU. 2015. The relationship between serum cortisol, adrenaline, blood glucose and lipid profile of undergraduate students under examination stress. African health sciences. **15**: 131-136.

Maradi R and Usha P. 2019. Effects of academic stress on lipid profile, liver function tests and electrolytes in healthy medical students. Int J Clin Biochem Res. **6**: 606-610.

Oliver W, Beer J , Rebecca P, and Camille RQ. 2021"Exploring stress, coping, and health outcomes among social workers. European Journal of Social Work. **24**:: 317-330.

Onyango AN. 2018.Cellular stresses and stress responses in the pathogenesis of insulin resistance. Oxidative medicine and cellular longevity Oxid Med Cell Longev.**2018**: 320-361.

Pickering G, André M, Marion T, Przemyslaw B, Natalia Y, Mohamed A, Lionel N and Etienne P. 2020. Magnesium status and stress: The vicious circle concept revisited." Nutrients. **12**: 3672.

Rahman M, Khandkar S, Sharnali D, Sushmita K, Elikanah OA, Md Ataur R, Abdul H and Myung P. 2021. Role of insulin in health and disease: an update. International journal of molecular sciences. **22**: 6403.

Seiler A, Christopher PF and Lisa M C. 2020. The impact of everyday stressors on the immune system and health. Stress challenges and immunity in space: From mechanisms to monitoring and preventive strategies : 71-92.

Sharma K, Shivani A, Swarupa C and Mayur BW. 2022. Stress-Induced Diabetes: A Review. Cureus **14**: 9

Singh S, Soumitra C and Rajajeyakumar M. 2022. Examination Stress and its Correlation with Cardiovascular Parameters and Lipid Profile. International Journal of Pharmaceutical and Clinical Research. **14**: 396-404

Stewart JG , Grant SS, Erika CE, Elizabeth AC, Nicholas BA, George MS and Randy P. 2019.. Life stress and suicide in adolescents Journal of abnormal child psychology. **47**: 1707-1722.

Stock AA, Soomi L, Nicole GN and Anne-Marie C. 2020. Effects of sleep extension on sleep duration, sleepiness, and blood pressure in college students. Sleep Health. **6:** 32-39.

Turner AI, Smyth N, Hall SJ, Torres SJ, Hussein M, Jayasinghe SU and Clow AJ. 2020. Psychological stress reactivity and future health and disease outcomes: A systematic review of prospective evidence. Psychoneuroendocrinology. **114**:104.

Wu D, Lingwei Y, Tingzhong Y, Randall C, Sihui P, Wei G, and Shuhan J. 2020. The impacts of uncertainty stress on mental disorders of Chinese college students: Evidence from a nationwide study." Frontiers in psychology. **11**: 243.

Wuthrich, VM, Tess J and Vanessa A. 2020. Academic stress in the final years of school: A systematic literature review. Child Psychiatry & Human Development. **51**: 986-1015.

Subscription

Jordan Journal of Biological Sciences

An International Peer – Reviewed Research Journal

Published by the Deanship of Scientific Research, The Hashemite University, Zarqa, Jordan

Name: ..... الاسم:

Specialty: ..... التخصص:

Address: ..... العنوان:

P.O. Box: ..... صندوق البريد:

City &Postal Code:..... المدينة: الرمز البريدي:

Country: ..... الدولة:

Phone: ..... رقم الهاتف

Fax No.: ..... رقم الفاكس:

E-mail: ..... البريد الإلكتروني:

Method of payment: ..... طريقة الدفع:

Amount Enclosed: ..... المبلغ المرفق:

Signature: ..... التوقيع:

Cheque should be paid to Deanship of Research and Graduate Studies – The Hashemite University.

I would like to subscribe to the Journal

For

- ☐ One year
- ☐ Two years
- ☐ Three years

One Year Subscription Rates

	Inside Jordan	Outside Jordan
Individuals	JD10	$70
Students	JD5	$35
Institutions	JD 20	$90

Correspondence

Subscriptions and sales:

The Hashemite University
P.O. Box 330127-Zarqa 13115 – Jordan
Telephone: 00 962 5 3903333
Fax no. : 0096253903349
E. mail: jjbs@hu.edu.jo

المجلة الأردنية للعلوم الحياتية
Jordan Journal of Biological Sciences (JJBS)

http://jjbs.hu.edu.jo

المجلة الأردنية للعلوم الحياتية: مجلة علمية عالمية محكمة ومفهرسة ومصنفة، تصدرعن الجامعة الهاشمية وبدعم من صندوق دعم البحث العلمي والإبتكار – وزراة التعليم العالي والبحث العلمي.

هيئة التحرير

رئيس التحرير

الأستاذ الدكتور محمد علي وديان
الجامعة الهاشمية، الزرقاء، الأردن

مساعد رئيس التحرير

الأستاذ الدكتور مهند عليان مساعدة
الجامعة الهاشمية، الزرقاء، الأردن

الأعضاء:

الأستاذ الدكتور خالد محمد خليفات
جامعة مؤتة

الأستاذ الدكتور ليث ناصر العيطان
جامعة العلوم و التكنولوجيا الأردنية

الأستاذة الدكتورة طارق حسن النجار
الجامعة الأردنية / العقبة

الأستاذ الدكتور وسام محمد هادي الخطيب
الجامعة اليرموك

الاستاذ الدكتور عبد اللطيف علي الغزاوي
الجامعة الهاشمية

الاستاذ الدكتور نضال احمد عودات
جامعة البلقاء التطبيقية

فريق الدعم:

المحرر اللغوي

الأستاذ الدكتور شادي نعامنة

تنفيذ وإخراج

م. مهند عقده

ترسل البحوث الى العنوان التالي:

رئيس تحرير المجلة الأردنية للعلوم الحياتية
الجامعة الهاشمية
ص.ب , 330127 , الزرقاء, 13115 , الأردن
هاتف: 0096253903333
E-mail: jjbs@hu.edu.jo, Website: www.jjbs.hu.edu.jo

المملكة الأردنية الهاشمية

المجلة الأردنية

للعلوم الحياتية

مجلة علمية عالمية محكمة

تصدر بدعم من صندوق دعم البحث العلمي و الابتكار

http://jjbs.hu.edu.jo/